Palaeoclimate reconstructions from the Antarctic Peninsula; linking marine and terrestrial records

Anna Rose Hey

May 2009

Thesis submitted for the degree of PhD



British Antarctic Survey
NATURAL ENVIRONMENT RESEARCH COUNCIL

CARDIFF UNIVERSITY
PRIFYSGOL CAERDYDD

UMI Number: U585235

All rights reserved

INFORMATION TO ALL USERS
The quality of this reproduction is dependent upon the quality of the copy submitted.

In the unlikely event that the author did not send a complete manuscript
and there are missing pages, these will be noted. Also, if material had to be removed,
a note will indicate the deletion.



UMI U585235
Published by ProQuest LLC 2013. Copyright in the Dissertation held by the Author.
Microform Edition © ProQuest LLC.
All rights reserved. This work is protected against
unauthorized copying under Title 17, United States Code.



ProQuest LLC
789 East Eisenhower Parkway
P.O. Box 1346
Ann Arbor, MI 48106-1346

Summary

The Antarctic Peninsula (AP) is one of the fastest-warming regions on Earth. To assess whether this warming is part of the natural variability in the climate system, palaeoclimate archives are used to document the character of past climate changes and constrain predictions for the future. This investigation integrates a suite of radiocarbon dated marine sediment records from the continental shelf of the AP to provide a critical assessment of the distribution, timing, magnitude and forcing of Holocene climatic events. Sedimentary logs, diatom assemblages, stable isotopes and pigments were used as proxies to reconstruct AP ice sheet retreat, fluctuations in sea ice extent, changes in water mass circulation and ice shelf collapse events. This has revealed the spatial and temporal heterogeneity of climate events through the Holocene. The marine environment of the western AP (WAP) experienced deglaciation; onset of the Mid Holocene climatic optimum; and climatic deterioration into the Late Holocene considerably earlier than the marine environment of the eastern AP (EAP) and AP terrestrial records. These differences suggest that the climate of the WAP has been more closely connected with the SE Pacific, through coupled ocean-atmosphere interactions (such as the position of Southern Westerlies and El Niño Southern Oscillation frequency), whereas the EAP displayed a closer affinity with AP terrestrial records and the cryospheric influences of the Weddell Sea. This investigation has emphasised the complexity of the climate system of the AP on a range of spatial and temporal scales and highlighted that no single record can adequately represent regional palaeoclimate; records must be developed from the oceans and continents and then interpreted as an assemblage.

Acknowledgements

I would like to express my thanks to the many people who have helped during the course of this project. I particularly thank my fantastic supervisors; Dr Jennifer Pike, Dr Claire Allen and Dr Dominic Hodgson. Jenny has been a constant source of support and advice; I truly could not have wished for a better supervisor. Claire was a fantastic mentor onboard the British Antarctic Survey cruise (JR149) that I was extremely privileged to have taken part in. Claire's constant enthusiasm for Antarctic research (and diatoms!) has been highly contagious. Dom's guidance during the sedimentary pigment component of this project and in the closing phases of the thesis has been invaluable.

Special thanks to Xavier Crosta for providing the facilities at Bordeaux to run stable isotope analyses; for hosting my visit in 2008, together with Delphine Denis; and for useful discussion regarding the interpretation of this dataset. Thanks also to Brendan Keeley and Matt Pickering at the University of York for providing training with the laboratory procedures to undertake sedimentary pigment analyses and for aiding pigment identification. I am also grateful to C.-D. Hillenbrand for chronology discussions and colleagues at Cardiff University who have developed my knowledge in the field of palaeoclimatology enormously.

This project was supported by NERC grant NER/S/A/2005/13132 and the British Antarctic Survey CACHE-PEP project. Thanks also to the Antarctic Science Bursary and The Micropalaeontological Society (TMS) for financial assistance to attend the ISAES X Conference in 2007.

Thanks to friends old and new for being there when I needed, particularly Wendy, Anna, Amy, Claire, Cass, Ruth, Cheryl, Alison, the 222'ers and Highfields Home Group. Finally, I thank my family (the Hey's and Haworth's) for their endless encouragement and support. Last (but by no means least), Gavin and Mungo – without you, this would have been so much harder. Thanks Mungo for facilitating all that thinking time at the park and Gav… what can I say?... you are the best!

List of abbreviations

AABW	Antarctic Bottom Water
AAIW	Antarctic Intermediate Water
AASW	Antarctic Surface Water
ACoastC	Antarctic Coastal Current
AP	Antarctic Peninsula
BAS	British Antarctic Survey
CDW	Circumpolar Deep Water
CRS	*Chaetoceros* species resting spores
EAP	East Antarctic Peninsula
EAIS	East Antarctic Ice Sheet
ENSO	El Niño Southern Oscillation
GC	Gravity core
HPLC	High performance liquid chromatography
HSSW	High Salinity Shelf Water
LCDW	Lower Circumpolar Deep Water
LGM	Last Glacial Maximum
mbsf	Metres below sea floor
MS	Magnetic susceptibility
Mv/g	Millions of valves / gram
NADW	North Atlantic Deep Water
PCA	Principal components analysis
PF	Polar Front
PFZ	Polar Frontal Zone
PGC	Prince Gustav Channel
RRS	Royal Research Ship
SAF	Subantarctic Front
SST	Sea Surface Temperature
TC	Trigger core
TOC	Total organic carbon
UCDW	Upper Circumpolar Deep Water
VC	Vibro core
WAIS	West Antarctic Ice Sheet
WAP	West Antarctic Peninsula
WSDW	Weddell Sea Deep Water
WSBW	Weddell Sea Bottom Water
WSTW	Weddell Sea Transitional Water
WW	Winter Water

Contents

Declaration..... i
Summary..... ii
Acknowledgements..... iii
List of abbreviations..... iv
Contents..... v
List of Contents..... vi
List of Figures..... xii
List of Tables..... xviii
List of Equations and Boxes..... xx

1 INTRODUCTION 1-1

1.1 Rationale 1-1
1.1.1 Why Antarctica? 1-1
1.1.2 Why the Antarctic Peninsula? 1-1
1.1.3 Why the Holocene? 1-2

1.2 Research questions 1-3

1.3 Project aims 1-3

1.4 Thesis format 1-3

2 LOCATION 2-1

2.1 Geological setting 2-1

2.2 Antarctic Ice Sheet history 2-2
2.2.1 Mesozoic – Cenozoic 2-2
2.2.2 Last Glacial Maximum and subsequent deglaciation 2-3
2.2.3 Present day 2-4

2.3 Antarctic palaeoclimate and present climate 2-5
2.3.1 Palaeoclimate proxies 2-6
2.3.2 Palaeoclimate reconstructions 2-8
2.3.2.1 Last Glacial Maximum (LGM) 2-8
2.3.2.2 Last deglaciation 2-10
2.3.2.3 Holocene 2-11
2.3.3 Present day climate 2-13

2.4 Southern Ocean oceanography 2-15
2.4.1 Southern Ocean zones 2-17
2.4.2 Southern Ocean currents and water masses 2-17
2.4.3 Southern Ocean sea ice 2-19

2.5 Antarctic Peninsula oceanography 2-20
2.5.1 West Antarctic Peninsula (WAP) 2-20
2.5.1.1 WAP water masses and currents 2-21
2.5.1.2 WAP sea ice 2-23
2.5.2 East Antarctic Peninsula (EAP) 2-25
2.5.2.1 EAP water masses and currents 2-25
2.5.2.2 EAP sea ice 2-26

2.6 Antarctic Peninsula study regions 2-26
2.6.1 WAP: GC114 – Boyd Strait; and GC047 – Anvers Trough 2-29
2.6.2 WAP: VC306 – Marguerite Bay 2-30
2.6.3 WAP: GC358 – Ronne Entrance 2-32
2.6.4 EAP: VC243 and VC237 – Prince Gustav Channel 2-33
2.6.5 EAP: VC205 – Erebus and Terror Gulf 2-33

2.7 Chapter summary 2-34

3 DIATOMS OF THE SOUTHERN OCEAN 3-1

3.1 Definition and physical form 3-1

3.2 Biology 3-2

3.3 Distribution and ecology 3-3

3.4 Diatom habitats 3-6
3.4.1 Open ocean 3-6
3.4.2 Sea ice 3-7
3.4.3 Benthic environments 3-8

3.5 Diatom species ecology 3-8
3.5.1 *Actinocyclus actinochilus* (Ehrenberg) Simonsen 3-9
3.5.2 Genus *Chaetoceros* Ehrenberg 3-9
3.5.2.1 Sub-genus *Hyalochaete Chaetoceros* Gran 3-10
3.5.2.2 *Chaetoceros* resting spores (CRS) 3-10
3.5.3 Genus *Cocconeis* Ehrenberg 3-10
3.5.4 *Eucampia antarctica* (Castracane) Mangin 3-11
3.5.5 *Fragilariopsis curta* (Van Heurck) Hustedt 3-12
3.5.6 *Fragilariopsis cylindrus* (Grunow) Krieger 3-13
3.5.7 *Fragilariopsis kerguelensis* (O'Meara) Hustedt 3-13
3.5.8 *Fragilariopsis obliquecostata* (Van Heurck) Heiden 3-14
3.5.9 *Fragilariopsis separanda* Hustedt 3-15
3.5.10 *Fragilariopsis sublinearis* (Van Heurck) Heiden 3-15
3.5.11 *Fragilariopsis vanheurckii* (M. Pergallo) Hustedt 3-15
3.5.12 Genus *Navicula* Bory de st-Vincent 3-16
3.5.13 *Odontella weissflogii* (Janisch) Grunow 3-16
3.5.14 Genus *Porosira* Jørgensen 3-16
3.5.15 Genus *Proboscia* Sunström 3-17
3.5.16 Genus *Rhizosolenia* Brightwell 3-17
3.5.17 *Thalassiosira antarctica* Comber 3-18
3.5.18 *Thalassiosira gracilis* (Karsten) Hustedt 3-19
3.5.19 *Thalassiosira lentiginosa* (Janisch) Fryxell 3-20

3.6 Diatoms as proxies 3-20
3.6.1 Diatom preservation in the sedimentary record 3-21
3.6.1.1 Advection 3-22
3.6.1.2 Aggregation 3-22
3.6.1.3 Dissolution 3-22
3.6.2 Diatom assumptions for this study 3-23
3.6.3 Total diatom abundance and CRS abundance 3-24
3.6.4 Non-CRS absolute abundance and species assemblage 3-24

3.7 Chapter summary 3-24

4 ADDITIONAL PROXIES 4-1

4.1 Stable isotopes 4-1
4.1.1 Rationale behind stable isotopes 4-1
4.1.2 Carbon isotopes 4-1
4.1.3 Nitrogen isotopes 4-4
4.1.4 Potential sources of alteration to the isotopic signal 4-4

4.2 Sedimentary pigments 4-7
4.2.1 Origin of sedimentary pigments 4-7
4.2.2 Chlorophylls 4-8
4.2.3 Chlorophyll degradation products 4-8
4.2.4 Carotenoids 4-9

4.3 Chapter summary 4-10

5 METHODS 5-1

5.1 Quantitative diatom analysis 5-1
5.1.1 Sampling strategy 5-1
5.1.2 Sample preparation 5-1
5.1.3 Data collection and format 5-4
5.1.4 Data analysis 5-7
5.1.5 Statistical interpretation 5-11
5.1.6 Characterising diatom assemblages 5-14
5.1.7 Defining diatom stratigraphic zones 5-14

5.2 Stable isotope analysis 5-16
5.2.1 Sampling strategy 5-16
5.2.2 Sample preparation 5-16
5.2.3 Data collection and format 5-17
5.2.4 Data analysis 5-17

5.3 Sedimentary pigment analysis 5-19
5.3.1 Sampling strategy 5-19
5.3.2 Sample preparation 5-21
5.3.3 Data collection and format 5-21
5.3.4 Data analysis 5-24

5.4 Chapter summary 5-24

6 CORE MATERIAL AND CHRONOLOGY 6-1

6.1 Core material 6-2
6.1.1 Antarctic marine sediments 6-2
6.1.2 GC114 6-3
6.1.3 GC047 6-4
6.1.4 VC306 6-4
6.1.5 GC358 6-4
6.1.6 VC243 6-4
6.1.7 VC237 6-5
6.1.8 VC205 6-6

6.2 Core chronology 6-9
6.2.1 ^{14}C dating 6-9
6.2.2 Problems with ^{14}C dating in the Southern Ocean 6-15
6.2.2.1 Reservoir age 6-16
6.2.2.2 Contamination 6-19
6.2.3 GC114 and GC047 6-24
6.2.4 VC306 6-26
6.2.5 GC358 6-29
6.2.6 VC243 and VC237 6-33
6.2.7 VC205 6-35
6.2.8 Composite age models and correction applied ..... 6 -36
6.2.9 Age calibration 6-40

6.3 Chapter summary 6-46

7 RESULTS 7-1

7.1 GC114 7-2
7.1.1 Diatom assemblage 7-2
7.1.2 Diatom stratigraphic zones 7-2
7.1.2.1 GC114-i: 3.3 – 1.3 m 7-3
7.1.2.2 GC114-ii: 1.3 – 0 m 7-4
7.1.3 Diatom summary 7-13

7.2 GC047 7-14
7.2.1 Diatom assemblage 7-14
7.2.2 Diatom stratigraphic zones 7-14
7.2.2.1 GC047-i: 3.8 – 3.5 m 7-16
7.2.2.2 GC047-ii: 3.5 – 2.75 m 7-16
7.2.2.3 GC047-iii: 2.75 – 0.8 m 7-17
7.2.2.4 GC047-iv: 0.8 – 0 m 7-18
7.2.3 Diatom summary 7-27

7.3 VC306 7-28
7.3.1 Diatom assemblage 7-28
7.3.2 Diatom stratigraphic zones 7-28
7.3.2.1 VC306-i: 1.8 – 1.1 m 7-29
7.3.2.2 VC306-ii: 1.1 – 0 m 7-30
7.3.3 Diatom summary 7-39
7.3.4 Stable Isotopes 7-40
7.3.4.1 VC306-i: 1.8 – 1.1 m 7-40
7.3.4.2 VC306-ii: 1.1 – 0 m 7-40

7.4 GC358 ..... **7-43**
7.4.1 Diatom assemblage 7-43
7.4.2 Diatom stratigraphic zones 7-43
7.4.2.1 GC358-i: 0.75 – 0.5 m 7-44
7.4.2.2 GC358-ii: 0.5 – 0 m 7-45
7.4.3 Diatom summary 7-52

7.5 VC243 ..... **7-53**
7.5.1 Diatom assemblage 7-53
7.5.2 Diatom stratigraphic zones 7-53
7.5.2.1 VC243-i: 5.8 – 4 m 7-54
7.5.2.2 VC243-ii: 4 – 1.5 m 7-55
7.5.2.3 VC243-iii: 1.5 – 0 m 7-56
7.5.3 Diatom summary 7-66
7.5.4 Stable Isotopes 7-67
7.5.4.1 VC243-i: 5.8 – 4 m 7-67
7.5.4.2 VC243-ii: 4 – 1.5 m 7-67
7.5.4.3 VC243-iii: 1.5 – 0 m 7-68
7.5.5 Sedimentary pigments 7-70
7.5.5.1 VC243-ii: 4 – 1.5 m 7-75
7.5.5.2 VC243-iii: 1.5 – 0 m 7-75

7.6 VC237 ..... **7-76**
7.6.1 Diatom assemblage 7-76
7.6.2 Diatom stratigraphic zones 7-76
7.6.2.1 VC237-i: 6 – 5.2 m 7-77
7.6.2.2 VC237-ii: 5.2 – 3.7 m 7-78
7.6.2.3 VC237-iii: 3.7 – 2.1 m 7-78
7.6.3 Diatom summary 7-88

7.7 VC205 ..... **7-89**
7.7.1 Diatom assemblage 7-89
7.7.2 Diatom stratigraphic zones 7-89
7.7.2.1 VC205-i: 5.1 – 3.5 m 7-90
7.7.2.2 VC205-ii: 3.5 – 2.2 m 7-91
7.7.2.3 VC205-iii: 2.2 – 0 m 7-91
7.7.3 Diatom summary 101

7.8 Antarctic Peninsula fossil diatom assemblages **7-102**
7.8.1 Regional trends 7-102
7.8.2 Species associations 7-105

7.9 Chapter summary **7-108**

8 PALAEOCLIMATE RECONSTRUCTIONS FROM THE ANTARCTIC PENINSULA 8-1

8.1 Regional patterns in the AP fossil diatom assemblages 8-2
8.1.1 Regional trends 8-2
8.1.2 Diatom habitat types 8-5
8.1.2.1 Sea ice type 1 8-6
8.1.2.2 Sea ice type 2 8-6
8.1.2.3 Cool open ocean 8-7
8.1.2.4 Ice melt 8-7
8.1.2.5 Pelagic open ocean 8-8

8.2 Stable isotope and sedimentary pigment analyses 8-11
8.2.1 Stable isotopes 8-11
8.2.2 Sedimentary pigments 8-12

8.3 Holocene palaeoclimate reconstructions for each core locality 8-13
8.3.1 GC114 8-13
8.3.2 GC047 8-15
8.3.3 VC306 8-19
8.3.4 GC358 8-23
8.3.5 VC243 and VC237 8-26
8.3.6 VC205 8-34

8.4 Discussion 8-38
8.4.1 Were Holocene climate events peninsula-wide and synchronous? 8-38
8.4.1.1 Deglaciation – Early Holocene transition 8-40
Retreat of grounded ice 8-40
The post-deglaciation marine environment 8-57
Occurrence of an Early Holocene "climatic reversal"? 8-61
Occurrence of an Early Holocene climatic optimum? 8-63
After the Early Holocene climatic optimum 8-65
8.4.1.2 Mid-Holocene climatic optimum 8-67
8.4.1.3 Late Holocene climatic deterioration (Neoglacial) 8-76
8.4.1.4 Summary 8-84
8.4.2 Do AP Holocene climate events display similar phasing and duration to circum-Antarctic and global trends? 8-87
8.4.2.1 Deglaciation – Early Holocene transition 8-87
Retreat of grounded ice 8-88
Occurrence of an Early Holocene "climatic reversal"? 8-90
Occurrence of an Early Holocene climatic optimum? 8-90
After the Early Holocene climatic optimum 8-93
8.4.2.2 Mid-Holocene climatic optimum 8-93
8.4.2.3 Late Holocene climatic deterioration (Neoglacial) 8-95
8.4.2.4 Summary 8-96

8.5 Chapter summary 8-97

9 CONCLUSIONS 9-1

9.1 Conclusions from AP palaeoclimate reconstructions 9-1

9.2 Future research 9-5

List of Figures

Figure 2.1	Antarctic continental blocks, topography and bathymetry.	2-1
Figure 2.2	The location of Antarctica within Gondwana.	2-2
Figure 2.3	Extent of grounded ice during the Last Glacial Maximum (LGM) along the Antarctic Peninsula (AP) continental shelf.	2-4
Figure 2.4	Antarctic palaeoclimate proxy records, colour-coded based on the proxy used.	2-7
Figure 2.5	LGM winter and summer sea ice extent.	2-9
Figure 2.6	A three-dimensional schematic showing the meridional overturning circulation in each of the ocean basins and the horizontal connection in the Southern Ocean.	2-15
Figure 2.7	Schematic block diagram showing the Subantarctic Zone and Antarctic Zone of the Southern Ocean, and associated oceanographic fronts.	2-16
Figure 2.8	Southern Ocean seasonal sea ice extents and the Antarctic Polar Front	2-20
Figure 2.9	Map of the Antarctic Peninsula (AP), showing core localities, together with: (a) Mean annual isotherms; (b) Position of the present day average summer and winter sea ice limits and Polar Front; (c) Regional bathymetry and oceanographic circulation patterns.	2-24
Figure 3.1	Schematic diagram of centric and pennates diatom sub-orders	3-2
Figure 3.2	Chlorophyll *a* distributions in the Southern Ocean show high spatial and temporal variability.	3-5
Figure 3.3	Relationships between sea ice and open ocean diatoms in surface waters, sediments and sea ice cover.	3-21
Figure 4.1	Transmission of the surface water isotopic signature to photosynthetic organisms (diatoms), which then accumulate in marine sediment to record the inorganic nutrient pool of the surface waters.	4-3
Figure 4.2	Structure of Chlorophyll *a*.	4-8
Figure 4.3	Structure of the carotenoid Diatoxanthin	4-9
Figure 5.1	Preparation method for diatom quantitative analysis, using water column settling technique.	5-3
Figure 5.2	Rarefaction test for core GC114, sample depths 1 m and 1.7 m.	5-4
Figure 5.3	Count methodology for individual and fragmented diatom valves	5-6
Figure 5.4	Comparisons of fragmentation indexes for core VC243	5-7
Figure 5.5	Comparison of diatom relative abundance percentages between CRS included and CRS-free counts for core GC047.	5-9
Figure 5.6	Core VC306: Magnetic susceptibility (SI), sedimentary log and total diatom abundance (Mv/g).	5-10
Figure 5.7	Core VC205: Non-CRS diatom assemblage absolute abundance (Mv/g) (Figure 5.7a) and relative abundance (%) (Figure 5.7b) for a selection of AP indicator species	5-10
Figure 5.8	The principle of PCA, with variables x and y.	5-13
Figure 5.9	Example of hierarchical cluster analysis, using the agglomerative cluster method for five two-dimensional data points to produce a dendrogram	5-14
Figure 5.10	Core GC047: Q-mode PCA component scores plotted stratigraphically for PCA axes 1 – 5.	5-15
Figure 5.11	Example chromatogram, with the relative elution times of carotenoids and chlorophylls shown on the *x*-axis, and relative absorbance on the *y*-axis.	5-22
Figure 6.1	Map of the Antarctic Peninsula, showing core localities, together with the position of the present day average summer and winter sea ice limits and Polar Front.	6-1

Figure 6.2	Schematic representation of sediment delivery and sources in: (a) Terrigenous-dominated regimes, with ice-rafting, aeolian and mass movement events forming the dominant sediment transport processes; (b) Biogenic-dominated regimes, with high levels of surface water primary productivity and transmission to the sediments.	6-3
Figure 6.3	Core GC114: Magnetic susceptibility curve and sedimentary log.	6-7
Figure 6.4	Core GC047: Magnetic susceptibility curve and sedimentary log.	6-7
Figure 6.5	Core VC306: Magnetic susceptibility curve and sedimentary log.	6-7
Figure 6.6	Core GC358: Magnetic susceptibility curve and sedimentary log.	6-7
Figure 6.7	Core VC243: Magnetic susceptibility curve and sedimentary log.	6-7
Figure 6.8	Core VC237: Magnetic susceptibility curve and sedimentary log.	6-7
Figure 6.9	Core VC205: Magnetic susceptibility curve and sedimentary log.	6-7
Figure 6.10	Geology of the areas adjacent to Prince Gustav Channel (PGC), with petrographic data from cores VC237 and VC243.	6-8
Figure 6.11	Composite uncorrected ^{14}C age-depth plot for all cores used in this investigation.	6-11
Figure 6.12	Map of AP showing published surface sediment ages.	6-12
Figure 6.13	Map of WAP showing spatial variability in published surface sediment ages.	6-13
Figure 6.14	Map of north WAP and EAP showing spatial variability in published surface sediment ages.	6-14
Figure 6.15	Map of Marguerite Bay and southern Bellingshausen Sea showing box, vibro and gravity core surface sediment ages.	6-15
Figure 6.16	Core top age ranges, divided by geographic region, and compared to the surface ages of GC114 and TC046 (GC047).	6-25
Figure 6.17	(a) Marine cores from Marguerite Bay corrected by subtracting core top ages; (b) Marine cores from Marguerite Bay corrected using a 2460 ^{14}C year reservoir age.	6-28
Figure 6.18	Uncorrected age-depth plot for core GC358, together with surface sediment age for core GC359 and box cores from the southern Bellingshausen Sea.	6-30
Figure 6.19	Uncorrected age-depth plot for cores VC243 and VC237, together with box core surface ages for cores from Prince Gustav Channel (PGC) and northern Larsen area.	6-35
Figure 6.20	Composite corrected ^{14}C age-depth plot for all cores used in this investigation.	6-39
Figure 6.21	Radiocarbon age versus calibrated age for ^{14}C-dated samples from cores GC114 and VC306 using CALIB (v5.0.1).	6-42
Figure 7.1	Map of the Antarctic Peninsula, showing core localities, together with the position of the present day average summer and winter sea ice limits and Polar Front.	7-1
Figure 7.2	a) Core GC114: Total diatom abundance, CRS absolute abundance (both from CRS-included counts) and non-CRS assemblage absolute abundance (from CRS-free counts) (millions of valves/g (Mv/g)). b) Core GC114: CRS relative abundance (%)	7-5
Figure 7.3	Core GC114: Diatom absolute abundance (from CRS-included counts; Mv/g).	7-6
Figure 7.4	Core GC114: Non-CRS diatom assemblage plots for AP indicator species: (a) Absolute abundance (Mv/g); (b) Relative abundance (%).	7-7
Figure 7.5	Core GC114: R-mode PCA variable loading on axes 1 and 2 for diatom relative abundance data (> 1 %).	7-8
Figure 7.6	Core GC114: R-mode PCA variable loading on axes 3 and 4 for diatom relative abundance data (> 1 %).	7-8
Figure 7.7	GC114: R-mode cluster analysis of diatom species relative abundance (>1 %).	7-9

Figure 7.8	Core GC114: Q-mode PCA component scores plotted stratigraphically for PCA axes 1 – 4; division of the record into stratigraphic zones GC114-i and GC114-ii.	7-11
Figure 7.9	a) Core GC114: Q-mode cluster analysis of core depths, using diatom species relative abundance (>1 %). b) Core GC114: Stratigraphic pattern of Q-mode cluster groups.	7-12
Figure 7.10	Core GC114: Schematic representation of the fossil diatom assemblage, highlighting the relative contribution of CRS to the total assemblage and stratigraphic changes in the diatom community.	7-13
Figure 7.11	a) Core GC047: Total diatom abundance, CRS absolute abundance (both from CRS-included counts) and non-CRS assemblage absolute abundance (from CRS-free counts) (millions of valves/g (Mv/g)). b) Core GC047: CRS relative abundance (%).	7-19
Figure 7.12	Core GC047: Non-CRS diatom assemblage plots for AP indicator species: (a) Absolute abundance (Mv/g); (b) Relative abundance (%).	7-20
Figure 7.13	Core GC047: R-mode PCA variable loading on axes 1 and 2 for diatom relative abundance data (> 1 %).	7-21
Figure 7.14	Core GC047: R-mode PCA variable loading on axes 3 and 3 for diatom relative abundance data (> 1 %).	7-21
Figure 7.15	Core GC047: R-mode PCA variable loading on axes 4 and 5 for diatom relative abundance data (> 1 %).	7-22
Figure 7.16	GC047: R-mode cluster analysis of diatom species relative abundance (>1 %).	7-23
Figure 7.17	Core GC047: Q-mode PCA component scores plotted stratigraphically for PCA axes 1 – 5; division of the record into stratigraphic zones GC047-i, GC047-ii, GC047-iii and GC047-iv.	7-25
Figure 7.18	a) Core GC047: Q-mode cluster analysis of core depths, using diatom species relative abundances (>1 %). b) Core GC047: Stratigraphic pattern of Q-mode cluster groups.	7-26
Figure 7.19	Core GC047: Schematic representation of the fossil diatom assemblage, highlighting the relative contribution of CRS to the total assemblage and stratigraphic changes in the diatom community.	7-27
Figure 7.20	a) Core VC306: Total diatom abundance, CRS absolute abundance (both from CRS-included counts) and non-CRS assemblage absolute abundance (from CRS-free counts) (millions of valves/g (Mv/g)). b) Core VC306: CRS relative abundance (%).	7-32
Figure 7.21	Core VC306: Non-CRS diatom assemblage plots for AP indicator species: (a) Absolute abundance (Mv/g); (b) Relative abundance (%).	7-33
Figure 7.22	Core VC306: R-mode PCA variable loading on axes 1 and 2 for diatom relative abundance data (>1 %).	7-34
Figure 7.23	Core VC306: R-mode PCA variable loading on axes 3 and 4 for diatom relative abundance data (>1 %).	7-34
Figure 7.24	Core VC306: R-mode PCA variable loading on axes 3 and 4 for diatom relative abundance data (>1 %).	7-35
Figure 7.25	Core VC306: R-mode cluster analysis of diatom species relative abundance (> 1 %).	7-36
Figure 7.26	Core VC306: Q-mode PCA component scores plotted stratigraphically for PCA axes 1 – 5; division of the record into stratigraphic zones VC306-i and VC306-ii	7-38
Figure 7.27	Core VC306: Q-mode cluster analysis of core depths, using diatom species relative abundances (> 1 %).	7-38
Figure 7.28	Core VC306: Schematic representation of the fossil diatom assemblage, highlighting the relative contribution of CRS to the total assemblage and stratigraphic changes in the diatom community.	7-39

Figure 7.29	Core VC306: Bulk organic material stable isotope (carbon (C) and nitrogen (N)) contents and composition. a) C_{org}/N_{org} ratio b) Elemental contents (C_{org} and N_{org}) (%) c) Isotopic composition ($\delta^{13}C_{org}$ and $\delta^{15}N_{org}$) (‰)	7-42
Figure 7.30	a) Core GC358: Total diatom abundance, CRS absolute abundance (both from CRS-included counts) and non-CRS assemblage absolute abundance (from CRS-free counts) (millions of valves/g (Mv/g)).	7-46
Figure 7.30	b) Core GC358: CRS relative abundance (%).	7-46
Figure 7.31	Core GC358: Non-CRS diatom assemblage plots for AP indicator species: (a) Absolute abundance (Mv/g); (b) Relative abundance (%).	7-47
Figure 7.32	Core GC358: R-mode PCA variable loading on axes 1 and 2 for diatom relative abundance data (> 1 %).	7-48
Figure 7.33	Core GC358: R-mode PCA variable loading on axes 3 and 4 for diatom relative abundance data (> 1 %).	7-48
Figure 7.34	Core GC358: R-mode cluster analysis of diatom species relative abundance (> 1 %).	7-49
Figure 7.35	Core GC358: Q-mode PCA component scores plotted stratigraphically for PCA axes 1 – 4. Positive loading (dark grey); negative loading (light grey). Division of the record into stratigraphic zones GC358-i and GC358-ii	7-51
Figure 7.36	Core GC358: Q-mode cluster analysis of core depths, using diatom species relative abundances (> 1 %).	7-51
Figure 7.37	Core GC358: Schematic representation of the fossil diatom assemblage, highlighting the relative contribution of CRS to the total assemblage and stratigraphic changes in the diatom community.	7-52
Figure 7.38	a) Core VC243: Total diatom abundance, CRS absolute abundance (both from CRS-included counts) and non-CRS assemblage absolute abundance (from CRS-free counts). b) Core VC243: CRS relative abundance (%).	7-58
Figure 7.39	Core VC243: Diatom fragmentation, using two measures: observational index and percentage of *Fragilariopsis* species whole.	7-59
Figure 7.40	Core VC243: Non-CRS diatom assemblage plots for AP indicator species: (a) Absolute abundance (Mv/g); (b) Relative abundance (%).	7-60
Figure 7.41	Core VC243: R-mode PCA variable loading on axes 1 and 2 for diatom relative abundance data (> 1 %).	7-61
Figure 7.42	Core VC243: R-mode PCA variable loading on axes 3 and 4 for diatom relative abundance data (> 1 %).	7-61
Figure 7.43	Core VC243: R-mode cluster analysis of diatom species relative abundance (>1 %).	7-62
Figure 7.44	Core VC243: Q-mode PCA component scores plotted stratigraphically for PCA axes 1 – 4; division of the record into stratigraphic zones VC243-i, VC243-ii and VC243-iii	7-64
Figure 7.45	a) Core VC243: Q-mode cluster analysis of core depths, using diatom species relative abundance (>1 %). b) Core VC243: Stratigraphic pattern of Q-mode cluster groups.	7-65
Figure 7.46	Core VC243: Schematic representation of the fossil diatom assemblage, highlighting the relative contribution of CRS to the total assemblage and stratigraphic changes in the diatom community.	7-66
Figure 7.47	Core VC243: Bulk organic material stable isotope (carbon (C) and nitrogen (N)) contents and composition. a) C_{org}/N_{org} ratio b) Elemental contents (C_{org} and N_{org}) (%) c) Isotopic composition ($\delta^{13}C_{org}$ and $\delta^{15}N_{org}$) (‰) Stratigraphic zones VC243-i, VC243-ii and VC243-iii identified using Q-mode PCA analysis of diatom relative abundance data.	7-69

Figure 7.48	Core VC243: HPLC chromatogram for core depth 2.31 m, with the principal pigment peaks highlighted and numbered.	7-72
Figure 7.49	Core VC243: Sedimentary pigments ratios between: (a) total carotenoids and total chlorophylls; (b) total chlorophylls and diatoxanthin (Diatox); (c) total chlorophylls and monadoxanthin (Monadox); (d) total chlorophylls and fucoxanthin (Fuco).	7-73
Figure 7.50	Core VC243: Standardised peak areas (μAUs) for chlorophylls and carotenoids.	7-74
Figure 7.51	a) Core VC237: Total diatom abundance, CRS absolute abundance (both from CRS-included counts) and non-CRS assemblage absolute abundance (from CRS-free counts) (millions of valves/g (Mv/g)). b) Core VC237: CRS relative abundance (%).	7-80
Figure 7.52	Core VC237: Diatom fragmentation, using two measures: observational index and percentage of *Fragilariopsis* species whole.	7-81
Figure 7.53	Core VC237: Non-CRS diatom assemblage plots for AP indicator species: (a) Absolute abundance (Mv/g); (b) Relative abundance (%).	7-82
Figure 7.54	Core VC237: R-mode PCA variable loading on axes 1 and 2 for diatom relative abundance data (> 1 %).	7-83
Figure 7.55	Core VC237: R-mode PCA variable loading on axes 2 and 3 for diatom relative abundance data (> 1 %).	7-83
Figure 7.56	Core VC237: R-mode cluster analysis of diatom species relative abundance (>1 %).	7-84
Figure 7.57	Core VC237 Q-mode PCA component scores plotted stratigraphically for PCA axes 1 – 3; division of the record into stratigraphic zones VC237-i, VC237-ii and VC237-iii.	7-86
Figure 7.58	a) Core VC237: Q-mode cluster analysis of core depths, using diatom species relative abundance (>1 %). b) Core VC237: Stratigraphic pattern of Q-mode cluster groups.	7-87
Figure 7.59	Core VC237: Schematic representation of the fossil diatom assemblage, highlighting the relative contribution of CRS to the total assemblage and stratigraphic changes in the diatom community.	7-88
Figure 7.60	a) Core VC205: Total diatom abundance, CRS absolute abundance (both from CRS-included counts) and non-CRS assemblage absolute abundance (from CRS-free counts) (millions of valves/g (Mv/g)). b) Core VC205: CRS relative abundance (%).	7-93
Figure 7.61	Core VC205: Diatom fragmentation, using two measures: observational index and percentage of *Fragilariopsis* species whole.	7-94
Figure 7.62	Core VC205: Non-CRS diatom assemblage plots for AP indicator species: (a) Absolute abundance (Mv/g); (b) Relative abundance (%).	7-95
Figure 7.63	Core VC205: R-mode PCA variable loading on axes 1 and 2 for diatom relative abundance data (> 1 %).	7-96
Figure 7.64	Core VC205: R-mode PCA variable loading on axes 2 and 3 for diatom relative abundance data (> 1 %).	7-96
Figure 7.65	Core VC205: R-mode cluster analysis of diatom species relative abundance (>1 %).	7-97
Figure 7.66	Core VC205: Q-mode PCA component scores plotted stratigraphically for PCA axes 1 – 3; division of the record into stratigraphic zones VC205-i, VC205-ii and VC205-iii.	7-99
Figure 7.67	a) Core VC205: Q-mode cluster analysis of core depths, using diatom species relative abundance (>1 %). b) Core VC205: Stratigraphic pattern of Q-mode cluster groups.	7-100
Figure 7.68	Core VC205: Schematic representation of the fossil diatom assemblage, highlighting the relative contribution of CRS to the total assemblage and stratigraphic changes in the diatom community.	7-101
Figure 7.69	All AP cores: Q-mode PCA component loading on axes 1 and 2 for diatom relative abundance data (>1 %).	7-103

Figure 7.70	Map of the AP showing spatial variability in: 1) mean total diatom assemblage (CRS versus non-CRS; left hand pie chart); and 2) non-CRS assemblage (>1 % from CRS-free counts; right hand pie chart).	7-104
Figure 7.71	All AP cores: R-mode PCA variable loading on axes 1 and 2 for diatom relative abundance data (> 1 %).	7-107
Figure 7.72	All AP cores: R-mode PCA variable loading on axes 2 and 3 for diatom relative abundance data (> 1 %).	7-107
Figure 8.1	All AP cores: Q-mode PCA component loading on axes 1 and 2 for diatom relative abundance data (>1 %), with different environmental parameters identified between core sites labelled.	8-4
Figure 8.2	Schematic plot summarising the main associations of diatom species analysed in this investigation and their relationship with environmental gradients.	8-5
Figure 8.3	Oceanographic variability in Marguerite Bay; competitive interactions between cool shelf waters and warm nutrient-rich UCDW. (a) Cool shelf water-dominated regime (zone VC306-i). (b) UCDW-dominated regime (zone VC306-ii).	8-23
Figure 8.4	Comparison of Holocene events between AP marine cores.	8-39
Figure 8.5	Minimum deglaciation ages from published marine records from the Antarctic Peninsula (AP) continental shelf, provided by dating the transition between sub-glacial and glacio-marine sediments.	8-41
Figure 8.6	Deglaciation history and ice sheet retreat rates for the southern Bellingshausen Sea and Marguerite Bay, inferred from deglaciation sediment transitions in marine cores.	8-47
Figure 8.7	Deglaciation history and ice sheet retreat rates for Anvers Trough, inferred from deglaciation sediment transitions in marine cores.	8-47
Figure 8.8	Regional outline of the ice stream outlet system in the vicinity of Anvers Island and reconstructed grounding line position of Antarctic Peninsula Ice Sheet during the LGM.	8-48
Figure 8.9	Forcing mechanisms contributing to Antarctic deglaciation.	8-53
Figure 8.10	Modelled Holocene monthly surface temperatures (°C), averaged over the area south of 60°S.	8-67
Figure 8.11	Compilation of Mid-Holocene climatic optimum records in the AP marine cores used in this investigation, together with published marine records.	8-76
Figure 8.12	Holocene palaeoclimate reconstructions for the AP during: a) Deglaciation – Early Holocene (12650 – 8450 yr BP; 15020 – 9500 cal. yr BP); b) Mid-Holocene (8450 – 3700 yr BP; 9500 – 4100 cal. yr BP); c) Late Holocene (3700 yr BP – present; 4100 cal. yr BP – present.	8-86
Figure 8.13	Circum-Antarctic LGM ice sheet reconstruction and oldest radiocarbon ages from glacial-marine deposits, representing approximate age of initial ice sheet retreat from the shelf	8-90
Figure 8.14	Holocene climatic events for the circum-Antarctic and South America. Antarctic ice core records.	8-92
Figure A1.1	Palaeoclimate proxy records from the Antarctic Peninsula (AP), surrounding Weddell Sea, Bellingshausen Sea, Drake Passage and Scotia Sea, colour-coded based on the proxy used and numbered.	A1-1
Figure A1.2	Palaeoclimate proxy records from the Ross Sea Embayment, colour-coded based on the proxy used and numbered.	A1-2
Figure A1.3	Palaeoclimate proxy records from the East Antarctic Margin, encompassing the George V and Adélie Coast, colour-coded based on the proxy used and numbered.	A1-3

Figure A1.4	Palaeoclimate proxy records from the East Antarctic Margin, encompassing Prydz Bay and the Mac. Robertson Shelf, colour-coded based on the proxy used and numbered	A1-4
Figure A2.1	Correlation of core GC358 and GC359, based on sand content, TOC and mineralogy, together with AMS ^{14}C ages.	A2-5
Figure A2.2	Core GC114: Non-CRS diatom assemblage plots for all the species used in statistical analysis (> 1 %). Absolute abundance (AA; Mv/g) and relative abundance (RA; %).	A2-6
Figure A2.3	Core GC114: PCA scree plot, showing the relative importance of the principal components.	A2-7
Figure A2.4	Core GC047: Non-CRS diatom assemblage plots for all the species used in statistical analysis (> 1 %). Absolute abundance (AA: Mv/g) and relative abundance (RA; %).	A2-10
Figure A2.5	Core GC047: PCA scree plot, showing the relative importance of the principal components.	A2-11
Figure A2.6	Core VC306: Non-CRS diatom assemblage plots for all the species used in statistical analysis (> 1 %). Absolute abundance (AA; Mv/g) and relative abundance (RA; %).	A2-14
Figure A2.7	Core VC306: PCA scree plot, showing the relative importance of the principal components.	A2-15
Figure A2.8	Core GC358: Non-CRS diatom assemblage plots for all the species used in statistical analysis (> 1 %). Absolute abundance (AA; Mv/g) and relative abundance (RA; %).	A2-18
Figure A2.9	Core GC358: PCA scree plot, showing the relative importance of the principal components.	A2-19
Figure A2.10	Core VC243: Non-CRS diatom assemblage plots for all the species used in statistical analysis (> 1 %).	A2-22
Figure A2.11	Core VC243: PCA scree plot, showing the relative importance of the principal components.	A2-23
Figure A2.12	Core VC237: Non-CRS assemblage plots for all the species used in statistical analysis (> 1 %).	A2-26
Figure A2.13	Core VC237: PCA: scree plot, showing the relative importance of the principal components.	A2-27
Figure A2.14	Core VC205: Non-CRS diatom assemblage plots for all the species used in statistical analysis (> 1 %).	A2-30
Figure A2.15	Core VC205: PCA scree plot, showing the relative importance of the principal components.	A2-31
Figure A2.16	Diatom plates	pdf

List of Tables

Table 2.1	Water masses of the Southern Ocean and Antarctic continent margin, detailing temperature and salinity characteristics, together with acronyms used throughout the thesis.	2-16
Table 2.2	Details of cores used in this investigation.	2-27
Table 4.1	Potential sources of alteration to the $\delta^{13}C_{org}$ signal.	4-5
Table 4.2	Potential sources of alteration to the $\delta^{15}N_{org}$ signal.	4-6
Table 5.1	Core length, diatom sampling interval and resolution.	5-1
Table 5.2	Pigment sample depths for core VC243.	5-20
Table 5.3	HPLC gradient elution program employed for total extract analysis (Method A, Airs et al., 2001).	5-20
Table 6.1	Uncorrected AMS radiocarbon dates on bulk organic carbon for all cores used in this investigation.	6-9
Table 6.2	Outputs of ^{14}C age of sedimentary mixed layer from steady state box model.	6-22

Table 6.3	Corrected AMS radiocarbon dates on bulk organic carbon for all cores used in this investigation.	6-37
Table 6.4	Radiocarbon and calibrated dates for all cores used in this investigation.	6-43
Table 7.1	Core GC114: Comparison of diatom PCA axis loading and cluster groupings.	7-10
Table 7.2	Core GC047: Comparison of diatom PCA axis loading and cluster groupings.	7-24
Table 7.3	Core VC306: Comparison of diatom PCA axis loading and cluster groupings.	7-37
Table 7.4	Core GC358: Comparison of diatom PCA axis loading and cluster groupings.	7-50
Table 7.5	Core VC243: Comparison of diatom PCA axis loading and cluster groupings.	7-63
Table 7.6	Core VC243: Analytical data for the major pigments identified.	7-71
Table 7.7	Core VC237: Comparison of diatom PCA axis loading and cluster groupings.	7-85
Table 7.8	Core VC205: Comparison of diatom PCA axis loading and cluster groupings.	7-98
Table 8.1	Habitat types for AP diatom assemblages, based on regional differences in sedimentary diatom assemblage; consistent diatom species associations; and by interpretation of previously published literature.	8-10
Table 8.2	Affinities and environmental interpretation of pigments preserved in core VC243.	8-12
Table A1.1	Antarctic palaeoclimate records; original site identification, source publication and brief summary. Colour-coded on Figures A1.1 – A1.4: Diatom = yellow; Geological = brown; Terrestrial / lake = green; Ice core = blue.	A1-5
Table A2.1	Published ^{14}C ages for box and piston core samples collected from WAP areas, working offshore from Gerlache Strait to Bransfield Strait.	A2-1
Table A2.2	Published ^{14}C ages for box and vibro core surface samples collected from Prince Gustav Channel (PGC), northern Larsen area and outer EAP continental shelf.	A2-2
Table A2.3	Published ^{14}C ages for box and piston core samples collected from Marguerite Bay.	A2-3
Table A2.4	Unpublished ^{14}C ages for box and gravity core samples from the southern Bellingshausen Sea.	A2-4
Table A2.5	Core GC114: R-mode PCA with component loading values.	A2-8
Table A2.6	Core GC114: Q-mode PCA with component loading values.	A2-9
Table A2.7	Core GC047: R-mode PCA with component loading values.	A2-12
Table A2.8	Core GC047: Q-mode PCA with component loading values.	A2-13
Table A2.9	Core VC306: R-mode PCA with component loading values.	A2-16
Table A2.10	Core VC306: Q-mode PCA with component loading values.	A2-17
Table A2.11	Core GC358: R-mode PCA with component loading values.	A2-20
Table A2.12	Core GC358: Q-mode PCA with component loading values.	A2-21
Table A2.13	Core VC243: R-mode PCA with component loading values.	A2-24
Table A2.14	Core VC243: Q-mode PCA with component loading values.	A2-25
Table A2.15	Core VC237: R-mode PCA with component loading values.	A2-28
Table A2.16	Core VC243: Q-mode PCA with component loading values.	A2-29
Table A2.17	Core VC205: R-mode PCA with component loading values.	A2-32
Table A2.18	Core VC205: Q-mode PCA with component loading values.	A2-33
Table A2.19	All AP cores: R-mode PCA with component loading values.	A2-34

Table A2.20	Published uncorrected and reservoir corrected radiocarbon ages representing minimum estimates of glacial retreat on the AP.	A2-35
Table A2.21	(i) Core GC114: Diatom count data (CRS included); (ii) Core GC114: Diatom count data (CRS free).	Excel
Table A2.22	(i) Core GC047: Diatom count data (CRS included); (ii) Core GC047: Diatom count data (CRS free).	Excel
Table A2.23	(i) Core VC306: Diatom count data (CRS included); (ii) Core VC306: Diatom count data (CRS free).	Excel
Table A2.24	(i) Core GC358: Diatom count data (CRS included); (ii) Core GC358: Diatom count data (CRS free).	Excel
Table A2.25	(i) Core VC243: Diatom count data (CRS included); (ii) Core VC243: Diatom count data (CRS free).	Excel
Table A2.26	(i) Core VC237: Diatom count data (CRS included); (ii) Core VC237: Diatom count data (CRS free).	Excel
Table A2.27	(i) Core VC205: Diatom count data (CRS included); (ii) Core VC205: Diatom count data (CRS free).	Excel
Table A2.28	Core VC306: Stable isotope raw data.	Excel
Table A2.29	Core VC243: Stable isotope raw data.	Excel
Table A2.30	Core VC243: Sedimentary pigment data (0.11-0.14 m)	pdf
Table A2.31	Core VC243: Sedimentary pigment data (0.21-0.23 m)	pdf
Table A2.32	Core VC243: Sedimentary pigment data (0.45-0.46 m)	pdf
Table A2.33	Core VC243: Sedimentary pigment data (0.62-0.64 m)	pdf
Table A2.34	Core VC243: Sedimentary pigment data (0.86-0.87 m)	pdf
Table A2.35	Core VC243: Sedimentary pigment data (1.1-1.11 m)	pdf
Table A2.36	Core VC243: Sedimentary pigment data (1.3-1.31 m)	pdf
Table A2.37	Core VC243: Sedimentary pigment data (1.5-1.51 m)	pdf
Table A2.38	Core VC243: Sedimentary pigment data (1.65-1.66 m)	pdf
Table A2.39	Core VC243: Sedimentary pigment data (1.9-1.91 m)	pdf
Table A2.40	Core VC243: Sedimentary pigment data (2.1-2.11 m)	pdf
Table A2.41	Core VC243: Sedimentary pigment data (2.3-2.31 m)	pdf
Table A2.42	Core VC243: Sedimentary pigment data (2.5-2.51 m)	pdf
Table A2.43	Core VC243: Sedimentary pigment data (2.7-2.71 m)	pdf
Table A2.44	Core VC243: Sedimentary pigment data (2.95-2.96 m)	pdf
Table A2.45	Core VC243: Sedimentary pigment data (3.2-3.21 m)	pdf
Table A2.46	Core VC243: Sedimentary pigment data (3.4-3.42 m)	pdf
Table A2.47	Core VC243: Sedimentary pigment data (3.6-3.61 m)	pdf
Table A2.48	Core VC243: Sedimentary pigment data (3.75-3.76 m)	pdf
Table A2.49	Core VC243: Sedimentary pigment data (4-4.02 m)	pdf

List of Equations and Boxes

Equation 5.1	Absolute diatom abundance calculation.	5-8
Equation 5.2	$\delta^{13}C_{org}$ calculation	5-18
Equation 5.3	$\delta^{15}N_{org}$ calculation	5-18
Box 6.1	One box model of the mixed layer.	6-21
Box 6.2	Calculation of missing core top material.	6-23
Box 6.3	Application of the linear regression trendline equation to calculate the age of the surface sediment if the missing material was in fact present (x) in core VC306.	6-24

1 Introduction

This research investigates Holocene palaeoclimate variability from the Antarctic Peninsula (AP), with emphasis placed on reconstructing changes in water mass circulation on the continental shelves of the AP, sea ice extent and ice shelf collapse events. This is achieved using fossil diatom assemblages preserved in marine sediments from a range of continental shelf settings along the AP, together with carbon and nitrogen stable isotope analyses of bulk organic matter and sedimentary pigment analyses. Sediment records are compared between several marine locations and integrated with published palaeoclimate data from the AP and Antarctic continent. This provides valuable information on the spatial variability (extent and propagation of climate events), temporal trends (phasing and duration) and the identification of forcing mechanisms. This type of study advances our understanding of the palaeoclimatic history of the AP in relation to global Holocene climate events.

This chapter outlines the rationale behind the project, the specific project aims and an outline of the structure of this thesis.

1.1 Rationale

1.1.1 Why Antarctica?

Antarctica is an intrinsic part of the global ocean and atmosphere system. The presence of extensive polar ice caps is a rare occurrence in Earth history and crucial in shaping the modern global climate; acting to create steep equator-pole thermal gradients which drive vigorous atmospheric and oceanic circulation. The Southern Ocean is a key and central feature of global thermohaline circulation, connecting each of the major ocean basins. The extent of Antarctic sea ice, migrations of the Polar Front and water mass interactions all influence the world's oceans (thermohaline circulation, deep and bottom water production and primary productivity) and climate (position of the westerly wind belt, pole-equator temperature gradient and albedo effects). The importance of studying climate change in Antarctica stems from the impacts that changes in the growth and decay of the Antarctic Ice Sheet, associated ice shelf extent and seasonal sea ice cover have on global climate, sea level, ocean circulation and planetary albedo.

1.1.2 Why the Antarctic Peninsula?

The AP is recognised as one of the most dynamic climate systems on Earth, situated in the transition between several different climate zones: maritime, continental temperate

glacial and polar. It is highly sensitive to climate change and identified as one of the fastest-warming regions on Earth, with temperatures over the last 50 years increasing at a rate of 3.7 °C century^{-1} (Vaughan et al., 2003; Turner et al., 2005), more than five times the global mean (0.6 ± 0.2 °C during the 20th Century; Houghton et al., 2001) and has led to shifts in species distributions (Convey, 2001; Walther et al., 2002; Montes-Hugo et al., 2009), catastrophic disintegration of ice shelves (Vaughan and Doake, 1996, Scambos et al., 2003; Skvarca and de Angelis, 2003), accelerated discharge of continental glaciers (Cook et al., 2005; Pritchard and Vaughan, 2007), decrease in sea ice coverage on both sides of the AP (Curran et al., 2003; Parkinson, 2004) and the possibility of increased rates of global sea level rise (Oppenheimer, 1998; Rott et al., 2002). A key question facing scientists and policy makers is whether this recent rapid warming is part of the natural variability in the climate system or are anthropogenic influences involved. To make accurate predictions for the future, it is critical to understand the periodicity, amplitude and rate of natural climate changes in the past.

1.1.3 Why the Holocene?

The Holocene interglacial, spanning from 11700 cal. yr BP to the present day, is widely viewed as a period of relatively stable global temperatures. However, globally distributed palaeoclimate records are revealing that rapid and significant climate excursions have occurred through the Holocene (Domack and Mayewski, 1999; Mayewski et al., 2004). To better understand natural climate variability, it is critical to look at these temperature excursions within the Antarctic climate record to determine what caused them and what effect they had around Antarctica. Studies of continental Antarctic ice cores have shown that the Early Holocene (11000 – 9500 cal. yr BP) and the Mid Holocene (4000 – 2000 cal. yr BP) both included periods that were warmer than present (Ciais et al., 1992; Masson et al., 2000; Masson-Delmotte et al., 2004). These warm periods have been linked with the disintegration of two AP ice shelves (Pudsey and Evans, 2001; Pudsey et al., 2006; Bentley et al., 2005; Smith et al., 2007). As Holocene climate records increase in number and distribution across the Antarctic continent and along the AP, it is becoming increasingly apparent that significant discrepancies exist in the exact timing (i.e. onset and termination) of such climate events.

1.2 Research questions

1) In the Antarctic Peninsula (AP), were Holocene climate events peninsula-wide and synchronous? Where spatial and temporal discrepancies exist, do these patterns provide clues to forcing mechanisms?

2) Do AP Holocene climate events display similar phasing and duration to circum-Antarctic and global trends?

1.3 Project aims

- To provide detailed and chronologically well-constrained records of Holocene oceanographic and climate variability from a suite of regionally representative AP marine cores. Down-core records of diatom abundance and assemblage composition will be generated for each of the AP marine cores, and complemented with bulk organic carbon and nitrogen stable isotope data and sedimentary pigment analyses on selected cores. These individual marine palaeoclimate records will be subsequently correlated to develop an understanding of the spatial and temporal variability in AP Holocene climate events.

- To compare the Holocene reconstructions generated through this investigation with other AP proxy records, circum-Antarctic and global climate archives.

- To propose possible forcing mechanisms for the observed Holocene climate variability on a regional AP level, circum-Antarctic and global scale.

1.4 Thesis format

This thesis is divided into nine chapters:

- **Introductory** chapters: Chapter 1 details the rationale and sets the context for the project; Chapter 2 outlines the geographic location, oceanographic and climatic regime of the study area; Chapter 3 introduces the use of the diatoms as proxies for palaeoecological reconstructions; and Chapter 4 describes the use of carbon and nitrogen stable isotopes of bulk organic matter and sedimentary pigments.

- **Methods**: Chapter 5 describes the methods used: quantitative diatom analysis; carbon and nitrogen isotopes on bulk organic material; and sedimentary pigment analysis.

- **Results** chapters: Chapter 6 describes the core sediment and stratigraphy, including the age-models developed; Chapter 7 presents diatom results, together with results from stable isotopes on bulk organic material and sedimentary pigments analyses (where applicable).
- **Discussion**: Chapter 8 discusses results from individual core localities and proposes local environmental interpretations. These records are subsequently compared and AP palaeoclimate reconstructions proposed; addressing the first research question outlined in section 1.2. The discussion then draws on published datasets to address the second research question outlined in section 1.2.
- **Conclusions**: Chapter 9 highlights the main conclusions from this investigation and suggests potential for further work.

This thesis also includes:

- **Appendix 1:** contains details of published Antarctic palaeoclimate datasets that are discussed in the text (marked with the prefix "#"). Table A1.1 contains a summary of the study and details of the source publication. These studies are also highlighted on a series of maps (Figures A1.1 – A1.4) for the AP region; Ross Sea; George V – Adélie Coast; and Prydz Bay – Mac. Robertson Shelf.
- **Appendix CD**: contains all the raw diatom count; stable isotope output data; chromatograms from sedimentary pigment analyses; light microscope images of diatom species and genera documented in this study; and supplementary data to support Chapters 6 – 8, including published radiocarbon data referred to in text, expanded diatom assemblage plots and output tables from diatom statistical analysis (labelled Table A2.* and Figure A2.*).

2 Location

This chapter outlines the geological, glaciological, climatic and oceanographic settings of the Southern Ocean, Antarctic continent and Antarctic Peninsula (AP). Focus is then placed on the physical environment of the West Antarctic Peninsula (WAP) and East Antarctic Peninsula (EAP), and describes the environmental setting at each of the marine core sites.

2.1 Geological setting

Antarctica consists of two continental regions (East and West Antarctica), separated by the Transantarctic Mountains (Figure 2.1). East Antarctica is a large stable continental craton composed mainly of Precambrian metamorphic basement rocks; whereas West Antarctica is an archipelago of several micro-plates with mountainous metamorphic and volcanic terranes, of predominately Mesozoic-Cenozoic age (Anderson, 1999), illustrated in Figure 2.2.

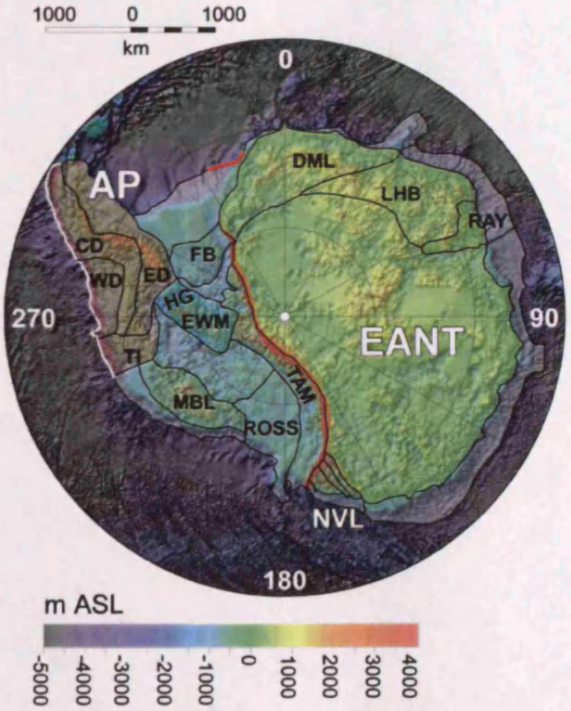


Figure 2.1
Antarctic continental blocks, topography and bathymetry. East Antarctica is sub-divided into four provinces: Dronning Maud Land (DML); Lützow-Holm Bay (LHB); Raynor Province (RAY); and the largely undivided unit of East Antarctica (EANT). West Antarctica consists of five major distinctive terranes: Antarctic Peninsula (AP) (comprising Eastern-Central-Western domains: ED-CD-WD); Thurston Island (TI); Filchner Block (FB); Marie Byrd Land (MBL); Haag (HG); and Ellsworth-Whitmore Mountains (EWM). The three northern Victoria Land (NVL) terranes are grouped together. ROSS = extended continental crust between MBL and EANT; TAM = Transantarctic Mountains (Source: Torsvik et al., 2007).



Figure 2.2
The location of Antarctica within Gondwana. The reconstruction shows the fragmentation of the supercontinent at 120 Ma, leaving East Antarctica as a large continent and West Antarctica as a collection of microplates (Source: Jamieson and Sugden, 2007).

The AP region encompasses geological terrain that is similar to the southern cordillera of the Andes. Before the break-up of Gondwana (which is believed to have commenced at ~160 Ma in the late Jurassic), the southern Andean arc complex was most likely contiguous with the linear trend of the AP (Domack et al., 2003). Palaeomagnetic pole data implies that the AP started to move away from East Antarctica (between 175 – 140 Ma) (Torsvik et al., 2007). The opening of Drake Passage (which is believed to have commenced by the Late Oligocene; ~26 Ma) led to the eastward propagation of shearing of both the Southern Andes (left lateral displacement) and the AP (Domack et al., 2003). Subsequent events have included creation of volcanic centres associated with the Bransfield Basin (a back arc spreading axis), the James Ross Island volcanic complex, and minor but more incompletely understood volcanism (Domack et al., 2003). Today, active tectonics and volcanism still occur in the South Shetland Trench and in the Bransfield Basin (Heroy and Anderson, 2005).

2.2 Antarctic Ice Sheet history

2.2.1 Mesozoic – Cenozoic

The long-term glacial history of Antarctica has been pieced together using a range of methods including: glacial sediments on the continent and its margins (e.g. Zachos et al., 1992; Troedson and Riding, 2002; Ivany et al., 2006); fossil biota preserved on the continent (e.g. Francis and Poole, 2002; Ashworth and Cantrill, 2004; Francis et al.,

2007); deep-sea $\delta^{18}O$ records (e.g. Kennett and Shackleton, 1976; Miller et al., 1991; Zachos et al., 1996; Lear et al., 2000); global sea level records (e.g. Miller et al., 2005; Kominz et al., 2008) and modelling studies (e.g. DeConto and Pollard, 2003; 2008).

The transition at the Eocene – Oligocene boundary (~34 Ma) from a greenhouse world to an icehouse world is believed to have culminated in the growth of a large (25 x 10^6 km^3) Antarctic Ice Sheet (Miller et al., 2007). This large ice sheet became a driver of climate change, not just a response to it, causing increased latitudinal thermal gradients and a spinning up of the oceans that, in turn, caused a dramatic reorganisation of ocean circulation and chemistry (Miller et al., 2007). Glaciation for the next ~20 million years (between ~34 – 14 Ma) was marked by ice volume fluctuations similar in scale to those of the Pleistocene ice sheets of the Northern Hemisphere (Jamieson and Sugden, 2007). A second glacial expansion is inferred in the middle Miocene (~14 Ma), with major growth of the East Antarctic Ice Sheet (EAIS) (Kennett, 1978; Flower and Kennett, 1994). The EAIS is believed to have been a permanent feature of the Antarctic continent since that time (Shackleton and Kennett, 1975; Sugden et al., 1993). In contrast, the West Antarctic Ice Sheet (WAIS) consisted of a number of isolated ice caps centred over islands and continental blocks between the Oligocene and early Miocene (~34 – 21 Ma) (Anderson and Shipp, 2001). These ice caps coalesced to form the WAIS, advancing onto the continental shelf on several occasions from late Miocene (~11 Ma) through to the Pleistocene (<0.1 Ma) (Anderson and Shipp, 2001).

2.2.2 Last Glacial Maximum and subsequent deglaciation

The Last Glacial Maximum (LGM) (23000 – 19000 cal. yr BP) was the most recent interval when global ice sheets reached their maximum integrated volume (Mix et al., 2001). The overall extent of LGM ice cover in Antarctica is not well known, however there is an emerging body of evidence that the EAIS and WAIS did not advance and retreat in concert during the last glacial period and subsequent deglaciation (Anderson et al., 2002).

Although data is much more sparse for the East Antarctic margin, it appears that ice sheet expansion achieved maximum extent at mid-shelf positions (e.g. Prydz Bay) and in some areas the ice terminus was situated near its present location (e.g. eastern Queen Maud Land) (Anderson et al., 2002). In the AP region, integration of recent modelling (Nakada et al., 2000) and marine geological data (Heroy and Anderson, 2005) suggest that the LGM ice sheet in this area was larger than indicated by previous studies, with a marine ice sheet grounded at the shelf edge (Sugden et al., 2006; Figure 2.3). The

deglaciation ice retreat of the EAIS retreat is inferred to have occurred significantly earlier (~22000 cal. yr BP for Prydz Bay) (Domack et al., 1998), potentially even prior to the LGM (Anderson et al., 2002), compared to the WAIS (between ~18000 and 9000 cal. yr BP for the WAP) (Heroy and Anderson, 2007). There are also clear differences in the timing of retreat between different sectors of the WAIS; in the AP, the ice sheet had withdrawn from offshore areas of the AP and approached its present configuration by the Early Holocene (~9500 cal. yr BP), whereas in the Ross Sea and Marie Byrd Land ice sheet thinning has persisted throughout the Holocene (Conway et al., 1999; Stone et al., 2003). Further, within the AP region, dynamics of retreat have varied from place to place, well illustrated by contrasts in the ice sheet retreat character between the western (e.g. Marguerite Bay; rapid) and eastern flanks of the AP (e.g. Larsen-A region; slow and steady) (Sugden et al., 2006). Full comparisons of the timing and character of ice sheet retreat for the AP and Antarctic continent will be discussed in Chapter 8, section 8.4.1.1 and 8.4.2.1 respectively.

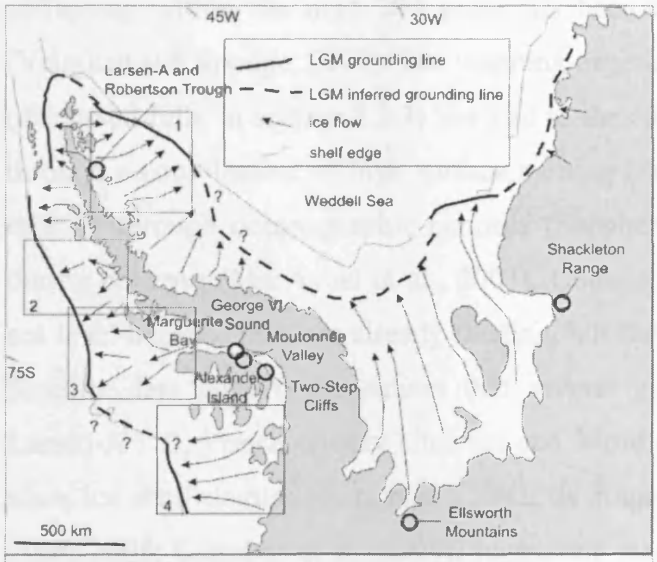


Figure 2.3
Extent of grounded ice during the Last Glacial Maximum (LGM) along the Antarctic Peninsula (AP) continental shelf (Source: Sugden et al., 2006).

2.2.3 *Present day*

The present day Antarctic ice sheet (including ice shelves and ice rises) covers an area of ~13 million km^2 (Fox and Cooper, 1994) and contains ~25.4 million km^3 of ice (Lythe et al., 2001), which is 90 % of all the freshwater ice on Earth (Vaughan and Spouge, 2002). The larger, EAIS rests on a large, high plateau that would be generally above sea level if the ice were removed; whereas the smaller, WAIS is a marine ice sheet, resting mainly on land that is far below present sea level. The WAIS is further

characterised by rapid ice flow and discharge, relative to the EAIS (Anderson et al., 2002). Most WAIS discharge occurs through ice streams that reach flow velocities of hundreds of metres per year (e.g. Rutford Ice Stream: 0.9 to 1.2 metres per day (Gudmundsson, 2006); 380 metres per year (Murray et al., 2007)). The WAIS is also mostly fringed by ice shelves, which form floating extensions of the ice sheets, moving seaward but confined horizontally by the rocky coastline. Most of the drainage from the WAIS is into the Ross and Weddell Seas, where there are extensive ice shelves (the Ross Ice Shelf and the Ronne-Filchner Ice Shelf, respectively) and into the Amundsen Sea in the vicinity of Pine Island Bay, where extensive ice shelves are not present (Oppenheimer, 1998).

The WAIS is considered much more unstable than the EAIS (Hughes, 1973), due to the differences in elevation of the grounding lines. There is increasing concern about the stability of the WAIS under current global warming; collapse of the WAIS would raise global eustatic sea level by around 5 m (Lythe et al., 2001). The risk of the entire WAIS collapsing within the next 200 years has been calculated at about 5 % probability (Vaughan and Spouge, 2002). The warming experienced on the AP over the last century (discussed fully in section 2.3.3) has lead to the collapse of several floating ice shelves, through a combination of high surface melting (Scambos et al., 2000), enhanced basal melting through oceanographic controls (Shepherd et al., 2003) and a domino effect during collapse (MacAyeal et al., 2003). Collapsing ice shelves do not displace mean sea level because they are already floating, but they may change glacier flow upstream. Satellite data have demonstrated that several glaciers which drain into the former Larsen-A / B, Prince Gustav Channel and Wordie Ice Shelf regions have accelerated since ice shelf demise (Rott et al., 2002; de Angelis and Skvarca, 2003; Rignot et al., 2004; 2005; Scambos et al., 2004), suggesting that ice shelf loss and thinning can lead immediately to rapid terrestrial ice discharge and thus sea level rise.

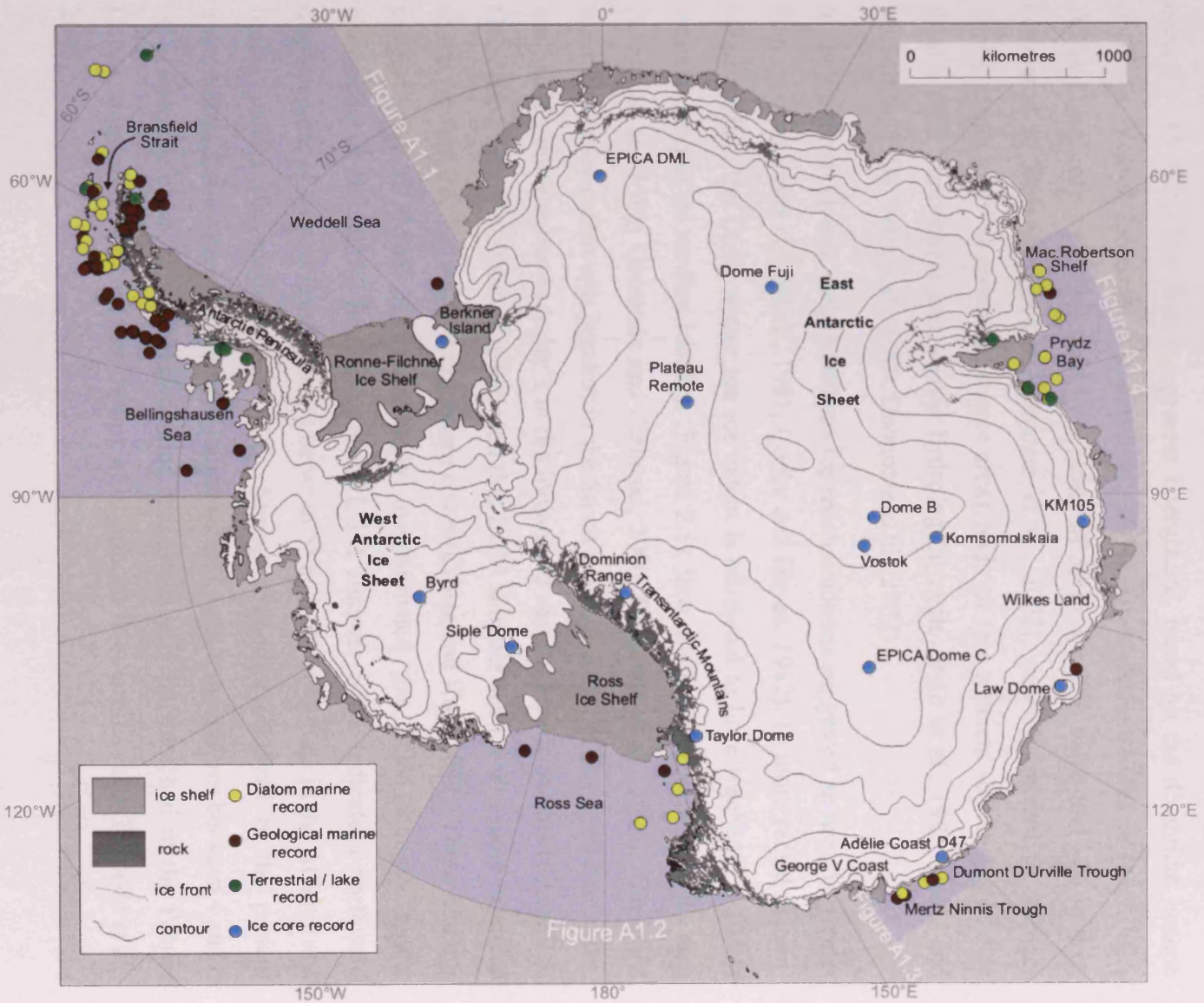
2.3 Antarctic palaeoclimate and present climate

The first part of this section briefly introduces the range of methods used for palaeoclimate reconstructions in Antarctica. The second part of this section introduces the broad-scale Antarctic climate trends since the demise of the last glacial period, through the current interglacial period (Holocene) and the present day climatic regime.

2.3.1 Palaeoclimate proxies

Palaeoclimate proxies use physical and biophysical principles to enable climate-related variations to be reconstructed back in time (IPCC, 2001). Careful calibration and cross-validation procedures are necessary to establish reliable relationships between proxy indicators and the climate variable they are assumed to represent. The distribution of some of the key Antarctic palaeoclimate proxy records are shown in Figure 2.4, colour-coded based on the proxy used. The main proxies used in Antarctic palaeoclimate studies are: (1) marine geological and geophysical records, providing information on the timing and character of deglaciation (e.g. Pope and Anderson, 1992; Pudsey et al., 1994; Evans et al., 2005; Ó Cofaigh et al., 2005a; Heroy and Anderson, 2005) and proximity and stability of ice shelves (e.g. Domack et al., 1995; 2005; Pudsey and Evans, 2001; Brachfeld et al., 2003); (2) diatom assemblages, reconstructing palaeoceanographic conditions (e.g. Leventer et al., 1996; 2002; Crosta et al., 1998; Cunningham et al., 1999; Armand, 2000; Taylor and Sjunneskog, 2002; Gersonde et al., 2005); (3) terrestrial records, including lake sediments (e.g. Hodgson et al., 2004; Bentley et al., 2005; Smith et al., 2007a; 2007b; Roberts et al., 2008); glacial stratigraphy and geomorphological (e.g. Sugden et al., 2006) and location of penguin rookeries (e.g. Baroni and Orombelli, 1994; Zale, 1994; Emslie, 2001); (4) ice core records, providing information about physical characteristics (e.g. temperature and dustiness) and composition of the atmosphere (e.g. CO_2 and CH_4) (e.g. Petit et al., 1999; Masson et al., 2000; EPICA Community Members, 2004; 2006). Ice cores provide some of the most accurately dated records of Antarctic palaeoclimate, but in contrast to marine and terrestrial records, the data is representative of very large regional areas. There are no long ice cores from the AP, due to shallow and complex topography along the spine of the AP and high heat flow in the northern parts (Bentley et al., 2009). This has meant that there is no regional record of atmospheric temperature and precipitation through the Holocene; instead reconstructions for the AP rely on core localities outside of the region (Figure 2.4), which may not fully capture patterns of AP spatial variability.

Figure 2.4 (next page)
Antarctic palaeoclimate proxy records, colour-coded based on the proxy used. Purple boxes indicate areas that are presented at larger scale in Appendix 1: Figure A1.1 (AP region); Figure A1.2 (Ross Sea Embayment); Figure A1.3 (George V – Adélie Coast); Figure A1.4 (Prydz Bay – Mac. Robertson Shelf), with full details of each proxy record and the source publication in Table A1.1. (Base map adapted from Sugden et al., 2006 and overlain with site localities using ESRI® ArcMap™ 9.2). Additional places mentioned in the thesis are also shown.


30°W
0°
30°E
60°W
60°E
90°W
90°E
120°W
120°E
150°W
180°
150°E
60°S
70°S
0
kilometres
1000
Figure A1.1
Figure A1.2
Figure A1.3
Figure A1.4
Bransfield Strait
Weddell Sea
Antarctic Peninsula
Bellingshausen Sea
Ronne-Filchner Ice Shelf
Berkner Island
EPICA DML
Dome Fuji
East Antarctic Ice Sheet
Plateau Remote
Mac.Robertson Shelf
Prydz Bay
West Antarctic Ice Sheet
Byrd
Dominion Range
Transantarctic Mountains
Siple Dome
Ross Ice Shelf
Ross Sea
Taylor Dome
Dome B
KM105
Komsomolskaia
Vostok
Wilkes Land
EPICA Dome C
Law Dome
Adélie Coast D47
George V Coast
Dumont D'Urville Trough
Mertz Ninnis Trough
ice shelf
rock
ice front
contour
Diatom marine record
Geological marine record
Terrestrial / lake record
Ice core record

2.3.2 Palaeoclimate reconstructions

2.3.2.1 Last Glacial Maximum (LGM)

During the LGM grounded ice extended onto the continental shelf around much of the continent. Mean annual surface temperatures in central Antarctica are proposed to have been 8 – 15 °C colder than the present interglacial, based on the deuterium isotope profile in Vostok ice cores (Blunier et al., 2004). Dust concentrations in the EPICA Dome C ice core were increased by a factor of 50 in absolute value and ~26 in flux, compared to Holocene levels (Delmonte et al., 2002), possibly related to stronger winds, larger and / or more arid source areas, and / or less efficient scavenging of dust from a drier atmosphere and weaker hydrological cycle (Petit et al., 1981; Hesse and McTainsh, 1999; Petit et al., 1999; Delmonte et al., 2002).

In the Southern Ocean, early LGM sea ice reconstructions suggested an area 5x greater than modern limits (CLIMAP, 1981; Cooke and Hayes, 1982). In more recent diatom-based studies, the LGM winter sea ice extent is estimated to have reached 5 – 10° of latitude north of its modern location (Figure 2.5), thus doubling the winter sea ice area (Crosta et al., 1998; Gersonde and Zielinski, 2000, Gersonde et al., 2005). The LGM summer sea ice extent was greatest in the South Atlantic sector of the Southern Ocean, but had a similar extent to today's in the Indian and eastern Pacific sectors (Figure 2.5; Gersonde et al., 2005) and it is believed that LGM summer sea ice was more extended in the western Pacific, relative to modern cover (Crosta and Koç, 2007). These findings suggest that CLIMAP (1981) strongly overestimated the LGM summer extent (Gersonde et al., 2005). Southern Ocean LGM summer SSTs indicate a northward displacement of Antarctic cold waters between 5° and 10° in latitude in the Atlantic and Indian sectors (Gersonde et al., 2005). Strongest cooling occurred in the present Subantarctic Zone in the Atlantic and Indian sectors, with temperatures between 4 and 6 °C (Gersonde et al., 2005). This cooling was potentially not matched in the Pacific Ocean, suggesting non-uniform cooling of the glacial Southern Ocean (Gersonde et al., 2005).

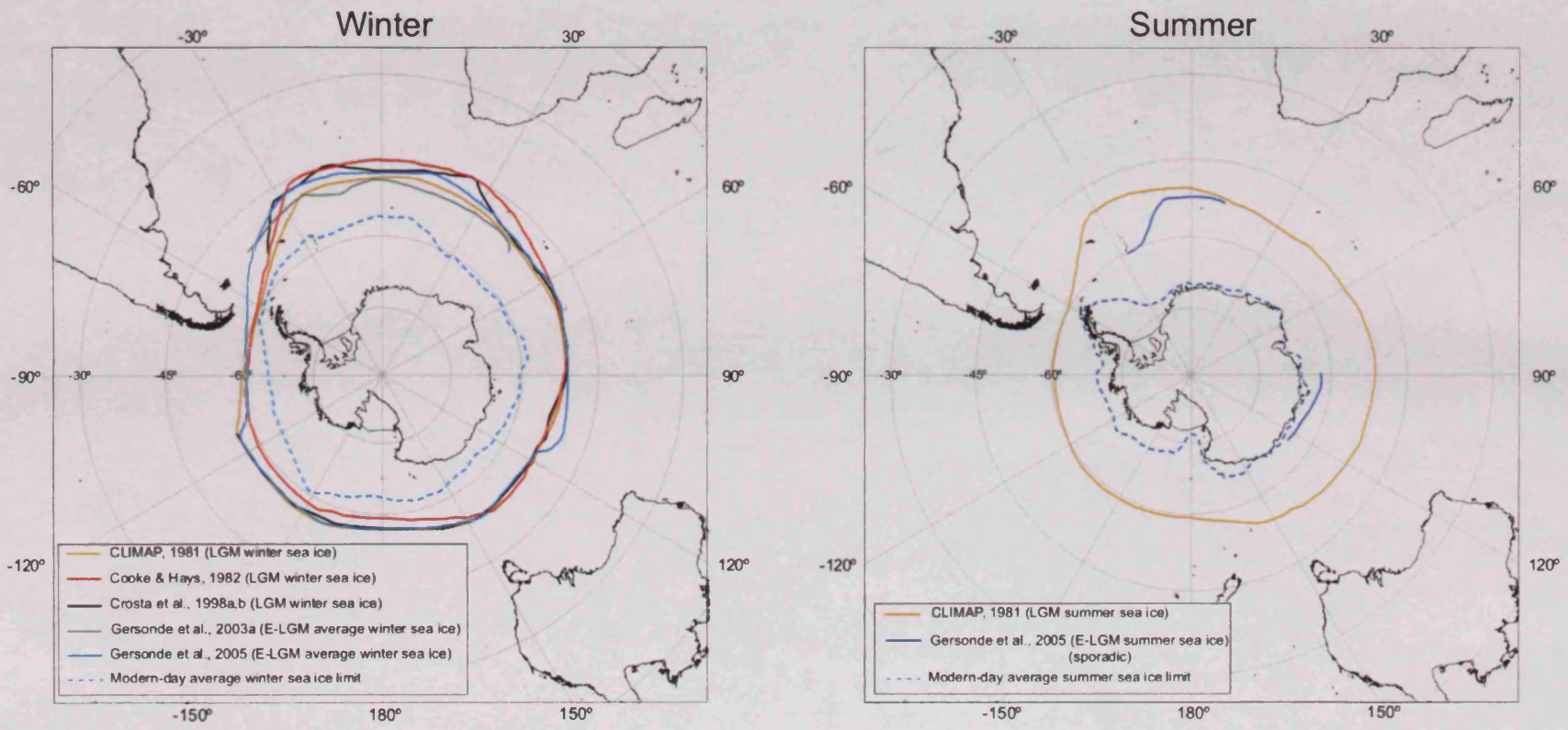


Figure 2.5

LGM winter and summer sea ice extent (adapted from Gersonde et al., 2005), with winter limits calculated from the *Fragilariopsis curta* group proxy (Gersonde and Zielinksi, 2000) and the modern analogy technique (MAT) (Crosta et al., 1998), and summer limits estimated from the *Fragilariopsis obliquecostata* proxy (Gersonde et al., 2005) and the MAT (Crosta et al., 1998). CLIMAP's winter and summer limits were located at the faunally identified winter and summer 0 °C isotherms, respectively (CLIMAP, 1981), and used lithogenic tracers such as changes in the sedimentation rate, presence of ice rafted debris, and geographical contact between diatom oozes and clayey sediments (Cooke and Hays, 1982). Positions of modern sea ice limits from Schweitzer (1995).

Compared to CLIMAP (1981) reconstructions, the more recent data of Gersonde et al. (2005) implies much less perennial sea ice cover, which has large implications for albedo effects, CO_2 transfer at the ocean-atmosphere interface, productivity and surface water stratification (Crosta and Koç, 2007).

As a result of the northward expansion of Antarctic cold waters and a relatively small displacement of the averaged Subtropical Front, pole-to-equator thermal gradients were steepened during the LGM in the northern zone of the Southern Ocean (Gersonde et al., 2005). This in turn drives more vigorous atmospheric circulation, with modelled increases in wind strength of ~70 % for the Southern Hemisphere westerlies (Brathauer and Abelmann, 1999) and 50 – 80 % for the Subantarctic glacial ocean (Petit et al., 1981), suggesting that the increased dust input in ice and marine cores during the LGM was mainly due to increased wind strength.

2.3.2.2 Last deglaciation

In Antarctica, the transition from glacial to interglacial conditions occurred over several millennia. Temperature changes through the last deglaciation were more gradual in the Southern Hemisphere (Blunier and Brook, 2001; EPICA Community Members, 2004) compared to the Northern Hemisphere (8 – 16 °C within a few decades; Huber et al., 2006). In the Southern Hemisphere, warming took place during a period of severe North Atlantic cold (Heinrich Stadial 1) and was followed by slight cooling, known as the Antarctic Cold Reversal (ACR), that occurred during the warm North Atlantic Bølling–Allerød period (Blunier and Brook, 2001). Completion of deglacial warming over Antarctica continued through the Younger Dryas (period of near-glacial conditions in the Northern Hemisphere between 12800 – 11500 cal. yr BP) (Barker et al., 2009). This global asynchronicity in deglaciation events has lead to the hypothesis of a bipolar seesaw, whereby changes in the strength of the Atlantic meridional overturning circulation (AMOC) affect the distribution of heat between the South Atlantic and North Atlantic (Broecker et al., 1998a; Vellinga et al., 2002). This mechanism is discussed further in Chapter 8.4.1.1.

Ice sheet retreat from the continental shelf of the WAIS occurred from ~18000 cal. yr BP, with retreat continuing throughout the Holocene. Ice sheet retreat was accompanied by an increase in eustatic sea level by just over 60 m, with the fastest rise termed melt-water pulse (MWP) 1A, beginning just before 14000 cal. yr BP (Fairbanks, 1989; Bard et al., 1990). Evidence from Barbados coral sequences (Fairbanks, 1989), marine

sediments from northwestern Australia (Yokoyama et al., 2001) and from the Irish Sea basin (Clark et al., 2004) shows a smaller meltwater pulse, around 19000 cal. yr BP (termed 19ka-MWP).

In the Southern Ocean, from 19000 cal. yr BP onwards, sea ice is proposed to have decreased from maximum LGM extent with periods of seasonal open water increasing in duration (Shemesh et al., 2002; Allen et al., 2005). Episodic shifts in the position of the Polar Front and main flow of the Antarctic Circumpolar Current (ACC) occurred during deglaciation, with increasing influence of NADW into the South Atlantic (Allen et al., 2005). Retreat of the Antarctic ice sheet and sea ice produced a habitat characterised by intense surface water stratification and increased nutrient inputs, enabling large phytoplankton blooms to develop (Leventer et al., 2002; Stickley et al., 2005; Leventer et al., 2006). In the some cases, immediate post-deglaciation diatom production and sedimentation were dramatically amplified above today's levels (e.g. Palmer Deep, AP: Leventer et al., 2002).

2.3.2.3 Holocene

As Antarctic palaeoclimate records increase in number and spatial distribution, it is becoming increasingly apparent that some Holocene climate events varied temporally between East and West Antarctica, whilst others are broadly synchronous; with the AP often being the most dynamic end-member. The timing of different Holocene events can be variable depending on the proxy, the resolution of the study and the studies stratigraphy.

The Holocene climate of the Southern Ocean and Antarctica commenced with an Early Holocene warm period between ~11000 – 9500 cal. yr BP, which is particularly evident in ice core records from East Antarctica (Ciais et al., 1992; Masson et al., 2000; Masson-Delmotte et al., 2004). Subsequently, there was cooling between 9000 – 8000 cal. yr BP, followed in some marine and ice core records by a warm Mid-Holocene period (also referred to as hypsithermal) between ~8000 – 3000 cal. yr BP (Cunningham et al., 1999; Masson et al., 2000; Hodell et al., 2001; Taylor et al., 2001; Masson-Delmotte et al., 2004) and in other ice core and terrestrial records between 4000 – 2000 cal. yr BP (Björck et al., 1991; Ciais et al., 1994; Mosley-Thompson, 1996; Jones et al., 2000; Hodgson and Convey, 2005). In the Late Holocene, there is a shift to cold conditions (also referred to as Neoglacial), although the timing and abruptness of this transition is highly diachronous around Antarctica; in the South Atlantic sector this

transition occurs at ~5000 cal. yr BP (Hodell et al., 2001), on the East Antarctic margin at ~4000 cal. yr BP (Crosta et al., 2007), in the West Antarctic sector at ~3000 cal. yr BP (Taylor et al., 2001; Brachfeld et al., 2002), and in AP terrestrial records after 2000 cal. yr BP (Bentley et al., 2009).

The Holocene climate framework for the AP is provided by the well-documented ODP Palmer Deep records (ODP Sites 1098 & 1099) (Domack et al., 2001; Leventer et al., 2002; Taylor and Sjunneskog, 2002; Sjunneskog and Taylor, 2002; Maddison et al., 2005), however, it is not representative of the whole region. Using magnetic susceptibility, mass accumulation rates, ice rafted debris and diatom assemblage data from Palmer Deep, five prominent LGM – Holocene palaeoenvironmental intervals have been proposed (Domack et al., 2001; Taylor and Sjunneskog, 2002; Sjunneskog and Taylor, 2002):

- LGM diamicton, deposited prior to 13180 cal. yr BP, recording presence of grounded ice over the core site;
- Deglaciation between 13180 cal. yr BP to 11460 cal. yr BP, with high primary production, iceberg rafting, and a sea ice-associated diatom assemblage;
- Climatic cooling (reversal) beginning at 11460 cal. yr BP and ending abruptly at 9070 cal. yr BP, characterised by intense ice rafting and reduced productivity, suggesting possible re-advance of glacial fronts;
- Mid-Holocene marine climatic optimum (hypsithermal) from 9070 – 3360 cal. yr BP; a prolonged period of enhanced productivity, maximum biogenic sediment accumulation and mass accumulation rates, plus minimum ice rafted debris flux and open water diatom assemblages;
- Late Holocene Neoglacial beginning at 3360 cal. yr BP, with increased concentration of ice rafted debris, decreasing sediment accumulation, high magnetic susceptibility and diatom assemblages suggesting more extensive sea ice and windier conditions. There is a further suggestion of a Little Ice Age signal, starting at ~700 cal. yr BP and ending ~100 cal. yr BP

Several studies have reconstructed the effects of Holocene climate variability on the stability of AP ice shelves. On the WAP, two cores from an epishelf lake suggest that the George VI Ice Shelf collapsed in the Early to Mid-Holocene (9595 – 7945 cal. yr BP) (Bentley et al., 2005; Smith et al., 2007a), immediately after the period of

maximum Holocene warmth and coinciding with an influx of warmer ocean water onto the WAP shelf (Smith et al., 2007a: 2007b). On the EAP, there is also evidence that the Prince Gustav Channel Ice Shelf and northern Larsen-A Ice Shelf disappeared in the Mid-Holocene (5000 – 2000 ^{14}C yr BP), based on ice rafted debris provenance studies (Pudsey and Evans, 2001; Pudsey et al., 2006). The collapse of these EAP ice shelves is possibly explained as a delayed response to the Mid-Holocene climatic optimum (Bentley et al., 2009). In comparison, the Larsen-B Ice Shelf is inferred to have been stable throughout the Holocene, attributed to its more southerly (colder) location (Domack et al., 2005).

Finally, some Antarctic marine and glacial records indicate Holocene rapid climate changes occurred on decadal-to-millennial timescales (Leventer et al., 1996; Masson et al., 2000; Nielsen et al., 2004; Delmonte et al., 2005; Bárcena et al., 2002; 2006; Crosta et al., 2007). These have been attributed to changes in the strength and extent of the polar vortex (Delmonte et al., 2005); solar activity (Leventer et al., 1996; Bárcena et al., 2002; 2006; Warner and Domack, 2002; Delmonte et al., 2005; Crosta et al., 2007); internal dynamics of the Southern Ocean thermohaline circulation (known as the "Southern Ocean flip-flop oscillator") (Pierce et al., 1995; Osborn, 1997; Crosta et al., 2007). Sediment accumulation rates in the cores analysed in this investigation are not high enough to resolve these events, so they are not discussed further.

2.3.3 Present day climate

Although Antarctica is dominated by cold temperatures, there are marked differences between the intense cold of the high plateau and the comparative mildness of the coast, and between the continental coast and the Subantarctic Islands.

On the continental high plateau, the lowest temperature recorded on Earth (-88 °C) were recorded at Vostok station. Weather fronts rarely penetrate far into the continent resulting in the high plateau also experiencing very low precipitation (38 mm/year) and light winds (18 km/hr) (for Vostok; http://www.aari.aq) due to a zone of high pressure that sits over the plateau most of the year. Katabatic winds carry dense air from the high plateau towards the coast, frequently reaching high velocities (e.g. 55 km/hr for Coats Land, on the southeast shore of the Weddell Sea; Renfrew and Anderson, 2002). These winds blow offshore affecting the build-up of sea ice in autumn and break-up in spring. In some areas, the strength of the winds pushing ice offshore sustains areas of semi-permanent open water (polynyas) close to the coast.

Antarctic coastal localities (including the AP) experience milder climates than the continental interior. Low cloud cover is persistent with precipitation often heavy, brought in by circling depressions (Stonehouse, 2002). Mean annual temperatures are ~ -15 °C, with summer temperatures close to 0 °C and winter temperatures between -20 °C to -30 °C (Anderson, 1999). The AP is one of the most dynamic climate systems on Earth, with the mountainous spine of the Peninsula and its associated ice sheets having a massive influence on the climate system. The unbroken mountain chain rises 1400 – 2000 m above sea level and forms a distinct climatic barrier, particularly to tropospheric circulation. The west and central AP experiences a mild maritime climate, dominated by conditions in the Bellingshausen Sea, and the southern AP and east coast a harsher continental climate, influenced by the cool waters of the Weddell Sea and associated cold, low-level barrier winds that develop over the ice covered sea (Smith et al., 1996a; King et al., 2003). Due to these influences, the coast of the WAP is generally ~7 °C warmer than the EAP coast (Smith et al., 1996a; Vaughan et al, 2003), and characterised by higher precipitation, caused by both the consistent westerly atmospheric flow generating cyclonic storms in the Bellingshausen Sea, and the rain shadow effect provided by the mountainous topography of the peninsula (Anderson, 1999; van Lipzig et al., 2004). Annual precipitation for the WAP is 0.45 – 0.80 m/year (Domack and Williams, 1990), compared to 0.1 – 0.15 m/year for the EAP (Draggan, 2009).

The AP is one of the fastest-warming regions in the world, with mean surface atmospheric warming of 3.7 ± 1.6 °C during the last century (Vaughan et al., 2003; Turner et al., 2005). The adjacent ocean is also changing with summer surface temperatures rising more than 1 °C since 1951 and a strong upper-layer stratification developing (Meredith and King, 2005). Of the 244 glaciers draining the AP ice sheet, 87 % have retreated in the period between 1940 and 2004 and retreat rates are accelerating (Cook et al., 2005). Another aspect of this warming has been the retreat or collapse of several of the regions ice shelves; Prince Gustav, Larsen-A and Larsen-B on the EAP, together with the Wordie and Wilkins on the WAP (Vaughan and Doake, 1996, Skvarca and de Angelis, 2003; Hodgson et al., 2006a; Vaughan, 2008). An ice shelf area of more than 14,000 km^2 has disappeared within the past two decades (Hodgson et al., 2006a), with retreat potentially driven by the southward progression of the -9 °C mean annual isotherm, which is regarded as a critical limit of ice shelf stability (Morris and Vaughan, 2003). Finally, sea ice extent has also declined by 20 % since 1950, although the decline is not uniform and displays large cyclical variations (Curran et al., 2003). Satellite data

reveals that sea ice concentrations (1979 – 2002) have dramatically increased (decreased) in the central Pacific sector (Bellingshausen / western Weddell sector) by ~4 – 10 % per decade (Liu et al., 2004).

2.2 Southern Ocean oceanography

Covering an area of approximately 36 million km^2, the Southern Ocean circles Antarctica, bound at the poleward edge by the Antarctic continent and its ice-shelves and marked at lower latitudes by the Subantarctic Front (SAF). The unique geography of the Southern Ocean means that ocean currents can flow uninterrupted around the continent, via the Antarctic Circumpolar Current (ACC), providing a connection between each of the major ocean basins and transferring heat and mass around the globe (Figure 2.6). The vigorous nature of this inter-ocean exchange enables oceanic teleconnections, where anomalies formed in one basin can be carried around the globe to influence climate in remote locations. This pattern of circum-polar circulation maintains the thermal isolation of the Antarctic continent, and its ice sheets, from subtropical waters to the north.

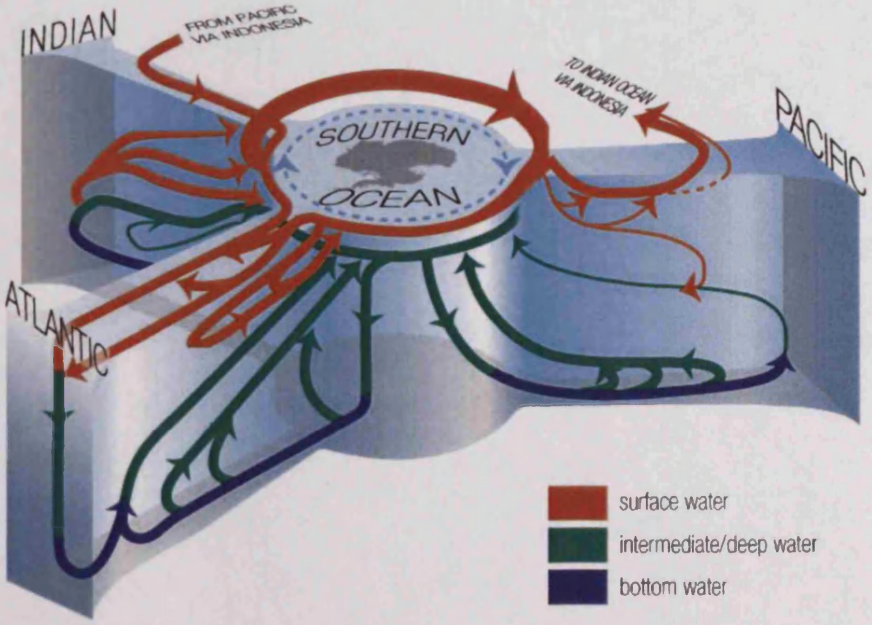


Figure 2.6
A three-dimensional schematic showing the meridional overturning circulation in each of the ocean basins and the horizontal connection in the Southern Ocean (Schmitz et al., 1996 adapted by Siedler et al., 2001).

CARDIFF UNIVERSITY
PRIFYSGOL CAERDYDD

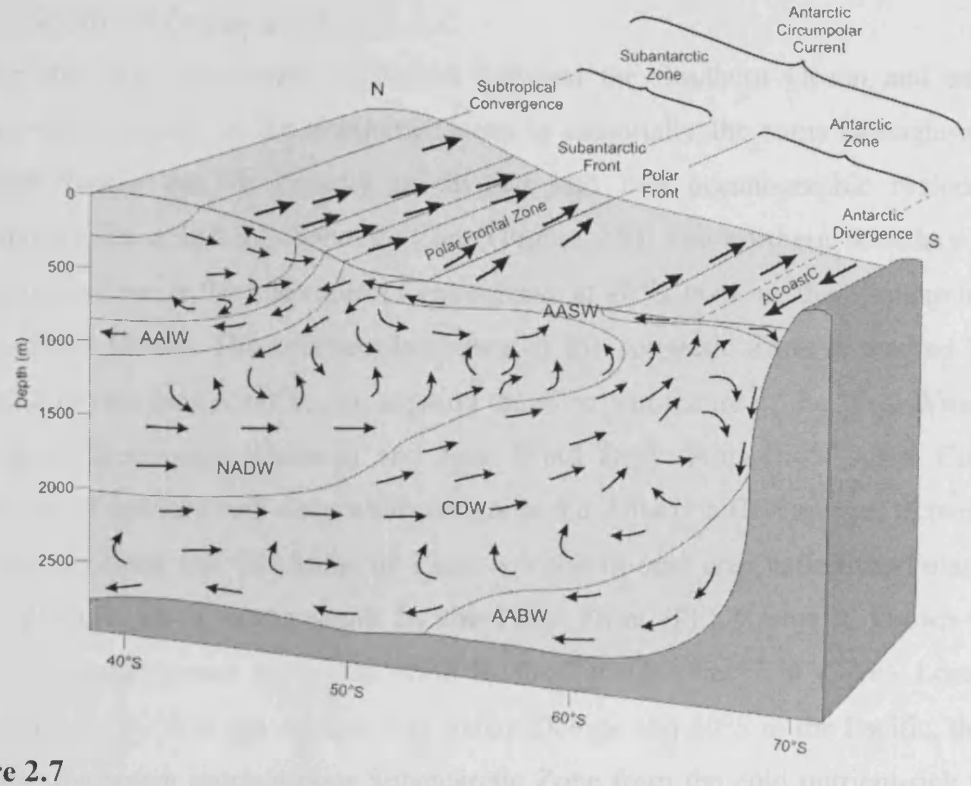


Figure 2.7
Schematic block diagram showing the Subantarctic Zone and Antarctic Zone of the Southern Ocean, and associated oceanographic fronts. Surface currents and vertical motion of water masses are also highlighted. AAIW = Antarctic Intermediate Water; NADW = North Atlantic Deep Water; CDW = Circumpolar Deep Water; AASW = Antarctic Surface Water; AABW = Antarctic Bottom Water; ACoastC = Antarctic Coastal Current (adapted from Open University Course Team, 1998).

Table 2.1
Water masses of the Southern Ocean and Antarctic continent margin, detailing temperature and salinity characteristics, together with acronyms used throughout the thesis. Source references: (1) Gordon et al. (2001); (2) Hofmann and Klinck (1998); (3) Foldvik et al. (2004).

Water mass	Acronym	Temperature (°C)	Salinity (PSU)	Reference
North Atlantic Deep Water	NADW	1 to 2	34.7 – 34.9	1
Circumpolar Deep Water	CDW	> 0	34.6 – 34.73	2
Upper Circumpolar Deep Water	UCDW	1.5 to 2.0	34.6 – 34.7	2
Lower Circumpolar Deep Water	LCDW	1.3 to 1.6	34.7 – 34.73	2
Modified Circumpolar Deep Water	-	1 to 1.4	34.6 – 34.7	2
Antarctic Intermediate Water	AAIW	3.8 to 4.8	34.2 – 34.4	2
Antarctic Surface Water	AASW	0 to -1.5	34.0 – 34.4	2
Winter Water	WW	< -1.5	34.0 – 34.4	2
High Salinity Shelf Water	HSSW	< -1.8	34.2 – 34.9	2
Antarctic Bottom Water	AABW	< -1	34.65 – 34.75	1
Weddell Sea Deep Water	WSDW	-0.7 to ≤ 0	34.58 – 34.7	3
Weddell Sea Bottom Water	WSBW	-0.7 to –1.3	< 34.67	3

2.4.1 Southern Ocean zones

Despite the large watermass exchanges between the Southern Ocean and adjacent oceans, the structure of the Southern Ocean is essentially the same throughout. The Southern Ocean can be broadly subdivided into two oceanographic regions: the Subantarctic Zone and the Antarctic Zone (Figure 2.7). The northern boundary of the Subantarctic Zone is the Subtropical Convergence at 40°S, marking the northern limit of the Southern Ocean. The southern boundary of the Antarctic Zone is marked by the Antarctic Divergence at 60°S, demarcating the divergent nature of the West Wind Drift (Antarctic Circumpolar Current) and East Wind Drift (Antarctic Coastal Current). Upwelling of nutrient-rich deep water occurs at the Antarctic Divergence. Between the Subantarctic Zone and the Antarctic Zone is a transitional area called the Polar Front Zone (PFZ), marked to the south by the Polar Front (PF) (formerly known as the Antarctic Convergence) and to the north by the Subantarctic Front (SAF). Located at approximately 50°S in the Atlantic and Indian Oceans and 60°S in the Pacific, the PFZ separates the warm nutrient-poor Subantarctic Zone from the cold nutrient-rich waters of the Antarctic Zone. Water temperature differs by about 2 °C across the PF (Scott and Marchant, 2005), which also marks one of the main jets of the ACC (Orsi et al., 1995). The position of both the SAF and PF is likely to be caused by topographic steering (Gille, 1994), yet they are not fixed in their location; changes in the configuration of currents and extent of seasonal sea ice will cause migration particularly of the PF.

2.4.2 Southern Ocean currents and water masses

On a broad scale, movement of water around the Antarctic continent is dominated by zonal circulation of the ACC (also known as the West Wind Drift). The ACC encompasses both the Subantarctic Zone and Antarctic Zone, and their associated circumpolar fronts, which correspond to water mass boundaries as well as deep-reaching jets of eastward flow (Rintoul et al., 2001) (Figure 2.7). The surface flow of the ACC is primarily driven by the frictional stress of westerly winds on the ocean surface. The voluminous nature of the ACC is attributed to the currents' large cross-sectional area (Priddle, 1990) and transport rates through the Drake Passage are between 100 – 134 Sv[1] (Orsi et al., 1995; Gordon, 2001; Meredith and King, 2005). Variability in ACC transport occurs due to wind and buoyancy forcing, stratification, the effect of eddy fluxes in the momentum and buoyancy budget, and by interactions between the strong deep currents and bottom topography (Rintoul et al., 2001). The role of

[1] Sv = Sverdrups (1 Sv = 10^6 m^3 s^{-1}).

topography in steering strong currents and eddies is a process central to the dynamics of the ACC (Rintoul et al., 2001). The ACC is continuously altered on its journey around the Southern Ocean. The Tasman Seaway, the Drake Passage and the Scotia Sea produce the most profound modifications to the water masses of the ACC (Orsi et al., 1995; Garabato et al., 2002). At the Drake Passage, the tip of South America and the AP split the circumpolar flow into three branches; a northward flowing component called the Peru-Chile Current, an eastward flowing portion which spills through the Drake Passage into the Scotia Sea, and an eddy flow which is peeled off to the south along the western AP (Orsi et al., 1995).

The most voluminous water mass in the ACC is Circumpolar Deepwater (CDW), which lies at depths between 1000 – 4000 m (Sievers and Nowlin, 1984). CDW is a relatively warm current composed of two prominent core layers: Upper Circumpolar Deep Water (UCDW), which is an oxygen minimum and high nutrient concentration layer; and Lower Circumpolar Deep Water (LCDW) at slightly deeper depths, with a salinity maximum (Orsi et al., 1995; Rintoul et al., 2001) (Table 2.1). CDW is derived from a mixture of Warm Deep Water (WDW) flowing in from the North Atlantic (North Atlantic Deep Water; NADW), Pacific and Indian Oceans and waters formed in the Antarctic region. WDW water dramatically shoals as it crosses the ACC, enabling deep waters originating far to the north to enter the sub-polar regime and mix laterally with Antarctic shelf waters (Orsi et al., 1995). Loss of NADW from the Atlantic through poleward flow into the Southern Ocean, and ultimately to the rest of the world oceans, is a crucial link in the global thermohaline circulation; this volume loss is replaced by Antarctic Intermediate Water (AAIW) and Antarctic Bottom Water (AABW) entering the Atlantic through its southern boundary.

Towards the Antarctic coast complex circulation occurs, comprising the Antarctic Coastal Current (ACoastC), also known as the East Wind Drift, and two major gyre systems in the Weddell and Ross Seas (Priddle, 1990). These gyre systems are cyclonic cells of re-circulating waters; the Weddell Sea Gyre will be discussed in further detail in section 2.5.2. The water mass associated with the continental margin is Antarctic Surface Water (AASW), whose properties are determined by cooling and ice formation in the winter and ice melt in the summer (Table 2.1) and will be described further in section 2.5.

2.4.3 Southern Ocean sea ice

Sea ice extent around Antarctica ranges from a minimum of 4 x 10^6 km^2 in February to a maximum extent of ~20 x 10^6 km^2 in September (Zwally et al., 1983; Stammerjohn and Smith, 1996; Parkinson, 2004), defining a seasonal sea ice zone (13.2 x 10^6 km^2) which is more than the area of the Antarctic continent itself (Stammerjohn and Smith, 1996; Parkinson, 2004) (Figure 2.8). Sea ice forms at – 1.8 °C (Ackley, 1996) and occurs just south of the – 1.8 °C surface-air-temperature isotherm (Zwally et al., 1983). Around Antarctica, mean ice thickness is 0.5 – 0.6 m (Wadhams, 2000); typical sea ice residence time is 1 – 2 years (Dieckmann and Hellmer, 2003); and first-year ice forms 80 % of the annual extent (15.5 x 10^6 km^2), compared to 3.5 x 10^6 km^2 for multi-year ice (Comiso, 2003). Ice cover is affected by many environmental factors such as surface air temperature, wind, ocean current, tides and sea surface temperature; the predominant factor is the seasonal cycle of solar insolation and temperature that drives the freezing and melting of ice around the continent (Zwally et al., 2002).

Antarctic sea ice has a major influence on global and regional climate, and is a key environmental variable shaping the ecosystems of the Southern Ocean. The extent of sea ice affects ocean-atmosphere exchanges (heat, salt flux, momentum transfers, CO_2 ventilation) (Stephen and Keeling, 2000), global albedo and ocean thermohaline circulation through the formation of AABW (Gordon and Comiso, 1988; Seidov et al., 2001; Stössel et al., 2002). From an ecological perspective, the presence / absence of sea ice causes variability in the heat and salinity balance of the upper ocean and, consequently, density gradients and the vertical structure of phytoplankton distribution and abundance. Further, sea ice is a habitat, feeding site, refuge and breeding ground for organisms at all trophic levels.

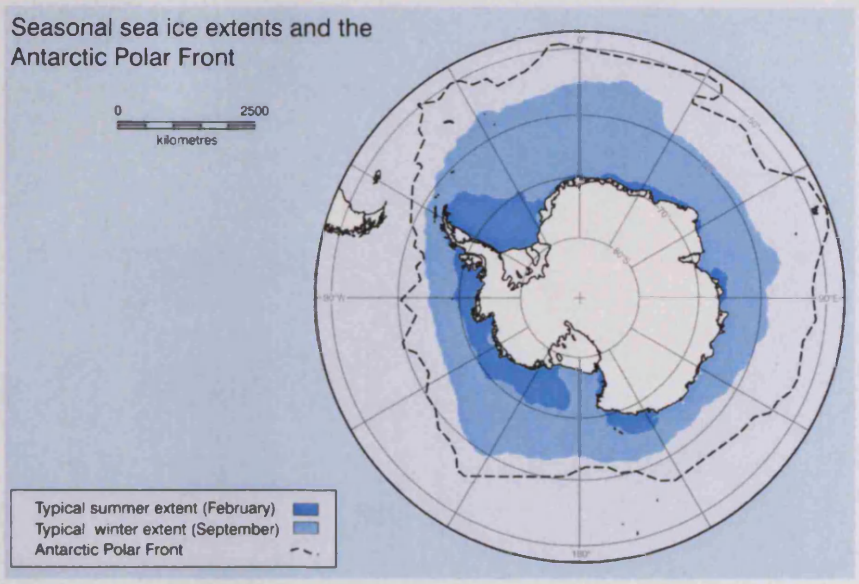


Figure 2.8
Southern Ocean seasonal sea ice extents and the Antarctic Polar Front (Source: BAS).

2.3 Antarctic Peninsula oceanography

Bathymetry, water masses and currents, sea ice and atmospheric processes are interconnected, but differentiated by the topography of the AP, producing very different environmental conditions either side of the AP. The WAP experiences a milder, maritime climate, whereas the EAP is under the influence of a harsher continental climate. Another characteristic feature setting the AP apart from the rest of the continent, and particularly important on the WAP, is the presence of numerous islands that create confined seas, in which strong stratification of the water column and surface warming occurs. This so called "island effect" (El-Sayed and Weber, 1982; Krebs, 1983), characterised by the addition of sea ice meltwater or continental glacial run-off and protection from storms, leads to an intense stabilisation of the surface water layer during austral summer and localised enhancements of primary productivity (El-Sayed and Weber, 1982; Amos, 1987; Crosta et al., 1997).

2.3.1 West Antarctic Peninsula (WAP)

The waters adjacent to the WAP are the result of a unique mixture of circumpolar and shelf water processes, with the presence of CDW being the most prominent oceanographic feature. The WAP shelf is deep compared with most of the world's shelf seas (much of the shelf is >500 m deep), and features rough bathymetry and numerous deep troughs (<1600 m) carved by glacial scouring. The troughs are one of the main factors facilitating intrusion of warm CDW onto the WAP shelf.

The WAP shelf has been extensively surveyed as part of the Palmer Long-Term Ecological Research (LTER) program (highlighted on Figure 2.9b), established in 1981 and based at Palmer Station on the southwest side of Anvers Island. This program brings together meteorological (Smith et al., 1996a), oceanographic (Hofmann et al., 1996; Martinson et al., 2008), sea ice (Stammerjohn and Smith, 1996), biological and ecological observations (Ross et al., 2008; Clarke et al., 2007), to provide a long term and integrated perspective for this region of the AP.

2.5.1.1 WAP water masses and currents

Along the continental shelf of the WAP, waters shallower than 100 – 150 m are composed of Antarctic Surface Water (AASW) and its end member winter water (WW) (Klinck, 1998; Smith et al., 1999; Moffat et al., 2008). Typically AASW has temperatures ranging between –1.8 °C to 1 °C and relatively low salinities (33.0 – 33.7 psu) (Smith et al., 1999). This water mass displays a broad range of characteristics because it is affected by atmospheric exchange, ice formation and melting, and exchange across the permanent pycnocline (Dierssen et al., 2002). By the end of autumn, strong surface heat loss, together with an increase in storm frequency, leads to the formation of a deep winter mixed layer (WW) and pack ice covers the shelf. WW is a well mixed (<100 m), has low temperatures (- 1.5 °C) and high salinity (33.8 – 34.0 psu) (Dierssen et al., 2002). As spring returns and summer progresses, sea ice retreats and the coastal waters become ice-free; the surface mixed layer is partially re-stratified by surface solar heating and freshening by sea ice melt (Klinck, 1998) and run-off from continental glaciers and ice shelves (Dierssen et al., 2002). In summer, these freshwater and shallow surface layers (20 – 30 m) overlie the remnant WW, which persists at depths between ~70 – 100 m (Klinck, 1998; Klinck et al., 2004).

Below AASW lies a permanent pycnocline at ~150 – 200 m (Hofmann and Klinck, 1998; Smith et al., 1999; Beardsley et al., 2004). The depth of this boundary is linked to sea ice conditions, with generally a deeper pycnocline in years with greater sea ice production (Smith and Klinck, 2002; Meredith et al., 2004). Below the pycnocline, waters are dominated by a modified version of CDW; a warm (1.5 °C) and salty (34.6 – 34.73 psu) water mass (Smith et al., 1999; Moffat et al., 2008). The close proximity of the ACC current and presence of deep glacial troughs results in intrusion of CDW, and the less-dense variety of this water mass (upper CDW; UCDW), onto the WAP shelf (Klinck et al., 2004). LCDW is present on the outer shelf edge, although this water mass has only been directly observed in the deep trough in Marguerite Bay (Klinck et al.,

2004). UCDW acts as a source of heat and nutrients for the biologically active upper layer of the shelf waters (Hofmann et al., 1996; Smith et al., 1999; Moffat et al., 2008). This vertical transfer across the pycnocline leads to relatively low rates of sea ice production along the WAP shelf (Martinson et al., 2008). Further, the presence of UCDW on the WAP shelf ensures that surface waters (under present climate conditions) do not become denser than the underlying modified UCDW and hence prohibit the formation of dense deep and bottom waters (Martinson et al., 2008; Wallace et al., 2008). Once on the shelf, UCDW mixes with AASW to produce modified UCDW, which has properties intermediate between the two water masses (i.e. cooler and fresher than UCDW) (Hofmann and Klinck, 1998; Klinck, 1998; Smith et al., 1999; Smith and Klinck, 2002; Martinson et al., 2008).

The physical process of getting UCDW onto the WAP shelf is predominately a result of alongshore wind stress and the divergence of Ekman transport at the coast (Hofmann et al., 1996; Stammerjohn and Smith, 1996; Wallace et al., 2008). Oceanographic modelling also suggests that offshore pressure gradients, similar to those created by northeastward ACC flow along the WAP, force upslope flow of UCDW onto the continental shelf via submarine canyon systems (Klinck and Smith, 1993). Further, momentum advection and the curvature of the shelf break are important in driving UCDW onto the shelf, following which the general shelf circulation can draw the UCDW into the interior (Dinniman and Klinck, 2004). Variability in the flux of UCDW onto the continental shelf is thought to be related to a combination of the continuity and strength of the ACC and the proximity of cross shelf troughs (Hofmann and Klinck, 1998). The latter factor means that certain areas of the WAP are more prone to intrusion of UCDW (e.g. Marguerite Bay).

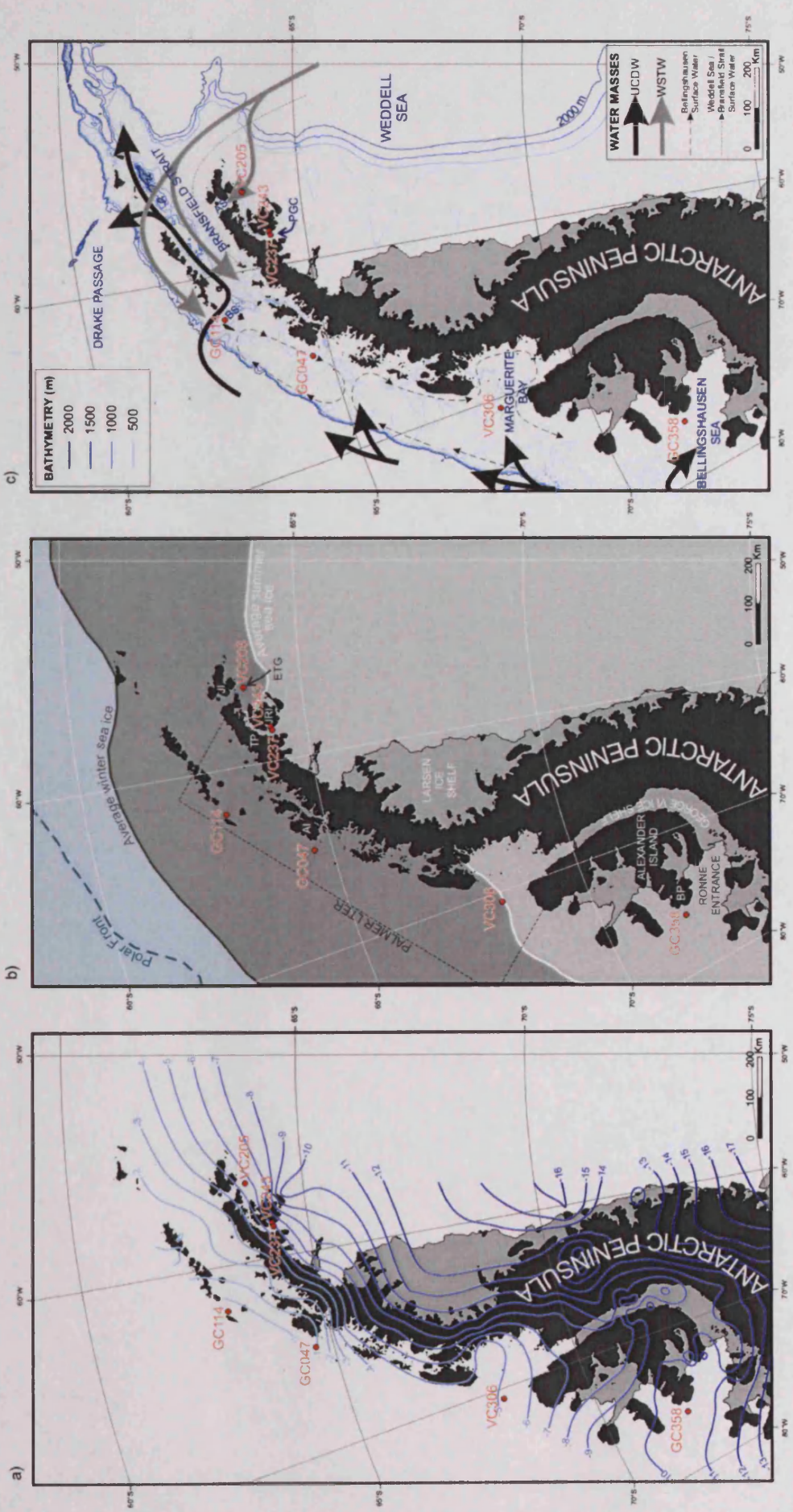
Over the WAP continental shelf, general circulation is clockwise, provided by outer northeasterly flowing ACC and inner southward coastal flow, caused by wind stress primarily being from the north-northeast (Hofmann et al., 1996) (Figure 2.9). Adjacent to the WAP coast, recent studies indicate the presence of an independent buoyancy-forced southward inner shelf current: the Antarctic Peninsula Coastal Current (APCC) (Beardsley et al., 2004; Klinck et al., 2004; Moffat et al., 2008). The APCC is strongly seasonal; forming during the spring / summer when the shelf is ice free and virtually disappearing during the winter months, when sea ice re-forms and meltwater fluxes from the coast are dramatically reduced (Moffat et al., 2008).

2.5.1.2 WAP sea ice

Relative to other places in the Southern Ocean, the WAP shelf region has relatively thin sea ice that displays considerable spatial and temporal (year-to-year) variability (Stammerjohn and Smith, 1996). There is little ice coverage in ~90 % of the Palmer LTER study area (highlighted on Figure 2.9b) between January to April, with March the mean month of minimum sea ice cover; ice decay is gradual (several months) and summers are long in this region (Stammerjohn and Smith, 1996). Highest sea ice growth rates occur in June and July, being a relatively brief event (several weeks), leading to maximum sea cover typically in August (Stammerjohn and Smith, 1996). Ice advances from the southwest to northeast and from the AP toward the northwest and in normal ice years, ice coverage advances to just south of Anvers Island and extends northwestwards across the WAP shelf (Stammerjohn and Smith, 1996). The vicinity of Anvers Island is often ice free during maximum ice coverage and in high ice years this area marks the location of a near coastal polynya (varying in size on a daily basis) (Stammerjohn and Smith, 1996). Linkages between air temperature and sea ice are proposed to be very strong for the WAP region (Smith et al., 1996a) and a further oceanographic control is provided by the upward flux of warm CDW, encouraging melting of the sea ice (Hofmann et al., 1996).

Figure 2.9 (next page)
Map of the Antarctic Peninsula (AP), showing core localities, together with:

- **a)** Mean annual isotherms (from Morris and Vaughan, 2003)
- **b)** Position of the present day average summer and winter sea ice limits and Polar Front (from Fetterer et al., 2002, updated 2007 and BAS); AI = Anvers Island; BP = Beethoven Peninsula; ETG = Erebus and Terror Gulf; JI = Joinville Island; JRI = James Ross Island; TP = Trinity Peninsula; PALMER Long-Term Ecological Research (LTER) area highlighted.
- **c)** Regional bathymetry and oceanographic circulation patterns; UCDW = Upper Circumpolar Deep Water; WSTW = Weddell Sea Transitional Water; AS = Antarctic Sound; BS = Boyd Strait; PGC = Prince Gustav Channel (modified from Hofmann et al., 1996; Zhou et al., 2002; Domack et al., 2003; and Moffat et al., 2008).


a)
b)
c)
ANTARCTIC PENINSULA
WEDDELL SEA
DRAKE PASSAGE
BRANSFIELD STRAIT
MARGUERITE BAY
BELLINGSHAUSEN SEA
LARSEN ICE SHELF
ALEXANDER ISLAND
RONNE ENTRANCE
PALMER LTER
ETG
PGC
BP
Polar Front
Average winter sea ice
Average summer sea ice
BATHYMETRY (m)
2000
1500
1000
500
WATER MASSES
UCDW
WSTW
Bellingshausen Surface Water
Weddell Sea / Bransfield Strait Surface Water
200 m
0
100
200
Km
GC114
VC205
GC047
VC306
GC358

2.5.2 East Antarctic Peninsula (EAP)

The oceanic system of the Weddell Sea embayment is governed by a cyclonic gyre (Weddell Sea Gyre) and sinking of AABW. The gyre extends from the western Weddell Sea (i.e. EAP) to ~20 – 30°E, with the Antarctic continent forming the southern and western boundary, while mid-ocean ridges and the ACC limit the gyre to the north (von Gyldenfeldt et al., 2002). The ACC is well removed from the EAP continental shelf due to the motion of the Weddell Sea Gyre. In addition, the glaciological regime is dramatically different to the WAP; on the EAP there are large, permanent ice fields, the Larsen and Ronne-Filchner Ice Shelves and high concentrations of multi-year sea ice. This exerts a large influence on atmospheric processes and shelf water masses.

2.5.2.1 EAP water masses and currents

Similar to the upper water column of the WAP, surface water in the western Weddell Sea exhibits distinct inter-seasonal variability, with the winter season characterised by WW (Gordon and Huber, 1984; 1990), subsequently diluted in summer by melting sea ice and warmed by solar radiation to give AASW in the upper 20 – 50 m (Foster and Carmack, 1976). A recent oceanographic study of the western Weddell Sea (offshore from Larsen-C Ice Shelf) highlighted the well-stratified nature of the upper ocean, developed through intense winter near-surface vertical fluxes (Absy et al., 2008). Below the well-developed surface mixed layer (< -1.8 °C) a pronounced pycnocline was present, which acted to isolate surface waters from the underlying Warm Deep Water (WDW) (< 0.5 °C) (Absy et al, 2008). WDW is a localised reflection of CDW, which enters the Weddell Sea from the eastern margin and extends to depths of 1500 m (Orsi et al., 1993; Rintoul et al., 2001). A large proportion of CDW that enters the Weddell Sea is quickly converted to Weddell Sea Deep and Bottom Water (WSDW and WSBW) through intense ice-ocean-atmosphere interactions along the southern margin (Ronne-Filchner Ice Shelf) and western margin (Orsi et al., 1993; Rintoul et al., 2001; von Gyldenfeldt et al., 2002; Foldvik et al., 2004). WSDW and WSBW is augmented by the addition of High Salinity Shelf Water (HSSW) formed as a bi-product of sea ice formation, via brine rejection (Foldvik et al., 2004). These deep water masses in the Weddell Sea are precursors to AABW, and it is believed that more than half of the total flux of AABW has origins in the Weddell Sea (Orsi et al., 1999).

2.5.2.2 EAP sea ice

The Weddell Sea is characterised by one of the most extensive annual and perennial sea ice regimes in the Southern Ocean (Stammerjohn and Smith, 1996), with sea ice present for 10 – 11 months/year (Sea Ice Climatic Atlas, 1985, cited in Crosta et al. 1997). Highest concentrations are observed in the western Weddell Sea (i.e. EAP), with perennial ice cover reaching 1.2 million km^2 (Gordon, 1998) and often remaining ice-covered even in summer (Eicken, 1992). Sea ice is concentrated in this area due to clockwise circulation of the Weddell Gyre, with sea ice transported via the westward flowing current of the southern gyre and packed against the eastern side of the AP (Venegas and Drinkwater, 2001). Further, the convergent flow regime in this area means that ice concentrations are much higher than in the seasonal pack ice, with perennial snow and ice thickness between 0.4 – 1.5 m (Lange and Eicken, 1991). Highest sea ice decay rates occur in December and January, with February (August) being the mean month of minimum (maximum) sea ice (Stammerjohn and Smith, 1996). In the western Weddell Sea, break-out generally occurs in November and re-formation in April (Scambos et al., 2001).

2.6 Antarctic Peninsula study regions

This research focuses on reconstructing regional oceanographic, biological and climate trends along a latitudinal transect of the AP and therefore spans a large geographical area. In total, seven cores have been investigated, on both sides of the AP and covering 9 degrees of latitude. Core locations are shown on Figure 2.9. Further details, including water depth and total core length, are presented in Table 2.2. The cores are from a range of depositional settings; channel, nearshore, bay and offshore continental shelf and were selected to be regionally representative, thereby affording the potential to assess the nature and phasing of Holocene climate change on both sides of the AP. This section describes the physical setting of each of the different core localities.

Table 2.2
Details of cores used in this investigation. Core number is generated by the coring technique (gravity core (GC); trigger core (TC); and vibro core (VC)) and unique site identification number. West Antarctic Peninsula (WAP); East Antarctic Peninsula (EAP); British Antarctic Survey (BAS); Royal Research Ship (RRS).

Core number	**Core site**	**Core type**	**Latitude** (decimal degrees)	**Longitude** (decimal degrees)	**Water depth** (metres)	**Core length** (metres)	**Cruise number & date**	**Previous work on the core**
GC114	Boyd Strait, WAP	Gravity core	-62.9339	-62.1185	772	3.4	BAS RRS *James Clark Ross* cruise JR19; 30th March 1997	- Splitting and sedimentary logging (BAS) - Volcanic glass shards within the sediment were analysed for major element compositions to assess potential tephrachronological correlations (Moreton, 1999; Moreton and Smellie, 1998)
GC047 TC046	Anvers Trough, WAP	Gravity core Trigger core	-64.5883	-64.805	536	3.8	BAS RRS *Discovery* cruise D172; 1987–1988	- Splitting and sedimentary logging (Pudsey et al., 1994) - Incorporated in a study to reconstructing ice sheet retreat from the AP shelf, using echo sounding and side scan sonar data, paired with sediment analysis of four cores (logging, grain size analysis, assessment of biogenic silica content, radiocarbon dating) (Pudsey et al., 1994)
VC306	Marguerite Bay, WAP	Vibro core	-68.1433	-70.5817	772	5.94	BAS RRS *James Clark Ross* cruise JR71; 20th February 2002	- Splitting and sedimentary logging (Ó Cofaigh et al., 2005a) - Part of a NERC Antarctic Funding Initiative project (AFI 48/02), reconstructing the configuration of palaeo-ice streams that drained the AP Ice Sheet during the last glacial cycle from geophysical and geological data; one such stream flowed to the edge of the continental shelf via Marguerite Trough (Ó Cofaigh et al., 2005a; 2007).
GC358	Ronne Entrance, WAP	Gravity core	-71.735	-76.0367	690	0.94	BAS RRS *James Clark Ross* cruise JR104; 31st January 2004	- Splitting and sedimentary logging (Hillenbrand et al., 2007) - Part of a NERC Antarctic Funding Initiative project (AFI4/17), studying glacial-interglacial changes in the southern Bellingshausen Sea and the presence of large outlet drainage basins during late Quaternary glacial periods (Hillenbrand et al., 2007).

Core number	Core site	Core type	Latitude (decimal degrees)	Longitude (decimal degrees)	Water depth (metres)	Core length (metres)	Cruise number & date	Previous work on the core
VC243	Prince Gustav Channel, EAP	Vibro core	-64.225	-58.305	649	5.86	BAS RRS *James Clark Ross* cruise JR48; 4th – 13th March 2000	- Splitting and sedimentary logging (Pudsey and Evans, 2001) - A suite of cores (including VC243 and VC237), together with bathymetric data, were collected from the PGC, Larsen Inlet and Larsen-A area to address questions regarding past ice shelf stability. From ice-rafted debris provenance analysis, linking rock types to different ice drainage basins, Pudsey and Evans, (2001) were able to conclude that during the Mid-Holocene (5-2 ka) the PGC Ice Shelf was absent. A further study of benthic foraminifera assemblages revealed a distinctive deglaciation signal present (occurring in the PGC at a minimum age of 9006 ^{14}C years (corrected)), which was repeated at the time of Mid-Holocene ice shelf break-up (Pudsey et al., 2006).
VC237	Prince Gustav Channel, EAP	Vibro core	-64.2232	-58.4778	816	6		
VC205	Erebus and Terror Gulf, EAP	Vibro core	-63.7404	-56.2189	498	5.42	BAS RRS *James Clark Ross* cruise JR29; 27th February 1998	- Splitting (BAS)

2.6.1 WAP: GC114 – Boyd Strait; and GC047 – Anvers Trough

Core GC114 is the most northerly core analysed on the AP transect (Figure 2.9). It was retrieved from Boyd Strait, which lies between Smith Island and Snow Island at the southern tip of the South Shetland Island chain. Boyd Strait is a NW-SE trending trough connecting Bransfield Strait with the continental slope, and ultimately to Drake Passage. Core GC047 was retrieved from Anvers Trough, ~25 km offshore from Anvers Island, which lies within the Palmer Archipelago (Figure 2.9).

Located at the northern tip of the AP, Bransfield Strait represents a series of semi-enclosed basins totalling ~450 km in length and 100 km wide. Three main sub-basins have been identified, between 1000 – 2000 m deep, separated by sills ~500 m deep, with a discontinuous chain of volcanoes and active hydrothermal vents along the axis of the central basin (Gràcia et al., 1996; Lawver et al., 1996). Bransfield Strait is bound to the north from the Drake Passage by the steep continental margin of the South Shetland Islands. To the south the boundary rises more gradually, with a wide portion of AP continental shelf (50 – 75 km) separating Bransfield Strait from the mountainous Trinity Peninsula at the northern tip of the AP. The Palmer Archipelago represents an island chain that sits on this wide portion of the AP continental shelf, to the south of Bransfield Strait and adjacent to the AP coastline (15 – 25 km), separated by narrow and deep straits and fjords (e.g. Gerlache Strait). Anvers Island forms the largest of the Palmer group (~60 km in length, highest peak ~2270 m).

The large-scale water mass distribution and circulation offshore of the Palmer Archipelago is very typical of the WAP region; dominated by UCDW below ~200 m (Hofmann et al., 1996) and surface waters influenced heavily by the seasonal cycle of sea ice advance and retreat (section 2.5.1.1). Southwest of Anvers Island, the Bismark Strait crosses the shelf at this latitude, extending landward from core site GC047 and providing a route for UCDW flow from the Bellingshausen Sea into Gerlache Strait (García et al., 2002). In contrast, Bransfield Strait experiences quite different oceanographic influences. Occupying a transitional zone between the Bellingshausen and the Weddell Seas, Bransfield Strait experiences both inflow of warm and relatively fresh water from the Bellingshausen Sea (typically 0.5–3.0°C and 33.1–33.9 psu in summer), and cool, relatively salty water from the Weddell Sea (typically with negative temperatures and salinity ranging from 34.1–34.6 psu in summer) (García et al., 2002). The two currents meet in the vicinity of Trinity Island, where they form a front of biological significance (Amos, 1987). A surface current (the Bransfield Strait Current)

flows along the shelf break to the south of the South Shetland Islands (Zhou et al., 2002). CDW does enter the western Bransfield Strait from the Bellingshausen Sea, but is blocked from entering the central and eastern basins by shallow sills (Zhou et al., 2002). The deep trough of Boyd Strait (core site GC114) provides a potential pathway for modified LCDW to flood into Bransfield Strait (Hofmann et al., 1996; García et al., 2002), as illustrated in Figure 2.9c. Deep and bottom waters of Bransfield Strait are formed through the sinking of surface waters and are characterised by their lower temperature and salinity, higher oxygen content and lower nutrient concentrations than deep waters outside the basin (e.g. WSDW) (Gordon and Nowlin, 1978; Hofmann et al., 1996).

Both core site GC114 and GC047 sit within the Palmer LTER study area, so the broad-scale WAP sea ice description (section 2.5.1.2) is applicable for these two localities. Core site GC114 lies between present-day winter and summer sea ice limits; with sea ice extending to ~57 °S at its maximum extent (September – October) and leaving Bransfield Strait completely ice free at its minimum extent (January – February) (N.O.C., 1985 cited in Bárcena et al., 2006). Based on summary satellite data from the Palmer Archipelago for the years 1978 – 1987 (Gloersen et al., 1992), Leventer et al. (1996) determined that the area offshore of Anvers Island has nearly open water with loose pack ice from February through to May and during some years the ice breaks up in December and January. Further, in the vicinity of Anvers Island year-to-year ice coverage can vary, ranging from being ice free, with a near coastal polynya, to ice coverage extending 200 km north and south from Anvers Island (Stammerjohn and Smith, 1996). Finally, Bransfield Strait and Palmer Archipelago are viewed as potentially the most sensitive portion of the AP, where the onset of modern glacial retreat has been well documented and observed to be propagating southwards (Cook et al., 2005).

2.6.2 WAP: VC306 – Marguerite Bay

Core VC306 was collected from the mid-shelf of Marguerite Bay, approximately 150 km northwest of the narrow entrance of George VI Sound, and within Marguerite Trough (Figure 2.9). Marguerite Bay is broad open bay bound by Adelaide Island to the north, the spine of the AP to the east and Alexander Island in the south. Outlet glaciers from the AP and Alexander Island drain into the northern, eastern and south-western parts of the bay. In the southern part of Marguerite Bay lies the George VI Ice Shelf in George VI Sound, which drains north into Marguerite Bay and south into the

Bellingshausen Sea embayment. Marguerite Trough extends from the mouth of George VI Sound, to the edge of the continental shelf. This trough is between 50 – 80 km in width and roughly 370 km in length and exhibits onshore over-deepening, with water depths of approximately 1500 m in the inner bay to roughly 500 m at the shelf edge (Ó Cofaigh et al., 2005a).

The water mass structure in Marguerite Bay is very typical of the WAP (section 2.5.1.1). UCDW intrudes onto the WAP shelf in this area, focused through Marguerite Trough (Meredith et al., 2008; Jenkins and Jacobs, 2008). This warm water mass flows all the way to the George VI Ice Shelf and forms the main inflow to the cavity beneath the ice shelf, resulting in basal melting (Jenkins and Jacobs, 2008). Much of the meltwater produced beneath the ice shelf appears to be carried northwards by the mean flow through the George VI Sound emerging in southern Marguerite Bay (Jenkins and Jacobs, 2008). Although, this meltwater currently only represents <3 % of the upper water column outflows from George VI Ice Shelf (the remainder (>97 %) consists primarily of UCDW), this is sufficient to lower the density of the UCDW/meltwater mixture to and below that of WW (i.e. <34 psu) (Jenkins and Jacobs, 2008). Outflows thus represent a flux of slightly modified UCDW to the surface layers of Marguerite Bay, with associated high temperature, low dissolved oxygen and high nutrient concentrations (Jenkins and Jacobs, 2008). Finally, the APCC has been observed to flow southwest along the west coast of Adelaide Island, into Marguerite Bay and exiting near Alexander Island (Beardsley et al., 2004; Klinck et al., 2004; Moffat et al., 2008) (Figure 2.9).

Marguerite Bay is seasonally ice covered, typically being ice-free (or with low concentrations) from December to March, although the start and end dates of the ice-free period can vary from November – January and March – May, respectively (Meredith et al., 2008). The presence of Rothera Research Station at Ryder Bay, on Adelaide Island, facilitates year-round in situ observations of coastal sea ice concentration and type (Clarke et al., 2008; Meredith et al., 2008). Ryder Bay is typically largely covered in fast ice from June to September, whereas ice free conditions or days with small concentrations of brash ice dominate the rest of the year; it is unusual for there to be multi-year ice (Meredith et al., 2008). Outer shelf settings (e.g. the mid shelf position of core site VC306) are likely to experience less temporally persistent and thinner sea ice cover than coastal settings (e.g. Ryder Bay).

Marguerite Bay is seen as a crucial area with respect to understanding the current climatic setting and oceanographic influences on the WAP. Ice shelves that have collapsed in the late 20th century lie within the key -5°C to -9°C isotherm boundaries (Hodgson et al., 2006a) and the present configuration of these boundaries straddles Marguerite Bay (Morris and Vaughan, 2003). Recent climate warming in the AP has resulted in the southerly propagation of ice shelf collapse, evidenced by the disintegration of nearby Wordie Ice Shelf in the late 1980s (Vaughan, 1993) and the breakout of Wilkins Ice Shelf in March 2008 (Vaughan, 2008). George VI Ice Shelf represents the northern limit of extant ice shelves on the WAP (Hodgson et al., 2006a).

2.6.3 WAP: GC358 – Ronne Entrance

GC358 represents the most southerly core analysed from the WAP. It was collected from the inner shelf of the southern Bellingshausen Sea, specifically the Ronne Entrance into which the George VI Ice Shelf discharges (Figure 2.9). The core site lies 30 km to the south of Alexander Island (Beethoven Peninsula), near several outlet glaciers and ice shelves which discharge into the Bellingshausen Sea. The small Bach Ice Shelf is particularly close to the core site (140 km) and is likely to exert the strongest influence on sediment and iceberg delivery to the site. Within the southern Bellingshausen Sea there is a major glacial trough (Belgica Trough), more than 550 m deep along its entire length from Eltanin Bay and Ronne Entrance to the continental shelf edge (Larter et al., 2004; Ó Cofaigh et al., 2005b). The inner shelf embayment is delimited by Alexander Island, the southern AP and Ellsworth Land.

The hydrographic regime of the southern Bellingshausen Sea is dominated by the ubiquitous presence of UCDW, characterised by relatively high temperature and salinity and low dissolved oxygen concentration (Jenkins and Jacobs, 2008). Similar to the Marguerite Bay Trough, it is likely that the presence of the Belgica Trough, and subsidiary cross-shelf channels, facilitates the intrusion of UCDW onto the continental shelf. Despite the deep water column being similar in character at both ice fronts of George VI Ice Shelf, temperatures at Ronne Entrance are ~0.1 °C lower than those found in Marguerite Bay, waters are less salty and dissolved oxygen is higher, suggesting that upwelling of UCDW is more pervasive in Marguerite Bay than Ronne Entrance (Jenkins and Jacobs, 2008).

Sea ice in the Bellingshausen / Amundsen Sea sector is characterised by substantial multi-year ice, often thick and impenetrable, occasionally causing ships to be beset for several months during winter (Zwally et al., 2002). However, from satellite observations

of sea ice cover between 1979 – 2002, the Bellingshausen Sea and Amundsen Sea have experienced the greatest decline in sea ice cover in Antarctica (Parkinson, 2004). The high sea ice concentration experienced in this region is likely to limit air-sea heat exchange, potentially causing reduced seasonal variability in thermohaline properties of AASW in this region, compared to more northerly WAP localities.

2.6.4 EAP: VC243 and VC237 – Prince Gustav Channel

PGC is a narrow channel, orientated north-south and bounded by James Ross Island to the east and the Trinity Peninsula on the AP to the west. Core VC237 was recovered from the deep central part of the channel, whilst core VC243 is from a comparable latitude, but lies 9 km closer towards the coast of James Ross Island and in shallower waters (Figure 2.9). In the narrowest section (which lies north of 64°10'S and these core sites), the channel is roughly 8 km wide, with steep sides (up to 8°), relatively flat to slightly hummocky floor and water depths typically between 700 – 850 m (Pudsey et al., 2001). The channel broadens to the south, reaching approximately 40 km at the southern entrance. From here, the channel feeds into a deep trough that extends onto the continental shelf, becoming shallower (~500 m) and smoother. Prior to 1995, an ice shelf was present in PGC and in the neighbouring Larsen-A embayment. Retreat of the PGC Ice Shelf sped up in the late 1980s and in 1995 a major breakout of both the PGC Ice Shelf and Larsen-A Ice Shelf occurred (Rott et al. 1996).

With respect to the oceanographic regime, the southern opening of PGC faces directly south and is fully exposed to the EAP open continental shelf. Within the Weddell Sea, water masses and currents flow clockwise within the Weddell Sea Gyre, bathing the eastern AP coastline in modified CDW (Gordon et al., 1993; Orsi et al., 1993) (section 2.5.2.1). Icebergs generally drift northwards along the EAP continental shelf, dropping ice rafted debris derived from the south within the PGC (Curry and Pudsey, 2007). Ice rafted debris is also derived locally from the tidewater glaciers discharging from James Ross Island and the Trinity Peninsula. There is no published data on the sea ice character within PGC, therefore only a generalised view of the sea ice extent and thickness for the EAP (section 2.5.2.2) can be applied to the PGC.

2.6.5 EAP: VC205 – Erebus and Terror Gulf

One core was analysed from a wide, flat basin (~500 m water depth) within the Erebus and Terror Gulf (core VC205) and is the most northerly core studied on the EAP (Figure 2.9). The continental shelf around this part of the Weddell Sea is wider in comparison to the WAP, with much more subdued topography and EAP inner shelf

troughs do not extend continuously out to the continental shelf break (Pudsey et al., 2006). A number of channels dissect this region of the shelf: the Antarctic Sound, connecting Bransfield Strait and the Weddell Sea, bounded by the tip of the AP to the south and Joinville Island to the north; and the PGC (see section 2.6.4) to the west. The Erebus and Terror Gulf forms a northerly extension of PGC, bordered to the northeast by Joinville Island and to the southwest by James Ross Island.

Both the Antarctic Sound and PGC are important features when considering the oceanographic and depositional environment of core VC205. The Antarctic Sound provides a subsidiary pathway for Weddell Sea Transitional Water to enter Bransfield Strait (Figure 2.9c); a potentially important connection between the east and west side of the AP. There is a consensus in the literature that Weddell Sea inflow enters Bransfield Strait as a weak and relatively shallow flow around Joinville Island and through the Antarctic Sound (López et al., 1999 and references therein). However, debate exists as to whether this also encompasses deep water components, as suggested by Gordon et al. (2000) and disputed by von Gyldenfeldt et al. (2002). PGC is potentially an important source region and route of terrigenous sediment and iceberg delivery from the outlet glaciers and ice shelves along the northern AP coast (Trinity Peninsula, western James Ross Island and the Larsen Ice Shelf regions). This delivery of terrigenous material may be highlighted in core VC205 as exaggerated inputs of ice rafted debris. There is no published data on the sea ice character in the Erebus and Terror Gulf, therefore only a generalised view of the sea ice extent and thickness for the EAP (section 2.5.2.2) can be applied to this region.

2.7 Chapter summary

This chapter presented the background context for this study, relating to Antarctica and the AP region. The regional geology, climate, oceanography and sea ice character have been presented for each of the core sites.

3 Diatoms of the Southern Ocean

This chapter provides background information on the use of diatoms as a proxy for palaeoceanographic and palaeoclimatic reconstructions. The modern-day distribution, habitats and ecology of diatoms used in this study are discussed, drawing on published surface water samples and core-top sediment studies from the Southern Ocean. This is followed by a brief summary of previous studies using diatoms to produce palaeoecological reconstructions in Antarctica. Factors that may complicate the signal preserved in the sediments (i.e. taphonomy, water column processes and transportation by currents) are also discussed. Finally, assumptions underlying the use of diatoms in this investigation are outlined, together with the parameters that can be inferred from the analysis of sedimentary diatoms.

3.1 Definition and physical form

Diatoms are unicellular, eukaryotic, micro-organisms, often occurring in colonies. Typically they range in size from ~2 to 200 μm, and they exhibit a wide variety of shapes. Their cell wall (frustule) is composed of silica (SiO_2) with an organic coating, and the degree of silicification varies. The frustules are variously ornamented with perforations, ribs, spines or minute processes. Diatom species classification is usually based on their gross morphology – shape, structure and ornamentation of the cell walls (Figure 3.1), although more recently, molecular techniques have been used. Many diatoms form colonies, held together by interlocking siliceous spines, processes or ridges; by pads or stalks of mucilage; or by threads of polysaccharide (chitinous material) (Round et al., 1990). Diatom colonies may aggregate to form floc particles several millimetres in diameter and form a component of marine snow (Priddle, 1990).

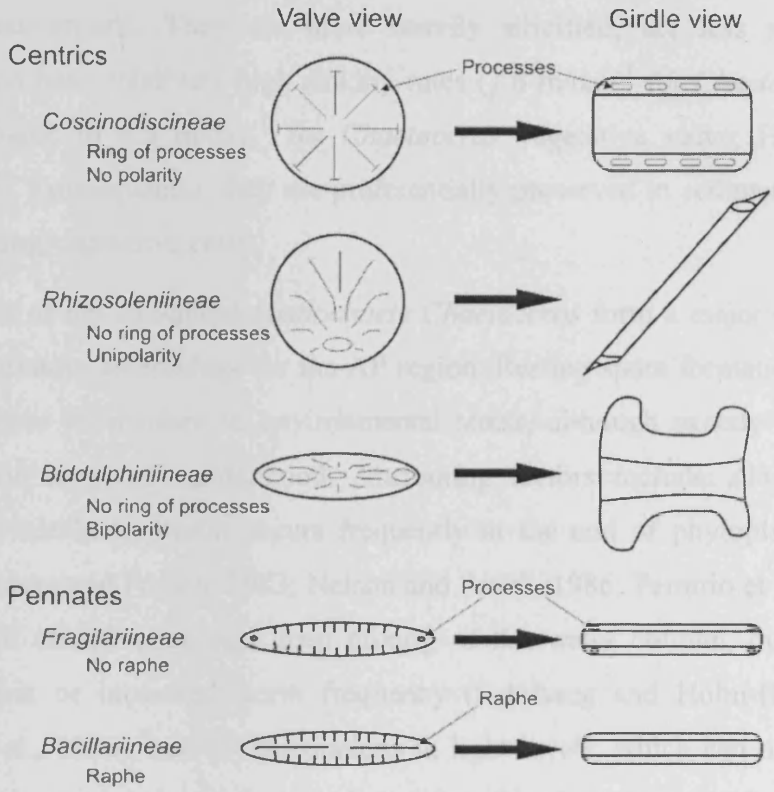


Figure 3.1
Schematic diagram of centric and pennates diatom sub-orders (redrawn from Hasle and Syvertsen, 1997). Centric diatoms have concentric or radial symmetry around a point or points; pennate diatoms have symmetry around a longitudinal axis.

3.2 Biology

Diatoms generally reproduce through vegetative fission at a rate of 0.1 – 8 times per day; this style of reproduction allows diatoms to build a very high biomass rapidly (Crosta and Koç, 2007). Vegetative reproduction involves the formation of two new individuals back-to-back within the parent cell frustule and typically leads to a decline in mean cell size of the offspring. At a given threshold, diatoms undergo sexual reproduction during which gametes, auxospores and full-sized vegetative cells are formed (Hasle and Syvertsen, 1997).

Some diatom species produce resting spores within the vegetative cell (e.g. *Hyalochaete Chaetoceros*, *Eucampia antarctica* and *Thalassiosira antarctica*) as a life cycle stage for maintaining populations during unfavourable conditions. The resting spore enhances the survival of a species under adverse conditions, serving as waiting or seeding populations (Ferrario et al., 1998). Regeneration of the resting spores requires re-suspension from the sediment or deep waters by mixing events or release from sea ice by melting. Resting spore valves are usually morphologically distinct from their

vegetative counterparts. They are more heavily silicified, are less susceptible to dissolution and have relatively high sinking rates (7.6 m/day^{-1} for *Chaetoceros* resting spores, compared to 4.8 m/day^{-1} for *Chaetoceros* vegetative valve; Hargraves and French, 1983). Consequently, they are preferentially preserved in sediments, compared to corresponding vegetative cells.

Resting spores of the sub-genus *Hyalochaete Chaetoceros* form a major component of the sediment diatom assemblage for the AP region. Resting spore formation is believed to be a response mechanism to environmental stress, although exactly what triggers their formation is poorly understood. Attributing factors include: (1) depletion of surface water nutrients, which occurs frequently at the end of phytoplankton bloom events (Hargraves and French, 1983; Nelson and Smith, 1986; Ferrario et al., 1998); (2) break-down of stratification and deep mixing of the water column, due to reduced meltwater input or increased storm frequency (Sakshaug and Holm-Hansen, 1984; Bodungen et al., 1986); and (3) fluctuations in light levels, which can occur when (i) cells are mixed or sink below the pycnocline; (ii) self-limitation occurs due to extremely high phytoplankton stocks; or (iii) sea ice cover increases and cells are advected under the ice (Fryxell, 1983; Hargraves and French, 1983; Nelson and Smith, 1991; Taylor and McMinn, 2001).

3.3 Distribution and ecology

The Southern Ocean is generally oligotrophic, with low biomass and productivity, but there are localised pulses of high productivity (Smith and Sakshaug, 1990). Diatom productivity is highest just south of the Polar Front, in a 900 – 2000 km broad circum-Antarctic belt (Burckle and Cirilli, 1987; Gersonde, 1990), depositing diatomaceous ooze between approximately 50°S and 60°S (Burckle, 1984a).

Sedimenting diatoms provide a reflection of productivity in surface waters (Leventer and Dunbar, 1996; Zielinski and Gersonde, 1997; Crosta et al., 2005); consequently, it is possible to map opal-rich sediments to provide information on the distribution of diatoms in surface waters. Using this technique, Crosta et al. (1997) noted very high variability in the distribution of total diatom abundance in the surface sediments of the Southern Ocean (2 – 1077 x 10^6 valves/g of dry sediment). Based on the distribution and relative abundance of *Hyalochaete Chaetoceros* resting spores (CRS), Crosta et al. (1997) divided the area into four biogeographic zones: (1) the AP sector; (2) the Embayment Systems (Ross Sea and Weddell Sea); (3) the Continental Shelf zone (water depth <2000 m); and (4) the Deep Ocean (water depth >2000 m). Spatially, the highest

abundances of CRS are found in the AP sector (<1000 x 10^6 valves/g of dry sediment) (Crosta et al., 1997).

The distribution of diatoms in the Southern Ocean is controlled by a combination of environmental factors, including water temperature and salinity (Neori and Holm-Hansen, 1982), water column stability (Leventer, 1991), ambient light levels (El Sayed, 1990), nutrient availability (Burckle and Cirilli, 1987) and proximity to sea ice (Cunningham and Leventer, 1998 and references therein). Near to the Antarctic continent, nutrient levels are high leading to favourable growth conditions and high primary production (Crosta et al., 1997); whereas beyond the coast, temperature, nutrient availability and stratification play an increasingly important role in regulating primary production (DeFelice and Wise, 1981). Arguably the most important physical determinant of spatial and temporal changes in the structure of the Antarctic coastal marine ecosystem is the annual advance and retreat of sea ice (discussed further in section 3.4.2). The relationship between Southern Ocean sea ice and primary productivity has been observed directly using satellite ocean colour scanners (e.g. SeaWiFS). Subtle changes in chlorophyll concentration reveal various types and quantities of marine phytoplankton. In the Southern Ocean, this phytoplankton is composed mainly of diatoms, with varying contributions of flagellates and other prymnesiophytes (i.e. *Phaeocystis*) (Holm-Hansen et al., 1977; Fryxell et al., 1984; Zielinski and Gersonde, 1997). Consequently, chlorophyll concentration is a realistic representation of diatom productivity and distribution in surface waters of the Southern Ocean (Figure 3.2).

Surface phytoplankton productivity around the Antarctic continent is largely restricted to ice-free periods, with highest productivity occurring in austral spring and summer (Figure 3.2). This has knock-on consequences for the export of biogenic particles to the sediment; over 95% of the annual flux at shallow and mid-depths occurs during December and January (austral summer), whereas during sea ice coverage, the vertical flux of siliceous organisms from the surface waters is extremely low (Wefer et al., 1988; Abelman and Gersonde, 1991; Leventer, 2003). Large blooms occur in the marginal sea ice zone because as the ice edge recedes, low-salinity meltwater produces a low-density surface lens that reduces vertical mixing and shallows the mixed layer; consequently phytoplankton are able to grow in a high-irradiance stable environment (Smith and Nelson, 1986; Sullivan et al., 1993; Arrigo and McClain, 1994; Marrari et al., 2008).

Additional factors can modify the distribution, timing, duration and magnitude of productivity pulses, including oceanographic processes (e.g. depth of water column, fronts, eddies, interleaving) and biological features (e.g. aggregation, grazing; section 3.6.1) (Smith and Sakshaug, 1990). A recent study of Chlorophyll *a* distribution along the AP, utilising SeaWiFS data, suggests that upwelling of iron-rich deep water, rather than the retreat of the ice edge, may be a major factor controlling phytoplankton bloom development during spring and summer in the vicinity of the shelf break, and in coastal waters along the northern AP (Marrari et al., 2008). Further, the seasonal variability in the amount and extent of glacial meltwater plumes influences the physical dynamics of the water (e.g. water column stratification, nearshore turbidity) and therefore primary productivity (Dierssen et al., 2002).

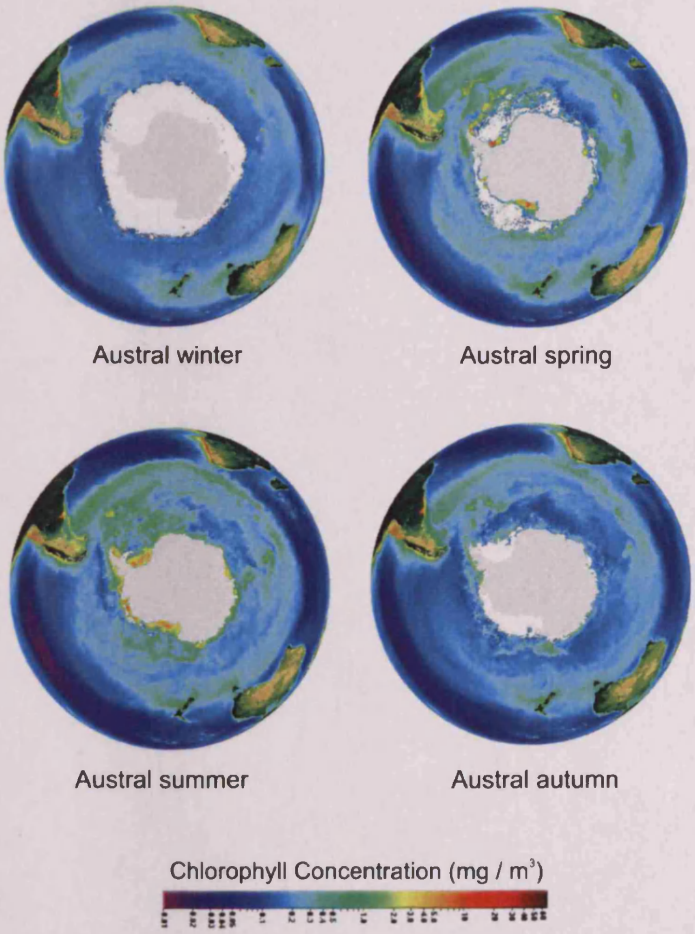


Figure 3.2
Chlorophyll *a* distributions in the Southern Ocean show high spatial and temporal variability (Source: http://oceancolor.gsfc.nasa.gov/SeaWiFS/BACKGROUND/). Most Antarctic open waters are relatively low chlorophyll concentrations despite the availability of nutrients, and thus the Southern Ocean is generally considered to be a high-nutrient low-chlorophyll region (Holm-Hansen et al., 1977). However, large phytoplankton blooms do occur during austral spring and summer (yellow – red), particularly in the marginal sea ice zone.

3.4 Diatom habitats

In the Antarctic marine setting, diatom habitats can be divided into three main types: (1) open ocean; (2) sea ice (both within the ice and in the adjacent water column); and (3) benthic.

3.4.1 Open ocean

Although nutrient-rich, the permanent open ocean zone of the Southern Ocean, north of the maximum winter sea ice edge, has been identified as an almost oligotrophic area (Smith and Sakshaug, 1990). As a habitat, the permanently open ocean zone is very different from the sea ice zone and continental shelf areas (which experience seasonally open water) being: (1) typically well-mixed and permanently ice free; and (2) experiencing a silicate gradient (from less than 10 μM-Si in the northern part to >50 μM-Si near the northern border with the sea ice zone) (Tréguer and Jacques, 1992).

In the permanently open ocean zone, the annual cycle of production is typically unimodal, with a delay in the spring bloom with increasing latitude due to the light effect (Tréguer and Jacques, 1992). Bloom development is a function of: (1) depth of the wind mixed layer (blooms are prevented from developing as soon as the mixed layer depth reaches 40 – 50 m); (2) light distribution in the water column; (3) local meterological conditions; (4) size of the initial standing stock of phytoplankton; and (5) loss rate (Tréguer and Jacques, 1992 and references therein). Irradiance and mixing regimes favourable for phytoplankton growth occur in spring and summer; spring is characterised by elevated primary production and biomass (typically with *Fragilariopsis kerguelensis* dominating surface assemblages), whereas summer primary production is relatively constant (with a more diverse diatom assemblage) (Crosta et al., 2005). Shade-adapted, large-celled, bloom-forming diatoms are dominant in the open ocean (Tréguer and Jacques, 1992) (e.g. *Thalassiosira lentiginosa*). In the oceanic region, including the Bransfield Strait shelf-break (WAP), deep chlorophyll *a* layers have been identified (Holm-Hansen et al., 1994; Kang and Lee, 1995; Prézelin et al., 2000; Garibotti et al., 2003), suggesting more vertically distributed phytoplankton compared to coastal areas (Garibotti et al., 2003), which display higher concentrations in the upper water column (Mitchell and Holm-Hansen, 1991; Smith et al., 1996b; Dierssen et al., 2002).

The seasonally open ocean zone (situated in coastal and continental shelf areas) is very different to the permanently open ocean zone, being strongly influenced by the annual contraction and expansion of sea ice. During spring and summer, retreat of sea ice

enables expansion of open ocean habitats along the WAP, and a patchier distribution along the EAP. The inter-relationship between Antarctic sea ice and the open ocean zone produces a gradation of habitats (and associated diatom communities) away from the continent: from cool open ocean conditions proximal to the sea ice margin, with diatom species displaying tolerance to sea ice (e.g. *Thalassiosira gracilis* and *Rhizosolenia* "pointed" group); through pelagic open ocean conditions typically found at the Antarctic Polar Front (e.g. *Fragilariopsis kerguelensis* and *Thalassiosira lentiginosa*); to warm open ocean conditions towards the Polar Front Zone (e.g. *Rhizosolenia* "rounded" group and *Thalassiothrix nitzschioides* group) (Crosta et al., 2005).

3.4.2 Sea ice

Sea ice plays a key role in biological processes, providing a habitat for organisms both within and attached to the under-surface of the ice, and through the hydrographic impacts imparted on the marginal sea ice zone (as discussed in section 3.3). The most conspicuous organisms in the ice are pennate diatoms, which reach such concentrations that their photosynthetic pigments discolour the ice brown (Thomas and Dieckmann, 2002). Even in areas of thick multi-year ice (e.g. western Weddell Sea), ice communities can still be found inside (Ackley et al., 1979; Hesgeth and von Quillfeldt, 2002).

During the initial stages of sea ice formation, diatom populations left over in surface waters from the preceding spring – summer blooms become trapped within newly forming frazil ice crystals and rise to the surface, where they accumulate in thick layers (Garrison et al., 1989; Arrigo, 2003). In regions where ice is most tightly coupled to the underlying or adjacent sea water, a special and protected habitat develops and facilitates intense diatom blooms (Eicken, 1992; Arrigo, 2003; Zemmelink et al., 2008). However, most sea ice habitats (strand layers, bottom ice, internal layers, near-surface and surface) are characterised by profound changes in abiotic conditions, including confinement to a small, yet dynamic pore system, salinity and light fluctuations, and a decrease in temperature (Gleitz and Thomas, 1992). Despite these environmental changes some diatoms remain metabolically active and growth may contribute significantly to the high algal standing stocks frequently observed in young sea ice (Gleitz and Thomas, 1992; 1993).

During sea ice melting, solutes and particles within sea ice, including nutrients and diatoms, are released to the upper water column, as a seeded population. Another

mechanism to remove diatoms from the sea ice is through grazing of the underside of the ice by krill; diatoms are exported into the water column due to rapid sinking of the faecal strings (Michels et al., 2008). Whether or not these diatoms function as a seed population depends on many factors, including the speed at which the particles settle through the water column, the presence of pelagic consumers and the viability of the cells once released from the sea ice (Leventer, 2003 and references therein).

3.4.3 Benthic environments

Diatoms occupy a range of benthic habitats, living either freely on or in the sediments or attached to the substratum, e.g., rocks (epilithic), sand grains, and plants (epiphytic) (Jones, 2007a), or attached to glacial and sea ice. Attached communities can be adnate (i.e. closely attached to the substrate, e.g. *Cocconeis*) or attached by mucilaginous stalks or pads (e.g. *Gomphonema*) (Jones, 2007a). Many factors interact to determine the distribution of benthic diatoms, the most important being substrate and the water depth (< 100 m), perhaps associated with irradiance penetration (Crosta and Koç, 2007). Benthic communities are likely to experience a strongly seasonal light regime, with low average irradiance; during periods of heavy ice cover little or no light reaches the communities and in summer light penetration is often reduced by particulate matter from glacial meltwater discharge (Longhi et al., 2003). Typically epiphytic and epilithic diatoms have been found to be predominant in the water column assemblages during spring and summer in inshore water near Davis Station, East Antarctica (Everitt and Thomas, 1986); Ellis Fjord, Vestfold Hills, East Antarctica (McMinn and Hodgson, 1993); Maxwell Bay, King George Island (AP) (Ahn et al., 1997); and Potter Cove, King George Island (AP) (Al-Handel et al., 2008), following ice break-out events and dispersal of the bottom sea ice strand community. Benthic diatoms are often very diverse and were grouped to genera level in this investigation, including *Achnanthes*, *Amphora*, *Cocconeis*, *Licmophora*, *Pinnularia*, *Pseudogomphonema*, *Melosira* and *Navicula*.

3.5 Diatom species ecology

Some diatom species thrive in very narrow ranges of environmental conditions, with some being endemic to single regions (e.g. *Fragilariopsis kerguelensis* and *Fragilariopsis curta* restricted to the Southern Ocean) (Crosta and Koç, 2007). For palaeoceanographic reconstruction purposes, species thriving in a limited range of conditions are obviously much more useful than widely distributed ones. There has been significant recent progress in assessing modern species distribution patterns

(biogeography); the most notable examples being the extensive coverage and detailed datasets presented in a set of linked research papers by Armand et al. (2005), Crosta et al. (2005) and Romero et al. (2005), focusing on the Antarctic sea ice zone, Antarctic open ocean zone and Tropical / Subtropical ocean, respectively. It is crucial to understand Antarctic diatom ecology for accurate Holocene reconstructions from fossil assemblages. This section describes the characteristics of diatom species that are identified as indicator species in this study (see Chapter 5.1.6). Photographs of the species can be found on the Appendix CD.

3.5.1 *Actinocyclus actinochilus* (Ehrenberg) Simonsen

Actinocyclus actinochilus is an endemic Antarctic species, associated with long periods of sea ice cover and cold water (Pichon et al., 1987; Zielinski and Gersonde, 1997; Armand et al., 2005). Geographically, the species distribution declines sharply from coastal regions to the maximum winter sea ice edge, and is ultimately limited to the north by the Polar Front (Armand et al., 2005). Maximum relative sedimentary abundances are associated with February SST between 0 and 1 °C and where sea ice duration is greater than 7 months/year, with an optimum of 8 – 9 months/year (Armand et al., 2005). Further, increasing sedimentary abundances falls in line with an ice-free region during summer (<40 % concentration) and a strongly compact sea ice covered region during winter (70 – 90 % concentration) (Armand et al., 2005). *A. actinochilus* has been observed in both open and ice-covered water in winter (Moisan and Fryxell, 1993), in newly formed spring sea ice (Gersonde, 1984) and in both fast and pack ice (Horner, 1985; Krebs et al., 1987; Garrison, 1991). The species has been noted to have higher presence in sea ice than in the adjacent water column (Garrison et al., 1983: 1987).

3.5.2 Genus *Chaetoceros* Ehrenberg

Chaetoceros is one of the most abundant, widespread and cosmopolitan diatom genera in the modern ocean, being present in most environments from coastal temperate to polar regions. The genus is composed of ~180 marine planktonic species, with around 75 of these forming resting spores as a survival phase (Stockwell and Hargraves, 1984) (section 3.2). In the Southern Ocean, *Chaetoceros* spp. are observed in temperature ranges between -2 to 12 °C (Zielinski and Gersonde, 1997). The two factors of primary importance to *Chaetoceros* spp. distribution are the influence of high productivity waters (Leventer, 1991; Zielinski and Gersonde, 1997) and surface water stratification produced by sea ice melt (Leventer et al., 1993: 1996). The genus is divided into two

sub-genera: *Hyalochaete* and *Phaeoceros*, which are distinguished by the ability to form resting spores or not, respectively (Priddle and Fryxell, 1985).

3.5.2.1 Sub-genus *Hyalochaete Chaetoceros* Gran

The distribution of *Hyalochaete Chaetoceros* spp. is circum-polar, with greatest abundance occurring in the AP region and the Ross Sea (Armand et al., 2005). They display a preference for the near coastal environment (Zielinski and Gersonde, 1997), in close proximity to sea ice (Leventer, 1991; Crosta et al., 1997), and even reported in winter sea ice (Ligowski et al., 1992). In coastal areas, they can achieve very high biomass (Armand et al., 2005) due to their ability to bloom rapidly when conditions are favourable. *Hyalochaete Chaetoceros* spp. have two forms: vegetative cells and robust resting spores (section 3.5.2.2). Modern sediment trap data from the AP suggests that *Hyalochaete Chaetoceros* spp. blooms are associated with melting of sea ice (reduced surface salinity, stratification and high nutrients) in austral spring (Leventer, 1991).

3.5.2.2 *Chaetoceros* resting spores (CRS)

Hyalochaete Chaetoceros spp. resting spores (CRS) are more heavily silicified than their vegetative counterparts and can remain viable for up to 2 years, which allows population re-seeding (Hargraves and French, 1983). The robust nature of the frustule and their associated high sinking rates makes CRS an extremely common component of sedimentary assemblages (<95 %; Crosta et al., 1997). The distribution of CRS is circumpolar, with little regard for zonal boundaries; greatest abundance occurs in the AP region and the Embayment systems (e.g. Ross and Weddell Seas) (Crosta et al., 1997). Such occurrences are associated with February SST between -1.3 and 3.5 °C, and where sea ice distribution is greater than 3 months/year, with 7 months/year at maximum abundance (Armand et al., 2005). Since CRS are formed within the vegetative cells when diatom blooms exhaust surface nutrients or when vegetative cells sink out of the photic zone (Hargraves and French, 1983), relative abundance of CRS has commonly been used to track high productivity events at the receding sea ice edge and periods of intense water column stratification (Leventer et al., 1993; 1996; Rathburn et al., 1997; Denis et al., 2006; Crosta et al., 2007; 2008).

3.5.3 Genus *Cocconeis* Ehrenberg

Cocconeis is a common benthic genus, living in water depths >9 m (Whitehead and McMinn, 1997). It is reported to be related to fast-ice, consisting of ~90 % congelation ice (Scott et al., 1994). From observations from Arthur Harbour (Anvers Island)

Cocconeis spp. were found to commonly form spring / summer blooms and benthic diatom mats in the sub-tidal zone (Krebs, 1983). In late spring as wind strength increases and sea ice breaks up, these mats disintegrate (Krebs, 1983). Sediment trap data from the northern AP recorded *Cocconeis* spp. as part of an autumn assemblage, interpreted to be coastal and ice related flora re-suspended by autumn storms (Leventer, 1991).

3.5.4 *Eucampia antarctica* (Castracane) Mangin

Early observations of *Eucampia antarctica* suggested a relationship with sea ice (Burckle, 1984b; Burckle et al., 1990), with much higher abundances noted in the adjacent water column than in the sea ice itself (Garrison et al., 1983; 1987). Generally, *E. antarctica* is associated with neritic (near-shore) environments, where floating sea ice is present and / or significant melting leads to a meltwater stratified water column (Cremer et al., 2003). However, in modern sediments higher occurrences of this species are typically found in the Antarctic Zone and Polar Front Zone (Zielinski and Gersonde, 1997), leading to questions regarding the proposed link with sea ice. A further suggestion is that *E. antarctica* exploits local lenses of cold, low-salinity water associated with iceberg melt, which occur in discharge alleys from the Weddell Sea and East Antarctic margin (Burckle, 1984). However, there are no direct observations of *E. antarctica* dominating the diatom assemblage in surface waters next to icebergs.

Two morphological varieties of *E. antarctica* exist, based on asymmetry and symmetry in girdle view (*E. antarctica* var. *antarctica* and *E. antarctica* var. *recta*, respectively) (Fryxell and Prasad, 1990). These two varieties have different distribution patterns; in Prydz Bay, *E. antarctica* var. *antarctica* was abundant far from sea ice edge, in open ocean assemblages during spring, whereas *E. antarctica* var. *recta* was abundant near sea ice during autumn (Fryxell, 1989). Consequently, *E. antarctica* var. *antarctica* is proposed to be a sub-polar form, associated with open water; *E. antarctica* var. *recta* is a polar form, associated with sea ice (Fryxell and Prasad, 1990; Kaczmarska et al., 1993). Both forms produce resting spores, which are more heavily silicified and robust, therefore being preferentially preserved in marine sediments.

The different morphologies of *E. antarctica* have been used as an indicator of oceanographic and sea ice conditions on the basis of morphology and chain length (Eucampia Index) (Kaczmarska et al., 1993; Leventer et al., 2002). The Eucampia Index compares the proportion of 'pointy' terminal valves (from the chain ends) to the flat intercalary valves (from the middle of the chain) (Kaczmarska et al., 1993). In theory,

warmer waters with less sea ice will be characterised by more intercalary valves (lower Eucampia Index) due to higher cell division (Kaczmarska et al., 1993). Although the Eucampia Index held much promise, it has not been employed in many sea ice estimation studies, simply due to the fact that the ratio has not been ground-truthed with respect to the distribution of *Eucampia* varieties in the surface sediments around Antarctica (Armand, 2000; Gersonde and Zielinski, 2000; Armand and Leventer, 2003). A recent study of Patterson et al. (2008) tried to improve understanding of the modern environmental constraints on the distribution of the different morphological forms of *E. antarctica*, using phytoplankton samples collected along five transits between South America and the AP. The data showed that under modern conditions, an overwhelming proportion of the cells were the polar variety, with sub-polar forms constituting an extremely minor component of phytoplankton samples and presumably located farther to the north (Patterson et al., 2008). A further finding of this study was that many living chains exhibited no terminal valves; consequently, the use of the Eucampia Index as a proxy for sea ice probably underestimates sea ice extent and should be used with caution (Patterson et al., 2008).

3.5.5 *Fragilariopsis curta* (Van Heurck) Hustedt

Fragilariopsis curta is an endemic, robust planktonic species in the Southern Ocean, occupying near-shore and open ocean environments. *F. curta* are common components of Antarctic pack ice (Garrison, 1991; Leventer, 1998; Hesgeth and Von Quillfeldt, 2002) and blooms subsequently develop in spring at the retreating sea ice edge, in relatively stable and nutrient-rich water column (Leventer and Dunbar, 1987; Fryxell, 1989; Kang and Fryxell, 1992; 1993; Cunningham and Leventer, 1998; Leventer, 1998; Hesgeth and Von Quillfeldt, 2002; Armand et al., 2005). These surface water observations in spring have been supported by sedimentary data; within laminated couplets, both *F. curta* and *F. cylindrus* appear first in early spring when sea ice is still present (Maddison et al., 2005; 2006; Denis et al., 2006). Surface water samples, sediment trap data and core-top assemblages have shown that *F. curta* is restricted to areas south of the Polar Front Zone, with relative abundances increasing southwards with increasing sea ice cover and decreasing temperature (Burckle et al., 1987; Gersonde and Zielinski, 2000; Armand et al., 2005). Highest sedimentary abundance occurs near the Antarctic coast (Truesdale and Kellogg, 1979; DeFelice and Wise, 1981; Gersonde and Wefer, 1987; Leventer, 1992; Taylor et al., 1997; Zielinski and Gersonde, 1997; Armand et al., 2005), with highest abundances in core-top sediment samples near

Prydz Bay, in the Ross Sea region and George V Coast (Armand et al., 2005). Excursions elsewhere are potentially linked to iceberg pathways (Armand et al., 2005). *F. curta* display a summer temperature preference of -1.3 to 2.5 °C, with maximum abundance falling within the temperature range of 0.5 and 1 °C and in locations that experience 9 – 11 months/year sea ice cover (Armand et al., 2005). *F. curta* and *F. cylindrus* have been successfully used to reconstruct presence of sea ice during the late Pleistocene through qualitative (Gersonde and Zielinski, 2000) or transfer function (Crosta et al., 2004) approaches. It is believed that higher relative abundances of *F. curta* in sediments indicates reduced growing season due to denser sea ice cover and late waning (Crosta et al., 2007) and / or increased coastal water stratification, through increased sea ice melt (Cunningham et al., 1999).

3.5.6 *Fragilariopsis cylindrus* (Grunow) Krieger

F. cylindrus is a bipolar species, found to occupy both sea ice habitats (land-fast and pack ice; Garrison and Buck, 1989; Garrison, 1991; Scott et al., 1994; Hesgeth and Von Quillfeldt, 2002) and well-stratified, stable open water in front of the sea ice edge near the Antarctic coast, as a seeded population from the ice (Garrison et al., 1987; Stockwell et al., 1991; Kang and Fryxell, 1992; Leventer et al., 1993; Armand, 2000; Hesgeth and von Quillfeldt, 2002). Maximum abundance is associated with February SSTs between 0.5 and 1 °C and sea ice duration greater than 8.5 months/year; further increased abundance are associated with heavily consolidated sea ice conditions during the winter (>70 – 90 %) (Armand et al., 2005). These environmental preferences mean that *F. cylindrus* is geographically limited to the area between the coast and the maximum summer sea ice edge (Armand et al., 2005). *F. cylindrus* is reported to form resting spores (McQuoid and Hobson, 1996), which are more dissolution resistant and well preserved in sediments (Leventer, 1992; Zielinski and Gersonde, 1997). *F. curta* and *F. cylindrus* have been used extensively as tools for reconstructions of sea ice distribution in the Southern Ocean (e.g. Leventer, 1998; Crosta et al., 1998; Gersonde and Zielinski, 2000; Gersonde et al., 2005).

3.5.7 *Fragilariopsis kerguelensis* (O'Meara) Hustedt

Fragilariopsis kerguelensis is a planktonic species endemic to the Southern Ocean, with a heavily silicified frustule. It thrives in the open ocean and is rare when sea ice is present during the growing season (Burckle et al., 1987; Zielinski and Gersonde, 1997; Crosta et al., 2005). Maximum abundances (70 – 80 %) are found in the zone between maximum winter sea ice edge and the Polar Front (coinciding with the main flow of the

ACC), where surface water temperatures range between 1 and 10 °C (Zielinski and Gersonde, 1997; Crosta et al., 2005). Towards neritic, shallow water and near-shore environments, abundance of *F. kerguelensis* in surface water and sedimentary assemblages decreases (Truesdale and Kellogg, 1979; Gersonde, 1984; Leventer, 1992; Zielinski and Gersonde, 1997). This well-constrained distribution pattern makes *F. kerguelensis* one of the most valuable indicators of open water deposition (Krebs et al., 1987; Leventer, 1992; Zielinski and Gersonde, 1997), used in coastal sediments to indicate oceanic conditions (Crosta et al., 2004); as a proxy for summer sea surface temperatures (Crosta et al., 2007); and possibly for the length of the growing season (Denis et al., 2006). A recent study has also highlighted that morphology of *F. kerguelensis* varies in space and time, related to the proximity of the Antarctic Polar Front (Cortese and Gersonde, 2007).

3.5.8 *Fragilariopsis obliquecostata* (Van Heurck) Heiden

Fragilariopsis obliquecostata is a planktonic species that has been observed in land-fast and pack ice and linked to ice surface melt pools (Gersonde, 1984; Garrison and Buck, 1989; Garrison, 1991). This species also displays increased abundance in the water column under sea ice (Garrison et al., 1983; 1987; Gersonde, 1984; Garrison, 1991). From sediment surface samples, the geographical range of *F. obliquecostata* appears to be confined to on or just north of the maximum summer sea ice extent (Armand et al., 2005) and extending north to the Antarctic Divergence (Gersonde, 1984; Gersonde and Wefer, 1987; Kellogg and Kellogg, 1987; Zielinski and Gersonde, 1997). Highest abundances are linked to SSTs below 2 °C and areas that experience >7 months/year sea ice cover and where highly consolidated ice conditions exist during winter (65 – 90 %); it is believed that winter sea ice concentration may play a greater role in the distribution pattern of *F. obliquecostata* than summer sea ice concentration (Armand et al., 2005). Highest abundances in core-top sediments have been observed in the Weddell Sea (Zielinski and Gersonde, 1997), Ross Sea region (Cunningham and Leventer, 1998) and in Prydz Bay (Armand et al., 2005), with the AP and George V Coast displaying lower abundances (Armand et al., 2005). *F. obliquecostata* has been used to infer summer sea ice cover (Gersonde and Zielinski, 2000; Bianchi and Gersonde, 2004), although application of this proxy is based on the understanding that the thickly silicified *F. obliquecostata* is apparent in conditions with markedly low sedimentation rates (Gersonde and Zielinski, 2000). Recent ground-truthing of the summer sea ice extent

method indicates that the proxy is unique to the Weddell Sea and perhaps should only be applied to this region (Armand and Leventer, 2003; Armand et al., 2005).

3.5.9 *Fragilariopsis separanda* Hustedt

Fragilariopsis separanda have been observed in highest abundances slightly offshore rather than inshore coastal environments (DeFelice and Wise, 1981; Gersonde and Wefer, 1987; Stockwell et al., 1991; Leventer, 1992; Taylor et al., 1997; Cunningham and Leventer, 1998). *F. separanda* displays a wider distribution and temperature range than the morphologically similar *F. rhombica*, although Armand et al. (2005) question whether some reports have misidentified the two species. In the South Atlantic sector, *F. separanda* is found to be confined to the south by the Polar Front (DeFelice and Wise, 1981; Zielinski and Gersonde, 1997). Highest abundances in core-top sediments are associated with February SSTs of -0.5 to 0 °C, although the species does exhibit a wide temperature range (-1 to 8 °C) (Armand et al., 2005). Where maximum abundances are observed sea ice duration lasts 4.5 – 9 m onths/year, with summer concentrations generally being ice-free or less than 30 % and September sea ice is highly consolidated (Armand et al., 2005).

3.5.10 *Fragilariopsis sublinearis* (Van Heurck) Heiden

Fragilariopsis sublinearis is reported as having a similar distribution in the Antarctic Zone as *F. ritscheri* and *F. obliquecostata* (Hasle, 1976; Tanimura, 1992; Zielinski and Gersonde, 1997). The species displays increased abundance in sediments south of the Antarctic Divergence (Gersonde, 1984; Gersonde and Wefer, 1987; Kellogg and Kellogg, 1987; Taylor et al., 1997; Zielinski and Gersonde, 1997). Maximum relative sedimentary abundances are associated with February SST between -1.3 and 2.5 °C, with sea ice concentration greater than 7.5 months/year (Armand et al., 2005). Plotted geographically, these major abundances of *F. sublinearis* are located almost exclusively in Prydz Bay, the Ross Sea and along Wilkes Land, within the maximum February sea ice extent (Armand et al., 2005). Leventer (1992) also noted high abundance along the George V Coast, with equal maximum proportions of *F. sublinearis* and *F. ritscheri* observed.

3.5.11 *Fragilariopsis vanheurckii* (M. Pergallo) Hustedt

Fragilariopsis vanheurckii is proposed to have a similar ecological preference to *F. curta* and *F. cylindrus* (Armand et al., 2005), observed near the spring ice margin (Garrison et al., 1987; Hesgeth and von Quillfeldt, 2002), suggesting a relationship with sea ice, but the species is not thought to live in the sea ice (Taylor and Sjunneskog,

2002). Following collapse of the ice shelf in the Larsen B embayment in 2002, *F. vanheurckii* was observed in unusually high abundance in modern phytoplankton assemblages and in the underlying sediments (Leventer, 2006). This observation, together with the higher than normal abundance in deglacial sediments from the Palmer Deep (WAP), led Leventer (2006) to suggest that potentially *F. vanheurckii* may be useful for tracking glacial ice melt in surface waters of the Southern Ocean.

3.5.12 Genus *Navicula* Bory de st-Vincent

Navicula spp., including *N. glaciei*, *N. gelida* var. *antarctica* and *N. directa*, are typical cryophilic benthic diatoms living in near-coastal sea ice. *N. glaciei* has been observed to be dominant in shore ice protected from wave turbulence (Krebs et al., 1987; Whitaker and Richardson, 1980; Riaux-Gobin et al., 2000) and as a significant component of the spring bloom when shore ice is released into the water column through melting (Krebs, 1983). *N. glaciei* is also a common component of sea ice and phytoplankton communities in fjords of the Vestfold Hills (East Antarctica) (McMinn, 2000) and King George Island (AP) (Kang et al., 2002). In Holocene sections, *N. glaciei* (together with *Fragilaria striatula*) was interpreted to reflect both the presence of winter sea ice and surface waters with variable salinity, resulting from ice melt during spring and summer (Cremer et al., 2003). Greatest abundances of *N. directa* (<1.7 %) have been found along the AP (Armand, 1997).

3.5.13 *Odontella weissflogii* (Janisch) Grunow

Odontella weissflogii is considered endemic to the Southern Ocean and occurs in Antarctic near-shore regions (Zielinski and Gersonde, 1997). It is characterised as a pack ice species (Garrison and Buck, 1989; Garrison, 1991), yet also observed in increased abundance in the adjacent water column (Garrison et al., 1983; Gersonde, 1984). The species is related to a February SST range between -2 and 5 °C (Zielinski and Gersonde, 1997), with highest abundances noted in cool waters of 1 °C (February SST) and -2.5 °C (August SST) (Armand, 1997). *O. weissflogii* is found with a near year round ice cover (10 – 11 months/year), with September maximum concentrations of 30 % and no ice cover in summer (Armand, 1997).

3.5.14 Genus *Porosira* Jørgensen

Two Antarctic planktonic species of *Porosira* are *P. glacialis* (Grunow) Jørgensen and *P. pseudodenticulata* (Hustedt) Jousé. The slightly different distribution observed between *Porosira glacialis* (open water) and *Porosira pseudodenticulata* (sea ice) can potentially act as an indicator for the proximity of the sea ice margin.

P. glacialis is bipolar species associated with coastal waters or sea ice (Hasle, 1973). There are also suggestions for a link with slush and wave exposed shore ice, but the species does not live within ice (Krebs, 1983; Scott et al., 1994). Core-top sediment data highlights that the species distribution is sharply confined to a small range of -1.3 to 2 °C, with maximum abundance occurring at an SST of 0 to 0.5 °C (Armand et al., 2005). Further, *P. glacialis* is found in sediments that have at least 7.5 months/year sea ice cover, with marginal to ice free conditions in summer (30 %) and relatively highly compacted sea ice cover in winter (65 – 80 %); abundances decrease notably when sea ice concentration is >85 % (Armand et al., 2005).

P. pseudodenticulata is observed in both pack and fast ice samples (Gersonde, 1984, Krebs, 1987) and in the adjacent water column (Garrison et al., 1987). Maximum abundance of *P. pseudodenticulata* is associated with February SST between -1.3 and 2 °C; and sea ice cover between 7.5 – 11 months/year, with <30 % sea ice concentration in summer and >70 % concentration in winter (Armand et al., 2005).

3.5.15 *Genus Proboscia* Sunström

Proboscia spp. are relatively abundant in Antarctic and sub-polar waters, with *P. truncata* (Karsten) Nöthig & Ligowski being endemic (Jordan et al., 1991). *P. inermis* (Castracane) Jordan & Ligowski forms a key component of the autumn assemblage from the Bellingshausen Sea, accounting for 21 % of phytoplankton carbon (Brichta and Nöthig, 2003). Both these *Proboscia* species possess elongate frustules, displaying positive buoyancy (Villareal, 1988) and an ability to form mats (Carpenter et al., 1977; Alldredge and Silver, 1982).

3.5.16 Genus *Rhizosolenia* Brightwell

Rhizosolenia are common components of Antarctic phytoplankton and are important contributors to sea floor sediments (Armand and Zielinski, 2001). *Rhizosolenia* spp. can form large blooms or mats in open water (Alldredge and Silver, 1982; Kemp et al., 1999) and have been reported in high abundances from Antarctica waters (Holm-Hansen et al., 1989; Leventer et al., 1996). *Rhizosolenia* spp. are generally absent from sea ice samples (Watanabe, 1982), therefore in the Atlantic sector this genus has been interpreted as an indicator of ice-free Weddell Sea outflow waters (Jordan and Pudsey, 1992).

R. antennata var. *semispina* Sundström is the most common *Rhizosolenia* species in the Southern Ocean (Armand, 1997), primarily linked to the open ocean water column and

not observed in sea ice conditions (Ligowski, 1993). *R. antennata* var. *semispina* is found to be dominant species in the open ocean waters of late summer (Froneman et al., 1995), as part of the shade flora (Crosta et al., 2005). Its distribution ranges from the Subantarctic to the Antarctic Zone, in temperatures between -1 and 12 °C, with highest abundances occurring in waters close to freezing point (-1 to 2 °C), in the northern Antarctic Zone (Zielinski and Gersonde, 1997). The related species, *R. antennata* var. *antennata*, is considered the resting spore of *R. antennata* var. *semispina* (Priddle et al., 1990; Hasle and Syvertsen, 1997; Crosta et al., 2005). *R. polydactyla* var. *polydactyla* has been found dwelling in several very different environments; in Antarctic and Subantarctic waters, with a maximum occurrence in the Polar Frontal Zone (Fenner et al., 1976); and in near coastal environments, being found in melted ice (Hasle, 1969). This wide distribution indicates that *R. polydactyla* var. *polydactyla* is eurythermal or that it has been confused with other taxa (Crosta et al., 2005).

3.5.17 *Thalassiosira antarctica* Comber

T. antarctica is widespread in Antarctica waters, occurring commonly in waters with SST between -2 to 1 °C (Zielinski and Gersonde, 1997). Previous studies have documented *T. antarctica* in coastal zones of loose platelet-ice crystals floating beneath coastal pack and fast ice, in polynyas and crack pools formed by disintegrating sea ice during summer (Horner, 1985; Smetacek et al., 1992; Gleitz et al., 1996). In Ross Sea surface sediments *T. antarctica* occurs in highest abundances close to the ice shelf front and is associated with the formation of platelet ice from super-cooled water masses that emerge from beneath the ice shelf (Cunningham and Leventer, 1998). It is rare to find *T. antarctica* in sea ice (Leventer and Dunbar, 1987; Fryxell and Kendrick, 1988; Zielinski and Gersonde, 1997), which is attributed to its inability to survive the low light intensities beneath and within sea ice (Fryxell et al., 1987; Fryxell and Kendrick, 1988). However, this species has been observed in some spring sea ice samples (Villareal and Fryxell, 1983), suggesting they over-wintered in the sea ice or were re-suspended from the sediments. *T. antarctica* also occurs in the Bransfield Strait (Gersonde and Wefer, 1987; Leventer, 1991), where its unusually high abundance is thought to be the result of surface water intrusion from the Weddell Sea (Gersonde and Wefer, 1987; Abelmann and Gersonde, 1991; Zielinski and Gersonde, 1997).

T. antarctica is believed to be a near-coastal species, for which production is related to open ocean conditions during autumn when sea ice re-advances and limits other species competitiveness (Cunningham and Leventer, 1998; Cunningham et al., 1999; Armand et

al., 2005). This suggestion of a relationship between *T. antarctica* and falling temperatures (freezing ice) and falling light levels is supported by observations in seasonally laminated coastal sediments, in which *T. antarctica* resting spores commonly dominate the last recorded bloom of the season (Maddison et al., 2005; Stickley et al., 2005). Relative abundances of *T. antarctica* have therefore been used to track productivity events at the advancing sea ice edge or in open ocean zones of sea ice (Taylor et al., 2001; Denis et al., 2006) and more specifically, as a proxy for sea ice presence and concentration during autumn (Crosta et al., 2008).

Two different morphology types of *T. antarctica* have been distinguished, termed T1 (or cold) and T2 (or warm) (Taylor et al., 2001; Domack et al., 2003; Buffen et al., 2007). The two types are distinguished by three features: valve diameter; relative coarseness of the areolae; and the presence or absence of marginal "shoe-like" processes (Villareal and Fryxell, 1983). *T. antarctica* T1 valves are generally smaller in diameter (usually <20 μm), have a greater number of areolae/10 μm (~10 – 12) and do not have these marginal processes. In contrast, *T. antarctica* T2 valves are generally larger (usually >20 μm), have fewer areolae/10 μm (~8 – 9) and have distinct marginal processes. This distinction was first noted by Villareal and Fryxell (1983) who cultured the species at two temperatures, -1.5 and 4.0 °C, and noted that smaller size, finer areolation and lack of marginal projections characterised specimens from the lower temperature culture. Both forms produce resting spores, which are more frequently preserved in the sedimentary assemblage than their vegetative counterparts.

3.5.18 *Thalassiosira gracilis* (Karsten) Hustedt

Thalassiosira gracilis is geographically widely distributed, with highest abundances noted along the Antarctic coast (Truesdale and Kellogg, 1979; Gersonde, 1984; Gersonde and Wefer, 1987; Kellogg and Kellogg, 1987; Leventer, 1992; Taylor et al., 1997; Zielinski and Gersonde, 1997; Cunningham and Leventer, 1998; Crosta et al., 2005). From core-top samples, abundances have been observed to increase towards the region of maximum winter sea ice extent and the Antarctic coast, with highest abundances found in February SSTs of 1 to 2 °C and increasing sea ice duration (to a maximum of 8.5 months/year) (Crosta et al., 2005). *T. gracilis* has been reported in sea ice samples (Gersonde, 1984; Krebs et al., 1987). Two morphologically different varieties exist: *T. gracilis* var. *expecta* (Van Landingham) Fryxell & Hasle and *T. gracilis* var. *gracilis* (Karsten) Hustedt. *T. gracilis* var. *expecta* is typically smaller in size, having smaller and more numerous areolae in the valve centre (14 – 15 in 10 μm),

compared to the heavily silicified *T. gracilis* var. *gracilis*, with larger and less numerous areolae in the valve centre (8 – 12 in 10 μm). However, the differing morphologies are gradational, making rigorous identification difficult. *T. gracilis* var. *gracilis* is considered the winter form of the species (Fryxell, 1990), observed in decreasing abundance in sediments away from the coast; whereas low coastal abundances of *T. gracilis* var. *expecta* suggest this variety is related to open primary productivity, rather than sea ice cover (Stockwell et al., 1991; Leventer, 1992; Cunningham and Leventer, 1998).

3.5.19 *Thalassiosira lentiginosa* (Janisch) Fryxell

Thalassiosira lentiginosa is a widely distributed planktonic species, believed to be truly pelagic (oceanic-inhabiting) (Crosta et al., 2005). Maximum surface sediment abundances are encountered in the permanently open ocean zone and Polar Front Zone (Fenner et al., 1976; DeFelice and Wise, 1981; Zielinski and Gersonde, 1997; Crosta et al., 2005). In general, lowest abundances are observed on the Antarctic continental shelf, most notably in the Ross Sea and AP region (Gersonde and Wefer, 1987; Kellogg and Kellogg, 1987; Taylor et al., 1997; Zielinski and Gersonde, 1997; Cunningham and Leventer, 1998; Crosta et al., 2005). *T. lentiginosa* prefers a temperature range of 0 to 8 °C (Zielinski and Gersonde, 1997; Crosta et al., 2005) and very low abundances occur below 1 °C (Crosta et al., 2005). Relative abundance of *T. lentiginosa* shows an inverse relationship with sea ice cover, with high occurrence between 0 to 4 months of sea ice per year and a decline towards prolonged sea ice duration (Crosta et al., 2005). *T. lentiginosa* is particularly resistance to dissolution (Shemesh et al., 1989; Pichon et al., 1992) increasing the species presence in sediments and potentially obscuring the true primary signal of distribution (Crosta et al., 2005).

3.6 Diatoms as proxies

Diatoms are excellent proxies for oceanographic and climate reconstructions because they commonly reflect the environment in which they live, responding to limiting factors and tracking changes in surface water mass character and sea ice extent (Figure 3.3). Fossil diatom assemblages have been used to reconstruct past fluctuations in sea surface temperature (SST), sea ice patterns, and latitudinal shifts in oceanic fronts. Factors affecting the sedimentary record, assumptions concerning the use of diatoms as proxies and some commonly used diatom-based parameters used in this investigation are described below.

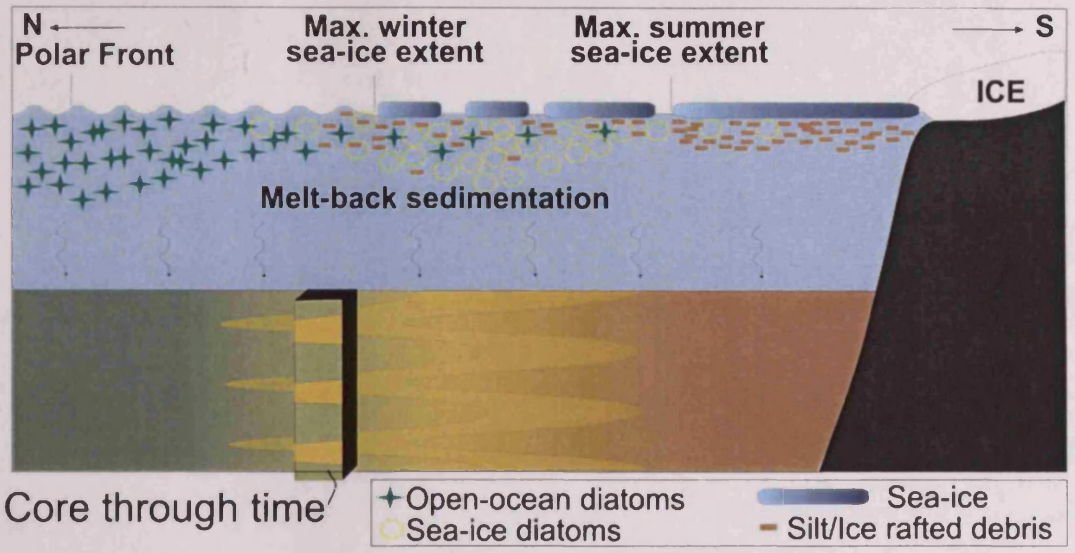


Figure 3.3
Relationships between sea ice and open ocean diatoms in surface waters, sediments and sea ice cover. The sedimentary signal provides basic reconstruction of Antarctic sea ice cover, based on the assumption that the greater the proportion of open ocean diatoms to sea ice diatoms, the longer the duration of open water conditions between winter and summer sea ice cover. By studying these open ocean and sea ice diatoms in sedimentary cores, past natural variability of sea ice cover can be estimated. (Source: Armand, 2000).

3.6.1 Diatom preservation in the sedimentary record

A key question about the use of diatoms as proxies is whether diatoms preserved in the sediment actually reflect the communities from which they are derived. In general, only 1 – 5 % of the diatom frustules produced in the surface water euphotic zone are preserved in the sedimentary record (Gersonde, 1990). The majority of phytoplankton in the upper ocean are recycled through microbial transformations (Thomas and Papadimitriou, 2003) and many processes such as lateral advection, mechanical break-down, zooplankton grazing, aggregation and differential dissolution (sections 3.6.1.1 to 3.6.1.3), also complicate the relationship between the living assemblage and that found in the underlying sediments. Consequently, sedimentary assemblages therefore represent average surface conditions (Crosta and Koç, 2007).

Despite these preservation issues, the pattern of diatom production in surface waters is often well conserved in modern sediments (Krebs, 1983; Bodungen et al., 1986; Gersonde and Wefer, 1987; Leventer and Dunbar, 1987; 1996; Crosta et al., 2005). The distribution of diatoms in Southern Ocean surface sediments show clear patterns that can be related to surface water properties and subsequently used to reconstruct changes in the past (Leventer and Dunbar, 1988; Leventer, 1992; Taylor et al., 1997; Zielinski

and Gersonde, 1997; Armand et al., 2005; Crosta et al., 2005; Romero et al., 2005). These studies provide an important validation of the use of diatoms as proxies.

3.6.1.1 Advection

Redistribution and transportation of diatoms occurs through hydrodynamic factors operating in the water column and at the sediment-water interface. Slow diatom sinking rates (1 – 10 m day^{-1} for single cells; Priddle, 1990) makes them susceptible to lateral advection and transport out of the area of production (Burckle and Stanton, 1975; Leventer and Dunbar, 1987; 1988). In areas where advection is a dominant process, small and lightly silicified diatoms are preferentially winnowed (Truesdale and Kellogg, 1979; Crosta et al., 1997).

3.6.1.2 Aggregation

Diatoms are more effectively exported from surface waters to the sea floor (increased sinking rates) when incorporated into pelagic grazer faecal pellets, millimetre-sized aggregates (marine snow) and by setae entanglement during super-blooms (Alldredge and Gotschalk, 1989; Jaeger et al., 1996). Many sediment trap studies have revealed that zooplankton faecal pellets are important components of rapid particulate flux to the seafloor (Turner, 2002). This is particularly important in the AP region, where high standing stocks of grazing zooplankton are responsible for the production of large numbers of faecal pellets comprised of organic material and fragmented diatom valves (Dunbar, 1984; Gersonde and Wefer, 1987). Marine snow refers to organic aggregates >500 μm in size (Alldredge and Silver, 1988) and such aggregates have been observed to be abundant and ubiquitous in the ocean (Turner, 2002). These large aggregations can occur under conditions of high phytoplankton biomass and low wind speeds (Riebesell, 1992); at water column density discontinuities (MacIntyre et al., 1995); or are related to diatom morphology (e.g. *Rhizosolenia* and *Corethron*) (Kemp et al., 1999; Pike and Kemp, 1999); and / or presence of sticky microbially-produced exopolmers (Palmisano and Sullivan, 1985; Thomas and Papadimitriou, 2003). Riebesell et al. (1991) observed that algae released from sea ice tended to form aggregates at a much higher rate than other algae.

3.6.1.3 Dissolution

The negative impacts of dissolution on the preserved sedimentary assemblage have long been suggested (Shemesh et al., 1989 and references therein), and potentially can account for the temporal and spatial variations in sedimentary diatom assemblages

observed in Southern Ocean Sediments (Shemesh et al., 1989). Sediment trap experiments indicate that dissolution of biogenic silica occurs predominately in the upper 50 m of the water column (Dunbar et al., 1989), and that higher temperatures promote faster dissolution rates of Antarctic diatom frustules (Tréguer et al., 1989). Typically diatoms from the open ocean zone are more robust and subject to less dissolution, compared to the lightly silicified forms from the Subantarctic and sea ice zone (Pichon et al., 1992a). Further, the high sinking rate of resting spores (particularly CRS), due to their heavily silicified frustule and formation of aggregates, leads to a short residence time in the water column and associated much lower dissolution rates; in contrast, more lightly silicified diatoms will sink more slowly and be more susceptible to dissolution (Crosta et al., 1997). This leads to an increase in the relative proportion of the more resistant tests (Gersonde and Wefer, 1987; Leventer and Dunbar, 1987; Shemesh et al., 1989). Indicators of good preservation include little frustule breakage, abundant whole valves, high diversity and the presence (although never in high abundance) of delicate weakly silicified forms; indicators of poor preservation include abundance of valves fragments, few whole valves, absence of delicate forms and apparent dissolution around broken valve margins (Burckle and Cirilli, 1987). Dissolution effects are therefore relatively easy to identify in sedimentary diatom studies.

3.6.2 Diatom assumptions for this study

This investigation of Holocene palaeoclimate in the AP region relies on three basic assumptions:

1) Diatom abundance in the sediment reflects changes in surface water properties, hence climate;

2) The relative abundance of CRS, together with the proportions of different diatom species, reflects different palaeoceanographic and palaeoclimatic regimes;

3) An refined climate signal can be obtained from the diatom assemblage by excluding CRS (CRS-free assemblage), since CRS are likely to reflect only a short period of the growth season and their dominance acts to obscure the signal of other ecologically interesting species.

The parameters used in this investigation are: total diatom abundance; CRS absolute and relative abundance; non-CRS abundance; and non-CRS species assemblage (i.e. individual species abundance).

3.6.3 Total diatom abundance and CRS abundance

Total diatom abundance in marine sediments is commonly used as a palaeoproductivity proxy and has been successfully used in Antarctic marine sediments (Gersonde, 1990; Leventer and Dunbar, 1996; Leventer et al., 1996; Zielinski and Gersonde, 1997; Crosta et al., 1997; Armand, 2000; Sjunneskog and Taylor, 2002; Heroy et al., 2008). In AP coastal sediments, the dominant component of diatom assemblages are CRS (Leventer et al., 1991; Crosta et al., 1997; Taylor and Sjunneskog, 2002). As a result, CRS exert a strong control on diatom absolute abundance so, similar to diatom absolute abundance, high concentrations of CRS in Antarctic sediments are considered to be indicative of high productivity (Leventer et al., 1996; 2002; Bàrcena et al., 1998; 2002; 2006; Taylor et al., 2001).

3.6.4 Non-CRS absolute abundance and species assemblage

Due to the dominance of CRS, non-CRS absolute abundance (from the CRS-free counts) is also used in this investigation. Through this measure, the aim is to assess whether total diatom abundance (mainly driven by CRS absolute abundance) is an accurate measure of productivity for the whole diatom assemblage. Since CRS generally form under bloom conditions at times when the water column is stratified, non-CRS absolute abundance will provide information about productivity under non-bloom conditions.

The purpose of assessing the non-CRS species assemblage (i.e. community composition) is to propose environmental conditions based on the known ecological preference of individual species. Using both previously published occurrences and interpretations of different species (as presented in section 3.5) and statistical analysis of the diatom data (Chapter 6.1.5), environmental information can be inferred.

3.7 Chapter summary

This chapter has introduced the use of diatoms as proxies in Southern Ocean palaeoceanographic and palaeoclimatic reconstructions. Species ecological information presented in section 3.5 will underpin the diatom-based interpretations in Chapter 8. The diatom measures used in this investigation to assess the overall diatom assemblage and species composition have been presented.

4 Additional proxies

This chapter introduces the use of carbon and nitrogen stable isotopes of bulk organic matter; and sedimentary pigments as proxies. Stable isotope analyses were performed on cores VC306 and VC243; a sedimentary pigment study was undertaken on core VC243.

4.1 Stable isotopes

Carbon and nitrogen isotope compositions of organic matter ($\delta^{13}C_{org}$ and $\delta^{15}N_{org}$ respectively) have been widely used to trace biogeochemical cycling in marine sediments (Altabet, 2005). The principles of the use of these proxies are described in sections 4.1.2 and 4.1.3, and potential sources of alteration to the isotopic signal are discussed in section 4.1.4.

4.1.1 Rationale behind stable isotopes

Diatoms preferentially assimilate light isotopes (^{12}C, ^{14}N) to build organic matter, thus leaving the nutrient pool in surface waters enriched in heavy isotopes (^{13}C, ^{15}N). As the initial pools are consumed during biomass production, their nutrient light to heavy isotope ratio progressively increases. This progressive increase is transferred to the biogenic material, thus leading to a parallel isotope enrichment of the organic matter (Figure 4.1). Stable isotope ratios of the particulate organic matter and of the buried organic matter therefore reflect the proportion of nutrients assimilated during phytoplankton development and can act as a measure of the balance between supply to the surface waters and biological uptake; therefore, they do not represent an absolute value of the assimilation but rather a relative uptake of the nutrient pool (Crosta and Koç, 2007).

4.1.2 Carbon isotopes

Carbon occurs in nature as a mixture of two stable isotopes, carbon-12 (^{12}C) and the much rarer carbon-13 (^{13}C). The primary fractionation process in the carbon cycle is photosynthesis, thereby enabling carbon isotopes to provide insights into past changes in ocean productivity (Maslin and Swann, 2005) [and possibly into past surface water CO_2 concentrations (e.g. Jasper and Hayes, 1990)]. All the common photosynthetic pathways discriminate against ^{13}C in favour of ^{12}C, so in areas where marine primary production is high, continuous uptake depletes surface waters in ^{12}C while enriching the surface water carbon pool in ^{13}C. The progressive increase in the ratio between ^{13}C to ^{12}C in the surface nutrient pool is transferred to the biogenic material subsequently

produced using the enriched pool, thus leading to a parallel isotope enrichment of the organic matter ($\delta^{13}C_{org}$) (summarised in Figure 4.1). In this explanation, the biogeochemical system is very much simplified; but assumes that the majority of carbon incorporated in the sediments is derived from photosynthetically produced material through passive diffusion (Laws et al., 1995; Maslin and Swann, 2005) and consequently $\delta^{13}C_{org}$ primarily reflects surface water productivity. Based on a given molecular dissolved CO_2 ($CO_{2(aq)}$) pool, $\delta^{13}C_{org}$ is less negative (enriched in ^{13}C; depleted in ^{12}C; isotopically heavier) when productivity is high and more negative (depleted in ^{13}C; enriched in ^{12}C; isotopically lighter) when productivity is lower. The $CO_{2(aq)}$ content of surface waters is less affected by variable inputs (than nitrate content, as discussed in section 4.1.3), due to active gas exchange with the atmosphere. Transfer of gases is a two-way process; exchange across the boundary is driven by concentration differences between air and surface seawater, with transport by molecular diffusion and wind-driven turbulent motion.

Unfortunately, this simplified theory of carbon isotopic fractionation during photosynthesis and the view that the primary carbon acquisition pathway is through passive diffusion into phytoplankton cells, is sometimes compromised. The $CO_{2(aq)}$ pool is dependent upon physical processes (SST and salinity, diffusivity, wind intensity) and biological processes (carbon uptake) (Crosta and Koç, 2007). Within a given ocean system other factors may influence uptake, such as growth rate, community structure (Popp et al., 1998), cell size / shape fraction (Pancost et al., 1997; Popp et al., 1998; Burkhardt et al., 1999; Trull and Armand, 2001), non-diffusive carbon uptake through carbon concentrating mechanisms[1] (Rau, 2001; Tortell et al., 2000; Cassar et al., 2004; Woodworth et al., 2004) and active uptake of bicarbonate (HCO_3^-) (Tortell et al., 1997; Keller and Morel, 1999). 90% of inorganic carbon in the sea is in the form of HCO_3^- ions, with less than 1% present as CO_2 (the form required by ribulose-1,5-bisphosphate carboxylase/oxygenase (Rubisco), the enzyme primarily responsible for photosynthetic carbon fixation) (Riebesell, 2000). At typical concentrations of CO_2 in sea water, Rubisco operates far below its optimum. Algae usually overcome the problem by increasing the CO_2 concentration at the site of carbon fixation through the active uptake of CO_2 or HCO_3^-, rather than relying on diffusion (Riebesell, 2000). Algae have two primary strategies to maximize the performance of Rubisco in photosynthetic CO_2

[1] Mechanisms for concentrating carbon around the Rubisco enzyme, which drives the carbon-reducing steps in photosynthesis (Keeley and Rundell, 2003).

fixation: either the development of a carbon concentrating mechanism (CCM), based at the level of the chloroplast, or the evolution of the kinetic properties of Rubisco (Badger et al., 1998). Acquisition of HCO_3^- strongly alters the fractionation process in phytoplankton (low fractionation factor) and causes enriched $\delta^{13}C_{org}$ values (Woodworth et al., 2004). However, active diffusion of HCO_3^- is enhanced at low CO_2 levels (Tortell et al., 2000), which is not the case in the Southern Ocean, where surface waters are saturated in CO_2. This would suggest that assimilation of HCO_3^- is not a major control in the sedimentary isotopic signal in this study area.

The processes outlined above, can in some cases strongly affect the carbon isotopic fractionation and weaken the relationship between $\delta^{13}C_{org}$ and $CO_{2(aq)}$ (Crosta and Koç, 2007). These, and other factors affecting interpretations of the sedimentary isotopic signal, are summarised in Table 4.1.

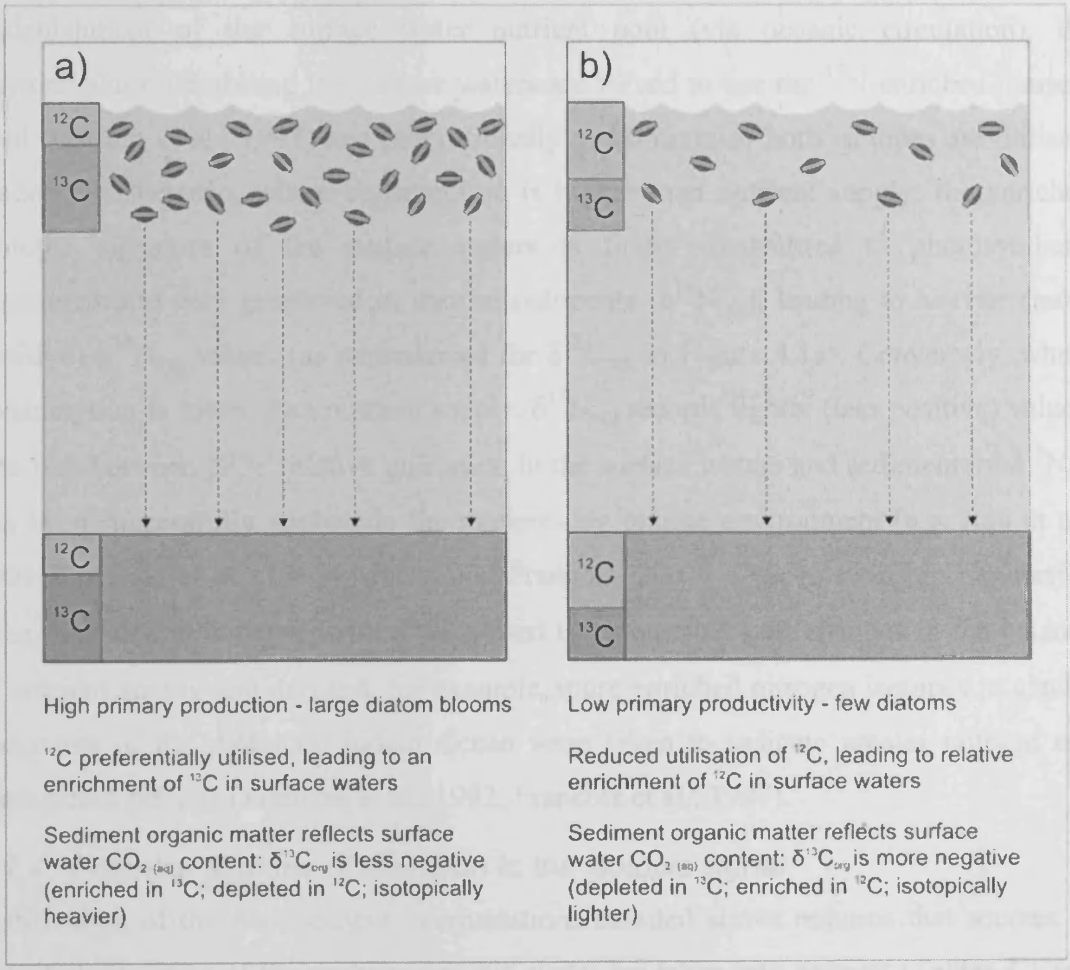


Figure 4.1
Transmission of the surface water isotopic signature to photosynthetic organisms (diatoms), which then accumulate in marine sediment to record the inorganic nutrient pool of the surface waters.
a) High primary production scenario;

b) Low primary production scenario.

4.1.3 Nitrogen isotopes

Nitrogen isotopes offer an insight into the relative utilisation of nitrate (NO_3^-), which is forced by shifts in the balance between the relative size of the nutrient pool (supplied through oceanic circulation processes) and biological consumption. Consequently, nitrogen isotopes provide information about both oceanographic influences and primary production. During periods of deep mixing in the modern ocean, NO_3^- concentrations are high; whereas during periods of thermal stratification and phytoplankton blooms, there is drawdown in near-surface nutrients (Altabet, 2005). The dominant isotope is nitrogen-14 (^{14}N), and this lighter isotope is preferentially fixed by photosynthesising organisms, leaving behind the much less abundant heavier isotope, nitrogen-15 (^{15}N). Within a given surface nutrient pool, higher productivity (i.e. consumption) leads to increased consumption of ^{14}N and enrichment of surface waters with ^{15}N. Assuming no replenishment of the surface water nutrient pool (via oceanic circulation), the phytoplankton inhabiting the surface waters are forced to use the ^{15}N-enriched nutrient pool (Ostrom et al., 1997) and proportionally much more of both isotopes are utilised. Under this scenario, where consumption is higher than nutrient supply, the enriched isotopic signature of the surface waters is firstly transmitted to photosynthetic organisms and then preserved in marine sediments ($\delta^{15}N_{org}$), leading to heavier (more positive) $\delta^{15}N_{org}$ values (as summarised for $\delta^{13}C_{org}$ in Figure 4.1a). Conversely, where consumption is lower than nutrient supply, $\delta^{15}N_{org}$ records lighter (less positive) values. The link between NO_3^- relative utilisation in the surface waters and sedimentary $\delta^{15}N_{org}$ has been successfully applied in the modern-day marine environment (e.g. Rau et al., 1991; Francois et al., 1993; Albatet and Francois, 2001). This relationship has further been extended down-core, with $\delta^{15}N_{org}$ used to reconstruct past changes in the balance of nutrient supply and demand; for example, more enriched nitrogen isotopes in glacial sediments of the Antarctic Indian Ocean were taken to indicate greater nutrient use during cold periods (Francois et al., 1992; Francois et al., 1997).

4.1.4 Potential sources of alteration to the isotopic signal

Justification of the two isotopic interpretations detailed above requires that sources of potential alteration of the primary isotopic signal are taken into account (Tables 4.1 and 4.2). A combined approach using elemental C/N ratios and isotopic signatures was therefore used in this study to assess these potential sources of alteration of both $\delta^{13}C_{org}$ and $\delta^{15}N_{org}$.

Table 4.1
Potential sources of alteration to the $\delta^{13}C_{org}$ signal.

Cause	Process	Effect	Examples of references
Physiological factors	Fractionation processes are different between phytoplankton communities and individual diatom species, dependant on light levels, cell size, nutritional status, growth rate and life history strategy.	- Cells with geometry that maximise surface-area-to-volume ratios (e.g. pennates) should have higher fractionation coefficients, leading to lighter $\delta^{13}C$ values. - Sedimentation of vegetative cells produced during spring bloom growth versus sedimentation of resting spores formed close to nutrient exhaustion (De la Rocha, 2005).	Laws et al. (1995); Ludlam et al. (1997); Popp et al. (1998); Burkhardt et al. (1999)a and b; Riebesell et al. (2000); De la Rocha, (2005).
	Active carbon uptake (carbon concentration mechanisms).	- Alteration of the fractionation factor (εp).	Rau, (2001); Cassar et al. (2004); Crosta and Koc, (2007).
Bacterial degradation	Aerobic and anaerobic microbial processes in the water column.	Oxidised recycled organic matter liberates ^{12}C.	Lehmann et al. (2002) and references therein; Maslin and Swann, (2005).
Reduced ocean-atmosphere gas exchange	Sea ice capping can isolate surface waters, preventing CO_2 equilibration between the two reservoirs.	Enriched CO_2 concentrations under the sea ice and in the surrounding waters; phytoplankton record depleted $\delta^{13}C$ values.	Crosta and Shemesh, (2002).
Terrigeneous input	From ice shelves, glaciers and fluvial outflow in the AP marine setting.	Such material has a heavier isotopic signature and higher C/N ratio, causing deviation from the Redfield ratio of 7 (Redfield et al., 1963).	Biddanda and Benner, (1997).
Ocean circulation	"Age" of the water affects the dissolved inorganic carbon content, with older waters incorporating $^{12}CO_2$ released by the degradation of organic matter.	Chemical ageing: older waters potentially contains lower $\delta^{13}C$ values, whereas relatively young water contains high $\delta^{13}C$ values.	Maslin and Swann, (2002).
Diagenetic alteration	May occur both pre- and postburial. Preferential remobilisation of light isotopes.	Will cause $^{12}CO_2$ enrichment in the $CO_{2\,(aq)}$ pool and $^{13}CO_2$ enrichment in the sedimentary record.	Lehmann et al. (2002) and references therein.

Table 4.2 Potential sources of alteration to the $\delta^{15}N_{org}$ signal (adapted from Ettwein et al., 2001). Full details of references found in original publication.

Cause	Process	Effect	Examples of references
Physiological factors*	Fractionation processes are different between phytoplankton communities and individual diatom species, dependant on light levels, cell size, nutritional status, growth rate and life history strategy.	Alteration of the fractionation factor (εp).	Popp et al. (1998); Laws et al. (2002); Cassar et al. (2006). Lourey et al. (2003); Robinson et al. (2008).
Denitrification	^{14}N returned to the atmosphere by denitrifying bacteria.	More ^{15}N enters smaller marine NO_3^- pool, thereby limiting supply for phytoplankton.	Holmes et al. (1998; 1997; 1996); Naqvi et al. (1998); Pride et al. (1999); François et al. (1993).
Nitrogen fixation	Cyanobacteria incorporate "new" nitrogen into system, for example.	More ^{14}N enters marine NO_3^- pool, thereby increasing the amount of utilizable NO_3^-.	Altabet and François (1994); Peters et al. (1978); Karl et al. (1997); Falkowski (1997).
Terrigeneous input	From ice shelves, glaciers and fluvial outflow in the AP marine setting.	Marine NO_3^- pool becomes typically enriched (but occasional depleted depending upon contaminant source).	Holmes et al. (1998; 1997; 1996); Peters et al. (1978); Capone and Carpenter (1982); Falkowski (1997).
Grazing and recycling	Enrichment in ^{15}N at each trophic level.	More ^{15}N enters marine NO_3^- pool, leading to a heavier isotopic signature.	Bronk and Ward (1999); Altabet et al. (1991).
Diagenetic alteration	May occur both pre- and postburial. Preferential remineralisation of ^{14}N during oxidative degradation of organic matter.	Will cause ^{14}N enrichment in the nitrate pool and ^{15}N enrichment in the sedimentary record.	Holmes et al. (1998; 1996); Altabet and François (1994); Altabet et al. (1991); Sigman et al. (1997); Farrell et al. (1995).

* More pronounced for carbon than nitrogen (Popp et al., 1998; Cassar et al., 2006).

4.2 Sedimentary pigments

Sedimentary pigments have been used as markers of the presence of photosynthetic organisms and environmental change in a number of lake settings on the Antarctic continent (Squier, 2003; Squier et al., 2002; 2005), however, with the exception of Hodgson et al. (2003), this is not a technique that has been applied extensively in the marine realm. The identification of fossil pigments in core VC243, from Prince Gustav Channel, is therefore a relatively novel application of the technique. The aim was to compare fossil pigment distributions and concentrations with the fossil diatom records, providing additional information on biological activity, phototrophic community composition and therefore environmental conditions at the time of deposition. The advantage of pigment analyses is that it provides a record of variations in the total primary producer community, rather than solely the diatom component.

4.2.1 Origin of sedimentary pigments

Sedimentary pigments (chlorophylls, carotenoids and biliproteins) are involved in light harvesting and photoprotection (Wright and Jeffrey, 2006). All phytoplankton contain chlorophyll *a* (Chl *a*); however many pigments are limited to particular classes allowing some discrimination of the taxonomic composition of the phytoplankton at class level (Jeffrey et al., 1997). The sedimentary pigments identified in this investigation were native chlorophyll, chlorophyll degradation products and carotenoids. The ecological affinities and environmental interpretation of individual pigments preserved in core VC243 are presented in Chapter 8 (Table 8.2).

Pigments are incorporated in marine sediments either directly, through deposition and / or burial of the remains of photoautotrophs (including diatoms), or indirectly via the actions of heterotrophic grazing (Squier, 2005). Pigments have often been shown to persist long after the disappearance of morphologically distinguishable remains of the organisms that produced them and are often the sole remnants of non-siliceous algae (Leavitt, 1993; Fietz et al., 2007). However, pigments are susceptible to diagenetic and catagenic transformations in which structural information can be lost, but the nature of these transformations can also provide useful information concerning the biological, chemical and physical processes that have operated either at or since the time when a particular sediment was deposited (Keeley, 2006). These chemical transformations commonly occur during senescence (cellular disruption associated with death), during grazing by zooplankton, and during sinking through the water column.

4.2.2 Chlorophylls

All photosynthetic phytoplankton contain one or more types of chlorophyll as part of the light-harvesting complexes in their chloroplasts. Chlorophylls are magnesium coordination complexes of conjugated cyclic tetrapyrroles[2], with a fifth isocyclic ring and often an esterified long-chain alcohol (Wright and Jeffrey, 2006) (Figure 4.2).

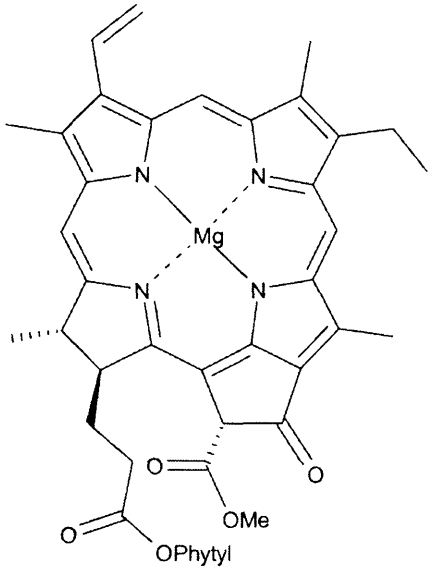


Figure 4.2
Structure of Chlorophyll *a*.

4.2.3 Chlorophyll degradation products

Depending on the type of degradation process, chlorophyll can degrade into various products, including phaeophytins, phaeoporphyrins, porphyrins and chlorophyllide, or ultimately to colourless compounds (Squier et al., 2005). The most common degradation products of chlorophylls occur through demetallation reactions, producing Mg-free phaeophytins and phaeoporphyrins, typically resulting from processes during or after senescence (Leavitt, 1993; Fietz et al., 2007), such as lowering of pH (Rowan, 1989). Loss of the phytyl chain by hydrolysis is another common degradation route, forming a chlorophyllide, and when both phytyl chain and Mg are lost, the product is phaeophorbide (Rowan, 1989). Phaeophorbide mainly results from zooplankton gut passage (Leavitt, 1993). Particular chemical structures can also be formed during these transformations including steryl chlorin esters (SCE) and oxidation products (e.g. purpurins). SCE are formed by esterification[3] from chlorophyll degradation products and are relatively stable compared to chlorophylls and other degradation products (Fietz

[2] Cyclic group of four linked nitrogen-containing rings (a tetrapyrrole nucleus), the nitrogen atoms of which are often coordinated to metal ions (Mg in the case of chlorophyll) (Daintith, 2008).
[3] A reaction of an alcohol with an acid to produce an ester (organic compound) and water (Daintith, 2008).

et al., 2007 and references therein). The formation of SCE has been observed during experiments in which diatoms were grazed by copepods (Harradine et al., 1996; Talbot et al., 1999) and it is widely accepted that SCE are markers of herbivory (Keeley, 2006). Purpurins are oxidation products of Chl *a*, and their occurrence provides evidence that, despite being subjected to oxidising conditions, the tetrapyrrole macrocycle, and hence chlorophyll signature is preserved (Squier et al, 2005).

4.2.4 Carotenoids

Unlike chlorophylls, carotenoids are very numerous, and over 600 are known in plants, fungi and animals (Wright and Jeffrey, 2006). Their function in the cell is either in light harvesting or protection of the chlorophylls from photo-oxidation (e.g. diatoxanthin). Nearly all carotenoids found in phytoplankton have the carbon atoms arranged around the skeletal double bonds, producing linear molecules (Wright and Jeffrey, 2006) (Figure 4.3). Carotenoids comprise two types, the carotenes and the xanthophylls. The carotenes are hydrocarbons and are few in number; the xanthophylls are oxygenated carotenoid derivatives, containing at least one atom of oxygen in the molecule, and make up the vast majority of the carotenoids. Carotenoids are taxonomically useful but quantitatively variable since their abundance can change dramatically in response to irradiance (Wright and Jeffrey, 2006).

General instability of carotenoids results from their double bond structure, being very susceptible to oxidation and free-radical reactions (Britton, 1993). Common carotenoid modifications include the degree of unsaturation of the isoprenoid skeleton, oxygen functional groups and esterification of hydroxyl derivatives (Wright and Jeffrey, 2006). Carotenoids are also particularly labile molecules, spontaneously rearranging in solution and esters can be easily hydrolysed (Wright and Jeffrey, 2006), forming derivatives that can complicate pigment analyses.

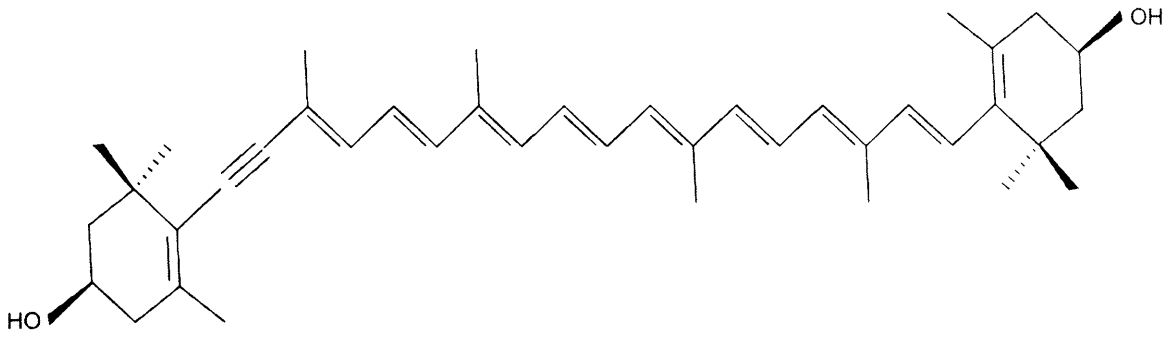


Figure 4.3
Structure of the carotenoid Diatoxanthin.

4.3 Chapter summary

This chapter has outlined the theory and assumptions behind the use of carbon and nitrogen stable isotopes as proxies for primary production (through the global carbon cycle) and utilisation of carbon nutrients and nitrate, respectively. Also discussed was the use of sedimentary pigments as markers for environmental change, providing records of variations in the total primary producer community.

5 Methods

This chapter describes the methods used for quantitative diatom analysis, nitrogen and carbon isotopes on bulk organic material, and sedimentary pigments.

5.1 Quantitative diatom analysis

5.1.1 Sampling strategy

Cores were sampled at intervals of between 5 and 10 cm (as detailed in Table 5.1), removing a small amount of sediment (~ 0.5 g) for diatom processing. The ends of the core liner and core sides were avoided to minimise possible contamination induced during the coring and splitting process.

Table 5.1 Core length, diatom sampling interval and resolution.

Core number	Core length (m)	Sampling interval (cm)	Sampling resolution (yrs)
GC114	3.4	10	108
GC047	3.8	8	234
VC306	5.94	10	455
GC358	0.94	5	862
VC243	5.86	10	109
VC237	6	10	156
VC205	5.42	10	189 (0 – 2.6 m); 24 (2.6 – 5.1 m)

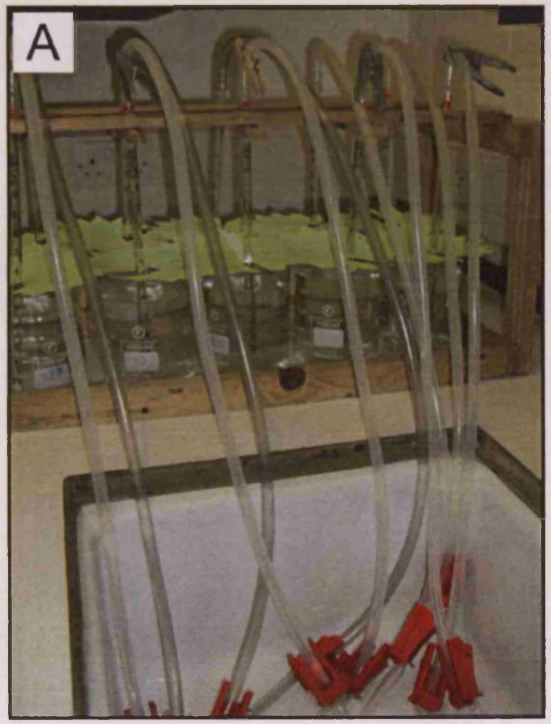
5.1.2 Sample preparation

Diatom slides were prepared following the random settling method of Scherer (1994), with minor modifications (Allen, 2003). The random settling technique has been shown to effectively distribute the biogenic particles randomly across the slide; produce an accurate sample of the original material; and be highly reproducible (Laws, 1983; Bodén, 1991; Scherer, 1994). Further, this technique has been successfully utilised on other Antarctic marine sediments (e.g. Leventer et al., 2002; Sjunneskog and Taylor, 2002; Allen et al., 2005; Heroy et al., 2008).

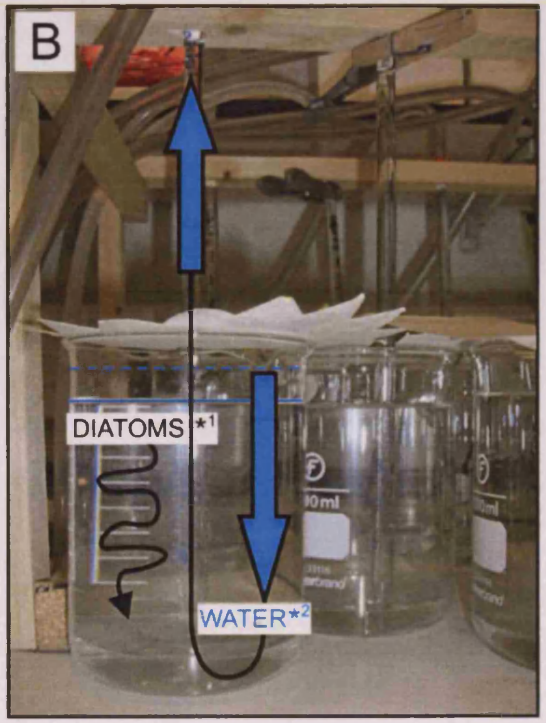
Sediment samples (weighing between 0.01 to 0.03 g, depending whether sediments were biogenic- or terrigenous-rich) were oven dried overnight in clean glass vials (20

ml). Dried samples were weighed using Mettler AE240 balance (standard deviation error ± 0.0002 g) and the dry weight noted. The vials were half filled with distilled water (10 ml) and 3 ml of hydrogen peroxide (30 %) plus 1 ml of hydrochloric acid (50 %) were added to remove organics and carbonates. The sample vials were left on a warm hotplate for a number of hours (< 5 hours), until the mixture was oxidised (reducing in volume and turn green-white in colour). After this oxidation step, 10 ml of calgon detergent (sodium hexametaphosphate) was added and the samples left to soak for an hour, further disaggregating the samples. Settling beakers were prepared, as illustrated in Figure 5.1. For each individual sample, a large beaker (1 litre) was filled with distilled water. On the base of the beaker, there was a modified petri dish (containing a hole), onto which a glass slide, with two glass coverslips temporarily glued on, was placed. A pipette was placed through the hole in the petri dish and siphon tube attached. Prior to adding sediment samples to the settling beaker, sample vials were dipped into an ultra sonic bath for 1-3 seconds, to disaggregate the samples but not long enough to break the diatom valves. Sediment samples were added to the settling beaker, vials rinsed with distilled water and water in the beaker homogenised with a glass stirrer. Settling beakers were covered to prevent contamination and left for 4 hours. In the settling beaker, diatom valves sink through the water column, to give an even distribution across the base of the beaker and on the glass coverslips (Figure 5.1B *[1]) (see section 5.1.4 and Equation 5.1 for absolute diatom abundance calculation). After 4 hours, valves were opened on the siphons, allowing the water to slowly drain out of the settling beaker (1 drip per 2 seconds) (Figure 5.1B *[2]). When the settling beakers had fully drained, glass slides, with diatom-coated coverslips, were removed and allowed to air dry. Coverslips were subsequently mounted onto microscope slides using Norland Optical Adhesive (Refractive Index 1.56) and cured under a UV light.

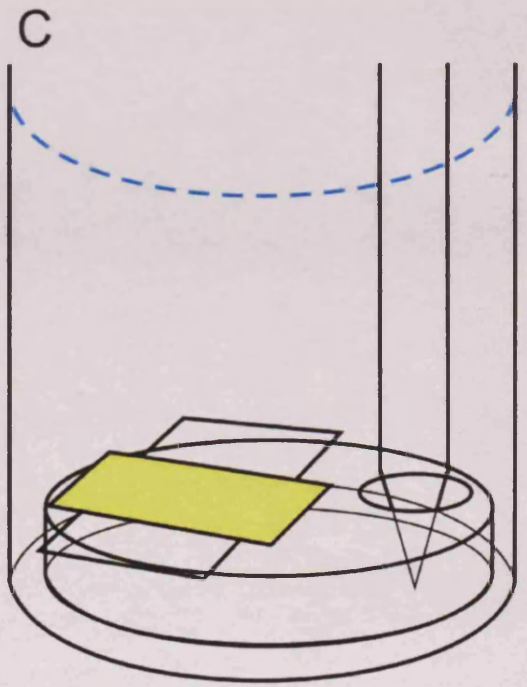
Figure 5.1
Preparation method for diatom quantitative analysis, using water column settling technique.



A: Settling beakers, each containing distilled water and clean (organic- and carbonate-free) diatom sediment sample. Siphon tubes and valves (red) allow the water to slowly drain from the base of the beaker. Two arrangements, each of 10 beakers, enables 20 samples to be processed at a time.



B: Diatoms sink through the water column (prior to valves on siphon being open) (*1). Diatom valves settle on the base of the beaker and on the glass coverslip, which is supported by the modified petri dish. Siphon taps are opened and the water drains slowly (*2), not disturbing the even distribution of valves at the base of the beaker.



C: Arrangement at the base of the beaker, showing the modified petri dish, (containing a hole for the tip of the siphon), which supports the glass slide and coverslip (yellow) for the diatoms to settle onto.

5.1.3 Data collection and format

Diatom slides were analysed with a Leica DM RX microscope with immersion oil at 1000x magnification, using differential interference contrast (or Nomarski) mode. A minimum of 400 diatom valves (including *Hyalochaete Chaetoceros* spp. resting spores (CRS)) were counted along measured transects (avoiding the outer 0.5 mm of the slide edge) to ensure the maximum inclusion of diatom species and statistical significance of the data. Figure 5.2 shows an initial rarefaction test on core GC114, which was carried out to ensure a sufficient number of cells were counted to capture the main species diversity.

CRS form a high proportion of diatom assemblages from the AP region (frequently 70 – 90 %) and the dominance of a single genus strongly biases the relative abundance data. Consequently, to assess the contribution, trends and ecological information of minor species, an additional set of counts (again >400 valves) was undertaken excluding CRS – hereafter referred to as the "CRS-free count". This is common practice for Antarctic sediments where CRS abundance frequently dominates the assemblage data and smothers the environmental significance of the minor species (see Leventer et al., 1996; Taylor et al., 2001; Taylor and Sjunneskog, 2002; Allen et al., 2005; Heroy et al., 2008).

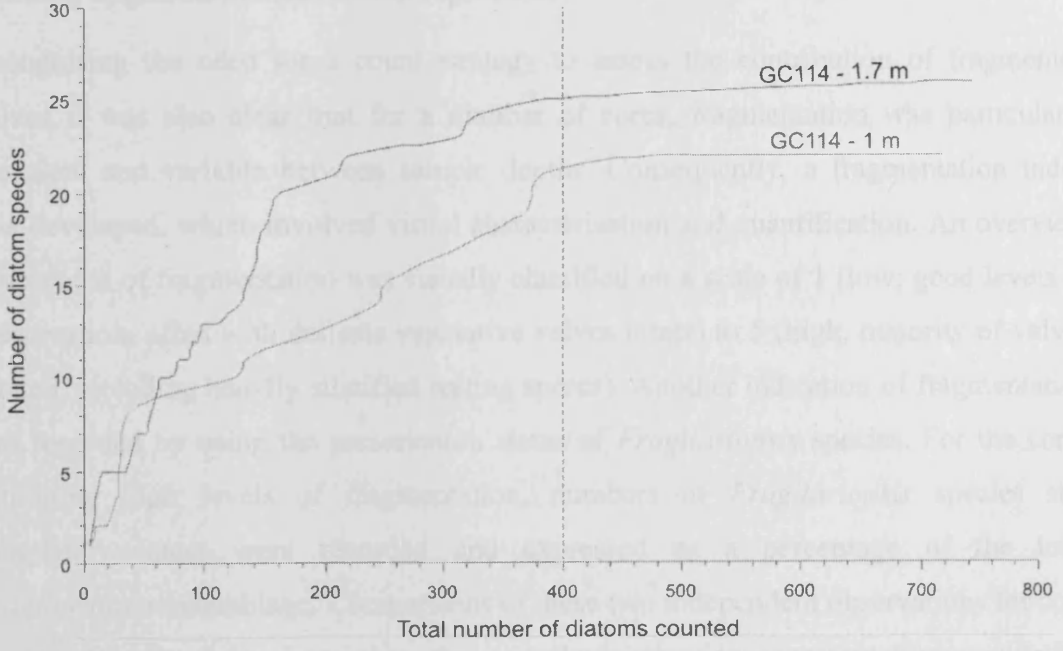


Figure 5.2
Rarefaction test for core GC114, sample depths 1 m and 1.7 m. Dashed line at 400 diatoms counted highlights a threshold at which the majority of the species diversity is captured.

Diatoms were identified using the general floristic studies of Hasle and Syvertsen (1997) and Antarctic species of Cremer et al. (2003) and Scott and Thomas (2005). Specific taxonomic references included Johansen and Fryxell (1985) for the genus *Thalassiosira* and Armand and Zielinski (2001) to separate species of *Rhizosolenia.* Where possible all valves were identified to species or genus level. If diatoms could not be identified to species level they were grouped by genus and if the valves were still unidentified, they were added to an unidentified centric or pennate group. Members of the subgenus *Hyalochaete* of the genus *Chaetoceros* were identified only as vegetative cells or resting spores due to difficulties distinguishing small scale morphological differences between vegetative valves under the light microscope. The raw count data therefore consists of the number of valves in the total assemblage and the number of individual species / genus groups, over a recorded transect area (and can be found on the appendix CD).

As all sediments are likely to have some fragmented frustules, a standard procedure for counting fragmented valves was implemented to ensure valve counts were not overestimated and to remove any bias resulting from the preferential fragmentation of certain morphologies (for example some of the more fragile pennates, such as *Pseudonitzschia* species and *Thalassionema* species). The criteria developed for counting fragments is illustrated in Figure 5.3.

Recognising the need for a count strategy to assess the contribution of fragmented valves it was also clear that for a number of cores, fragmentation was particularly prevalent and variable between sample depths. Consequently, a fragmentation index was developed, which involved visual characterisation and quantification. An overview assessment of fragmentation was visually classified on a scale of 1 (low; good levels of preservation, often with delicate vegetative valves intact) to 5 (high; majority of valves broken, including heavily silicified resting spores). Another indication of fragmentation was recorded by using the preservation status of *Fragilariopsis* species. For the cores exhibiting high levels of fragmentation, numbers of *Fragilariopsis* species still completely intact were recorded and expressed as a percentage of the total *Fragilariopsis* assemblage. Comparisons of these two independent observations for core VC243 (Figure 5.4) show that these methods provide representative qualitative measures of fragmentation.

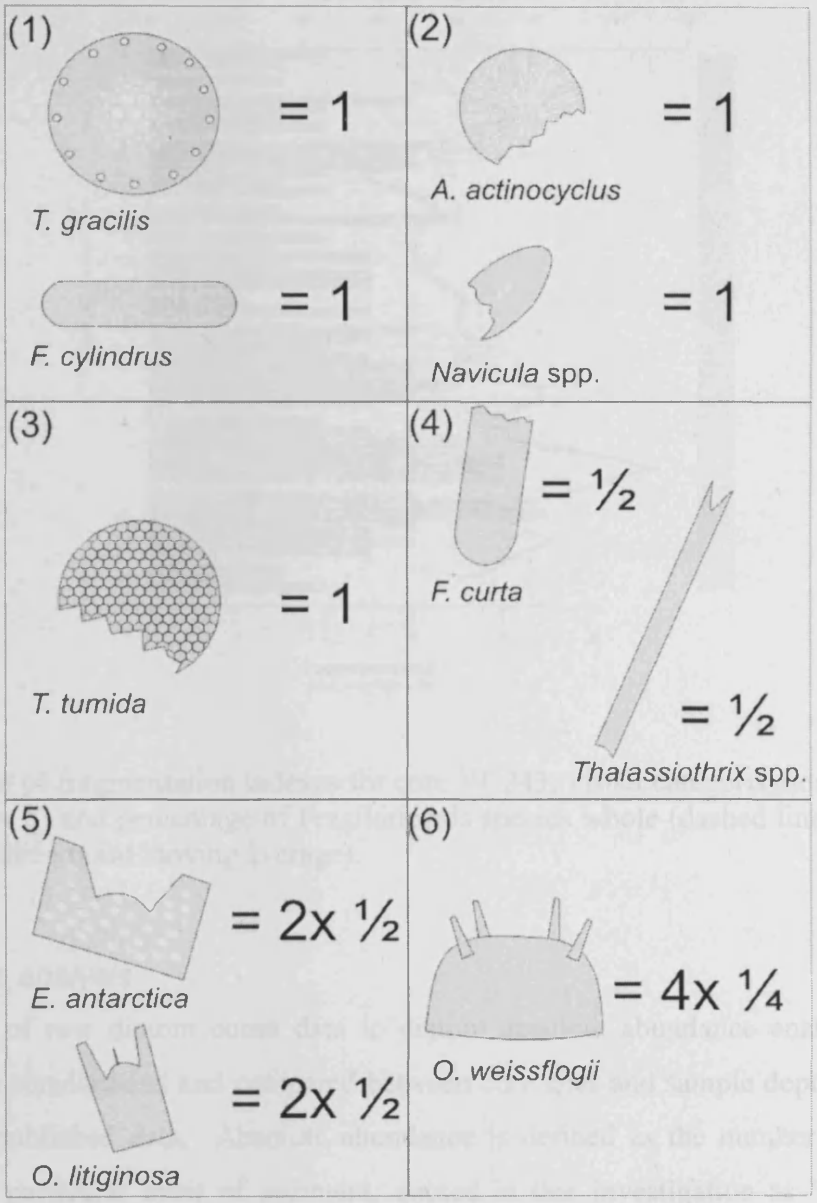


Figure 5.3
Count methodology for individual and fragmented diatom valves: (1) complete diatom valves counted as one valve; (2) fragmented centrics and pennates possessing visible, distinctive central features (for example *Actinocyclus* species and *Navicula* species) counted as one valve; (3) fragmented centrics that lack such a feature, but with more than half the valve face intact counted as one valve; (4) valve ends of fragmented pennates, again lacking such a feature (for example *Fragilariopsis* species and *Thalassiothrix* species), counted as ½ valve (counting poles); (5) *Eucampia antarctica* and *Odontella litiginosa* "horns" individually, counted as ½ valve; (6) *Odontella weissflogii* protrusions individually, counted as ¼ valve.

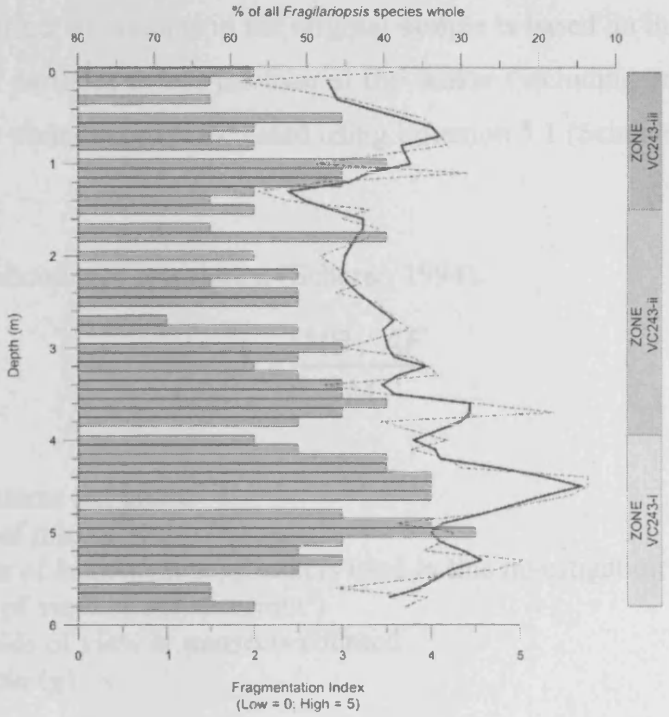


Figure 5.4
Comparisons of fragmentation indexes for core VC243; visual categorisation (bars: low = 0 to high = 5) and percentage of Fragilariopsis species whole (dashed line = original; solid line = three point moving average).

5.1.4 Data analysis

Conversion of raw diatom count data to diatom absolute abundance enables diatom counts to be standardised and compared between core sites and sample depths, together with other published data. Absolute abundance is defined as the number of diatoms valves in a particular mass of sediment, quoted in this investigation as "millions of valves per gram of dry sediment" (Mv/g). As a consequence, diatom absolute abundances are directly controlled by processes influencing sediment accumulation rate, such as export production, dissolution of biogenic silica both in the water and in the sediment, and inputs of terrigenous material (Meng, 1994). These processes are interpreted and discussed in context to provide information on past ocean conditions and more specifically, surface water palaeoproductivity. In addition, absolute abundance of the non-CRS assemblage is also calculated in this investigation using CRS-free count totals, which addresses whether productivity signals are similar between *Hyalochaete Chaetoceros* species (which overwhelming dominate total diatom abundance as CRS, as discussed in section 5.1.3) and the remainder of the diatom assemblage.

Estimating the number of diatoms in the original sample is based on the assumption that the distribution of particles across the base of the beaker (including on the coverslip) is uniform. Absolute abundance is calculated using Equation 5.1 (Scherer, 1994).

Equation 5.1
Absolute diatom abundance calculation (Scherer, 1994).

$$T = \frac{NB / AF}{M}$$

where:
T = number of diatoms per gram
N = total number of microfossils counted
B = area of bottom of beaker (mm^2) [beakers used in this investigation = 7854 mm^2]
A = area per field of view or transect (mm^2)
F = number of fields of view or transects counted
M = mass of sample (g)

Numerous studies have tested and documented the reproducibility and high accuracy of this random settling method for calculating diatom absolute abundance and relative abundance (Moore, 1973; Laws, 1983; Bodén, 1991; Scherer, 1994). By counting multiple slides from the same sediment sample, Bodén (1991) quantified errors to be ± 5 % for absolute abundance data (after a count of 400 valves).

Further information about the diatom community can be revealed by relative abundance data, highlighting the importance of specific phytoplankton species and their inter-relationships. This is expressed as a percentage of the total CRS-free assemblage. The use of the CRS-free assemblage is justified when comparisons are made between the CRS-included and CRS-free relative abundance data, as exemplified for core GC047 in Figure 5.5. As illustrated, the three most abundant species in this core show similar trends in percentage values between the two counts. Correlation coefficients (described in section 5.1.5) of the relative abundance data between the total diatom assemblage and CRS-free assemblage for these three species reveal highly significant correlations (at the 99 % confidence level): *F. curta* = 0.51; *F. kerguelensis* = 0.56; and *T. antarctica* warm resting spores = 0.5. Such correlations do not render CRS-free counts as obsolete; instead the purpose of the CRS-free count is to assess the contribution, trends and ecological information of minor species. The correlation in Figure 5.5 shows that the two counting methods produce similar stratigraphic patterns.

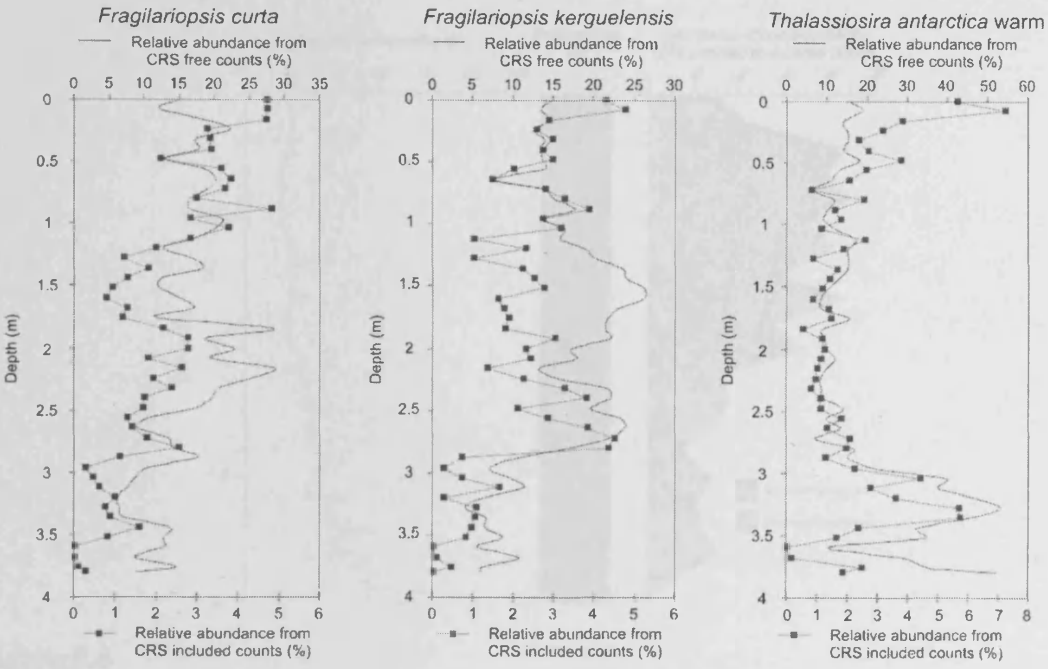


Figure 5.5
Comparison of diatom relative abundance percentages between CRS included and CRS-free counts for core GC047.

Both measures (diatom absolute abundance and relative abundance) have advantages and disadvantages. With diatom absolute abundance, caution is needed as this value is influenced by the terrigenous fraction, which can change significantly through time, for example during deglaciation. Using core VC306 as an example (Figure 5.6), although productivity was probably lower during early deglaciation (2 – 1.5 m), some of the diatom absolute abundance signal may be controlled by the amount of terrigenous material through this interval (recorded on the sedimentary log and magnetic susceptibility values). Relative abundance is also partly driven by the patterns exhibited by other species in the assemblage. Using core VC205 as an example, (Figure 5.7), the low absolute and relative abundance of *F. curta*, *F. cylindrus* and *F. vanheurckii* recorded in zone VC205-ii, results in a dramatic increase in the relative abundance of *T. antarctica* warm resting spores, which is not matched by increased absolute abundance of this species through this zone. However, such changes in community structure are related to environmental parameters, generally more favourable conditions for the dominant species (in the example given in Figure 5.7, *T. antarctica* warm resting spores). To extract the maximum amount of information on oceanographic, sedimentary processes and primary productivity, both diatom absolute and relative abundance data have been compared in tandem in this investigation.

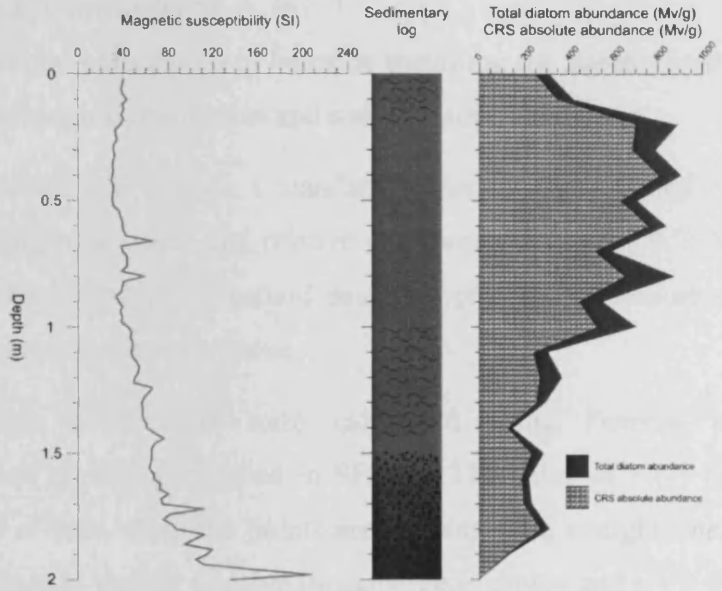


Figure 5.6
Core VC306: Magnetic susceptibility (SI) (see Chapter 6.1.1), sedimentary log and total diatom abundance (Mv/g). As highlighted, the lower-most deglaciation portion of the core (2 – 1.5 m), potentially records dilution of diatom absolute abundance by the terrigenous fraction of the sediment (recorded by high magnetic susceptibility).

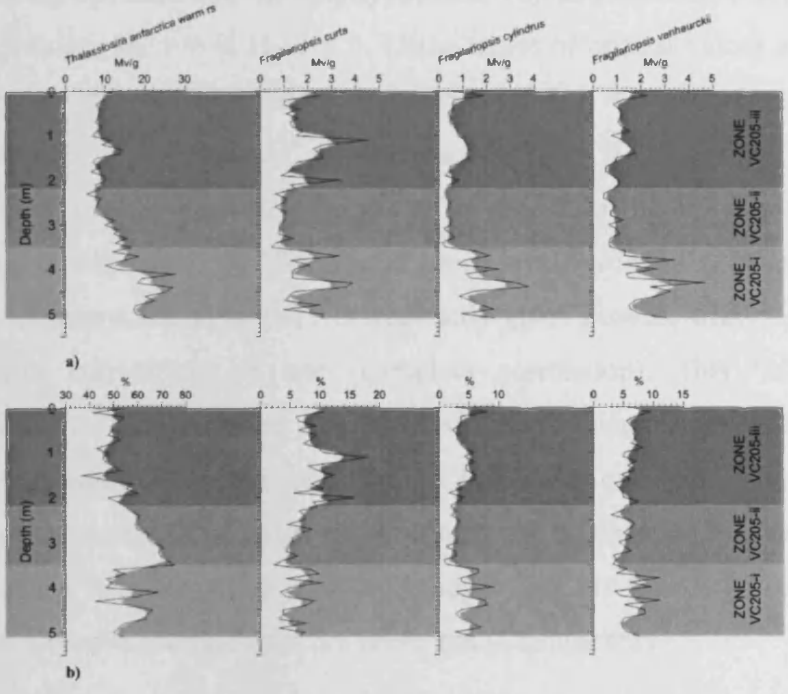


Figure 5.7
Core VC205: Non-CRS diatom assemblage absolute abundance (Mv/g) (Figure 5.7a) and relative abundance (%) (Figure 5.7b) for a selection of AP indicator species (c.f. Figure 7.62). These four species were selected as they are the most abundant non-CRS species in core VC205. As highlighted, decrease in the relative abundance of the three *Fragilariopsis* species in zone VC205-ii, results in a dramatic increase in *Thalassiosira antarctica* warm resting spore relative abundance, not matched by increased absolute abundance of this species. This emphasises the importance of comparing absolute and relative abundance data in tandem.

5.1.5 Statistical interpretation

A number of general points need to be made regarding the standardised presentation of diatom, sedimentological, biomarker and stable isotope results:

- Mean values will include 1 standard deviation (1σ), quoted in brackets (e.g. "diatom mean absolute and relative abundances of 1.8 (± 0.7) Mv/g and 4.6 (± 2.1) %, respectively"). Standard deviation provides a measure of the spread of the data around the mean value.

- Correlation coefficients were calculated using Pearson product-moment correlation (r) and performed in SPSS©. The value of r ($-1 \leq r \leq 1$) gives a measure of how close the points are to lying on a straight line; $r = 1$ ($r = -1$) corresponds to perfect positive (negative) correlation and $r = 0$ reveals that there is no connection between the two sets of data. Assessing whether the observed patterns can or cannot be explained by chance is based on the significance level (Mayhew, 2004); in all calculations the significance level was set at 5 %. To apply a significance test, the null hypothesis (H_0) and alternative hypothesis (H_1) were defined: H_0: $r = 0$; H_1: $r \neq 0$. Using tables of critical values and using the appropriate degrees of freedom, H_0 is rejected if $r <$ - critical value or $r >$ + critical value. A "significant" result has a 1 in 20 (5 % / 0.05 significance level) probability of the observation occurring by chance; a "highly significant" result has only a 1 in 100 (1 % / 0.01 significance level) probability (Mayhew, 2004). In the literature, the square of r is frequently given instead, with r^2 ranging from zero (no correlation) to one (complete correlation). This "coefficient of determination" indicates the proportion of variance that can be explained by the linear association (Hammer and Harper, 2006). For example, if r^2 is 0.90, then 90% of the variance of y can be accounted for by changes in x and the linear relationship between x and y. In this study, r^2 is only quoted when age models and linear sedimentation rates are presented (Chapter 6.2).

Statistical examination of the diatom data was carried out using two multivariate data analyses; principal components analysis (PCA) and hierarchical cluster analysis. This was performed using the program MVSP© (Kovach, 2002). Both methods are data exploration and visualisation tools, highlighting associations between both diatom species (R-mode) and between core depths (Q-mode), providing information on common environmental controls and temporal associations, respectively. In all PCA and

cluster analyses, diatom relative abundances were used as it was considered a more appropriate measure to assess changes in the diatom community, than absolute abundance data which is to some degree influenced by the terrigenous fraction. Only species comprising greater than 1 % abundance in any one sample were included, thus reducing the noise in the dataset.

PCA is a technique used for data reduction and interpretation. It is a form of ordination where each individual (species or sample depth) is placed to one or more constructed axes, so that its geometrical position relative to its fellows reflects its similarity to them. The application to species abundance data is based on the assumption that species distribute themselves in nature so as to fully exploit the ecological factors shaping their environment, and that their distribution thus carries information about these factors (e.g. temperature, nutrient levels) (Dale and Dale, 2002). A further assumption is that the majority of species are responding to a few main ecological gradients, so that complex sets of data may be reduced to a few main elements, which can be represented by axes in a geometrical bi-plot (Dale and Dale, 2002) (Figure 5.8). PCA assesses total variance in the diatom assemblage and acts to reduce the number of species (independent variables) to groups of species (composite variables), which are subsequently compared based on a similarity associated variable (principal component variable), likely to be related to ecological gradients (e.g. temperature, nutrient levels).

Application of PCA to this dataset was preceded by a square-root transformation of the diatom data in order to decrease the dominance of the major taxa and increase the importance of the minor taxa (Cunningham and Leventer, 1998), and data centring to ensure that the independence of the data was maintained (Kovach, 2002). Output from PCA analysis includes: (1) an eigenvalue, which indicates the relative proportion of the overall variance explained by that component and for convenience is also shown as a percentage sum; (2) component loading, reflecting the relative strength of the relationship between a composite variable and the component, which can be positive or negative. A decline in variance is experienced with increasing principal component number and it is rare for more than the first two or three principal components to be easily interpreted – the rest will often represent "noise" (Hammer and Harper, 2006). To define which principal components to focus on, eigenvalues were plotted as a descending curve (scree-plot); where the curve flattens out, or if no obvious change in gradient is visible, when a threshold eigenvalue of 2 is reached no further principal components are considered.

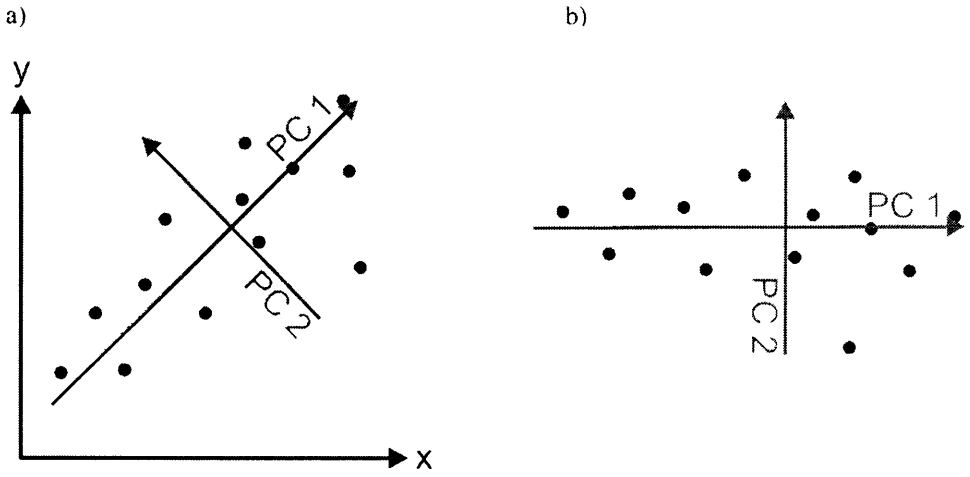


Figure 5.8
The principle of PCA, with variables x and y. a) Data points plotted in the co-ordinate system spanned by the original variables. PC1 is the direction along which variance is largest. PC2 is the direction along which variance is second to largest, and normal to PC1. b) Data plotted in a co-ordinate system spanned by the principal components (Hammer and Harper, 2006).

Hierarchical cluster analysis involves classification; the division of a large set of observations into a number of smaller distinct groups, so that observations within the same (different) group possess similar (dissimilar) characteristics (Jones, 2007b). The identification of groups and subgroups is based on a given distance or similarity measure between observations. In the agglomeration method, all observations are treated as separate clusters initially and then successively combined with the most similar samples until all are encompassed within a single hierarchical level, forming a dendrogram as illustrated in Figure 5.9 (Hammer and Harper, 2006). Each branching point corresponds to a joining event during the agglomeration and the branching point is drawn at a level corresponding to the similarity between the joined observations (Hammer and Harper, 2006). During cluster analysis, the distance measure and clustering algorithm need to be selected. The distance measure will determine how the similarity of the two observations is calculated and in this investigation the Spearman Coefficient was used. This measures the similarity between samples, irrespective of the observation value (clusters based on similarity, rather than absolute values) (Jones, 2007b). The clustering algorithm defines the distance between clusters and the method applied in this analysis was Unweighted Pair Group Method with Arithmetic Mean (UPGMA) (Sneath & Sokal, 1973) (also known as average linkage clustering or mean linkage). This approach takes into account all the points within a cluster and averages the distance between pairs of samples (Jones, 2007b).

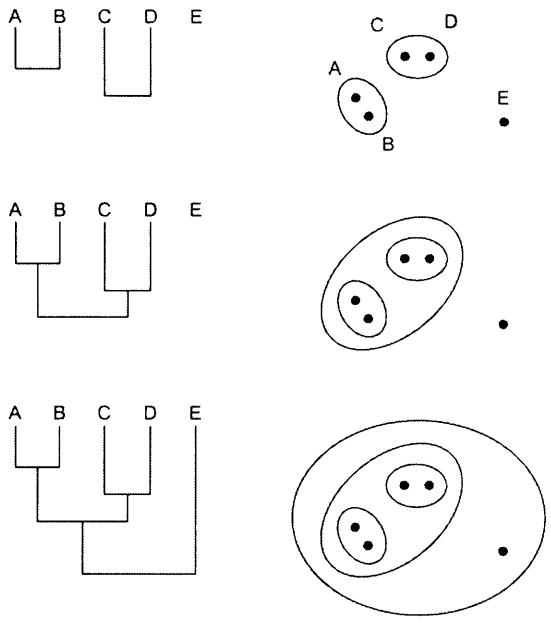


Figure 5.9
Example of hierarchical cluster analysis, using the agglomerative cluster method for five two-dimensional data points to produce a dendrogram (Hammer and Harper, 2006).

5.1.6 Characterising diatom assemblages

Presentation of diatom results includes total diatom abundance data, individual species absolute and relative abundance data, supplemented by R-mode PCA and cluster analysis. Application of these statistical techniques highlights species associations (and disassociations), reflecting preference for (and intolerance of) similar environmental conditions. Indicator species are defined as those species with high scores on high eigenvalue axes and with high statistical weights (top quartile of absolute abundance across all samples) (Pike et al., 2008). In other words, species *x* might have high scores on several PCA axes, but only be present in one or two samples, and conversely, species *y* might not have particularly high scores on PCA axes, but is abundant in numerous samples; neither would provide particularly useful ecological information. Species *x* is potentially linked to a specific habitat, but is too rare to argue statistical significance, whereas species *y* is too cosmopolitan, reaching high abundance but displaying little environmental preference. An ideal indicator species is one that is intimately linked to an ecological gradient and in adequate abundance to remain statistically significant.

5.1.7 Defining diatom stratigraphic zones

Presentation of diatom results for each core record then focuses on stratigraphic (i.e. temporal) zones. These are defined based on Q-mode PCA analyses, paired with visual examination of the diatom data. Primary and secondary PCA axes (i.e. those

incorporating the largest amount of the original variance in the data) were chosen and zones defined based on positive and negative component loading between sample depths (Figure 5.10). The exception to these criteria would be if the stratigraphic division on the primary axis was particularly complex (e.g. PCA axis 1 for cores GC114 and VC243); in this case, the next most important PCA axis was chosen. These diatom PCA based stratigraphic zones form the structure within which all other proxy data are described.

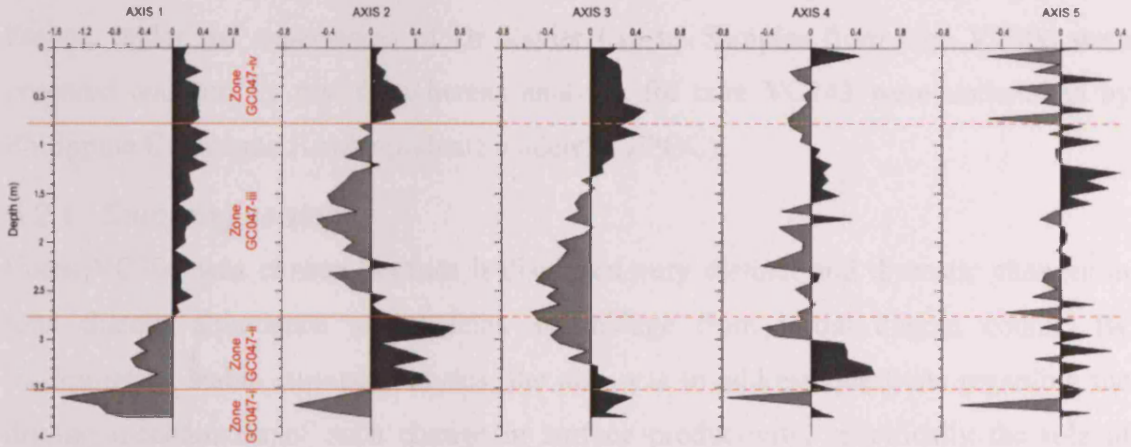


Figure 5.10
Core GC047: Q-mode PCA component scores plotted stratigraphically for PCA axes 1 – 5 (same as Figure 7.17). Stratigraphic zones defined by associations of positive loading (dark grey) and negative loading (light grey), in this case on axes 1 and 2.

5.2 Stable isotope analysis

Carbon (C) and nitrogen (N) elemental contents (C_{org} and N_{org}) and stable isotopic composition ($\delta^{13}C_{org}$ and $\delta^{15}N_{org}$) were measured on the bulk organic material in cores VC306 (Marguerite Bay) and VC243 (Prince Gustav Channel; PGC). The aim of incorporating results from these two elements was to provide additional information on palaeoproductivity and palaeoceanography, to supplement the diatom and sedimentary pigment datasets.

All stable isotope laboratory work and analysis was undertaken at Bordeaux I University, Environnements et Paléoenvironnements OCéaniques (EPOC) department, France, under the supervision of Dr Xavier Crosta. Samples from core VC306 were prepared and run by myself, whereas analyses for core VC243 were undertaken by Philippine Campagne (Undergraduate student at EPOC).

5.2.1 Sampling strategy

Cores VC306 was chosen because it displayed very distinct and dramatic changes in total diatom abundance and species assemblage from initial diatom counts. By incorporating stable isotope analyses, the aim was to address questions regarding the driving mechanisms of such change in surface productivity, specifically the role of different water masses (circumpolar deep water versus shelf waters) in the Marguerite Bay region; a theory proposed as a possible causal mechanism for the collapse of George VI Ice Shelf in the Early Holocene (Smith et al., 2007a). Core VC243 was chosen because it has been used in a number of previous investigations, reconstructing the PGC Ice Shelf history through the Holocene (Pudsey and Evans, 2001; Pudsey et al., 2006). By integrating stable isotope analyses additional information about oceanographic influences can be inferred.

Both cores were sampled at 10 cm intervals, which is an identical resolution to the diatom analyses (Table 5.1). Approximately 5 g of sediment was removed using a spatula and sealed in Whirlpack™ bags.

5.2.2 Sample preparation

Sediment samples from core VC306 were treated in the bulk, raw state to measure nitrogen isotopes, then decarbonated to analyse carbon. In comparison, measurement of both carbon and nitrogen isotopes in core VC243 were made on decarbonated samples. It is believed that decarbonation, if too harsh, can slightly enrich $\delta^{15}N_{org}$ values (X.

Crosta, pers. comm.) [It is worth noting that for the core VC243 decarbonation was relatively smooth, suggesting that the sediments contained very little carbonate.]

Raw sediment samples were oven dried overnight (60 °C) and ground into a fine powder using a pestle and mortar to break clumps and homogenise the sediment. Initial measurements of nitrogen isotopes for core VC306 were undertaken at this stage (using the set-up described below). Further decarbonation steps were performed on the bulk dry sediment, using 10 % HCl. When the sample stopped effervescing (10 – 15 minutes), acid was removed by successive centrifuge cycles with de-ionised water. The sediment was dried again in the oven overnight and crushed to obtain a homogeneous powder. This powder was analysed for carbon isotopes in core VC306 and nitrogen and carbon isotopes in core VC243.

The sediment was packed and sealed into a pre-weighed tin foil capsule (5 mm x 9 mm). Approximately 20 mg and 5 mg are required for measurement of $\delta^{15}N_{org}$ and the $\delta^{13}C_{org}$, respectively, although the sediment weight was increased for terrigenous-rich sediments (> 60 mg and < 15 mg). The majority of the samples were re-run to check the reproducibility of measurements. The standard errors are ~ 0.3 ‰ for the $\delta^{15}N_{org}$ and 0.01% for N_{org}, 0.2 ‰ for $\delta^{13}C_{org}$ and 0.1% for C_{org} (X. Crosta, pers. comm). Isotope measurements were compared to reference standards. The standards used in the EPOC laboratory are Acetanilide (0.4 – 0.45 mg), Glycine (0.3 mg) and Casein (0.35 – 0.4 mg), which have isotopic values bracketing the C_{org} and N_{org} isotopic ratio values of the sediments.

5.2.3 Data collection and format

Isotopic measurements of bulk organic matter were performed using a NC2500 CARLO-ERBA chemical analyser in line with a Micromass OPTIMA-IRMS stable isotope ratio mass spectrometer.

5.2.4 Data analysis

Three outputs from stable isotope analysis are assessed in this investigation: C_{org} content and N_{org} content (both expressed as %); the ratio of C_{org} to N_{org} (abbreviated to C_{org}/N_{org}); and $\delta^{13}C_{org}$ and $\delta^{15}N_{org}$ (both expressed as ‰).

The main purpose for studying elemental carbon and nitrogen contents is to have insight into palaeoproductivity and nutrient utilisation histories, respectively. Further, the ratio of C_{org} to N_{org} gives an indication of the source of the organic matter and whether contamination has occurred. The average molar ratio of carbon to the two principal

nutrient elements in organic matter – nitrogen and phosphorous – is close to 106:16:1 (C:N:P) and this is the basic Redfield ratio (Redfield et al., 1963). Deviation away from the Redfield value implies that consumption, decomposition, recycling of organic particles or contamination from terrigenous sources has occurred (see Chapter 4.1.3 for further details). C_{org} to N_{org} contents of the sediment samples were measured simultaneously with the isotopic ratios by integrating the voltage of the main ion beam.

For convenience, the small but robust nature of variations in the stable isotopic compositions of low-mass (light) elements such as carbon and nitrogen, are normally reported as delta (δ) values in parts per thousand (denoted as ‰) enrichments or depletions relative to international standards. All results were reported versus Pee Dee Belenmite (PDB) for carbon and versus Air for nitrogen. Standardisation enables inter-comparisons to be made between samples. Calculation of $\delta^{13}C_{org}$ and $\delta^{15}N_{org}$ is achieved using Equation 6.3 and Equation 6.4, respectively. A positive δ value means that the sample contains more of the heavy isotope than the standard; a negative δ value means that the sample contains less of the heavy isotope than the standard. For example, a $\delta^{15}N_{org}$ value of +30 ‰ means that there are 30 parts per thousand or 3 % more ^{15}N in the sample relative to the standard.

Equation 5.2 $\delta^{13}C_{org}$ calculation.

$$\delta^{13}C\ ‰ = [(^{13}C/^{12}C \text{ sample} - {}^{13}C/^{12}C \text{ standard}) / (^{13}C/^{12}C \text{ standard})] \times 1000$$

Equation 5.3 $\delta^{15}N_{org}$ calculation.

$$\delta^{15}N\ ‰ = [(^{15}N/^{14}N \text{ sample} - {}^{15}N/^{14}N \text{ standard}) / (^{15}N/^{14}N \text{ standard})] \times 1000$$

There are several commonly used conventions for making comparisons between the δ values of two materials:

- higher vs. lower values
- heavier vs. lighter (the "heavier" material is the one with the higher δ value)
- more/less positive vs. more/less negative (e.g. -10‰ is more positive than -20‰)

- enriched vs. depleted, although it is always necessary to state what isotope is in short supply (e.g. a material is enriched in ^{13}C or ^{12}C relative to some other material) and that the enrichment or depletion is a result of some reaction or process.

5.3 Sedimentary pigment analysis

Sedimentary pigments were identified in core VC243, from Prince Gustav Channel (PGC). All sample preparation, sediment extractions and High Performance Liquid Chromatography (HPLC) were undertaken by me at The University of York Chemistry Department, under the supervision of Dr Brendan Keeley and Matthew Pickering (PhD student).

5.3.1 Sampling strategy

Core VC243 was chosen for pigment analysis for a number of reasons. Firstly, the core has been used in a number of previous investigations, reconstructing the PGC Ice Shelf history through the Holocene (Pudsey and Evans, 2001; Pudsey et al., 2006) and the incorporation of a marine pigment dataset was designed to provide additional information on the ecological conditions that occurred during a known period of ice shelf retreat and reformation. For example, ice thickness and distribution could be inferred through changing productivity levels, associated with different groups of phototrophs from their pigment distributions and concentrations. Secondly, diatom analysis in core VC243 highlighted clear and dramatic down-core fluctuations in diatom flux. Important questions to address are whether these maxima in diatom flux coincide with significant peaks in other phototrophs and can pigments be used as an additional proxy for changes in total primary production, as suggested by Harris et al. (1996)?

Within core VC243, 20 samples were taken from upper 4 m of the core (Table 5.2). These sample depths took sediment below, through and above an interval of elevated diatom absolute abundance. Using a metal spatula, >12 g (wet weight) of sediment was removed from the core, taking care to avoid exposed sediment surfaces so that photo-induced degradation of the pigments was minimised. The sediment samples were placed in sterile Whirlpack^{TM} bags and stored in the dark, frozen at –20°C. The samples were transported frozen from BAS headquarters in Cambridge to the Organic Geochemistry Laboratory at The University of York.

Table 5.2 Pigment sample depths for core VC243.

Sample no	Sample interval (m)	Sample interval (average) (m)
1	0.11-0.14	0.125
2	0.21-0.23	0.22
3	0.45-0.46	0.455
4	0.62-0.64	0.63
5	0.86-0.87	0.865
6	1.10-1.11	1.105
7	1.3-1.31	1.305
8	1.50-1.51	1.505
9	1.65-1.66	1.655
10	1.9-1.91	1.905
11	2.10-2.11	2.105
12	2.3-2.31	2.305
13	2.50-2.51	2.505
14	2.7-2.71	2.705
15	2.95-2.96	2.955
16	3.20-3.21	3.205
17	3.4-3.42	3.41
18	3.60-3.61	3.605
19	3.75-3.76	3.755
20	4.00-4.02	4.01

Table 5.3
HPLC gradient elution program employed for total extract analysis (Method A, Airs et al., 2001).

Time (min)	% ammonium acetate (0.01 M)	% methanol	% acetonitrile	% ethyl acetate
0	5	80	15	0
5	5	80	15	0
100	0	20	15	65
105	0	1	1	98
110	0	1	1	98
115	5	80	15	0

5.3.2 Sample preparation

Glassware was prepared by soaking overnight in a 1% solution of Decon90™ followed by thorough rinsing under tap water, deionised water and finally analytical grade acetone. Pigments were extracted from the sediment using the methods described in Airs et al. (2001) and utilised by Squier (2003) and others. In all phases of the laboratory procedure, the sediment and extracts were manipulated in low light conditions to minimise photo-induced degradation.

To extract pigments, sediment was thawed in the dark and ~10 g of wet sediment was weighed into a plastic centrifuge tube and 20 cm^3 of analytical grade acetone was added. The sediment was sonicated for 10 minutes and subsequently centrifuged (5 minutes, 30,000 rpm, 2000 g). The supernatant (liquid) was extracted using a pipette and filtered into a round-bottomed flask, through DCM washed cotton wool to remove any insoluble residues. The solvent (acetone) was removed on a rotary evaporator to leave the dry pigments in the flask. The extraction procedure was repeated until a colourless supernatant was obtained (up to a maximum of 10 extractions) and each extraction was combined in the round-bottomed flask, to be subsequently dried by a rotary evaporator. Dried extracts were re-dissolved in a small amount of acetone (~ 2 ml) and transferred to a glass vial. Acetone was removed under a slow stream of nitrogen gas and the dry pigment sample was stored at –20°C. To prolong the storage life and prevent degradation of the sample, extracts were treated with a solution of diazomethane (prepared by Matthew Pickering, using the method and appropriate safety precautions of Black, 1983), which acts to methylate any free acid groups. The sediment from which the pigments were extracted was left to dry in the air, weighed and stored in Whirlpack™ bags at –20 °C.

5.3.3 Data collection and format

The samples were prepared for HPLC by re-dissolving the dry pigments in 200 µl of analytical grade acetone, transferred into glass vials and loaded into an autosampler carousel. Extracts were injected (20 µl) and analyses were performed with a 115 minute gradient elution programme that is detailed in Table 5.3. HPLC was performed using a Waters (Milford, MA USA) HPLC system comprising a 717 autosampler and 996 photodiode array detector. Instrument control, data processing and analysis were performed using Waters Millennium software (Millennium[32]). A solvent system comprising methanol, acetonitrile, ethyl acetate and 0.01M ammonium acetate solution was used in all HPLC separations (Airs et al., 2001). All solvents used were HPLC

grade or of the highest analytical grade available. Solvents were degassed using a Phenomened Degasex DG-4000 vacuum degasser. Separation of the components in the extract was achieved using two Waters Spherisorb ODS2 columns (150 x 4.6 mm; 3 μm; Elstree, UK) coupled in series and a flow rate of 0.7 ml min^{-1}. UV/Vis absorbance was determined using Hitachi U-3000 spectrophotometer with slit width of 2 nm, cell path length of 1 cm and scanning in the 350-800 nm range.

The principle of reverse-phase HPLC is that analytes are separated based on their polarity. The stationary phase (column packing) is non polar and the mobile phase (eluent) is polar; consequently individual components are retarded by the stationary phase differently and separate from each other while they are travelling at different speeds through the column with the eluent (Skoog et al., 2000). More polar / hydrophilic components interact strongly with the mobile phase and consequently elute first, whereas less polar / hydrophobic components prefer the greasy C-18 carbon chains on the stationary phase and subsequently elute later. The solvent composition (Table 5.3) changes from polar to less polar over the course of the run to get all components through the column in a reasonable time. The time each component takes to pass through the column is termed the retention time (t_R) (minutes). The output data from the HPLC included UV-Vis spectrum index plots, detailing retention times and peak area, for each individual pigment detected and a chromatogram (Figure 5.11), where the area under the pigment peaks is linearly related to their concentration.

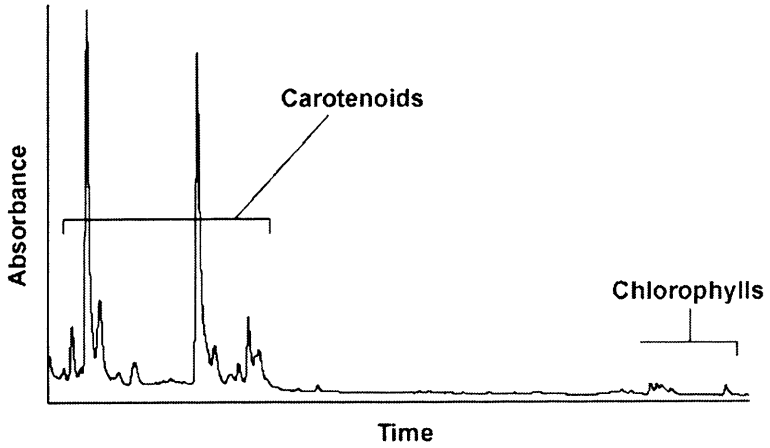


Figure 5.11
Example chromatogram, with the relative elution times of carotenoids and chlorophylls shown on the *x*-axis, and relative absorbance on the *y*-axis.

A series of standards were prepared and run in tandem with HPLC analysis of the sediment extracts. These standards were prepared using a stock standard solution containing an equimolar amounts of chlorophyll *a*, phaeophytin *a*, and phaeophorbide *a* in acetone. Absolute amounts were determined by UV/vis spectroscopy using molar absorption coefficients: chlorophyll *a* ε_{662}= 7.88×10^4 l mol^{-1} cm^{-1}; phaeophytin *a* ε_{667}= 4.45×10^4 l mol^{-1} cm^{-1}; phaeophorbide *a* ε_{667}= 4.40×10^4 l mol^{-1} cm^{-1} (obtained from Jeffery and Humphrey, 1975) before mixing. A sequence of serial dilutions were then carried out on the stock solution to produce 6 solutions at 100 %, 75 %, 50 % 25 %, 12.5 % and 6.25 % strength. 100 µl aliquots of each solution were divided into sample vials and acetone removed under a gentle stream of nitrogen. One of each of the 6 standard strengths was reconstituted in 100 µl of acetone and run using Method A (Airs et al., 2001) (injection volume 20 µl). This allowed a standard curve to be constructed for chlorophyll *a*, phaeophytin *a* and phaeophorbide *a*. The concentrations of pigments in sediment samples could then be determined from the standard curve of its respective standard (or the standard it shares the closest structural similarity with).

Generally, the analytical procedure shows very good reproducibility between HPLC runs (Airs, 2002) and samples are not usually re-run. The only inherent error occurs at lower pigment concentration, as the signal to noise ratio becomes greater leading to more inaccuracy in integrations and the quantification of absolute abundance. This was addressed for core VC243 by using a larger initial sediment sample weight (> 12 g) than previous sedimentary pigment studies, resulting in a corresponding increase in extracted pigment concentration. Coelutions (where two or more components elute from the column at the same time) can also affect integrations, rendering identification and quantification problematic.

Liquid Chromatography Mass Spectrometry (LC-MS) was used in tandem with photodiode array detection to aid in the identification of a number of pigments in core VC243. This method was employed because some components show indistinguishable or very similar UV-Vis spectra and retention times. LC-MS provides a lot more security in pigment assignments, through its ability to select and fragment individual ions. LC-MS was performed using a Finnigan (San Jose, CA, USA) system comprising a Thermo Separations AS3000 auto-sampler, P4000 gradient pump, UV2000 UV-Vis detector (Thermo Quest, Hemel Hempstead, UK) and a Finnigan MAT LCQ ion trap mass spectrometer equipped with an Atmospheric Pressure Chemical Ionization (APCI)

source operated in the positive ion mode. Ion traps function by temporal separation; increasing the amplitude of the radio frequency (R*f*) voltage destabilises the trajectories of the trapped ions and they are ejected from the trap (Squier, 2003). Ions are scanned out of the trap and detected according to their mass/charge (*m/z*) value. Instrument settings were as follows: capillary temperature 150°C, APCI vapouriser temperature 450°C, discharge current 5 μA, sheath gas flow 60 (arbitrary units). On-line demetallation of chlorophylls in LC-MS was achieved by introducing methanoic acid (98 %) into the eluent flow post-column at a rate of 5 μL min^{-1} via a syringe pump (Hamilton 1750 fixed needle syringe, Waters, Watford, UK). Demetallation following separation is advantageous because the chromatographic properties of the metallated and free-base components are retained, providing retention times and abundance information, while also enhancing the sensitivity of the detection of the metallated components (Airs and Keeley, 2000).

5.3.4 Data analysis

Pigments were identified on the basis of their retention time, UV-Vis spectra and mass. These were compared with previously published data (e.g. Airs et al., 2001; Jeffrey et al., 1997). Pigment relative abundances were calculated from the peak areas on the chromotograms, standardised to sample dry weights. The majority of components were plotted as peak areas (microabsorbance/second; μAUs), together with the ratios between different pigments. For several pigments, absolute concentrations (mol dm^{-3}) were calculated using calibration lines. Individual pigment abundance and concentration were compared between sample depths to provide information on stratigraphic variability. Several compounds were grouped during data analysis (e.g. native vs. degradation products) providing more general information about overall biological, chemical and physical processes that have operated either at or since the time of sediment deposition.

5.4 Chapter summary

This chapter has presented methods used in the investigation of AP marine sediment cores; quantitative diatom analysis, nitrogen and carbon isotopes on bulk organic material, and sedimentary pigments.

6 Core material and chronology

This chapter provides a description of the core sedimentary material and chronological controls. The core locations are shown in Figure 6.1, with place names referred to in the text highlighted. The regional setting of each core has previously been reviewed in Chapter 2.

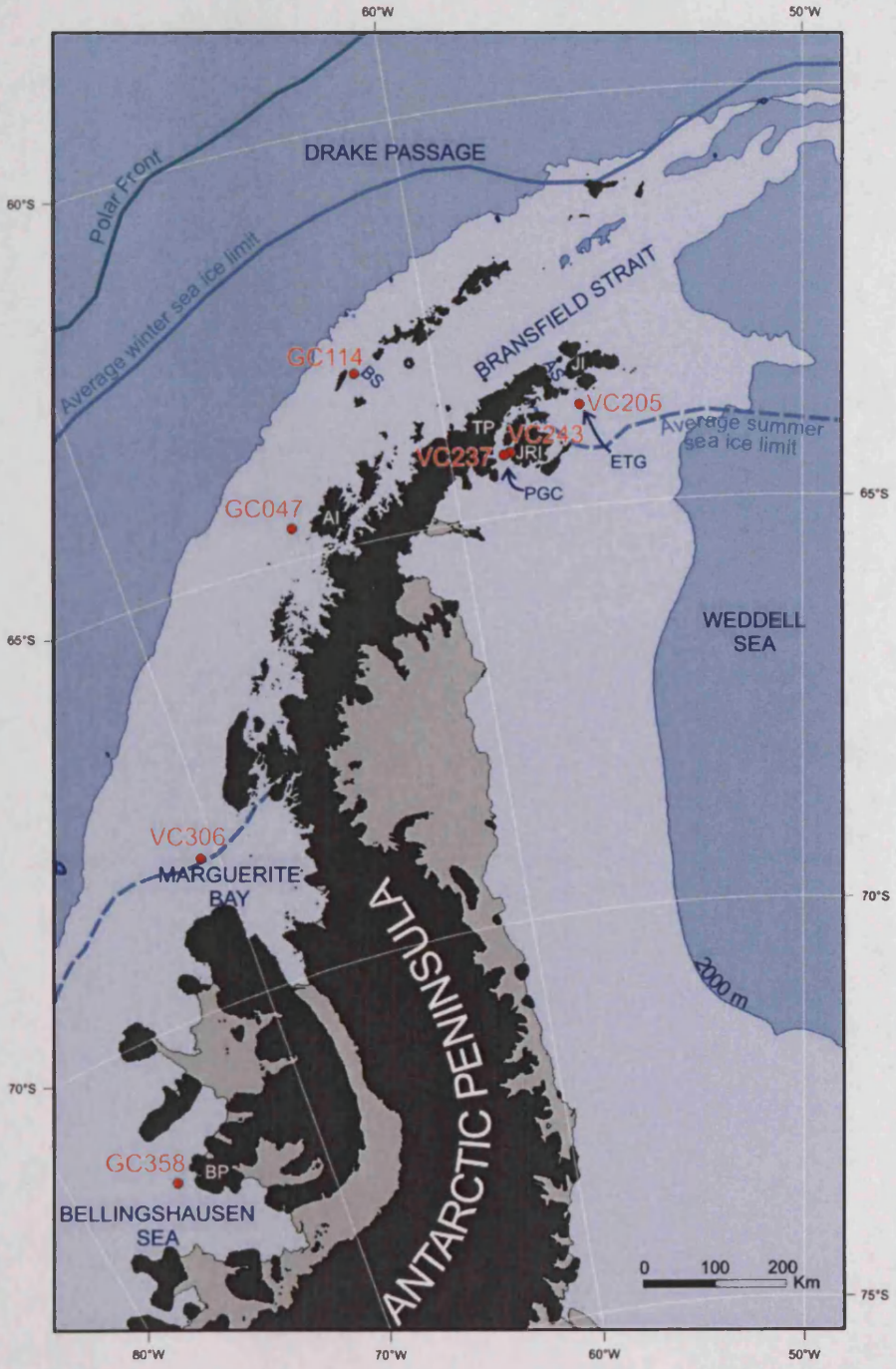


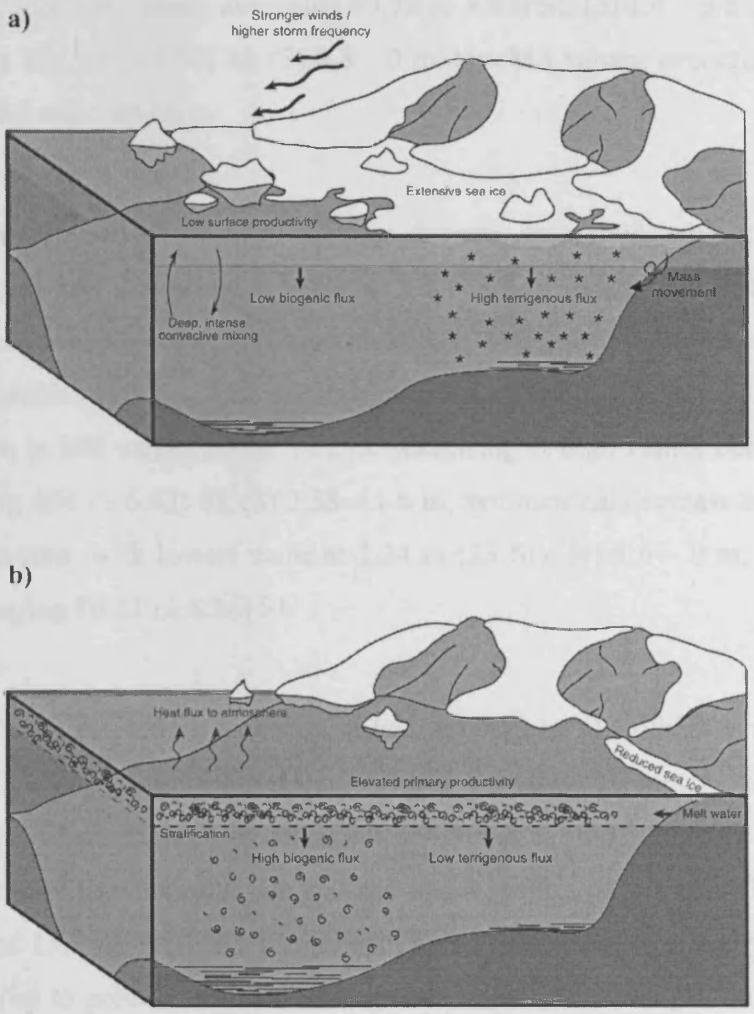
Figure 6.1 Map of the Antarctic Peninsula, showing core localities, together with the position of the present day average summer and winter sea ice limits and Polar Front (cf. Figure 2.9). AI = Anvers Island; AS = Antarctic Sound; BP = Beethoven Peninsula; BS = Boyd Strait; ETG = Erebus and Terror Gulf; JI = Joinville Island; JRI = James Ross Island; PGC = Prince Gustav Channel; TP = Trinity Peninsula.

6.1 Core material

6.1.1 Antarctic marine sediments

The Antarctic continental shelf includes a wide range of glacial-marine environments, which result in deposition of an equally diverse range of marine sediments. The Holocene sediments analysed in this investigation were deposited in seasonal sea ice, glacio-marine, pro-glacial and sub-ice shelf environments along the AP. The sediments comprise draped units which blanket the irregular, glacially scoured underlying surfaces (Anderson, 1999). In ice-dominated (typically nearshore) environments, ice-rafting, aeolian and mass movement events are the dominant sediment transport processes, delivering large amounts of terrestrially-derived material (Figure 6.2a); whereas in more ice-free environments, high levels of primary productivity mean that the dominant flux to the sediments is biogenic (Figure 6.2b). The resulting spectrum of sediment types includes: (1) glacio-marine sediments (>10 % ice-rafted debris); (2) terrigenous silt and clay (<10 % ice-rafted debris or biogenic silica); (3) distinctively olive green siliceous mud (10 – 30 % biogenic silica) and siliceous ooze (>30 % biogenic silica), with only small quantities of ice-rated debris (usually <10 %) (Dunbar et al., 1989; Anderson, 1999). Diatoms form the dominant source of biogenic siliceous material and can constitute a significant portion of the sediment; 10 – 30 % and >30 %, resulting in the respective descriptive names "diatomaceous mud" and "diatomaceous ooze" (Anderson, 1999).

Details of the sedimentary character of each of the cores examined in this investigation are presented in section 6.1.2 to 6.1.8, in the form of sediment logs and magnetic susceptibility (MS) plots. MS is a proxy for the stratigraphic variations in the relative inputs of terrestrial and biogenic sediments. High (low) MS values typically correspond to high (low) terrigenous and low (high) biogenic content. Using this principle, magnetic susceptibility plots have been widely used to reconstruct changes in depositional environments, specifically variations in terrigenous and biogenic sediment inputs (e.g. Domack and Ishman, 1992; Leventer et al., 1996; Kirby et al., 1998; Domack et al., 2001).



(adapted from Shevenell and Kennett, 2002)

Figure 6.2
Schematic representation of sediment delivery and sources in:

a) Terrigenous-dominated regimes, with ice-rafting, aeolian and mass movement events forming the dominant sediment transport processes;
b) Biogenic-dominated regimes, with high levels of surface water primary productivity and transmission to the sediments.

6.1.2 GC114

Core GC114 comprises 3.35 m of diatomaceous mud, with discrete volcanic ash horizons (between 3.02 – 3 m and 0.13 – 0.11 m) (Figure 6.3). Other notable features include faint bioturbation at 1.4 m and between 1 – 0.6 m and monosulphidic knots / patches between 2 – 1.65 m. Increased sulphur content in other AP marine cores have been found to be coincident with total organic carbon maximum, suggesting the occurrence of bacterial degradation (Yoon, 1999; Yoon et al., 2002). The MS record (Figure 6.3) shows a moderately noisy signal, although three units can be highlighted:

(1) 3.35 – 1.6 m, mid MS values, averaging 90.78 (± 8.81) SI; (2) 1.6 – 0.8 m, high MS values, averaging 105.08 (± 6.57) SI; (3) 0.8 – 0 m, low MS values, averaging 84.63 (± 13.2) SI, which decrease up-core.

6.1.3 GC047

Core GC047 is composed of 3.8 m of uniform diatomaceous mud, with a sub-unit of interlaminated mud and diatom ooze between 3.8 – 3.5 m (described on the original sedimentary log as "rainbow core") (Figure 6.4). The MS record demarcates a number of stratigraphic units: (1) 3.8 – 3.22 m, very low MS, averaging 6.16 (± 4.14) SI; (2) dramatic increase in MS values above 3.22 m, stabilising at high values between 3 and 2.58 m, averaging 104 (± 6.62) SI; (3) 2.58 – 1.6 m, symmetrical decrease and increase in MS values up-core, with lowest value at 2.24 m (33 SI); (4) 1.6 – 0 m, stable, mid MS values, averaging 80.31 (± 8.36) SI.

6.1.4 VC306

Core VC306 is 5.94 m in length and is described in detail by Ó Cofaigh et al. (2005a), specifically grain size, sedimentary structures, bed contacts, geometry, sorting, clast shape and texture. Diatoms are only abundant above 1.8 m (Ó Cofaigh et al., 2005a); therefore the focus of this investigation was the upper section of this core (Figure 6.5). Between 1.99 and 1.62 m, there is a prominent unit of grey massive gravelly clay, with abundant clasts (up to pebble size) and average MS value of 124.42 (± 24.02) SI. This pebbly unit grades upwards into a unit of olive-grey massive, bioturbated diatomaceous mud, with dispersed coarse grained material. Bioturbation is evident between 1.52 – 1 m and 0.2 – 0 m. MS values gradually decrease up-core, from >70 SI below 1.62 m to low values averaging 37.38 (± 6.73) SI between 1 and 0 m (Figure 6.5).

6.1.5 GC358

Core GC358 is 0.94 m in length, composed of a unit of gravely sandy mud between 0.94 – 0.79 m (MS >28 SI), overlain by diatomaceous mud between 0.79 – 0 m (Figure 6.6). The MS record for the upper mud unit can be divided into two intervals: (1) 0.7 – 0.4 m, stable mid MS values, averaging 23.5 (± 1.02) SI; (2) 0.4 – 0 m, low MS values decreasing up-core, from 23.8 SI at 0.38 m to 10.2 SI at 0.03 m.

6.1.6 VC243

Core VC243 comprises a 5.86 m unit of diatom-bearing silty clay (Pudsey and Evans, 2001; Pudsey et al., 2006). Using the sedimentary log and MS record (Figure 6.7), VC243 can be divided into a number of sub-units: (1) 6 – 1.87 m, silty clay, typically

clast-poor to clast-free; intermittent horizons of bioturbation (burrows infilled by black organic material) and sporadic diffuse, planar laminations; MS averaging 16.13 (± 3.21) SI; (2) 1.87 – 0.65 m, massive clayey silt, rare small dropstones, which increase in frequency upwards from 1.4 m, occasional burrows; MS averaging 14.65 (± 1.63) SI; (3) 0.65 – 0.5 m, distinct horizon with pronounced concentration of clasts; MS averaging 24 (± 1.85) SI; (4) 0.5 – 0 m, massive clayey silt, no dropstones observed, lack of mottling (implying no bioturbation) and lamination; MS averaging 13.64 (± 1.33) SI.

Previously published petrographic clast provenance analysis (Pudsey et al., 2006; Figure 6.10) revealed a very clear stratigraphic signal of changing ice-rafted debris source areas. The lower part of VC243 records higher abundance of Trinity Peninsula plutonic rocks and phyllites, peaking between 4 – 3 m, whereas the upper part of the core is dominated by fresh James Ross Island volcanic rocks (Pudsey and Evans, 2001). The observation of ice-rafted debris from the opposite side of the PGC (Trinity Peninsula) was used to infer the disappearance of the ice shelf and seasonally open marine conditions in the channel, enabling icebergs carrying debris from different sources to drift freely over the site (Pudsey and Evans, 2001). Based on this evidence, the ice shelf was considered absent over core site VC243 between 5350 – 1930 ^{14}C years BP (Pudsey et al., 2006).

6.1.7 VC237

Core VC237 comprises a 6 m unit of diatom-bearing silty clay (Pudsey et al., 2006) (Figure 6.8), similar in character to core VC243. Throughout the core, bioturbation is common, as are small quantities of poorly sorted gravel sized clasts (dropstones). Increased concentrations of gravel sized clasts are particularly obvious between: 5.68 – 5.56 m; 5 – 4.55 m; and 2.62 – 2.5 m. The MS record shows significant variability between 6 – 1.97 m, with two broad peaks of high MS values centred at 4.73 m (33 SI) and 3.21 m (26 SI), together with an additional spike at 2.05 m (24 SI). Up-core of 1.97 m, MS values are stable, averaging 14.33 (± 1.07) SI.

Similar to core VC243, core VC237 provides clear evidence for changing supply of ice-rafted debris from either side of PGC (Figure 6.10). Pudsey et al. (2006) observed that the lowest 1.2 m (core depth 6 – 4.8 m) and the uppermost 1 m contained almost entirely Trinity Peninsula derived fragments, whereas the middle part of the core contains a mixed ice-rafted debris assemblage. The presence of this mixed ice-rafted

debris was used to infer disintegration of the ice shelf and open water over core site VC237 between 9300 – 3500 ^{14}C years BP (Pudsey et al., 2006).

6.1.8 VC205

Core VC205 consists of 5.1 m of homogenous diatomaceous mud, with minor to moderate amounts of silts and fine sands (Figure 6.9). In the upper 3 m, small gravel sized clasts (dropstones) are common, associated with isolated lenses of fine sand. From the MS record (Figure 6.9), two units can be resolved: (1) 5.1 – 3.6 m, MS values are consistently low, averaging 22.32 (± 12.34) SI; (2) 3.6 – 0 m a "saw-tooth" MS pattern exists, composed of a dramatic increase (> 130 SI units) up-core of 3.6 m, followed by a gradual decrease (~ 90 SI units) between 3.4 – 1.2 m, followed by a second dramatic increase to ~140 SI above 1.2 m, followed by a second gradual decrease between 1 and 0 m (from ~140 – 70 SI).

Figure 6.3
Core GC114: Magnetic susceptibility curve and sedimentary log.

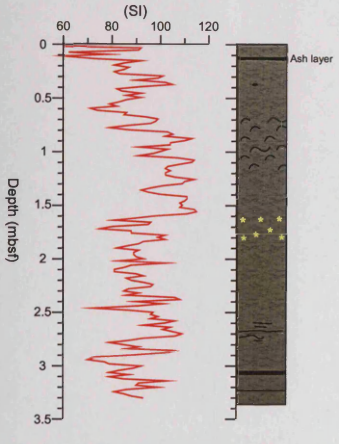


Figure 6.4
Core GC047: Magnetic susceptibility curve and sedimentary log.

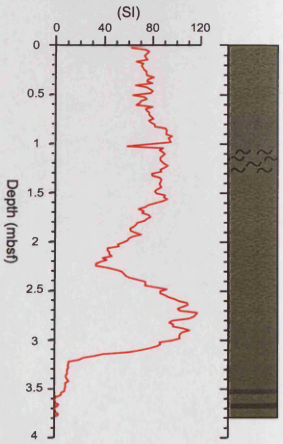


Figure 6.5
Core VC306: Magnetic susceptibility curve and sedimentary log.

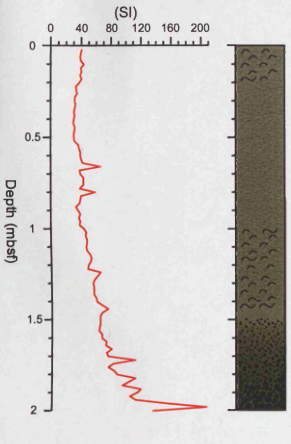


Figure 6.6
Core GC358: Magnetic susceptibility curve and sedimentary log.

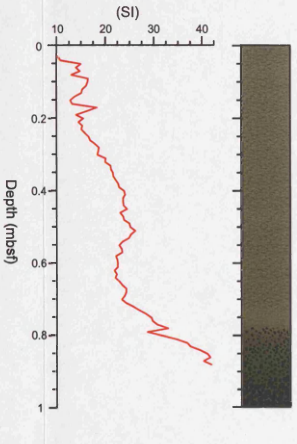


Figure 6.7
Core VC243: Magnetic susceptibility curve and sedimentary log.

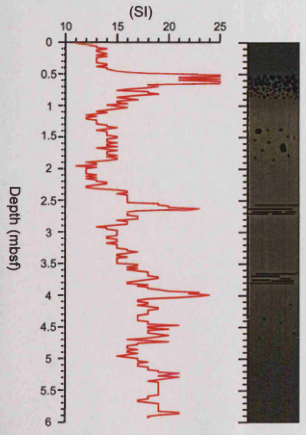


Figure 6.8
Core VC237: Magnetic susceptibility curve and sedimentary log.

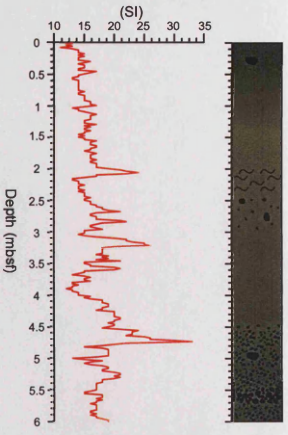
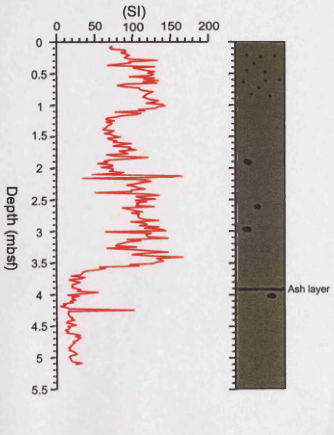
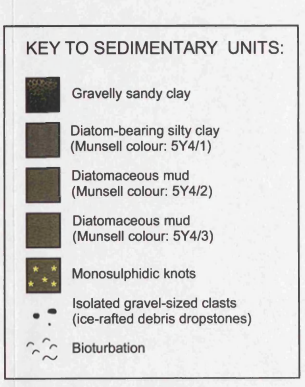


Figure 6.9
Core VC205: Magnetic susceptibility curve and sedimentary log.





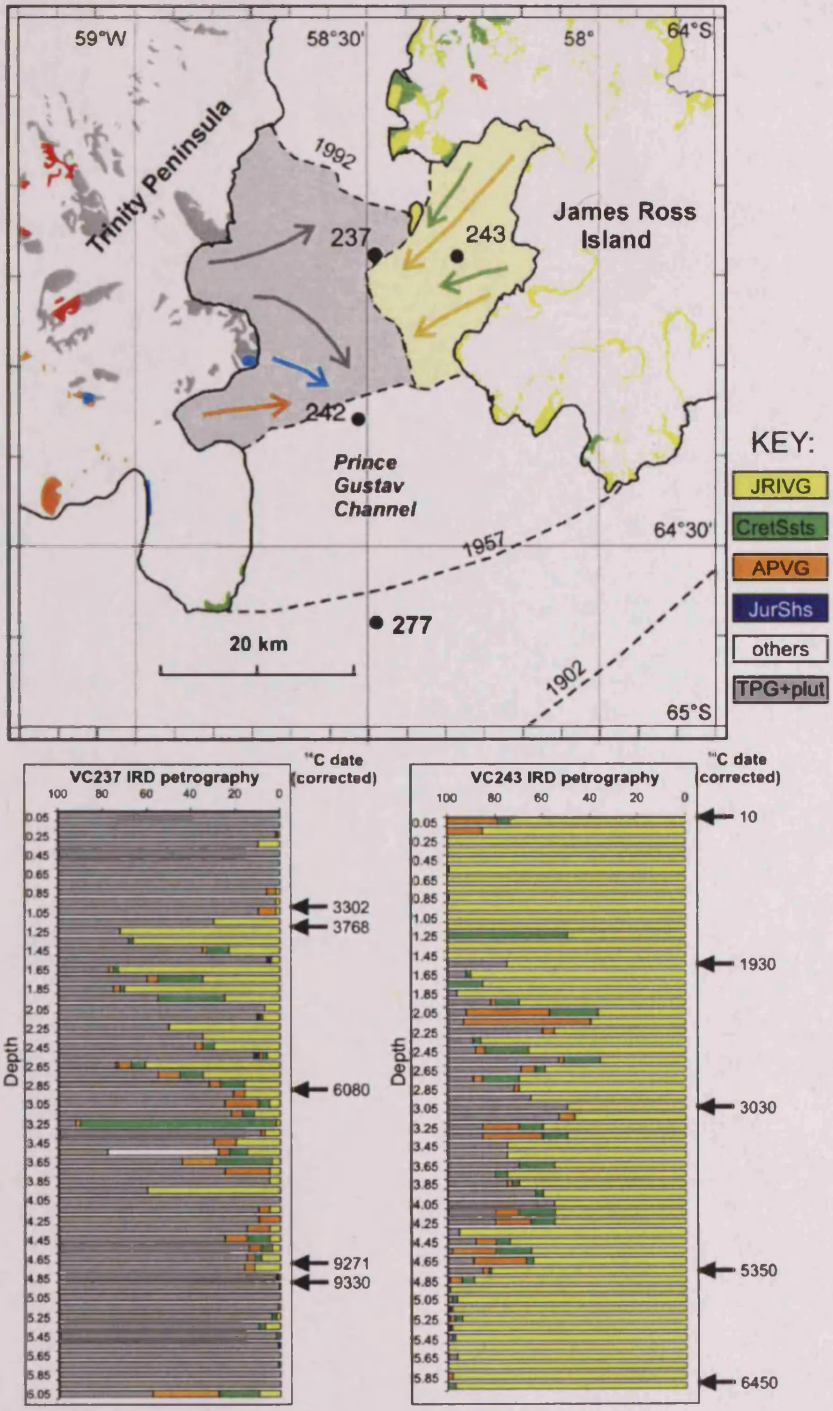


Figure 6.10
Geology of the areas adjacent to Prince Gustav Channel (PGC), with petrographic data from cores VC237 and VC243 (adapted from Pudsey et al., 2006). Grey indicates ice derived from Trinity Peninsula and yellow indicates ice derived from James Ross Island. Coloured arrows: suggested derivation of corresponding rock types. ^{14}C dates (corrected) as detailed in Table 6.3. Key to rock types: JRIVG = James Ross Island Volcanic Group; CretSsts = Cretaceous sandstones; APVG = Antarctic Peninsula Volcanic Group; JurShs = Jurassic sediments; TPG+plut = Trinity Peninsula Group, plus plutonic rocks. Intervals of mixed IRD occur mainly from 9300 – 3500 yrs BP in VC237 and from 5350 – 1930 yrs BP in VC243 (Pudsey et al., 2006).

6.2 Core chronology

6.2.1 ^{14}C dating

All the cores included in this investigation were ^{14}C-dated by accelerator mass spectrometry (AMS) on the acid-insoluble organic (AIO) carbon fraction. The advantage of this technology is that sediments containing only small amounts of organic carbon, which is often the case in Antarctic marine settings, can often yield accurate ages (Domack et al., 2001). The carbon is thought to be derived largely from marine phytoplankton, mainly diatoms (Harden et al., 1992; Pudsey et al., 1994; Pudsey and Evans, 2001). Uncorrected radiocarbon dates for all cores used in this investigation are presented in Table 6.1 and on a composite age-depth plot in Figure 6.11. The ^{14}C AMS dates were corrected for the difference in ^{14}C composition between the atmosphere and ocean surface – the reservoir effect (Bard, 1988). The scale of this correction varies geographically and temporally, mainly as a function of ocean circulation (upwelling and mixing of intermediate and deep waters) frontal positions and sea ice extent (Bard, 1988; Stuiver et al., 1991). The corrections applied to each core are discussed in sections 6.2.3 – 6.2.7.

Table 6.1
Uncorrected AMS radiocarbon dates on bulk organic carbon for all cores used in this investigation.

Core	Sample depth (m)	Laboratory code	Conventional Radiocarbon Age (^{14}C years BP ± 1σ)	Carbon content (% by wt.)	$\delta^{13}C$ (‰)
GC114	0.05	Beta - 213285	2620 (± 40)	N/A	N/A
GC114	0.75	SUERC-11836	2934 (± 35)	0.6	-26.0
GC114	1.25	-	3515 (± 38)	N/A	N/A
GC114	1.52	Beta - 213286	4230 (± 40)	N/A	N/A
GC114	1.99	-	4279 (± 39)	N/A	N/A
GC114	2.48	SUERC-11837	4669 (± 35)	0.5	-26.9
GC114	3.28	Beta - 213287	5980 (± 40)	N/A	N/A
TC046	0	[1]OxA-3249	1870 (± 70)	N/A	N/A
GC047	2.4	[1]OxA-3250	7780 (± 90)	N/A	N/A
GC047	3.6	SUERC-15254	12768 (± 76)	0.76	-22.8
GC047	3.79	[1]OxA-3251	12280 (± 150)	N/A	N/A

Core	Sample depth (m)	Laboratory code	Conventional Radiocarbon Age (^{14}C years BP ± 1σ)	Carbon content (% by wt.)	δ^{13}C (‰)
VC306	0	[2]OxA-13409	4560 (± 40)	1.54	-25.8
VC306	1.1	SUERC-16451	10041 (± 50)	0.7	-23.9
VC306	1.62	[2]OxA-13410	12010 (± 80)	N/A	-27.0
VC306	1.8	[2]OxA-13411	12610 (± 110)	N/A	-25.8
GC358	0	*Erl-10830	11246 (± 91)	N/A	-25.7
GC359	0	Erl-9304	5131 (± 50)	N/A	-25.8
GC358	0.245	Erl-10831	9570 (± 82)	N/A	-24.4
GC358	0.465	Erl-10832	13076 (± 95)	N/A	-24.8
GC358	0.735	Erl-10832	21433 (± 168)	N/A	-24.3
VC243	0.01	[3, 4]CAMS-68472	6010 (± 50)	0.9	-22.7
VC243	0.51	SUERC-15260	10984 (± 61)	0.7	-24.5
VC243	0.65	SUERC-15261	10767 (± 60)	0.7	-24.3
VC243	1.55	[3, 4]CAMS-68473	7930 (± 40)	0.9	-23.0
VC243	3.05	[3, 4]CAMS-68474	9030 (± 40)	0.9	-22.8
VC243	4.76	[3, 4]CAMS-68475	11350 (± 60)	0.8	-23.1
VC243	5.92	[3, 4]CAMS-68476	12450 (± 40)	0.7	-23.1
BC314	0	[4]AA-51695	6022 (± 40)	0.8	-24.6
VC237	1	[4]AA-50486	9302 (± 41)	0.8	-23.8
VC237	1.2	[4]AA-50487	9768 (± 43)	0.9	-24.2
VC237	2.9	[4]AA-50488	12080 (± 120)	0.6	-24.4
VC237	4.7	[4]AA-50489	15271 (± 75)	0.6	-24.6
VC237	4.9	[4]AA-50490	15330 (± 80)	0.7	-24.5
VC205	0	SUERC-16443	5234 (± 35)	1.0	-23.7
VC205	1.3	SUERC-16444	8354 (± 41)	0.8	-23.7
VC205	2.1	SUERC-16445	9590 (± 43)	0.6	-23.8
VC205	2.8	SUERC-16446	10280 (± 44)	0.7	-23.8
VC205	4	SUERC-16447	10669 (± 45)	0.8	-23.7
VC205	5.1	SUERC-16450	10798 (± 47)	1.0	-23.5

Dates marked ([1]) have been previously published by Pudsey et al. (1994); dates marked ([3]) by Ó Cofaigh et al. (2006); dates marked ([3]) by Pudsey and Evans (2001); dates marked ([4]) by Pudsey et al. (2006). Core top age for GC358 (*) is believed to be contaminated.

Laboratory codes: NSF-Arizona AMS Facility (**AA**); Beta Analytic Radiocarbon Dating Laboratory, Miami (**Beta**); Center for Accelerator Mass Spectrometry, Lawrence Livermore National Laboratory (**CAMS**); Erlangen AMS Laboratory, Germany (**Erl**); Oxford Radiocarbon Accelerator Unit (**OxA**); Scottish Universities Environmental Research Centre, East Kilbride (**SUERC**).

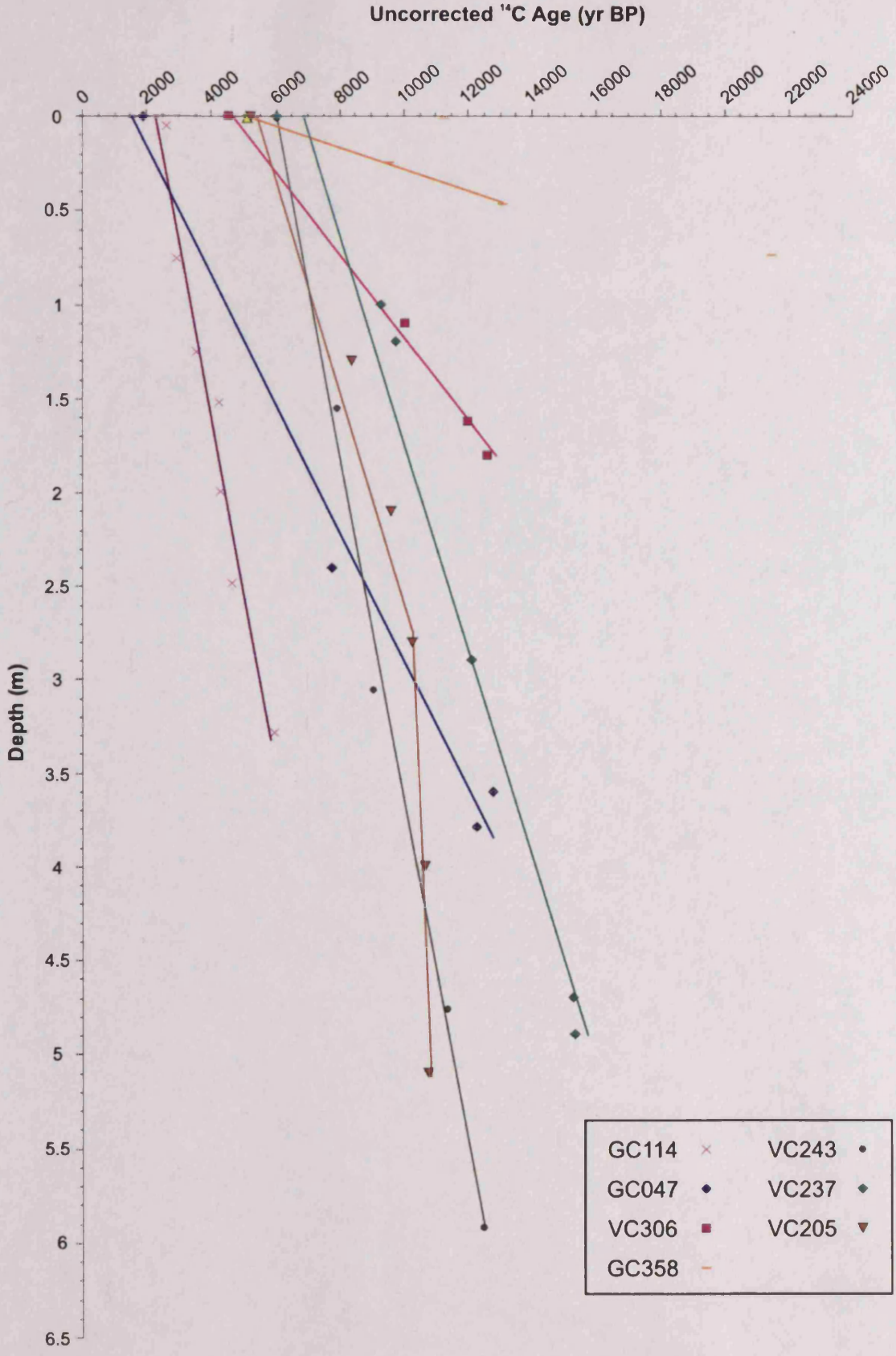


Figure 6.11
Composite uncorrected ^{14}C age-depth plot for all cores used in this investigation (Table 6.1). Error bars fall within the size of the point. Solid lines represent linear regressions. Yellow triangle is the core top age for core GC359, used as a chronological control for core GC358 (see section 6.2.5).

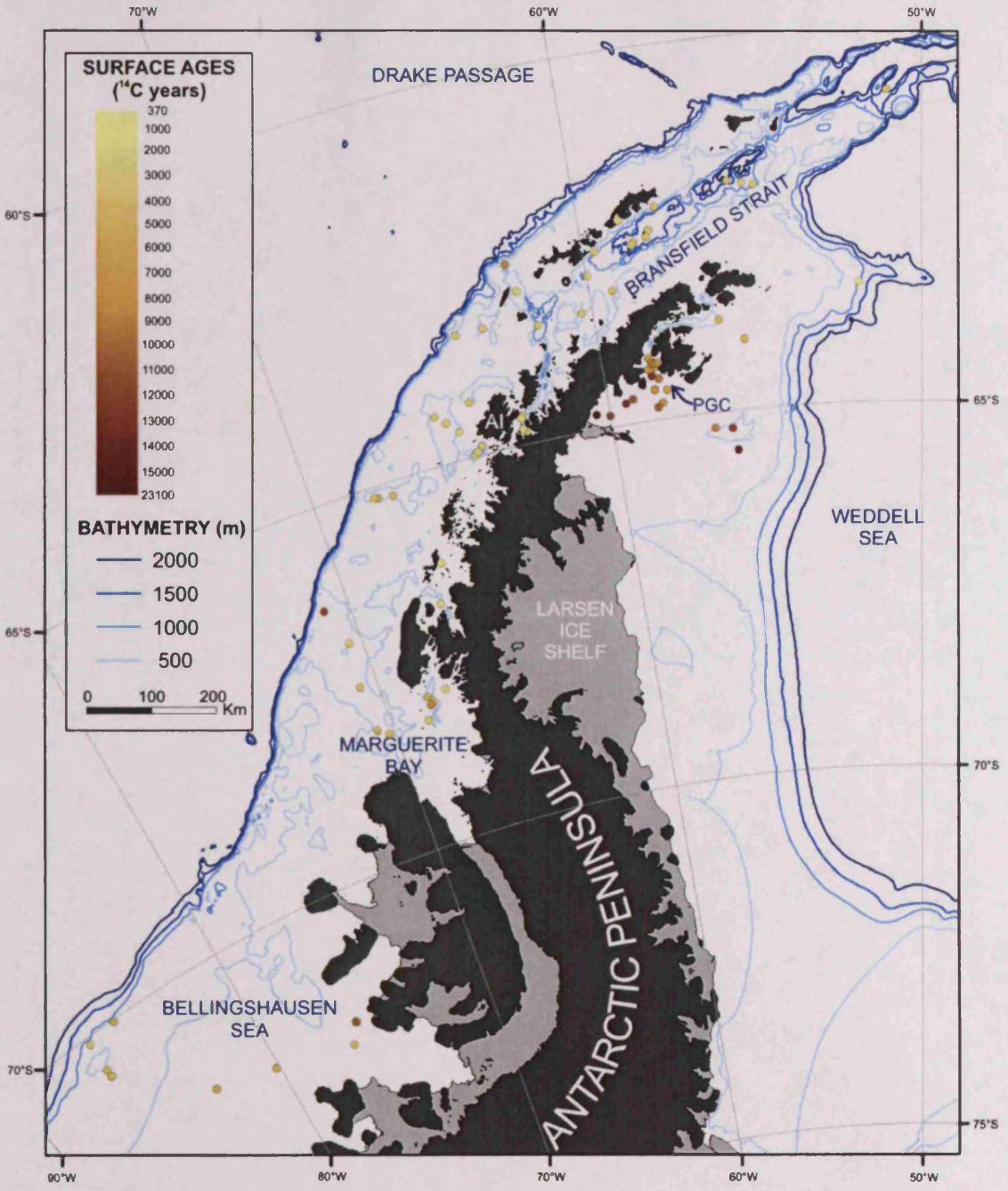


Figure 6.12
Map of AP showing published surface sediment ages. This provides information on the spatial variability of the Antarctic marine reservoir effect and local carbon contamination influences, discussed in sections 6.2.2.1 and 6.2.2.2 respectively. For more detailed information on the spatial variability in core top ages and data source information for: (1) WAP, specifically Bransfield Strait, Anvers Island (AI) and associated coastal localities, see Figure 6.13 and Table A2.1; (2) north WAP and EAP, specifically Bransfield Strait, Prince Gustav Channel (PGC) and Larsen A embayment, see Figure 6.14, Table A2.1 and Table A2.2; and (3) Marguerite Bay and southern Bellingshausen Sea, see Figure 6.15, Table A2.3 and Table A2.4.

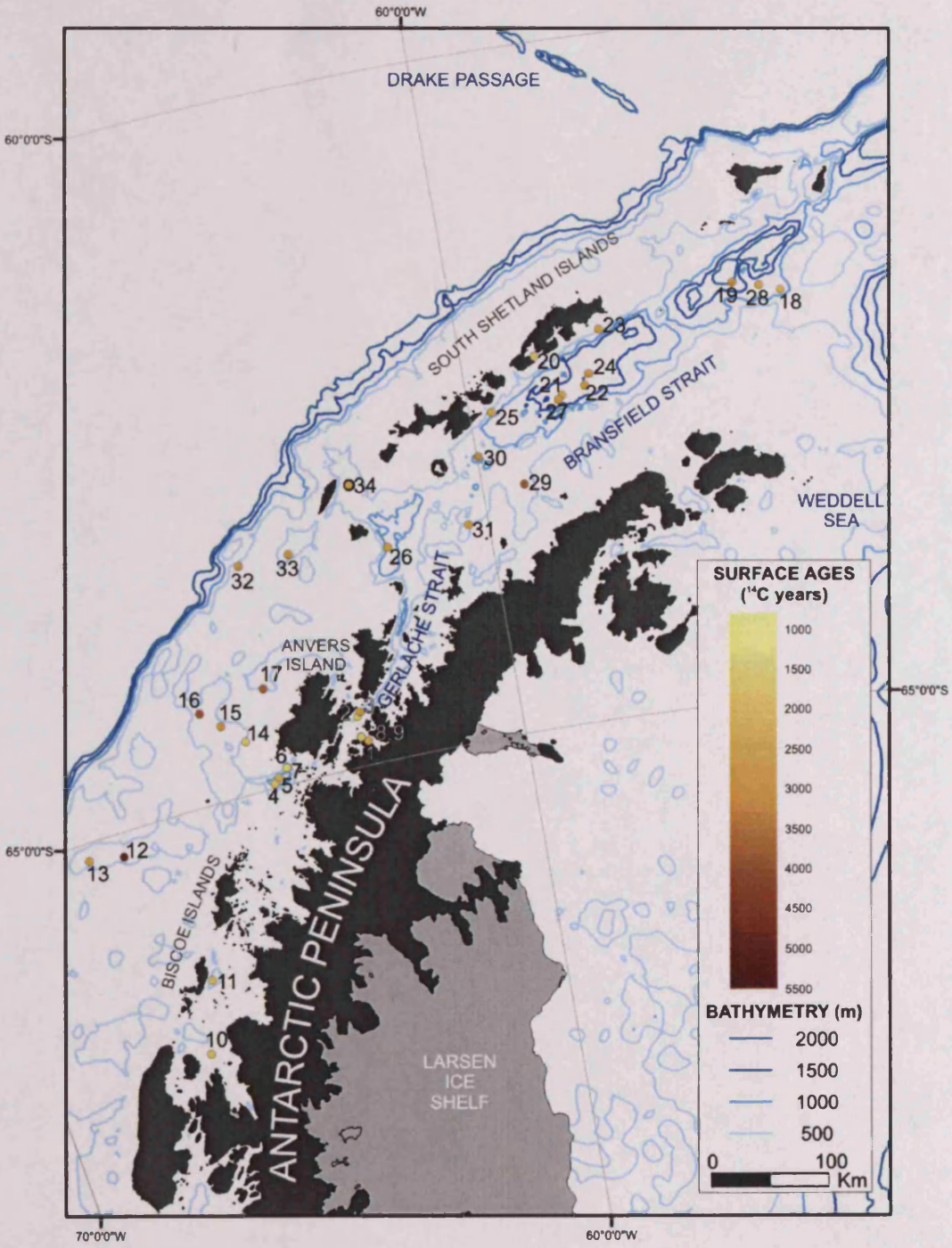


Figure 6.13
Map of WAP showing spatial variability in published surface sediment ages. Core numbering refers to Table A2.1, where details of publication, sample interval and conventional ^{14}C age the can be found.

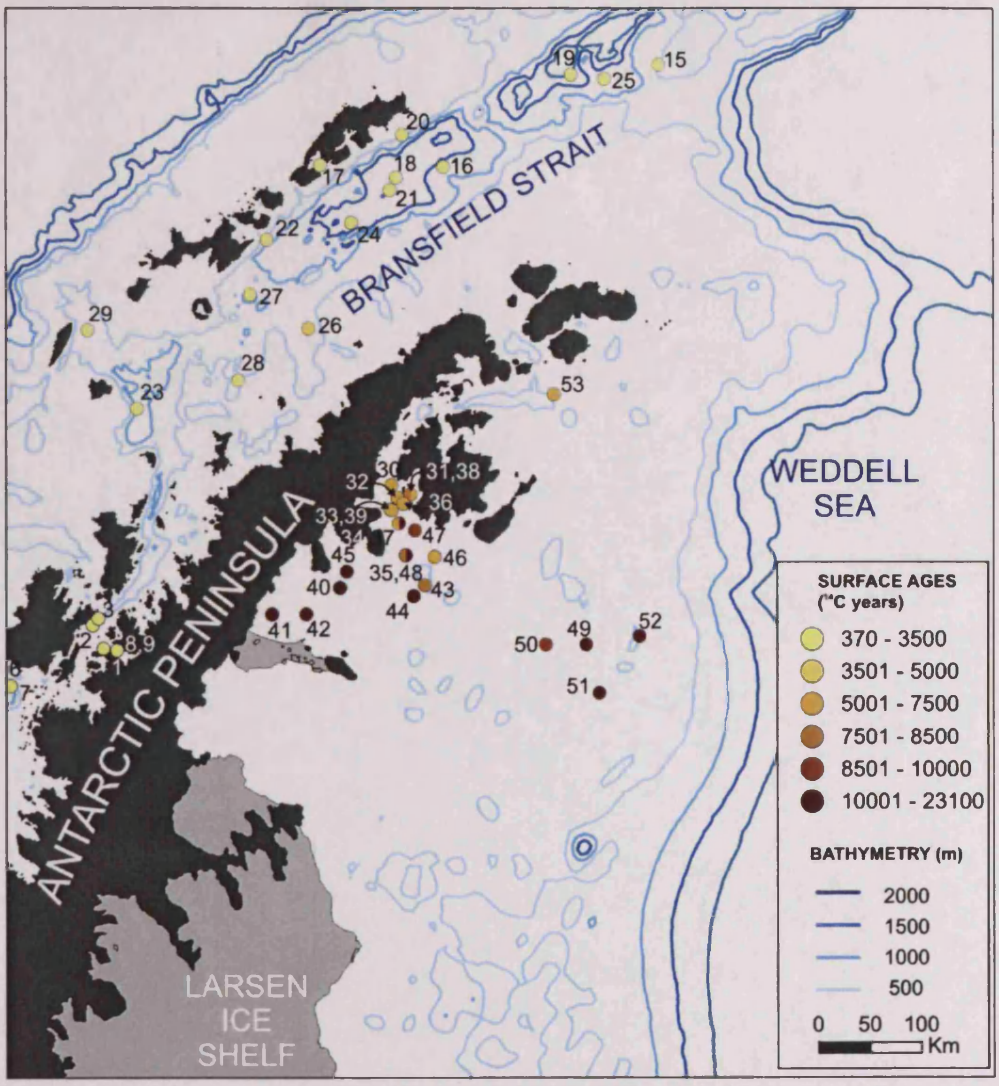


Figure 6.14
Map of north WAP and EAP showing spatial variability in published surface sediment ages. Note the surface age disparity between different sides of the AP; EAP marine cores exhibit significantly older surface ages than WAP cores. Core numbering refers to Table A2.2, where details of publication, sample interval and conventional ^{14}C age can be found.

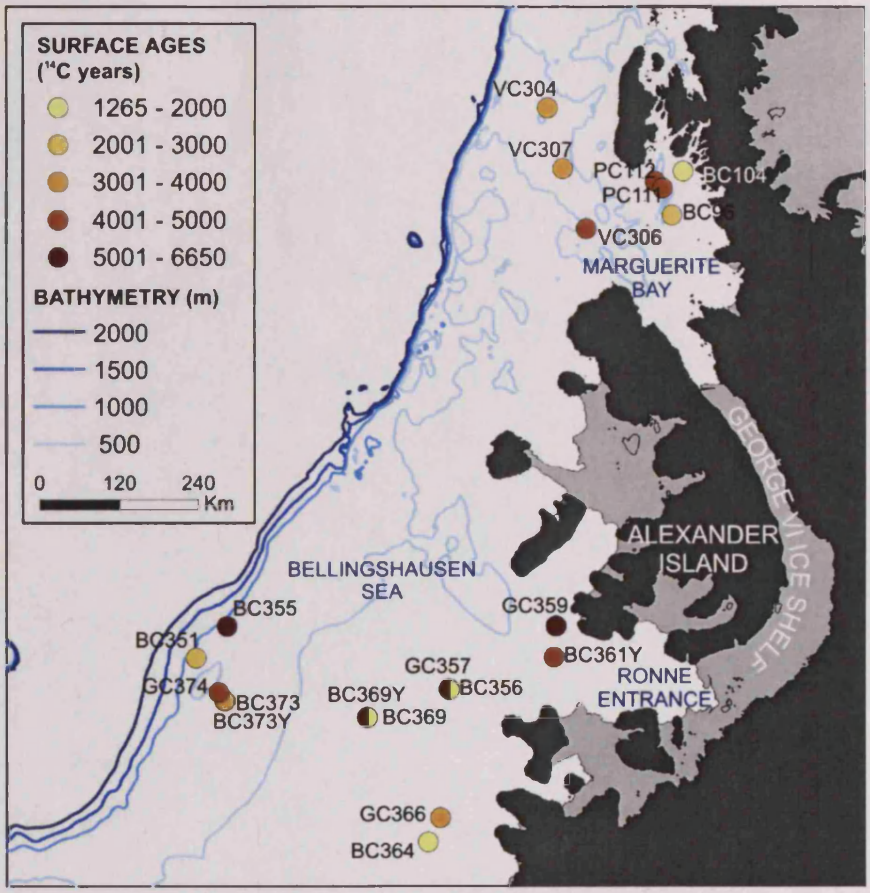


Figure 6.15
Map of Marguerite Bay and southern Bellingshausen Sea showing box (BC), vibro (VC) and gravity core (GC) surface sediment ages (Table A2.3 and Table A2.4, published in Harden et al., 1992; Ó Cofaigh et al., 2005a and unpublished from C.-D. Hillenbrand).

6.2.2 *Problems with ^{14}C dating in the Southern Ocean*

Accurate dating of Antarctic marine sediments remains one of the greatest challenges in palaeoenvironmental research, often limiting our ability to confidently assign leads and lags between proxies from different geographic areas. Erroneously old ^{14}C ages, in some cases by as much as a several thousand years, are frequently derived from carbonate material and AIO material in Antarctic sediments (Gordon and Harkness, 1992; Berkman and Forman, 1996; Andrews et al., 1999; Domack et al., 1999; Brachfeld et al., 2003). For example, radiocarbon dating of living Antarctic coastal molluscs yields average ages of 1100 – 1400 ^{14}C years (Stuiver et al., 1981; Björck et al., 1991; Gordon and Harkness, 1992; Berkman and Forman, 1996). Further, significant spatial variability exists in Antarctic surface sediment ages, as highlighted in Figure 6.11. For example, in semi-enclosed bay systems, channels and fjords surface sediment ages can be as high as 6000 ^{14}C years (Gerlache Strait: Domack, 1992; PGC: Pudsey and Evans, 2001; Pudsey

et al., 2006). The unusually old ages result from the local oceanographic conditions, together with terrestrial inputs of ancient carbon-rich material from the Antarctic continent and reworking of old marine carbon, and will now be discussed under the respective headings of reservoir age (section 6.2.2.1) and contamination (section 6.2.2.2).

6.2.2.1 Reservoir age

The age difference between the atmosphere and the surface ocean is termed the "apparent age" or "reservoir age" (Suess and Revelle, 1957; Craig, 1957; Bard, 1988). The reservoir ages of waters around Antarctica are particularly old due to the unique nature of Southern Ocean circulation and spatially highly variable due to regional differences in upwelling; inputs of depleted ^{14}C CO_2 from glacier meltwater; and sea ice capping through the occurrence of perennial ice cover (Omoto, 1983; Domack et al., 1989; Melles et al., 1994; Ingólfsson et al., 1998; 2004). These factors influencing the reservoir age of Antarctic coastal waters will now be discussed, although it needs stressing that large uncertainties are still associated with a number of these variables and quantifying their affect is difficult.

a) Southern Ocean circulation and regional differences in upwelling

Although there is rapid global mixing in the atmosphere (instantaneous) and terrestrial biosphere (years), mixing rates in the deep ocean are slow (millennia for global overturning circulation), so that radioactive decay becomes an important factor in the mixing between incoming modern carbon dioxide from the surface layers and outgoing old carbon dioxide from the deep layers (Bowman, 1990). As a consequence, deep ocean waters at the present day can show a radiocarbon age of a few millennia (Broecker and Peng, 1982). This is compounded in the Southern Ocean because circum-polar waters can remain out of contact with the atmosphere for extended periods, resulting in the continued decay and ageing of the carbon signal. From ocean-only models, Matsumato and Key (2004) propose that CDW influences natural ^{14}C abundance in the Southern Ocean, leading to $\delta^{14}C$ >200 ‰, which equates to >1400 conventional ^{14}C years. The subsequent upwelling of ^{14}C-depleted CDW at the Antarctic Divergence (see Chapter 2.4.1) brings inorganic carbon pools with old ^{14}C ages onto the Antarctic shelf. These carbon pools are utilised by living Antarctic marine organisms (including marine phytoplankton), which then record an apparent old age relative to the atmosphere (Stuiver et al., 1981; Björck et al., 1991; Gordon and

Harkness, 1992; Berkman and Forman, 1996). The circum-Antarctic reservoir age is variable, but typically 1230 – 1300 ^{14}C years (Berkman et al., 1998; Ingólfsson et al., 1998; 2004) and more specifically for the AP region, ~1260 ^{14}C years (Domack et al., 2001). Due to the paucity of carbonate microfossils, the chronology of the cores used in this investigation was generated by dating the AIO material in the sediment; it is assumed that the AIO material originates entirely from marine phytoplankton and consequently, if living marine organisms are utilising carbon pools with old ^{14}C ages, it follows that dates derived from their fossil counterparts will be comparably old too. Radiocarbon dating using AIO material is less desirable than carbonate because of unquantifiable contamination issues from inputs of old carbon (see section 6.2.2.2).

Regional differences in upwelling of CDW along the AP may account for some of the spatial variability in core top ages shown in Figure 6.12. Focusing on the WAP (Table A2.1 and Figure 6.13) and using this as a regional case study to exemplify the spatial variability in core top ages, a number of features can be highlighted:

- Youngest core top ages (<2000 ^{14}C years BP) are found closest to the western AP coastline (specifically the Palmer Deep basin and inland of the Biscoe Islands), with the exception of Gerlache Strait and associated fjords (<2760 ^{14}C years BP);
- With increasing distance offshore from Anvers Island, core top ages increase;
- Oldest WAP core top ages (>2100 years ^{14}C years BP) are located in Bransfield Strait.

These spatial patterns might provide clues as to the processes and carbon inputs that are affecting the ^{14}C concentration in these AP marine sediments. Several possibilities might explain the discrepancy between the proposed Antarctic reservoir correction (1230 – 1300 years) and the surface ^{14}C ages detailed in Table A2.1 and Figure 6.13, including variability in the reservoir effect and contamination. In this example from the northern WAP, emphasis will be placed on oceanographic influences and current configuration for this area of the AP. As shown in Figure 2.9 and discussed in Chapter 2.5, a branch of the ACC passes through Bransfield Strait and the dominant water mass associated with this current is CDW. Therefore, for the purpose of this study, it is proposed that the spatial variability shown in the surface ages of northern WAP marine sediment (Figure 6.13) can be explained by local primary producers utilising different water masses with different ^{14}C concentrations; Bransfield Strait organisms grow in ^{14}C

depleted water (thus recording older reservoir ages), whereas coastal sites are under the influence of coastal currents, which are better equilibrated with the atmosphere and so have more enriched ^{14}C values (thus recording younger reservoir ages).

Often assumptions are made that there has been no change in the reservoir effect through time (Bowman, 1990). However, Sikes et al. (2000) found evidence for considerably older surface and deep ocean reservoir ages near New Zealand during the last glaciation; a volcanic ash layer dated on land at 22590 yr BP exhibited a reservoir age of 2000 years or more, compared to a reservoir age of a few hundred years for the period 15000 – 0 yr BP. Similarly, using ^{226}Ra decay in barite from a deep sea core from the Southern Ocean and subsequent comparison with ^{14}C ages measured in planktonic foraminifera, van Beek et al. (2002) found that throughout the middle to late Holocene, the reservoir age was comparable to modern estimates (~1100 years); whereas during the early Holocene, a higher reservoir age (~1900 years) was observed. The higher sea surface reservoir age documented in the Early Holocene may be attributed to a change in the Southern Ocean circulation, specifically mixing with deeper waters (van Beek et al., 2002). This temporal heterogeneity further compounds the problems of radiocarbon dating Antarctic marine sediments.

Unfortunately, with only several samples dated (maximum 7) for each core in this investigation and a lack of terrestrial or tephra-based calibration, addressing questions of reservoir age variability is not feasible. The generally smooth age-depth curves exhibited by all cores (Figure 6.11), suggests that no sudden changes in the reservoir effect have occurred in these coastal marine settings through the Holocene. Changes in reservoir effects through time are worth considering in higher resolution studies, focused on transitional time periods and in marine settings likely to be affected by major changes in ocean circulation (e.g. Bølling/Allerød to Younger Dryas transition in the North Atlantic, see Bondevik et al., 2006).

b) Glacier meltwater

The addition of CO_2 deficient in ^{14}C by the submarine melting of old glacial ice has been suggested as another factor affecting the reservoir age of Antarctic surface waters (Domack et al., 1989). From the Wilkes Land continental shelf, Domack et al. (1989) observed a surface sediment ^{14}C age of approximately 5500 ^{14}C years BP and used this as the down-core reservoir correction. The authors proposed that summer primary production in this region occurs in a stable surface layer that contains significant amounts of winter basal meltwater (containing old CO_2), which has had no exchange

with the atmosphere because of sea ice coverage. However, building on the reasoning of Harden et al. (1992), if submarine melting of glaciers in AP bays and fjords is a large enough component to offset seawater ^{14}C activities, then one should expect to see older ages at sites closer to land. For the WAP, the general pattern is the reverse; youngest core top ages are found closest to the AP coast (Figure 6.13). The exceptions are the samples from Gerlache Strait and associated fjords (cores 1, 2, 3, 8 & 9 on Figure 6.13), but they do not exhibit such large reservoir ages (5500 years) as the cores Domack et al. (1989) analysed. The old surface ages in these near coast settings may be a function of distance from glacier grounding lines (Domack, 1992) and will be discussed in section 6.2.2.2. In the northern AP and on coastal islands, glaciers are smaller and have quicker through-flow of ice, compared with the larger and older AP glaciers that discharge into fjords and southern AP embayments. Meltwater from the smaller northern AP glaciers is therefore likely to be derived from ice of more recent origin and exposed to the present atmosphere before entering the marine environment, consequently less likely to offset seawater ^{14}C concentrations dramatically. The influence of glacier meltwater on the reservoir effect is presumed to be a function of site and glacier speed/ice residence times, and is a potentially important factor for high latitude environments. However, this theory remains to be systematically tested.

c) Sea ice capping

The presence of extensive sea ice severely limits ocean-atmosphere gas exchange, thus reducing the potential for ^{14}C in surface waters to equilibrate with the atmosphere and increasing the sea surface ^{14}C reservoir age (Bard et al., 1994; Schlosser et al., 1994). Changes in sea ice cover through time, both in geographic extent and duration, will affect the marine reservoir age. Potentially the latitudinal trend of older sediment core tops towards the southern AP and on the EAP may in part be caused by more extensive sea ice cover in these areas. Sea ice capping is worth considering for time periods where sea ice concentration and extent were dramatically enhanced compared with today (e.g. glacial periods, as discussed in Chapter 2.3.2.1); such factors are unlikely to strongly influence regional reservoir effects during the Holocene.

6.2.2.2 Contamination

Contamination of the original carbon signature preserved in marine sediments can take place either during original sediment deposition, with inputs and re-working of fossil carbon; or during the coring process and subsequent sectioning and splitting, when potentially sediment is lost, over-penetrated, compressed or disturbed.

a) Fossil carbon

Dating of AIO material can sometimes be further complicated by varying degrees of fossil carbon contamination, which can locally be highly variable (Harden et al., 1992; Pudsey et al., 1994; Andrews et al., 1999; Pudsey and Evans, 2001). Fossil carbon can be delivered from terrestrial sources, undergoing transportation and deposition into the marine realm, or through erosion of older marine sediments and subsequent re-deposition, by processes of lateral transport, current winnowing and mass movement.

On the AP coast and islands there is very little terrestrial vegetation and the bedrock is predominantly igneous, so contamination by land-derived carbon is believed to be negligible (Pudsey et al., 1994). Although this proposition is supported by the data in Figure 6.13 for the WAP, showing that surface sediments closest to the WAP coast generally display young ^{14}C ages (which would not be the case if inputs of older organic matter from terrestrial source were substantial), local geology is an important contamination factor in a number of localities. For example, outcrops of Trinity Peninsula upper Palaeozoic marine shales at the northern tip of the AP (Fleming and Thomson, 1979) may result in input of reworked carbon material (radiocarbon dead, i.e. where ^{14}C is no longer detectable) (Pudsey and Evans, 2001; Pudsey et al., 2006; Heroy et al., 2008). This has been used to explain the significantly old surface sediment ages found in PGC (Pudsey and Evans, 2001; Pudsey et al., 2006), as highlighted in Figure 6.14. Another example is provided from the Gerlache Strait, where there is published data showing a clear relationship of decreasing surface sediment age with distance from the coast (Domack, 1992). Comparable carbonate dated samples display uniformity of ages, regardless of distance from the coast (Domack, 1992). The older ages (generated from AIO material) near the coast might reflect reworking of old organic carbon, leading to contamination of the original carbon signature.

Another possible source of old organic carbon is erosion and re-deposition of older sediments, by processes of lateral transport, current winnowing and mass movement; "Deposition of reworked material from upslope and lateral transport of organic matter appear to be the most reasonable explanation for the anomalously old ^{14}C ages at the sediment-water interface in continental shelf sediments of the Antarctic Peninsula" (Harden et al., 1992; p93). Mass movement is not believed to be an important process in the open shelf setting (Pudsey et al., 1994) and within the cores used in this investigation (with the exception of VC243), as evidenced by the lack of substantial age reversals and sedimentary structures associated with flow. An example where erosion

processes may influence surface sediment ages is provided by the age progression (1870 – 3200 – 4020 ^{14}C years BP) onshore to offshore of Anvers Island (cores 14-16 in Table A2.1 and Figure 6.13); towards the shelf edge deposition may be less continuous, and material reworked by grounded icebergs and shelf currents (Pudsey et al., 1994).

Another mechanism of contamination is bioturbation, whereby benthic fauna displace and mix sediment particles between horizons. For example, even with a hypothetical reservoir age of zero, surface sediment ages would not record zero radiocarbon years, due to mixing of modern and older sediment in the mixed layer. Using steady state modelling (Box 6.1), Barker et al. (2007) predict ^{14}C age differences in the sedimentary mixed layer of up to several thousand years, attributing this to the effects of bioturbation and dissolution. Application of the steady state models detailed in Barker et al. (2007) to the cores used in this investigation (Table 6.2), results in only relatively small ^{14}C age differences between the surface ocean age and that of the sedimentary mixed layer. The exception is core GC358, which records a significant difference (1786 ^{14}C years), highlighting the observations of Peng and Broecker, (1984) and Barker et al. (2007) that cores with low sedimentation rates are particularly vulnerable to age offsets through bioturbation. As illustrated by the AP cores in this study, there is a direct association between sedimentation rate and ^{14}C age of the sedimentary mixed layer; high (low) sedimentation rate result in small (large) differences in ^{14}C age (Table 6.2). The effect bioturbation has on the true age of the sediment is worth acknowledging, particularly with cores experiencing very low sedimentation rates, however mixing of material is already taken into account by using the common Antarctic method based on a uniform application of a surface sediment age correction down-core.

Box 6.1
One box model of the mixed layer (Barker et al., 2007).

At steady state:
^{14}C of sedimentary mixed layer = 8033 x ln (1 + τ/8033) + Age of surface ocean

where τ = Residence time of silt grains in mixed layer (years)
= 1000 x thickness of mixed layer (8 cm) / sediment accumulation rate (cm/kyr)

Table 6.2
Outputs of ^{14}C age of sedimentary mixed layer from steady state box model (Box 6.1), using age of the surface ocean inferred from three-dimensional global ocean circulation model outputs described in Butzin et al. (2005) and generated using the searchable (latitude and longitude) reservoir age dataset at: http://radiocarbon.ldeo.columbia.edu/research/resage2.htm (Fairbanks, 2005) and linear sedimentation rate generated from Figure 6.11.

Core	^{14}C age of surface ocean (years) (Butzin et al., 2005) [1]	Sedimentation rate (cm/kyr); high ([1]) to low ([7])	^{14}C age of sedimentary mixed layer (years) [2]	Difference in ^{14}C age [2-1] (due to mixing in surface layer) (years); small ([1]) to large ([7])
GC114	1117	93 [1]	1203	86 [1]
GC047	1236	34 [5]	1468	232 [5]
VC306	1794	22 [6]	2150	356 [6]
GC358	1816	6 [7]	3050	1234 [7]
VC243	1575	92 [1]	1661	86 [2]
VC237	1575	64 [3]	1699	124 [3]
VC205	1449	53 [4]	1599	150 [4]

b) Coring contamination

Methods used to obtain marine cores frequently disturb, compress or smear the sediment stratigraphy, with surface sediments most likely to be severely disrupted or not recovered (McCoy and Von Herzen, 1971; McCoy, 1980; Skinner et al., 2003). A summary of the main sediment coring techniques and details of their relative merits and drawbacks is provided by Weaver and Schultheiss (1990). It is essential to assess the coring method used for each core in this investigation, to determine whether coring artefacts are likely to affect the reliability of information obtained from the sediment record.

The biggest issue with respect to marine sediment coring is the possibility of disruption or loss of surface sediments. Preservation of the sediment-water interface is crucial to provide accurate assessment of regional reservoir effects and subsequently applying them as a down-core correction on radiocarbon dates. Box corers and multi corers provide the most reliable method for recovering surface sediments, often retrieving the sediment-water interface (Weaver and Schultheiss, 1990), but frequently they are not taken in tandem with longer coring devices (piston corer, gravity corer and vibro corer). For example, both gravity corers and piston corers, with their linked trigger corer, are capable of disturbing surface sediments, over-penetration or even repeat penetration

(McCoy, 1980), with the respective consequences being disturbance of surface sediment, loss of sediment out of the top of the coring barrel and / or compression of the sedimentary sequence, and multiple sampling of surface sediments (Weaver and Schultheiss, 1990). To further compound the problem, as witnessed from personal cruise and coring experience, Antarctic diatomaceous sediments are frequently waterlogged and hence "soupy" in character in the uppermost core section (approximate depth <0.5 m). This means that the uppermost sediments are easily mixed during recovery and extracting an accurate core top sample for dating is often difficult to obtain.

To address the issue of non-recovery or loss of surface sediment, Harden et al. (1992) developed a calculation to estimate how much surface material was not recovered in piston cores from the AP. In their study, the authors utilised a number of piston and box cores (in the latter, the sediment-water interface is more likely to be preserved) from the Bransfield Strait, Gerlache Strait (core locations for these areas are shown in Table A2.1 and Figure 6.13) and Marguerite Bay (Table A2.3 and Figure 6.15), dating them using ^{210}Pb and ^{14}C methods. The amount of missing core top material was estimated by subtracting the average surface age, as determined from the box cores, from the surface age for each piston core and multiplying the difference by the ^{14}C sediment accumulation rate (Harden et al., 1992). Although it is possible that surface sediment was lost from several of the cores used in this investigation, the principle of calculation of missing core material was only applied to core VC306. It is highly likely that surface sediment was not recovered during coring of VC306 (see section 6.2.4) and box cores of sufficient quantity and quality exist for Marguerite Bay (Table A2.3) to apply the calculation. The amount of surface material lost during coring is calculated (Box 6.2), then by using linear regression equation generated by a trendline through core dates (Figure 6.11) enables a potential surface age to be generated (assuming the missing sediment was infact present) (Box 6.3).

Box 6.2
Calculation of missing core top material (after Harden et al., 1992).

Missing core top material =
[Surface age for core – Average surface age from box cores] x Sediment accumulation rate

VC306:
[4560 years – 2335 years] x 0.022 cm/year = **48.95 cm**

Box 6.3
Application of the linear regression trendline equation to calculate the age of the surface sediment if the missing material was in fact present (x) in core VC306.

VC306:
$y = 0.00022\ x - 1.030683$
$-0.4895 = 0.00022\ x - 1.030683$

$$\frac{-0.4895 + 1.030683}{0.00022} = x$$

$x =$ **2460 years**

Sediments can also be contaminated during sectioning and splitting once the core has been recovered. From personal cruise and coring experience, remnants of plastic liner (swarf) can easily be entrained in the core material; precautions should be taken during core handling and processing to minimise this possible contamination source, which being a petrochemical adds material of infinite age. If contamination is suspected, this information is normally noted on original core sedimentary logs.

Given the competing influences on the ^{14}C record and the need for a robust chronology in order to make core comparisons, details of the dating methods applied to each core used will now be discussed in detail.

6.2.3 GC114 and GC047

Both core GC114 and GC047 are situated in the northern sector of the AP, experiencing similar oceanographic influences and sedimentary depositional processes. Consequently, the magnitude of correction to account for the regional marine reservoir effect should be similar.

The chronology for core GC114 is based on six AMS radiocarbon dates (Figure 6.11). Dates are in chronological order and age reversals do not occur. The age-depth relationship is approximately linear (r^2 = 0.96). Likewise for core GC047, the three ages, plus the surface age from a small pilot corer (TC046) used to obtain an undisturbed surface sample at the same site (Pudsey et al., 1994), display a linear age-depth relationship (r^2 = 0.98). A small age reversal exists between samples 3.6 m and 3.79 m, but assuming minimum and maximum errors in the two dates, the reversal corresponds to 262 years or 714 years respectively. This is considered a relatively minor reversal and could be explained by short-term variations in surface mixing, bioturbation or sampling error. As Figure 6.11 highlights, the two cores experience different average

sedimentation rates: GC114 = 93 cm ky^{-1} and GC047 = 34 cm ky^{-1}. The rate of accumulation for GC114 is comparable with published rates for this region of the AP, ranging between 72 – 262 cm ky^{-1} (Harden et al., 1992; Leventer et al., 1996; Bárcena et al., 1998; 2002; 2006; Masque et al., 2002; Heroy et al., 2008), whereas the sedimentation rate for GC047 falls below this general range. The higher accumulation rates at GC114 are expected close to the Bransfield Strait area, where high biogenic fluxes are common (Abelmann and Gersonde, 1991), controlled in part by the highly productive phytoplankton blooms at the confluence of cold Weddell Sea water and warmer water from the Gerlache and Bellingshausen Sea areas (Bárcena et al., 2002).

The core top ages for GC114 and TC046 are 2620 (± 40) and 1870 (± 70) ^{14}C years respectively and lie outside of the mean age suggested as representing the reservoir age of Antarctic shelf waters (1230 – 1300 ^{14}C years) (Gordon and Harkness, 1992; Berkman and Forman, 1996; Domack et al., 2001). However, exploration of the spatial variability in core top ages from Bransfield Strait, Gerlache Strait and Anvers Island area, including Palmer Deep, suggests that these ages are within the published ranges for these areas. Table A2.1 shows conventional ^{14}C ages for surface box and piston core samples collected from these areas, from a variety of publications. Details of the range and average surface ages, divided by geographic region, are also given in Table A2.1. As highlighted in Figure 6.16, when the range values are plotted against core top ages for GC114 and TC046, these surface ages fall within the published range and there appears to be a progression in core top ages working away from the AP coast.

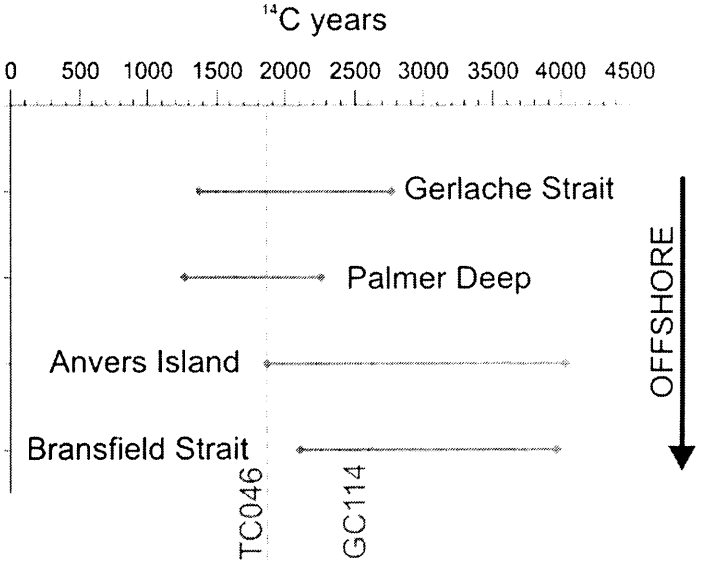


Figure 6.16
Core top age ranges, divided by geographic region, and compared to the surface ages of GC114 and TC046 (GC047).

In light of the spatial variability observed in core top ages from the WAP, the reservoir correction and down-core adjustment applied to both cores is a subtraction of the core top age: **2620 ^{14}C years** for core GC114; and **1870 ^{14}C years** for core GC047. The corrected core chronologies are shown in Table 6.3 and Figure 6.20. The record for core GC114 is truncated, spanning the Mid to Late Holocene (3360 ^{14}C years BP – present), whereas GC047 covers most of the Holocene (10410 ^{14}C years BP – present).

6.2.4 VC306

Four samples were ^{14}C dated from core VC306 and exhibit a linear age-depth relationship (r^2 = 0.99), with no age reversals (Figure 6.11). This implies that sediment delivery to the site has been constant through time. The average sedimentation rate for core VC306 is 22 cm ky^{-1}, which falls at the lower end of published rates (12 – 50 cm ky^{-1}) from Marguerite Bay (Harden et al., 1992; Ó Cofaigh et al., 2005a).

The old surface sediment age in core VC306 (4560 ^{14}C years BP (± 40)) was unexpected. However, this age is comparable with dates from two other piston cores from Marguerite Bay (Table A2.3: PC111 and PC112); 4260 ^{14}C years (± 160) and 4100 ^{14}C years (± 150) (Harden et al., 1992) and vibro cores VC304 (3473 ^{14}C years (± 39)) and VC307 (3710 ^{14}C years (± 45)). These ages fall significantly outside the suggested reservoir age for Marguerite Bay, which ranges between 1200 – 2818 ^{14}C years, based on planktonic foraminifera from cores in the middle and outer shelf trough (Pope and Anderson, 1992). Clearly, there are additional factors affecting the AIO-based age of surface sediments in Marguerite Bay, most likely to include: loss of core top material during coring; input of old organic carbon from terrestrial sources; or regional variability in the Antarctic marine reservoir effect due to the particular oceanographic influences present in the Marguerite Bay area (and the southern Bellingshausen Sea; core GC358), with upwelling of ^{14}C-depleted CDW onto the continental shelf (Jenkins and Jacobs, 2008; Meredith et al., 2008).

Information in the original cruise report for core VC306 provides supporting evidence of loss of core top material during the coring process: "The penetrometer on the BGS vibro-corer did not work properly for several days, so a guess had to be made at the length of vibration time required to collect a core" (British Antarctic Survey JR71 cruise report, 2002; p8). A penetrometer is an instrument that measures sediment penetration and without this functioning it is difficult to assess the depth the corer has reached. Core VC306 recovered 5.95 m of sediment and the maximum the vibro-corer could contain was 6 m, therefore it is not unreasonable to suggest that over-penetration occurred

during the coring process, resulting in surface sediment loss from the coring barrel. As presented in Boxes 6.2 and 6.3, it is estimated that roughly 50 cm was lost, equating ~ 2500 ^{14}C years. This leads to a more realistic surface sediment age, and down-core radiocarbon correction value, of 2460 ^{14}C years for core VC306. Performing the same calculations detailed in Boxes 6.2 and 6.3 on comparable cores from Marguerite Bay (VC304 and VC307) yields similar surface ages (and hence reservoir correction) to that proposed for VC306 (2564 and 1675 ^{14}C years, respectively). Averaging the corrections above for cores VC304, VC306 and VC307 gives 2233 ^{14}C years, which is close to the 2460 ^{14}C year correction calculated for VC306. This brings the core top age of VC306 in line with the suggested marine reservoir age of shelf waters in Marguerite Bay (1200 – 2818 years), put forward by Pope and Anderson (1992) from foraminifera.

The other method used to correct radiocarbon dates in the Antarctic is to assume the core top age represents the modern sediment surface and subtract this age from down-core ^{14}C dates (Bentley and Anderson, 1998; Cunningham et al., 1999; Domack et al., 1999; Taylor and McMinn, 2002; Heroy and Anderson, 2007). This is not appropriate for VC306, due to age constraints imposed by the known deglaciation history of the Marguerite Bay area. Working from the outer shelf in towards the AP coastline, the progression of dates for deglaciation should go from older to younger, recording the retreat of the ice sheet from the continental shelf edge. As the ice sheet retreated, sediment composition changed from glacial till into glacio-marine sediments; recording the ice sheet lifting off the seafloor sediments, becoming a floating ice shelf and eventually retreating, leaving open water at the site (Kennedy and Anderson, 1989; Pope and Anderson, 1992; Anderson, 1999). Published data on the deglaciation history of Marguerite Bay is shown in Figure 6.17; these are minimum deglaciation ages. This data provides temporal and spatial tie points, with which to compare the radiocarbon dates from VC306. As highlighted in Figure 6.17a), the method of age correction based on the core top age can immediately be discredited because the timings of deglaciation of cores VC306, VC304, PC111 and PC112 (latter two published in Bentley and Anderson, 1999) are coeval or postdate when George VI Ice Shelf was absent (Clapperton and Sugden, 1982; Smith et al., 2007). In comparison, Figure 6.17b shows application of a correction value of 2460 ^{14}C years seems feasible as there is a roughly chronological progression of dates towards the coast.

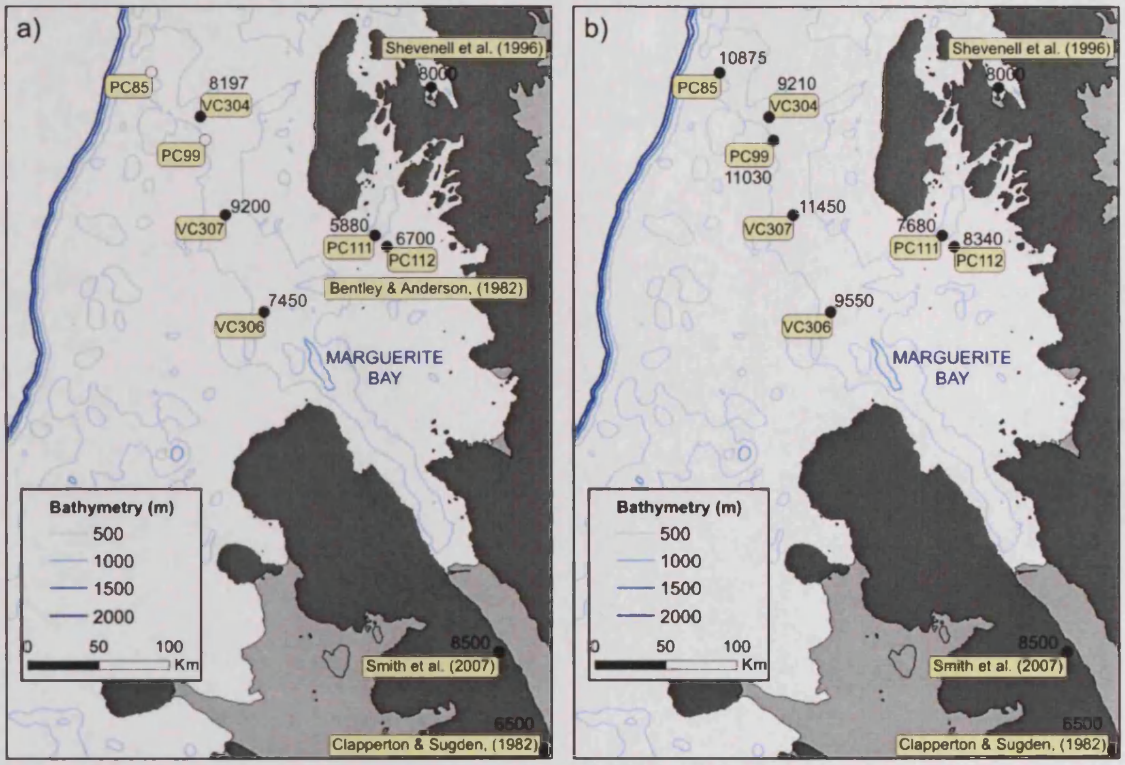


Figure 6.17
a) Marine cores from Marguerite Bay corrected by subtracting core top ages;
b) Marine cores from Marguerite Bay corrected using a 2460 ^{14}C year reservoir age.
Dates next to localities relate to the minimum timing of deglaciation in each of the records, given in ^{14}C years BP. Tie points on the AP coast are: 1) marine record from Lallemand Fjord (Shevenell et al., 1996); 2) lake cores from Alexander Island recording a marine incursion at that time (corrected by 1300 ^{14}C years) and the first absence of George VI Ice Shelf (Smith et al., 2007); 3) presence of pelecypod shells of that age (corrected by 750 ^{14}C years) in a moraine on Alexander Island, suggesting George VI Sound was ice-free (Clapperton and Sugden, 1982); 4) core VC304 (Ó Cofaigh et al., 2005); 5) core VC306 (Ó Cofaigh et al., 2005); 6) core VC307 (Ó Cofaigh et al., 2005); 7) core PC111 (Harden et al., 1992; Bentley and Anderson, 1999); 8) core PC112 (Harden et al., 1992; Bentley and Anderson, 1999); 9) core PC85 (Pope and Anderson, 1992) 10) core PC99 (Pope and Anderson, 1992). No core top samples were dated for PC85 and PC99, hence these points are absent on Figure 6.17a).

In light of the reconstructions of deglaciation in Marguerite Bay and the suggestion that surface sediments from core VC306 are missing (as explained in section 6.2.2.2 and above), the reservoir correction and down-core adjustment proposed for this core is **2460 ^{14}C years**. The corrected core chronology is shown in Table 6.3 and Figure 6.20. The record for core VC306 spans the Early to Late Holocene, from 10150 ^{14}C years BP to 2100 ^{14}C years BP.

6.2.5 GC358

Three of the four AMS radiocarbon ages for core GC358 show a linear age-depth relationship (r^2 = 0.97) (Figure 6.11 and Figure 6.18). The average sedimentation rate for core GC358 is 6 cm ky^{-1}, which is significantly lower than rates exhibited by other cores used in this investigation. However, this low rate of sedimentation is considered to be regionally representative; a nearby core (GC359) displays a Holocene sedimentation rate of 3.7 cm ky^{-1}. The chronology of core GC358 has been problematic for two reasons: (1) proposing an accurate surface sediment age (and hence down-core reservoir, plus local source correction) has been difficult; (2) even assuming a large correction value, doubts exist as to the accuracy of the timing of deglaciation (provided by the lowermost radiocarbon date at 0.735 m).

Firstly, addressing the issue regarding the surface sediment age, the radiocarbon date at the core top of GC358 is unusually old (11246 (± 91) ^{14}C years). It is believed that this age is a result of contamination introduced during core handling and cutting (C.-D. Hillenbrand, pers. comm.) and will therefore be excluded from further analysis. Unfortunately, there are very few published dates for marine cores from the southern Bellingshausen Sea, so application of a representative sediment correction for this area is difficult.

Surface sediment ages of box and gravity cores from the southern Bellingshausen Sea may provide information on an appropriate core top age for core GC358 (Table A2.4, Figure 6.15 and Figure 6.18). A comparable core (GC359), located just 1.9 km from GC358, displays a surface sediment age of 5131 (± 50) ^{14}C years. When comparisons are made with other AIO generated core-top ages from the area, this surface sediment age appears to be regionally representative; box core and gravity core surface ages average ~4800 and ~5000 ^{14}C years respectively. Further, the similarity between average box core surface ages (which typically preserve the sediment-water interface) and gravity core ages suggests that the core top age from GC359 is likely to represent modern sedimentation. For these reasons, the core top age of core GC359 (5131 ^{14}C years) is proposed as a comparable surface sediment age for core GC358.

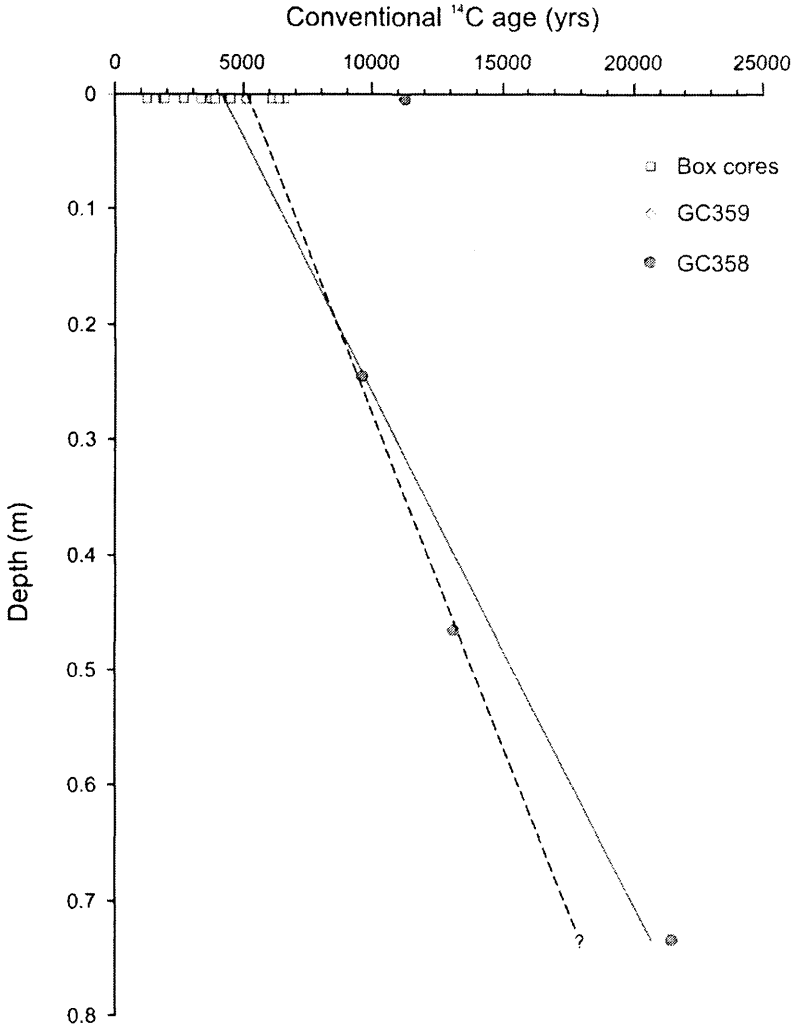


Figure 6.18
Uncorrected age-depth plot for core GC358, together with surface sediment age for core GC359 and box cores from the southern Bellingshausen Sea, as detailed in Table A2.4 and Figure 6.15. Solid line = GC358 linear regression using core top age of GC359; Dashed line = GC358 linear regression using core top age of GC359 and excluding lowermost ^{14}C date from core GC358 (0.735 m) (suspected to be contaminated by reworked organic carbon from terrestrial inputs following deglaciation).

Clues as to the processes and influences affecting ^{14}C ages of southern Bellingshausen Sea sediments are provided by age comparisons based on the material dated (Table A2.4). Carbonate material provides the most reliable assessment of the marine reservoir effect, which in this area appears larger than the accepted age of Antarctic shelf waters. This age mismatch is likely to result from regional variability in the Antarctic marine reservoir effect, due to the oceanographic influences in the southern Bellingshausen Sea and the glaciological regime of the southern AP (discussed in section 6.2.2.1). Also highlighted in Table A2.4 is the observation that AIO dated material records an older age than carbonate, averaging ~4800 – 5000 ^{14}C years from sediment samples,

compared to ~3000 ^{14}C years from carbonate samples. The disparity between ages provided from AIO material versus carbonate could be interpreted as contamination of the AIO derived age, due to reworking of fossil carbon. In summary, the variable, yet consistently old surface ages in the southern Bellingshausen Sea (from box and gravity cores) suggests that the reservoir effect, plus local contamination influences, are higher in this area than elsewhere on the WAP, yet comparable with corrections applied in coastal EAP settings (e.g. PGC, cores VC243 and VC237; see section 6.2.6).

For the reasons outlined above, **5131 ^{14}C years** is proposed as a representative core-top and down-core correction value for core GC358. Using this correction, the record spans from 16302 ^{14}C years BP to present. However, this leads to the second problem with this cores' chronology; the timing of deglaciation for this southerly latitude and coastal core locality is several thousand years earlier than other AP regions (reviewed fully in Chapter 8.4.1). Is this likely to be an accurate reflection of the deglaciation history of the southern Bellingshausen Sea or an artefact developed because of the difficulties in radiocarbon dating in Antarctica?

In a study by Hillenbrand et al. (2007), a suite of cores proximal to core GC358 were used to reconstruct glacial dynamics of the West Antarctic Ice Sheet at the LGM and during deglaciation. The post-glacial onset of seasonal open-water conditions is recorded as a change in sediment from glacial diamictons to diatomaceous muds and by tracking this change in sediment character across the shelf core site deglaciation histories were proposed. The reconstructions of Hillenbrand et al. (2007) do suggest an early onset of deglaciation ages for the southern Bellingshausen Sea, as follows: outer shelf ~26000 years BP; middle part of the shelf ~19000 years BP; Eltanin Bay ~12000 years BP and Ronne Entrance ~7000 years BP. The timing proposed for deglaciation of Ronne Entrance is based on the ^{14}C age at 0.25 m in core GC359 (11736 (± 120) ^{14}C years), corrected by subtracting the core top age (5131 (± 50) ^{14}C years). The radiocarbon age at the same sediment transition in core GC358 (0.735 m) (Figure A2.1) should be comparable between this core and GC359; this is not the case. The apparent timing of deglaciation of core site GC358 is 16302 ^{14}C years BP, assuming a correction value of 5131 years. This age is ~9000 ^{14}C years different from the age proposed from GC359; furthermore, this inner shelf core is recording a deglaciation age comparable with that of the middle shelf.

It is difficult to explain the mismatch in deglaciation ages at these two very proximal, inner shelf core localities. A possible scenario relates to local differences in the core site bathymetry. Core GC358 was recovered from a trough and core GC359 a ridge (1.9 km apart); potentially the ice shelf could have lifted off GC358 sediments earlier, enabling advection of open marine sediments into the trough, whilst the grounding line was still pinned to the ridge sediments of GC359. This is unlikely because water depths between the two core sites are only 5 m difference, and furthermore, prolonged standstill of the ice shelf edge (~9000 ^{14}C years) is unlikely.

As highlighted in Figure 6.18, the deglaciation age of core GC358 can be reduced slightly if a linear sedimentation rate is assumed from the core-top age (provided by core GC359), through the middle two radiocarbon dates (0.245 m and 0.465 m in core GC358) and extrapolated down-core to the deglaciation sediment transition. This method involves discrediting the radiocarbon age provided by 0.735 m. However, it is not unreasonable to assume that this lowermost radiocarbon sample is contaminated with reworked organic carbon from terrestrial inputs following deglaciation, thus yielding a date that potentially is too old. Other researchers have found a similar jump in age, referred to as a "dog leg", and also argue that these dates are contaminated with reworked (dead) carbon and therefore unreliable (Pudsey and Evans, 2001; Pudsey et al., 2006; Heroy and Anderson, 2007). For core GC358, extrapolation of the linear sedimentation rate for the upper core leads to an alternative and conservative minimum age for the sediment transition at 0.735 m of 12650 ^{14}C years BP (corrected by 5131 ^{14}C years) (Figure 6.18). This is still considerably older than that proposed from core GC359, but is a more plausible age when considering the regional deglacial history proposed by Hillenbrand et al. (2007).

In summary, the age model proposed for core GC358 assumes:

- the core-top of GC358 is contaminated and that the proximal core GC359 records a true surface sediment age. This age (5131 (± 50) ^{14}C years) is considered as an appropriate reservoir, plus local source correction;
- the lowermost radiocarbon sample in core GC358 (0.735 m) is contaminated with fossil carbon due to terrestrial inputs following deglaciation, leading to an anomalously old deglaciation age (16300 ^{14}C years BP). A more realistic age (12650 ^{14}C years BP) is provided by extrapolation of the linear sedimentation

rate for the upper core. This equates to a reservoir, plus local source correction for this sample depth of 8783 ^{14}C years;

- the corrected core chronology shown in Table 6.3 and Figure 6.20 chronology is accurate and that deglaciation of this coastal site occurred considerably earlier than other AP shelf settings (several thousand years for northern WAP sites and >7000 years for coastal EAP sites). This finding is discussed further in Chapter 8.3.4 and 8.4.1.

6.2.6 VC243 and VC237

Both core VC243 and VC237 were recovered from PGC (EAP); oceanographic influences and sedimentary inputs through the Holocene would have acted in a similar manner at both localities. The similar geographic setting of these two cores means that the magnitude of correction to account for the Antarctic marine reservoir effect should also be similar. The average sedimentation rate for core VC243 is 92 cm ky^{-1} and for VC237 64 cm ky^{-1}.

Five of the seven AMS radiocarbon ages for core VC243 show a linear age-depth relationship (r^2 = 0.99); the exceptions to this linear trend are core depths 0.51 m and 0.65 m, where large age reversals exist (Figure 6.11 and Figure 6.19). From the sedimentary log (Figure 6.7), these depths correspond to a horizon with pronounced concentrations of clasts. The sedimentary structure and anomalously old radiocarbon ages suggest localised reworking of older fossil carbon. Anomalously old ages were reported from AIO material in the Ross Sea and attributed to reworking of fossil carbon by iceberg plowing or gravity driven sediment flows, possibly through collapse of steep sided levees generated along the trends of iceberg scours (Domack et al., 1999). Both these mechanisms are applicable in the PGC; however, it is more likely that this clast-rich horizon originates from gravity flow because the PGC Ice Shelf had reformed by the Late Holocene, limiting iceberg movement over the core sites. Due to fossil carbon contamination of these two dates (0.51 m and 0.65 m), they were ignored during construction of the age model for this core. Lastly, it is worth noting that the surface sediment age for core VC243 is significantly older (6010 ^{14}C years) than the accepted marine reservoir age of Antarctic shelf waters.

The chronology for core VC237 is based on five AMS radiocarbon samples and box core BC314. Ages are in chronological order and age reversals do not occur (Figure 6.11 and Figure 6.19). The age-depth relationship shows a good linear correlation (r^2 =

0.997). No surface sediment sample was dated for core VC237, consequently the surface sediment age is derived from box core BC314 (Table A2.2), from the same locality.

The chronology of cores VC243 and VC237 has previously been published in Pudsey and Evans (2001) and Pudsey et al. (2006). ^{210}Pb and AMS ^{14}C dating techniques were employed on a total of six box cores and 14 vibro cores from the PGC and northern Larsen area (Pudsey et al., 2006). Figure 6.19 shows an uncorrected age depth-plot for cores VC243 and VC237, together with surface ages for box cores from the PGC and Larsen-A area, detailed in Table A2.2 and Figure 6.14. As highlighted on Figure 6.19, surface ^{14}C ages are consistently older than 5491 ^{14}C years, suggesting ageing of surface sediments is common in this region. Pudsey et al. (2006) gain further confidence in the accuracy of the surface ages from ^{210}Pb ages, which are comparable with ages from PGC and Larsen-A reported by Gilbert and Domack (2003). This demonstrates that the core-top material is of geologically recent age and consequently a reservoir plus local source correction of 6000 ^{14}C year was proposed (Pudsey and Evans, 2001; Pudsey et al., 2006). The local source effect relates to the input of organic carbon not of recent marine origin (Evans et al., 2005). The sediments must contain some old carbon (~44 %) from some of the source rocks, i.e., the Cretaceous sediments on James Ross Island, the Jurassic near Cape Longing or the Trinity Peninsula Group metasediments (Pudsey et al., 2006).

Due to the robust nature of the combined AMS ^{14}C and ^{210}Pb chronology proposed by Pudsey and colleagues (Pudsey and Evans, 2001; Pudsey et al., 2006), a reservoir plus local source correction of **6000 ^{14}C years** is also applied, which produces a surface age of 10 and 22 years for VC243 and VC237 respectively. The corrected core chronologies are shown in Table 6.3 and Figure 6.20. The record from core VC243 is truncated, covering the Mid to Late Holocene (6450 ^{14}C years BP to present), whereas VC237 covers nearly the full Holocene (11130 ^{14}C years BP to present). Only the lowermost 4 metres of core VC237 were analysed for diatoms, with results spliced to core VC243 to provide a full Holocene diatom record for PGC.

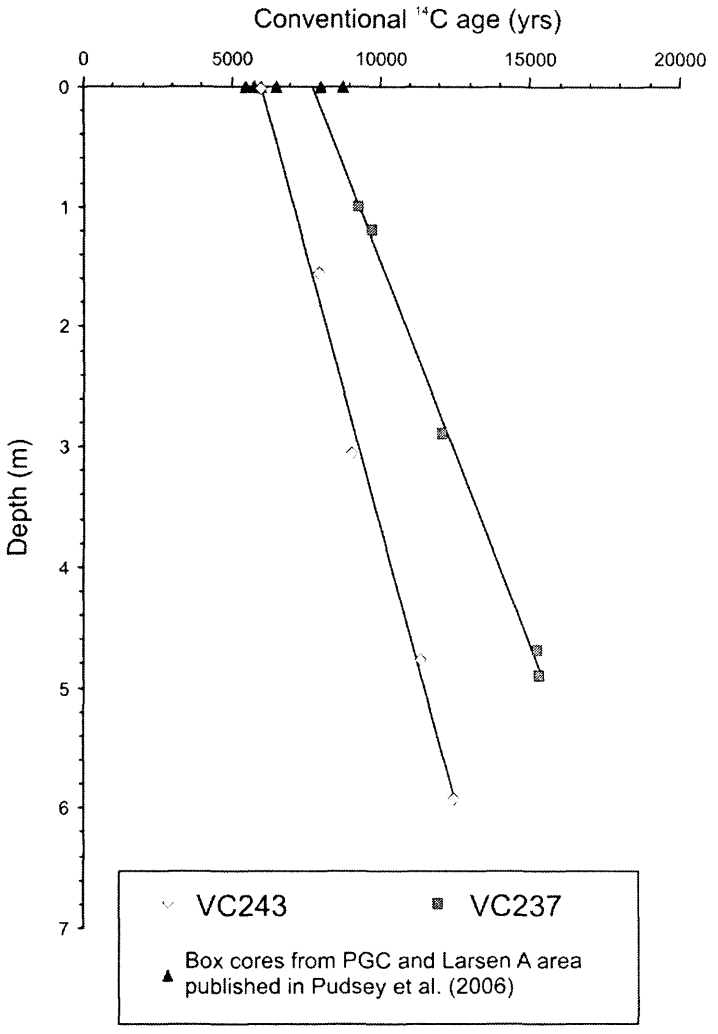


Figure 6.19
Uncorrected age-depth plot for cores VC243 and VC237, together with box core surface ages for cores from Prince Gustav Channel (PGC) and northern Larsen area.

6.2.7 VC205

The chronology for core VC205 is based on six AMS radiocarbon samples; ages are in chronological order and age reversals do not occur (Figure 6.11). However, two sedimentation rates are evident; 413 cm ky^{-1} between 5.1 – 2.6 m and 53 cm ky^{-1} between 2.6 – 0 m. The extremely high sedimentation in the lower section of the core is comparable with the rate for laminated sections of Palmer Deep sediment core (250 – 400 cm ky^{-1}) (Leventer et al., 1996; 2002) and implies that terrigenous and / or biogenic delivery to the core site is elevated during this interval. Magnetic susceptibility values between 5.1 – 3.6 m are extremely low (Figure 6.9), suggesting that the dominant source is biogenic. In the Erebus and Terror Gulf setting, such a rapid increase in sedimentation could result from: sediment focusing because of changes in ocean current configurations; elevated primary productivity in the area; and / or PGC Ice Shelf

collapse-driven mass sedimentation. Dramatically increased sedimentation rates were found in shallow marine records during the Mid-Holocene collapse of George VI Ice Shelf, with almost instantaneous deposition of ~2 m of ice-rafted debris (Smith et al., 2007a). Magnetic susceptibility values do dramatically increase up-core of 3.6 m (Figure 6.9), suggesting increased terrigenous and / or reduced biogenic flux to the sediment. The dog-leg in the age-depth profile for core VC205 could potentially be an artefact of influx of reworked organic carbon from the Mesozoic rocks in this region (as observed in cores from the PGC; see section 6.2.6), resulting in radiocarbon samples above 3.6 m yielding an apparently older age. MS values are higher between 3.6 – 2.2 m (Figure 6.9) suggesting that increased terrigenous input is a likely scenario. Conditions in the nearby PGC will clearly affect sedimentation processes at core site VC205, particularly whether the channel was open and ice free or closed due the presence of an ice shelf. Each of these scenarios will be explored in more detail in Chapter 8.3.6.

The surface sediment age for core VC205 is significantly older (5234 ^{14}C years BP) than the suggested Antarctic marine reservoir age of shelf waters (Gordon and Harkness, 1992; Berkman and Forman, 1996; Domack et al., 2001). Unfortunately, there are no published surface sediment dates for other marine cores from this area of EAP continental shelf, so assessment as to whether this surface age is comparable with regional trends is difficult. The nearest available surface sediment ages are provided by the cores from the PGC and northern Larsen area (presented in section 6.2.6), where there is accepted contamination of fossil carbon, leading to a reservoir plus local source correction of 6000 ^{14}C years. Due to a lack of alternative corrections and supporting radiocarbon data from this area, correction of radiocarbon dates in core VC205 is done by assuming the core top age represents modern sediment surface and subtract this age from down-core ^{14}C ages. This leads to a reservoir plus local source correction of **5234 ^{14}C years** and the corrected core chronology is shown in Table 6.3 and Figure 6.20. The record from core VC205 therefore covers the Mid to Late Holocene (5564 ^{14}C years BP to present).

6.2.8 Composite age models and correction applied

Correction for the Antarctic marine reservoir effect and local source factors leads to the surface and down-core ages detailed in Table 6.3 and illustrated in Figure 6.20. Interpretation and cross-correlation of the cores studied in this investigation is based on corrected ^{14}C ages (yr BP) (as opposed to calibrated age, as discussed in section 6.2.9).

Table 6.3
Corrected AMS radiocarbon dates on bulk organic carbon for all cores used in this investigation.

Core	Sample depth (m)	Laboratory code	Conventional ^{14}C Age (^{14}C years BP ± 1σ)	Reservoir plus local source correction (years)	Corrected ^{14}C Age (^{14}C years BP ± 1σ) †
GC114	0.05	Beta - 213285	2620 (± 40)	2620	0 (± 108)
GC114	0.75	SUERC-11836	2934 (± 35)	2620	314 (± 106)
GC114	1.25	-	3515 (± 38)	2620	895 (± 107)
GC114	1.52	Beta - 213286	4230 (± 40)	2620	1610 (± 108)
GC114	1.99	-	4279 (± 39)	2620	1659 (± 107)
GC114	2.48	SUERC-11837	4669 (± 35)	2620	2049 (± 106)
GC114	3.28	Beta - 213287	5980 (± 40)	2620	3360 (± 108)
TC046	0	OxA-3249	1870 (± 70)	1870	0 (± 122)
GC047	2.4	OxA-3250	7780 (± 90)	1870	5910 (± 135)
GC047	3.6	SUERC-15254	12768 (± 76)	1870	10898 (± 126)
GC047	3.79	OxA-3251	12280 (± 150)	1870	10410 (± 180)
VC306	0	OxA-13409	4560 (± 40)	2460	2100 (± 108)
VC306	1.1	SUERC-16451	10041 (± 50)	2460	7581 (± 112)
VC306	1.62	OxA-13410	12010 (± 80)	2460	9550 (± 80)
VC306	1.8	OxA-13411	12610 (± 110)	2460	10150 (± 128)
GC358	0	Erl-10830	11246 (± 91)	N/A	Contaminated
GC359	0	Erl-9304	5131 (± 50)	5131	0 (± 112)
GC358	0.245	Erl-10831	9570 (± 82)	5131	4439 (± 129)
GC358	0.465	Erl-10832	13076 (± 95)	5131	7945 (± 138)
GC358	0.735	Erl-10832	21433 (± 168)	8783	12650 (± 195)
VC243	0.01	CAMS-68472	6010 (± 50)	6000	10 (± 112)
VC243	1.55	CAMS-68473	7930 (± 40)	6000	1930 (± 108)
VC243	3.05	CAMS-68474	9030 (± 40)	6000	3030 (± 108)
VC243	4.76	CAMS-68475	11350 (± 60)	6000	5350 (± 117)
VC243	5.92	CAMS-68476	12450 (± 40)	6000	6450 (± 108)
BC314	0	AA-51695	6022 (± 40)	6000	22 (± 108)
VC237	1	AA-50486	9302 (± 41)	6000	3302 (± 108)
VC237	1.2	AA-50487	9768 (± 43)	6000	3768 (± 109)
VC237	2.9	AA-50488	12080 (± 120)	6000	6080 (± 120)
VC237	4.7	AA-50489	15271 (± 75)	6000	9271 (± 125)
VC237	4.9	AA-50490	15330 (± 80)	6000	9330 (± 128)

Core	Sample depth (m)	Laboratory code	Conventional ^{14}C Age (^{14}C years BP ± 1σ)	Reservoir plus local source correction (years)	Corrected ^{14}C Age (^{14}C years BP ± 1σ) †
VC205	0	SUERC-16443	5234 (± 35)	5234	0 (± 106)
VC205	1.3	SUERC-16444	8354 (± 41)	5234	3120 (± 108)
VC205	2.1	SUERC-16445	9590 (± 43)	5234	4356 (± 109)
VC205	2.8	SUERC-16446	10280 (± 44)	5234	5046 (± 109)
VC205	4	SUERC-16447	10669 (± 45)	5234	5435 (± 110)
VC205	5.1	SUERC-16450	10798 (± 47)	5234	5564 (± 110)

Laboratory codes: NSF-Arizona AMS Facility (**AA**); Beta Analytic Radiocarbon Dating Laboratory, Miami (**Beta**); Center for Accelerator Mass Spectrometry, Lawrence Livermore National Laboratory (**CAMS**); Erlangen AMS Laboratory, Germany (**Erl**); Oxford Radiocarbon Accelerator Unit (**OxA**); Scottish Universities Environmental Research Centre, East Kilbride (**SUERC**).

† Error on corrected ^{14}C age was calculated through summing in quadrature, (i.e. the reported date error and error on the Antarctic reservoir correction of Berkman et al. (1998) (± 100 years), using the following equation: sqrt((date error)^2+(100)^2)).

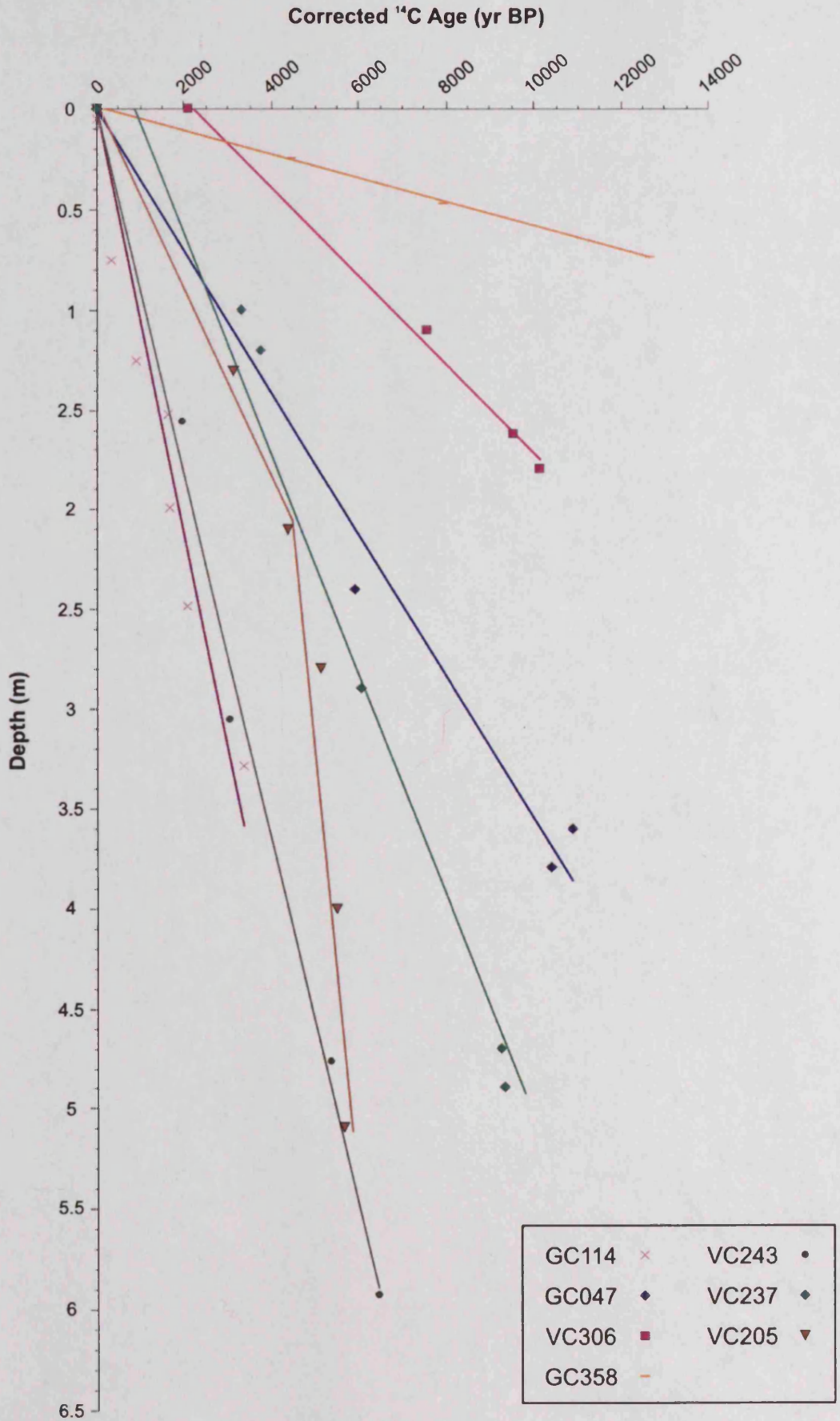


Figure 6.20
Composite corrected ^{14}C age-depth plot for all cores used in this investigation (Table 6.3). Solid lines represent linear regressions.

6.2.9 Age calibration

In palaeoclimatology, ^{14}C age calibration is needed because radiocarbon ages are not equivalent to calendar age. The calculation of the radiocarbon age of a sample assumes that the specific activity of the ^{14}C in atmospheric CO_2 has been constant. However, production of ^{14}C in the atmosphere varies through time due to changes in the Earth's geomagnetic field intensity, and in its concentration, which is regulated by the carbon cycle (specifically storage of carbon in reservoirs such as the ocean, ocean sediments and sedimentary rocks). For the past 11000 years, fluctuations in atmospheric ^{14}C have been largely produced by changes in the solar magnetic field (de Vries, 1958: 1959; Stuiver, 1961; Stuiver and Quay, 1980). For the period 14500 – 11000 years BP, many researchers believe that carbon cycle changes tied to deep ocean circulation are a significant cause of atmospheric ^{14}C fluctuations (Edwards et al., 1993; Stocker and Wright, 1996; Hughen et al., 2000; Delaygue et al., 2003).

In this investigation, correlation of events in the sediment cores was based on a corrected ^{14}C chronology (Table 6.3). This was deemed most favourable because ^{14}C ages of specific sample intervals are absolute (within laboratory errors). Although normally necessary to correct for reservoir effects, as soon as these corrections (which are highly variable and relatively unknown in the Antarctic regions), together with age calibrations (which are probabilistic (Sewell, 1998)) are applied to core chronologies, additional uncertainties and errors are introduced. Such errors should be kept to a minimum; hence in this investigation correlations are based primarily on corrected ^{14}C ages; an approach used by other Antarctic researchers (e.g. Leventer et al., 1996; Taylor and McMinn, 2002; Domack et al., 2005; Maddison et al., 2006; Bárcena et al., 1998; 2002; Yoon et al., 2007). However, because calendar ages are frequently used for other palaeoclimate records, it is necessary to also present a calibrated radiocarbon chronology for these marine cores. Calibrated ages were calculated as "cal. yr BP", quoted in brackets after the ^{14}C ages. Three different calibration tools are explored in this section: (1) CALIB (v5.0.1) (Stuiver and Reimer, 1993; Stuiver et al., 2005) using the IntCal04 dataset (Reimer et al., 2004); (2) CALIB (v5.0.1) (Stuiver and Reimer, 1993; Stuiver et al., 2005) using the Marine04 dataset (Hughen et al., 2004); and (3) CalPal online (Danzeglocke et al., 2008). The purpose of this comparison is to assess variability in output calendar ages between calibration datasets and programs, and whether any discrepancy is substantial.

When entering the radiocarbon dates into CALIB calibration software, there are several calibration datasets to choose from. To assess variability in output calendar ages between calibration datasets both IntCal04 (Reimer et al., 2004) and Marine04 (Hughen et al., 2004) were compared for all cores used in this investigation, together with an independent program CalPal online (Danzeglocke et al., 2008) (Figure 6.21). Both IntCal04 and Marine04 are constructed in two parts using a combination of tree-ring and marine datasets. IntCal04 draws on tree-ring data between 0 and 12400 cal. years BP and beyond that, because terrestrial data is sparse, IntCal04 converts coral and foraminifera data to atmospheric equivalent by subtracting a site-specific reservoir correction (R) and input into a random walk model (Reimer et al., 2004). The reverse is the case for Marine04; because high-resolution marine data are lacking between 0 – 10500 cal. years BP, Marine04 utilises the dendrochronology-based curve of IntCal04, which is then converted with an ocean-atmosphere box diffusion model (Stuiver and Braziunas, 1993) to yield mixed-layer ^{14}C ages (Hughen et al., 2004). Between 10500 and 26000 cal. years BP, Marine04 relies on direct measurements of ^{14}C ages from corals and foraminifera (Hughen et al., 2004). These data are normalised to the global ocean mixed layer reservoir age (R) (405 years), therefore no marine reservoir correction should be made to the sample radiocarbon age prior to calibration (Hughen et al., 2004; Stuiver and Reimer, 2005; Stuiver et al., 2005). However, the difference between the regional reservoir age and the mixed layer reservoir age (ΔR) is entered in CALIB; in this study, this value is the reservoir correction detailed in Table 6.3, minus 405 years. CalPal uses calibration curve "CalPal-2007-Hulu" based on Hulu-referenced Cariaco data by Hughen et al. (2006), together with numerous other calibration datasets (tree-ring, marine, coral, lacustrine; for full review see www.calpal.de/calpal/manual/index) (Danzeglocke et al., 2008). As Figure 6.21 and Table 6.4 highlights, frequently age ranges are overlapping between IntCal04 and Marine04, and CalPal is always within the 2 σ calibrated age range and frequently within the 1 σ range. As a consequence, age calibrations in this investigation were performed using the CalPal online software. This program was preferred as it has a very easy user interface, allowing quick, yet accurate age calibration.

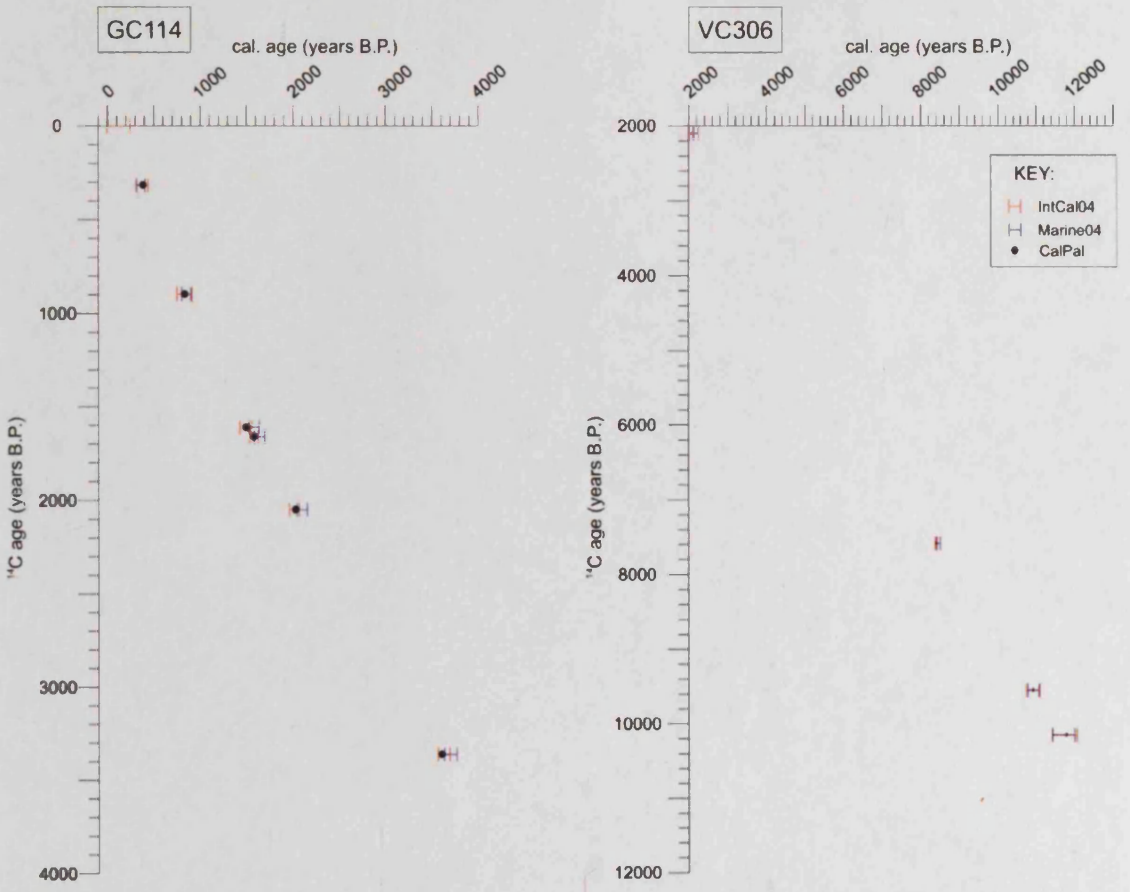


Figure 6.21
Radiocarbon age versus calibrated age for ^{14}C-dated samples from cores GC114 and VC306 using CALIB (v5.0.1) (Stuiver and Reimer, 1993). Red = calibrated age range (1 σ) generated by IntCal04 calibration dataset (Reimer et al., 2004) (inputting corrected ^{14}C age as detailed in Table 6.4); Blue = calibrated age range (1 σ) generated by MarineCal04 calibration dataset (Hughen et al., 2004) (inputting uncorrected ^{14}C age and ΔR value of individual reservoir ages detailed in Table 6.4 minus 405 years); grey circle = calibrated age (1 σ error falls with size of circle) generated by CalPal online (Danzeglocke et al., 2008) (inputting corrected ^{14}C age as detailed in Table 6.4).

Table 6.4
Radiocarbon and calibrated dates for all cores used in this investigation.

Core	Sample depth (m)	Conventional ^{14}C Age (^{14}C years BP ± 1σ)	Corrected ^{14}C Age (^{14}C years BP ± 1σ) [1]	ΔR (years) [2]	Calibrated age range (cal. years BP) [2]		Median probability (cal. years BP) [2]	CalPal online (cal. years BP)
					1 σ range	2 σ range		
GC114	0.05	2620 (± 40)	0 (± 108)	2215	X	X	X	X
GC114	0.75	2934 (± 35)	314 (± 106)	2215	313 – 407	285 – 444	364	323 (± 142)
GC114	1.25	3515 (± 38)	895 (± 107)	2215	796 – 894	744 – 923	843	826 (± 91)
GC114	1.52	4230 (± 40)	1610 (± 108)	2215	1519 – 1631	1474 – 1697	1581	1529 (± 121)
GC114	1.99	4279 (± 39)	1659 (± 107)	2215	1578 – 1691	1523 – 1747	1636	1570 (± 126)
GC114	2.48	4669 (± 35)	2049 (± 106)	2215	2034 – 2149	1985 – 2244	2099	2038 (± 130)
GC114	3.28	5980 (± 40)	3360 (± 108)	2215	3633 – 3764	3582 – 3823	3703	3623 (± 134)
TC046	0	1870 (± 70)	0 (± 122)	1465	X	X	X	X
GC047	2.4	7780 (± 90)	5910 (± 135)	1465	6665 – 6884	6547 – 7005	6780	6748 (± 169)
GC047	3.6	12768 (± 76)	10898 (± 126)	1465	12832 – 12909	12791 – 12990	12875	12872 (± 118)
GC047	3.79	12280 (± 150)	10410 (± 180)	1465	12046 – 12414 (68 %) 12440 – 12628 (32 %)	11745 – 12785	12291	12223 (± 322)
VC306	0	4560 (± 40)	2100 (± 108)	2055	2116 – 2252	2054 – 2296	2177	2107 (± 146)
VC306	1.1	10041 (± 50)	7581 (± 112)	2055	8389 – 8499	8349 – 8556	8446	8381 (± 121)
VC306	1.62	12010 (± 80)	9550 (± 80)	2055	10780 – 11070	10650 – 11131	10907	10908 (± 153)
VC306	1.8	12610 (± 110)	10150 (± 128)	2055	11597 – 12009 (86 %) 11418 – 11503 (14 %)	11291 – 12125 (98 %) 12130 – 12185 (2 %)	11764	11784 (± 287)

Core	Sample depth (m)	Conventional ^{14}C Age (^{14}C years BP ± 1σ)	Corrected ^{14}C Age (^{14}C years BP ± 1σ) [1]	ΔR (years) [2]	Calibrated age range (cal. years BP) [2]		Median probability (cal. years BP) [2]	CalPal online (cal. years BP)
					1 σ range	2 σ range		
GC358	0	11246 (± 91)	Contaminated	X	X	X	X	X
GC359	0	5131 (± 50)	0 (± 112)	4726	X	X	X	X
GC358	0.245	9570 (± 82)	4439 (± 129)	4726	5031 – 5267	4863 – 5323	5134	5090 (± 177)
GC358	0.465	13076 (± 95)	7945 (± 138)	4726	8761 – 9055	8617 – 9196	8914	8810 (± 178)
GC358	0.735	21433 (± 168)	12650 (± 195)	8378	14572 – 15160 (94 %) 14491 – 14547 (6 %)	14167 – 15345	14823	15010 (± 424)
VC243	0.01	6010 (± 50)	10 (± 112)	5595	X	X	X	X
VC243	1.55	7930 (± 40)	1930 (± 108)	5595	1888 – 2000	1849 – 2079	1953	1880 (± 130)
VC243	3.05	9030 (± 40)	3030 (± 108)	5595	3261 – 3362	3204 – 3412	3314	3204 (± 140)
VC243	4.76	11350 (± 60)	5350 (± 117)	5595	6112 – 6258	5999 – 6285	6174	6130 (± 126)
VC243	5.92	12450 (± 40)	6450 (± 108)	5595	7331 – 7414	7280 – 7449	7372	7365 (± 91)
BC314	0	6022 (± 40)	22 (± 108)	5595	X	X	X	X
VC237	1	9302 (± 41)	3302 (± 108)	5595	3564 – 3681	3488 – 3758	3625	3554 (± 121)
VC237	1.2	9768 (± 43)	3768 (± 109)	5595	4182 – 4336	4124 – 4397	4257	4160 (± 162)
VC237	2.9	12080 (± 120)	6080 (± 120)	5595	6852 – 7143	6699 – 7250	6984	6967 (± 160)
VC237	4.7	15271 (± 75)	9271 (± 125)	5595	10457 – 10609	10339 – 10720	10536	10477 (± 160)
VC237	4.9	15330 (± 80)	9330 (± 128)	5595	10507 – 10685	10420 – 10893	10603	10549 (± 180)

Core	Sample depth (m)	Conventional ^{14}C Age (^{14}C years BP ± 1σ)	Corrected ^{14}C Age (^{14}C years BP ± 1σ) [1]	ΔR (years) [2]	Calibrated age range (cal. years BP) [2]		Median probability (cal. years BP) [2]	CalPal online (cal. years BP)
					1 σ range	2 σ range		
VC205	0	5234 (± 35)	0 (± 106)	4829	X	X	X	X
VC205	1.3	8354 (± 41)	3120 (± 108)	4829	3356 – 3453	3319 – 3531	3410	3315 (± 132)
VC205	2.1	9590 (± 43)	4356 (± 109)	4829	4911 – 5079 (95 %) 5097 – 5111 (5 %)	4864 – 5203	5013	5024 (± 171)
VC205	2.8	10280 (± 44)	5046 (± 109)	4829	5767 – 5885	5709 – 5921	5824	5792 (± 111)
VC205	4	10669 (± 45)	5435 (± 110)	4829	6206 – 6296	6171 – 6367	6259	6198 (± 132)
VC205	5.1	10798 (± 47)	5564 (± 110)	4829	6315 – 6426	6278 – 6486	6378	6371 (± 107)

[1] Dates are corrected using the reservoir, plus local source corrections detailed in Table 6.3.

[2] Calibration was carried-out using CALIB (v5.0.1) (Stuiver and Reimer, 1993), Marine04 calibration dataset (Hughen et al., 2004) and a ΔR value of individual reservoir ages detailed in Table 6.3 minus 405 years. X = beyond CALIB calibration curve. Where more than one calibrated range is given, the figure in parentheses indicates the percentage of the area under the probability distribution. All other ranges constitute 100 % of the probability distribution over the stated 1σ or 2σ range.

6.3 Chapter summary

This chapter has described the core sedimentary material, outlined some of the chronology issues associated with dating Antarctic marine sediments and presented the age-models for each of the cores used in this investigation.

7 Results

This chapter presents the results of analyses performed on each core, including diatoms, and where applicable, stable isotopes and pigments. Supplementary data are on the enclosed appendix CD, including full diatom assemblage plots (with all species used during statistical analysis) and outputs from diatom statistical analysis (PCA tables, with eigenvalues, percentage variance and component loading) (labelled Figure A2.* and Table A2.*). In section 7.8, diatom assemblage data from individual core records is compared between the core locations to reveal differences in assemblages and local environmental conditions.

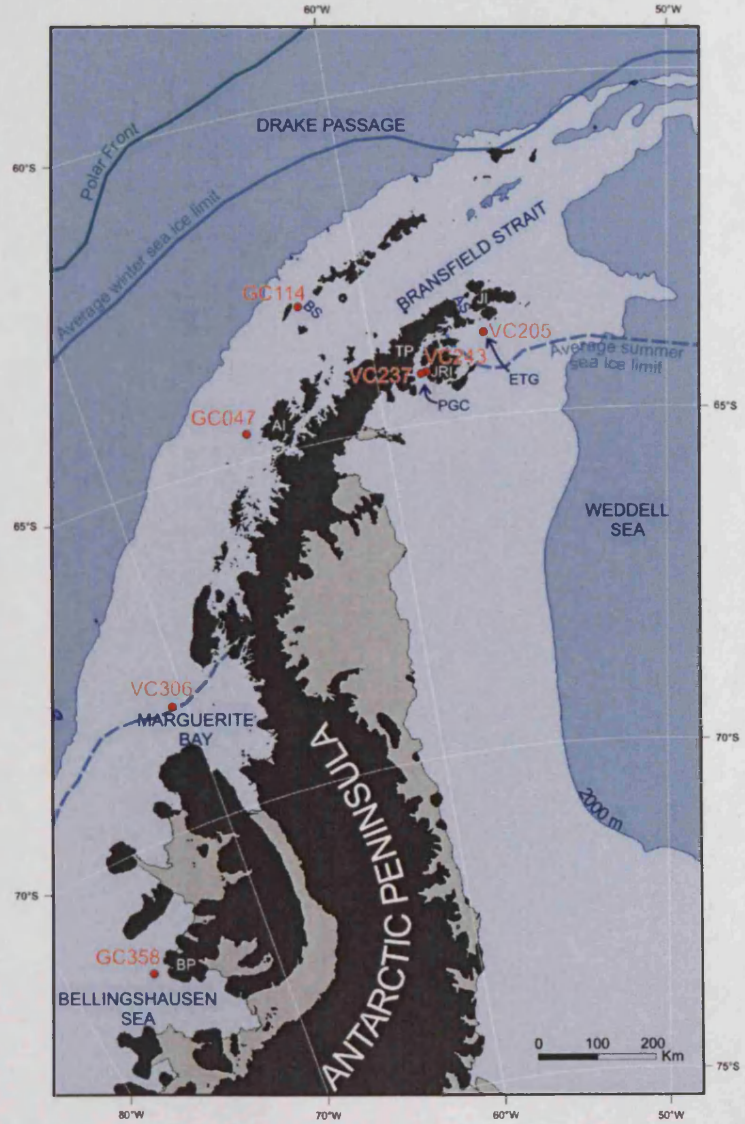


Figure 7.1 Map of the Antarctic Peninsula, showing core localities, together with the position of the present day average summer and winter sea ice limits and Polar Front (cf. Figure 2.9). AI = Anvers Island; AS = Antarctic Sound; BP = Beethoven Peninsula; BS = Boyd Strait; ETG = Erebus and Terror Gulf; JI = Joinville Island; JRI = James Ross Island; PGC = Prince Gustav Channel; TP = Trinity Peninsula.

7.1 GC114

7.1.1 Diatom assemblage

In core GC114, diatom absolute abundance is relatively constant along the core length (Figure 7.2a), suggesting reasonably stable biogenic inputs to the sediment through time. The sedimentary diatom assemblage is dominated by CRS, averaging 71.16 (± 8.5) % of the total diatom assemblage (Figure 7.2b). There is an overall trend of decreasing CRS relative abundance up-core. The non-CRS assemblage (Figure 7.4) is dominated by *F. kerguelensis* and *F. curta*, in roughly equal proportions; respective mean absolute abundance of 10 (± 2.7) Mv/g and 8.8 (± 3.4) Mv/g, and mean relative abundance of 24.6 (± 3.6) % and 20.9 (± 4.4) %. The remainder of the non-CRS assemblage includes moderate contributions from *T. gracilis* var. *gracilis* (mean absolute abundance, 2.7 (± 1.3) Mv/g; mean relative abundance, 6.5 (± 2.1) %), *F. separanda* (mean absolute abundance, 2.5 (± 1.6) Mv/g; mean relative abundance, 5.7 ± (2.3) %), *P. inermis* (mean absolute abundance, 1.8 (± 1.3) Mv/g; mean relative abundance, 4.5 (± 2.9) %) and *R. antennata* var. *semispina* (mean absolute abundance, 1.8 (± 1.3) Mv/g; mean relative abundance, 4.4 (± 2.9) %), together with minor contributions from *T. gracilis* var. *expecta*, *T. antarctica* warm rs, *T. lentiginosa* and *F. cylindrus*.

R-mode PCA analysis highlights several diatom species associations within core GC114; species with high positive and negative loadings on axes 1 – 4 are highlighted in bold and the variance explained by each PCA axis is also presented (Figure 7.5, Figure 7.6 and Table A2.5). R-mode cluster analysis of diatom species relative abundance effectively identified four distinct assemblages, of roughly equal size, at 5 % similarity (Figure 7.7). Comparison of the species associations revealed by PCA and cluster analysis are presented in Table 7.1, with indicator species highlighted.

7.1.2 Diatom stratigraphic zones

Q-mode PCA analysis reveals that stratigraphic component scores for axis 1 show much more variability than those for axes 2, 3 and 4 (Figure 7.8 and Table A2.6). Axis 2 (and to a lesser extent, axis 4) displays a distinct stratigraphic separation, with typically negative component loadings below 1.3 m and positive component loading above 1.3 m. This division at 1.3 m reflects changes in the diatom assemblage from typically *T. antarctica* warm rs, *P. inermis* and *R. antennata* species between 3.3 and 1.3 m, to *F. curta*, *F. cylindrus*, *T. gracilis* and *Navicula* species between 1.3 and 0 m. This observation is further strengthened by the presence of negative component loading

between 1.9 and 0.7 m on axis 3, reflecting the higher abundance of *F. cylindrus*, *F. vanheurckii*, *F. ritscheri* and *T. antarctica* cold rs at these depths.

Q-mode cluster analysis of sample depths reveals two main clusters at 69 % similarity (Figure 7.9a), labelled GC114-A and GC114-B, together with two outlier sample depths (2.1 and 0.4 m). Exploration of the stratigraphic associations of these clusters is achieved by plotting the cluster groups on a sedimentary log (Figure 7.9b). In core GC114, neighbouring sample depths are frequently from different cluster groups and there appears to be little order and structure to the stratigraphic pattern. This is not entirely unexpected as both total diatom abundance and individual species abundances show fluctuating stratigraphic patterns, making obvious associations between core depths difficult.

Using the criteria of core zonation (Chapter 5.1.7) based on identification of a PCA axis with simplified component loading along the core length, immediately excludes axis 1 (Figure 7.8). As highlighted in Table 7.1, all the species on axis 1 are not considered indicator species and in the example of non-indicator species given in Chapter 5.1.6, it is likely that these species are typical "species *x*" – they are potentially linked to a specific habitat but their rarity in sample depths produces a very complex stratigraphic component loading. This complexity, paired with the lack of indicator species, results in exclusion of axis 1 in core zonation. Axis 2 still encompasses a large proportion of the total variance in the data (13 %; Table A2.6) and provides two clear zones (GC114-i (3.3 – 1.3 m) and GC114-ii (1.3 – 0 m)) with distinct differences in the diatom community structure. These two zones are described below and highlighted on total diatom abundance plot (Figure 7.2) and individual species absolute and relative abundance plots (Figure 7.4).

It is worth noting that diatom absolute abundance is relatively constant (averaging 159.2 (± 56.61) Mv/g) along the core length, yet overprinted by small scale variability (Figure 7.2). A three-point moving average reveals regular cyclicity around the mean (Figure 7.3). These cycles have a periodicity of 0.4 – 0.6 m (~440 – 660 ^{14}C years). Further, each peak and trough in the cycle is composed of several data points, indicating that the cycles are a genuine feature.

7.1.2.1 GC114-i: 3.3 – 1.3 m

Total diatom abundance in this zone is relatively constant. At the base of zone GC114-i (3.3 – 2.6 m), relative abundance of CRS is high (averaging 81.34 (± 6.2) %), falling to

mid-range values (averaging 69.12 (± 4.84) %) for the remainder of this zone (2.6 – 1.3 m) (Figure 7.2b). Generally peaks and troughs in total diatom abundance coincide with peaks and troughs in non-CRS absolute abundance, except between 2.6 and 1.8 m.

Several pronounced shifts in the non-CRS species assemblage occur in zone GC114-i. Abundances of *T. antarctica* warm rs are elevated at the base (3.3 – 2.5 m), recording mean absolute and relative abundances of 2.4 (± 1.2) Mv/g and 6.6 (± 2.33) %, respectively. *T. gracilis* var. *gracilis* exhibits elevated abundances between 2.6 – 2.1 m, with average absolute abundance of 3.5 (± 0.6) Mv/g and average relative abundance of 7.4 (± 0.8) %. In the upper section of zone GC114-i (2.6 – 1.4 m), *P. inermis* displays elevated absolute and relative abundance, averaging 2.9 (± 1.4) Mv/g and 6.9 (± 3.2) %, respectively. Likewise, *P. truncata* also shows increased absolute and relative abundance between 2.6 – 1.6 m, averaging 0.71 (± 0.24) Mv/g and 1.6 (± 0.5) %, respectively. Finally, *R. antennata* group records elevated absolute and relative abundances between 2 – 1.4 m, averaging 3.8 (± 1.5) Mv/g and 9.4 (± 2.1) %, respectively. The high abundances of both these three species rapidly diminish at the transition into zone GC114-ii.

7.1.2.2 GC114-ii: 1.3 – 0 m

Total diatom abundance in the upper section of this zone (0.6 – 0 m) progressively decreases up-core, to reach a minimum at 0.1 m (66.62 Mv/g) (Figure 7.3). CRS relative abundance also shows a decline up-core of 0.6 m, to relatively low abundance at 0 m (56 %). The non-CRS absolute abundance does not record a comparable decline through this section of zone GC114-ii (0.6 – 0 m), maintaining fluctuating mid-range values (42.27 (± 13.14) Mv/g).

F. curta, *F. cylindrus* and *T. gracilis* var. *expecta* show pronounced elevated absolute and relative abundances between 1.3 and 0 m. Grouped *F. curta* and *F. cylindrus* absolute and relative abundance total 11.18 (± 4.15) Mv/g and 26.08 (± 4.65) % respectively. *T. gracilis* var. *expecta* reaches mean absolute and relative abundances of 1.8 (± 0.7) Mv/g and 4.6 (± 2.1) %, respectively. *T. gracilis* var. *gracilis* exhibits elevated abundances in the upper section of this zone (0.8 – 0 m), with average absolute abundance of 3.6 (± 1.5) Mv/g and average relative abundance of 8.3 (± 2.4) %. As described in section 7.1.2.1, *P. inermis*, *P. truncata* and *R. antennata* group are present in notably diminished numbers throughout zone GC114-ii.

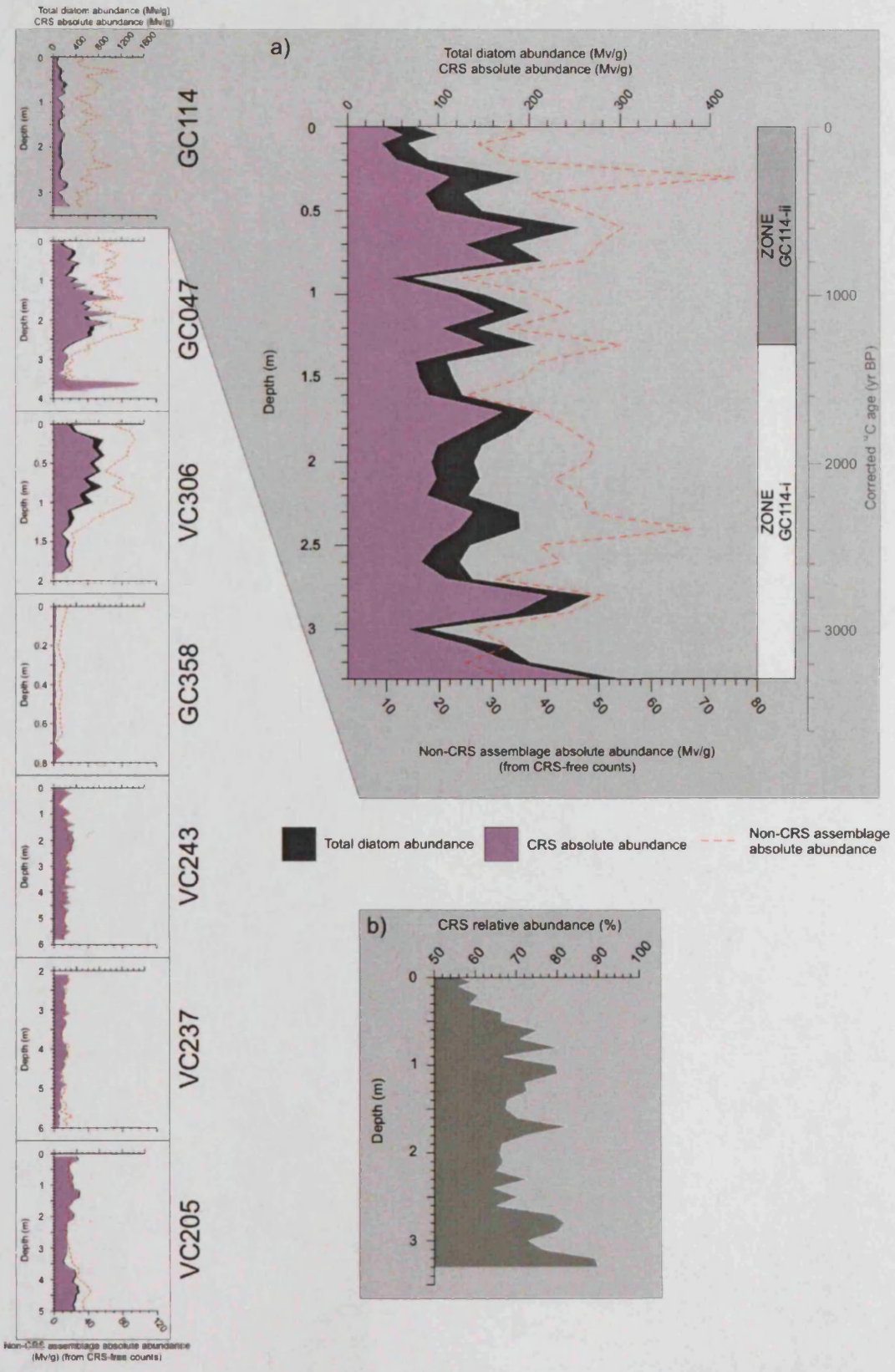


Figure 7.2

a) Core GC114: Total diatom abundance, CRS absolute abundance (both from CRS-included counts) and non-CRS assemblage absolute abundance (from CRS-free counts) (millions of valves/g (Mv/g)). Stratigraphic zones GC114-i and GC114-ii identified using Q-mode PCA analysis of diatom relative abundance data.

b) Core GC114: CRS relative abundance (%).

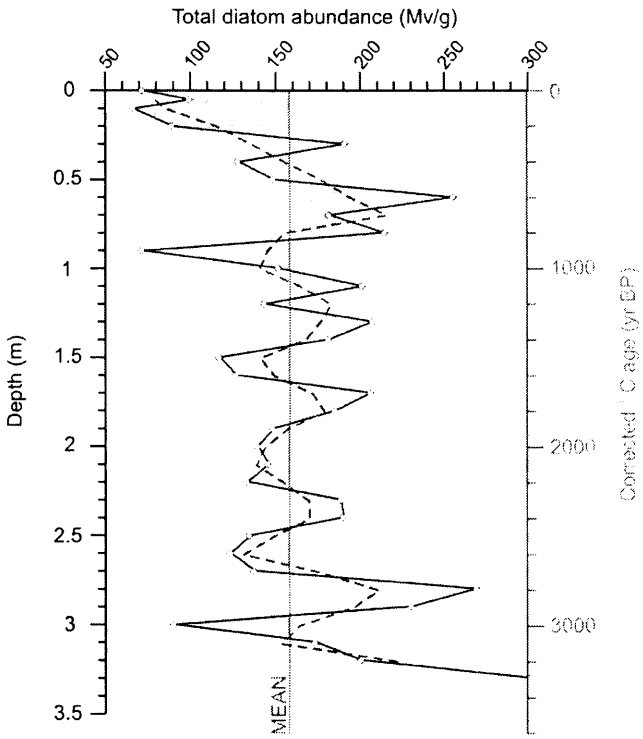


Figure 7.3
Core GC114: Diatom absolute abundance (from CRS-included counts; Mv/g). Three point moving average (dashed line), sample depths (white dots) and mean absolute abundance (grey solid line).

Figure 7.4
CoreGC114:Non-CRS diatom assemblage plots forAP indicator species: (a)Absolute abundance (Mv/g); (b) Relative abundance (%).
Three point average (white); original abundance (dark grey line). Stratigraphic zones GC114-i andGC114-ii identified usingQ-mode PCA analysis of diatom relative abundance data.

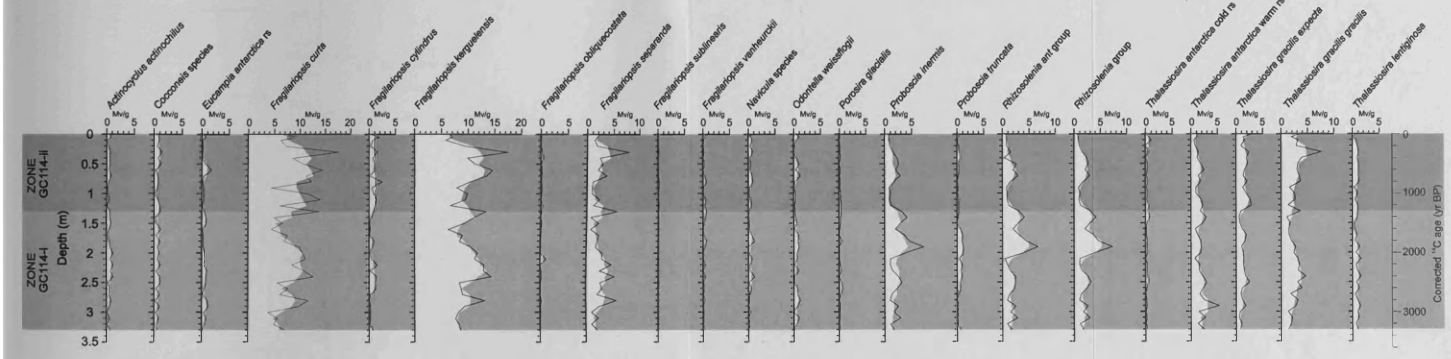


Figure 7.4 (a)

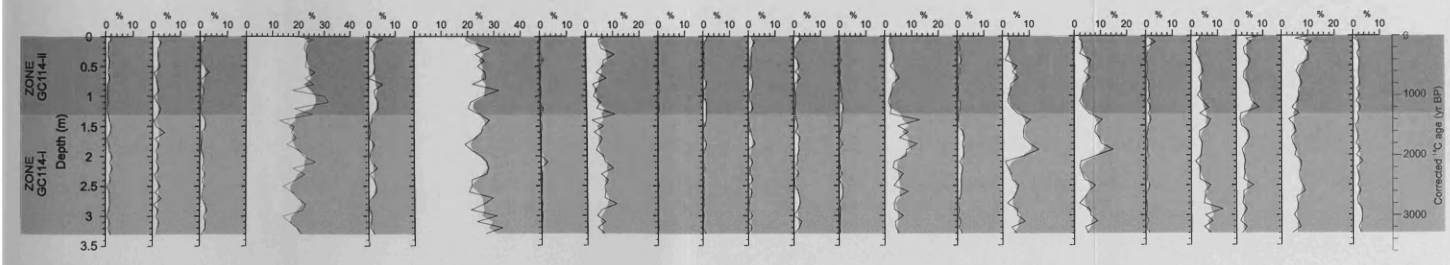


Figure 7.4 (b)

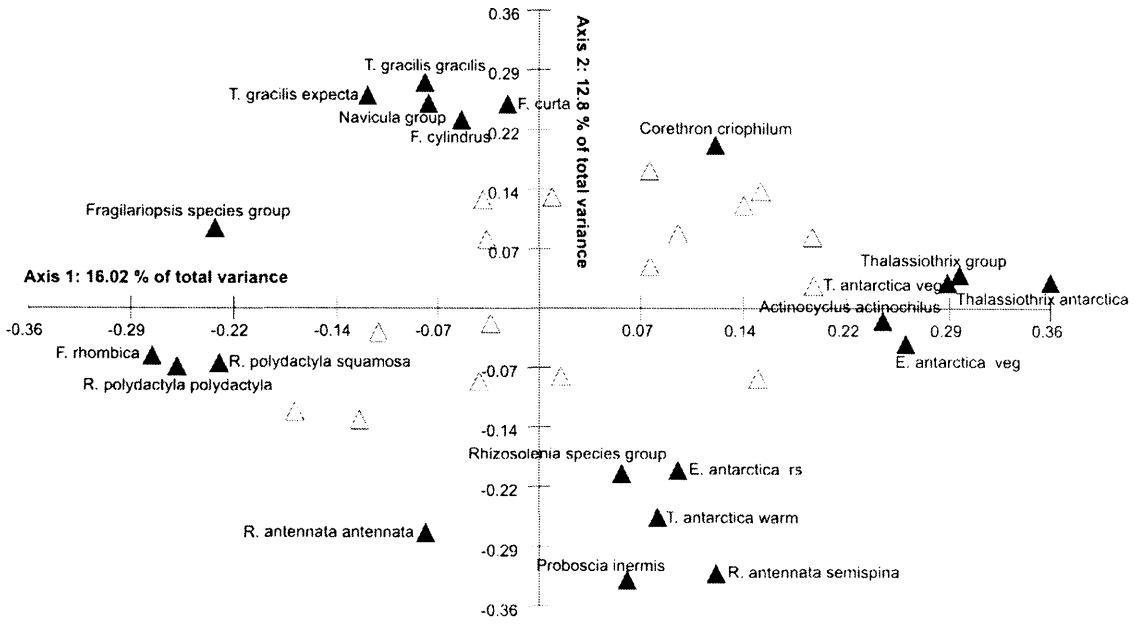


Figure 7.5
Core GC114: R-mode PCA variable loading on axes 1 and 2 for diatom relative abundance data (> 1 %). Data square-root transformed and standardised. Tolerance of eigenanalysis set at 1 x 10^{-10}. Highlighted species are those that have component loading ≥ + 0.20 or ≤ – 0.20.

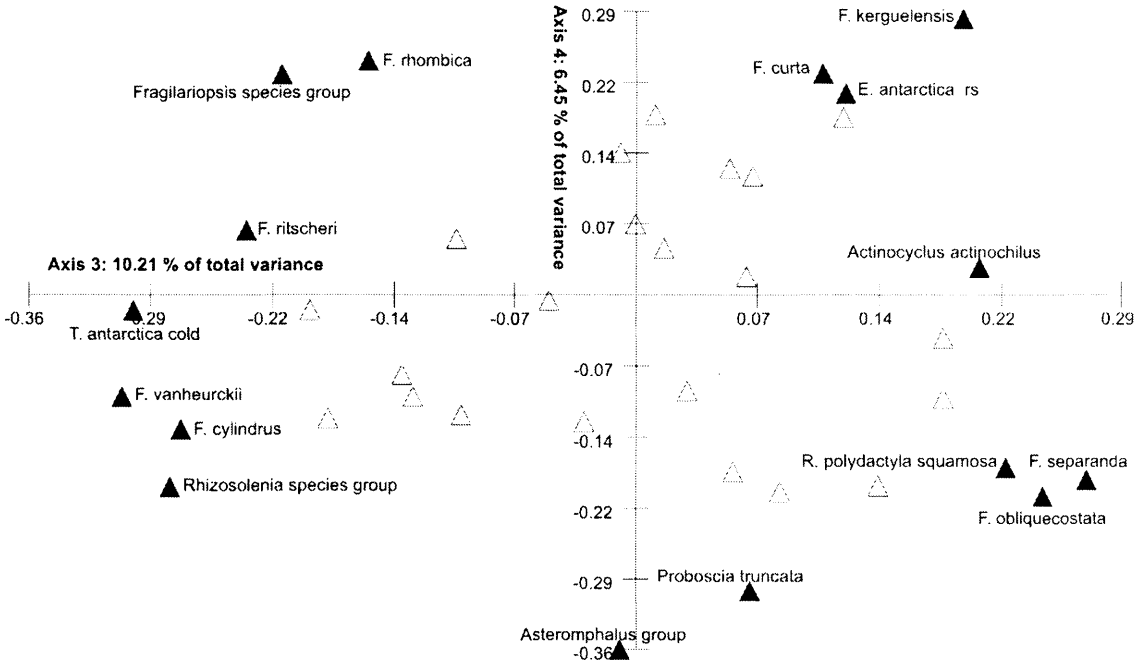


Figure 7.6
Core GC114: R-mode PCA variable loading on axes 3 and 4 for diatom relative abundance data (> 1 %). Data square-root transformed and standardised. Tolerance of eigenanalysis set at 1 x 10^{-10}. Highlighted species are those that have component loading ≥ + 0.20 or ≤ – 0.20.

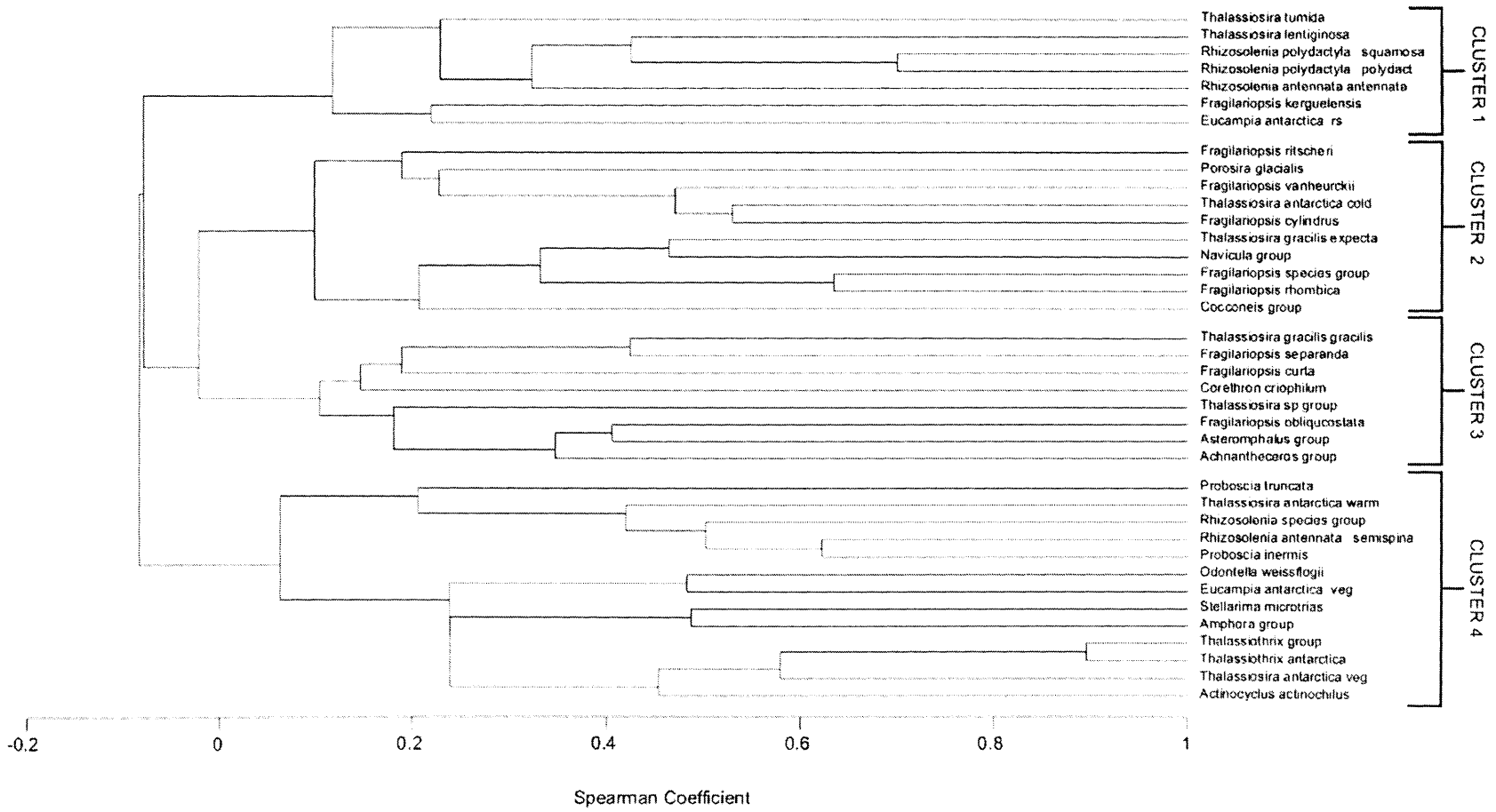


Figure 7.7

GC114: R-mode cluster analysis of diatom species relative abundance (>1 %). UPGMA clustering method; data square-root transformed; and Spearman Coefficient similarity measure.

Table 7.1
Core GC114: Comparison of diatom PCA axis loading and cluster groupings. Indicator species denoted with *. Grouped indicator species shown in grey box and relate to diatom assemblages highlighted on Figure 7.10.

Axis 1 Positive	Cluster group		**Axis 1 Negative**	Cluster group	
A. actinochilus	4	**None**	*F. rhombica*	2	**None**
E. antarctica veg	4		*Fragilariopsis* species gp	2	
T. antarctica veg	4		*R. polyd polydactyla*	1	
Thalassiothrix group	4		*R. polyd squamosa*	1	
Axis 2 Positive	Cluster group		**Axis 2 Negative**	Cluster group	
*F. curta**	3	**F. curta – F. cylindrus; T. gracilis**	*P. inermis**	4	**Rhizosolenia – Proboscia**
*F. cylindrus**	2		*R. antennata* f. *antennata*	1	
Navicula group	2		*R. antennata* f. *semispina**	4	
*T. gracilis expecta**	2		*R.* species group	4	
T. gracilis var. *gracilis**	3		*T. antarctica* warm rs*	4	
Axis 3 Positive	Cluster group		**Axis 3 Negative**	Cluster group	
A. actinochilus	4	**F. separanda**	*F. cylindrus**	2	**F. cylindrus**
F. obliquecostata	3		*F. ritscheri*	2	
*F. separanda**	3		*F. vanheurckii*	2	
R. polydactyla f. *squamosa*	1		*Fragilariopsis* species gp	2	
			Rhizosolenia species gp	4	
			T. antarctica cold rs	2	
Axis 4 Positive	Cluster group		**Axis 4 Negative**	Cluster group	
E. antarctica rs	1	**F. curta; F. kerguelensis**	*Asteromphalus* group	3	**None**
*F. curta**	3		*F. obliquecostata*	3	
*F. kerguelensis**	1		*P. truncata*	4	
F. rhombica	2				
Fragilariopsis species gp	2				

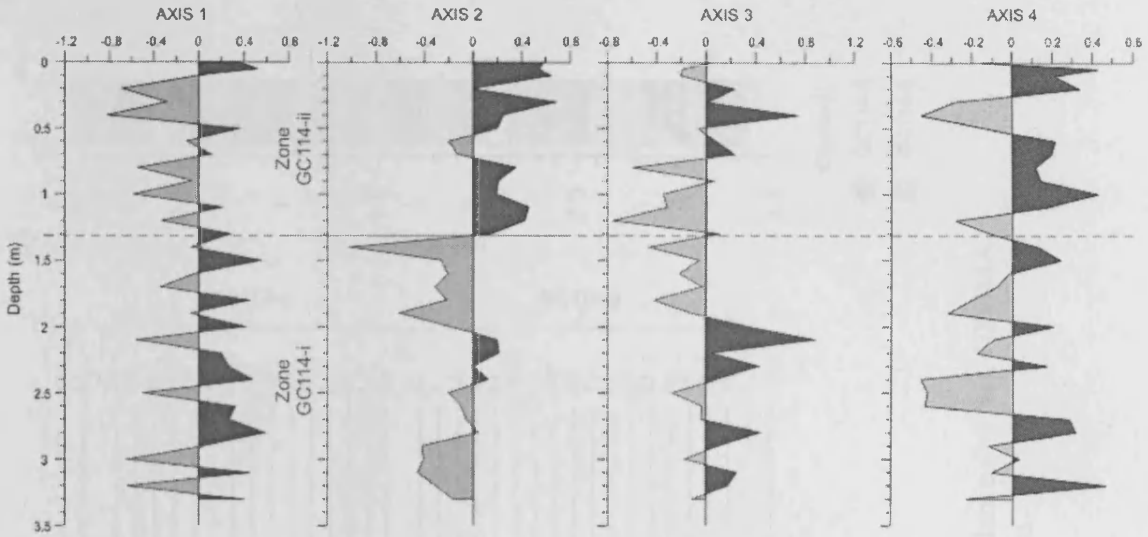


Figure 7.8
Core GC114: Q-mode PCA component scores plotted stratigraphically for PCA axes 1 – 4. Positive loading (dark grey); negative loading (light grey). Division of the record into stratigraphic zones GC114-i and GC114-ii was based on component loading on axis 2.

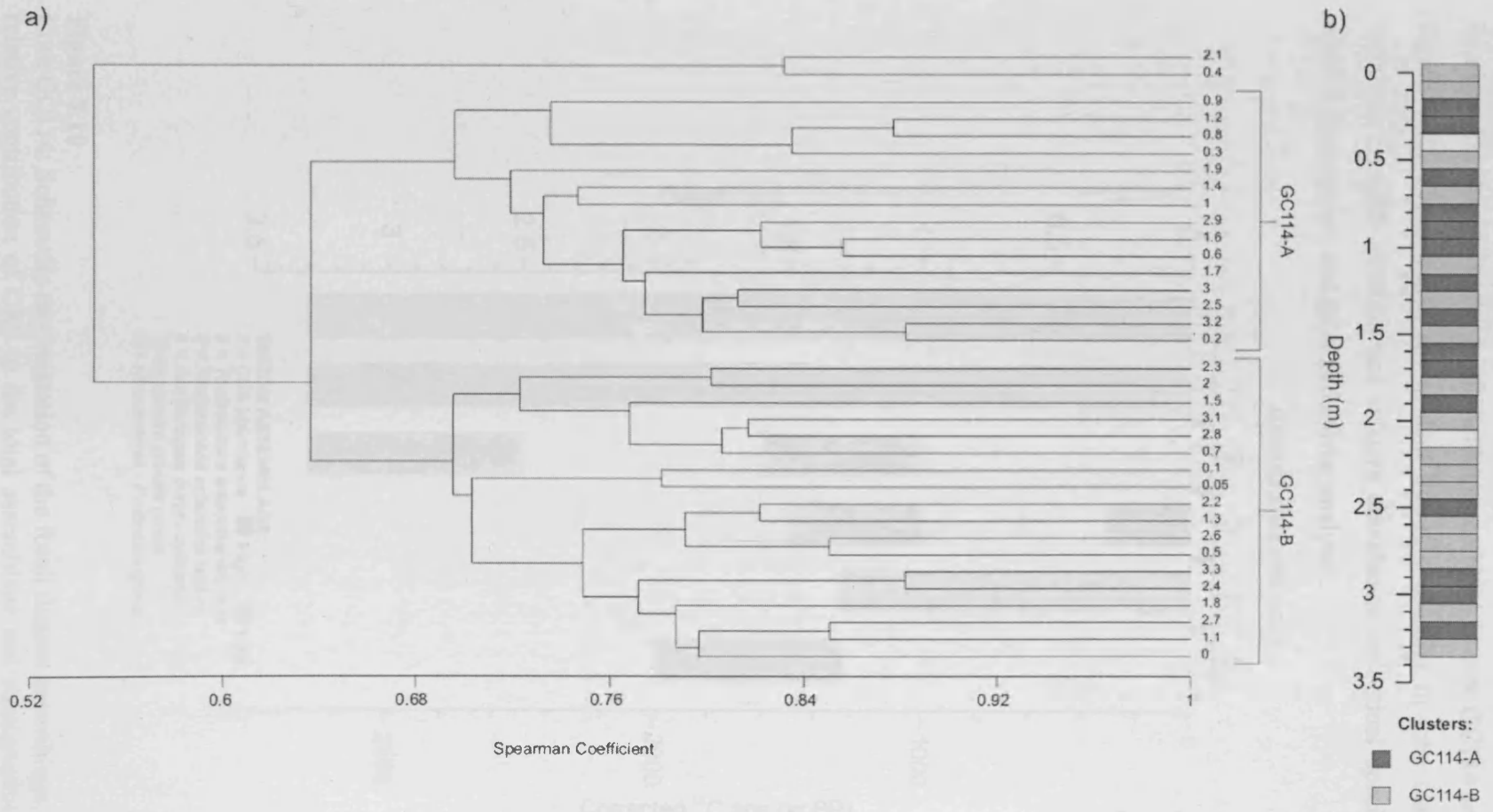


Figure 7.9

a) Core GC114: Q-mode cluster analysis of core depths, using diatom species relative abundance (>1 %). UPGMA clustering method; data square-root transformed; and Spearman Coefficient similarity measure.

b) Core GC114: Stratigraphic pattern of Q-mode cluster groups.

7.1.3 Diatom summary

Stratigraphic changes in the fossil diatom assemblage in core GC114 are summarised in Figure 7.10. These trends are evident through: changes in total diatom abundance; variations in CRS absolute and relative abundance; individual species absolute and relative abundances; and PCA and cluster analyses.

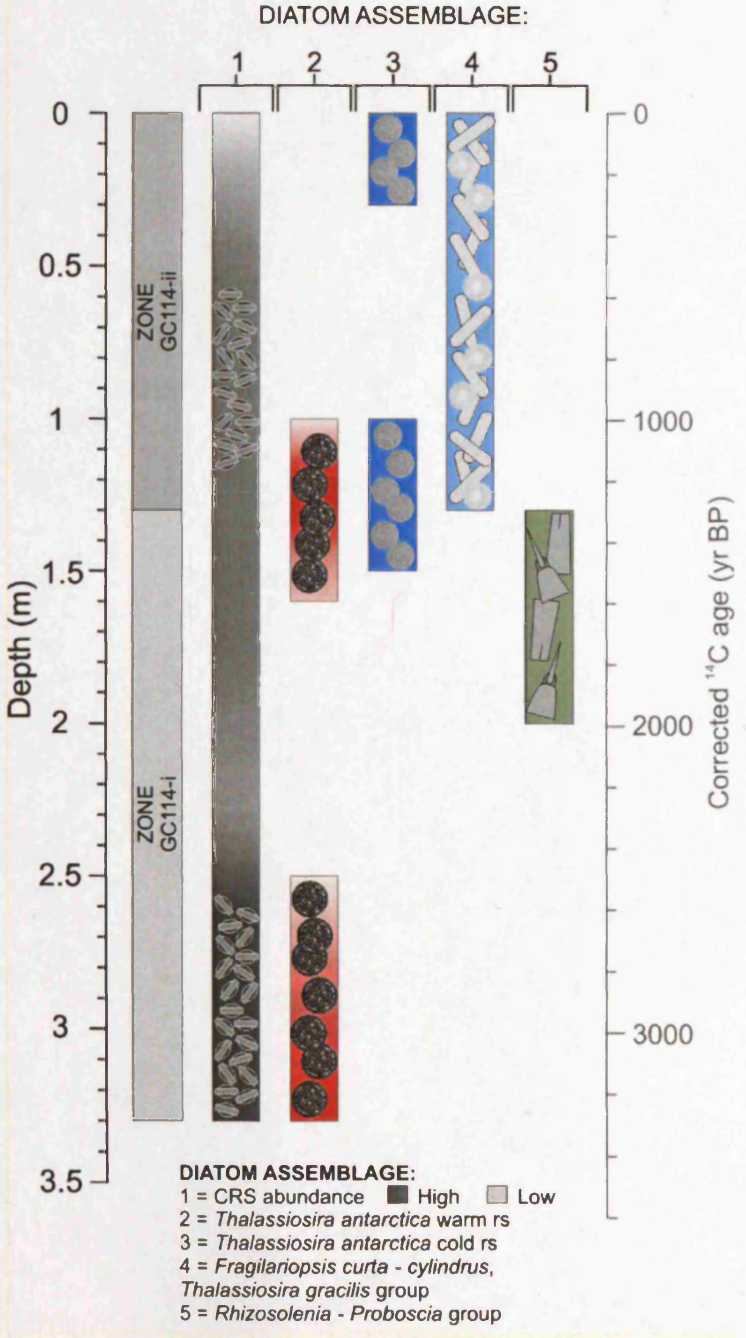


Figure 7.10
Core GC114: Schematic representation of the fossil diatom assemblage, highlighting the relative contribution of CRS to the total assemblage and stratigraphic changes in the diatom community. Stratigraphic zones GC114-i and GC114-ii identified using Q-mode PCA analysis of diatom relative abundance data. Darker tones indicate elevated abundance.

7.2 GC047

7.2.1 Diatom assemblage

Diatom absolute abundance in core GC047 shows significant variation, recording fluctuating biogenic inputs into the sediment (Figure 7.11a). CRS constitute a large proportion of the total diatom assemblage (averaging 86.32 ± 7.07 %) (Figure 7.11b). Although variations in the non-CRS species assemblage are pronounced (Figure 7.12), typically the assemblage is dominated by *F. curta*, *F. kerguelensis* and *T. antarctica* warm rs in roughly equal proportions; respective mean absolute abundance of 9.2 (± 6.5) Mv/g, 8.9 (± 5.5) Mv/g and 7.4 (± 2.6) Mv/g, and mean relative abundance of 15.6 (± 5.3) %, 15.3 (± 6.2) % and 18.2 (± 12.4) %. The remainder of the non-CRS assemblage includes moderate contributions from *T. gracilis* var. *gracilis* (mean absolute abundance, 2.1 (± 1.5) Mv/g; mean relative abundance, 3.5 (± 2.1) %), *T. gracilis* var. *expecta* (mean absolute abundance, 1.5 (± 0.9) Mv/g; mean relative abundance, 3 (± 1.4) %), *R. antennata* group (mean absolute abundance, 1.9 (± 1.6) Mv/g; mean relative abundance, 3.2 (± 1.9) %), *T. lentiginosa* (mean absolute abundance, 1.7 (± 1.2) Mv/g; mean relative abundance, 2.7 ± (1.8) %) and *P. inermis* (mean absolute abundance, 1.4 (± 1.2) Mv/g; mean relative abundance, 2.5 (± 1.9) %), together with minor contributions from *O. weissflogii*, *A. actinochilus* and *F. vanheurckii*.

R-mode PCA analysis highlights several diatom species associations within core GC047; species with high positive and negative loadings on axes 1 – 5 are highlighted in bold and the variance explained by each PCA axis is also presented (Figure 7.13, Figure 7.14, Figure 7.15 and Table A2.7). R-mode cluster analysis of diatom species relative abundance highlighted four diatom assemblages, at 10 % similarity (Figure 7.16). Comparison of the species associations revealed by PCA and cluster analysis are presented in Table 7.2, with indicator species highlighted.

7.2.2 Diatom stratigraphic zones

Q-mode PCA analysis reveals interesting stratigraphic patterns, particularly fluctuations from one dominant component loading to another along the core length (Figure 7.17 and Table A2.8). Axes 1, 2 and 3 record clear groupings along the core length, whereas axes 4 and 5 are more variable. Axis 1 displays solely highly negative loading below 2.7 m, with a transition to positive loading above 2.7 m. This reflects the dominance of *T. antarctica* warm rs, *F. cylindrus* and *F. vanheurckii* (all displaying high negative

loading on axis 1) between 3.8 – 2.7 m, and an increasing contribution from *T. gracilis* var. *gracilis*, *T. lentiginosa* and *R. antennata* (all displaying high positive loading on axis 1) between 2.7 – 0 m. Similarly, on axis 2 there is a fluctuating pattern with high negative loading (*F. kerguelensis*, *F. rhombica* and *F. separanda*) at the base of the core and between 2.5 – 0.8 m and high positive loading (*Rhizosolenia* species, *Proboscia* species, *T. gracilis* var. *expecta* and *O. weissflogii*) between 3.5 – 2.5 m and 0.8 – 0 m. Finally, axis 3 also provides interesting information on species groupings stratigraphically, with solely negative loading between 3.3 – 1.3 m, sandwiched by positive loading between 3.8 – 3.3 m and 1.3 – 0 m. This records higher relative abundance of *E. antarctica* rs and vegetative valves, *F. kerguelensis* and *Thalassiothrix antarctica* (all displaying high negative loading on axis 3) between 3.3 m – 1.3 m, higher relative abundance of *T. antarctica* cold rs, *S. microtrias*, *A. actinochilus*, *C. pennatum* and *P. inermis* (all displaying high positive loading on axis 3) occur immediately up-core of this interval.

Q-mode cluster analysis on sample depths in core GC047 revealed several high level groupings between core depths, at 60 % similarity, together with two outlier sample depths (3.68 m and 3.6 m) (Figure 7.18a). These groups are labelled GC047-A, GC047-B and GC047-C. Cluster group GC047-C can be further sub-divided into 5 smaller clusters, labelled i – v. When individual sample depths within each cluster and sub-cluster are plotted on a sedimentary log for core GC047 (Figure 7.18b) it is apparent that neighbouring sample depths are frequently from the same cluster group. These groups highlight clear temporal associations of similar diatom species. Cluster group GC047-A and cluster group GC047-B occur solely between 3.8 and 3.52 m and 3.44 and 2.72 m respectively; cluster group GC047-C is solely between 2.64 and 0 m. Between core depths 2.64 and 0 m (cluster group GC047-C), there is a progression up-core from sub-cluster ii and iii (2.64 – 1.28 m) to iv and v (1.2 – 0 m).

Using the method of core zonation (Chapter 5.1.7), the primary and secondary PCA axes were chosen to form the basis of stratigraphic division of core GC047 (Figure 7.17). Combined axis 1 and 2 explain 34.41% of the total variance in the diatom data, with axis 1 explaining 22.71% of the variance (Table A2.8). Four clear zones are highlighted (GC047-i (3.8 – 3.5 m), GC047-ii (3.5 – 2.75 m), GC047-iii (2.75 – 0.8 m) and GC047-iv (0.8 – 0 m)) with distinct differences in the diatom community structure. These four zones are described below and highlighted on total diatom abundance plot

(Figure 7.11) and individual species absolute and relative abundance plots (Figure 7.12).

7.2.2.1 GC047-i: 3.8 – 3.5 m

The highest values of diatom absolute abundance are found in this zone, with a distinctive peak between 3.68 and 3.6 m (1540 Mv/g) (Figure 7.11), corresponding to the CRS ooze described on the sedimentary log (Figure 6.3). This CRS ooze layer represents a complete dominance of the diatom assemblage by CRS, with relative abundance reaching 99.19 % at 3.68 m. Conversely, non-CRS absolute abundance is low throughout this zone, averaging 16.4 (± 4.5) Mv/g.

Paired with the extremely high abundance of CRS between 3.68 and 3.6 m, *F. cylindrus*, *F. vanheurckii* and *Pseudonitzschia* species also are found in elevated abundances in this zone, reaching relative abundance levels of >26 %, >12 % and >8 % respectively, together with elevated absolute abundance (2.56, 1.33 and 1.43 Mv/g respectively). *Corethron pennatum*, together with grouped *F. rhombica*, *F. separanda* and *F. ritscheri* also show an association at this core depth, but to a lesser extent, with relative abundances of >5%, >6 % and >3 %, and absolute abundance values of 0.65, 1.07 and 0.36 Mv/g.

Overall, *T. antarctica* warm rs dominate the non-CRS diatom assemblage throughout this zone and into zone GC047-ii, with a mean relative abundance of 33.6 (± 13.6) %. In contrast, lowest absolute and relative abundances of *T. antarctica* cold rs are observed in this zone and into GC047-ii, averaging 0.25 (± 0.15) Mv/g and 1.34 (± 0.82) %, respectively. Further, abundances of both *F. curta* and *F. kerguelensis* are comparatively low in zones GC047-i and GC047-ii; *F. curta* records mean absolute and relative abundances of 2.09 (± 1.08) Mv/g and 10.71 (± 3.53) and *F. kerguelensis* of 1.67 (± 1.11) Mv/g and 8.36 (± 3.39) % (c.f. core average for these species in section 7.2.1).

7.2.2.2 GC047-ii: 3.5 – 2.75 m

From the extremely high total diatom abundance witnessed in zone GC047-i, there is a dramatic decrease to low abundances (200 (± 48) Mv/g) at the transition between the zones and throughout zone GC047-ii. Non-CRS absolute abundance maintains low from zone GC047-i into GC047-ii, averaging 19.74 (± 4.8) Mv/g.

As discussed in section 6.2.2.1, *T. antarctica* warm rs dominate the non-CRS assemblage throughout this zone, with relatively low concentrations of *F. curta* and *F. kerguelensis*. *E. antarctica* rs show an interesting pattern in this zone and into zone GC047-iii, with pronounced higher absolute (7.07 (± 5.26) Mv/g) and relative (12.25 (± 3.54) %) abundances between 3.2 and 1.9 m.

7.2.2.3 GC047-iii: 2.75 – 0.8 m

At the transition into zone GC047-iii, total diatom abundance gradually increases, reaching fluctuating mid-values (728 (± 163) Mv/g) between 2.4 m and 1.28 m. Up-core of 1.28 m, there is a symmetrical, yet less smooth, decline in abundance into zone GC047-iv. Concurrent with the increase in total diatom abundance at 2.75 m, absolute abundance of the non-CRS assemblage also increases, reaching maximum values for the core between 2.24 and 2 m of ~100 Mv/g. Up-core of this maximum, non-CRS absolute abundance falls slightly to mid-levels (63 (± 9.9) Mv/g), which are sustained throughout zone GC047-iii and GC047-iv. CRS relative abundance is relatively stable in the lower section of zone GC047-iii (2.75 – 1.28 m), averaging 88.31 (± 3.1) %. Up-core of 1.28 m, CRS relative abundance decreases gradually through the upper section of zone GC047-iii.

Several species exhibit a change in abundance at the transition between zone GC047-ii and GC047-iii. Abundance of *F. curta* increases dramatically, reaching highest abundance for the core between 2.5 – 1.8 m (18.68 (± 5.68) Mv/g and 22.22 (± 4.22) %). Paired with this, *E. antarctica* rs also reach maximum abundance for the core in near identical core depths to *F. curta* (3.2 – 1.9 m, as described in section 7.2.2.2). *F. kerguelensis* abundance also increases sharply at the base of zone GC047-iii, reaching maximum values at 2.32 m (18.3 Mv/g and 21.76 %). The elevated abundance of these two species of *Fragilariopsis* is sustained throughout zone GC047-iii and into GC047-iv. They form a significant and roughly equal proportion of the non-CRS assemblage in these upper two zones, with absolute and relative abundances averaging 11.73 (± 3.45) and 12.7 (± 5.33) Mv/g, and 18.12 (± 4.61) and 18.15 (± 4.26) %, for *F. kerguelensis* and *F. curta*, respectively. It is worth noting that the increase in *F. kerguelensis* abundance (at core depths <2.88 m) precedes the comparable increase in *F. curta* abundance (at core depths <2.56 m).

Other species recording a change at the transition into zone GC047-iii are *T. gracilis* var. *gracilis* and *T. lentiginosa*. Both these species record comparatively high absolute

and relative abundances between throughout zone GC047-iii and GC047-iv, of ~2.6 Mv/g and ~4 %, respectively.

7.2.2.4 GC047-iv: 0.8 – 0 m

Total diatom abundance decreases from the core maximum at 1.28 m, reaching comparatively low diatom abundance in zone GC047-iv (averaging, 326 (± 94.2) Mv/g). In contrast, abundance of the non-CRS assemblage does not fall dramatically in zone GC047-iv, maintaining mid-range values (averaging, 65.1 (± 6.83) Mv/g) towards the core top. CRS relative abundance continues the decreasing trend initiated at 1.28 m (zone GC047-iii) towards the core top, reaching lowest value at 0.08 m (62.36 %).

Along the full core length, *T. antarctica* cold rs exhibit an up-core trend of gradually increasing absolute and relative abundance, reaching highest abundances in zone GC047-iv (averaging, 3.09 (± 1.46) Mv/g and 4.63 (± 1.92) %). *P. inermis* and grouped *Rhizosolenia* species also record elevated abundances in zone GC047-iv, with mean absolute abundances of 2.85 (± 1.37) Mv/g and 5.03 (± 1.26) Mv/g, respectively, and mean relative abundance of 4.35 (± 1.94) % and 7.69 (± 1.65) %, respectively.

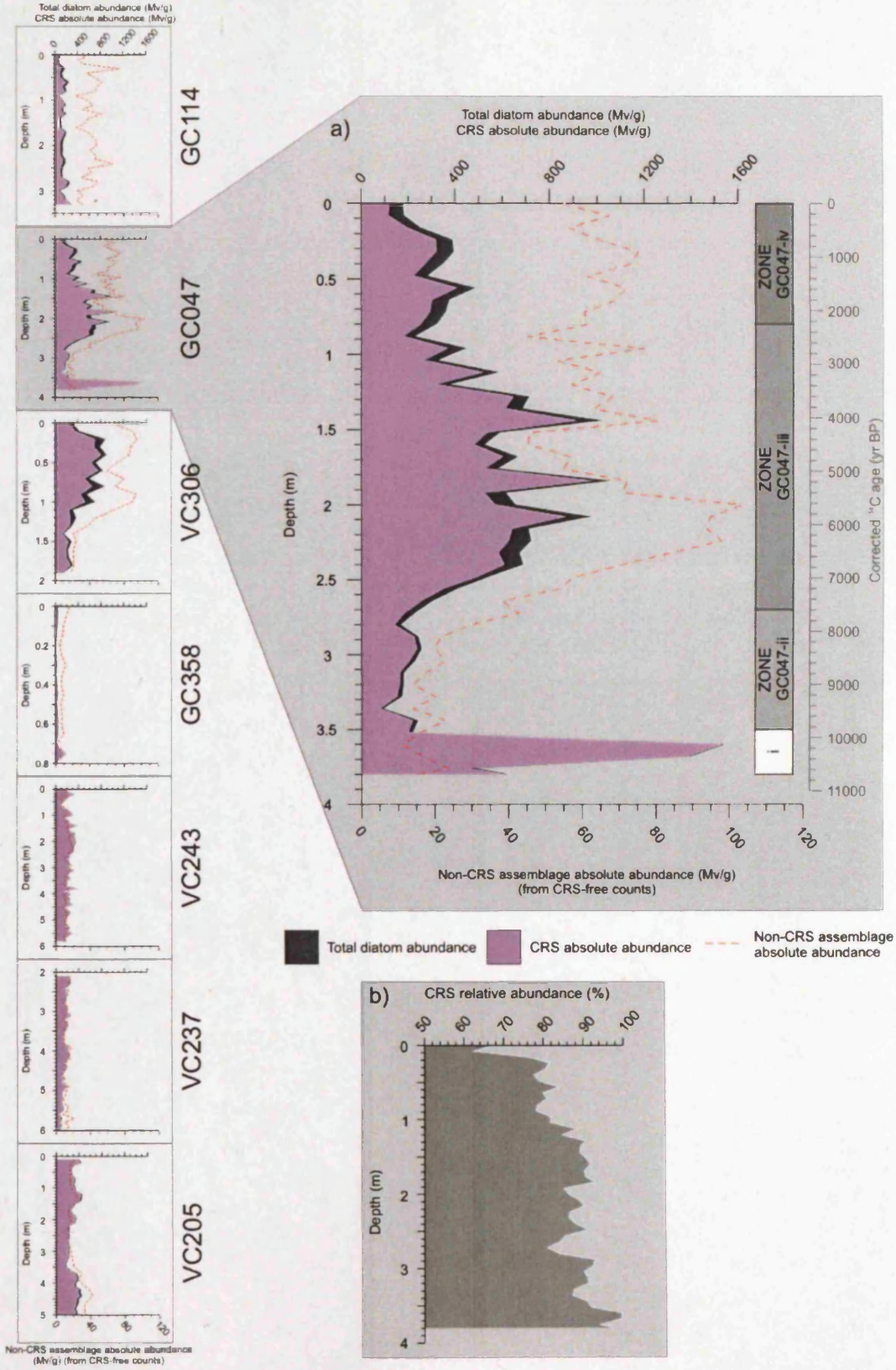


Figure 7.11

a) Core GC047: Total diatom abundance, CRS absolute abundance (both from CRS-included counts) and non-CRS assemblage absolute abundance (from CRS-free counts) (millions of valves/g (Mv/g)). Stratigraphic zones GC047-i, GC047-ii, GC047-iii and GC047-iv identified using Q-mode PCA analysis of diatom relative abundance data.

b) Core GC047: CRS relative abundance (%).

Figure 7.12
CoreGC047: Non-CRS diatom assemblage plots forAP indicator species: (a)Absolute abundance (Mv/g); (b) Relative abundance (%).
Stratigraphic zones GC047-i to GC047-iv identified using Q-mode PCA analysis of diatom relative abundance data.

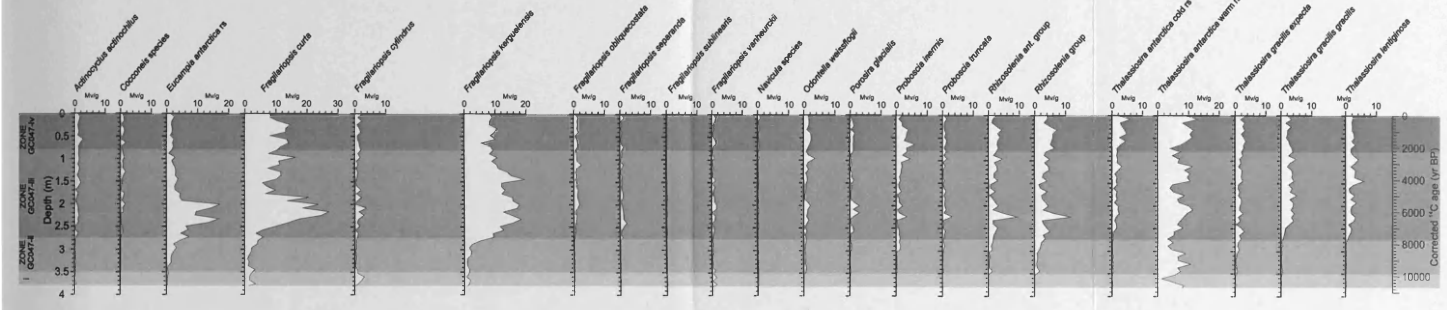


Figure 7.12 (a)

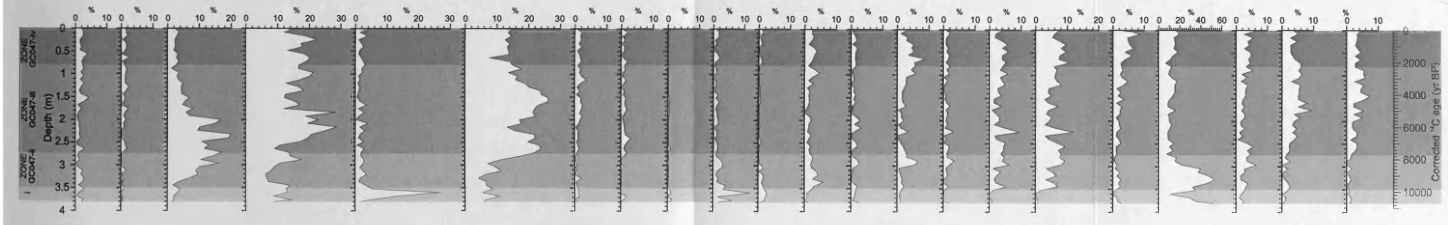


Figure 7.12 (b)

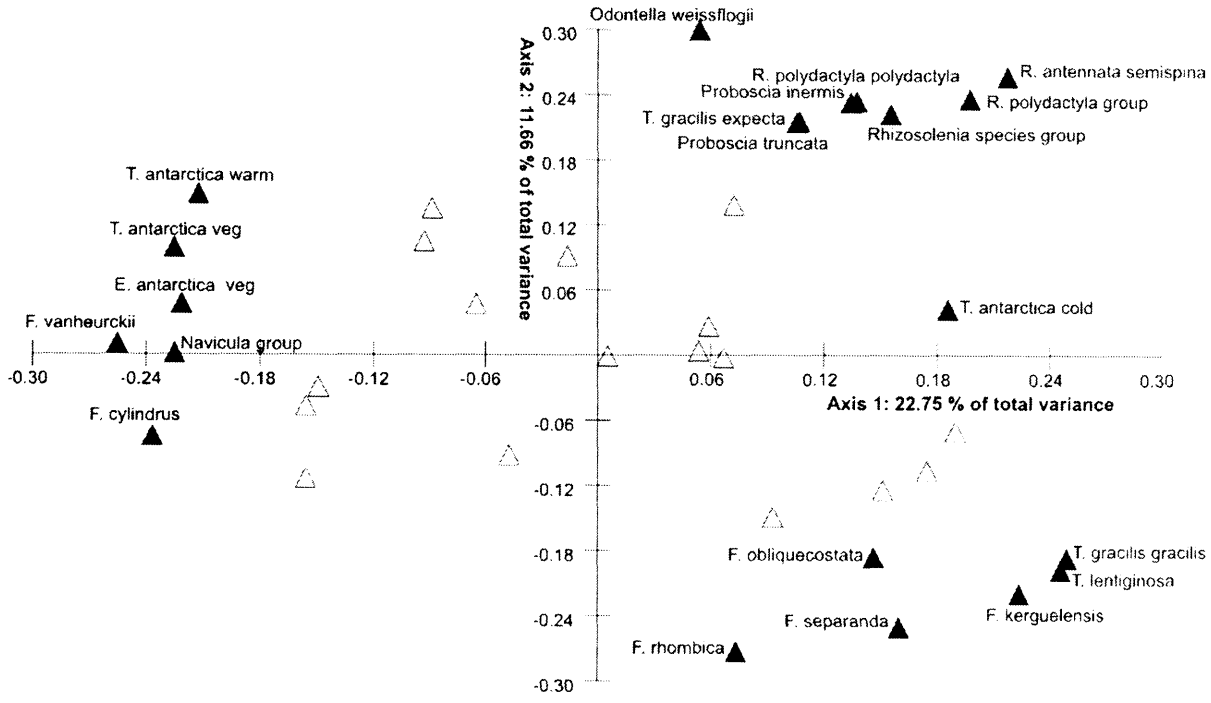


Figure 7.13
Core GC047: R-mode PCA variable loading on axes 1 and 2 for diatom relative abundance data (> 1 %). Data square-root transformed and standardised. Tolerance of eigenanalysis set at 1 x 10^{-10}. Highlighted species are those that have component loading ≥ + 0.20 or ≤ – 0.20.

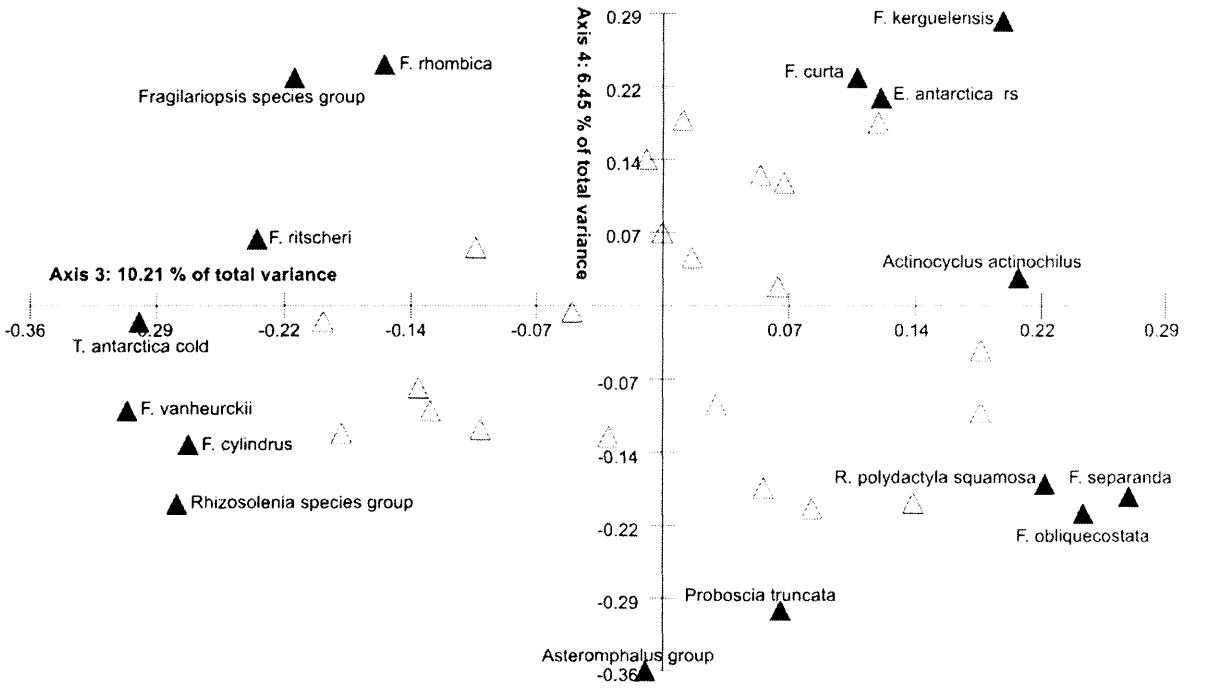


Figure 7.14
Core GC047: R-mode PCA variable loading on axes 3 and 4 for diatom relative abundance data (> 1 %). Data square-root transformed and standardised. Tolerance of eigenanalysis set at 1 x 10^{-10}. Highlighted species are those that have component loading ≥ + 0.20 or ≤ – 0.20.

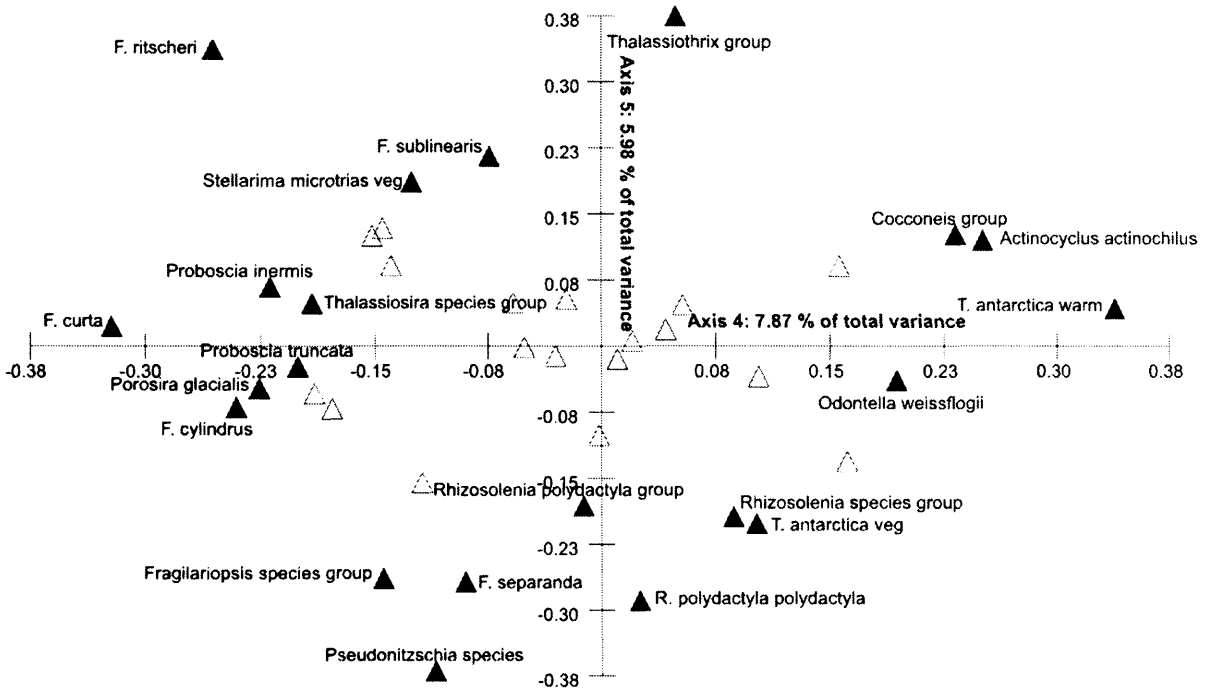


Figure 7.15
Core GC047: R-mode PCA variable loading on axes 4 and 5 for diatom relative abundance data (> 1 %). Data square-root transformed and standardised. Tolerance of eigenanalysis set at 1 x 10^{-10}. Highlighted species are those that have component loading $\geq +0.20$ or ≤ -0.20.

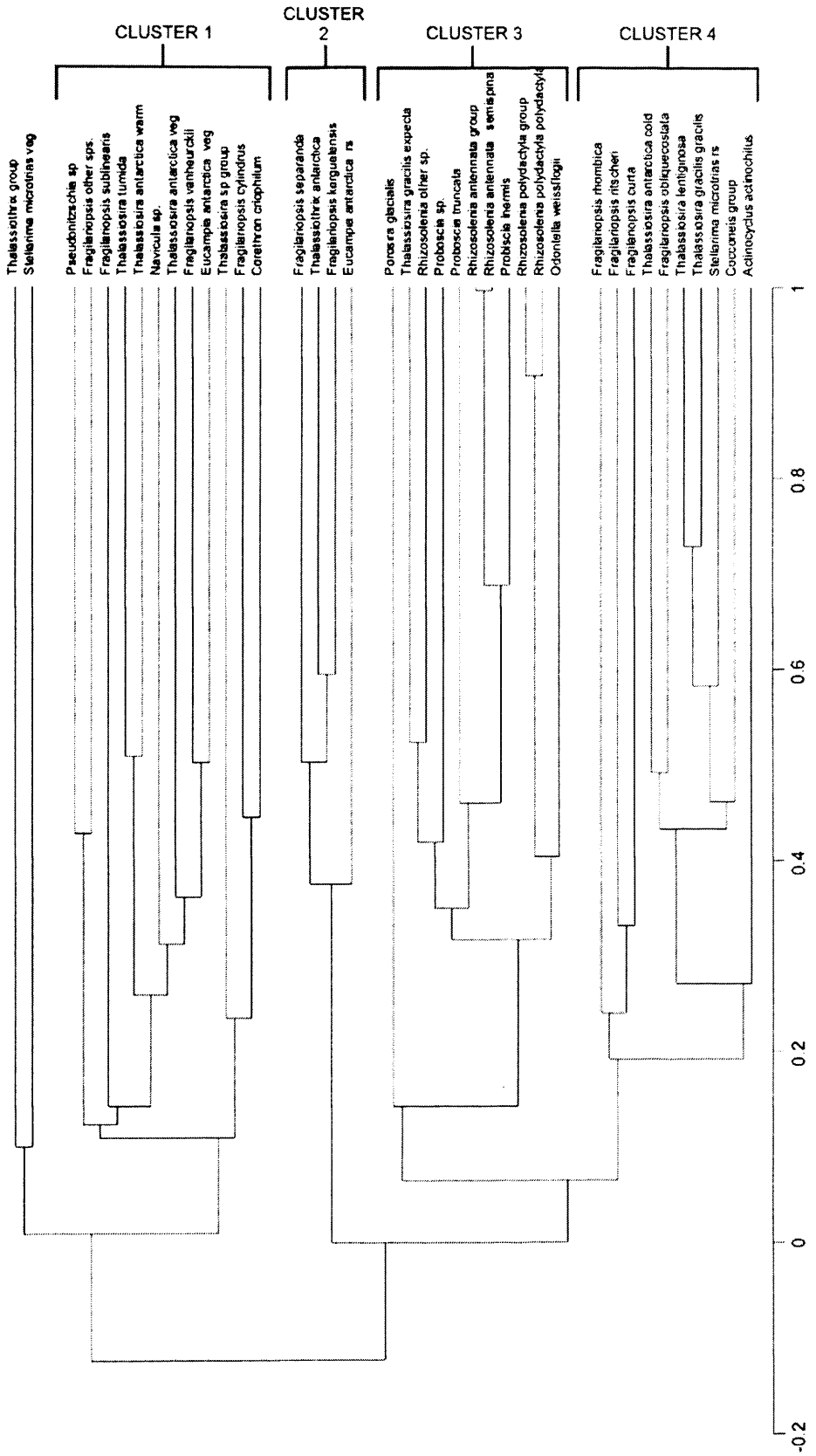


Figure 7.16
GC047: R-mode cluster analysis of diatom species relative abundance (>1 %). UPGMA clustering method; data square-root transformed; and Spearman Coefficient similarity measure.

Table 7.2
Core GC047: Comparison of diatom PCA axis loading and cluster groupings. Indicator species denoted with *. Grouped indicator species shown in grey box and relate to diatom assemblages highlighted on Figure 7.19.

Axis 1 Positive	Cluster group		**Axis 1 Negative**	Cluster group	
R. ant. f. *semispina**	3	**T. gracilis var. gracilis – T. lentiginosa**	*E. antarctica* veg	1	**T. antarctica warm rs**
T. gracilis var. *gracilis**	4		*F. cylindrus*	1	
*T. lentiginosa**	4		*F. vanheurckii*	1	
			Navicula group	1	
			T. antarctica veg	1	
			T. antarctica warm rs*	1	
Axis 2 Positive	Cluster group		**Axis 2 Negative**	Cluster group	
O. weissflogii	3	**Rhizosolenia - Proboscia**	*F. kerguelensis**	2	**F. kerguelensis**
*P. inermis**	3		*F. rhombica*	4	
P. truncata	3		*F. separanda*	2	
R. antennata f. *semispina**	3				
R. polydactyla f. *polydactyla*	3				
Rhizosolenia species group	3				
T. gracilis var. *expecta**	3				
Axis 3 Positive	Cluster group		**Axis 3 Negative**	Cluster group	
*P. inermis**	3	**T. antarctica cold rs**	*E. antarctica* rs*	2	**E. antarctica**
A. actinochilus	4		*E. antarctica* vegetative	1	
T. antarctica cold rs*	4		*Thalassiothrix* group	2	
C. pennatum	1				
S. microtrias	4				
Axis 4 Positive	Cluster group		**Axis 4 Negative**	Cluster group	
A. actinochilus	4	**T. antarctica warm rs**	*F. curta**	4	**F. curta**
Cocconeis group	4		*F. cylindrus*	1	
T. antarctica warm rs*	1		*F. ritscheri*	4	
			P. glacialis	3	
			*P. inermis**	3	
			P. truncata	3	
Axis 5 Positive	Cluster group		**Axis 5 Negative**	Cluster group	
F. ritscheri	4	**None**	*F. separanda*	2	**None**
F. sublinearis	1		*Fragilariopsis* species group	1	
Thalassiothrix group	N/A		*Pseudonitzschia* species	1	
			R. polydactyla f. *polydactyla*	3	
			T. antarctica veg	1	

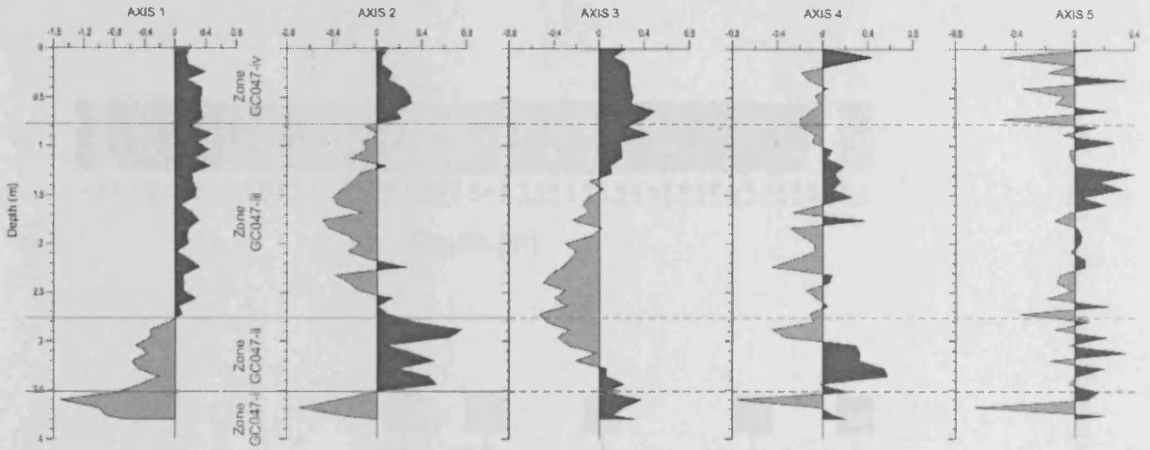


Figure 7.17
Core GC047: Q-mode PCA component scores plotted stratigraphically for PCA axes 1 – 5. Positive loading (dark grey); negative loading (light grey). Division of the record into stratigraphic zones GC047-i, GC047-ii, GC047-iii and GC047-iv was based on component loading on axes 1 and 2.

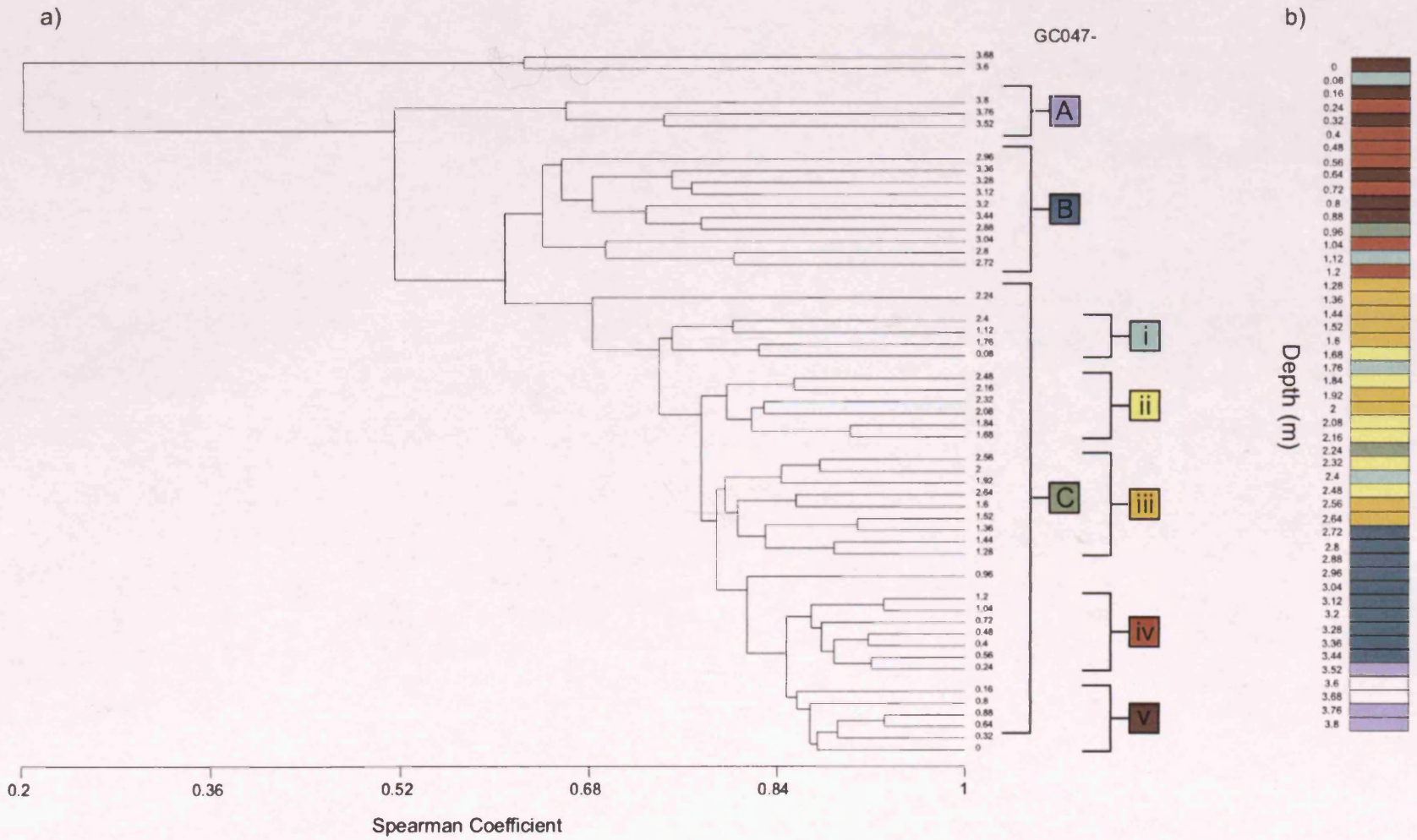


Figure 7.18

a) Core GC047: Q-mode cluster analysis of core depths, using diatom species relative abundances (>1 %). UPGMA clustering method; data square-root transformed; and Spearman Coefficient similarity measure.

b) Core GC047: Stratigraphic pattern of Q-mode cluster groups.

7.2.3 *Diatom summary*

Stratigraphic changes in the fossil diatom assemblage in core GC047 are summarised in Figure 7.19. These trends are evident through: changes in total diatom abundance; variations in CRS absolute and relative abundance; individual species absolute and relative abundances; and PCA and cluster analysis.

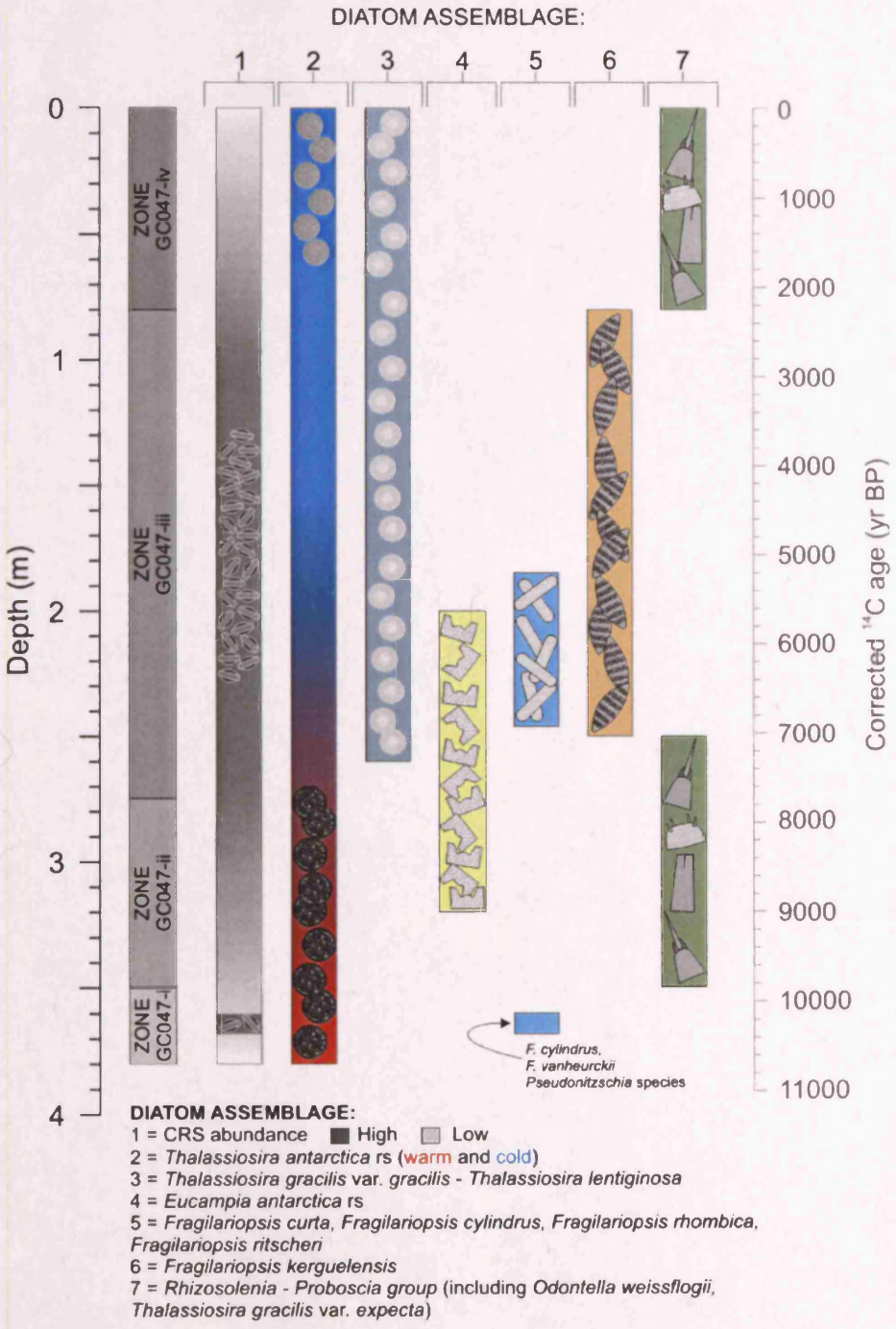


Figure 7.19
Core GC047: Schematic representation of the fossil diatom assemblage, highlighting the relative contribution of CRS to the total assemblage and stratigraphic changes in the diatom community. Stratigraphic zones GC047-i, GC047-ii, GC047-iii and GC047-iv identified using Q-mode PCA analysis of diatom relative abundance data.

7.3 VC306

7.3.1 Diatom assemblage

In core VC306, total diatom abundance, CRS and non-CRS absolute abundance display considerable stratigraphic variability (Figure 7.20a). However, in relative abundance terms, CRS constitute a large and reasonably constant proportion of the total diatom assemblage (averaging 81.73 (± 5.27) %) (Figure 7.20b). Individual diatom species show dominance at different core intervals (Figure 7.21), but typically, the non-CRS assemblage is dominated by *T. antarctica* warm rs, *F. curta* and *E. antarctica* rs in roughly equal proportions; respective mean absolute abundance of 12.16 (± 6.84) Mv/g, 11.72 (± 8.2) Mv/g and 7.86 (± 7.15) Mv/g, and mean relative abundance of 21.64 (± 4.6) %, 16.57 (± 5.79) % and 14.31 (± 10.58) %. The remainder of the non-CRS assemblage includes moderate contributions from *T. antarctica* cold rs (mean absolute abundance, 5.6 (± 4.79) Mv/g; mean relative abundance, 7.32 (± 5.59) %), grouped *Rhizosolenia* species (mean absolute abundance, 1.98 (± 1.12) Mv/g; mean relative abundance, 3.18 (± 1.19) %), *P. inermis* (mean absolute abundance, 1.77 (± 1.96) Mv/g; mean relative abundance, 2.34 (± 2.23) %), *F. vanheurckii* (mean absolute abundance, 1.59 (± 1.15) Mv/g; mean relative abundance, 2.65 (± 1.35) %) and *F. cylindrus* (mean absolute abundance, 1.89 (± 2.59) Mv/g; mean relative abundance, 2.46 (± 2.71) %), together with minor contributions from both varieties of *T. gracilis*, *P. truncata*, *O. weissflogii* and *F. obliquecostata*.

R-mode PCA analysis highlights several diatom species associations within core VC306; species with high positive and negative loadings on axes 1 – 5 are highlighted in bold and the variance explained by each PCA axis is also presented (Figure 7.22, Figure 7.23, Figure 7.24 and Table A2.9). R-mode cluster analysis of diatom species relative abundance highlighted three diatom assemblages, of roughly equal size, at 7 % similarity (Figure 7.25). Comparison of the species associations revealed by PCA and cluster analysis are presented in Table 7.3, with indicator species highlighted.

7.3.2 Diatom stratigraphic zones

Q-mode PCA analysis reveals clear stratigraphic groupings of similar component scores (Figure 7.26 and Table A2.10). These associations between core depths are most pronounced on axis 1, with exclusively negative scores below 1.1 m and solely positive scores above 1.1 m. This division at 1.1 m results from explicit change in the diatom community, from a mixed assemblage with *T. gracilis*, *E. antarctica* rs, *F. kerguelensis* and *T. tumida* (all with high negative loading on axis 1), to an assemblage dominated by

F. curta, *F. cylindrus*, *F. sublinearis*, *T. antarctica* cold rs, grouped *Navicula* species and *Proboscia* species (all with high positive loading on axis 1). Axis 2 also reveals interesting stratigraphic groupings, with solely positive scores between 1.6 and 0.65 m, sandwiched by negative loading above and below. The positive score on axis 2 is driven by elevated abundance of *E. antarctica* rs between 1.6 and 0.8 m, whereas the negative score reflects increased contribution from *T. antarctica* warm rs, *F. vanheurckii*, *F. obliquecostata*, *P. glacialis* and *S. microtrias* rs at the base of the core (1.8 – 1.6 m) and towards the core-top (0.65 – 0 m). Component scores on axes 3, 4 and 5 show much more stratigraphic variability, which consequently makes extracting meaningful associations between core depths difficult.

Q-mode cluster analysis on sample depths in core VC306 revealed two distinct cluster groups at 60 % similarity (Figure 7.27), labelled VC306-A and VC306-B. Group VC306-A contains all sample depths between 0 and 1 m and group VC306-B contains all sample depths between 1.1 and 1.8 m.

Using the method of core zonation based on Q-mode PCA component loading (Chapter 5.1.7), axis 1 is used as a basis for core stratigraphic division (Figure 7.26). This axis explains 27.24 % of the variance in the data and provides two clear zones (VC306-i (1.8 – 1.1 m) and VC306-ii (1.1 – 0 m)). Differences in total diatom abundance and species assemblage between these zones is described and highlighted on total diatom plot (Figure 7.20) and individual species abundance plots (Figure 7.21).

7.3.2.1 VC306-i: 1.8 – 1.1 m

Diatom absolute abundance in zone VC306-i is relatively low (260 (± 80) Mv/g). CRS form a particularly high proportion of the total diatom assemblage between 1.7 – 1.2 m (averaging 80.37 (± 4.81). Into the transition with zone VC306-ii and the lower of portion of zone VC306-ii (1.2 – 0.8 m) CRS records slightly lower relative abundance (averaging 76.09 (± 2.75) %). Similar to total diatom abundance, absolute abundance of non-CRS assemblage is lowest in the basal section of the core (1.9 – 1.4 m), averaging 21.3 (± 1.9) Mv/g. Non-CRS assemblage increases up-core from 1.4 m, which is prior to the increase in total diatom abundance (at ~1.1 m).

There are several notable features of the non-CRS species assemblage through zone VC306-i. Firstly, *F. curta* absolute and relative abundance are comparatively low, averaging 3.85 (± 1.7) Mv/g and 10.74 (± 3.36) %, respectively. In contrast, *F. kerguelensis* relative abundance is very high between 1.8 – 1.6 m (18.5 (± 3.93) %) and

displays a trend of decreasing relative abundance through zone VC306-i, reaching abundance of ~10 % at the transition into zone VC306-ii. In addition, *E. antarctica* rs absolute and relative abundance both show clear peaks between 1.3 – 0.8 m and 1.6 – 0.8 m, respectively. During this interval of elevated abundance, *E. antarctica* rs mean absolute and relative abundance are 16.25 (± 7.18) Mv/g and 24.44 (± 5.25) %, respectively. Finally, both varieties of *T. gracilis*, together with *T. tumida*, record elevated abundances throughout zone VC306-i. Grouped *T. gracilis* mean absolute and relative abundances is 1.77 (± 0.99) Mv/g and 5.09 (± 0.99) %, respectively. *T. tumida* absolute and relative abundance is 0.81 (± 0.38) Mv/g and 2.52 (± 0.97) %.

7.3.2.2 VC306-ii: 1.1 – 0 m

Diatom absolute abundance increases dramatically up-core of the transition into zone VC306-ii (1.1m), to fluctuate at high values between 1 – 0.2 m (765 (± 129) Mv/g). Up-core of 0.2 m total diatom abundance falls significantly, to mid-values between 0.1 – 0 m (370 (± 78) Mv/g). Non-CRS absolute abundance displaying a more gradual increase to high absolute abundances between 1.1 – 0 m (79.8 (± 12.2) Mv/g). There is a short interval of reduced non-CRS absolute abundance between 0.8 – 0.5 m (70.3 (± 8.6) Mv/g), together with a reduction at the core-top (66.5 Mv/g).

The most striking feature of the non-CRS assemblage in core VC306 is the dramatic and significant shift in *F. curta* absolute and relative abundance at 1.1 m, from low abundances below to high abundances above. In contrast to the lower zone, mean absolute and relative abundance of *F. curta* in zone VC306-ii is 18.15 (± 4.92) Mv/g and 20.37 (± 4.06) %, respectively. Further, two maxima occur in *F. curta* abundances, between 0.9 – 0.8 m and between 0.2 – 0.1 m; these peaks are interestingly coeval with maxima in *F. cylindrus* (together with *Pseudonitzschia* group), at 1 m and 0.2 m. The peak in *F. cylindrus* at 1 m is particularly large, with absolute and relative abundances increasing to 10.89 Mv/g and 12.23 %, compared to the baseline levels of 1.35 (± 1.42) Mv/g and 1.91 (± 1.36) %, respectively. *F. kerguelensis* absolute abundance follows a similar trend to *F. curta*, with elevated abundances in zone VC306-ii (5.67 (± 1.61) Mv/g), compared to zone VC306-ii (3.25 (± 0.99) Mv/g). This is also the case for grouped *Navicula* species, showing elevated mean absolute and relative abundance between 0.9 – 0.1 m of 0.85 (± 0.43) Mv/g and 1.12 (± 0.42) % respectively.

Similarly, *T. antarctica* cold rs exhibit a trend of increasing absolute and relative abundance progressively through zone VC306-ii, from low values at 1.2 m (0.36 Mv/g

and 0.76 %, respectively) to high values at 0.1 m (14 Mv/g and 15.49 %, respectively). *T. antarctica* warm rs absolute abundance shows a similar up-core trend to *T. antarctica* cold rs, from relatively low values in zone VC306-i (2.04 Mv/g), increasing throughout zone VC306-ii, to maximum abundance at 0.1 m (14 Mv/g). In addition, two species of *Proboscia* (*P. inermis* and *P. truncata*), together with grouped *Rhizosolenia* species, display elevated abundances in zone VC306-i. Between 0.7 – 0 m, grouped *Proboscia* species absolute and relative abundance is 5.45 (± 2.26) Mv/g and 6.54 (± 2.54) % respectively. Between 1.2 – 0 m grouped *Rhizosolenia* species absolute abundance is 2.6 (± 0.73) Mv/g, compared to 0.63 (± 0.21) Mv/g in zone VC306-i. Relative abundance of grouped *Rhizosolenia* species is reasonably constant along the core length (averaging 3.18 (± 1.19) %).

Finally, summed vegetative valve abundance (for *E. antarctica*, *T. antarctica* and *S. microtrias*) (Figure A2.6) display two peaks in zone VC306-ii: between 1.1 – 0.6 m; and between 0.1 – 0 m. These peaks are interestingly coincident with periods of elevated abundance of *F. curta* and *F. cylindrus*.

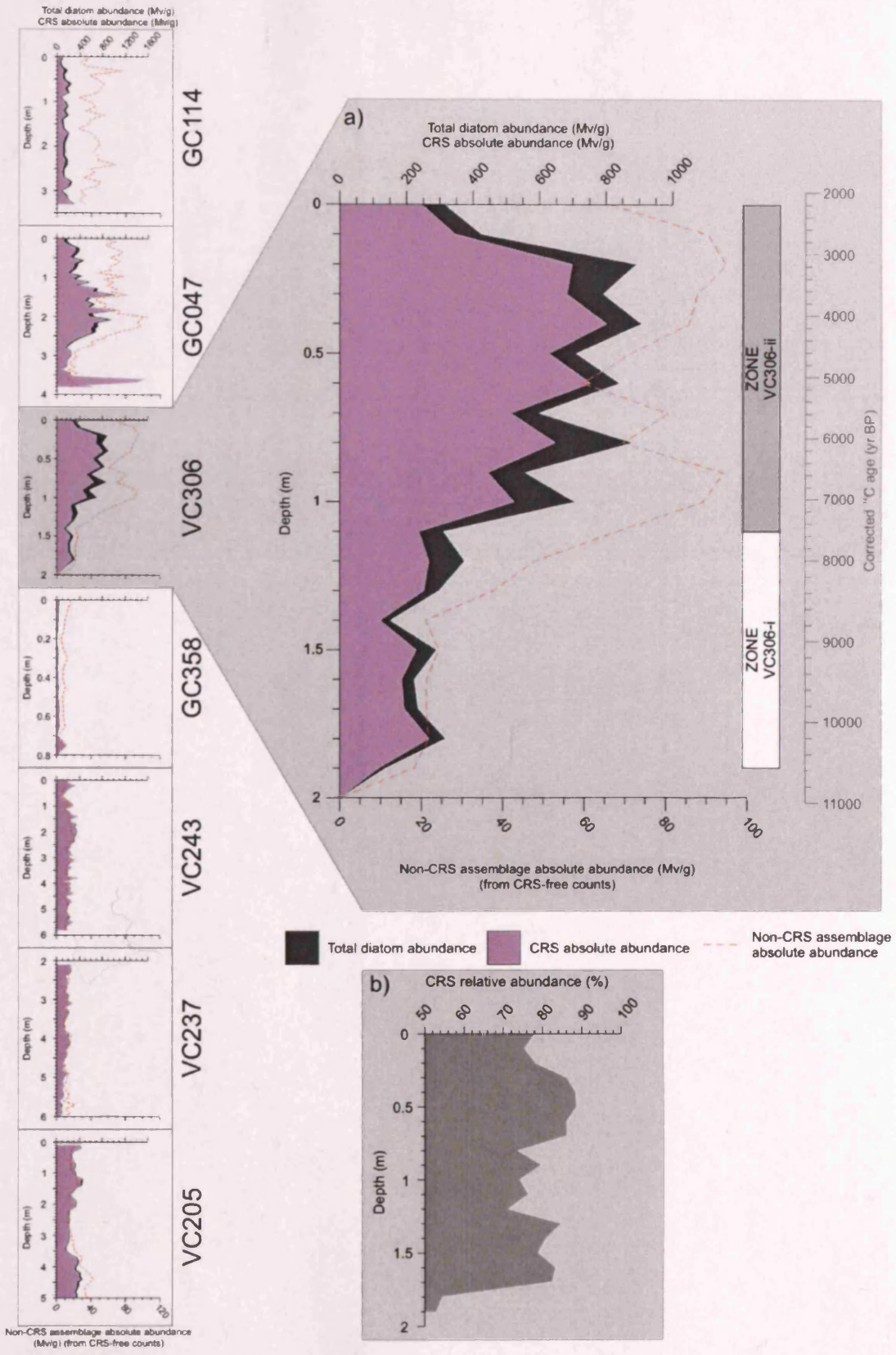


Figure 7.20

a) Core VC306: Total diatom abundance, CRS absolute abundance (both from CRS-included counts) and non-CRS assemblage absolute abundance (from CRS-free counts) (millions of valves/g (Mv/g)). Stratigraphic zones VC306-i and VC306-ii identified using Q-mode PCA analysis of diatom relative abundance data.

b) Core VC306: CRS relative abundance (%).

Figure 7.21
Core VC306: Non-CRS diatom assemblage plots for AP indicator species: (a) Absolute abundance (Mv/g); (b) Relative abundance (%). Stratigraphic zones VC306-i and VC306-ii identified using Q-mode PCA analysis of diatom relative abundance data.

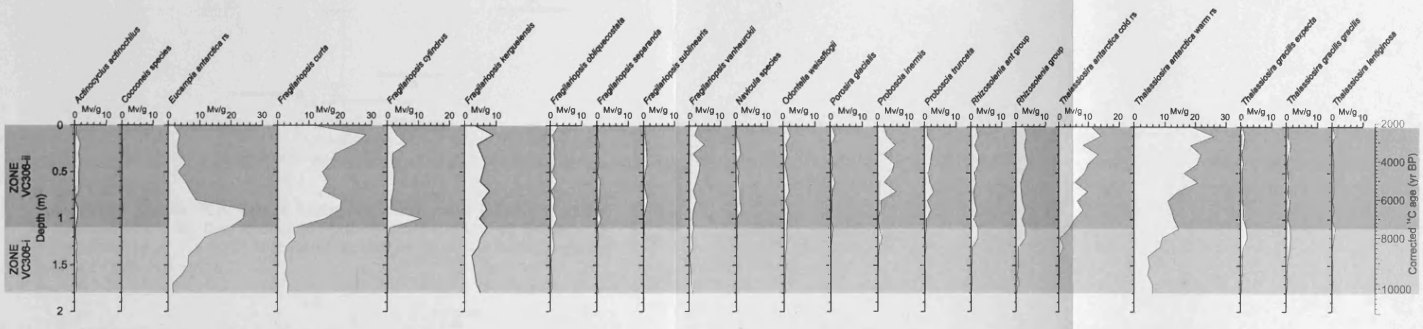


Figure 7.21 (a)

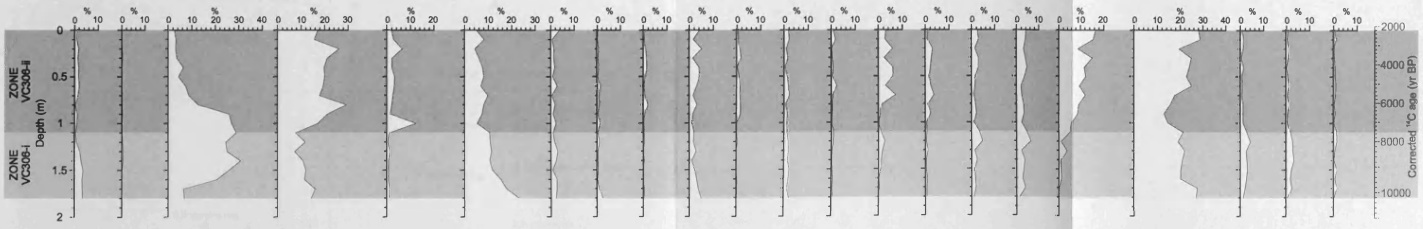


Figure 7.21 (b)

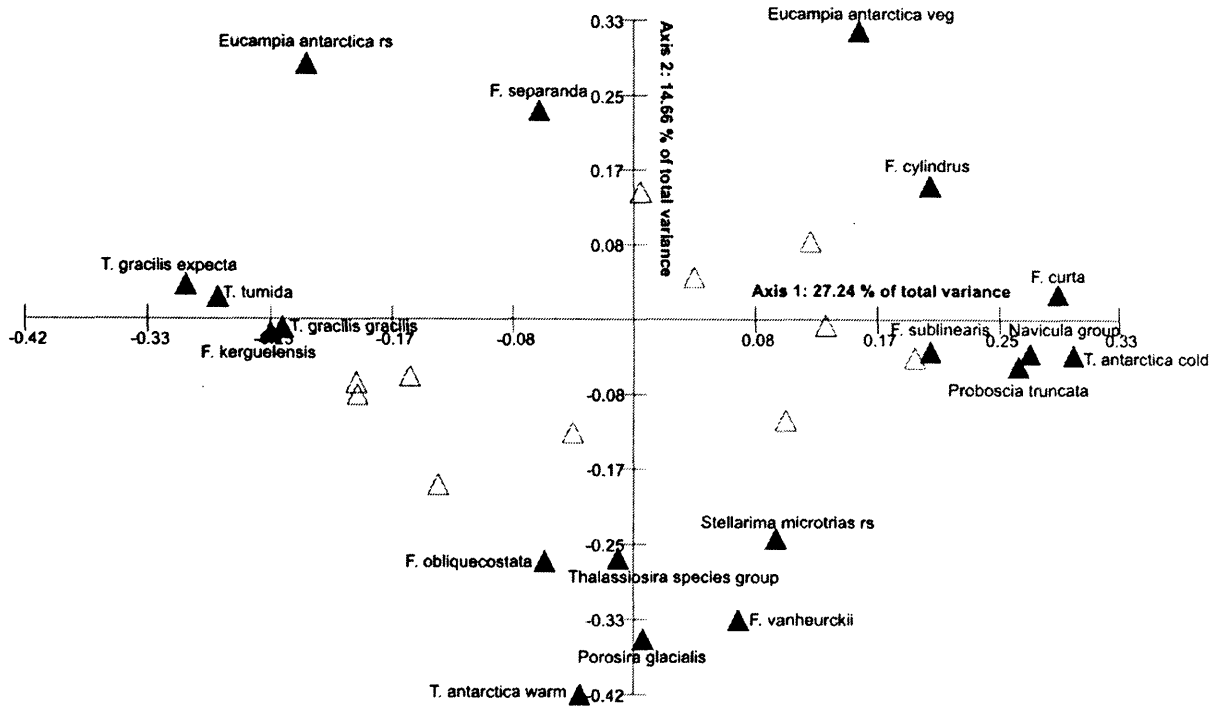


Figure 7.22
Core VC306: R-mode PCA variable loading on axes 1 and 2 for diatom relative abundance data (>1 %). Data square-root transformed and standardised. Tolerance of eigenanalysis set at 1 x 10^{-10}. Highlighted species are those that have component loading ≥ + 0.20 or ≤ – 0.20.

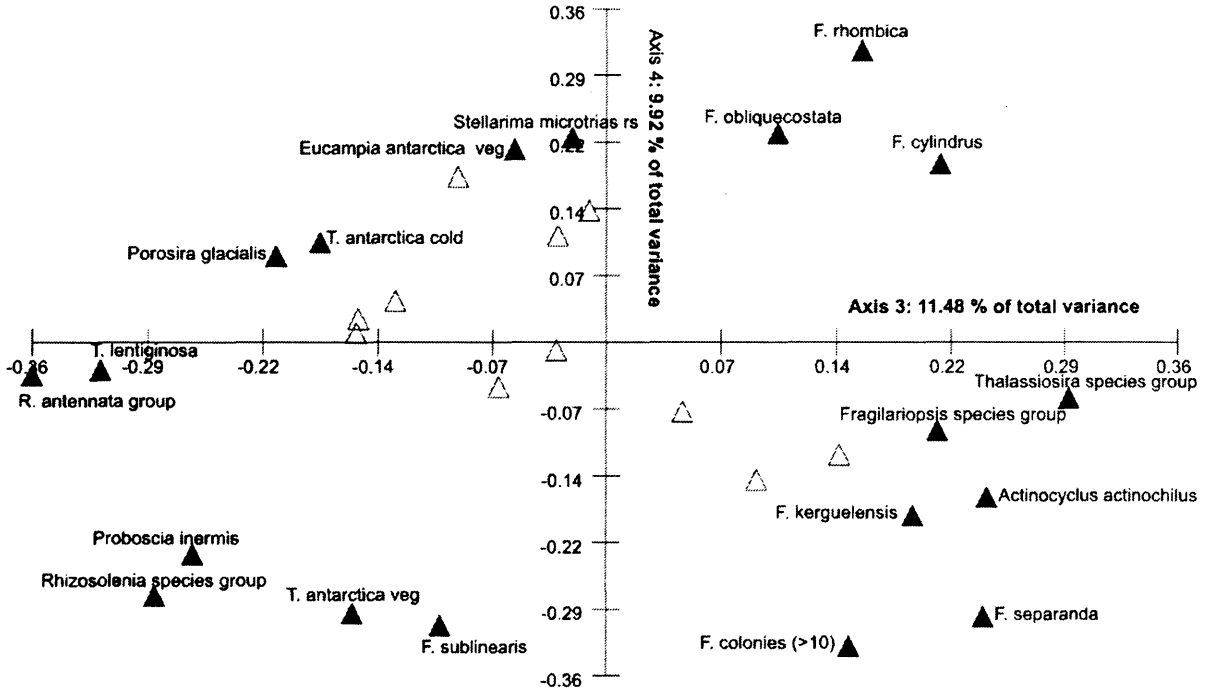


Figure 7.23
Core VC306: R-mode PCA variable loading on axes 3 and 4 for diatom relative abundance data (>1 %). Data square-root transformed and standardised. Tolerance of eigenanalysis set at 1 x 10^{-10}. Highlighted species are those that have component loading ≥ + 0.20 or ≤ – 0.20.

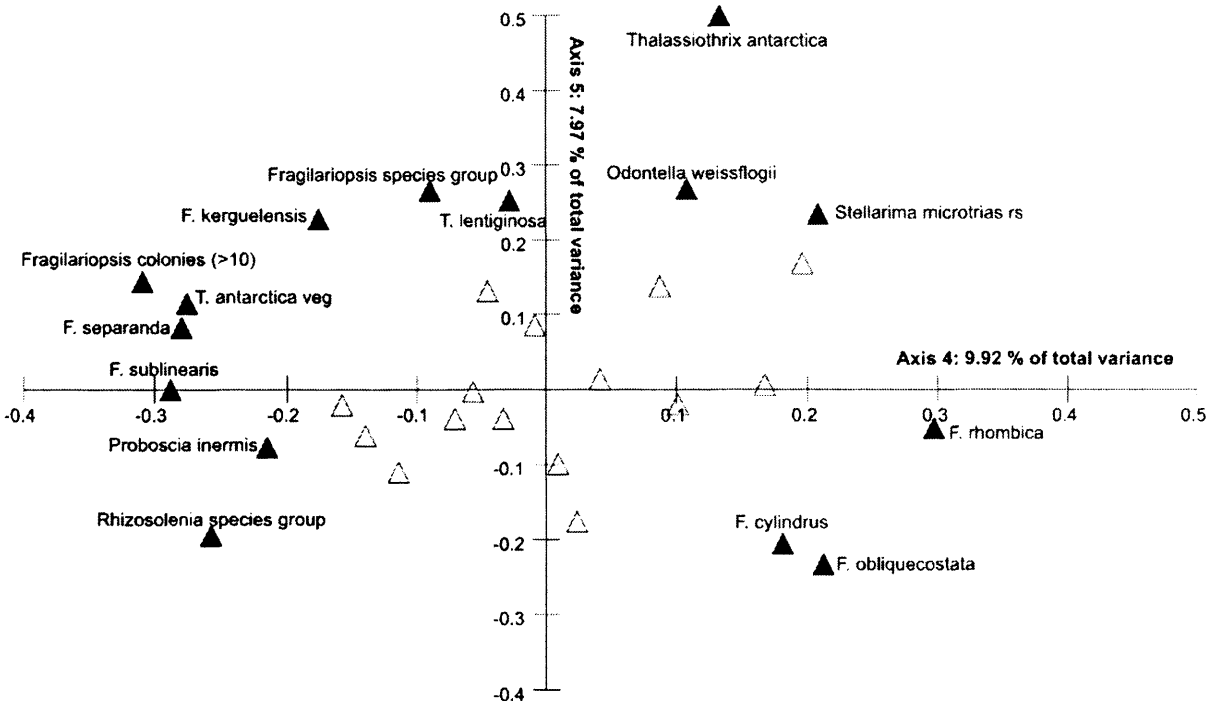


Figure 7.24
Core VC306: R-mode PCA variable loading on axes 4 and 5 for diatom relative abundance data (>1 %). Data square-root transformed and standardised. Tolerance of eigenanalysis set at 1 x 10^{-10}. Highlighted species are those that have component loading $\geq +0.20$ or ≤ -0.20.

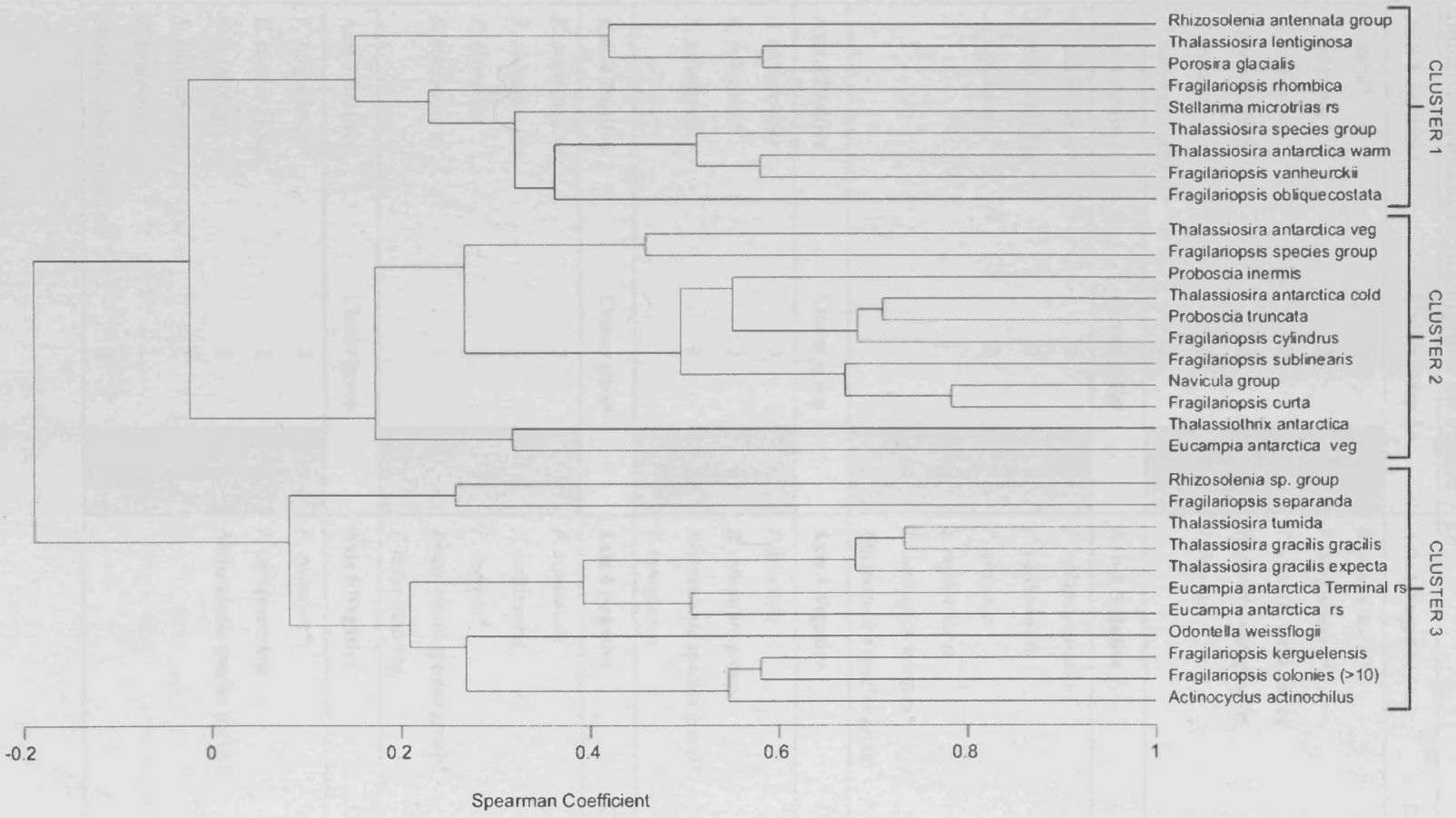


Figure 7.25
Core VC306: R-mode cluster analysis of diatom species relative abundance (> 1 %). UPGMA clustering method; data square-root transformed; and Spearman Coefficient similarity measure.

Table 7.3
Core VC306: Comparison of diatom PCA axis loading and cluster groupings. Indicator species denoted with *. Grouped indicator species shown in grey box and relate to diatom assemblages highlighted on Figure 7.28.

Axis 1 Positive	Cluster group		**Axis 1 Negative**	Cluster group	
*F. curta**	2	**F. curta – F. cylindurs; T. antarctica cold rs**	*E. antarctica* rs*	3	**E. antarctica rs; F. kerguelensis**
*F. cylindrus**	2		*F. kerguelensis**	3	
F. sublinearis	2		*T. gracilis* var. *expecta*	3	
Navicula group	2		*T. gracilis* var. *gracilis*	3	
P. truncata	2		*T. tumida*	3	
T. antarctica cold rs*	2				
Axis 2 Positive	Cluster group		**Axis 2 Negative**	Cluster group	
E. antarctica rs*	3	**E. antarctica rs**	*F. obliquecostata*	1	**T. antarctica warm rs**
E. antarctica veg	2		*F. vanheurckii*	1	
F. separanda	3		*P. glacialis*	1	
			S. microtrias rs	1	
			T. antarctica warm rs*	1	
			Thalassiosira species group	1	
Axis 3 Positive	Cluster group		**Axis 3 Negative**	Cluster group	
A. actinochilus	3	**F. cylindrus**	*P. glacialis*	1	**Rhizosolenia**
*F. cylindrus**	2		*R. antennata* group	1	
F. separanda	3		*Rhizosolenia* species group*	3	
			T. lentiginosa	1	
Axis 4 Positive	Cluster group		**Axis 4 Negative**	Cluster group	
E. antarctica veg	2	**None**	*F. separanda*	3	**Rhizosolenia – Proboscia**
F. obliquecostata	1		*F. sublinearis*	2	
F. rhombica	1		*P. inermis**	2	
S. microtrias rs	1		*Rhizosolenia* species group*	3	
			T. antarctica veg	2	
Axis 5 Positive	Cluster group		**Axis 5 Negative**	Cluster group	
*F. kerguelensis**	3	**F. kerguelensis**	*F. cylindrus**	2	**F. cylindrus; Rhizosolenia**
F. species group	2		*F. obliquecostata*	1	
O. weissflogii	3		*Rhizosolenia* species group*	3	
S. microtrias rs	1				
T. lentiginosa	1				
Thalassiothrix antarctica	2				

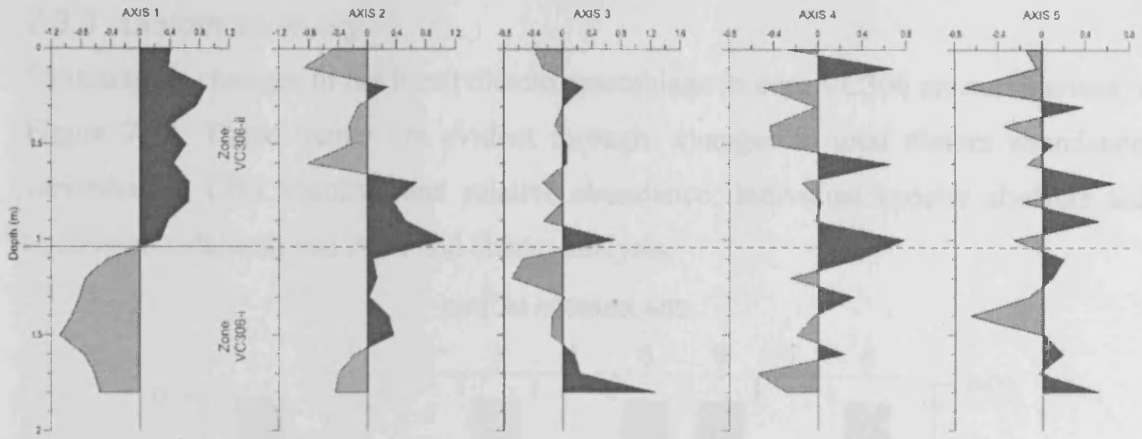


Figure 7.26
Core VC306: Q-mode PCA component scores plotted stratigraphically for PCA axes 1 – 5. Positive loading (dark grey); negative loading (light grey). Division of the record into stratigraphic zones VC306-i and VC306-ii is based on component loading on axis 1.

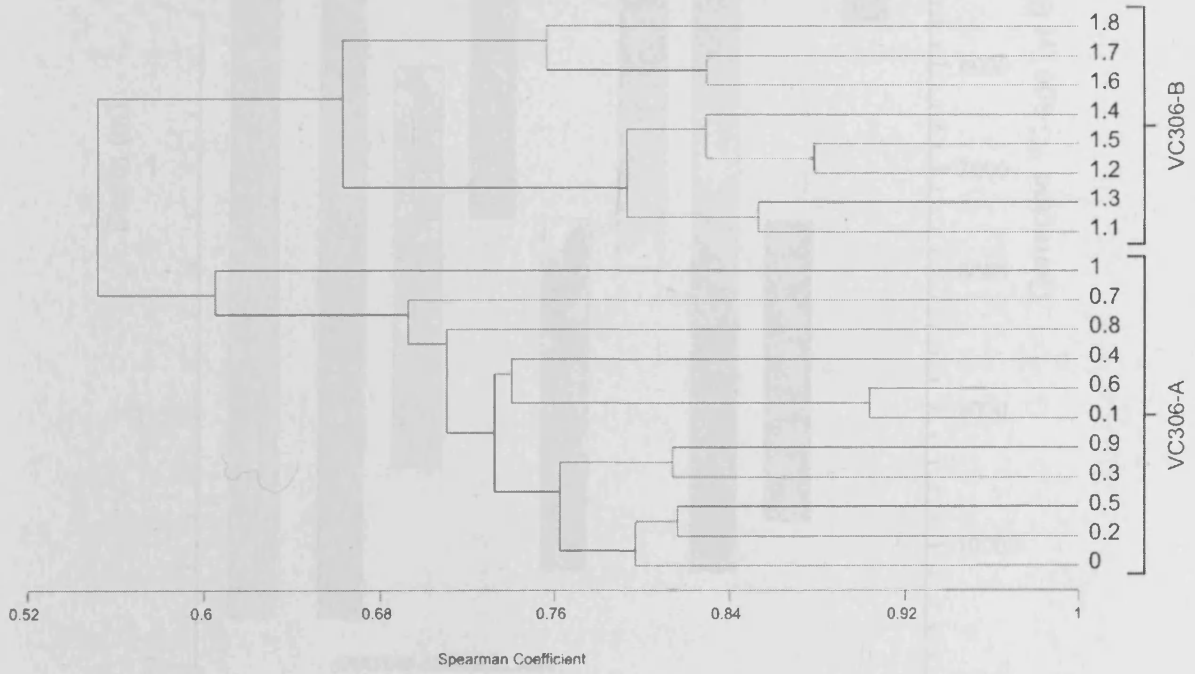


Figure 7.27
Core VC306: Q-mode cluster analysis of core depths, using diatom species relative abundances (> 1 %). UPGMA clustering method; data square-root transformed; and Spearman Coefficient similarity measure.

7.3.3 Diatom summary

Stratigraphic changes in the fossil diatom assemblage in core VC306 are summarised in Figure 7.28. These trends are evident through: changes in total diatom abundance; variations in CRS absolute and relative abundance; individual species absolute and relative abundances; and PCA and cluster analysis.

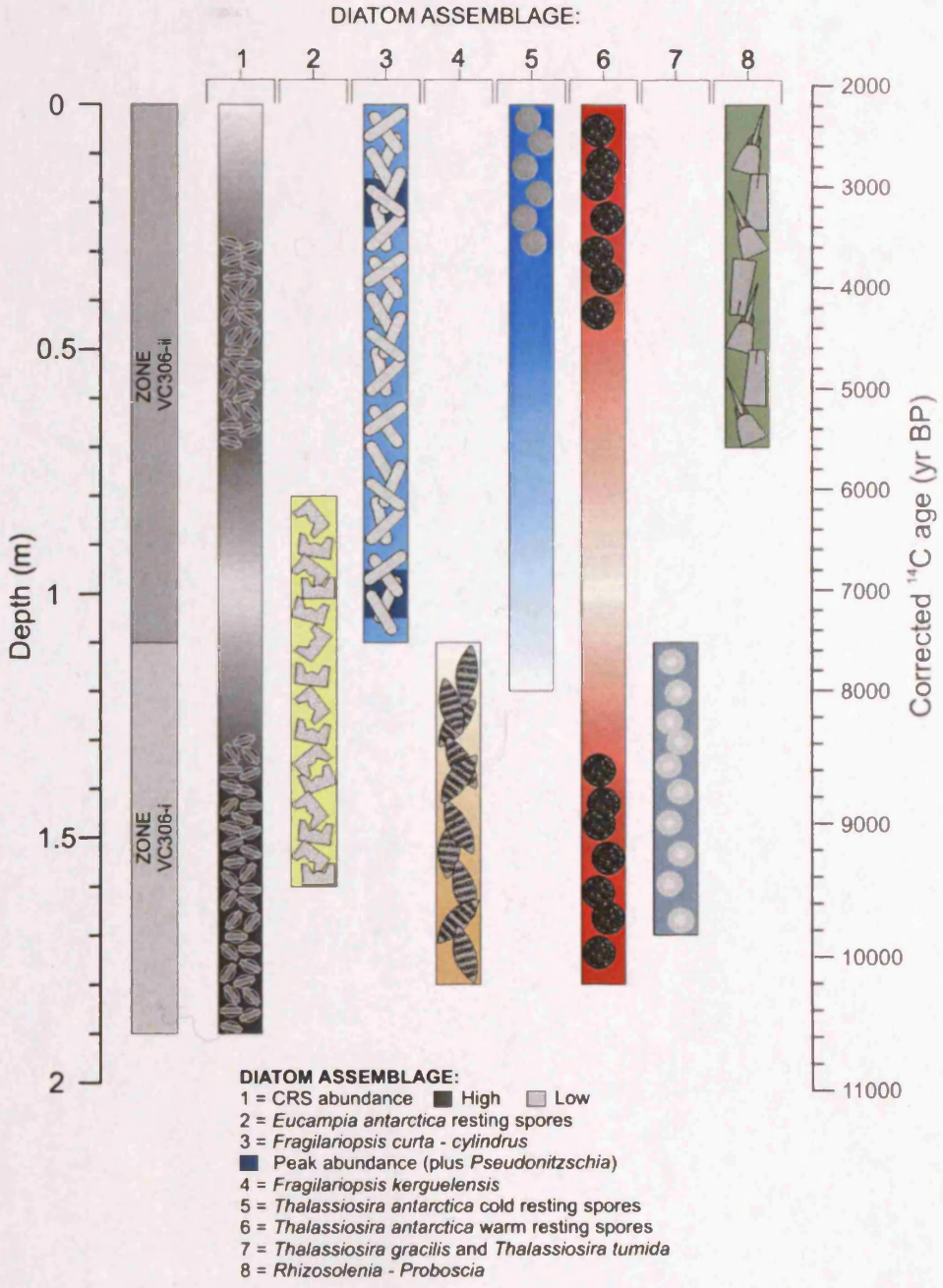


Figure 7.28
Core VC306: Schematic representation of the fossil diatom assemblage, highlighting the relative contribution of CRS to the total assemblage and stratigraphic changes in the diatom community. Stratigraphic zones VC306-i and VC306-ii identified using Q-mode PCA analysis of the diatom relative abundance data. Darker tones indicate elevated abundance.

7.3.4 Stable Isotopes

In core VC306, carbon and nitrogen elemental contents (C_{org} and N_{org}) and isotopic composition ($\delta^{13}C_{org}$ and $\delta^{15}N_{org}$) record significant stratigraphic variability (Figure 7.29). Isotope contents and composition are described using the diatom PCA based stratigraphic zones described in section 7.3.2. On a broad scale, both C_{org} and N_{org} show very similar stratigraphic trends, with lower content in zone VC306-i and elevated content in VC306-ii. Conversely, $\delta^{13}C_{org}$ and $\delta^{15}N_{org}$ display moderate anti-correlation along the core length, although this trend is less applicable in the lower portion of zone VC306-ii (1 – 0.2 m), where both isotopes show an up-core trend of progressive depletion. Along the core length, $\delta^{13}C_{org}$ is more negative (depleted in ^{13}C; lighter) in zone VC306-i and less negative (enriched in ^{13}C; heavier) in zone VC306-ii. In contrast, $\delta^{15}N_{org}$ is more positive (enriched in ^{15}N; heavier) in zone VC306-i and less positive (depleted in ^{15}N; lighter) in zone VC306-ii. The details of these trends will be described in more detail below. The ratio of C_{org}/N_{org} is constant throughout core VC306 (7 – 8), with the exception of 0.85 m, where the ratio drops to 6.

7.3.4.1 VC306-i: 1.8 – 1.1 m

C_{org} and N_{org} are low and relatively constant between 1.85 and 1.45 m, with mean contents of 0.493 (± 0.047) % and 0.069 (± 0.005) %, respectively. Up-core of 1.45 m, both isotopes display a short-lived increase to 0.819 % for C_{org} and 0.105 % for N_{org} at 1.15 m. $\delta^{13}C_{org}$ records depleted values throughout zone VC306-i, typically more negative than -23.5 ‰. Mirroring the low C_{org} and N_{org} content between 1.85 – 1.45 m, $\delta^{13}C_{org}$ is also heavily depleted, averaging -23.89 (± 0.41) ‰ through these depths. Into the transition with VC306-ii, $\delta^{13}C_{org}$ increases sharply at 1.15 m, recording a shift of 1.28 ‰ (from -23.66 ‰ at 1.15 m to -22.38 ‰ at 1 m). $\delta^{15}N_{org}$ shows a broad trend of enrichment through zone VC306-i, from relatively low values at 1.85 m (5.01 ‰) to high values at 1.1 m (6.03 ‰).

7.3.4.2 VC306-ii: 1.1 – 0 m

In the lower section of zone VC306-ii, C_{org} and N_{org} contents display a decreasing trend between 1.1 – 0.85 m. Through the mid-to-upper portion of VC306-ii, both contents increase in a broad peak, centred at roughly 0.4 m, where C_{org} reaches 1.02 % and N_{org} 0.131 %. In the upper-most 0.2 m of the core, C_{org} and N_{org} decrease once again, averaging 0.821 (± 0.102) % and 0.109 (± 0.01) %, respectively. $\delta^{13}C_{org}$ and $\delta^{15}N_{org}$ both show a comparable trend of progressive depletion through zone VC306-ii, from -23.24

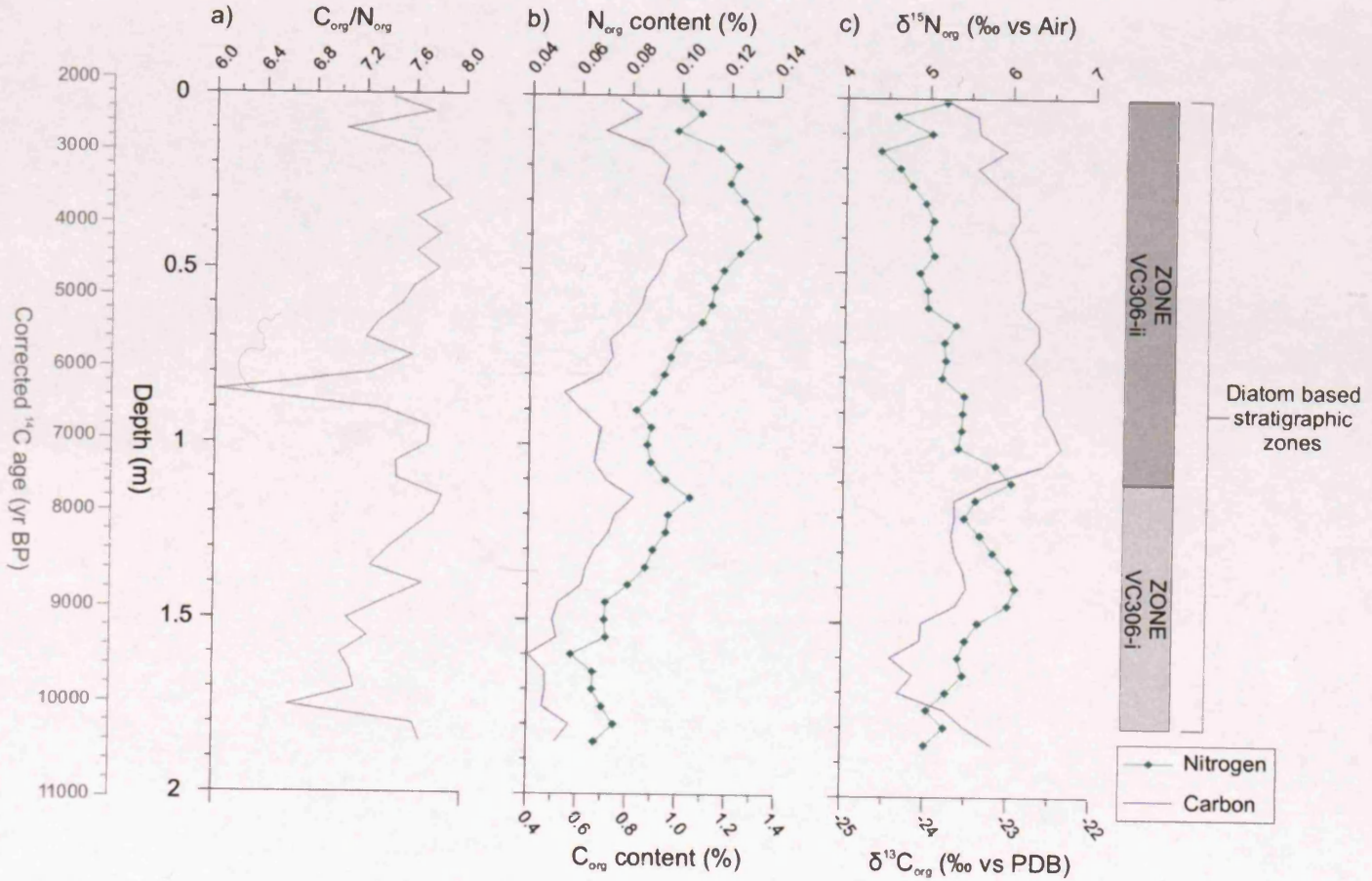


Figure 7.29
Core VC306: Bulk organic material stable isotope (carbon (C) and nitrogen (N)) contents and composition.
a) C_{org}/N_{org} ratio
b) Elemental contents (C_{org} and N_{org}) (%)
c) Isotopic composition ($\delta^{13}C_{org}$ and $\delta^{15}N_{org}$) (‰)
Stratigraphic zones VC306-i and VC306-ii identified using Q-mode PCA analysis of diatom relative abundance data.

7.4 GC358

7.4.1 Diatom assemblage

It is worth noting that overall diatom absolute abundance in core GC358 is considerably lower than the absolute abundance found in other WAP cores studied in this investigation (Figure 7.30a); mean diatom absolute abundance is 43 (± 39) Mv/g, compared to 159 (± 57) Mv/g for GC114; 490 (± 39) Mv/g for core GC047; and 498 (± 269) Mv/g for core VC306. This restricted diatom community still witnesses a dominance of CRS, with relative abundance averaging 72.86 (± 10.23) % (Figure 7.30b). Although the non-CRS species assemblage shows significant variability (Figure 7.31), typically *E. antarctica* rs and *F. curta* dominate, with respective mean absolute abundance of 2.25 (± 0.91) Mv/g and 1.52 (± 1.39) Mv/g, and mean relative abundance of 27.82 (± 11.73) % and 16.47 (± 9.05) %. Numerous other species (*T. antarctica* warm rs and cold rs, *F. kerguelensis*, *F. obliquecostata*, together with grouped *Rhizosolenia* species and *T. gracilis* species) represent a significant and roughly equal proportion of the remainder of the fossil assemblage, with mean absolute and relative abundance ranging between 0.8 – 0.33 Mv/g and 9.3 – 4 % respectively.

R-mode PCA reveals several diatom species associations within core GC358; species with high positive and negative loadings on axes 1 – 4 are highlighted in bold and the variance explained by each PCA axis is also presented (Figure 7.32, Figure 7.33 and Table A2.11). R-mode cluster analysis of diatom species relative abundance highlighted four diatom species groupings, at 10 % similarity (Figure 7.34). Comparison of the species associations revealed by PCA and cluster analysis are presented in Table 7.4, with indicator species highlighted.

7.4.2 Diatom stratigraphic zones

Q-mode PCA analysis reveals several associations between sample depths in core GC358 (Figure 7.35 and Table A2.12). A clear stratigraphic pattern is evident on axis 1, with exclusively positive loading between 0.8 – 0.5 m and negative loading between 0.5 and ~0 m. This reflects changes in the diatom community, from *T. tumida*, *Thalassiothrix* species, *F. sublinearis* and grouped *Fragilariopsis* species (all with high positive loading on axis 1) below 0.5 m to an assemblage with increased contribution from *Rhizosolenia* species and *A. actinochilus*. Further information is provided by axes 2 and 3: negative loading on axis 2 between 0.75 – 0.35 m reflects higher abundance of *T. tumida*, *T. lentiginosa*, *T. gracilis* var. *expecta* and *F. obliquecostata* at these depths, whereas positive loading on axis 2 between 0.35 – 0 m records the elevated abundances

of *F. cylindrus*, *F. vanheurckii*, *F. sublinearis*, *F. separanda*, *F. kerguelensis*, *S. microtrias* rs and grouped *Navicula* species; negative loading on axis 3 towards the base (0.75 – 0.6 m) and at the core top (0.1 – 0 m) reflects the increased abundance of *T. antarctica* cold rs, *F. curta*, *F. obliquecostata* and *P. truncata* during these intervals, whereas positive loading in the middle portion of the core (0.6 – 0.15 m) reflects dominance particularly of *E. antarctica* rs through this interval, together with *T. antarctica* warm rs, *F. kerguelensis*, *F. sublinearis* and *Pseudogomphonema* species. Axis 4 shows a more variable stratigraphic pattern of component loading, therefore summarising trends is difficult and unlikely to be meaningful.

Q-mode cluster analysis on core GC358 sample depths reveals two groupings, at 75 % similarity, plus an isolated sample depth (0.75 m) (Figure 7.36). The groups are labelled GC358-A and GC358-B. Studying the sample depths within each cluster group, there is clear division; typically samples below 0.4 m form cluster group GC358-A, whereas core depths between 0.35 and 0 m are solely part of cluster group GC358-B.

Using the method of core zonation based on PCA component loading (Chapter 5.1.7), axis 1 (which explains 26.14 % of the total variance in the data (Table A2.12)) clearly divides core GC358 into two zones (GC358-i (0.75 – 0.5 m) and GC358-ii (0.5 – 0 m)) Figure 7.35). These two zones are described below and highlighted on total diatom and CRS abundance plots (Figure 7.30) and individual species abundance plots (Figure 7.31).

7.4.2.1 GC358-i: 0.75 – 0.5 m

At the base of zone GC358-i (0.75 m), extremely high diatom absolute abundance is found in a single spike (179 Mv/g); a level unprecedented for the remainder of the core, which in general, shows limited variability in either zone. In zone GC358-i, CRS relative abundance is high (averaging 81.07 (± 6.31) %) and decreases up-core (Figure 7.30b).

The non-CRS species assemblage in zone GC358-i displays several interesting features. Firstly, *F. kerguelensis* records maximum abundance in a clear spike at the base of the core (0.75 m), with absolute and relative abundance reaching 1.05 Mv/g and 13.32 %. Secondly, *F. curta* abundance is high throughout zone GC358-i, with absolute and relative abundances ranging between 0.64 – 5.55 Mv/g and 12.77 – 34.6 % respectively, compared to levels through the lower section of zone GC358-ii (0.5 – 0.2 m) of 0.79 (± 0.58) Mv/g and 9.33 (± 3.77) %. Similarly, abundances of *F. obliquecostata*, *F.*

cylindrus and *F. vanheurckii* are also elevated in this zone. Relative abundance of *F. obliquecostata* is particularly high between 0.7 – 0.55 m, with mean abundances of 9.47 (± 1.42) %. In addition, *T. gracilis* var. *expecta* and *T. tumida* both show elevated abundance in zone GC358-i. Both species show maximum abundances at 0.65 / 0.7 m: *T. gracilis* var. *expecta* and *T. tumida* absolute abundance is 0.64 Mv/g and 0.33 Mv/g; relative abundance is 6.7 % and 4.76 % respectively. Although overall abundances of *T. gracilis* var. *gracilis* are lower than those displayed by *T. gracilis* var. *expecta*, the trends are similar, with slightly elevated abundance in zone GC358-i. *O. weissflogii* shows elevated absolute and relative abundance between 0.65 – 0.45 m, averaging 0.16 (± 0.06) Mv/g and 2.1 (± 0.96) % respectively, compared to average levels for the remainder of the core of 0.08 (± 0.03) Mv/g and 1 (± 0.32) %. Finally, *E. antarctica* rs display a distinctive peak in the non-CRS assemblage between 0.65 – 0.15 m, with mean absolute and relative abundances of 2.56 (± 0.75) Mv/g and 33.13 (± 10.05) % respectively.

7.4.2.2 GC358-ii: 0.5 – 0 m

Total diatom abundance displays limited stratigraphic variability in core GC358. CRS relative abundance is typically low in zone GC358-ii, averaging 67.61 (± 7.15) %). Conversely, the non-CRS assemblage exhibits a trend of increasing absolute abundance through zone GC358-ii, most marked up-core of 0.2 m, where abundance progressively increases, reaching a maximum at the core top (16 Mv/g).

Several species display a change in abundance at the transition into zone GC358-i. Firstly, grouped *Rhizosolenia* species shift from low abundances below to higher abundance above, with absolute and relative abundance averaging 0.6 (± 0.28) Mv/g and 6.57 (± 2.78) % through zone GC358-ii. *A. actinochilus* shows a similar trend, from low abundance at the base of zone GC358-i (0.75 m; ~ 0.06 Mv/g and ~ 2 %), progressively increasing in abundance up-core, reaching maximum abundance at the top of zone GC358-ii (0.15 – 0 m; ~ 0.6 Mv/g and ~ 5 %). *T. gracilis* var. *expecta* and *T. tumida* show the converse pattern; both these species exhibited elevated abundances at the base of zone GC358-i; progressively decreasing in abundance up-core, reaching low abundances in zone GC358-ii (<0.15 Mv/g and <1.7 %).

A peak exists in *F. cylindrus* (and *F. curta* to a lesser extent) abundance between 0.4 – 0.25 m, with absolute and relative abundance reaching 0.26 Mv/g and 3.43 % at 0.35 m.

F. curta abundance is high at the top of core GC358 (0.15 – 0 m), with mean absolute and relative abundance of 2.99 (± 2.03) Mv/g and 23.63 (± 9.82) %.

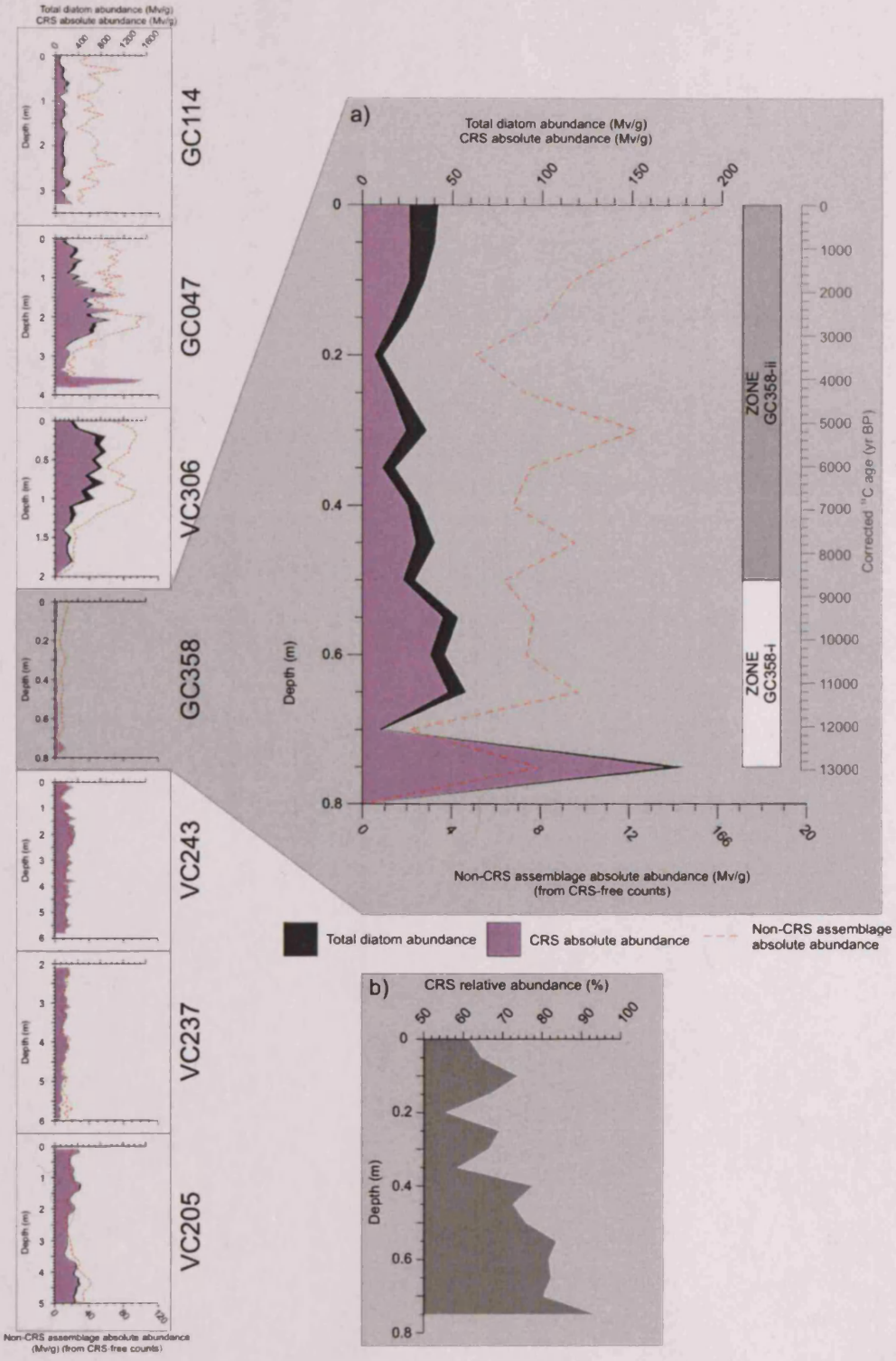


Figure 7.30

a) Core GC358: Total diatom abundance, CRS absolute abundance (both from CRS-included counts) and non-CRS assemblage absolute abundance (from CRS-free counts) (millions of valves/g (Mv/g)). Stratigraphic zones GC358-i and GC358-ii identified using Q-mode PCA analysis of diatom relative abundance data.

b) Core GC358: CRS relative abundance (%).

Figure 7.31
CoreGC358: Non-CRS diatom assemblage plots for AP indicator species: (a) Absolute abundance (Mv/g); (b) Relative abundance (%). Stratigraphic zones GC358-i and GC358-ii identified using Q-mode PCA analysis of diatom relative abundance data.

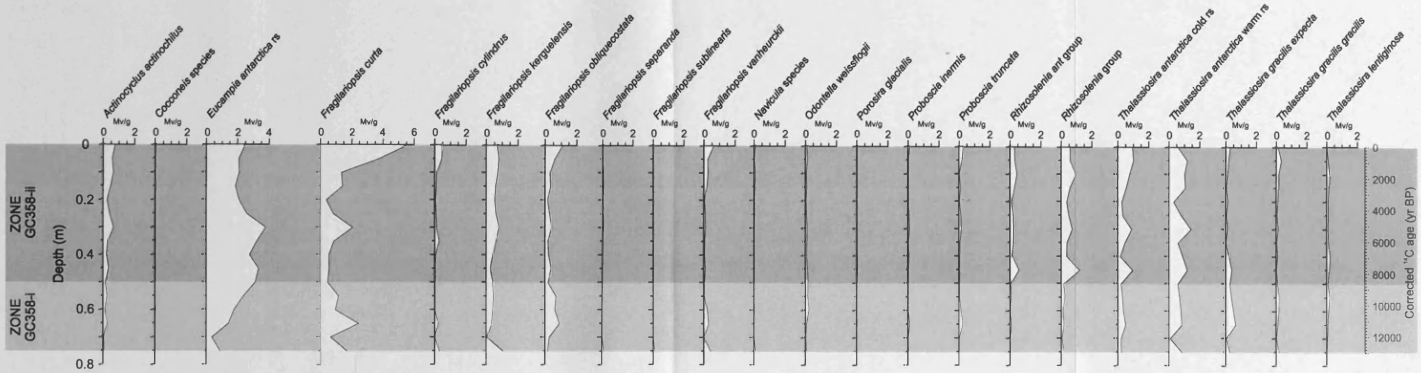


Figure 7.31 (a)

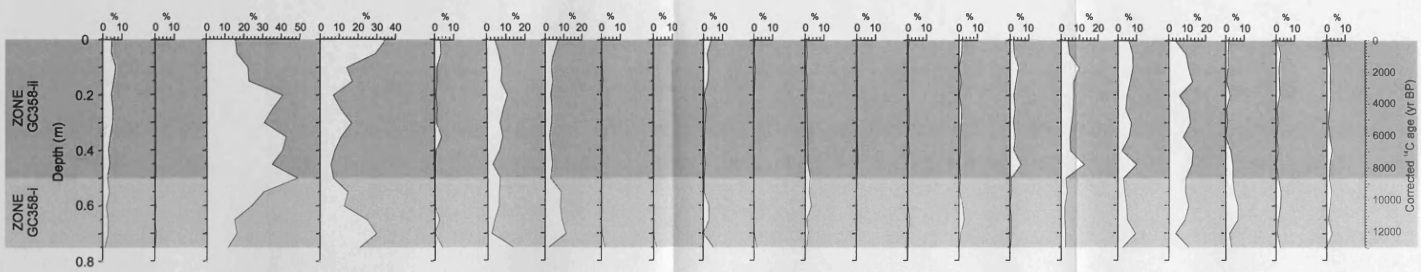


Figure 7.31 (b)

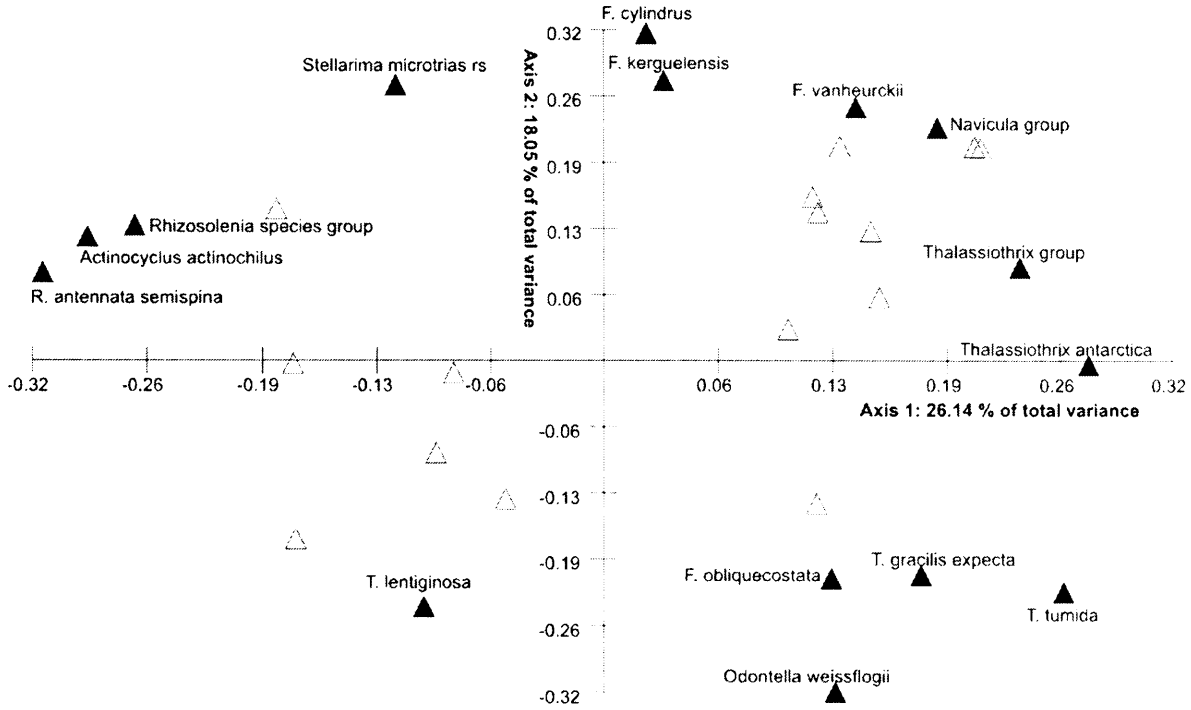


Figure 7.32
Core GC358: R-mode PCA variable loading on axes 1 and 2 for diatom relative abundance data (> 1 %). Data square-root transformed and standardised. Tolerance of eigenanalysis set at 1 x 10^{-10}. Highlighted species are those that have component loading ≥ + 0.20 or ≤ – 0.20.

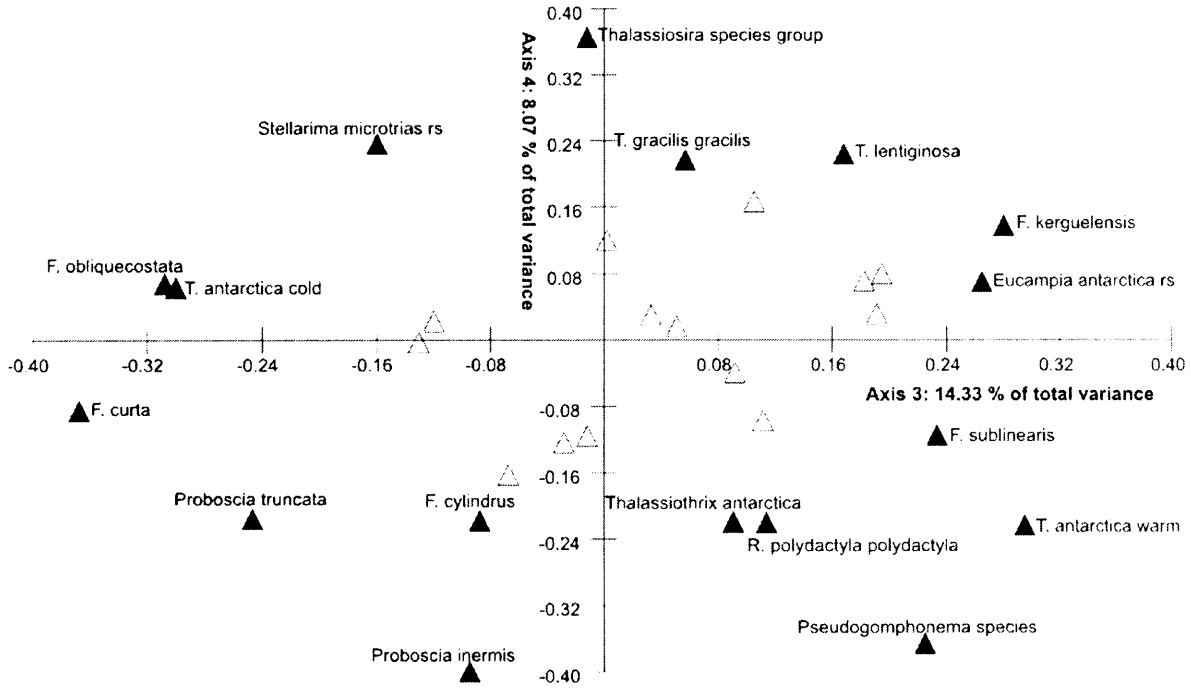


Figure 7.33
Core GC358: R-mode PCA variable loading on axes 3 and 4 for diatom relative abundance data (> 1 %). Data square-root transformed and standardised. Tolerance of eigenanalysis set at 1 x 10^{-10}. Highlighted species are those that have component loading ≥ + 0.20 or ≤ – 0.20.

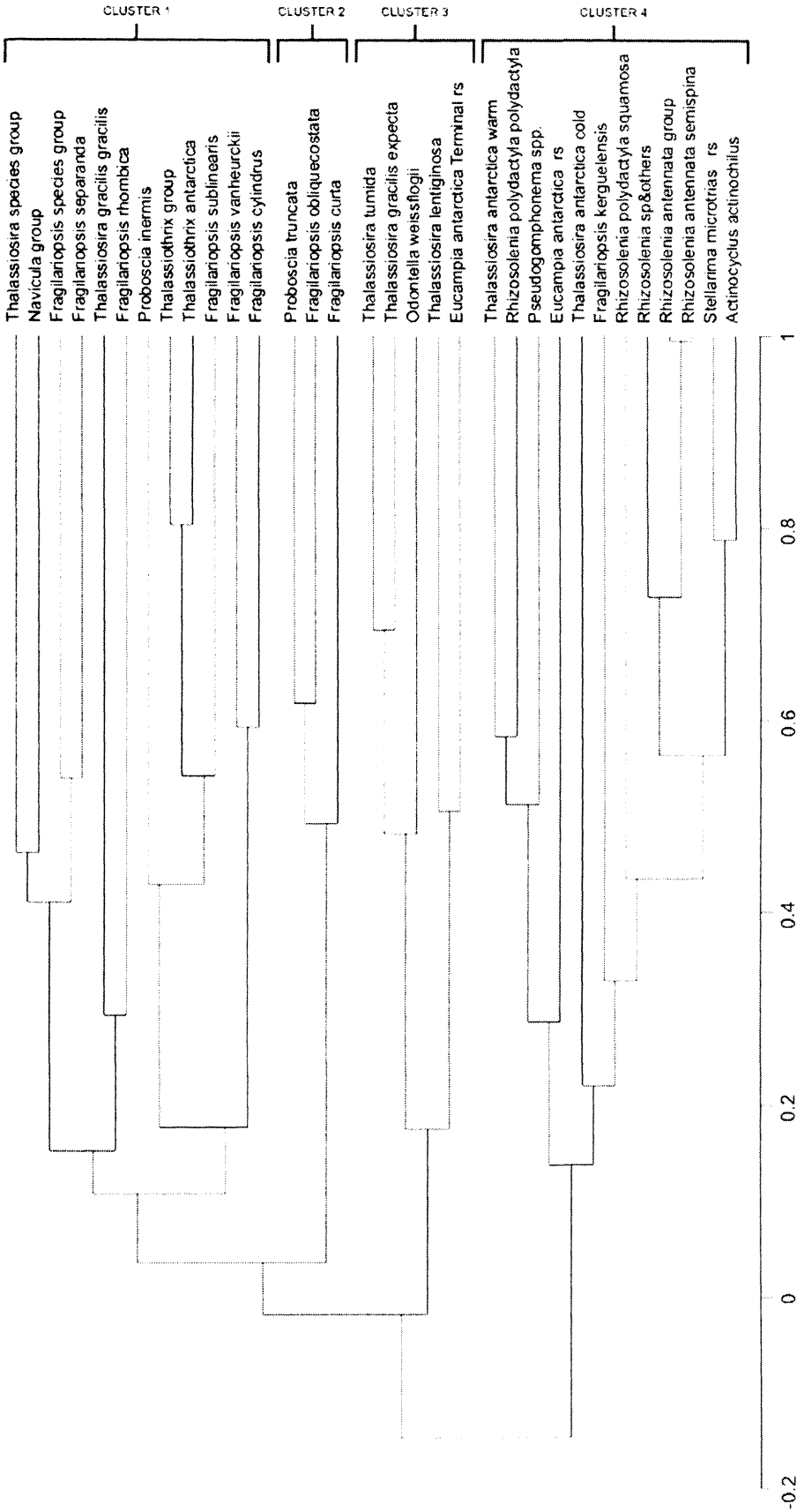


Figure 7.34
Core GC358: R-mode cluster analysis of diatom species relative abundance (> 1 %). UPGMA clustering method; data square-root transformed; and Spearman Coefficient similarity measure.

Table 7.4 Core GC358: Comparison of diatom PCA axis loading and cluster groupings. Indicator species denoted with *. Grouped indicator species shown in grey box and relate to diatom assemblages highlighted on Figure 7.37.

Axis 1 Positive	Cluster group		**Axis 1 Negative**	Cluster group	
F. sublinearis	1	**None**	*A. actinochilus**	4	**A. actinochilus**
Fragilariopsis species group	1		*R. antennata* f. *semispina*	4	
T. tumida	3		*R. antennata* group	4	
Thalassiothrix antarctica	1		*Rhizosolenia* species group	4	
Axis 2 Positive	Cluster group		**Axis 2 Negative**	Cluster group	
F. cylindrus	1	**F. kerguelensis**	*O. weissflogii*	3	**T. gracilis var. expecta**
*F. kerguelensis**	4		*T. gracilis* var. *expecta**	3	
F. separanda	1		*T. lentiginosa*	3	
Fragilariopsis species group	1		*T. tumida*	3	
F. sublinearis	1				
F. vanheurckii	1				
Navicula group	1				
S. microtrias rs	4				
Axis 3 Positive	Cluster group		**Axis 3 Negative**	Cluster group	
E. antarctica rs*	4	**E. antarctica rs; F. kerguelensis; T. antarctica warm**	*F. curta**	2	**F.curta; F. obliquecostata; T. antarctica cold rs**
*F. kerguelensis**	4		*F. obliquecostata**	2	
F. sublinearis	1		*P. truncata*	2	
Pseudogomphonema species	4		*T. antarctica* cold rs*	4	
T. antarctica warm rs*	4				
Axis 4 Positive	Cluster group		**Axis 4 Negative**	Cluster group	
S. microtrias rs	4	**None**	*F. cylindrus*	1	**T. antarctica warm rs**
T. gracilis var. *gracilis*	1		*P. inermis*	1	
T. lentiginosa	3		*P. truncata*	2	
Thalassiosira species group	1		*Pseudogomphonema* species	4	
			R. polydactyla f. *polydactyla*	4	
			T. antarctica warm rs*	4	
			Thallassiothrix antarctica	1	

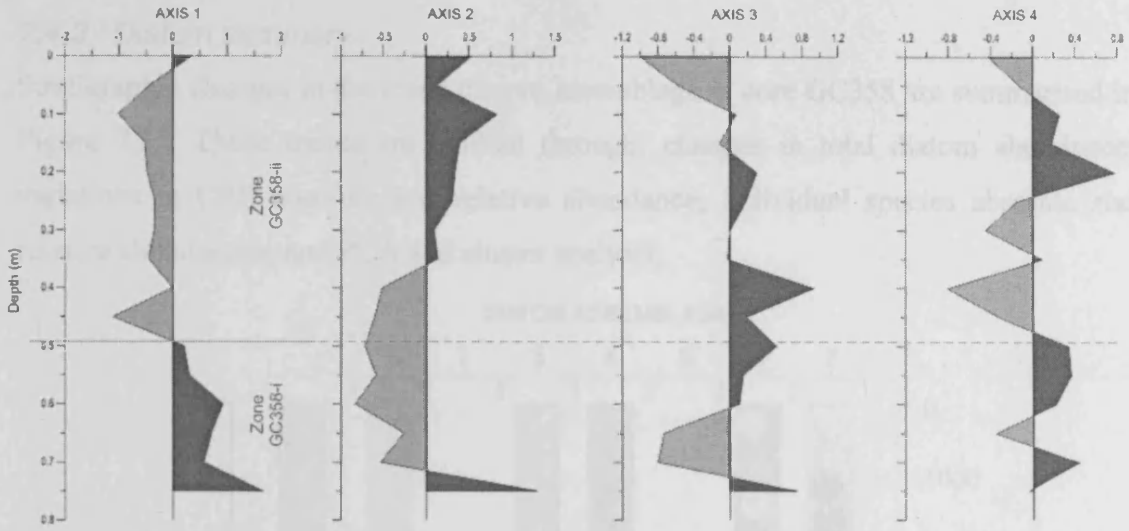


Figure 7.35
Core GC358: Q-mode PCA component scores plotted stratigraphically for PCA axes 1 – 4. Positive loading (dark grey); negative loading (light grey). Division of the record into stratigraphic zones GC358-i and GC358-ii is based on component loading on axis 1.

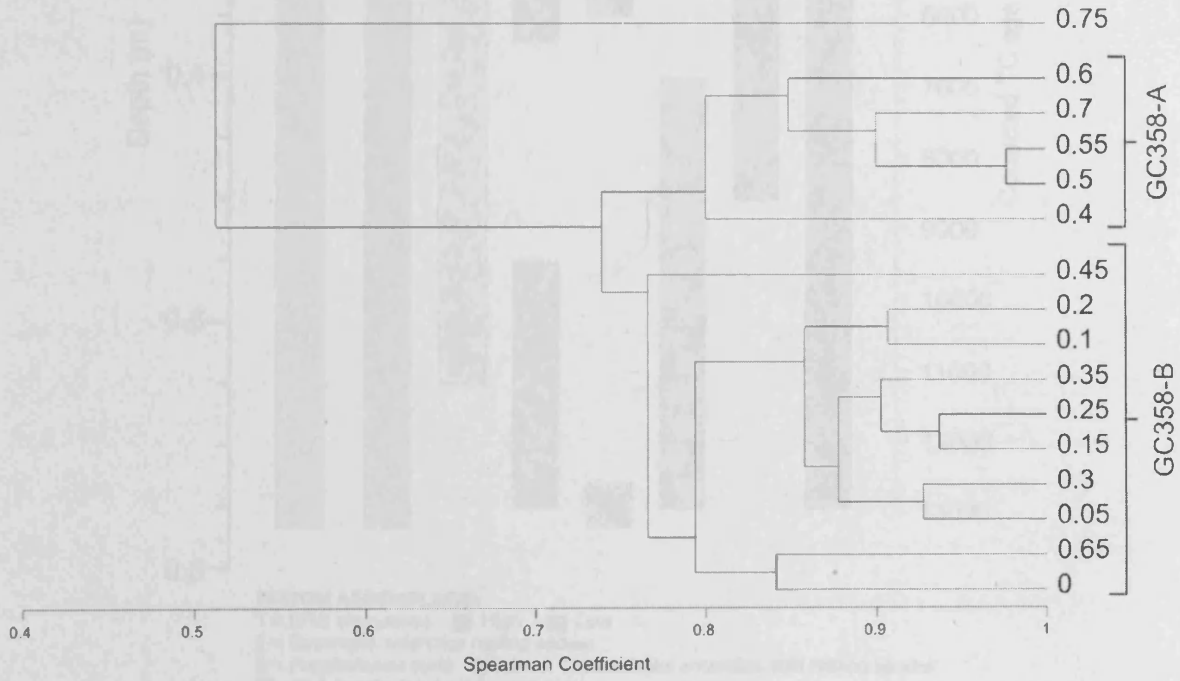


Figure 7.36
Core GC358: Q-mode cluster analysis of core depths, using diatom species relative abundances (> 1 %). UPGMA clustering method; data square-root transformed; and Spearman Coefficient similarity measure.

7.4.3 Diatom summary

Stratigraphic changes in the fossil diatom assemblage in core GC358 are summarised in Figure 7.37. These trends are evident through: changes in total diatom abundance; variations in CRS absolute and relative abundance; individual species absolute and relative abundances; and PCA and cluster analysis.

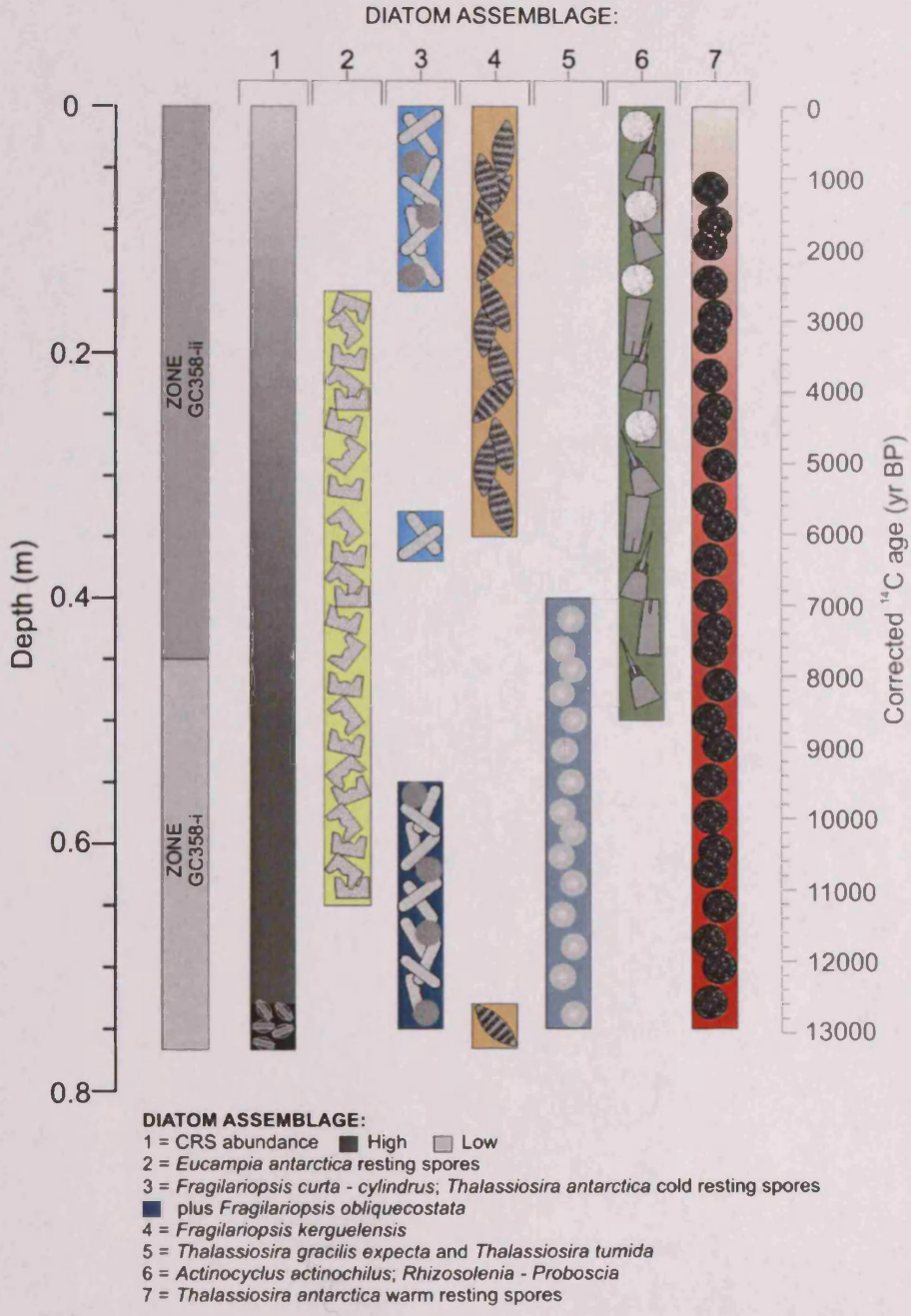


Figure 7.37
Core GC358: Schematic representation of the fossil diatom assemblage, highlighting the relative contribution of CRS to the total assemblage and stratigraphic changes in the diatom community. Stratigraphic zones GC358-i and GC358-ii identified using Q-mode PCA analysis of the diatom relative abundance data. Darker tones indicate elevated abundance.

7.5 VC243

7.5.1 Diatom assemblage

Total diatom abundance is relatively constant along the core length, although intervals of higher abundance are present in the record (Figure 7.38a). In general, the sedimentary assemblage is reasonably fragmented in core VC243, although fragmentation is variable between sample depths (Figure 7.39). Throughout the core, CRS form the most abundant and consistent proportion of the total diatom assemblage, with concentrations ranging between 90.5 – 97.4 % (Figure 7.38b). Stratigraphic variations in the non-CRS species assemblage are pronounced in core VC243 (Figure 7.40). By far the most abundant non-CRS species throughout the core is *T. antarctica* warm rs, with mean absolute and relative abundances of 6.69 (± 1.65) Mv/g and 53.83 (± 7.69) % respectively. The remainder of the non-CRS assemblage includes moderate contributions from *F. curta* (mean absolute abundance, 1 (± 0.58) Mv/g; mean relative abundance, 7.77 (± 3.47) %), *F. vanheurckii* (mean absolute abundance, 0.69 (± 0.27) Mv/g; mean relative abundance, 5.56 (± 1.64) %), *O. weissflogii* (mean absolute abundance, 0.59 (± 0.3) Mv/g; mean relative abundance, 4.6 ± (2.23) %) and *F. cylindrus* (mean absolute abundance, 0.3 (± 0.24) Mv/g; mean relative abundance, 2.38 ± (1.88) %), together with minor contributions from *P. glacialis*, *T. antarctica* cold rs and benthic diatoms, including *Navicula*, *Achnanthes*, *Amphora* and *Cocconeis* species.

R-mode PCA analysis highlights several diatom species associations in core VC243; species with high positive and negative loadings on axes 1 – 4 are highlighted in bold and the variance explained by each PCA axis is also presented (Figure 7.41, Figure 7.42 and Table A2.13). R-mode cluster analysis of diatom species relative abundance displays rather complex species associations (Figure 7.43). The assemblage can be divided into two large groups, at 2 % similarity, together with two isolated individuals (*T. antarctica* warm rs and vegetative). Comparison of the species associations revealed by PCA and cluster analysis are presented in Table 7.5, with indicator species highlighted.

7.5.2 Diatom stratigraphic zones

Q-mode PCA analysis reveals complex stratigraphic component loading, particularly on axes 1 and 3 (Figure 7.44 and Table A2.14). On axis 2, a more straight forward pattern exists with typically negative component scores between 5.8 – 4 m and positive component scores between 4 – 0 m, becoming more pronounced above 1.5 m. The division at 4 m reflects the change in diatom assemblage, from dominance of *T.*

antarctica warm rs and *O. weissflogii* (both with negative loading on axis 2) at the base of the core (5.8 – 4 m), to a more mixed assemblage, with increased contributions from *F. curta*, *F. cylindrus*, *P. glacialis*, *Nitzschia* species, *Achnanthes* group and *Cocconeis* group (all with positive loading on axis 2) in the middle-upper core (4 – 0 m). The stratigraphic pattern on axis 4, with positive loading between 4.5 – 2.4 m records the increased abundance of *E. antarctica* rs, *O. weissflogii*, *O. litigiosa*, *T. gracilis* group and *S. microtrias* through this interval.

Q-mode cluster analysis on sample depths reveals an equally complex grouping system in core VC243 (Figure 7.45a). Three cluster groups can be identified (VC243-A, VC243-B and VC243-C), at 70 % similarity, plus several outlier sample depths. When individual sample depths within each cluster group are plotted stratigraphically for core VC243, there appears to be little association based on sample depth, with neighbouring depths frequently forming part of different cluster groups (Figure 7.45b). The only observation of note is that below 1.8 m, sample depths typically form part of cluster group VC243-A and VC243-B, whereas above 1.8 m, sample depths are more likely to fall into cluster group VC243-C.

Using the criteria of core zonation (Chapter 5.1.7) based on identification of a PCA axis with simplified component loading along the core length immediately excludes axis 1 (Figure 7.45). As highlighted in Table 7.5, with the exception of *F. vanheurckii*, all the species on axis 1 are not considered indicator species and in the example of non-indicator species given in Chapter 5.1.6, it is likely that these species are typical "species *x*" – they are potentially linked to a specific habitat but their rarity in sample depths produces a very complex stratigraphic component loading. This complexity, paired with the lack of indicator species, results in exclusion of axis 1 in core zonation. Axis 2 still encompasses a large proportion of the total variance in the data (13 %, Table A2.14) and provides three clear zones (VC243-i (6 – 4 m), VC243-ii (4 – 1.5 m) and VC243-iii (1.5 – 0 m)) (Figure 7.44) with distinct differences in the diatom community structure. These three zones are described below and highlighted on total diatom abundance plot (Figure 7.38), Fragmentation Index plot (Figure 7.39) and individual species absolute and relative abundance plots (Figure 7.40).

7.5.2.1 VC243-i: 5.8 – 4 m

Total diatom abundance in this zone displays fluctuating mid-range values (217.3 (± 38.57) Mv/g). The mean proportion that CRS form of the total assemblage is 93.68 (±

1.59) %. Non-CRS absolute abundance exhibits a similar pattern to total diatom abundance; fluctuating mid values (11.2 (± 1.38) Mv/g). Zone VC243-i experiences the highest levels of diatom fragmentation for the core, with typically <35 % of *Fragilariopsis* species intact between 5.8 – 3.6 m.

There are several notable features of the non-CRS species assemblage through zone VC243-i. *T. antarctica* warm rs relative abundance is high between 5.8 and 4.1 m (averaging 61.72 (± 5.46) %). In comparison, absolute abundance of *T. antarctica* warm rs displays mid-range values between 5.8 – 3.2 m (averaging 6.57 (± 0.96) Mv/g). *O. weissflogii* shows an increase in absolute and relative abundances between 4.6 and 3.7 m, averaging 0.92 (± 0.24) Mv/g and 8.03 (± 1.73) % respectively, compared to average values of 0.52 (± 0.27) Mv/g and 3.91 (± 1.58) %, for the remainder of the core. Although average abundances of *E. antarctica* rs are low throughout core VC243, this species shows a similar pattern to that of *O. weissflogii*. *E. antarctica* rs record elevated abundances between 4.5 and 3 m, with mean absolute abundances of 0.13 (± 0.05) Mv/g and mean relative abundances of 0.97 (± 0.25) %. Finally, it is worth noting that lowest abundances of *F. curta* for the whole of the core occur between 5.8 – 4.1 m, with absolute abundance averaging 0.59 (± 0.26) Mv/g and relative abundance averaging 5.31 (± 2) %.

7.5.2.2 VC243-ii: 4 – 1.5 m

Between 4 – 2.6 m, total diatom abundance remains relatively low, with similar values to zone VC243-i (averaging 232.21 (± 59.42) Mv/g). At 2.5 m, diatom absolute abundance exhibits a dramatic and progressive increase up-core, peaking at 2 m (354.99 Mv/g). Between 2.5 – 1.3 m, highest diatom absolute abundances for the core are found, averaging 305.62 (± 50.07) Mv/g. CRS relative abundance is stable through zone VC243-ii, averaging 93.57 (± 0.94) %. Similar to total diatom abundance, absolute abundance of non-CRS assemblage is highest in the middle section of the core, although values are elevated in two peaks (between 3.2 – 2.8 m and 2.5 – 1.6 m), compared to the single peak for total diatom abundance (between 2.5 – 1.3 m). Non-CRS absolute abundance is highest at 2.3 m (21.95 Mv/g), which is slightly earlier than the peak of total diatom absolute abundance, at 2 m. Diatom fragmentation in zone VC243-ii is moderate-low, with typically 35 – 55 % of *Fragilariopsis* species intact between 3.5 – 1.5 m.

Several species exhibit a change in abundance at the transition between zone VC243-i and VC243-ii, with the total assemblage becoming more mixed, with greater contributions from a number of species. Firstly, the high relative abundance of *T. antarctica* warm rs seen in zone VC243-i reduces slightly in zone VC243-ii (averaging 51.19 (± 3.75) %). In comparison, *T. antarctica* warm rs absolute abundance is high in zone VC243-ii, as observed in two peaks between 3.1 – 2.1 m (averaging 8.46 (± 1.86) Mv/g); and progressively decreasing values up-core of 2 m. Secondly, absolute and relative abundances of *F. curta* increase dramatically at the transition at 4 m and progressively increase up-core, to reach highest levels between 2.5 – 1.8 m, averaging 1.73 (± 0.31) Mv/g and 10.47 (± 2.01) % respectively. Similarly *F. cylindrus* exhibits elevated abundances up-core of 2.5 m, in a series of peaks. Absolute and relative abundance of *F. cylindrus* average 0.44 (± 0.14) Mv/g and 3.37 (± 1.05) % between 2.5 and 0 m, compared to 0.2 (± 0.08) Mv/g and 1.61 (± 0.58) % between 5.8 – 2.6 m. Like-wise, *T. antarctica* cold rs show elevated absolute and relative abundance between 2.5 – 1.3 m, averaging 0.36 (± 0.13) Mv/g and 2.27 (± 0.77) % respectively. Grouped *Navicula* species show a roughly symmetrical increase and decrease in abundance up-core, with maximum absolute and relative abundances between 2.3 – 1.8 m, averaging 0.78 (± 0.12) Mv/g and 4.59 (± 0.69) %, respectively. *P. glacialis* and *S. microtrias* rs both exhibit an up-core increasing abundance trend between 3.9 – 0 m. *P. glacialis* absolute and relative abundances between this interval average 0.27 (± 0.1) Mv/g and 2.12 (± 0.8) %, respectively, whilst *S. microtrias* rs absolute and relative abundances between 3.9 – 0 m average 0.1 (± 0.07) Mv/g and 0.89 (± 0.64) %, respectively. Finally, both varieties of *T. gracilis* show elevated absolute and relative abundances between ~3.5 – 2.5 m, with grouped absolute abundance averaging 0.28 (± 0.1) Mv/g and 2.05 (± 0.56) %, respectively.

7.5.2.3 VC243-iii: 1.5 – 0 m

Total diatom abundance decreases from maximum levels at ~2 m, in a series of steps towards the core top. Lowest absolute abundances occur between 0.7 m and 0.5 m (115.13 (± 28.5) Mv/g), which is coincident with lowest relative CRS values, between 0.8 m – 0.5 m (averaging 91.4 (± 0.6) %). This interval corresponds to a horizon with a pronounced concentration of clasts (see Figure 6.6). Non-CRS species absolute abundance falls from maximum values at 2.3 m progressively up-core to 0.9 m. Mirroring the period of lowest CRS abundance, non-CRS absolute abundance also falls significantly to a minimum of 5.7 Mv/g at 0.4 m. The uppermost 0.2 m and core top

record mid-range non-CRS abundance, averaging 12.4 (± 1.4) Mv/g. Diatom fragmentation increases again in zone VC243-iii, and is most apparent between 1.1 – 0.5 m, where typically 35 – 45 % of *Fragilariopsis* species are intact.

The transition from zone VC243-ii into VC243-iii is not particularly marked. *T. antarctica* warm rs continue their observed progressive up-core decrease in absolute and relative abundance, with lowest absolute abundance at 0.6 m (2.13 Mv/g) and lowest relative abundance at 0.2 m (34.98 %). In contrast, *P. glacialis* continue their increase in abundance up-core, with highest abundances of this species occurring between 0.5 – 0 m (3.33 (± 0.72) Mv/g). Both varieties of *T. gracilis* decrease in abundance in zone VC243-iii, with mean absolute abundance 0.1 (± 0.06) Mv/g and mean relative abundance 0.91 (± 0.44) % through zone VC243-iii. Although highly variable, *F. curta* and *F. cylindrus* maintain moderate abundances throughout this zone. *F. curta* absolute abundance ranges between 2.61 Mv/g (0.2 m) and 0.34 Mv/g (0.4 m); relative abundance between 18.97 % (0.2 m) and 3.99 % (0.7 m). *F. cylindrus* absolute abundance ranges between 1.18 Mv/g (0.9 m) and 0.1 Mv/g (0.6 m); relative abundance between 10.73 % (0.4 m) and 1.27 % (1.1 m). Finally, grouped *Cocconeis* species also exhibit elevated absolute and relative abundances between 1.6 and 0 m, averaging 0.28 (± 0.08) Mv/g and 2.64 (± 0.53) %, respectively.

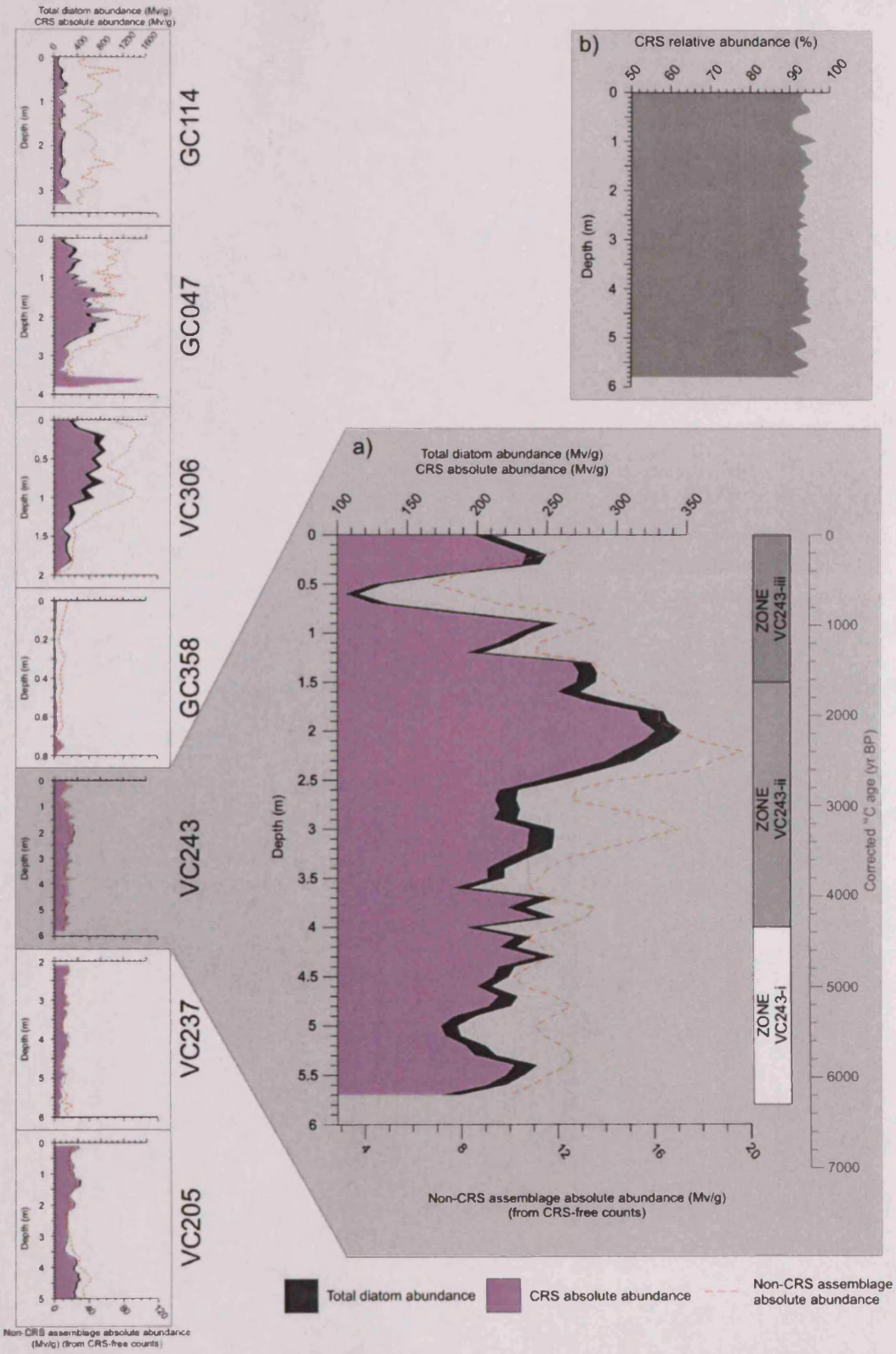


Figure 7.38

a) Core VC243: Total diatom abundance, CRS absolute abundance (both from CRS-included counts) and non-CRS assemblage absolute abundance (from CRS-free counts) (millions of valves/g (Mv/g)), smoothed using a three point moving average. Stratigraphic zones VC243-i, VC243-ii and VC243-iii identified using Q-mode PCA analysis of diatom relative abundance data.

b) Core VC243: CRS relative abundance (%).

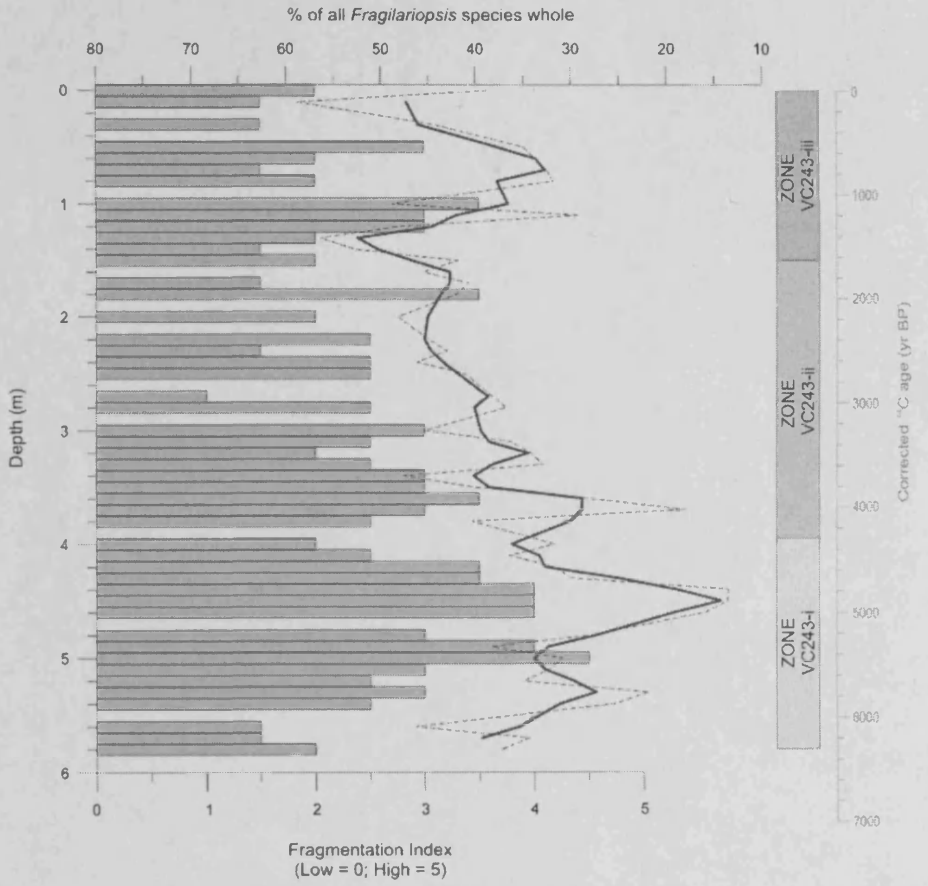


Figure 7.39
Core VC243: Diatom fragmentation, using two measures: observational index (bars: low = 0 to high = 5); and percentage of *Fragilariopsis* species whole (dashed line = original; solid line = three point moving average).
Stratigraphic zones VC243-i, VC243-ii and VC243-iii identified using Q-mode PCA analysis of diatom relative abundance data.

Figure 7.40
Core VC243: Non-CRS diatom assemblage plots for AP indicator species: (a) Absolute abundance (Mv/g); (b) Relative abundance (%).
Three point average (white); original abundance (dark grey line). Stratigraphic zones VC243-i to VC243-iii identified using Q-mode PCA analysis of diatom relative abundance data.

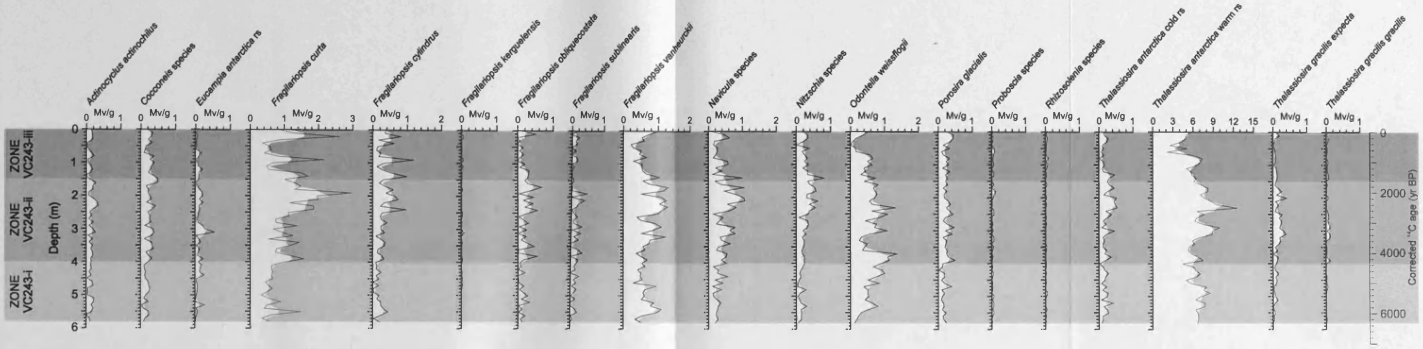


Figure 7.40 (a)

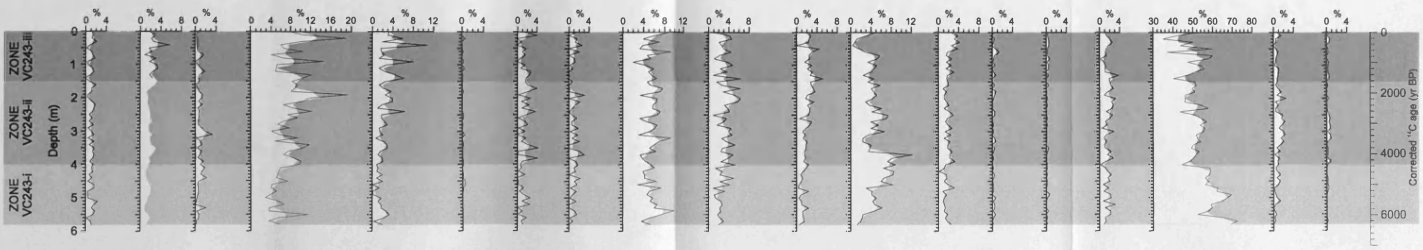


Figure 7.40 (b)

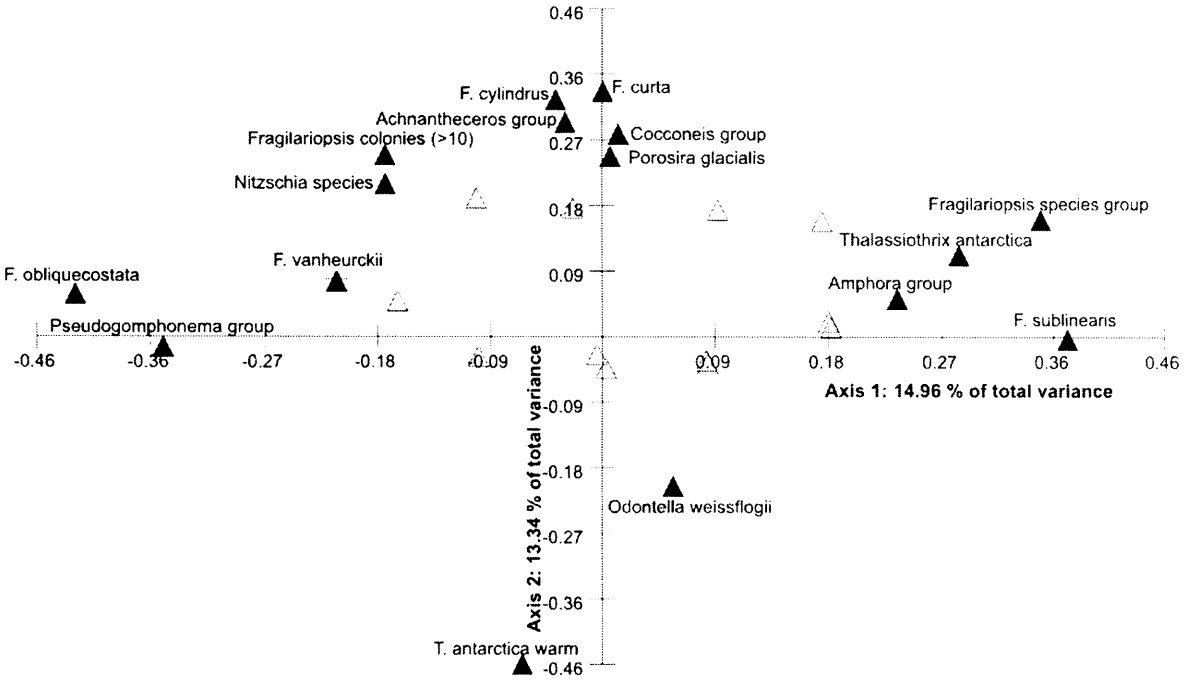


Figure 7.41
Core VC243: R-mode PCA variable loading on axes 1 and 2 for diatom relative abundance data (> 1 %). Data square-root transformed and standardised. Tolerance of eigenanalysis set at 1 x 10^{-10}. Highlighted species are those that have component loading ≥ + 0.20 or ≤ – 0.20.

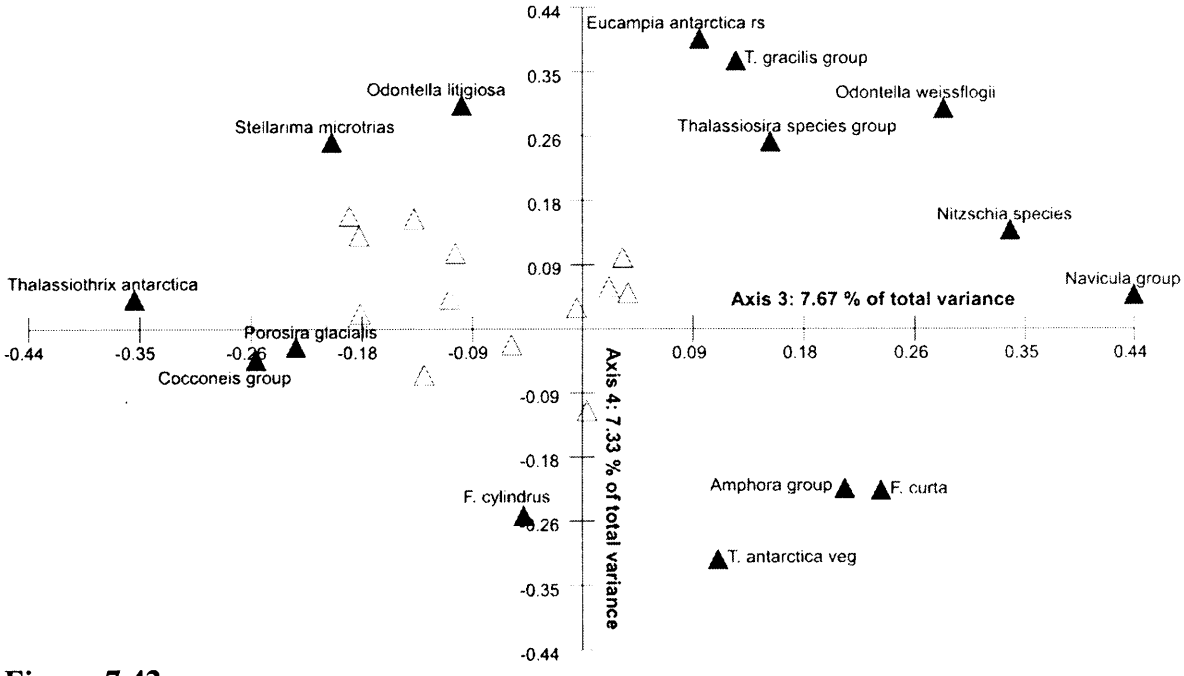


Figure 7.42
Core VC243: R-mode PCA variable loading on axes 3 and 4 for diatom relative abundance data (> 1 %). Data square-root transformed and standardised. Tolerance of eigenanalysis set at 1 x 10^{-10}. Highlighted species are those that have component loading ≥ + 0.20 or ≤ – 0.20.

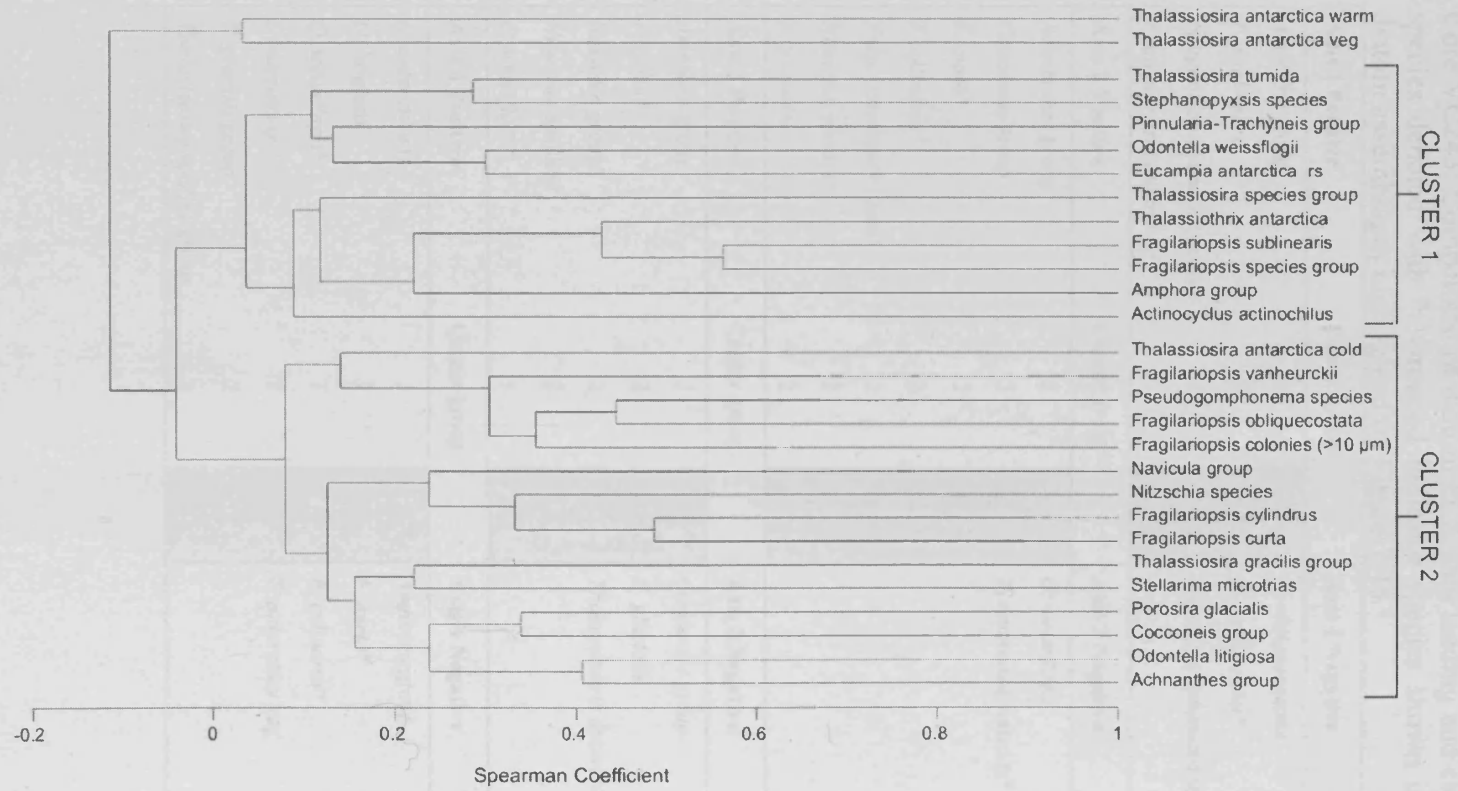


Figure 7.43
Core VC243: R-mode cluster analysis of diatom species relative abundance (>1 %). UPGMA clustering method; data square-root transformed; and Spearman Coefficient similarity measure.

Table 7.5

Core VC243: Comparison of diatom PCA axis loading and cluster groupings. Indicator species denoted with *. Grouped indicator species shown in grey box and relate to diatom assemblages highlighted on Figure 7.46.

Axis 1 Positive	Cluster group		**Axis 1 Negative**	Cluster group	
Amphora group	1	None	*F. obliquecostata*	2	F. vanheurckii
F. sublinearis	1		*F. vanheurckii**	2	
Fragilariopsis species group	1		*Pseudogomphonema* species	2	
Thalassiothrix antarctica	1				
Axis 2 Positive	Cluster group		**Axis 2 Negative**	Cluster group	
Achnanthes group	2	F. curta – F. cylindrus; Nitzschia	*O. weissflogii*	1	T. antarctica warm rs
Cocconeis group	2		*T. antarctica* warm rs*	N/A	
*F. curta**	2				
*F. cylindrus**	2				
Frag. colonies (>10µm)	2				
Nitzschia species*	2				
P. glacialis	2				
Axis 3 Positive	Cluster group		**Axis 3 Negative**	Cluster group	
Amphora group	1	F. curta; Navicula; Nitzschia; O. weissflogii	*Cocconeis* group	2	None
*F. curta**	2		*P. glacialis*	2	
Navicula group*	2		*Thalassiothrix antarctica*	1	
Nitzschia species*	2				
*O. weissflogii**	1				
Axis 4 Positive	Cluster group		**Axis 4 Negative**	Cluster group	
E. antarctica rs	1	O. weissflogii	*Amphora* group	1	F. curta – F. cylindrus
O. litigiosa	2		*F. curta**	2	
*O. weissflogii**	1		*F. cylindrus**	2	
S. microtrias	2		*T. antarctica* veg	N/A	
T. gracilis group	2				
Thalassiosira species group	1				

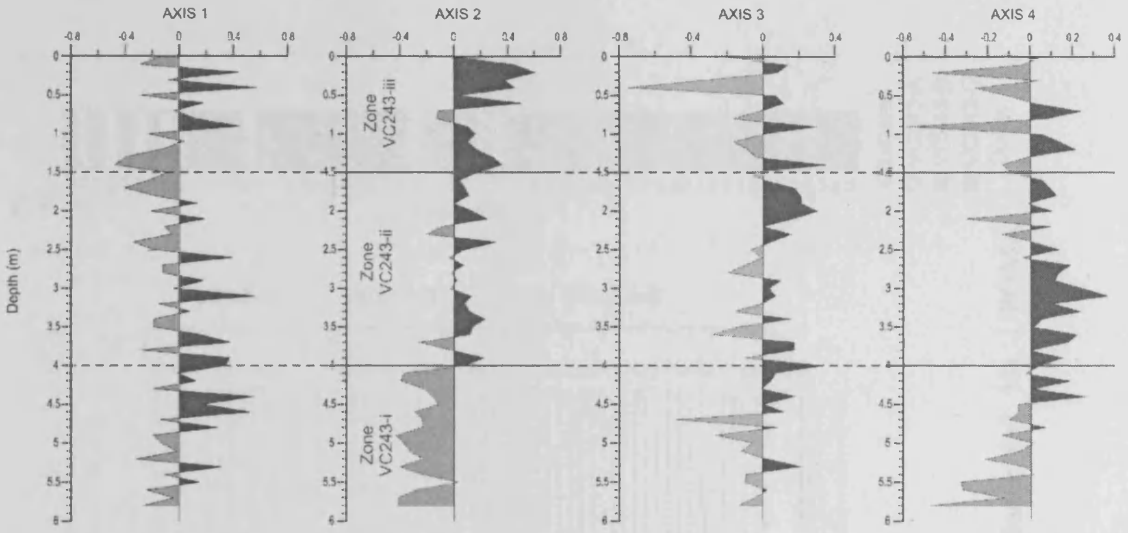


Figure 7.44
Core VC243: Q-mode PCA component scores plotted stratigraphically for PCA axes 1 – 4. Positive loading (dark grey); negative loading (light grey). Division of the record into stratigraphic zones VC243-i, VC243-ii and VC243-iii was based on component loading on axis 2.

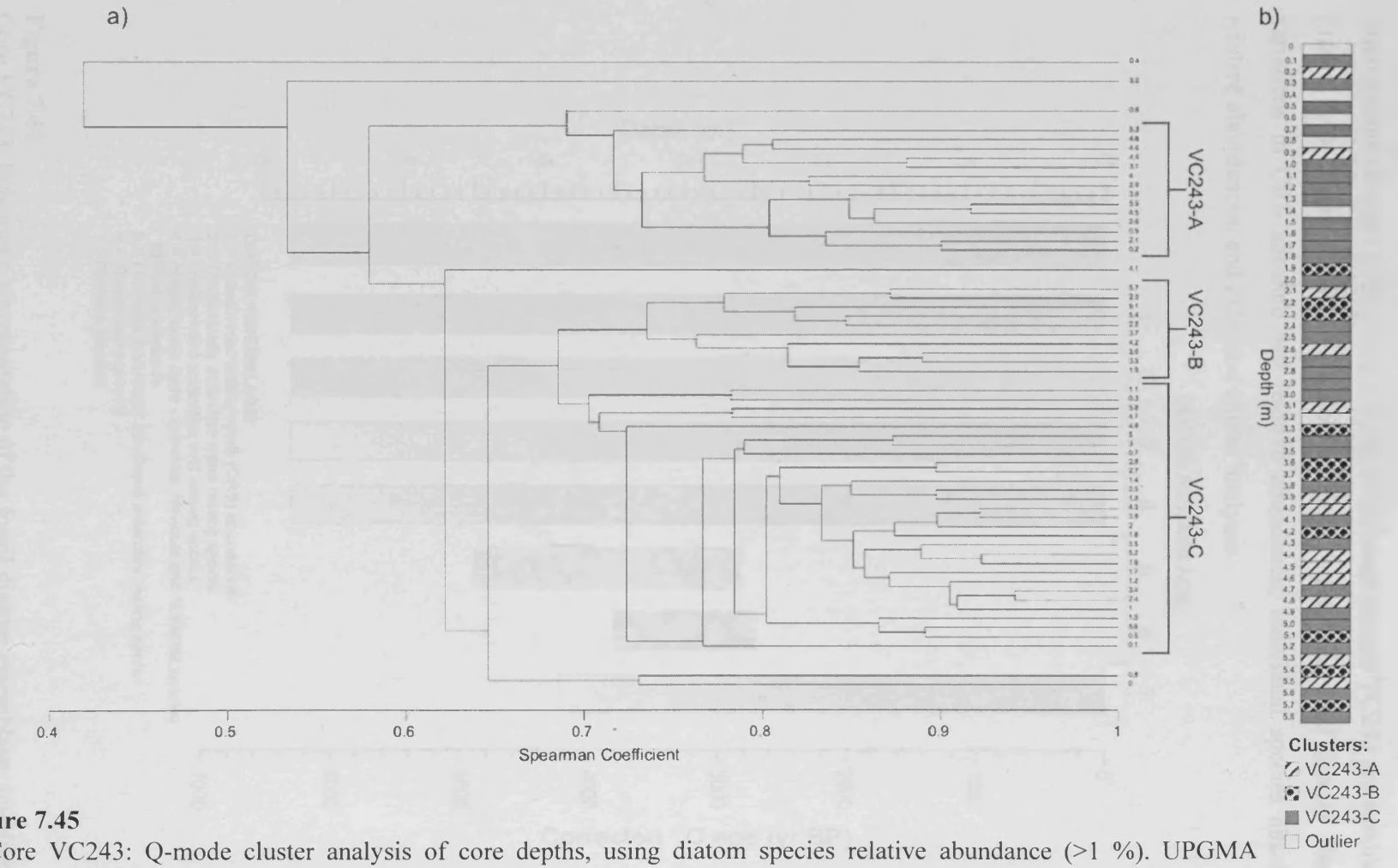


Figure 7.45

a) Core VC243: Q-mode cluster analysis of core depths, using diatom species relative abundance (>1 %). UPGMA clustering method; data square-root transformed; and Spearman Coefficient similarity measure.

b) Core VC243: Stratigraphic pattern of Q-mode cluster groups.

7.5.3 Diatom summary

Stratigraphic changes in the fossil diatom assemblage in core VC243 are summarised in Figure 7.46. These trends are evident through: changes in total diatom abundance; variations in CRS absolute and relative abundance; individual species absolute and relative abundances; and PCA and cluster analyses.

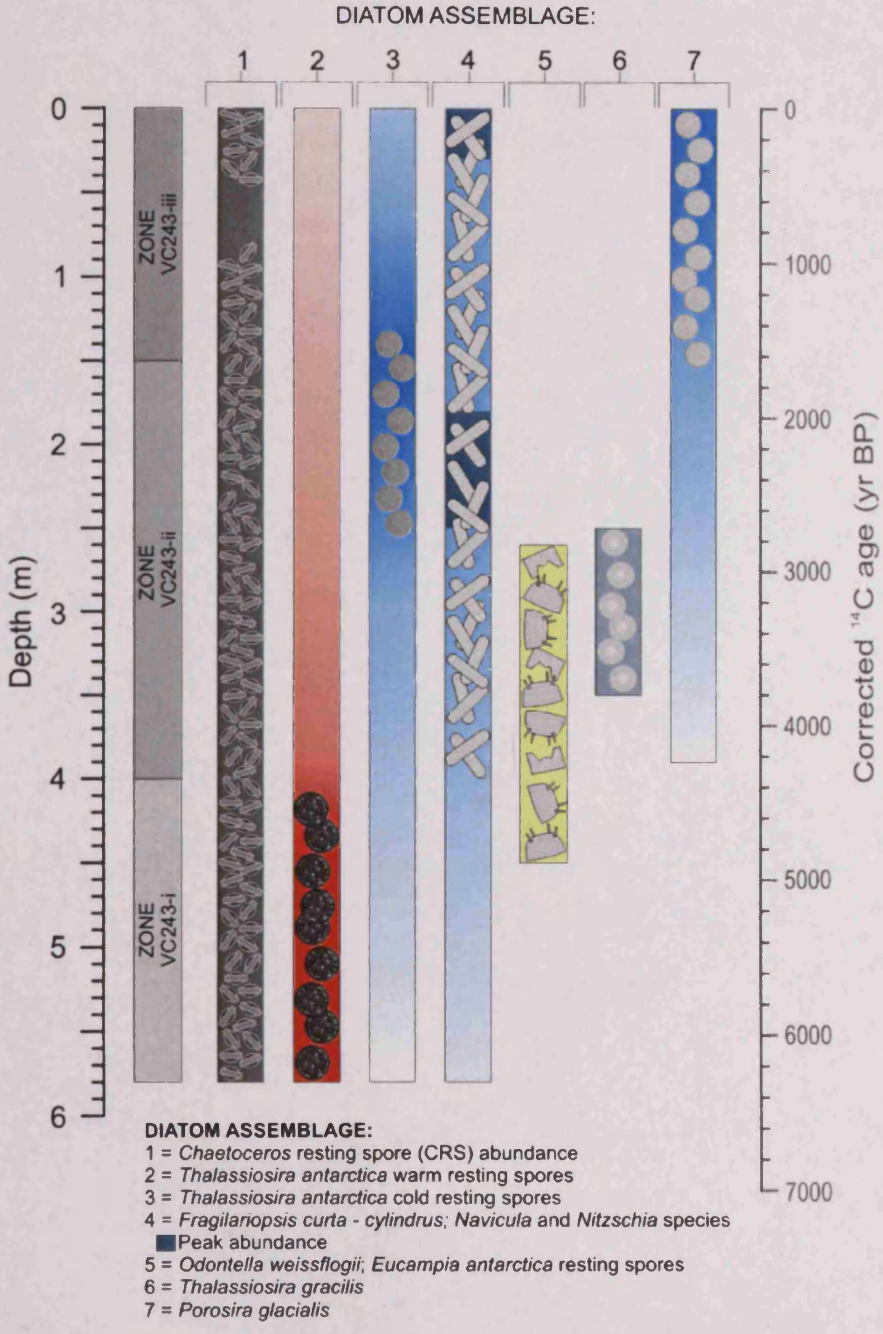


Figure 7.46
Core VC243: Schematic representation of the fossil diatom assemblage, highlighting the relative contribution of CRS to the total assemblage and stratigraphic changes in the diatom community. Stratigraphic zones VC243-i, VC243-ii and VC243-iii identified using Q-mode PCA analysis of diatom relative abundance data. Darker shading indicates elevated abundance.

7.5.4 Stable Isotopes

In core VC243, bulk organic matter carbon and nitrogen elemental contents (C_{org} and N_{org}) and isotopic composition ($\delta^{13}C_{org}$ and $\delta^{15}N_{org}$) record considerable stratigraphic variability, frequently between neighbouring sample depths (Figure 7.47). Isotope contents and composition are described using the diatom PCA based stratigraphic zones described in section 7.5.2. Typically along the core length, both C_{org} and N_{org} show very similar stratigraphic patterns, displaying a general trend of increasing content through zone VC243-i and VC243-ii. In zone VC243-iii, C_{org} and N_{org} both record much more variable values, but the overall trend is towards lower content. Stratigraphic patterns are less similar between $\delta^{13}C_{org}$ and $\delta^{15}N_{org}$. $\delta^{13}C_{org}$ displays an up-core trend through zones VC243-i and VC243-ii of progressively less negative values (enriched in ^{13}C; heavier), whereas $\delta^{15}N_{org}$ displays a reasonably gradual trend of less positive values (depleted in ^{15}N; lighter) along the whole core length. In zone VC243-iii, $\delta^{13}C_{org}$ matches the trend of $\delta^{15}N_{org}$, recording a slight shift to more negative values (depleted in ^{13}C; lighter). The ratio of C_{org}/N_{org} oscillates between 7 – 9 throughout the core, although three peaks are observed at 5.7 m, 0.6 m and 0.2 m, where the ratio jumps to ~12.

7.5.4.1 VC243-i: 5.8 – 4 m

C_{org} and N_{org} are low and relatively constant between 5.9 – 5.1 m, with mean contents of 0.73 (± 0.05) % and 0.09 (± 0.01) %, respectively. Up-core of 5.1 m, both isotopes display a short-lived increase to 0.85 % for C_{org} and 0.11 % for N_{org} at 4.6 m. In the upper-most portion of zone VC243-i, both C_{org} and N_{org} display a slight decrease reaching 0.74 % and 0.09 % respectively at the transition with zone VC243-ii (4 m). $\delta^{13}C_{org}$ and $\delta^{15}N_{org}$ are relatively stable through zone VC243-i, with respective mean values of -23.66 (± 0.15) ‰ and 4.58 (± 0.28) ‰.

7.5.4.2 VC243-ii: 4 – 1.5 m

Both C_{org} and N_{org} show a progressive increase in content through zone VC243-ii, from 0.74 % and 0.09 % at 4 m, to maximum values of 1.01 % and 0.12 % respectively at 1.9 m. This depth marks the initiation of the downward trend towards lower contents witnessed in zone VC243-iii. $\delta^{13}C_{org}$ and $\delta^{15}N_{org}$ display opposing trends in zone VC243-ii. $\delta^{13}C_{org}$ remains relatively stable through the lower portion of zone VC243-ii (4 – 3.1 m), with mean content of -23.72 (± 0.16). Up-core of 3.1 m, $\delta^{13}C_{org}$ display a jump to less negative values, remaining relative stable for the remainder of zone VC243-ii, averaging -23.15 (± 0.16) ‰. $\delta^{15}N_{org}$ display a gradual trend towards less

positive values through zone VC243-ii, from 4.18 ‰ at the base (4 m) to 3.36 ‰ at the top (1.5 m).

7.5.4.3 VC243-iii: 1.5 – 0 m

In zone VC243-iii, both C_{org} and N_{org} record much greater variability, although both show a slight decrease to lower contents. Through this zone, C_{org} content averages 0.9 (± 0.06) % and N_{org} content averages 0.1 (± 0.01) %. At 0.6 m, both isotopes show a dramatic shift to lower contents, although this drop is more pronounced in N_{org}, with content falling to 0.07 %. Similarly, $\delta^{13}C_{org}$ and $\delta^{15}N_{org}$ are much more variable through zone VC243-iii, than VC243-i and VC243-ii. Mean $\delta^{13}C_{org}$ values through this zone are -23.43 (± 0.29) ‰ and there is a weak up-core trend towards more negative values. In general, $\delta^{15}N_{org}$ continue on the gradual up-core trend towards less positive values, witnessed in zones VC243-i and VC243-ii, reaching 3.61 ‰ at the core top. The exception to this trend is sample depth 1.4 m, where there is a dramatic shift to less positive $\delta^{15}N_{org}$ values (2.78 ‰).

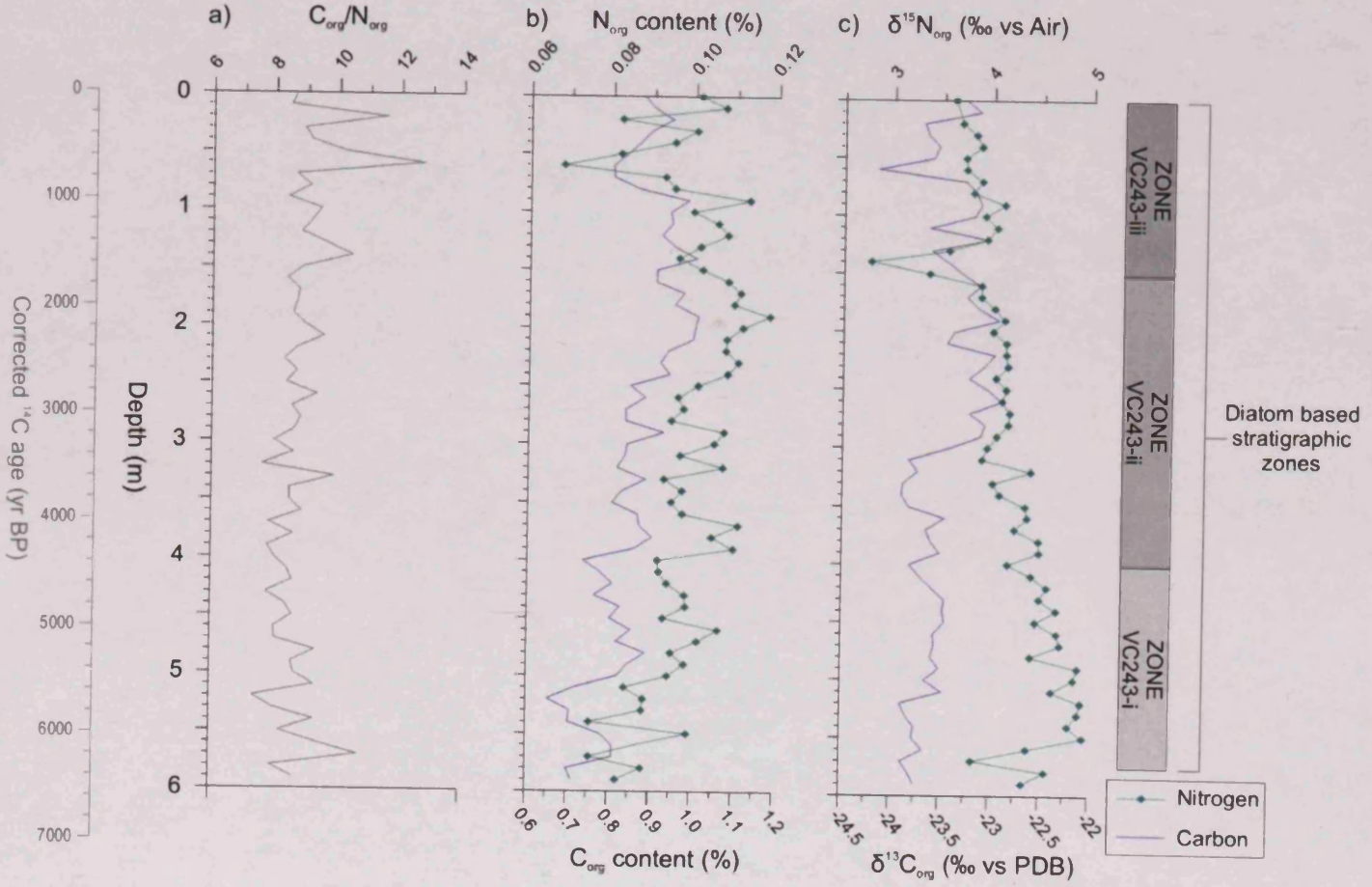


Figure 7.47
Core VC243: Bulk organic material stable isotope (carbon (C) and nitrogen (N)) contents and composition.
a) C_{org}/N_{org} ratio
b) Elemental contents (C_{org} and N_{org}) (%)
c) Isotopic composition ($\delta^{13}C_{org}$ and $\delta^{15}N_{org}$) (‰)
Stratigraphic zones VC243-i, VC243-ii and VC243-iii identified using Q-mode PCA analysis of diatom relative abundance data.

7.5.5 Sedimentary pigments

HPLC analyses revealed a mixture of chlorophylls and carotenoids preserved in core VC243. Full details of the main pigments, their retention times (tR), main UV/Vis absorption bands, *m/z* value of the protonated molecule $[M+H]^{+a}$ and diagnostic fragmentation ions can be found in Table 7.6. A representative chromatogram is given in Figure 7.48 (chromatogram VC243_2.31 m). Native chlorophyll *a* (Chl *a*) is present in the upper two samples (0.13 m and 0.22 m) and three intermediate sample depths (3.41 m, 2.31 m and 1.66 m), but elsewhere is transformed into chlorophyll derivatives, including phaeophytin *a* (Phe *a*), phaeophorbide *a* (Phorb *a*), pyrophaeophytin (PPhe *a*) and pyrophaeophorbide *a* (PPhorb *a*), chlorophyllone (Chlphy), together with purpurin-7 (Pup-7) and purpurin-18 (Pup-18). For ease of comparison between sample depths chlorophyll and chlorophyll derivatives have been grouped to Σ of chlorophyll *a* (Chl *a*, Chl *a*'), Σ of phaeophytins (Phe *a*, Phe *a*', Phe-Chl type), Σ of phaeophorbides (Phorb *a*, Phorb *a*'), Σ of hydroxyl products (HO-Chl, HO-Phe) and Σ of purpurins (Pup-7, Pup-18). Reference to "total chlorophylls" represents a sum of the above compounds. Carotenoids, including fucoxanthin (Fuco), diatoxanthin (Diatox) and monadoxanthin (Monadox) are common at all sample depths and their relative proportions vary stratigraphically. "Total carotenoids" refers to the sum of the above three compounds.

Pigment distribution in core VC243 is described using the diatom PCA based stratigraphic zones described in section 7.5.2. No samples were analysed for pigments below 4 m depth, therefore zone VC243-i is not included in the following description. Overall trends are revealed through analysis of the ratio between total carotenoids and total chlorophylls, together with individual carotenoids and total chlorophyll (Figure 7.49). Between 4 m – 0 m the general trend is an up-core decrease in the ratio between total carotenoids and total chlorophylls, reflecting the higher relative abundance of carotenoids to chlorophyll pigments in zone VC243-ii. Both ratios of Diatox and Monadox to total chlorophyll show the same trend, decreasing up-core from 47:53 to 30:70 for Diatox, and from 23:77 to 8:92 for Mondax. Fucox to total chlorophyll ratio shows limited stratigraphic trend because in a number of the samples Fucox was below detection limits.

Table 7.6

Core VC243: Analytical data for the major pigments identified. Pigments and their transformation products were identified from their HPLC retention time (t_R), on-line UV/Vis spectra and *m/z* value of protonated molecule $[M+H]^{+a}$ through LC-MS. A number of pigments are highlighted on the chromatogram for sample depth 2.31 m (Figure 7.48).

t_R (min)	Main UV/Vis spectra (nm)	$[M+H]^{+a}$	Diagnostic fragment ions	Assignment	Esterifying alcohol	Abbreviation	Figure 7.48 ref
9.5	449	659	641, 623, 581	Fucoxanthin		Fuco	1
10	447,	601		Unknown carotenoid			2
13	451	599		Unknown carotenoid			3
14	455	581		Unknown carotenoid			4
21	409, 665	533	515, 505	Chlorophyllone	N/A	Chlphy	5
22	407, 665	623	605, 545	Hydroxy Phaeophorbide *a*	Methanol	HO Phorb *a*	6
22	425, 452, 480	567	549	Diatoxanthin		Diatox	7
25.5	401, 671	653		Purpurin 7	Methanol	Pup-7	8
27.5	425, 447, 475	567		Monadoxanthin		Monadox	9
28.5	408, 665	607	547, 461	Phaeophorbide *a*	Methanol	Phorb *a*	10
30	409, 666	607	547, 461	Phaeophorbide *a* epimer	Methanol	Phorb *a'*	11
37	409, 669	549	521, 435	Pyrophaeophorbide *a*	Methanol	Pphorb *a*	12
40	449	585	567	Unknown carotenoid			13
43	450	581		Unknown carotenoid			14
45	430, 668			Hydroxy Chlorophyll a??		HO Chl a??	15
47.5	430, 665	887	609	Hydroxy Chlorophyll a??	Phytol	HO Chl a	16
51.5	432, 665	871	593, 533	Chlorophyll *a*	Phytol	Chl *a*	17
54.5	431, 665	871	593, 533	Chlorophyll *a* epimer	Phytol	Chl *a'*	18
58	409, 668	871	593, 533	Unidentified Phaeophytin-Chlorophyll type		Phe-Chl type	19
61.5	409, 667	871	593, 533	Unidentified Phaeophytin-Chlorophyll type		Phe-Chl type	20
66.5	408, 667	887	869, 609	Hydroxy phaeophytin *a*	Phytol	HO-phe *a*	21
67.5	399, 664	903	625,	15 ^{1} hydroxylactonephaeophytin a			22
68.5	339, 663	917	857, 639	Purpurin 7	Phytol	Pup-7	23
71.5	408, 666	871	893, 533	Phaeophytin *a*	Phytol	Phe *a*	24
74	409, 666	871	893, 533	Phaeophytin *a* epimer	Phytol	Phe *a'*	25
78.5	358, 407, 545, 697	843	565, 503	Purpurin 18	Phytol	Pup-18	26
80	410, 666	813	535	Pyrophaeophytin *a*	Phytol	Pphe *a*	27
	410, 667	901	535	Steryl chlorin ester	C_{27} steryl		28
	410, 668	901	535	Steryl chlorin ester	C_{27} steryl		29
90.57	410, 663	915	535	Pyrophaeophorbide *a*	C_{28} steryl	Pphorb *a*	30
	410, 667	915	535	Steryl chlorin ester	C_{28} steryl		31
	410, 667	903	535	Steryl chlorin ester	C_{27} steryl		32
	410, 668	917	535	Steryl chlorin ester	C_{28} steryl		33
		945	535	Steryl chlorin ester	C_{30} steryl		34
		931	535		C_{27} steryl		35

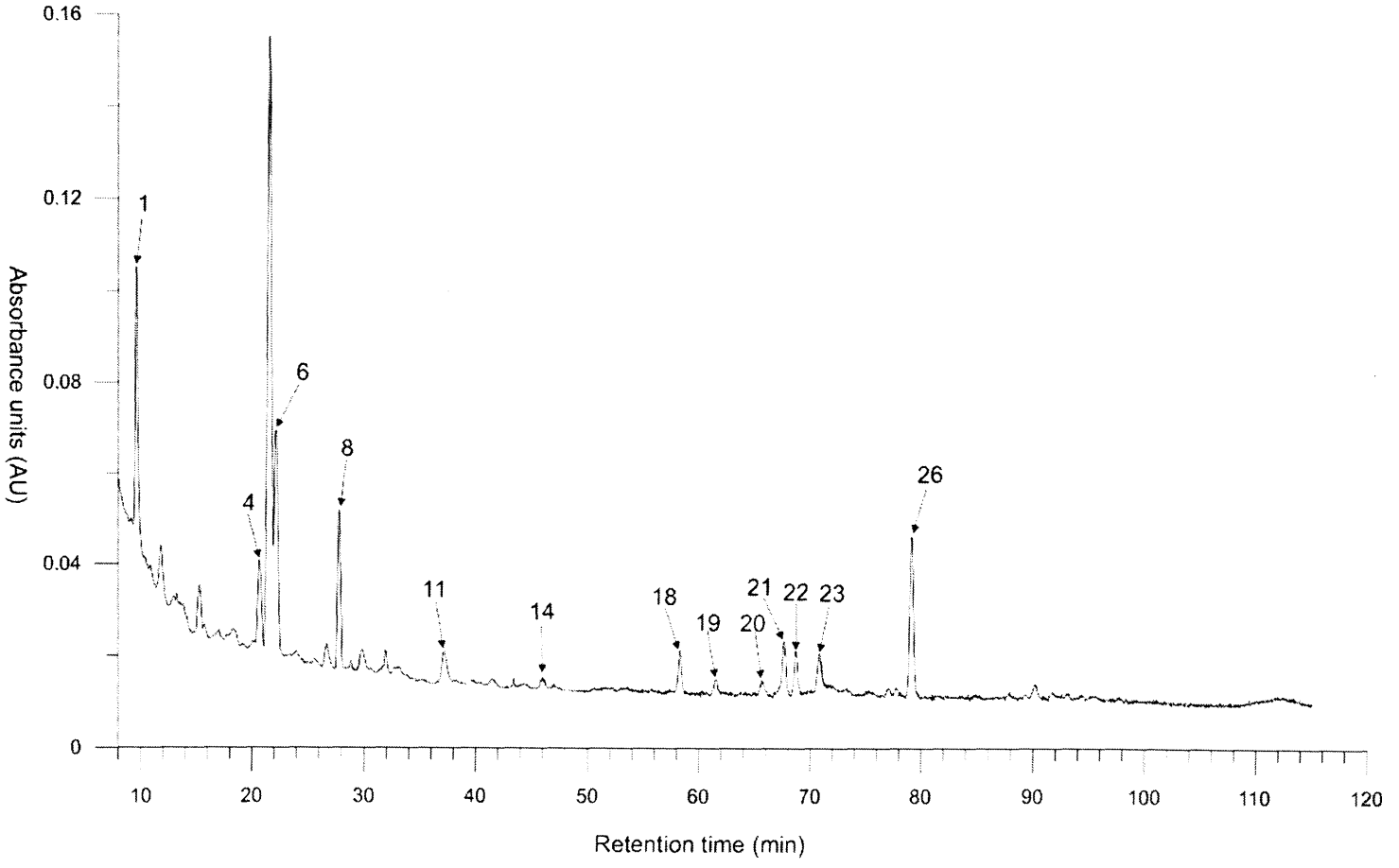


Figure 7.48
Core VC243: HPLC chromatogram for core depth 2.31 m, with the principal pigment peaks highlighted and numbered (pigment identification can be found in Table 7.6).

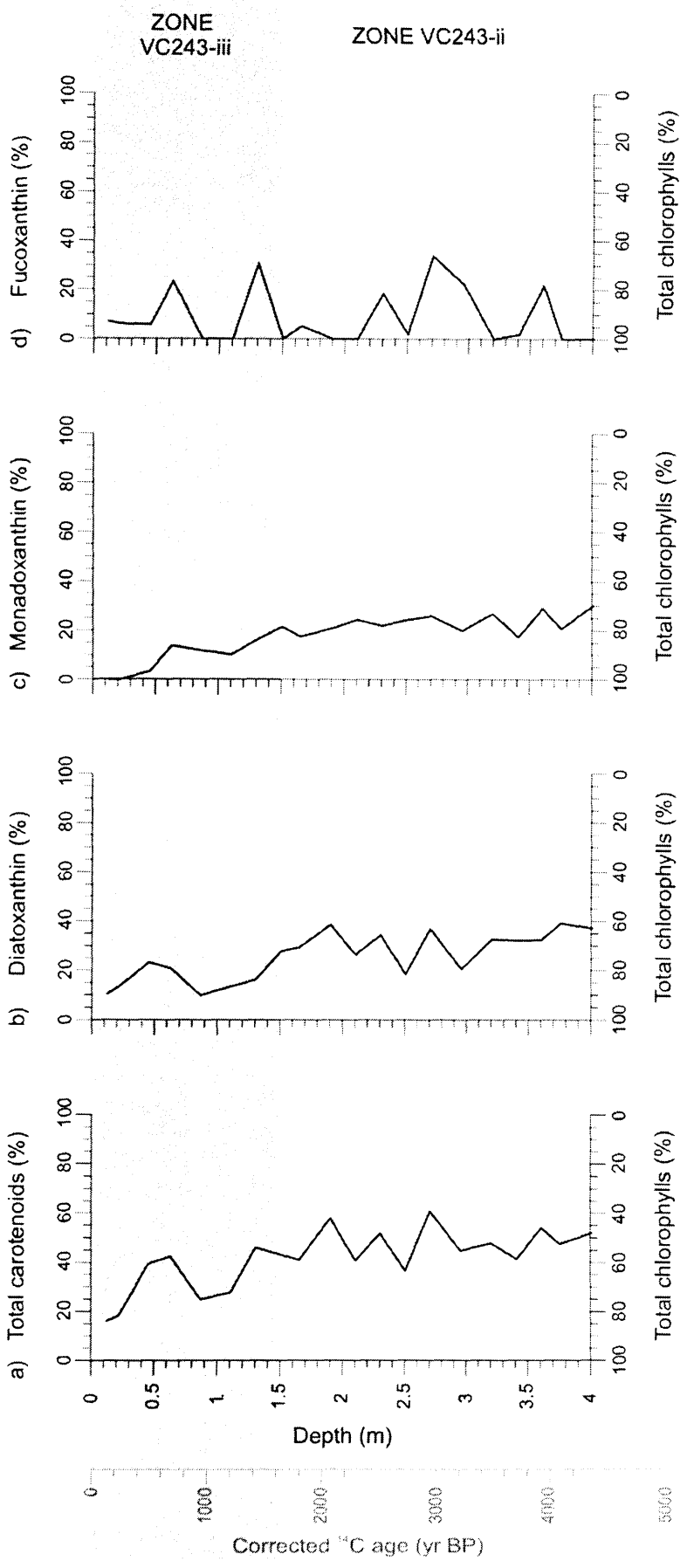


Figure 7.49
Core VC243: Sedimentary pigments ratios between: (a) total carotenoids and total chlorophylls; (b) total chlorophylls and diatoxanthin (Diatox); (c) total chlorophylls and monadoxanthin (Monadox); (d) total chlorophylls and fucoxanthin (Fuco).

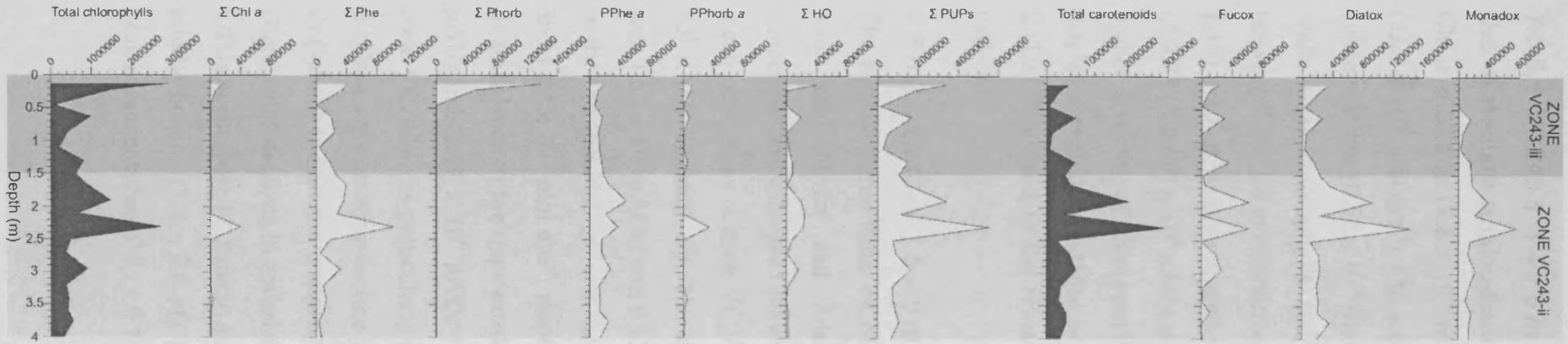


Figure 7.50

Core VC243: Standardised peak areas (μAUs) for total chlorophylls and total carotenoids (on same scale); standardised peak areas for Σ of chlorophyll *a* (Chl *a*, Chl *a*'), Σ of phaeophytins (Phe *a*, Phe *a*', Phe-Chl type), Σ of phaeophorbides (Phorb *a*, Phorb *a*'), pyrophaeophytin (PPhe *a*) and pyrophaeophorbide *a* (PPhorb *a*), Σ of hydroxyl products (HO-Chl, HO-Phe) (all on same scale) and Σ of purpurins (Pup-7, Pup-18) (note different scale); standardised peak area for fucoxanthin (Fucox), diatoxanthin (Diatox) and monadoxanthin (Monadox) (all on same scale).

7.5.5.1 VC243-ii: 4 – 1.5 m

One of the most striking features through this zone is the high concentration of native Chl *a* at 2.31 m (7.8 x 10^{-6} mol dm^{-3}), coincident with higher concentrations of Phe *a* (3.27 x 10^{-6} mol dm^{-3}). Chl *a* is also preserved at 3.41 m and 1.66 m, but in much lower concentrations (0.56 x 10^{-6} mol dm^{-3} and 0.28 x 10^{-6} mol dm^{-3}, respectively). On a broad scale, total chlorophylls and carotenoids are preserved in elevated concentrations between 2.5 – 1.6 m (respective mean peak areas of 1.25 (± 0.9) x 10^6 µAUs and 1.26 (± 1.16) x 10^6 µAUs) compared to the remainder of the core (respective mean peak areas of 0.73 (± 0.69) x 10^6 µAUs and 0.43 (± 0.22) x 10^6 µAUs) (Figure 7.50). There is also higher diversity of chlorophyll derivatives in zone VC243-ii. The Σ of purpurins also display elevated abundance between 2.5 – 1.6 m (mean peak area 2.46 (± 1.99) x 10^6 µAUs) compared to the remainder of the core (mean peak area 1.14 (± 0.81) x 10^6 µAUs).

7.5.5.2 VC243-iii: 1.5 – 0 m

The transition into zone VC243-iii is marked by a decline in the concentration of both total chlorophylls and total carotenoids (Figure 7.50). From the maximum concentrations witnessed between 2.5 and 1.6 m, total chlorophyll and total carotenoid mean peak areas in zone VC243-i fall to 0.95 (± 0.91) x 10^6 µAUs and 0.38 (± 0.27) x 10^6 µAUs, respectively. The spike in total chlorophyll at sample depths 0.22 m (peak area 1.52 x 10^6 µAUs) and 0.13 m (peak area 2.89 x 10^6 µAUs) (which is not witnessed in the carotenoids), reflects the increased concentration of Phorb *a* at these depths (5.15 and 1.38 x 10^{-6} mol dm^{-3}, respectively). Like-wise the Σ of purpurins shows an increase in abundance in the uppermost sample depths (0.22 m – 0.13 m) (peak area 1.85 x 10^6 µAUs and 3.45 x 10^6 µAUs respectively). The decline in carotenoid abundance into zone VC243-iii is particularly prominent in Monadox and Diatox abundance. Monadox displays a progressive decline up-core from peak area of 1.7 at the base of zone VC243-iii (1.5 m) to become completely absent in the uppermost 0.5 m of the core. Similarly, Diatox also declines in abundance through zone VC343-iii, from peak area of 0.24 x 10^6 µAUs at the base (1.5 m) to mean peak areas of 0.12 (± 0.11) x 10^6 µAUs through the middle portion (1.3 – 0.6 m), then displaying a recovery up-core of 0.5 m, with mean peak area measuring 0.2 (± 0.16) x 10^6 µAUs.

7.6 VC237

7.6.1 Diatom assemblage

Total diatom abundance in core VC237 is relatively constant along the core length, although there is a broad stratigraphic trend towards higher abundance up-core (Figure 7.51a). Similar to core VC243, generally the sedimentary assemblage is reasonably fragmented in core VC237 (Figure 7.52). Again, CRS compose the largest proportion of the total diatom assemblage, ranging between 77.61 – 95.59 % (Figure 7.51b). Throughout the core, undoubtedly the most abundant non-CRS species is *T. antarctica* warm rs, with mean absolute and relative abundances of 6.88 (± 2.54) Mv/g and 56.31 (± 11.06) % respectively (Figure 7.53). The remainder of the non-CRS assemblage includes moderate contributions from *F. vanheurckii* (mean absolute abundance, 0.82 (± 0.3) Mv/g; mean relative abundance, 6.85 (± 2.22) %), *F. curta* (mean absolute abundance, 0.78 (± 0.38) Mv/g; mean relative abundance, 6.6 (± 3.18) %), *F. cylindrus* (mean absolute abundance, 0.39 (± 0.18) Mv/g; mean relative abundance, 3.37 (± 1.63) %) and *O. weissflogii* (mean absolute abundance, 0.31 (± 0.21) Mv/g; mean relative abundance, 2.58 (± 1.68) %), together with minor contributions from *F. obliquecostata*, *P. glacialis*, *T. antarctica* cold rs, *T. gracilis expecta* and benthic diatoms, including *Navicula*, *Cocconeis* and grouped *Pinnularia-Trachyneis* species.

R-mode PCA analysis highlights several diatom species associations in core VC237; species with high positive and negative loadings on axes 1 – 3 are highlighted in bold and the variance explained by each PCA axis is also presented (Figure 7.54, Figure 7.55 and Table A2.15). R-mode cluster analysis of diatom relative abundance results in division of the assemblage into several groups, at 12 % similarity (Figure 7.56), labelled 1 – 5. Comparison of the species associations revealed by PCA and cluster analysis are presented in Table 7.7, with indicator species highlighted.

7.6.2 Diatom stratigraphic zones

Q-mode PCA analysis reveals interesting stratigraphic associations between sample depths, which are particularly evident on axes 1 and 2 (Figure 7.57 and Table A2.16). On axis 1, there are negative component scores between 6 – 5.2 m (relating to high abundance of *T. antarctica* rs), overlain by more variable scores between 5.2 – 3.7 m, and positive component scores between 3.7 – 2.1 m (relating to increased relative abundance of *F. curta*, *F. cylindrus*, *F. obliquecostata*, *T. gracilis* group, *Proboscia* group, *Pinnularia-Trachyneis* group, *Navicula* and *Nitzschia* species). On axis 2, negative component scores between 5.3 – 3.8 m reflects higher abundance of *F.*

cylindrus, *F. vanheurckii* and *T. antarctica* vegetative, whereas positive loading between 3.3 – 2.1 m records the increased contribution from *E. antarctica* rs, *P. glacialis*, *T. tumida*, *A. actinochilus* and *Achnanthes* group.

Q-mode cluster analysis on sample depths reveals a rather complex grouping system in core VC237 (Figure 7.58a). Four cluster groups can be identified, at 71 % similarity, (VC237-A, VC237-B, VC237-C and VC237-D), plus a couple of outlier sample depths (4.9 m and 4.8 m). When individual sample depths are plotted on a sedimentary log for core VC237 (Figure 7.58b), a couple of observations become apparent: cluster VC237-A is confined to sample depths between 5.9 and 5.6 m; cluster VC237-D is clearly the most dominant, with the majority of sample depths between 5.5 and 2.1 m falling into this group.

Using the method of core zonation described in Chapter 5.1.7, axes 1 and 2 (explaining 34.93 % of the total variance, Table A2.16) were used to divide core VC237 into three stratigraphic zones (VC237-i (6 – 5.2 m), VC237-ii (5.2 – 3.7 m) and VC237-iii (3.7 – 2.1 m)) (Figure 7.57). Each zone displays distinct differences in the diatom community structure, which are described below and highlighted on total diatom abundance plots (Figure 7.51), Fragmentation Index plot (Figure 7.52) and individual species absolute and relative abundance plots (Figure 7.53).

7.6.2.1 VC237-i: 6 – 5.2 m

Diatom absolute abundance in core VC237 shows a general trend of increasing values up-core, from 60 Mv/g at the 6 m to 210 Mv/g at 2.1 m (Figure 7.51). The majority of the up-core increase in absolute abundance occurs predominantly in zone VC237-i (between 6 m – 4.2 m), with abundance increasing progressively through these core depths. CRS relative abundance shows a similar trend, recording lowest values in zone VC237-i (87.27 (± 4.42) %). Unlike total diatom abundance and CRS absolute abundance, non-CRS absolute abundance does not show a trend of increasing abundance up-core; values at the base of the core (6 m) are similar to those at the core top (2.1 m). In zone VC237-i, non-CRS absolute abundance averages 12.33 (± 4.15) Mv/g, with slightly higher values in a broad peak centred at ~5.7 m (21.3 Mv/g).

The non-CRS species assemblage in zone VC237-i is overwhelmingly dominated by *T. antarctica* warm rs, with absolute and relative abundance averaging 8.8 (± 3.46) Mv/g and 70.27 (± 4.78) %, respectively. From these maximum abundances in zone VC237-i, there is a general trend of decreasing *T. antarctica* warm rs abundance up-core. *P.*

glacialis also displays slightly elevated abundances in zone VC237-i, with mean absolute abundance of 0.33 (± 0.15) Mv/g and mean relative abundance of 2.66 (± 0.42) %, compared to 0.19 (± 0.09) Mv/g and 1.6 (± 0.68) % for the zone VC237-ii. Further, *A. actinochilus* displays elevated abundances in the lower section of zone VC237-i (6 – 5.6 m), with absolute and relative abundance averaging 0.23 (± 0.11) Mv/g and 1.71 (± 0.38) %, respectively.

F. vanheurckii, *F. curta* and *F. cylindrus* all display comparatively low abundance in zone VC237-i, with respective mean absolute abundance of 0.59 (± 0.16) Mv/g, 0.37 (± 0.13) Mv/g, and 0.22 (± 0.09) Mv/g respectively, with mean relative abundances of 5.06 (± 1.3) %, 3.11 (± 1.15) % and 1.94 (± 1.06) %.

7.6.2.2 VC237-ii: 5.2 – 3.7 m

Zone VC237-ii is characterised by increasing diatom abundance up-core, reaching high abundance in a broad peak centred at 4 m (~248 Mv/g), which is coincident with a peak in non-CRS absolute abundance (~15 Mv/g). Throughout this zone, CRS relative abundance is high, yet somewhat variable (92.38 (± 2.29) %).

The non-CRS assemblage changes in zone VC237-ii, to include an increased contribution from *F. vanheurckii*, *F. curta* and *F. cylindrus*. This shift in the diatom community structure was first initiated at the transition into zone VC237-ii (5.2 m). Through this zone *F. vanheurckii*, *F. curta* and *F. cylindrus* respective mean absolute abundances are 0.91 (± 0.29) Mv/g, 0.76 (± 0.29) Mv/g, and 0.49 (± 0.18) Mv/g and mean relative abundances are 7.78 (± 2.6) %, 6.36 (± 1.91) % and 4.1 (± 1.32) %. In addition, *O. weissflogii* display an increase in zone VC237-ii; between 4.3 – 2.1 m mean absolute and relative abundance are 0.43 (± 0.19) Mv/g and 3.51 (± 1.55) %.

T. antarctica warm rs temporarily reverse their up-core trend of decreasing abundance between 4.2 – 3.9 m, where there is a short interval of slightly elevated abundances (mean absolute abundances of 9.43 (± 1.65) Mv/g; mean relative abundances of 59.34 (± 7.07) %). This interval is coincident with a spike in *T. antarctica* vegetative valves, occurring between 4 – 3.8 m and recording absolute and relative abundances of 0.26 (± 0.19) Mv/g and 1.74 (± 0.86) %.

7.6.2.3 VC237-iii: 3.7 – 2.1 m

In zone VC237-iii, total diatom abundance displays fluctuating high-range values (194 (± 39.2) Mv/g). Non-CRS absolute abundance is equally as variable, but displays mid-

range values (12.11 (± 2.83) Mv/g). There is a noticeable decrease in absolute abundance between 3.8 – 3.5 m (averaging 144 (± 11) Mv/g).

With respect to the non-CRS species assemblage, generally trends initiated in zone VC237-ii continue into zone VC237-iii. *F. curta* and *F. cylindrus* maintain their high abundances across the transition, with respective mean absolute abundances of 1.04 (± 0.34) Mv/g and 0.4 (± 0.16) Mv/g respectively, with mean relative abundances of 8.8 (± 3.1) % and 3.5 (± 1.7) %. Abundances of *F. vanheurckii* decline slightly into zone VC237-iii, with absolute and relative abundances averaging 0.86 (± 0.33) Mv/g and 6.98 (± 1.67) %. In addition, *T. antarctica* warm rs conform to the up-core trend of decreasing abundance in zone VC237-iii; between 3.7 – 2.1 m mean absolute abundance is 5.67 (± 1.63) Mv/g and mean relative abundance is 47.25 (± 7.41) %.

Throughout core VC237, *T. gracilis* var. *expecta* displays higher abundances than *T. gracilis* var. *gracilis*, however it is worth noting that both varieties of *T. gracilis* increase significantly in abundance in the upper part of zone VC237-iii (2.7 – 2.1 m), with grouped mean absolute and relative abundance totalling 0.45 (± 0.34) Mv/g and 3.1 (± 2.16) % respectively. *E. antarctica* rs also typically have low abundances through core VC237; average absolute and relative abundance are 0.09 (± 0.07) Mv/g and 0.74 (± 0.47) % respectively. However, between 2.5 – 2.1 m *E. antarctica* rs mean absolute and relative abundance increase to 0.22 (± 0.06) Mv/g and 1.5 (± 0.53) %. Finally, benthic diatom species (*Achnanthes*, *Amphora*, *Cocconeis*, *Navicula* and grouped *Pinnularia-Trachyneis* species) all show a trend of gradually increasing abundance up-core, with peak abundances typically found between 3 – 2.5 m.

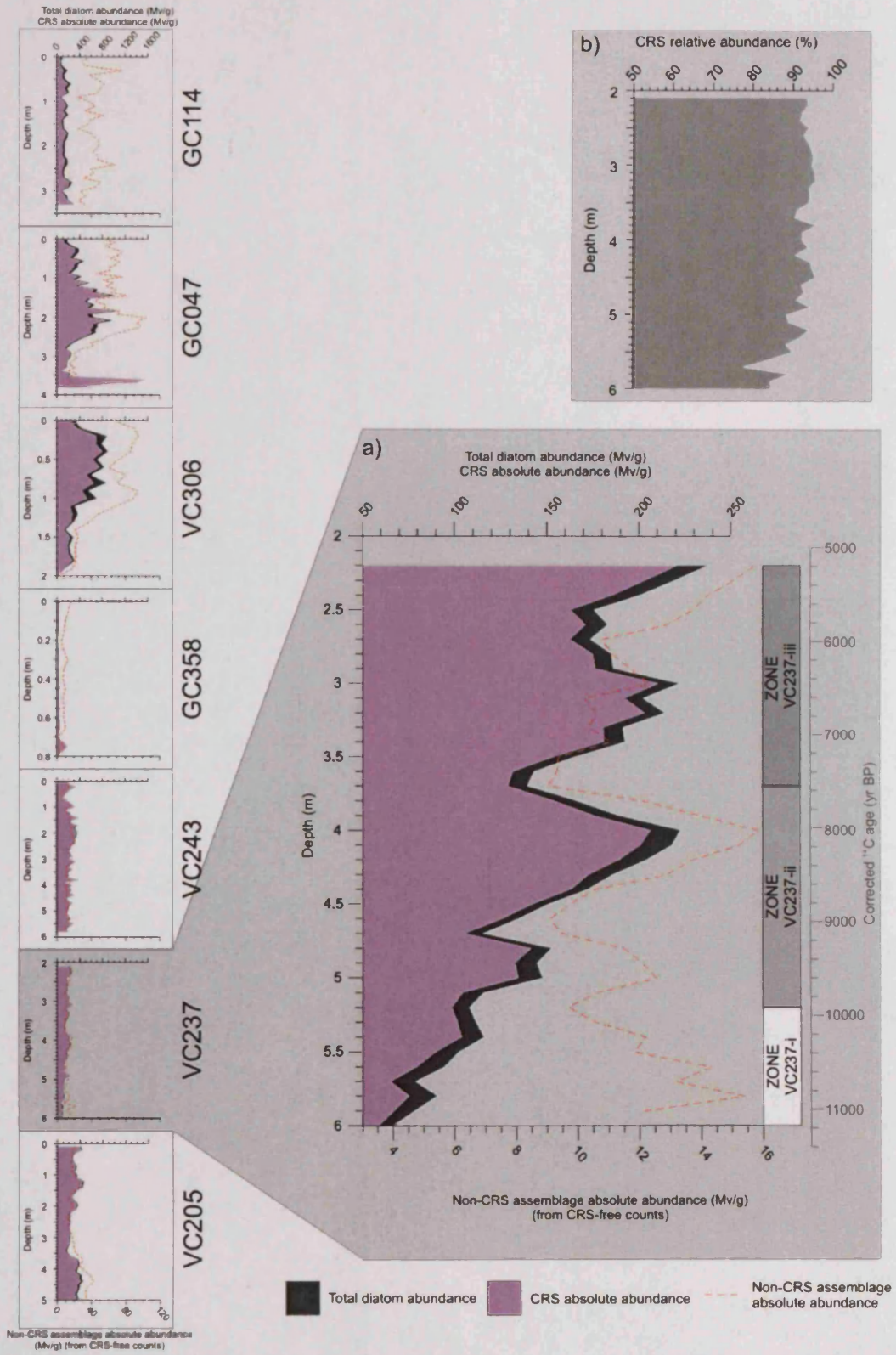


Figure 7.51

a) Core VC237: Total diatom abundance, CRS absolute abundance (both from CRS-included counts) and non-CRS assemblage absolute abundance (from CRS-free counts) (millions of valves/g (Mv/g)), smoothed using a three point moving average. Stratigraphic zones VC237-i, VC237-ii and VC237-iii identified using Q-mode PCA analysis of diatom relative abundance data.

b) Core VC237: CRS relative abundance (%).

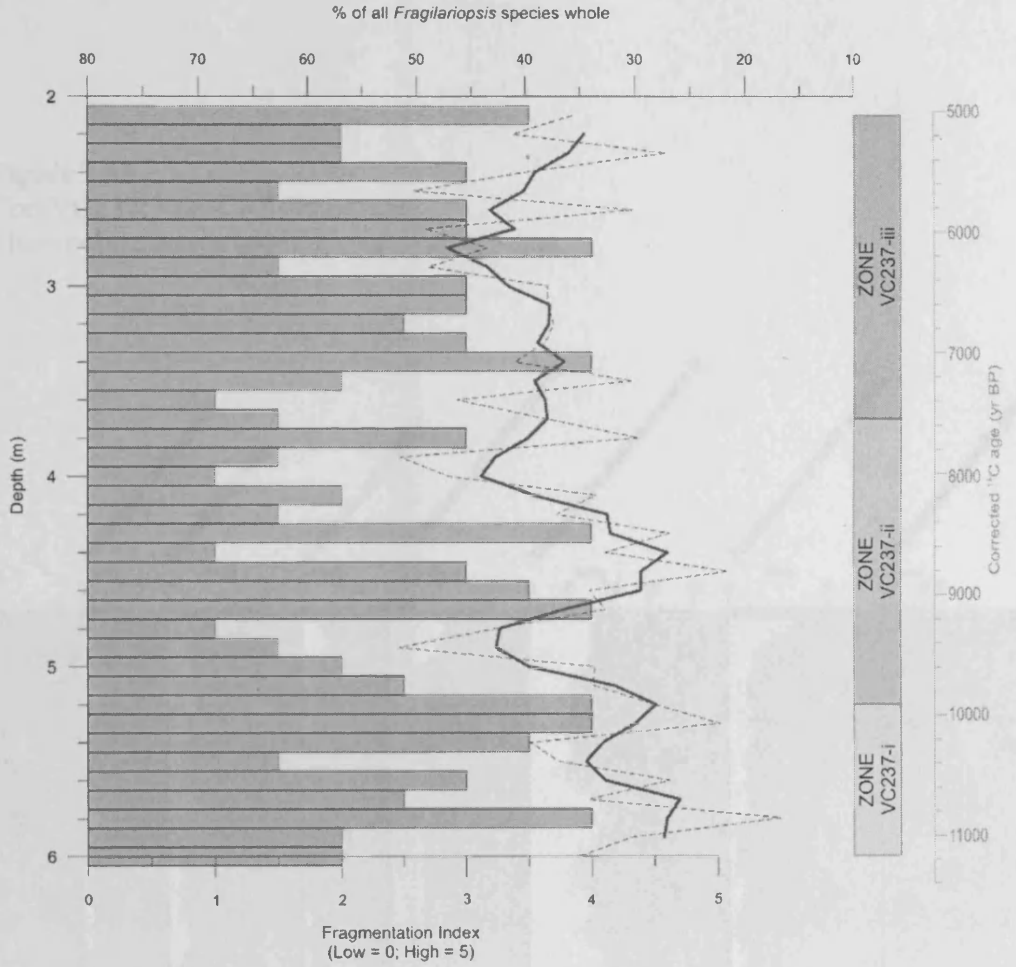


Figure 7.52
Core VC237: Diatom fragmentation, using two measures: observational index (bars: low = 0 to high = 5); and percentage of *Fragilariopsis* species whole (dashed line = original; solid line = three point moving average). Stratigraphic zones VC237-i, VC237-ii and VC237-iii identified using Q-mode PCA analysis of diatom relative abundance data.

Figure 7.53
CoreVC237:Non-CRS diatom assemblage plots forAP indicator species: (a)Absolute abundance (Mv/g); (b) Relative abundance (%).
Three point average (white); original abundance (dark grey line). Stratigraphic zonesVC237-i toVC237-iii identified usingQ-mode PCA analysis of diatom relative abundance data.

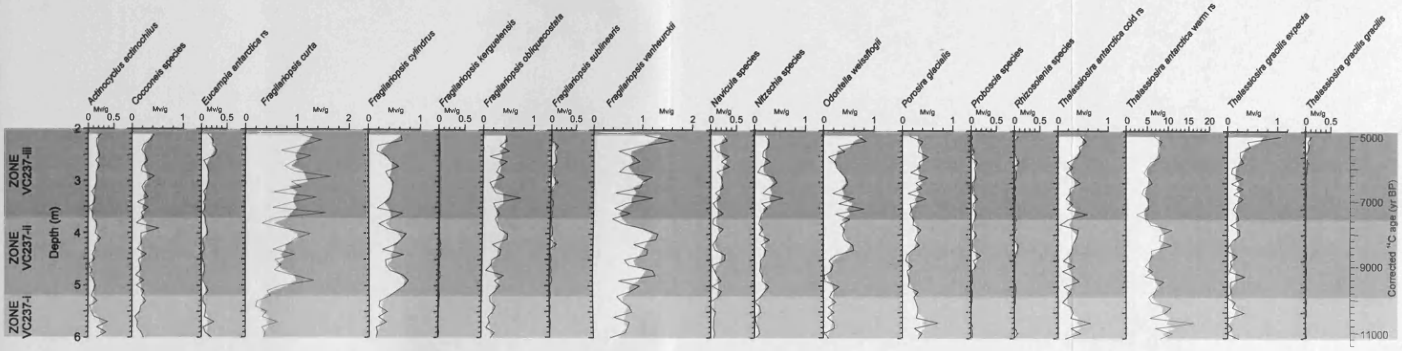


Figure 7.53 (a)

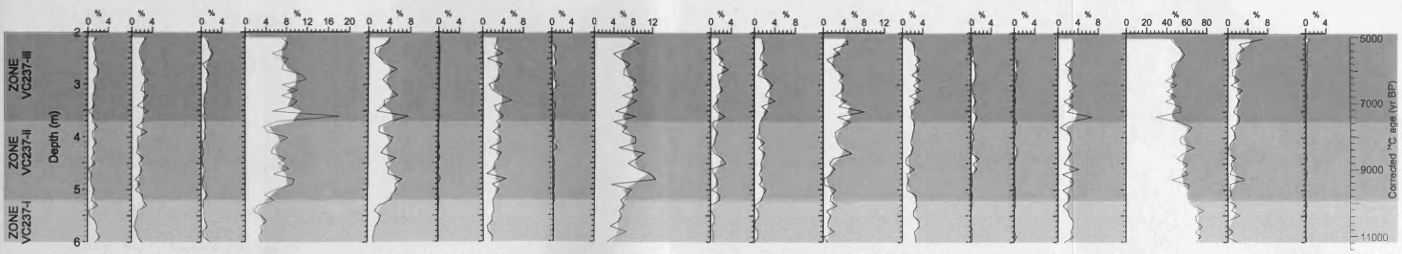


Figure 7.53 (b)

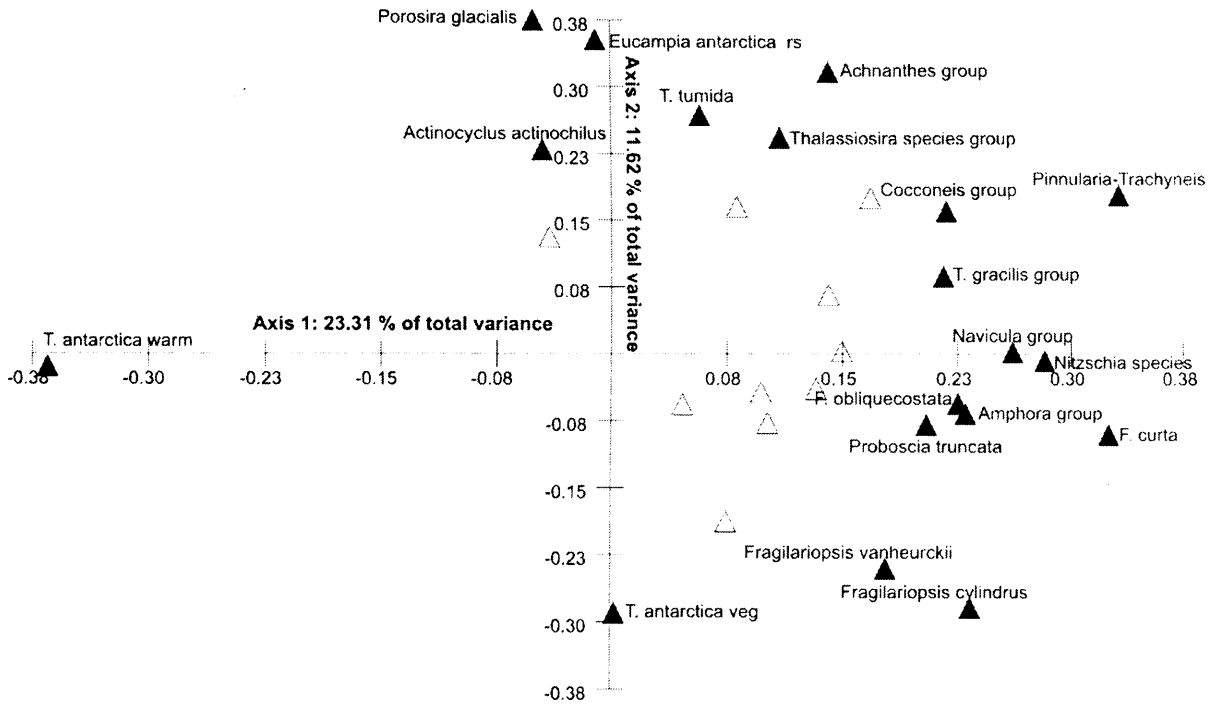


Figure 7.54
Core VC237: R-mode PCA variable loading on axes 1 and 2 for diatom relative abundance data (> 1 %). Data square-root transformed and standardised. Tolerance of eigenanalysis set at 1 x 10^{-10}. Highlighted species are those that have component loading ≥ + 0.20 or ≤ – 0.20.

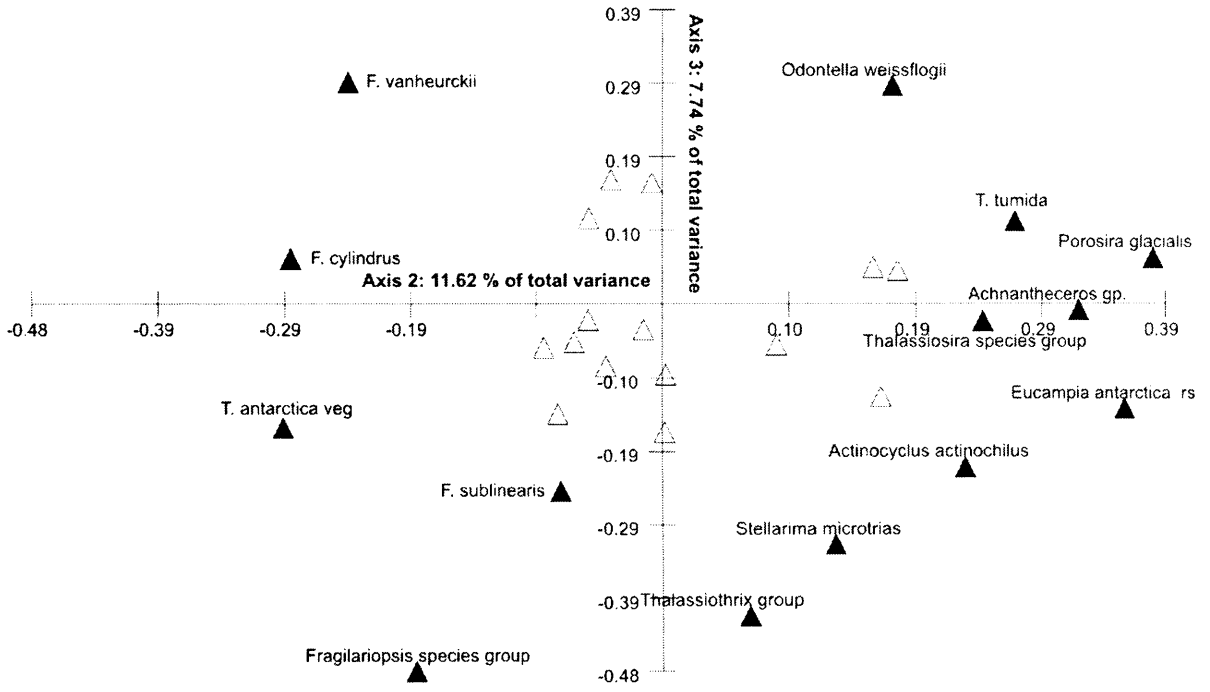


Figure 7.55
Core VC237: R-mode PCA variable loading on axes 2 and 3 for diatom relative abundance data (> 1 %). Data square-root transformed and standardised. Tolerance of eigenanalysis set at 1 x 10^{-10}. Highlighted species are those that have component loading ≥ + 0.20 or ≤ – 0.20.

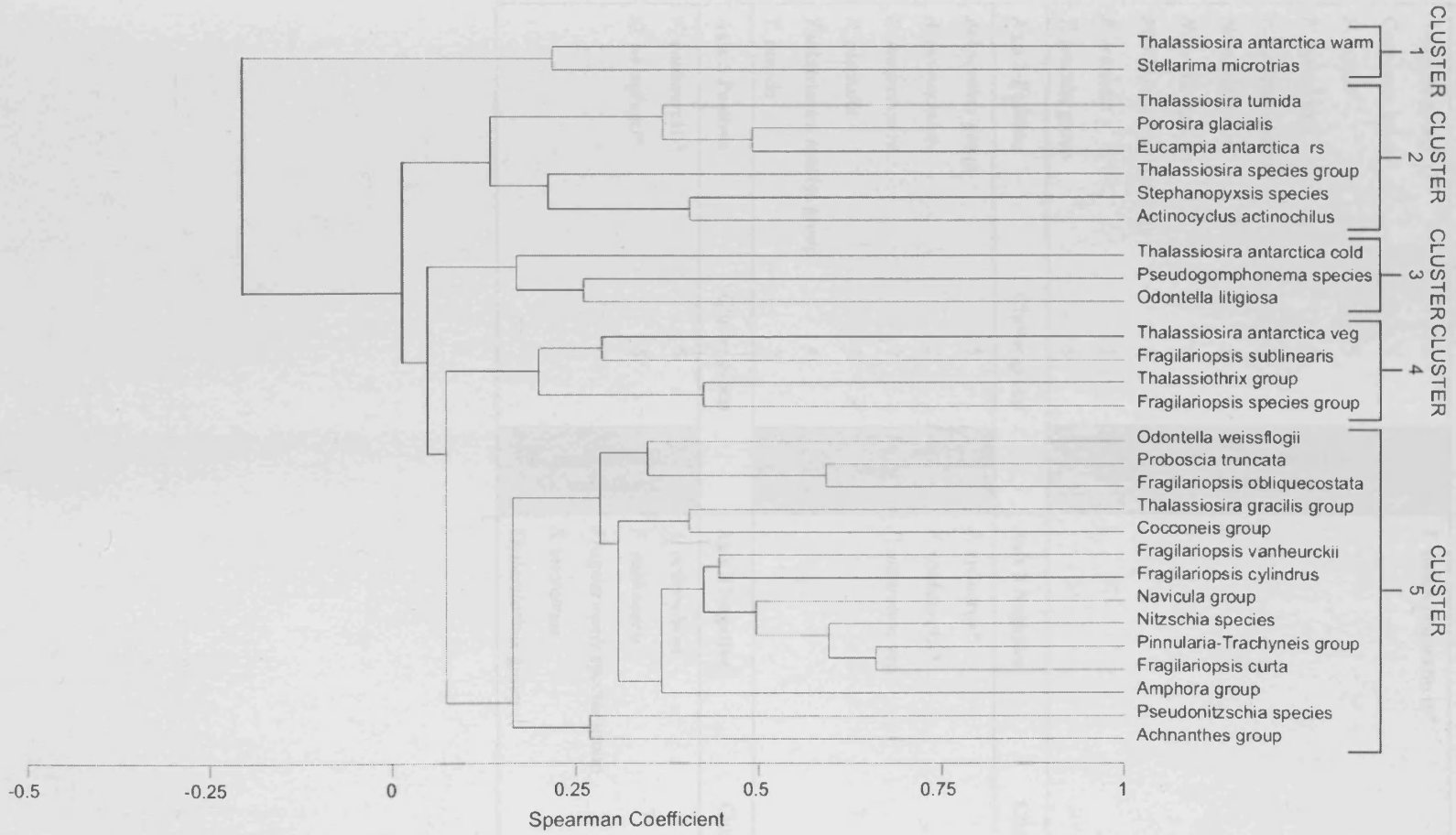


Figure 7.56
Core VC237: R-mode cluster analysis of diatom species relative abundance (>1 %). UPGMA clustering method; data square-root transformed; and Spearman Coefficient similarity measure.

Table 7.7
Core VC237: Comparison of diatom PCA axis loading and cluster groupings. Indicator species denoted with *. Grouped indicator species shown in grey box and relate to diatom assemblages highlighted on Figure 7.59.

Axis 1 Positive	Cluster group		**Axis 1 Negative**	Cluster group	
Amphora group	5	**F. curta – F. cylindrus – F. obliquecostata**	*T. antarctica* warm rs*	1	**T. antarctica warm rs**
Cocconeis group	5				
*F. curta**	5				
*F. cylindrus**	5				
*F. obliquecostata**	5				
Navicula group	5				
Nitzschia species	5				
Pinnularia-Trachyneis gp	5				
P. truncata	5				
T. gracilis group	5				
Axis 2 Positive	Cluster group		**Axis 2 Negative**	Cluster group	
Achnanthes group	5	**None**	*F. cylindrus**	5	**F. cylindrus – F. vamheurckii**
A. actinochilus	2		*F. vanheurckii**	5	
E. antarctica rs	2		*T. antarctica* veg	4	
P. glacialis	2				
Thalassiosira species group	4				
T. tumida	2				
Axis 3 Positive	Cluster group		**Axis 3 Negative**	Cluster group	
*F. vanheurckii**	5	**F. vanheurckii; O. weissflogii**	*A. actinochilus*	2	**None**
*O. weissflogii**	5		*F. sublinearis*	4	
			Fragilariopsis species group	4	
			S. microtrias	1	
			Thalassiothrix group	4	

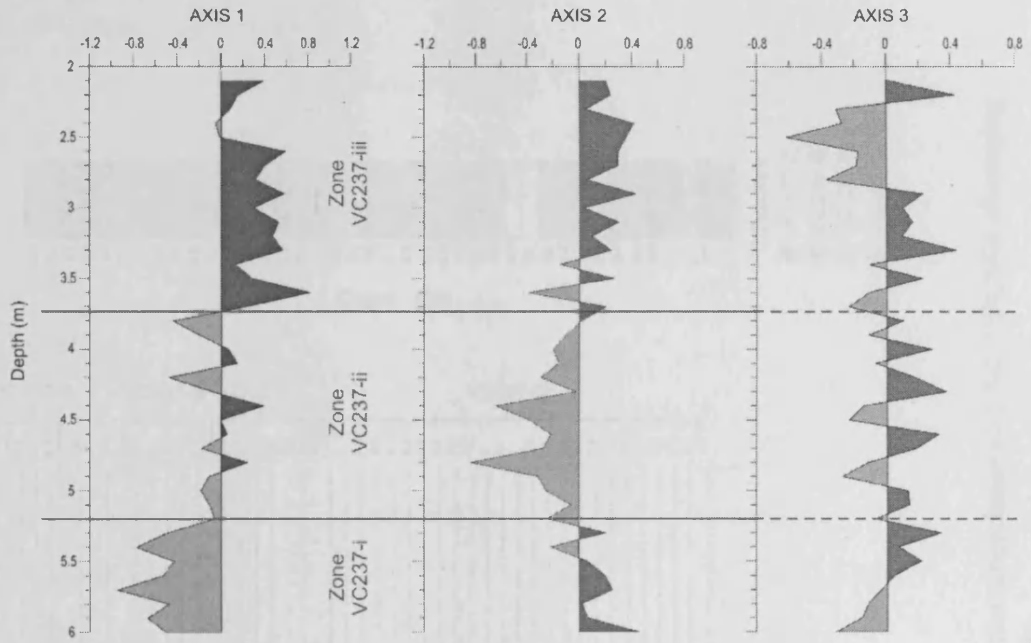


Figure 7.57
Core VC237 Q-mode PCA component scores plotted stratigraphically for PCA axes 1 – 3. Positive loading (dark grey); negative loading (light grey). Division of the record into stratigraphic zones VC237-i, VC237-ii and VC237-iii is based on component loading on axis 1.

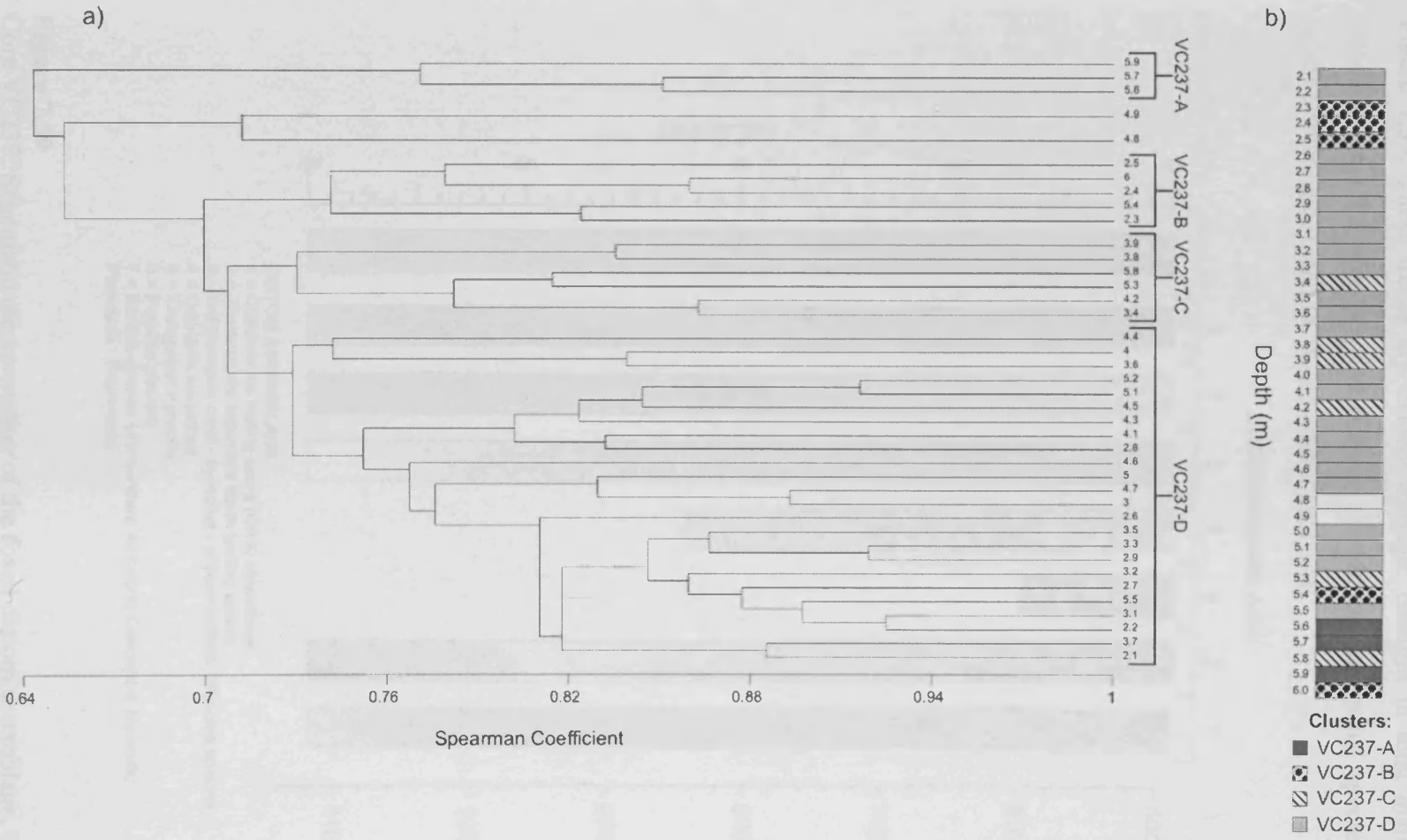


Figure 7.58

a) Core VC237: Q-mode cluster analysis of core depths, using diatom species relative abundance (>1 %). UPGMA clustering method; data square-root transformed; and Spearman Coefficient similarity measure.

b) Core VC237: Stratigraphic pattern of Q-mode cluster groups.

7.6.3 Diatom summary

Stratigraphic changes in the fossil diatom assemblage in core VC237 are summarised in Figure 7.59. These trends are evident through: changes in total diatom abundance; variations in CRS absolute and relative abundance; individual species absolute and relative abundances; and PCA and cluster analyses.

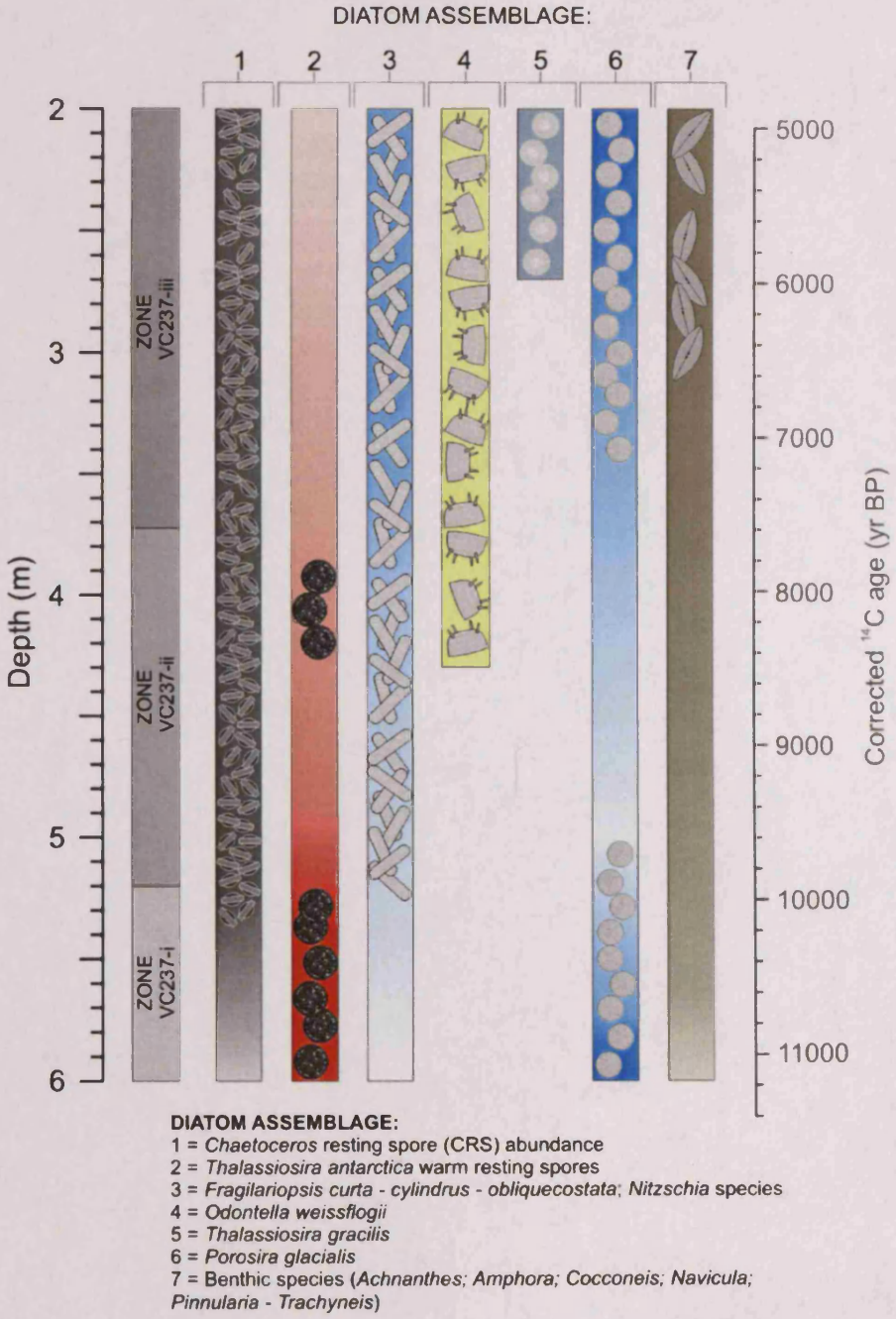


Figure 7.59
Core VC237: Schematic representation of the fossil diatom assemblage, highlighting the relative contribution of CRS to the total assemblage and stratigraphic changes in the diatom community. Stratigraphic zones VC237-i, VC237-ii and VC237-iii identified using Q-mode PCA analysis of diatom relative abundance data. Darker tones indicate elevated abundances.

7.7 VC205

7.7.1 Diatom assemblage

In core VC205, total diatom abundance displays moderate stratigraphic variability (Figure 7.60a), suggesting fluctuating biogenic inputs to the sediment. Similar to the other two EAP cores, the sedimentary assemblage in core VC205 is reasonably fragmented (Figure 7.61). CRS constitute a significant and reasonably constant proportion of the total diatom assemblage (range 85.8 – 95.86 %; average 92.06 (± 2.64) %) (Figure 7.60b). By far the most abundant non-CRS species throughout the core is *T. antarctica* warm rs, with mean absolute and relative abundances ranging between 5.31 – 27.6 Mv/g and 36.83 – 74.97 %, respectively (Figure 7.62). The remainder of the non-CRS assemblage includes moderate contributions from *F. curta* (mean absolute abundance, 1.66 (± 0.91) Mv/g; mean relative abundance, 7.57 (± 3.22) %), *F. vanheurckii* (mean absolute abundance, 1.39 (± 0.84) Mv/g; mean relative abundance, 5.95 (± 1.88) %) and *F. cylindrus* (mean absolute abundance, 0.97 (± 0.78) Mv/g; mean relative abundance, 3.9 (± 1.89) %), together with minor contributions from *P. glacialis*, *O. weissflogii*, *T. antarctica* cold rs, *F. obliquecostata*, *F. sublinearis* and benthic diatoms, including grouped *Cocconeis* and *Navicula* species.

R-mode PCA analysis highlights a series of diatom species associations in core VC205; species with high positive and negative loadings on axes 1 – 3 are highlighted in bold and the variance explained by each PCA axis is also presented (Figure 7.63, Figure 7.64 and Table A2.17). R-mode cluster analysis of diatom relative abundance results in division of the assemblage into several groups, at 8 % similarity, (Figure 7.65), labelled 1 – 5. Comparison of the species associations revealed by PCA and cluster analysis are presented in Table 7.8, with indicator species highlighted.

7.7.2 Diatom stratigraphic zones

Q-mode PCA analysis reveals several stratigraphic groupings (Figure 7.66 and Table A2.18). Clear divisions of positive and negative component loading exist on axis 1; typically between 5.1 – 3.5 m loading is negative, whereas between 3.2 – 0.2 loading is positive. This transition at ~3.5 m reflects a change in the diatom assemblage, from *E. antarctica*, *Corethron pennatum*, *T. antarctica* vegetative, *F. cylindrus*, *F. kerguelensis* and *F. ritscheri* assemblage below, to increased contribution from *S. microtrias*, *Nitzschia* species, *Melosira* species grouped *Cocconeis* and *Achnanthes* species above. Axis 2 provides further information about the transition at 3.5 m; loading between 3.5 – 2.2 m is positive (reflecting higher abundance of *T. antarctica warm* rs), whereas

between 2.2 – 0 m loading is negative (reflecting higher abundance of *F. curta*, *F. cylindrus*, *F. rhombica*, *F. sublinearis*, *T. gracilis* group and *Navicula* species). Axis 3 shows much more stratigraphic variability in component scores, which consequently makes extracting meaningful associations between core depths difficult.

Q-mode cluster analysis reveals relatively complex associations between core depths (Figure 7.68a). However, on a broad scale, core VC205 can be divided into two cluster groups, at 60 % similarity (VC205-A and VC205-B), plus an outlier sample depths (4.9 m). When individual sample depths are plotted on a sedimentary log for core VC205 (Figure 7.68b), a clear division along the core length exists, with typically samples below 3.5 m forming cluster group VC205-A and those above 3.5 m forming part of cluster group VC205-B.

Using the method of core zonation described in Chapter 5.1.7, core VC205 is divided into three stratigraphic zones (VC205-i (5.1 – 3.5 m), VC205-ii (3.5 – 2.2 m) and VC205-iii (2.2 – 0 m)) based on PCA loading on the primary and secondary axes (Figure 7.66 and Table A2.18). Each zone displays distinct differences in the diatom community structure, which are described below and highlighted on total diatom abundance plots (Figure 7.60), Fragmentation Index plot (Figure 7.61), individual species absolute and relative abundance plots (Figure 7.62).

7.7.2.1 VC205-i: 5.1 – 3.5 m

Total diatom abundance in zone VC205-i is high and relatively stable (averaging 389 (± 78) Mv/g). At 3.7 m, just prior to the transition into zone VC205-ii, total abundance decreases rapidly. Non-CRS absolute abundance displays a similar trend, with comparatively high values in zone VC205-i (averaging 33.29 (± 7.14) Mv/g). CRS relative abundance is slightly lower and more variable than during other core zones, averaging 90.21 (± 2.62) %.

Several diatom species record elevated abundance in zone VC205-i. Firstly, *T. antarctica* warm rs display a trend of decreasing absolute abundance up-core, with very high values (21.61 (± 3.86) Mv/g) in zone VC205-i. Relative abundance of this species shows a slightly different trend, with highest values at a slightly shallower depth than peak absolute abundance; between 3.5 and 2.8 m (68.68 (± 3.82) %). Similar to *T. antarctica* warm rs absolute abundance, *T. antarctica* cold rs display elevated abundances in zone VC205-i, which is also coincident with peak *T. antarctica* vegetative abundances. Between 5.1 – 3.7 m, mean absolute and relative abundance of

T. antarctica cold rs are 0.91 (± 0.77) Mv/g and 2.62 (± 2.24) %. Secondly, *E. antarctica* rs record maximum abundances in zone VC205-i, with absolute and relative abundances of 1.46 Mv/g and 3.66 % respectively, and display a step-wise decrease towards the transition with zone VC205-ii, where this species becomes very rare. In addition, the majority of *Fragilariopsis* species display a similar up-core trend, with elevated abundance in zone VC205-i most pronounced in *F. cylindrus*, *F. obliquecostata*, *F. sublinearis* and *F. vanheurckii*, with abundances through this zone nearly double that of the remainder of the core.

In core VC205, *T. gracilis* var. *expecta* shows consistently higher abundances than *T. gracilis* var. *gracilis*, however both show broadly similar stratigraphic trends. Grouped abundance is elevated between 5 – 4.6 m, with mean absolute and relative abundance of 0.49 (± 0.12) Mv/g and 1.48 (± 0.41) %, respectively. Finally, *O. weissflogii* displays moderate abundance between 5.1 – 3.6 m (mean absolute abundance, 0.43 (± 0.15) Mv/g; mean relative abundance, 1.32 (± 0.48) %).

7.7.2.2 VC205-ii: 3.5 – 2.2 m

Total diatom abundance and non-CRS absolute abundance in zone VC205-ii are both low, averaging 219 (± 33) Mv/g and 16.13 (± 3.68) Mv/g, and display abrupt transitions with the lower (VC205-i) and upper zones (VC205-iii). With the exception of *T. antarctica* warm rs, all indicator species show low abundance through zone VC205-ii. This is reflected in the relative abundance of *T. antarctica* warm rs, which increase to 64.24 (± 6.16) % through this zone.

7.7.2.3 VC205-iii: 2.2 – 0 m

Total diatom abundance through zone VC205-iii is more variable, recording fluctuating values between 198 – 659 Mv/g. Similarly, non-CRS absolute abundance mirrors diatom absolute abundance, showing a step-wise increase to higher abundances, peaking at 1.3 m (28 Mv/g), then stabilising at mid-range values between 1 – 0 m (17.7 (± 2.6) Mv/g). CRS relative abundance is extremely high and relatively stable through zone VC205-iii, with mean abundance of 93.56 (± 1.46) %.

Compared to the high abundance of *Fragilariopsis* species in zone VC205-i, there is a subsidiary peak in zone VC205-i, centred at approximately 1.1 m. Elevated abundance at this depth is most obvious in *F. curta*, *F. cylindrus* and *F. sublinearis*. Using *F. curta* and *F. cylindrus* as an example, grouped absolute and relative abundance of these species between 1.6 – 0.9 m is 3.47 (± 1.17) Mv/g and 16.52 (± 3.93) %, respectively.

Likewise there are subsidiary peaks for *T. antarctica* cold rs, which records elevated abundances at 1.4 m, (0.6 Mv/g; 2.33 %) and grouped *T. gracilis*, with a distinctive spike at 1.5 m (0.84 Mv/g; 3.93 %). In addition, *O. weissflogii* record elevated abundances in zone VC205-iii, in a roughly symmetrical, broad peak, with maximum values at 1.1 m (1.26 Mv/g; 4.96 %). Finally, benthic species, specifically grouped *Achnanthes*, *Cocconeis* and *Pinnularia-Trachyneis* species, show a trend of increasing abundance up-core. Grouped *Cocconeis* species form a significant proportion of the non-CRS assemblage, with absolute and relative abundance typically >0.8 Mv/g and >4 % in zone VC205-iii.

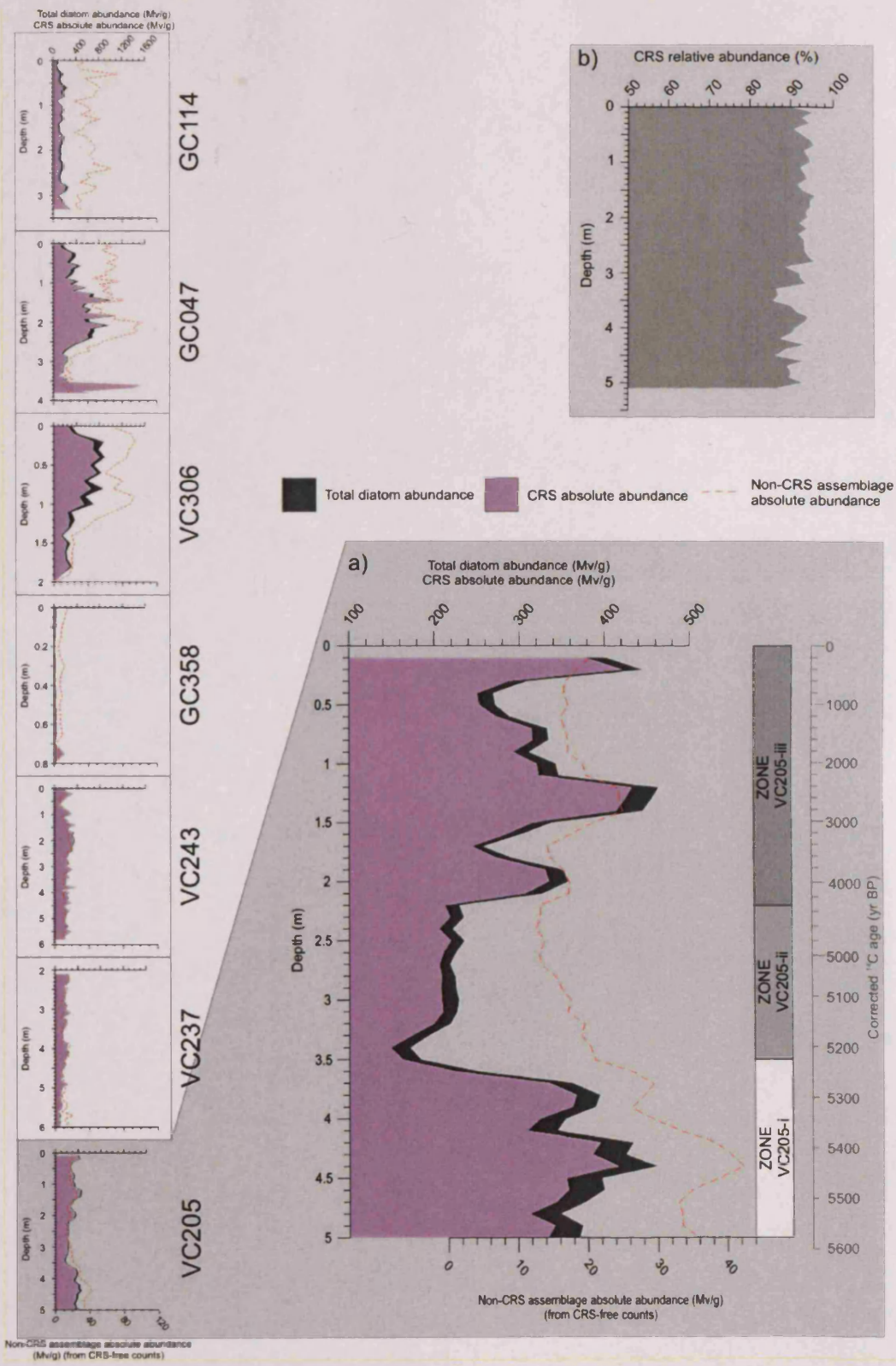


Figure 7.60

a) Core VC205: Total diatom abundance, CRS absolute abundance (both from CRS-included counts) and non-CRS assemblage absolute abundance (from CRS-free counts) (millions of valves/g (Mv/g)), smoothed using a three point moving average. Stratigraphic zones VC205-i, VC205-ii and VC205-iii identified using Q-mode PCA analysis of diatom relative abundance data.

b) Core VC205: CRS relative abundance (%).

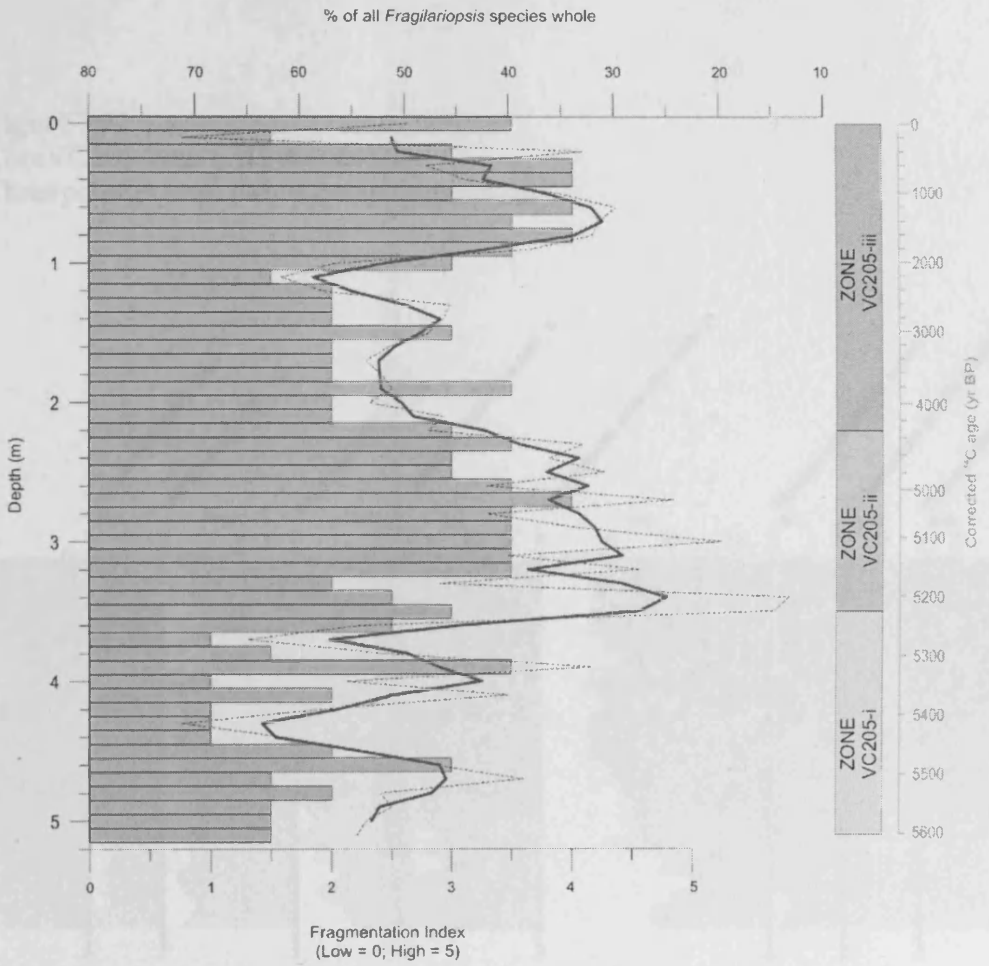


Figure 7.61
Core VC205: Diatom fragmentation, using two measures: observational index (bars: low = 0 to high = 5); and percentage of *Fragilariopsis* species whole (dashed line = original; solid line = three point moving average). Stratigraphic zones VC205-i, VC205-ii and VC205-iii identified using Q-mode PCA analysis of diatom relative abundance data.

Figure 7.62
Core VC205: Non-CRS diatom assemblage plots for AP indicator species: (a) Absolute abundance (Mv/g); (b) Relative abundance (%).
Three point average (white); original abundance (dark grey line). Stratigraphic zones VC205-i to VC205-iii identified using Q-mode PCA analysis of diatom relative abundance data.

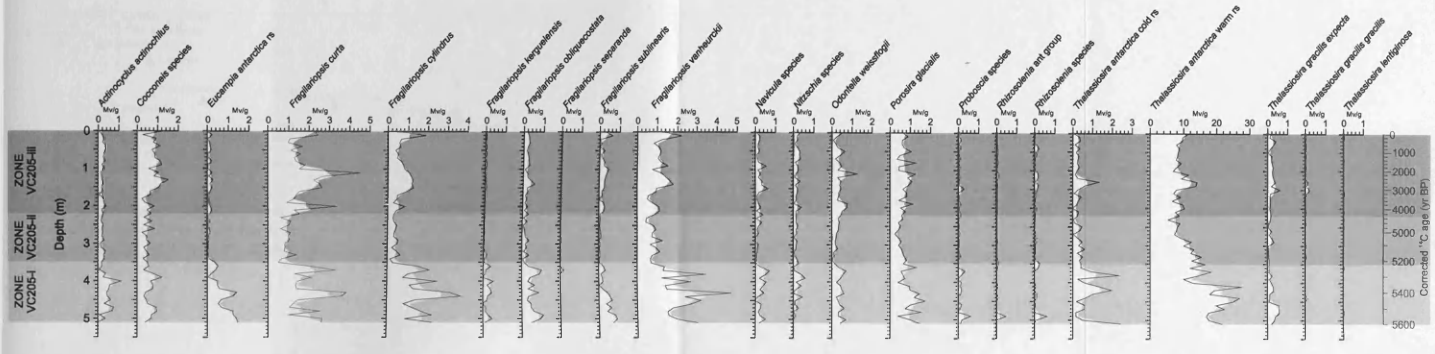


Figure 7.62 (a)

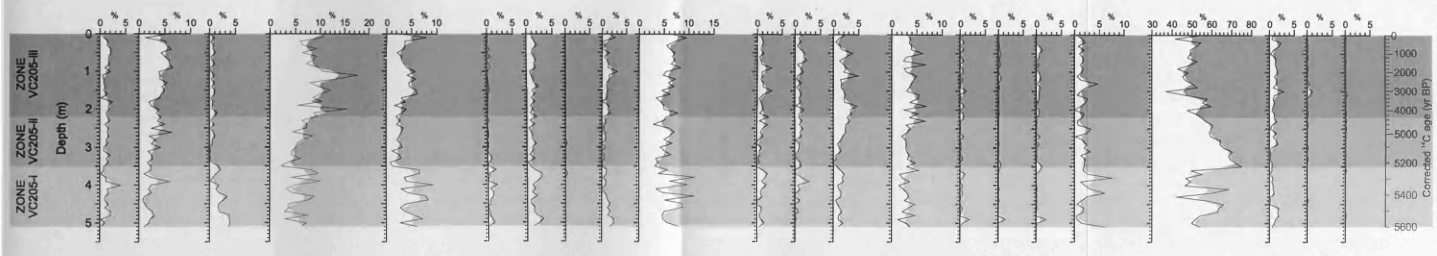


Figure 7.62 (b)

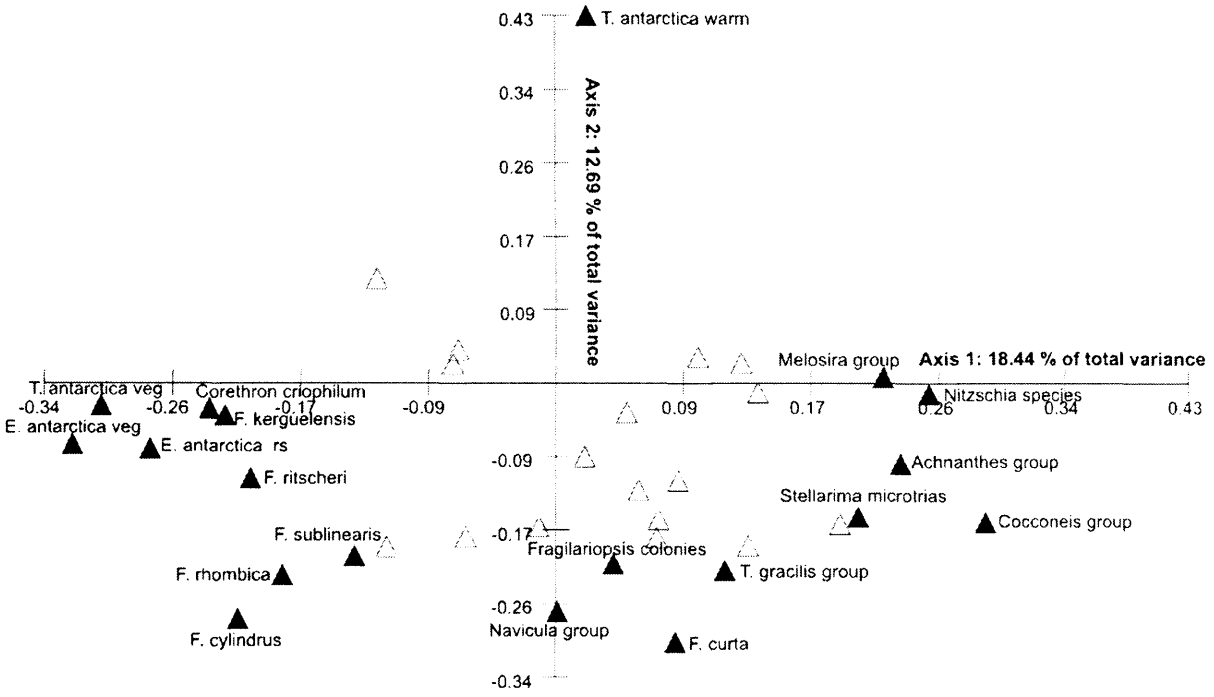


Figure 7.63
Core VC205: R-mode PCA variable loading on axes 1 and 2 for diatom relative abundance data (> 1 %). Data square-root transformed and standardised. Tolerance of eigenanalysis set at 1 x 10^{-10}. Highlighted species are those that have component loading ≥ + 0.20 or ≤ – 0.20.

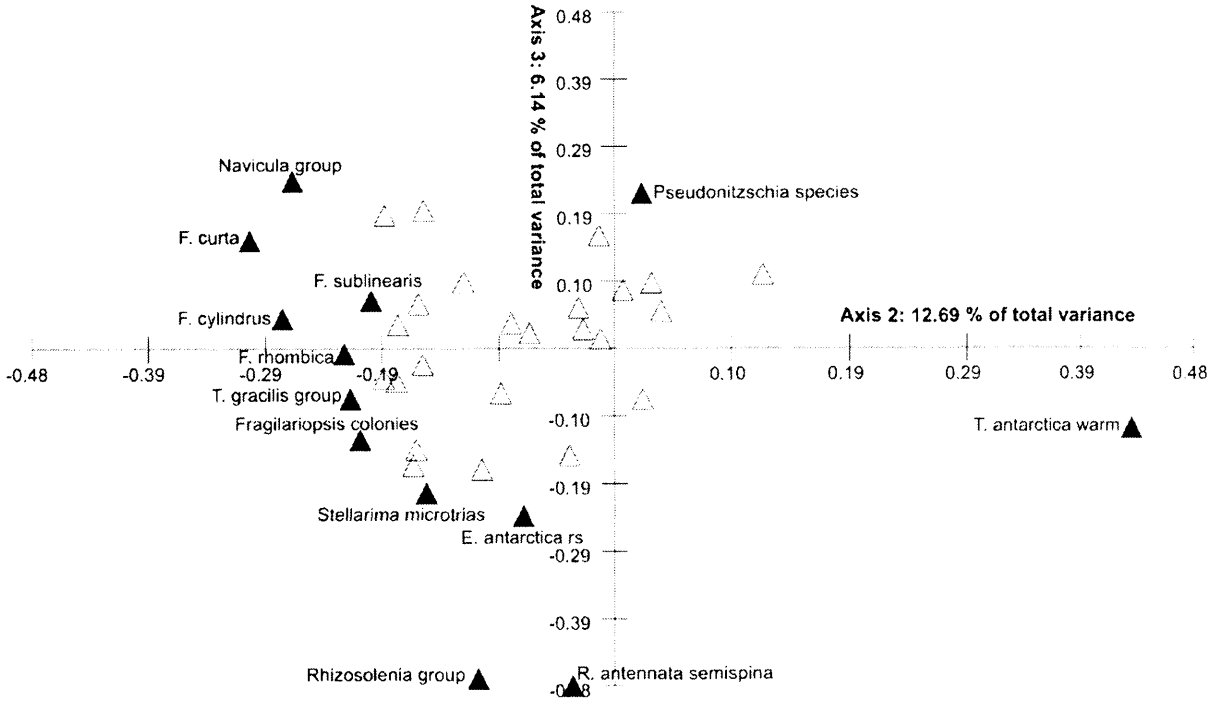


Figure 7.64
Core VC205: R-mode PCA variable loading on axes 2 and 3 for diatom relative abundance data (> 1 %). Data square-root transformed and standardised. Tolerance of eigenanalysis set at 1 x 10^{-10}. Highlighted species are those that have component loading ≥ + 0.20 or ≤ – 0.20.

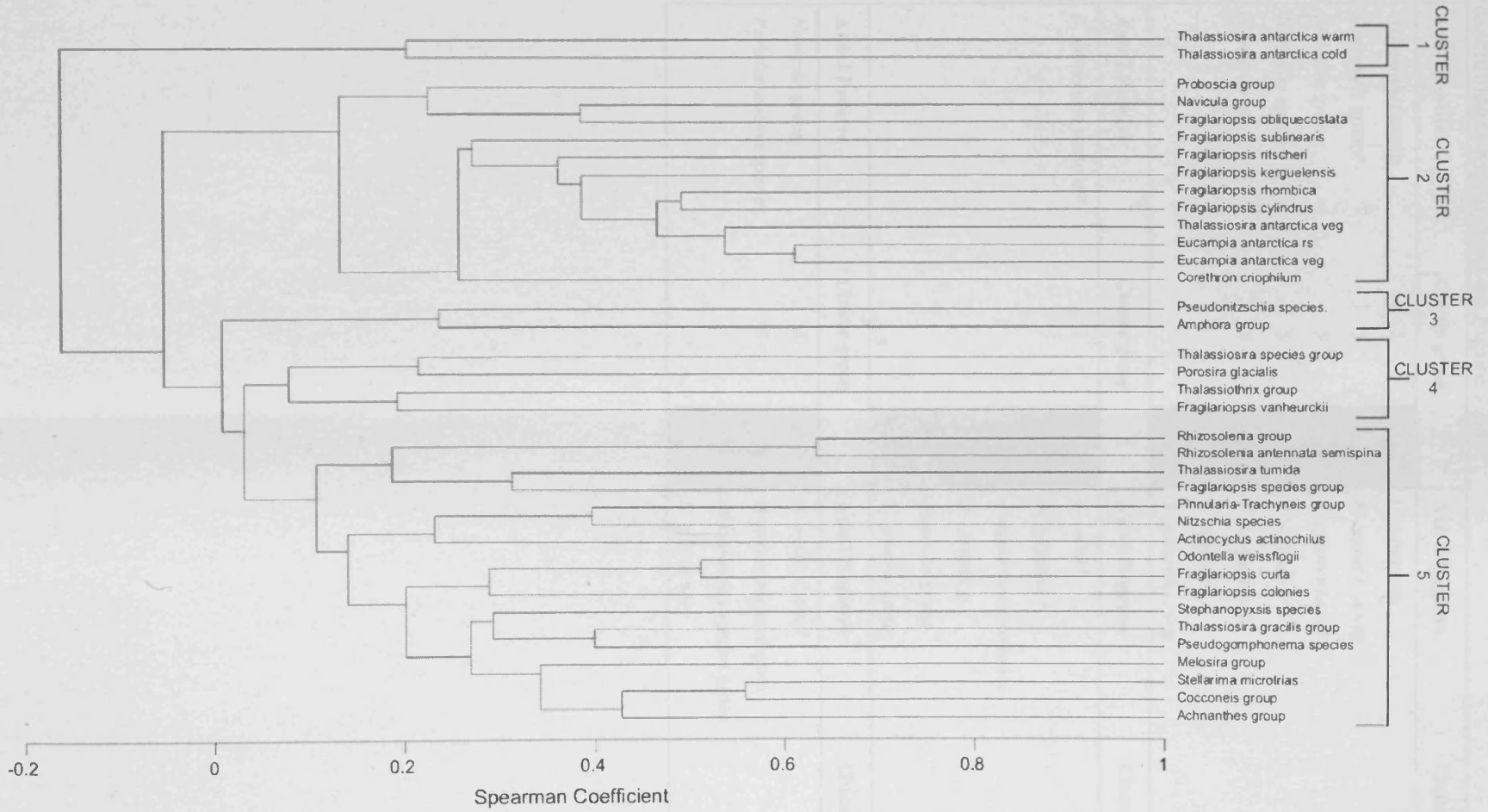


Figure 7.65
Core VC205: R-mode cluster analysis of diatom species relative abundance (>1 %). UPGMA clustering method; data square-root transformed; and Spearman Coefficient similarity measure.

Table 7.8
Core VC205: Comparison of diatom PCA axis loading and cluster groupings. Indicator species denoted with *. Grouped indicator species shown in bold and relate to diatom assemblages highlighted on Figure 7.68.

Axis 1 Positive	Cluster group		**Axis 1 Negative**	Cluster group	
Achnanthes group	5	**Cocconeis group**	*C. pennatum*	2	**E. antarctica rs; F. cylindrus**
Cocconeis group*	5		*E. antarctica* veg	2	
Melosira group	5		*E. antarctica* rs*	2	
Nitzschia species	5		*F. cylindrus**	2	
S. microtrias	5		*F. kerguelensis*	2	
			F. ritscheri	2	
			T. antarctica veg	2	
Axis 2 Positive	Cluster group		**Axis 2 Negative**	Cluster group	
T. antarctica warm rs*	1	**T. antarctica warm rs**	*F. curta**	5	**F. curta – F. cylindrus**
			*F. cylindrus**	2	
			Fragilariopsis colonies	5	
			F. rhombica	2	
			Navicula group	2	
			T. gracilis group	5	
Axis 3 Positive	Cluster group		**Axis 3 Negative**	Cluster group	
Navicula group	2	**None**	*E. antarctica* rs*	2	**E. antarctica rs**
Pseudonitzschia species	3		*R. antennata semispina*	5	
			Rhizosolenia species group	5	
			S. microtrias	5	

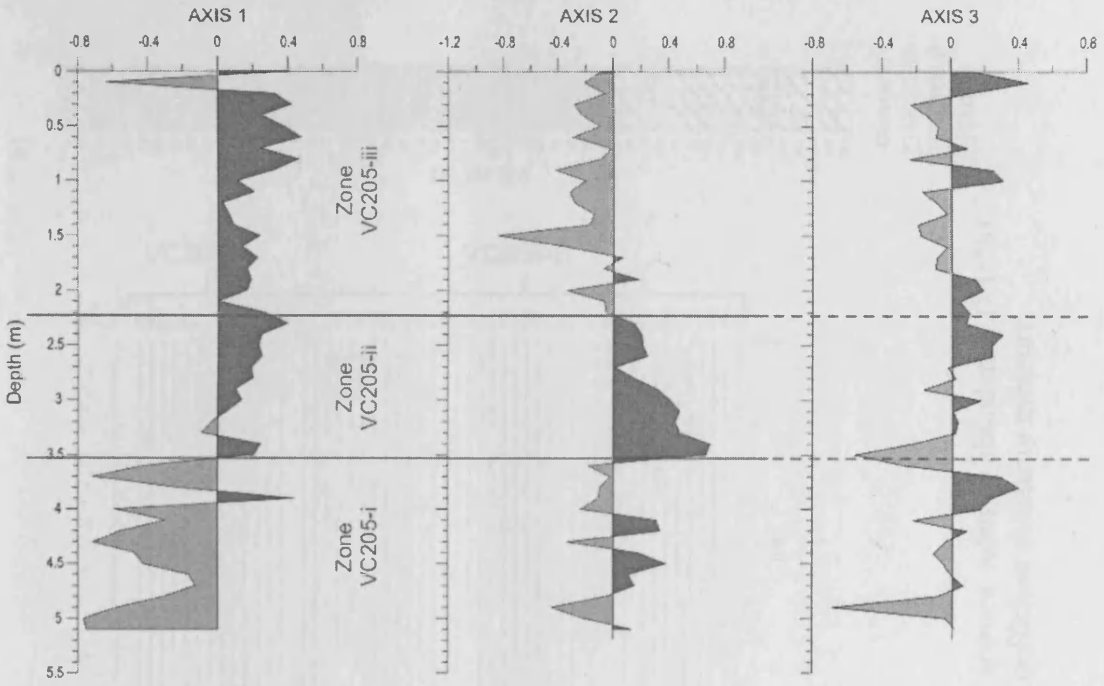


Figure 7.66
Core VC205: Q-mode PCA component scores plotted stratigraphically for PCA axes 1 – 3. Positive loading (dark grey); negative loading (light grey). Division of the record into stratigraphic zones VC205-i, VC205-ii and VC205-iii is based on component loading on axes 1 and 2.

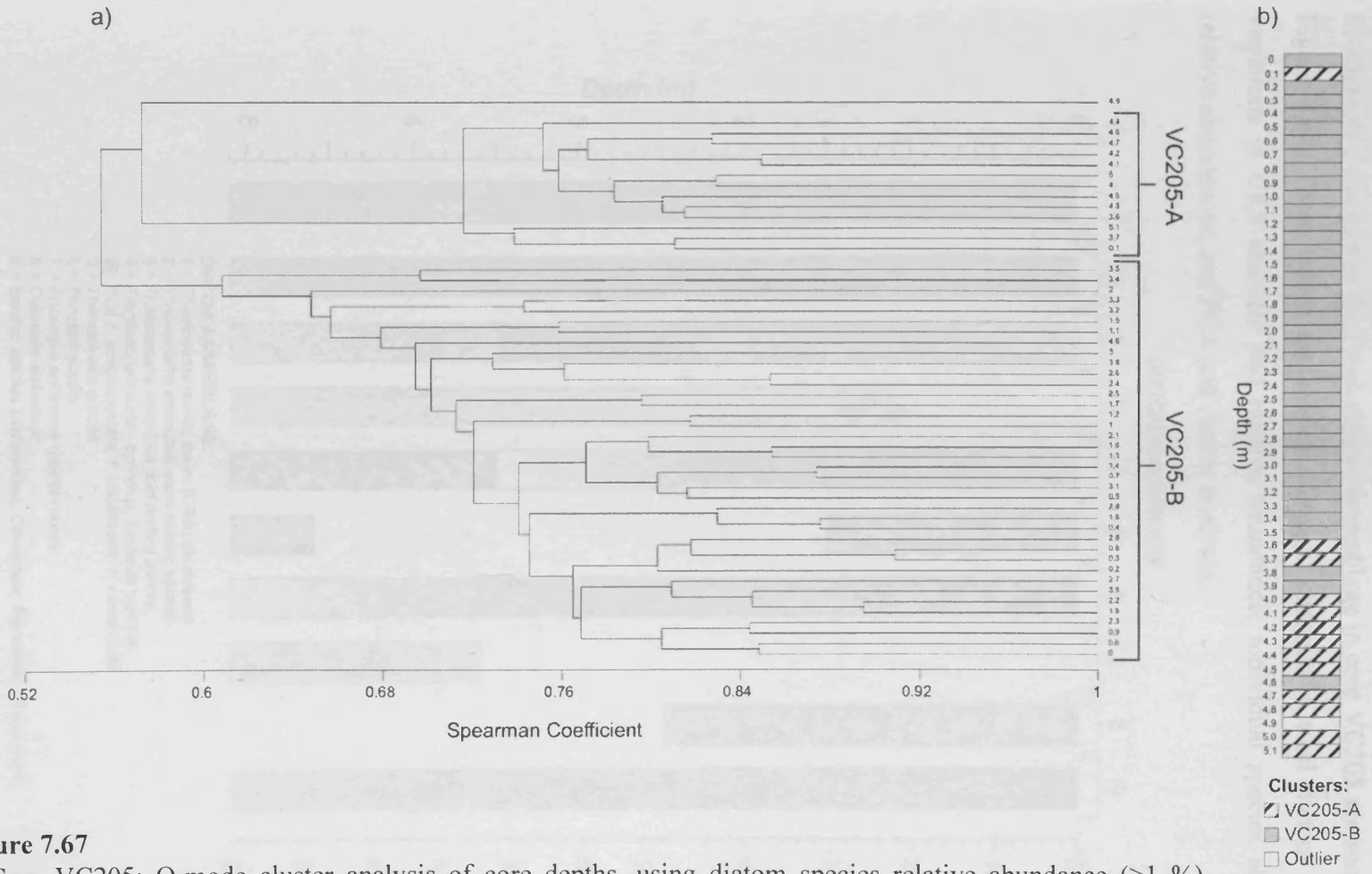


Figure 7.67
a) Core VC205: Q-mode cluster analysis of core depths, using diatom species relative abundance (>1 %). UPGMA clustering method; data square-root transformed; and Spearman Coefficient similarity measure.
b) Core VC205: Stratigraphic pattern of Q-mode cluster groups.

7.7.3 Diatom summary

Stratigraphic changes in the fossil diatom assemblage in core VC205 are summarised in Figure 7.68. These trends are evident through: changes in total diatom abundance; variations in CRS absolute and relative abundance; individual species absolute and relative abundances; and PCA and cluster analyses.

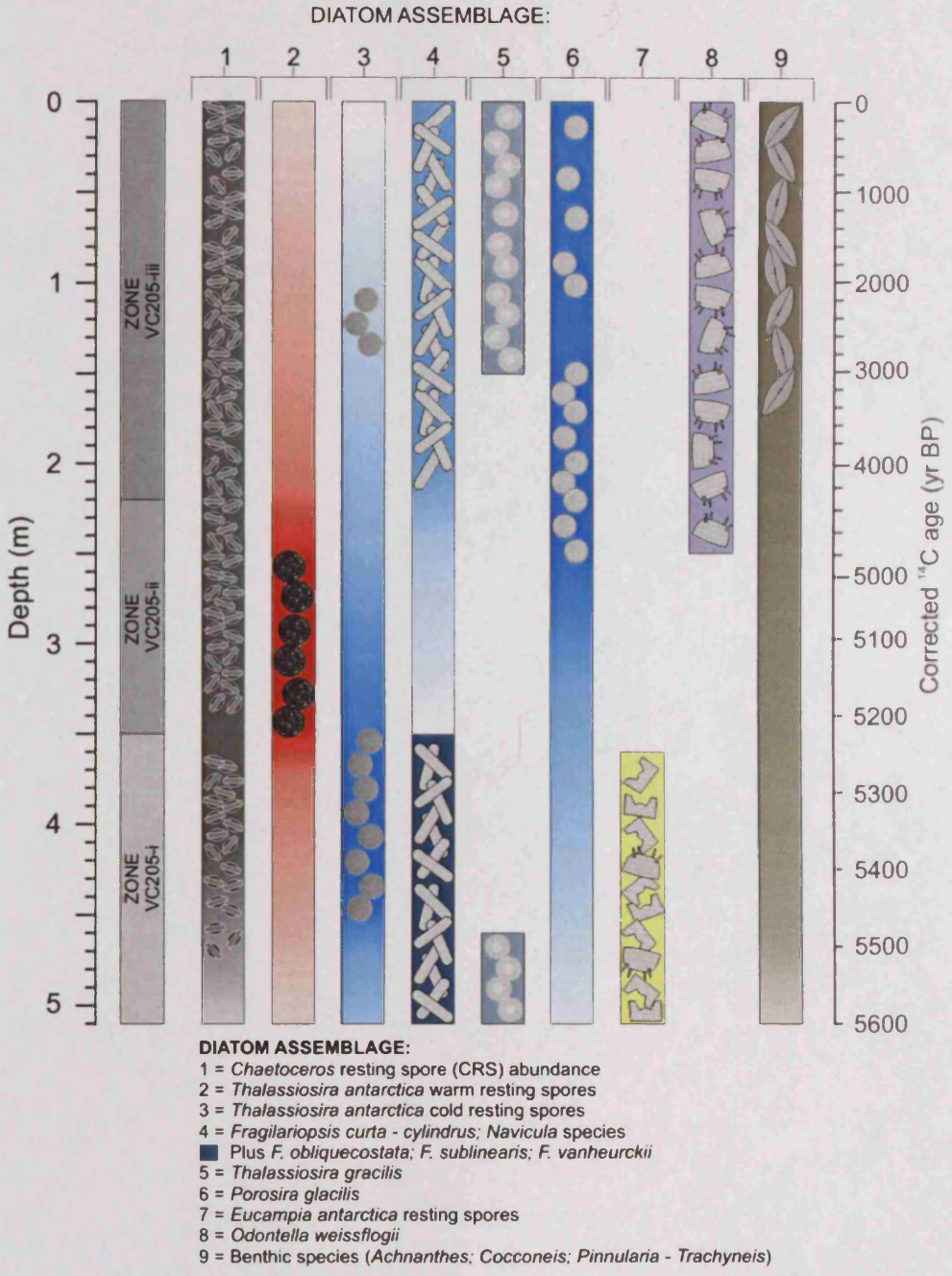


Figure 7.68
Core VC205: Schematic representation of the fossil diatom assemblage, highlighting the relative contribution of CRS to the total assemblage and stratigraphic changes in the diatom community. Stratigraphic zones VC205-i, VC205-ii and VC205-iii identified using Q-mode PCA analysis of diatom relative abundance data. Darker tones indicate elevated abundance.

7.8 Antarctic Peninsula fossil diatom assemblages

7.8.1 Regional trends

In the suite of AP cores studied in this investigation, Holocene diatom assemblages display distinct regional patterns. A combined Q-mode PCA analysis of diatom relative abundance data (>1 %) for all sample depths in all cores (Figure 7.69), and plots of mean diatom relative abundance data within individual cores (Figure 7.70) reveals some of these patterns. Both plots highlight the striking cross-peninsula differences in diatom assemblages and further, an obvious latitudinal trend along the WAP. On Figure 7.69, the EAP cores are clustered towards the positive end of axis 1, whereas the WAP cores are generally towards the negative end of axis 1 and arranged along axis 2 in a clear north-to-south latitudinal trend: from core GC114 (negative loading on axis 1; positive on axis 2), through core GC047 and VC306 (progressively less negative on axis 1 and more negative on axis 2), to core GC358 (negative on both axis 1 and 2). The spatial arrangement of core samples on Figure 7.69 reflects variability in the non-CRS sedimentary assemblage either side of the AP, and latitudinally between WAP core sites. Individual core pie-charts (Figure 7.70) and R-mode PCA analysis (Figure 7.71; Figure 7.72 and Table A2.19) highlights which species are responsible for these spatial trends. The cross-peninsula pattern is driven by the heavy sedimentary dominance of *T. antarctica* warm rs (strong positive loading on axis 1) in the EAP cores, compared to the more mixed sedimentary assemblage in the WAP cores. In the northern WAP (cores GC114, GC047 and VC306), the non-CRS assemblage is characterised by roughly equal dominance of *F. kerguelensis* (strong negative loading on axis 1) and *F. curta* (negative loading on axis 1). Towards the southern WAP, this assemblage is supplemented by *T. antarctica* warm rs (strong positive loading on axis 1), *T. antarctica* cold rs (negative loading on axis 2) (particularly in cores GC047 and VC306) and *E. antarctica* rs (strong negative loading on axis 2) (particularly in core GC358), together with the decreased contribution from *F. kerguelensis* (strong negative loading on axis 1). Figure 7.70 also highlights that *F. curta*, *F. vanheurckii*, *F. cylindrus*, *O. weissflogii* and benthic species constitute a moderate portion of the non-CRS assemblage on the EAP side, whereas *F. kerguelensis* and *E. antarctica* rs are notably absent.

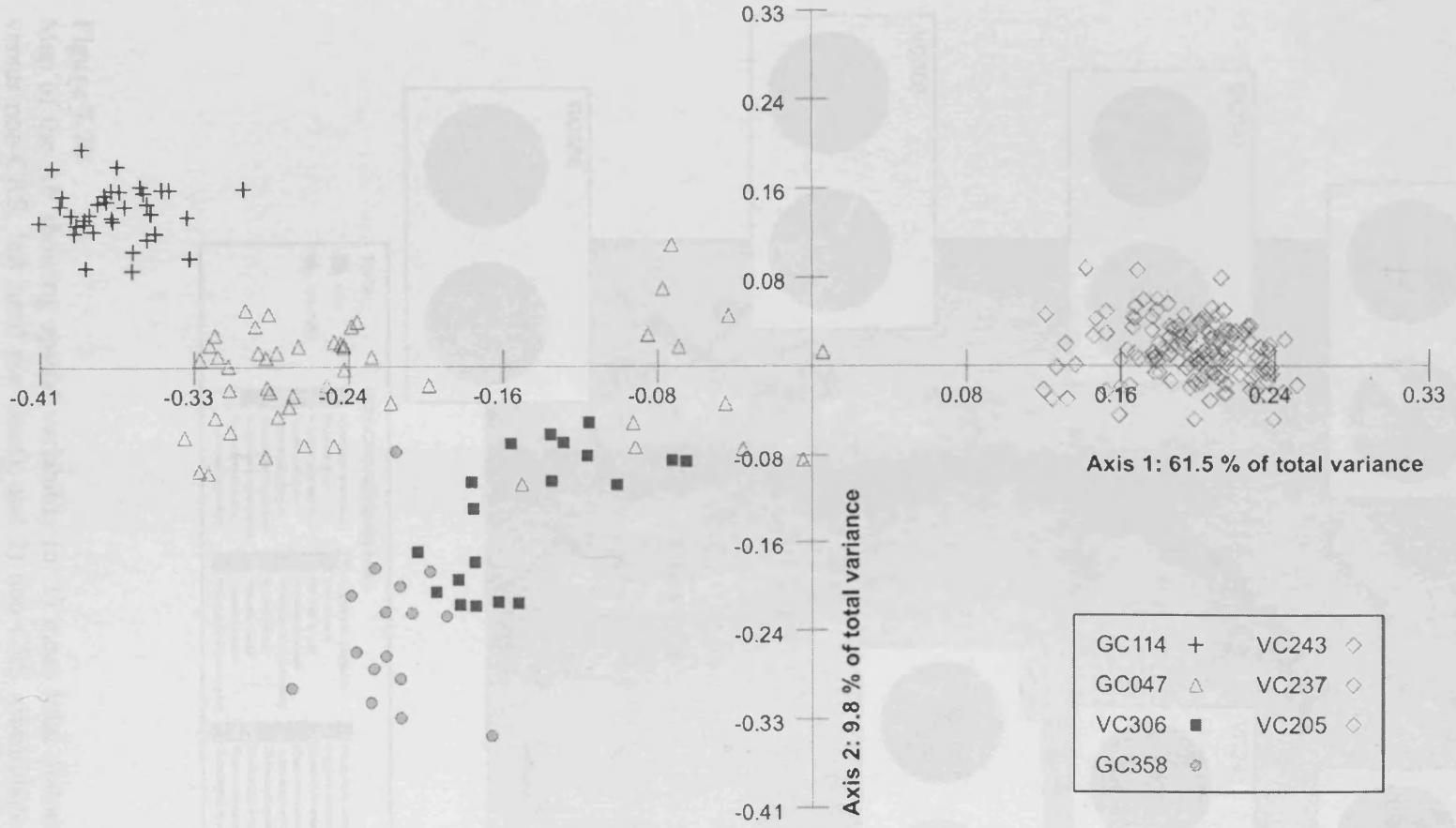


Figure 7.69
All AP cores: Q-mode PCA component loading on axes 1 and 2 for diatom relative abundance data (>1 %). Data square-root transformed and standardised. Tolerance of eigenanalysis set at 1 x 10^{-10}.

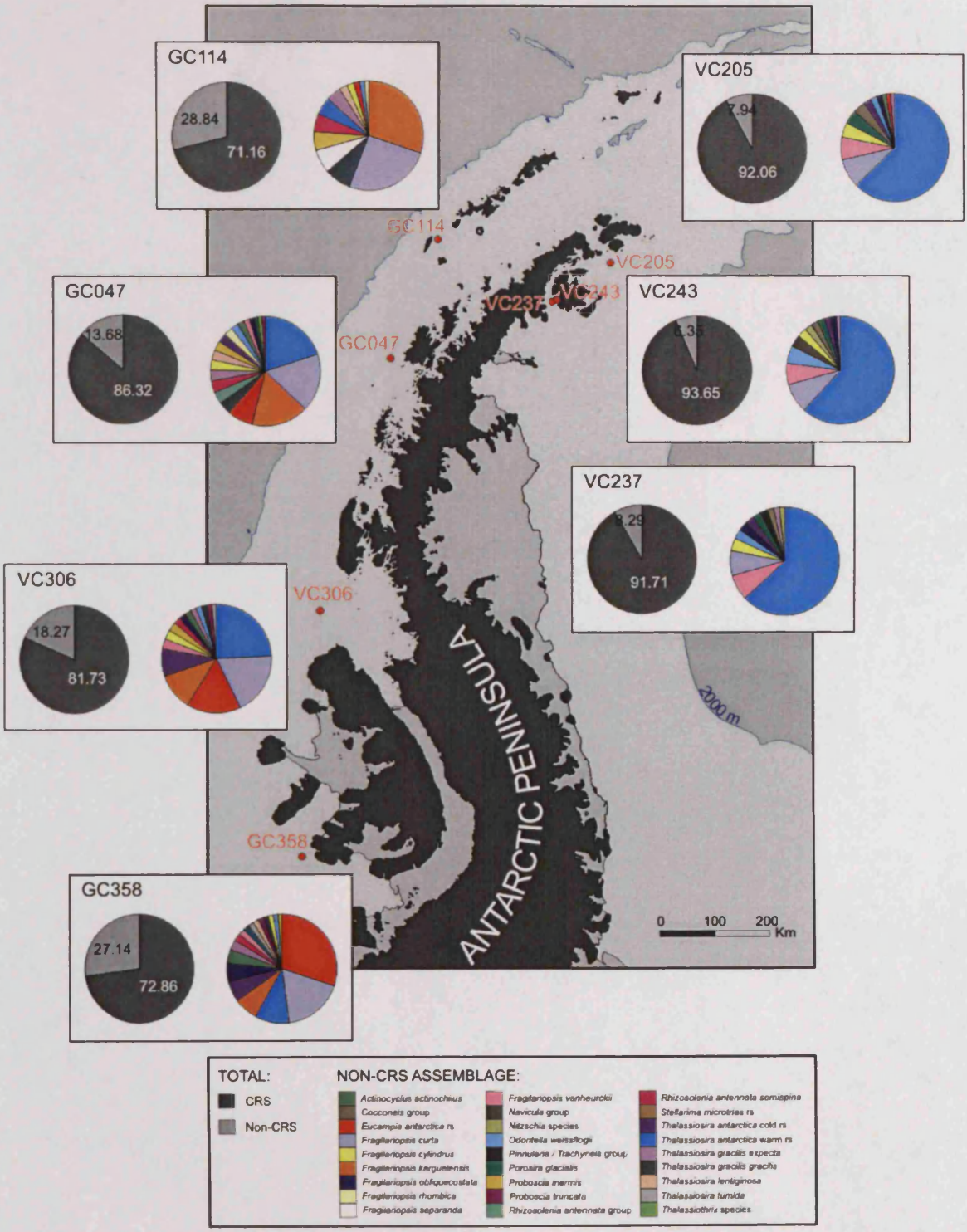


Figure 7.70
Map of the AP showing spatial variability in: 1) mean total diatom assemblage (CRS versus non-CRS; left hand pie chart); and 2) non-CRS assemblage (>1 % from CRS-free counts; right hand pie chart). Both measures were calculated by averaging the diatom relative abundance data along the cores. Throughout the Holocene and at all core localities, CRS are the most abundant diatom in the sediment and are particularly dominant in the EAP cores.

7.8.2 Species associations

The large quantitative diatom dataset generated in this study also reveals further important information about the AP diatom community structure and species associations. This is revealed through R-mode PCA of the diatom relative abundance data (>1 %) for all samples depths in all cores (Figure 7.71, Figure 7.72 and Table A2.19), paired with visual examination of the diatom assemblage data presented in all of the sections 7.*.1. In the AP cores analysed the following diatom species associations are evident:

- In all cores, *T. antarctica* rs display directly opposite PCA loading (and occur in separate cluster groups) to *T. gracilis* species (either both varieties, or solely *T. gracilis* var. *gracilis*). With the exception of core VC306, this is observed in the *T. antarctica* warm rs variety.
- In all cores, *T. antarctica* warm rs display directly opposite PCA loading (and occur in separate cluster groups) to *F. curta*.
- In all cores, *F. curta* and *F. cylindrus* display similar PCA loading (and occur in the same cluster groups) to grouped *Navicula* species.
- In all cores, *F. curta* or *F. cylindrus* display similar PCA loading (and occur in the same cluster groups) to *T. antarctica* cold rs (cores GC114, VC306, GC358) or *T. antarctica* vegetative valves (cores VC243, VC237 and VC205).
- In all the WAP cores, *Proboscia* species and *Rhizosolenia* species display similar PCA loading (and occur in the same cluster groups). In EAP cores, *Proboscia* species and *Rhizosolenia* species either do not reach sufficient relative abundance (> 1 %) to be included in statistical analysis or do not show particular striking PCA loading or patterns.
- In all the WAP cores, *E. antarctica* species display directly opposite PCA loading (and occur in separate cluster groups) to *Proboscia* species (*P. inermis* or *P. truncata*).
- In all the cores (excluding GC114, GC047 and VC205, from the north-west and north-east AP respectively), *E. antarctica* displays directly opposite PCA loading (and occur in separate cluster groups) to *F. curta* and *F. cylindrus*.
- In three of the WAP cores (GC047, VC306 and GC358), *E. antarctica* rs display directly opposite PCA loading (and occur in separate cluster groups) to *T.*

antarctica cold rs. In core VC243, *E. antarctica* rs display directly opposite PCA loading (and in separate cluster groups) to *T. antarctica* vegetative valves.

- In three of the WAP cores (GC047, VC306 and GC358), *F. kerguelensis* displays directly opposite PCA loading (and occur in separate cluster groups) to *T. gracilis* species.
- In cores VC306, GC358 and VC205, *E. antarctica* rs display similar PCA loading (and occur in the same cluster groups) to *F. kerguelensis*.
- In cores GC047, GC358 and VC243, *O. weissflogii* display similar PCA loading (and occur in the same cluster groups) to *T. gracilis* var. *expecta*.
- In cores VC243 and VC237 (from Prince Gustav Channel), *F. curta* display similar PCA loading (and occur in the same cluster groups) to *Amphora* and *Achnanthes* species.

In theory, opposite PCA loading (positive versus negative, or vice versa) on individual axes, and different cluster groupings, suggests contrasting environmental preferences; whereas comparable PCA loading (positive or negative) on individual axes, and similar cluster groupings implies similar environmental preferences.

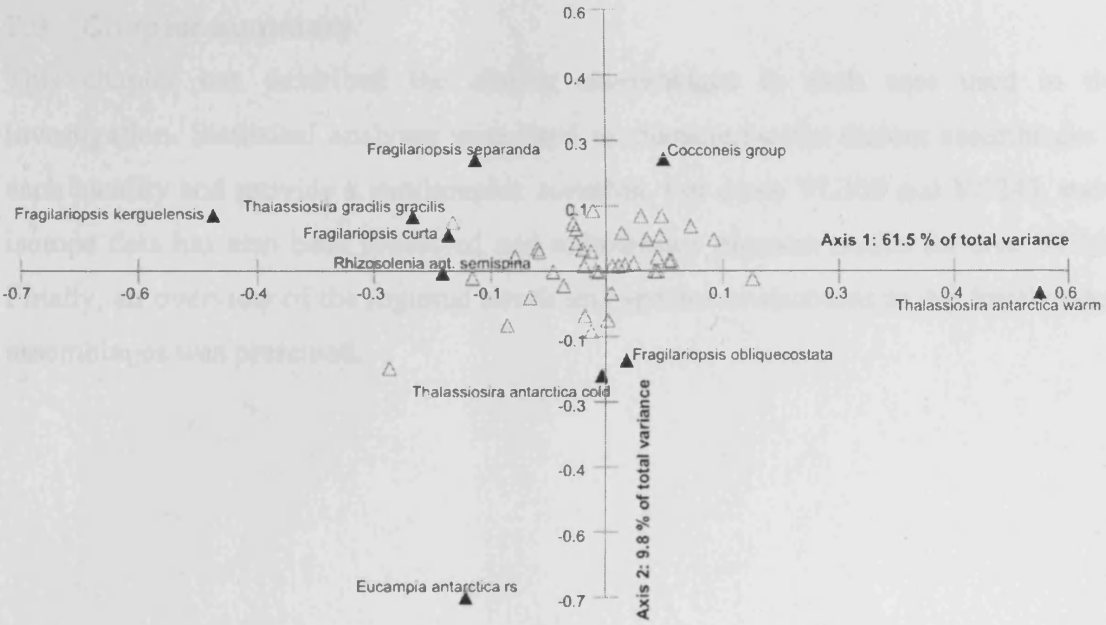


Figure 7.71
All AP cores: R-mode PCA variable loading on axes 1 and 2 for diatom relative abundance data (> 1 %). Data square-root transformed and standardised. Tolerance of eigenanalysis set at 1 x 10^{-10}. Highlighted species are those that have component loading ≥ + 0.20 or ≤ – 0.20.

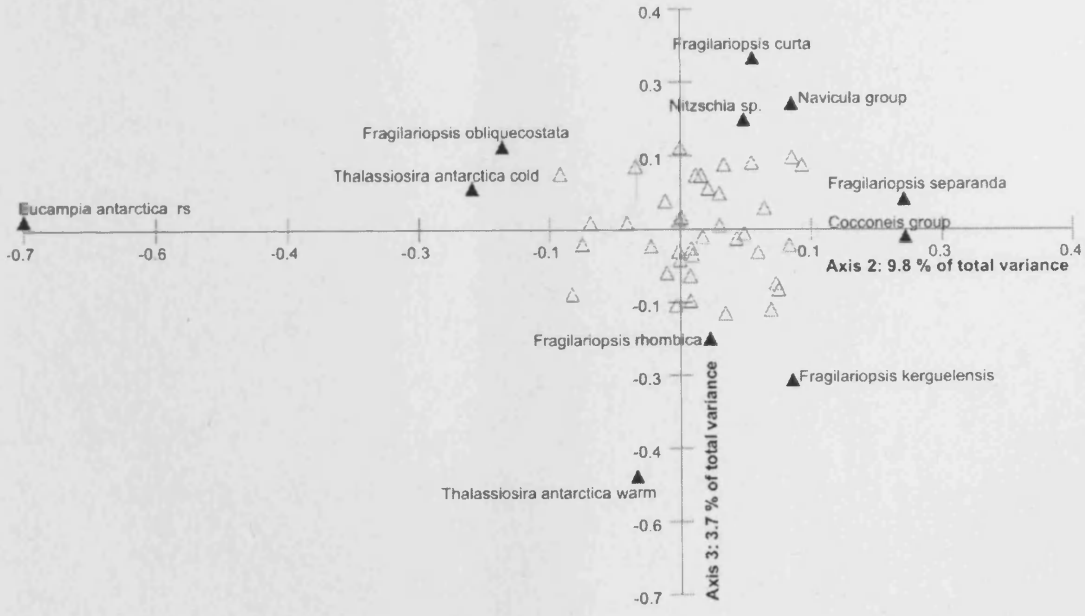


Figure 7.72
All AP cores: R-mode PCA variable loading on axes 2 and 3 for diatom relative abundance data (> 1 %). Data square-root transformed and standardised. Tolerance of eigenanalysis set at 1 x 10^{-10}. Highlighted species are those that have component loading ≥ + 0.20 or ≤ – 0.20.

7.9 Chapter summary

This chapter has described the diatom assemblages in each core used in this investigation. Statistical analyses were used to characterise the diatom assemblages at each locality and provide a stratigraphic zonation. For cores VC306 and VC243, stable isotope data has also been presented and sedimentary pigment results for core VC243. Finally, an overview of the regional trends and species associations in AP fossil diatom assemblages was presented.

8 Palaeoclimate reconstructions from the Antarctic Peninsula

The diatom assemblages preserved in the seven regionally representative marine sediment cores from the Antarctic Peninsula (AP), together with nitrogen and carbon stable isotope and sedimentary pigment analyses, enable local and regional (AP) reconstructions of past ocean and climate conditions. Radiocarbon dated stratigraphic shifts in diatom abundance and species assemblages reflect changes in oceanographic conditions, including sea ice duration and extent, over the core sites.

This discussion chapter is divided in four sections:

- Section 8.1 describes the broad-scale regional patterns in the AP diatom assemblages. An overview of latitudinal and cross-peninsula trends is presented (sub-section 8.1.1) and explained by regional scale differences in the oceanographic and cryospheric environment between localities. A description is then provided of the consistent species associations (or disassociations), revealed through statistical analysis of the fossil diatom data (sub-section 8.1.2). Using this information, coupled with diatom ecological data presented in the literature, distinct habitat types are identified and typical community members proposed (sub-section 8.1.3). These diatom habitat types are later used to define changes in the Holocene environment at each core locality (section 8.4).

- Section 8.2 discusses some of the assumptions with stable isotope and sedimentary pigment analyses and justifies the palaeoenvironmental interpretations based on these proxies.

- Section 8.3 proposes Holocene palaeoclimate reconstructions for each core locality, based on environmental proxies analysed. The results are discussed using the core zonations described in Chapter 7.*.2 and dated using corrected ^{14}C ages (yr BP) and corresponding calibrated ages (cal. yr BP) (both rounded to the nearest 10 years).

- Section 8.4 addresses the broader research questions posed in Chapter 1.2: (1) In the AP, were Holocene climate events peninsula-wide and synchronous? Where spatial and temporal discrepancies exist, do these patterns provide clues to the forcing mechanisms? (sub-section 8.4.1); (2) Do AP Holocene climate events display similar phasing and duration to circum-Antarctic and global trends? (sub-section 8.4.2). Emphasis is placed on three climatic episodes, and their associated

transitions: (1) Deglaciation – Early Holocene transition, including the variable occurrence of a climatic reversal and Early Holocene climatic optimum; (2) Mid-Holocene Climatic Optimum; and (3) Late Holocene climatic deterioration (Neoglacial). For the AP, schematic maps are included representing each of the three main Holocene time-slices. Additional published proxy records (other marine records, ice core and terrestrial datasets) are incorporated to address these broad research questions. In the discussion text, additional Antarctic proxy records are marked with the prefix "#", relating to Table A1.1 and Figure A1.1 – A1.4, where a summary of the study, details of the source publication and location can be found. Where published marine and terrestrial datasets are used, the age model provided in the original publication is presented, usually as calibrated age (cal. yr BP), and where applicable the equivalent reservoir corrected ^{14}C ages (yr BP) are quoted in brackets.

8.1 Regional patterns in the AP fossil diatom assemblages

8.1.1 Regional trends

Although individual diatom species abundance varies temporally through the Holocene in all cores, some regionally consistent patterns have emerged. CRS are the most abundant diatoms in the cores. Although this dominance may in part be due to their heavily silicified frustule and therefore resistance to dissolution, and relatively high sinking rates (discussed in Chapter 3.5.3.3 and 3.6.2), they are also likely to reflect high dominance of their vegetative counterparts (*Hyalochaete Chaetoceros*) in surface waters. *Hyalochaete Chaetoceros* are abundant in these coastal areas due to their ability to bloom rapidly in favourable conditions, particularly in stratified, nutrient-rich waters, following sea ice melt and / or stabilisation resulting from low wind intensity (Leventer, 1991; 1998; Armand et al., 2005). Such conditions are common in the AP region; macro-nutrients (N, P, Si) are generally far in excess of phytoplankton requirements (Holm-Hansen et al., 1994; Dierssen et al., 2002) and the seasonal cycle of sea ice advance and retreat leads to strong surface water stratification during spring. As such, the variability witnessed in CRS abundance in Holocene sediments probably reflects changing nutrient availability (particularly immediately following ice sheet retreat) and sea ice conditions (both seasonal duration and geographical extent).

In the non-CRS assemblage, the clear cross-peninsula and WAP latitudinal differences (presented in Chapter 7.8) reflect gradients of different environmental parameters at the core sites (labelled on Figure 8.1). In the EAP cores, the non-CRS assemblage is overwhelmingly dominated by *T. antarctica* warm rs. Understanding the ecological preferences of *T. antarctica* (vegetative or rs) is challenging due to the paucity of direct observations in modern surface water blooms, together with lack of consistency in published identifications of the warm and cold varieties of resting spores. However, this study suggests that *T. antarctica* warm rs clearly favours the much colder surface waters and heavier sea ice conditions found on the EAP, compared to the WAP (Figure 8.1). Further clues to the environmental preference of *T. antarctica* warm rs will be discussed later in section 8.1.2.2. On the WAP, the latitudinal trend in the non-CRS assemblage (described in Chapter 7.8.1) may in part reflect the different shelf settings of the cores; from the outer continental shelf in the north (GC114), which is more oceanic in nature, to progressively inner coastal settings towards the south (GC047 – VC306 – GC358), that are influenced by more persistent sea ice and continental ice, and their associated meltwater inputs. However, latitudinal differences in shelf water masses and their respective temperatures, together with variability in sea ice extent and temporal duration, are likely to be equally important in controlling diatom community structure at individual sites on the WAP (Figure 8.1).

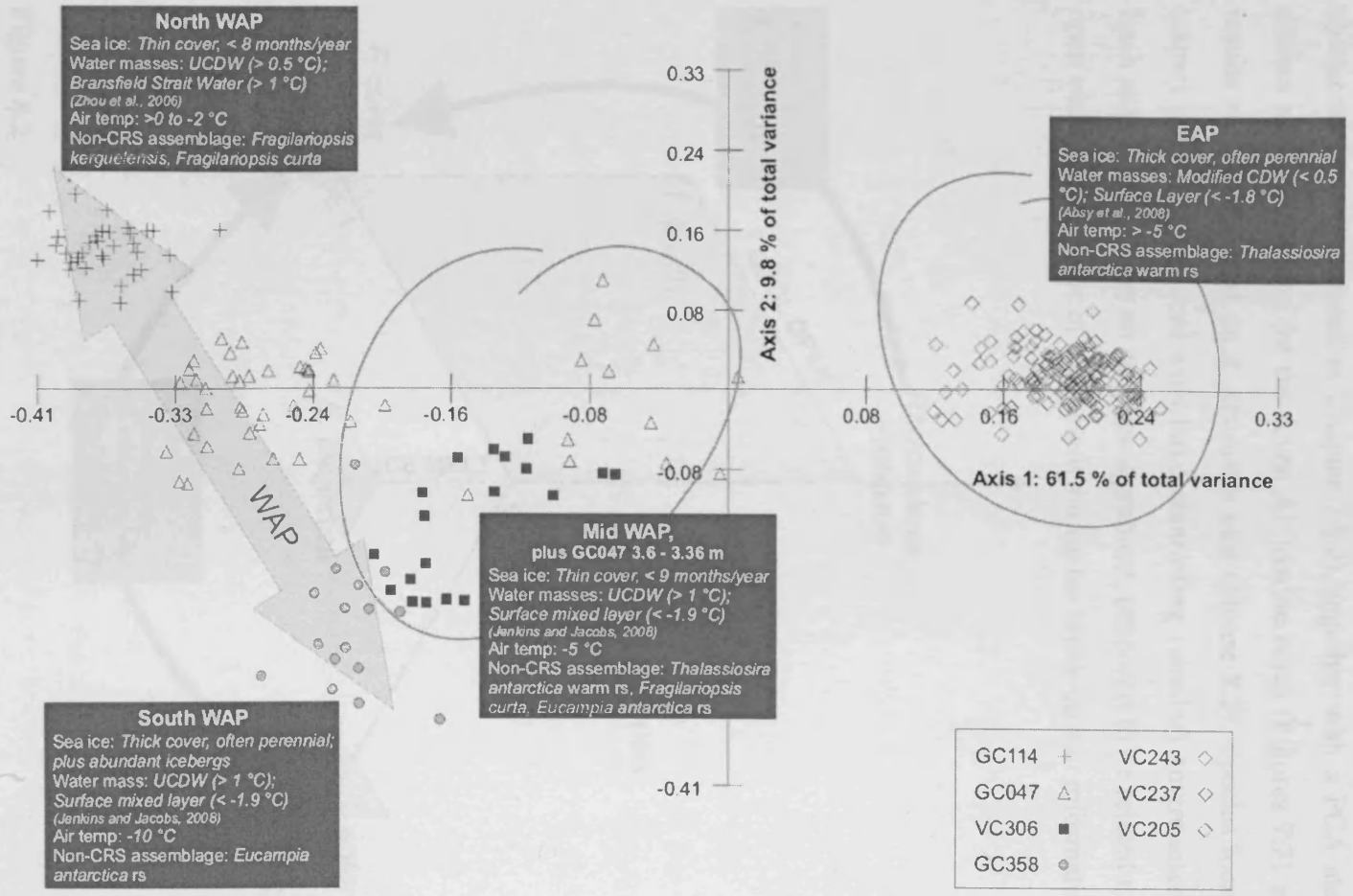


Figure 8.1

All AP cores: Q-mode PCA component loading on axes 1 and 2 for diatom relative abundance data (>1 %) (Figure 7.85), with different environmental parameters identified between core sites labelled. The obvious cross-peninsula and WAP latitudinal differences in diatom assemblage reflect a combination of forcing factors, including: sea ice character (Stammerjohn and Smith, 1996); dominant water masses (individually referenced on plot); and mean annual air temperature (Morris and Vaughan, 2003) (all discussed in detail in Chapter 2).

8.1.2 Diatom habitat types

Combining observations of regional differences in the diatom assemblages (Chapter 7.8.1 and Chapter 8.1.1) with trends of consistent diatom species associations present in the AP marine cores (Chapter 7.8.2), several diatom habitat types are proposed. These diatom habitat types have been revealed through comparison of R-mode PCA and cluster analysis (presented in Chapter 7.8.2), together with a PCA analysis of all the diatom assemblage data for the seven AP marine cores (Figures 7.71 and 7.72). These results are summarised on a schematic plot (Figure 8.2). Species located on opposite (same) ends of individual axes have contrasting (similar) environmental preferences. Each axis approximates an ecological gradient, proposed to be related to the duration of open water and the type of ice present during ice break-up and reformation.

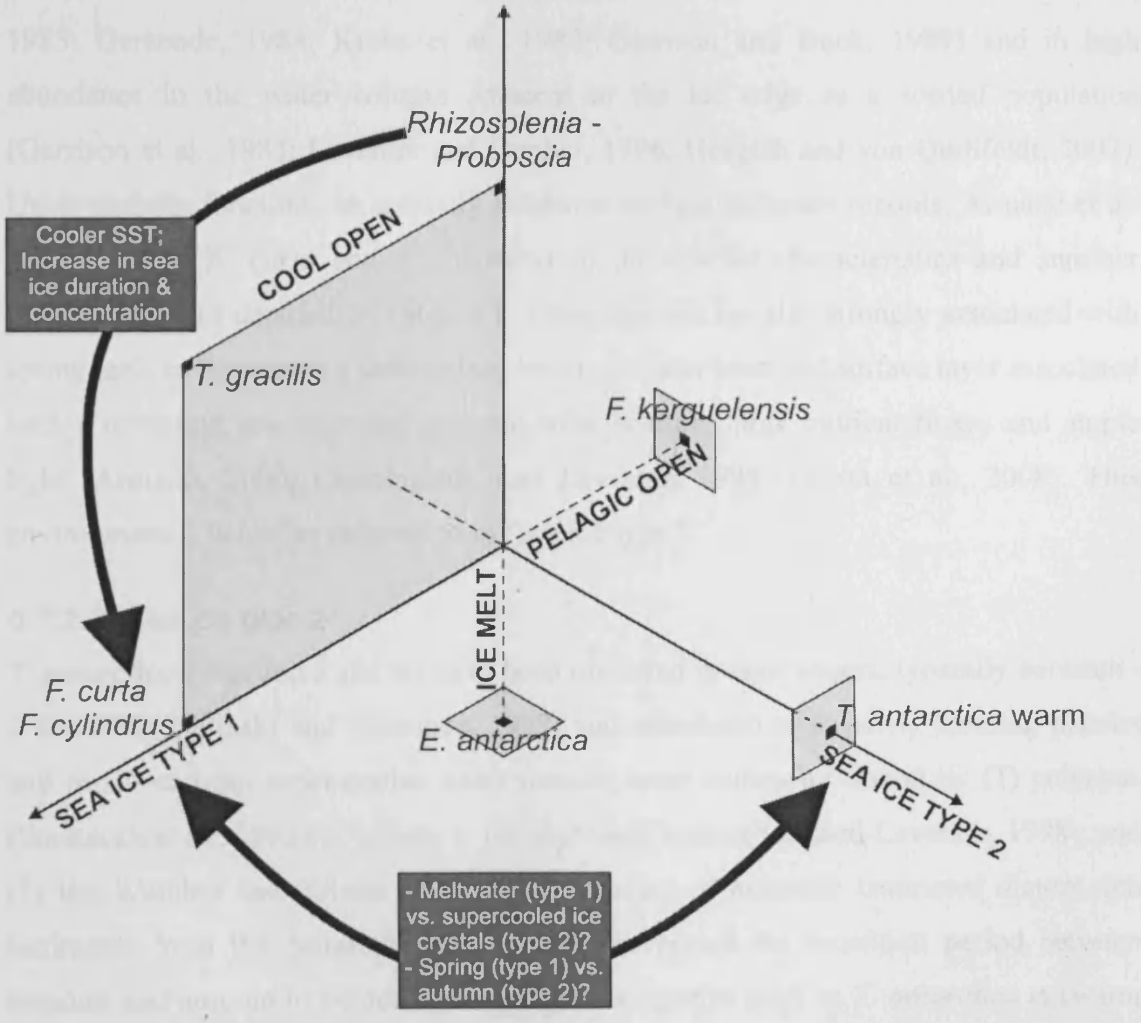


Figure 8.2
Schematic plot summarising the main associations of diatom species analysed in this investigation and their relationship with environmental gradients (e.g. sea ice type 1). These gradients are described in further detail in Table 8.1, together with associated diatom community members.

The most distinctive feature of the AP diatom assemblages is the consistent anti-correlation between *F. curta – F. cylindrus* and *T. antarctica* warm rs on individual core PCA plots, particularly those from the EAP, and on the composite PCA plot for all cores (Figure 7.71 and 7.72). Both are traditionally considered sea ice-associated diatoms (as discussed in Chapter 3.5.5 – 3.5.6 and 3.5.17, respectively), which leads to the question: why are these two species frequently not preserved in equal abundance in same sediment samples? I propose that these species are associated with different types of sea ice (sea ice type 1 and sea ice type 2 in Figure 8.2), related to subtly different water column conditions.

8.1.2.1 Sea ice type 1

F. curta and *F. cylindrus* are commonly found in pack and fast ice (Garrison et al., 1983; Gersonde, 1984; Krebs et al., 1987; Garrison and Buck, 1989) and in high abundance in the water column adjacent to the ice edge as a seeded population (Garrison et al., 1983; Leventer and Dunbar, 1996; Hesgeth and von Quillfeldt, 2002). Using transfer functions on spatially extensive surface sediment records, Armand et al. (2005) linked *F. curta* and *F. cylindrus* to the sea ice characteristics and summer (February) SSTs detailed in Table 8.1. These species are also strongly associated with spring melt environment, characterised by a meltwater stratified surface layer associated with a retreating ice edge and seasonal solar heating, large nutrient fluxes and ample light (Armand, 2000; Cunningham and Leventer, 1998; Crosta et al., 2008). This environment is hereafter referred to as "sea ice type 1".

8.1.2.2 Sea ice type 2

T. antarctica (vegetative and rs) have been observed in cool waters, typically between -2 and 2°C (Zielinski and Gersonde, 1997) and associated with newly forming platelet and frazil ice from super-cooled water masses, most commonly found in: (1) polynyas (Smetacek et al., 1992); (2) close to ice shelves (Cunningham and Leventer, 1998); and (3) the Weddell Sea (Gleitz et al., 1998). Studies of annually laminated diatom-rich sediments from the Antarctic margin have interpreted the transition period between summer and autumn to be dominated by centric species such as *T. antarctica* rs (warm and cold varieties not defined) and *P. glacialis* (Maddison et al., 2005; 2006; Denis et al., 2006). This observation of *T. antarctica* rs dominating the last recorded bloom of the season, strongly indicates a relationship with falling temperatures (forming ice) and falling light levels (Maddison et al., 2005; Stickley et al., 2005). This observation has

lead to the use of *T. antarctica* (rare vegetative cells and dominant rs) as a proxy for sea ice presence and concentration in autumn (Crosta et al., 2008), as first suggested by Cunningham and Leventer (1998).

The observation of *T. antarctica* warm rs dominating the non-CRS assemblage in the EAP suggests that phytoplankton productivity in this region is characterised by large blooms of *T. antarctica* vegetative cells in late summer. This species clearly favours the much colder surface waters developed through interaction with the large ice shelves on the EAP (including the Ronne-Filchner Ice Shelf). Their sedimentary dominance is also probably a function of the extensive and persistent sea ice cover, leading to the reduced length of the diatom growing season and prevents typical open ocean diatoms from reaching large biomass. In the Weddell Sea, sea ice formation commences in late summer and autumn by frazil ice production in the upper water column, becoming concentrated in the surface water as grease ice and subsequently developing in extent through the pancake ice cycle, frequently forming closed pack ice within weeks (Lange et al., 1989). The autumn sea ice environment, characterised by high salinities, cold, non-stratified surface waters, with abundant ice crystals and rapid development of closed sea ice, is hereafter referred to as "sea ice type 2".

8.1.2.3 Cool open ocean

"Cool open ocean" species are represented as a plane between two axes on Figure 8.2, signifying a continuum along which SST decrease and sea ice duration and concentration increase (Table 8.1), from *Rhizosolenia – Proboscia* species at one end, through *T. gracilis*, *A. actinochilus* and *S. microtrias*, to *T. tumida*, *T. antarctica* cold rs and *F. curta – F. cylindrus* (typical sea ice type 1 species) at the other end. This group of cool open ocean species displays a preference for the marginal ice zone.

8.1.2.4 Ice melt

E. antarctica is situated at the extreme of another ecological gradient (PCA axis 2 on Figures 7.71 and 7.72; and represented schematically on Figure 8.2). The environmental preference of *E. antarctica* is mostly speculative, being observed in a range of different environments, and is further complicated by the occurrence of two morphological varieties. In the majority of counts for these cores, the variety present was the polar form (*E. antarctica* var. *recta*). This species is typically found in nearshore environments, adjacent to / beneath pack-ice or in a meltwater stratified water column (Fryxell and Prasad, 1990; Cremer et al., 2003). The origin of meltwater stratification

could be iceberg melt, with *E. antarctica* var. *recta* potentially exploiting these pseudoneritic conditions (Burckle, 1984), although there is no published confirmation. Icebergs have been observed as hot spots of primary productivity, due to nutrient enrichment and the development of localised surface water stratification through the addition of cold, fresh meltwater (de Baar et al., 1995; Smith et al., 2007c; Schwarz and Schodlok, 2008). Stratification and surplus nutrients enable phytoplankton cells to remain in the well-lit surface layers and bloom. Although there are no direct observations of *E. antarctica* dominating the diatom assemblage in surface waters next to icebergs, higher cell concentrations are recorded following localised iron enrichment at Kerguelen Plateau (Armand et al., 2008). This observation potentially acts as a simulation of the addition of nutrients (originating from dust accumulation on land-based and sea ice) to the ocean through melting of glacial and sea ice.

The opposite PCA loadings between *E. antarctica* and *Proboscia* species in several cores potentially provides additional information regarding the preferred habitat of *E. antarctica*. As discussed in section 8.1.2.3 and presented in Table 8.1, *Proboscia* is proposed to be a cool open ocean species, associated with the marginal ice zone, so *E. antarctica* is unlikely to be heavily linked to this habitat. Similarly, in a number of cores *E. antarctica* has directly opposite PCA loading to *T. antarctica* cold rs, *F. curta* and *F. cylindrus*. This suggests that *E. antarctica* is not solely linked with the sea ice type 1 habitat, supporting the hypothesis of Zielinski and Gersonde (1997). Potentially the most useful observation regarding *E. antarctica* from this study is that a number of cores (GC047, VC306 and GC358) record a large and sustained peak in *E. antarctica* abundance immediately following ice sheet retreat (discussed further for individual records in section 8.3). This observation leads to the suggestion that the environment following ice sheet retreat, characterised by localised meltwater lenses from glacial melt and surface water nutrient enrichment, acted to sustain large populations of *E. antarctica*; this supports the proposition of Burckle (1984) that *E. antarctica* var. *recta* has a strong affinity with iceberg melt.

8.1.2.5 Pelagic open ocean

The position of *F. kerguelensis* at the extreme of another axis on the schematic plot (Figure 8.2) results from the species negative loading on the composite PCA plot (Figure 7.71). Although no explicit species associations are evident, *F. kerguelensis* does reach high abundances in several of the WAP cores (<28 % of the non-CRS assemblage). As discussed in Chapter 3.5.10, *F. kerguelensis* has a well constrained

distribution in the Southern Ocean and thrives in the open ocean, usually dominant in the region of the ACC (Zielinski and Gersonde, 1997), and is rare when sea ice is present during the growing season (Crosta et al., 2005). This is consistent with the regional patterns in the diatom assemblages in these AP cores (Chapter 7.8); highest abundances are found in the outer continental shelf and oceanic setting of core GC114, decreasing in abundance towards the southern AP (core GC358), where the heavier sea ice conditions produce a growing season that is too short to allow *F. kerguelensis* to bloom. This interpretation is supported by the observation that in several of the WAP cores, *F. kerguelensis* displayed opposite PCA loading to *T. gracilis* (typical cool open ocean species, with a preference for the marginal ice zone). The term "pelagic open ocean" was therefore used to define the ecological preference of *F. kerguelensis* by Crosta et al. (2005), distinguished as being far from the coast and / or not on the continental shelf. Consequently, the presence of *F. kerguelensis* in coastal sediments is used here to indicate increased influence of open ocean conditions (Leventer et al., 1992; Taylor et al., 1997; Crosta et al., 2004; Heroy et al., 2008).

Table 8.1
Habitat types for AP diatom assemblages, based on regional differences in sedimentary diatom assemblage (Chapter 7.8.1 and Chapter 8.1.1); consistent diatom species associations (Chapter 7.8.2); and by interpretation of previously published literature (presented in Chapter 3.5). Preferences for summer sea surface temperature (February SST) and open water / sea ice characteristics taken from Armand et al. (2005) and Crosta et al. (2005).

Sea ice type 1	
Characteristics:	Spring sea ice melt conditions; characterised by a meltwater stratified surface layer associated with a retreating ice edge. - Sea ice: >7.5 months/year; typically 9-11 months/year; winter concentrations 65 – 90 % and summer concentrations variable - February SST: -1.3 to 3.5 °C
Community members:	*F. curta, F. cylindrus, F. sublinearis, F. obliquecostata, F. ritscheri, F. vanheurckii, P. glacialis, T. antarctica* cold rs, *Navicula* spp., *S. microtrias, A. actinochilus, T. tumida,* CRS
Sea ice type 2	
Characteristics:	Autumn sea ice reformation conditions, characterised by high salinities, cold, non-stratified surface waters, with abundant ice crystals and rapid development of closed sea ice. - Sea ice: >6 months/year; winter concentrations >70 % and unconsolidated summer (15 – 40 %) - February SST: 0 to 0.5 °C
Community members:	*T. antarctica* warm rs
Cool open ocean	
Characteristics:	Open water – sea ice interface, with tolerance to withstand varying degrees of sea ice consolidation. - Sea ice: <8.5 month/year; spectrum in winter, from unconsolidated (*R. antennata* f. *semispina*) – to consolidated (*T. gracilis*); whereas in summer, all members display preference for unconsolidated ice (<40 % concentration) - February SST: 1 to 2 °C (<8 °C)
Community members:	*R. antennata* f. *semispina, P. inermis, P. truncata* (environmental parameters for *Proboscia* species inferred through consistent association in sediments with *R. antennata* f. *semispina*), *T. gracilis*
Ice melt	
Characteristics:	Iceberg and spring sea ice melt associated, characterised by localised lenses of cold, low salinity, stratified water and nutrient enrichment (particularly iron), originating from dust accumulation on glacial and sea ice.
Community members:	*E. antarctica* rs
Pelagic open ocean	
Characteristics:	Oceanic preference, particularly for warmer SST and minimal sea ice conditions typically found between winter sea ice edge and Subantarctic Front (although *F. kerguelensis* and *T. lentiginosa* can withstand minimal sea ice). - Sea ice: 0 – 4 months/year (<8 months/year for *F. kerguelensis*); open water in winter – consolidated sea ice (<70 % for *F. kerguelensis*); open water in summer (<20 % sea ice for *F. kerguelensis*); - February SST: 1 – 8 °C (>0 °C and <20 °C)
Community members:	*F. kerguelensis, T. lentiginosa, Thalassiothrix* group, *R. polydactyla*

8.2 Stable isotope and sedimentary pigment analyses

8.2.1 Stable isotopes

The interpretation of stable isotopes as palaeoenvironmental indicators were discussed in Chapter 4.1.3, and potential sources of alteration to the primary signal have been addressed in this study in collaboration with X. Crosta and P. Campagne (pers. comm.); the conclusions of which are presented below.

Early diagenesis and contamination by terrigenous organic matter are believed to have had little impact on the isotopic signal in cores VC306 and VC243, on account of the C_{org}/N_{org} ratios of 7 – 7.6 in core VC306 and 8 – 9 in core VC243 (Figure 7.37 and 7.59), which are relatively close to initial Redfield values of 7 (Redfield et al., 1963). The more pronounced deviation away from the Redfield Ratio in core VC243 may in part reflect a degree of contamination by terrigenous organic matter; a conclusion Pudsey and Evans (2001) reached based on the anomalously old ^{14}C dates in this core. An increase in the C_{org}/N_{org} ratio to ~11 is observed in core VC243 between 700 – 200 yr BP (635 – 170 cal yr BP; 0.6 m and 0.2 m); this deviation suggests contamination may have occurred through this interval, which is supported by a pronounced concentration of clasts at these core depths. The origin and implication of these observations in the uppermost portion of core VC243 are discussed later in section 8.3.5.

The impacts of stratigraphic diatom community changes are also unlikely to have impacted the isotopic signal in either core. Using core VC306 as an example, there is a clear change in the diatom community composition between zones VC306-i and VC306-ii (presented in Chapter 7.3.2), with a dramatic increase in the abundance of pennates of the genus *Fragilariopsis* through zone VC306-ii. Pennates have a geometry that maximise surface area-to-volume ratios, which should lead to higher isotopic fractionation and a lighter (depleted in ^{13}C) $\delta^{13}C_{org}$ signature (Popp et al., 1998). In zone VC306-ii, the reverse is observed; $\delta^{13}C_{org}$ is heavier (enriched in ^{13}C). This is also seen in the upper portion of zone VC243-ii, where a slight increase in *Fragilariopsis* species abundance is not matched by a lighter $\delta^{13}C_{org}$ signature. For this reason, species-specific fractionations are not considered to be driving the isotopic records.

Unfortunately, there is no way of controlling for active carbon uptake processes and carbon concentration mechanisms from fossil assemblages. Further, it is also difficult to gauge whether the nitrate source has changed from nitrates (NO_3^-) to ammonia (NH_4^+),

which would occur if decomposition was acting to break down the organic molecules into non-organic substances.

Given that the potential sources of alteration (presented in Chapter 4.1.4) seem secondary, the Holocene isotopic records from cores VC306 and VC243 are interpretated as proxies for the relative utilisation of nutrients and primary production. Specifically, isotopic records track the balance between input by water masses for both carbon and nitrogen, plus exchanges at the atmosphere-ocean interface for CO_2, and uptake by phytoplankton. Based on these assumptions, detailed isotopic interpretations are discussed in tandem with diatom-based results for the two specific sites in section 8.3.3 for core VC306 and section 8.3.5 for core VC243.

8.2.2 Sedimentary pigments

The changing distribution of pigments derived from primary producers reflects changes in the overall community composition and ecology of surface waters. The ecological affinities and environmental interpretation assigned to individual pigments preserved in core VC243 are detailed in Table 8.2.

Table 8.2
Affinities and environmental interpretation of pigments preserved in core VC243. Modified from Jeffrey et al. (1997) and Hodgson et al. (2003). Organisms unlikely to be important at this core site are quoted in brackets.

Pigment	Abbreviation	Affinity / Interpretation
Chlorophyll *a*	Chl *a*	All photosynthetic algae
Phaeophorbide *a*	Phorb *a*	Chl *a* derivative; general marine detritus, zooplankton faecal pellets
Pyrophaeophorbide *a*	Pphorb *a*	Marine detritus, zooplankton faecal pellets
Phaeophytin *a*	Phe *a*	Chl *a* derivative; general algal detritus
Pyrophaeophytin *a*	Pphe *a*	Derivatives of *a*-phorbins; zooplankton faecal pellets
Purpurin 7	Pup-7	Chlorophyll oxidation product
Purpurin 18	Pup-18	Chlorophyll oxidation product
Fucoxanthin	Fuco	Major pigments in diatoms, prymnesiophytes, (brown seaweeds), (raphidophytes), some dinoflagellates
Diatoxanthin	Diatox	Diatoms, prymnesiophytes, chrysophytes, dinoflagellates
Monadoxanthin	Monadox	Cryptophytes

8.3 Holocene palaeoclimate reconstructions for each core locality

8.3.1 GC114

The record for core GC114 spans the Mid–Late Holocene (~3360 yr BP – present; 3600 cal. yr BP – present). Comparing core GC114 with some of the more coastal sites along the WAP, two general observations are worth highlighting (Figure 7.2): (1) total diatom abundance is lower; (2) the variability of diatom abundance is more subdued, with no distinct intervals of elevated primary production or dramatic shifts in the diatom assemblage. The first observation can be explained by the exposed outer shelf setting of this core site; situated in a ~20 km wide trough, connecting waters from the shelf break with Bransfield Strait, means conditions that promote large *Chaetoceros* species blooms (stable, well stratified surface water) are less likely to develop. The second observation either suggests that the site makes core GC114 insensitive to regional changes in production, potentially due to consistent warm CDW influences; or that Late Holocene environmental changes are not well preserved in the sediment record. Nevertheless, subtle environmental changes are evident in the Mid–Late Holocene; PCA analysis of the diatom assemblage divides the stratigraphy into two intervals. Furthermore, total diatom abundance displays distinct cycles, with a periodicity of ~440 – 660 ^{14}C years (Figure 7.3); different to those observed in magnetic susceptibility, organic carbon, nitrogen and diatom data by Leventer et al. (1996) (#25; Table A1.1 and Figure A1.1) and Bárcena et al. (1998; 2002; 2006) (#1, #7, #8 and #10) (200 – 300 years), attributed to solar forcing and reduction in sunspot activity. This suggests either a different forcing mechanism is driving total diatom abundance in core GC114 or that the cycles represent harmonics of the initial sunspot activity cycle.

- **Zone GC114-i: Mid-Late Holocene transition**
  ^{14}C age = 3360 – 1220 yr BP
  Cal. Age = 3600 – 1090 cal. yr BP
  Depth = 3.3 – 1.3 m

This zone post-dates the Mid-Holocene climatic optimum identified in this area of Bransfield Strait by Heroy et al. (2008; #14). Nevertheless, it is still characterised by comparatively high diatom primary production, inferred from relatively low MS values (Figure 6.3) and generally higher total diatom abundance (particularly between 3360 – 2620 yr BP; 3600 – 2750 cal. yr BP; 3.3 – 2.8 m) (Figure 7.2). This zone therefore marks a period of transition from the end of the Mid-Holocene climatic optimum in Bransfield Strait, with the diatom assemblage progressively changing through time. The sequence of events starts with sea ice type 2 conditions and cool open waters between

3360 – 2620 yr BP (3600 – 2750 cal. yr BP; 3.3 – 2.8 m), based on elevated abundances of *T. antarctica* warm rs and *T. gracilis* var. *gracilis* (Figure 7.4). As suggested from other datasets in this area (e.g. Abelmann and Gersonde, 1991; Bárcena et al., 1998; Heroy et al., 2008), these species possibly suggest intrusion of colder Weddell Sea waters into Bransfield Strait and greater connectivity with the northern EAP. Between 1870 – 1220 yr BP (1800 – 1090 cal. yr BP; 2 – 1.3 m) (Figure 7.4) increased contribution from *Proboscia* and *Rhizosolenia* species suggests the onset of changes in large scale water column structure, with deeper mixing and reduced surface water stratification during the growing season. Both these genera have an ability to adjust their buoyancy and tolerate low light levels (Kemp et al., 2000), enabling them to survive at deeper water depths. Reduced surface water stratification and deeper mixing could originate from: (i) reduced meltwater inputs from a decline in spring sea ice melt over the core site; (ii) increased storm frequency; or (iii) increased strength of the Bransfield Strait Surface Current (described in Chapter 2.6.1). There is also an increased input of terrigenous or magnetic-rich material to the sea floor between ~1500 – 750 yr BP (1410 – 700 cal. yr BP; 1.6 – 0.8 m), shown by increased MS values (Figure 6.3), possibly caused by: (i) increased iceberg frequency, resulting in more "rain out" of terrigenous material; (ii) increased storm frequency and precipitation and / or glacier melt; or (iii) an increase in atmospheric sourced dust particles. The combined evidence of deep mixing and increased terrigenous particles means the most likely forcing mechanisms are increased storm frequency and precipitation; consistent with a transition into Late Holocene Neoglacial.

- **Zone GC114-ii: Late Holocene Neoglacial**
  ^{14}C age = 1220 – 0 yr BP
  Cal. Age = 1090 – 0 cal. yr BP
  Depth = 1.3 – 0 m

This zone is initially characterised by a period of increasing surface water stratification between 1220 – 560 yr BP (1090 – 590 cal. yr BP; 1.3 – 0.6 m), evidenced from increased CRS relative abundance and increased abundance of typical sea ice type 1 species (e.g. *F. curta*, *F. cylindrus* and *T. antarctica* cold rs). This assemblage reflects seeding from sea ice and subsequent dominance in the spring meltwater stratified surface waters, suggesting an increased influence of seasonal sea ice cover over the core site. There is also a clear trend of increasing abundance of *T. gracilis* species from 1220 yr BP (1090 cal. yr BP; 1.3 m) towards the present, indicating the influence of the marginal sea ice zone, which would have oscillated over the core site to the same

rhythm as the seasonal sea ice cycle. From 560 yr BP (590 cal. yr BP; 0.6 m) to the present day, terrigenous inputs have decreased, based on the reduction of MS values (Figure 6.3). The origin of reduced terrigenous inputs could be: (1) reduction in iceberg frequency due to more extensive sea ice cover; (2) reduced run-off from the South Shetland Islands, as climatic cooling manifests itself in the expansion of ice fields and reduced calving from ice fronts. Of these, increased sea ice cover, both spatially and temporally, would produce the observed reduction in total diatom abundance, as the length of the growing season at this core site is protracted. This suggests that a climatic cooling signal was sustained through the Late Holocene in Bransfield Strait.

8.3.2 GC047

Sediment core GC047 provides a complete Holocene palaeoclimate record (~10750 yr BP – present; 12720 cal. yr BP – present). It is not possible to pin-point the exact time of ice sheet retreat at the core site as coring did not penetrate into glacial till. However, Pudsey et al. (1992) propose that ice sheet recession west of Anvers Island commenced before 11000 yr BP and at the nearby Palmer Deep Basin (#24) open marine / neretic deposition commenced at 13180 cal. yr B.P (~11300 yr BP) (Domack et al., 2001; Sjunneskog and Taylor, 2002). Palmer Deep is situated landward of core site GC047, which would suggest retreat of the ice sheet over core site GC047 (minimum age 10750 yr BP; 12720 cal. yr BP) pre-dates that of Palmer Deep. This does not support a recent deglaciation model ("calving bay re-entrant") developed for several bays on the East Antarctic margin, proposing earlier and more rapid ice retreat in deep basins and troughs, with ice grounded on surrounding shallower bathymetric areas (Leventer et al., 2006), and also proposed as a plausible mechanism for deglaciation of the Palmer Deep Basin (Domack et al., 2006).

- **Zone GC047-i: Immediate post-deglaciation and Early Holocene warmth**
  ^{14}C age = 10750 – 9870 yr BP
  Cal. Age = 12720 – 11280 cal. yr BP
  Depth = 3.8 – 3.5 m

Sedimentology, MS (Figure 6.4), diatom absolute abundance (Figure 7.11), community structure (Figure 7.12) and preservation all reveal that immediately following ice sheet retreat, the marine environment was characterised by very high diatom primary production, recorded in the sediment by high diatom absolute abundance, with the preservation of laminae, and extremely low MS values. A distinctive spike in total diatom abundance and CRS absolute abundance between 10400 – 10160 yr BP (12330

– 11830 cal. yr BP; 3.68 – 3.6 m) (Figure 7.11), implies large blooms of *Chaetoceros* spp. exploited the stable, stratified and nutrient-rich waters following ice sheet retreat, formed by increased sea ice melt and glacial run-off. Such intense diatom accumulation immediately following deglaciation has been observed in other Antarctic marine settings (e.g. Leventer et al., 2002; Taylor et al., 1999) and is discussed further in section 8.4.1.1. The CRS ooze is coincident with peaks in the relative abundance of *Corethron pennatum*, several *Fragilariopsis* species (*F. cylindrus*, *F. rhombica*, *F. ritscheri* and *F. vanheurckii*), together with grouped *Pseudonitzschia* species and *E. antarctica* vegetative valves (Figures 7.12 and A2.4). This assemblage is very similar in composition to the deglacial "Assemblage 1" described by Stickley et al. (2005) from the East Antarctic margin (#136; Iceberg Alley) and "Laminae Type 2" described by Maddison et al. (2006) from the East Antarctic margin (#108; Mertz Ninnis Trough). Through analysis of numerous seasonally laminated sediments, Stickley et al. (2005) and Maddison et al. (2005; 2006) reconstructed discrete productivity events, with the assemblages mentioned above indicative of deglacial spring blooms, characterised by sea ice melt, stratification, exceptionally high primary production and rapid opal flux to the seafloor. A similar Early Holocene environmental reconstruction is therefore proposed for core site GC047, with sea ice type 1 conditions prevailing. Throughout this interval, preservation is very good; numerous *Fragilariopsis* species are still in colonies, occasionally delicate *Rhizosolenia* girdle bands and *C. pennatum* spines are present and the abundance of vegetative valves (*E. antarctica* vegetative, *S. microtrias* vegetative and *T. antarctica* vegetative) reaches relatively high abundance (Figure A2.4). This is consistent with extremely high primary productivity, with efficient and rapid export of diatoms from the surface waters to the sea floor.

- **Zone GC047-ii: Occurrence of a "climatic reversal"?**
  ^{14}C age = 9870 – 7680 yr BP
  Cal. Age = 11280 – 8280 cal. yr BP
  Depth = 3.5 – 2.75 m

The transition into this zone is marked by a rapid decrease in primary production, recorded by lower total diatom abundance, CRS absolute and relative abundance (Figure 7.11), together with increased inputs of terrigenous particles, recorded by a dramatic rise in MS values (Figure 6.4). The reduction in diatom productivity is likely to result from reduced surface water stratification, which is controlled by the volume of meltwater inputs, the strength and distribution of ocean currents and vigour of surface mixing by storms. Breakdown in stratification at the transition into this zone could have

resulted from one of two conflicting scenarios: (1) sustained warming trend – reduced meltwater inputs as the proximal ice sheet retreated sufficiently towards the AP coastline, together with disintegration of ice present in fjords and inland straits (e.g. Gerlache Strait), leading to reconfiguration and increased vigour of coastal currents; (2) climatic cooling – reduced meltwater inputs due to either a stand-still event of the ice front, or the expansion of sea ice cover and duration over coastal sites. Incorporating the MS data of increased terrigenous inputs and diatom assemblage data, the second scenario is most likely, with a resurgence of ice fronts and associated increase in iceberg frequency from 9870 yr BP (11280 cal. yr BP; 3.5 m). The non-CRS assemblage (Figure 7.12) in this zone is dominated by *T. antarctica* warm rs, suggesting presence of sea ice type 2 conditions, together with increased abundance of *T. gracilis* var. *expecta, T. tumida* , *Rhizosolenia* and *Proboscia* species, whose preference is for cool open water. Typical sea ice type 1 taxa (*F. curta* and *F. cylindrus*) are not in high abundance, nor is there a particularly strong pelagic open ocean signal (*F. kerguelensis*). Instead, the proxies suggest the presence of well-mixed, supercooled shelf waters. This is supported by higher abundances of *E. antarctica* rs, specifically the symmetric, polar form, from ~9000 yr BP (~10200 cal. yr BP; 3.2 m) and bridging the transition into GC047-iii. This species is likely to be exploiting the cool waters derived from the close proximity of the ice sheet and / or localised meltwater lenses associated with freshly calved icebergs; both consistent with increased inputs of terrigenous particles.

- **Zone GC047-iii: Mid-Holocene climatic optimum into Mid-Late Holocene transition**
  ^{14}C age = 7680 – 2260 yr BP
  Cal. Age = 8280 – 2260 cal. yr BP
  Depth = 2.75 – 0.8 m

From the onset of this zone towards ~5490 yr BP (6300 cal. yr BP; 2 m), total diatom abundance, CRS absolute and relative abundance increase steadily (Figure 7.11), indicating the return of more productive, stable waters offshore from Anvers Island and ameliorating climatic conditions. Regular seasonal cycles of sea ice are established and there is greater oceanographic connection with typically outer continental shelf water masses, specifically UCDW. These interpretations are based on the equal contribution of *F. curta* (typical sea ice type 1 species) and *F. kerguelensis* (typical pelagic open ocean species) to the non-CRS assemblage (Figure 7.12). Higher absolute and relative abundances of *F. curta*, *F. cylindrus* and *E. antarctica* rs, particularly between 6950 – 5190 yr BP (7780 – 5960 cal. yr BP; 2.5 – 1.9 m), indicate extended spring-like

conditions, characterised by meltwater-driven stratification of the water column, and sustained nutrient fluxes from melting glaciers and sea ice. Further, a much higher percentage of *E. antarctica* var. *antarctica* (asymmetric, possible sub-polar form) is observed around 5490 yr BP (6300 cal. yr BP; 2 m). Although the environmental preference of this form is still debated, it has previously been used to infer the southward incursion of warm, northern surface water into coastal AP settings (Leventer et al., 2002; Smith et al., 2007a); a similar oceanographic interpretation is proposed for offshore Anvers Island at ~5490 yr BP (6300 cal. yr BP; 2 m). Minor diatom fragmentation and good preservation of delicate diatom frustules at this time (Figure A2.4) also suggests rapid transport of the diatoms from surface waters to the seafloor.

From 5190 yr BP (5960 cal. yr BP; 1.9 m), the environmental reconstruction suggests shorter seasonal duration of typical sea ice type 1 conditions, being progressively replaced by longer periods of seasonally open water conditions. This suggestion is based on the decline in absolute abundance of sea ice type 1 species and *E. antarctica* rs (Figure 7.12), representing the diminished influence of melting glacier and sea ice, and reduced nutrient fertilisation processes. *F. kerguelensis* absolute and relative abundance remains high through this upper interval, inferring a continued influence of outer shelf waters (UCDW). This shift from sea ice type 1 to more prolonged seasonally open ocean conditions could represent a progressive southward and landward migration of the marginal sea ice zone, oscillating to the south of Anvers Island by 5190 yr BP (5960 cal. yr BP; 1.9 m) and signify peak Mid-Holocene climatic optimum conditions for this core locality. The decline in total diatom, CRS absolute and relative abundance from 3950 yr BP (4400 cal. yr BP; 1.4 m) (Figure 7.11), likely to be driving the associated increase in MS values (Figure 6.4), is thought to represent the start of the transition into a Late Holocene Neoglacial. This transitional period is characterised by a reduction in primary production, likely linked to reduced surface water stability. *F. kerguelensis* absolute and relative abundance also diminishes after 3950 yr BP (4400 cal. yr BP; 1.4 m), suggesting that (i) seasonally pelagic open ocean conditions were becoming more distant from the core site and / or present for a shorter duration in the annual cycle of sea ice advance and retreat; and (2) that incursions of UCDW were potentially decreasing in volume and frequency.

- **Zone GC047-iv: Late Holocene Neoglacial**
  ^{14}C age = 2260 – 0 yr BP
  Cal. Age = 2260 – 0 cal. yr BP
  Depth = 0.8 – 0 m

This zone is characterised by proxies indicative of more turbulent oceanographic conditions, with increased storm frequency and wave action potentially causing reduced surface water stratification and deeper mixing. Sea ice type 1 is still present, highlighted by the stabilised, mid-range abundance values of *F. curta*, together with increased abundances of *S. microtrias* rs, *A. actinochilus* and *T. antarctica* cold rs (Figure 7.12); however, extended periods of surface stratification are not considered likely, due to the active and rapid disintegration of pack ice and deeper mixing of the water column in the stormier conditions, implied by the reduction in total diatom abundance, CRS absolute and relative abundance (Figure 7.11). The remainder of the non-CRS assemblage is similar in structure to zone GC047-ii (Figure 7.12). There is an increased abundance of *Rhizosolenia* and *Proboscia* species; abundance of *T. gracilis* var. *gracilis* declines, being replaced by *T. gracilis* var. *expecta*. These cool open water species suggest that the continental shelf offshore Anvers Island was bathed in well-mixed cool shelf waters, potentially developed through increased influence of cold Weddell Sea Waters around the tip of the AP. This could imply greater oceanographic connection between the northern WAP (cores GC047 and GC114) and the northern EAP in the Late Holocene.

8.3.3 VC306

The full deglaciation sequence preserved at the base of core VC306 includes the transition from sub-ice sheet terrigenous-rich glacial tills to seasonally open marine diatomaceous muds. The gradual decrease in MS values up-core (Figure 6.5) reflects the retreat of the ice sheet landward, as terrigenous sedimentary inputs diminish. The minimum age for onset of marine deposition for this Marguerite Bay site is 10150 yr BP (11800 cal. yr BP; 1.8 m). The ensuing sedimentation history of this site covers the Mid-Holocene and transitional period into the Late Holocene. The loss of core top material (discussed in Chapter 6.2.4) means that the last 2100 yr BP (2080 cal. yr BP) of this palaeoclimate record are missing. The Holocene record for this site is divided into two zones, with distinct differences in diatom assemblage and stable isotope signals. As discussed in section 8.2.1, stable isotope results are used as proxies for the relative utilisation of nutrients, i.e. the balance between input by water masses and uptake by phytoplankton.

- **Zone VC306-i: Deglaciation – Early Holocene**
  ^{14}C age = 10150 – 7580 yr BP
  Cal. Age = 11800 – 8390 cal. yr BP
  Depth = 1.8 – 1.1 m

The marine environment at core site VC306 following ice sheet retreat is characterised by low diatom primary production, based on the low total diatom and CRS absolute abundance (Figure 7.20), together with low C_{org} and N_{org} contents (Figure 7.29). Evidence of an immediate post-retreat peak in diatom production seen further north at core site GC047 is notably absent. The trough setting of core site VC306 could mean that the ice sheet retreated earlier from this locality, yet ice fronts remained in close proximity, grounded on surrounding bathymetric highs; a similar scenario to the "calving bay re-entrant" model (Leventer et al., 2006). This situation would explain the high relative abundance of *T. antarctica* warm rs (Figure 7.21), with sea ice type 2 conditions developing through interaction with the surrounding grounded ice sheet. Further, the constricted shape of the bay, bound by Adelaide Island to the north and Alexander Island to the south, together with the shallowing offshore profile, may have prevented calved material and icebergs from the collapsing ice sheet and nearby George VI Ice Shelf from exiting the bay. Using epishelf lake sediments (#55 and #56), Smith et al. (2007a) dated the onset of George VI Ice Shelf retreat to 8170 yr BP (9600 cal. yr BP) and its partial or complete reformation to 7300 yr BP (7730 cal. yr BP). Building on the study of Smith et al. (2007a), Roberts et al. (2008) analysed clast provenance in the same and additional epishelf lake records (#57 and #58), revealing that during periods of ice-shelf loss, the lithological assemblage was dominated by a range of exotic clasts, presumed to be transported by iceberg rafting processes. The high abundance of *E. antarctica* rs from 9500 yr BP (10860 cal. yr BP; 1.6 m) (Figure 7.21), with the dominant form being *E. antarctica* var. *recta* (symmetrical, polar), represents this ice-dominated environment, with development of localised meltwater lenses and high nutrient inputs from melting glacier and sea ice. Although nutrient inputs are suggested to have been elevated, overall productivity still remains low through this zone due to other limiting factors (e.g. surface water instability, consolidated ice cover). This presence of multi-year sea ice and stagnating icebergs may have further prevented a major increase in production and instead facilitated the development of a cool shelf water-dominated regime, exemplified by increased relative abundance of typical cool open ocean species (both varieties of *T. gracilis*, *T. tumida* and *A. actinochilus*) (Figures 7.21 and A2.6). Addition of ice has been shown by modelling to cool surface waters by three distinct processes: heat conduction from water to ice that served to warm the ice; absorption of latent heat during the phase change; and subsequent mixing of the meltwater (which has a temperature equal to the freezing point) with the ambient water

(Jenkins, 1999). The modern-day seasonal cycle of sea ice advance and retreat was not developed in Marguerite Bay during this zone and surface water stratification was poorly developed, inferred from the low abundances of typical sea ice type 1 species (*F. curta – F. cylindrus*) (Figure 7.21).

Carbon and nitrogen stable isotope results provide further details about the oceanographic conditions during the process of ice sheet retreat in Marguerite Bay (Figure 7.29). $\delta^{15}N_{org}$ typically has an inverse relationship with diatom abundance and productivity, suggesting high nutrient utilisation. The notion of greater nutrient utilisation at a time when overall productivity was low requires nutrient inputs to be much smaller, suggesting either a smaller volume of upwelling water reaching the surface or the presence of different water masses (with low NO_3^- pool). The cool shelf water-dominated regime, characterised by the presence of persistent ice and a pervasive cool water cap may have restricted oceanographic circulation and prevented nutrient-rich UCDW encroaching onto the continental shelf (Figure 8.3). The lack of warm UCDW influences may have provided a positive feedback, further accentuating the cooling of surface waters in Marguerite Bay and dominance of multi-year sea ice.

- **Zone VC306-ii: Mid-Holocene climatic optimum into Late Holocene transitional period**
  ^{14}C age = 7580 – 2100 yr BP
  Cal. Age = 8390 – 2080 cal. yr BP
  Depth = 1.1 – 0 m

The transition into this zone represents a distinct change in oceanographic, particularly sea ice, conditions in Marguerite Bay. At 7580 yr BP (8390 cal. yr BP; 1.1 m), total diatom abundance, CRS absolute abundance (Figure 7.20) and carbon and nitrogen stable isotope contents (Figure 7.29) increase rapidly, plus there are very distinctive changes in the diatom assemblage and isotopic values of these two elements (Figures 7.21 and 7.29, respectively). The rapid changes in diatom community structure in response to changing environmental conditions are believed to result from the establishment of regular seasonal sea ice in Marguerite Bay and surface water stability linked to the reformation of George VI Ice Shelf (Smith et al., 2007a). Although elevated diatom abundance could be a product of reduced dilution by terrigenous particles, based on the rapidity of changes in the diatom assemblage, it is proposed that this is primarily a productivity signal, linked to the establishment of regular seasonal sea ice cycles and associated surface water stability. The marginal sea ice zone is therefore inferred to be oscillating in Marguerite Bay during the Mid-Holocene, with spring

meltwater stratified surface waters being a common feature. This inference is based on the dramatic increased absolute and relative abundance of sea ice type 1 species (*F. curta*, *F. cylindrus* and *T. antarctica* cold rs) at 7580 yr BP (8390 cal. yr BP; 1.1 m) (Figure 7.21). Associated with this, increased abundances of *P. inermis* and *P. truncata* suggests that cool, and more importantly, open ocean conditions were present in Marguerite Bay during part of the year. These cool waters could be derived from the Antarctic Peninsula Coastal Current (observed in the modern-day circulation of Marguerite Bay (Moffat et al., 2008; Chapter 2.6.2)), entering Marguerite Bay when Mid-Holocene sea ice extent was at its annual minimum. Further, increased absolute abundance of *F. kerguelensis* through this zone suggests increased influence of typically outer shelf water masses, specifically UCDW. The dominance of this water mass could provide a driving mechanism for the rapid environmental changes in Marguerite Bay at 7580 yr BP (8390 cal. yr BP; 1.1 m), now experiencing a UCDW-dominated regime (Figure 8.3). This scenario is supported by the carbon and nitrogen stable isotopic signature in this zone (Figure 7.29). $\delta^{15}N_{org}$ becomes less positive up-core, when productivity is seen to increase. This suggests the balance between nutrient inputs (size of NO_3^- pool) and outputs (utilisation by phytoplankton) has shifted towards a larger nutrient supply relative to phytoplankton uptake. The increased supply of nutrients is potentially explained by intensified UCDW intrusion onto the continental shelf in Marguerite Bay, contrasting with the shelf water-dominated regime in zone VC306-i. The presence of UCDW would prevent multi-year ice becoming established, in favour of a recurrent cycle of sea ice advance and retreat. $\delta^{13}C_{org}$ becomes dramatically less negative at the transition into zone VC306-ii, remaining enriched through the rest of zone VC306-ii. This enrichment results from higher demand (through increased productivity) on a relatively constant $CO_{2(aq)}$ pool. The $CO_{2(aq)}$ pool is much less variable than NO_3^- due to active gas exchange at the ocean-atmosphere interface when not covered by perennial sea ice; a similar trend to that observed on glacial-interglacial timescales (Crosta and Shemesh, 2002). This suggestion of active gas exchange provides another argument for the establishment of an annual cycle of sea ice cover and open ocean conditions during spring and summer in Marguerite Bay during the Mid-Holocene.

The transitional period into the Late Holocene Neoglacial is also recorded in this zone, characterised by lower primary production and representing more unstable surface water conditions. Between 3130 – 2100 yr BP (3360 – 2080 cal. yr BP; 0.2 – 0 m), total

diatom abundance, CRS absolute and relative abundance declines (Figure 7.20), as do N_{org} and C_{org} contents (Figure 7.29). Diatom assemblage data imply a progressive increase in perennial sea ice cover, with typical sea ice type 1 assemblage (*F. curta – F. cylindrus*) declining towards 2100 yr BP (2080 cal. yr BP; 0 m) (Figure 7.21). Both *T. antarctica* warm rs and *T. antarctica* cold rs record increasing absolute and relative abundance throughout zone VC306-ii, out-competing other diatom species as sea ice type 2 conditions, decreased sea surface temperatures and increased multi-year ice coverage became established in Marguerite Bay towards 2100 yr BP (2080 cal. yr BP; 0 m). This is proposed to mark the beginning of the Late Holocene Neoglacial in Marguerite Bay.

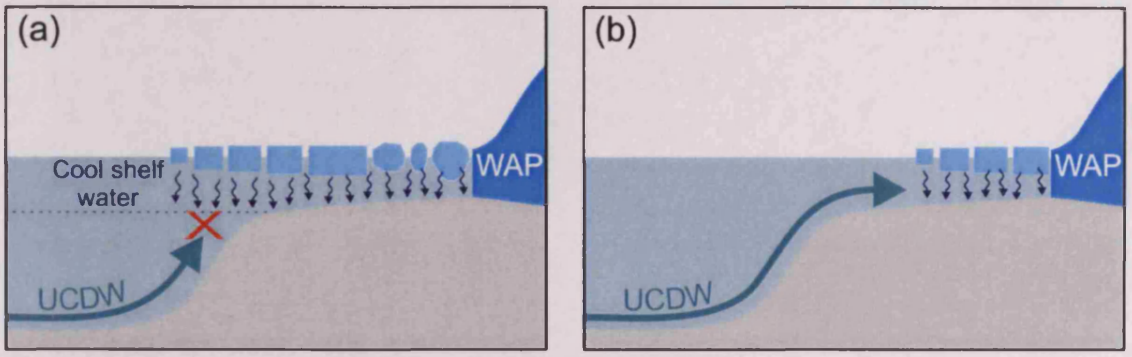


Figure 8.3
Oceanographic variability in Marguerite Bay; competitive interactions between cool shelf waters and warm nutrient-rich UCDW.
(a) Cool shelf water-dominated regime (zone VC306-i). Persistent icebergs and multi-year sea ice acts to cool surface waters and active surface water overturning develops. This may have restricted large-scale oceanographic circulation and prevented warm nutrient-rich UCDW flooding the shelf.
(b) UCDW-dominated regime (zone VC306-ii). Presence of UCDW on the shelf (discussed in section 8.5.2) prevents multi-year ice becoming established and the recurrent annual cycle of sea ice advance and retreat is established in the Mid-Holocene.

8.3.4 GC358

Compared to other cores used in this investigation, total diatom abundance in core GC358 is significantly lower (Figure 7.30), suggesting subdued primary production. The reason for this lower diatom productivity in the southern Bellingshausen Sea is likely to be associated with an increased duration and extent of sea ice at this more southerly latitude. The low biogenic sedimentary inputs also help explain the comparably thin accumulation of Holocene sediments in this area. Nevertheless, the palaeoclimate record provided by core GC358 contains the full sequence of ice sheet retreat, including the transition from sub-ice sheet terrigenous-rich glacial tills to

seasonally open marine diatomaceous muds. Inconsistencies in the chronology of cores from the southern Bellingshausen Sea (discussed in Chapter 6.2.5) means that providing a precise deglaciation date is not possible. However, based on the chronological model for core GC358, removal of grounded ice from this core site is proposed to have occurred at 12650 yr BP (15020 cal. yr BP), although it could have been as late as ~7000 yr BP (~7840 cal. yr BP) (Hillenbrand et al., 2007), based on the deglaciation sediment transition in a proximal core (GC359). The gradual decrease in MS values up-core (Figure 6.6) reflects the retreat of the ice sheet landward, as terrigenous sedimentary inputs diminish.

- **Zone GC358-i: Deglaciation – Early Holocene**
  ^{14}C age = 12650 – 8600 yr BP
  Cal. Age = 15020 – 9570 cal. yr BP
  Depth = 0.75 – 0.5 m

This zone records the development of the marine environment in Ronne Entrance following ice sheet retreat; environmental changes at this locality are proposed to have been slower-paced compared to more northerly WAP localities. The initial retreat of grounded ice from this core site at 12650 yr BP (15020 cal. yr BP; 0.75 m) is likely to have been marked by large nutrient and meltwater inputs, together with increased light levels. As in core GC047, these conditions promoted extremely high primary production, with initial post-deglaciation sedimentation of a CRS ooze (Figure 7.30) and elevated abundances of numerous *Fragilariopsis* species (particularly *F. cylindrus, F. separanda, F. sublinearis* and *F. vanheurckii*), together with *Navicula* species (Figure 7.31). High primary production was short-lived, as the initial influx of nutrients was quickly exhausted and not replenished; the remainder of this zone is characterised by lower diatom productivity, highlighted by reduced total diatom abundance and CRS absolute abundance. However, relative abundance of CRS remains high (Figure 7.30b) suggesting that although productivity was lower, surface stratification was occurring, caused by a steady supply of meltwater from slow ice sheet retreat and / or periodic disintegration of the sea ice pack. The latter suggestion is based on higher abundances of sea ice type 1 species throughout this zone (particularly *F. curta*, *F. cylindrus*, *F. obliquecostata* and *T. tumida*) (Figures 7.31 and A2.8), representing spring meltwater conditions, together with increased abundance of cool open ocean species (*P. truncata*, *P. inermis* and *T. gracilis* var. *expecta*), representing the development of cool shelf waters, through interaction with the proximal grounded ice and ice shelves at times when open ocean conditions were more extensive.

Towards the transition into zone GC358-ii, glacier-derived meltwater and nutrient fluxes are proposed to have increased, representing a re-initiation of ice sheet retreat. This is based on the dramatic increase in *E. antarctica* rs absolute and relative abundance (Figure 7.31). This interval coincides with a phase of more rapid ice sheet retreat on the WAP (e.g. Marguerite Bay and Anvers Trough; discussed fully in section 8.4.1.1) and collapse of the George VI Ice Shelf between 8170 and 7300 yr BP (9600 – 7730 cal. yr BP) (Smith et al., 2007a). The *E. antarctica* rs assemblage may suggest that retreat of the George VI Ice Shelf also occurred at the southern exit of George VI Sound in the southern Bellingshausen Sea, as well as the northern one (Marguerite Bay). Several highly asymmetrical (possible sub-polar) forms of *E. antarctica* var. *antarctica* are noted around 9460 yr BP (10710 cal. yr BP; 0.55 m), coincident with a period of lower absolute and relative abundance of typical sea ice type 1 species (*F. curta* and *F. cylindrus*) between 10320 – 7730 yr BP (12210 – 8510 cal. yr BP; 0.6 – 0.45 m). Both these observations allude to an environment with minimal seasonal sea ice (type 1), under the influence of outer shelf oceanographic inputs, driving active melt of glacial ice. *E. antarctica* rs dominates the non-CRS diatom assemblage in the southern Bellingshausen Sea between 10320 – 4290 yr B.P (12210 – 4870 cal. yr BP; 0.6 – 0.25 m). The extended duration of the *E. antarctica* rs peak (~8000 years, compared to ~3600 years for core VC306) may be a function of the more southerly latitude of core site GC358, promoting the longevity of ice within the confinements of the Ronne Entrance. Again similar to core VC306, the period of elevated *E. antarctica* rs abundance bridges the transition into zone GC358-ii.

- **Zone GC358-ii: Mid-Holocene climatic optimum into Late Holocene climatic deterioration**
  ^{14}C age = 8600 – 0 yr BP
  Cal. Age = 9570 – 0 cal. yr BP
  Depth = 0.5 – 0 m

Reconstructions for this zone suggest a comparatively less ice-dominated regime than the previous zone, exposed to more open ocean and outer shelf oceanographic influences during the diatom growing season. Absolute abundance of CRS remains reasonably constant through this zone (Figure 7.30a), whereas relative abundance decreases (Figure 7.30b), suggesting CRS productivity events (characterised by strong stratification) were becoming less common and environmental conditions instead favoured non-bloom species. As discussed for zone GC358-i, this non-CRS assemblage is dominated by *E. antarctica* rs until 4290 yr BP (4870 cal. yr BP; 0.25 m) (Figure

7.31), representing glacial ice stagnation due to the southerly latitude of this core site. From this data, the Ronne Entrance is proposed to have experienced less extensive sea ice and more frequent and / or extensive periods of open water between 8600 – 1700 yr BP (9570 – 1620 cal. yr BP; 0.5 – 0.1 m), suggesting prolonged climatic optimum conditions. Although *Fragilariopsis* species (particularly *F. curta*, *F. obliquecostata*, *F. vanheurckii*) still record moderate contributions to the non-CRS assemblage, their absolute and relative abundance is reduced compared to zone GC358-i and the uppermost 0.1 m of this zone (1700 yr BP – present; 1620 cal. yr BP – present) (Figure 7.31). *F. kerguelensis* also displays elevated absolute and relative abundances through this zone, suggesting an open ocean influence and possible intrusion of UCDW. The inference of open ocean influences is further supported by the marked increased abundance of *Rhizosolenia* species, observed in both *R. antennata* f. *semispina* and *R. polydactyla* f. *polydactyla*, at 7730 yr BP (8512 cal. yr BP; 0.45 m). These two species have slightly different environmental preferences; *R. antennata* f. *semispina* being a cool open ocean species linked to the marginal ice zone, whereas *R. polydactyla* f. *polydactyla* being a pelagic open ocean species, preferring warmer temperatures and very little sea ice.

Another environmental change occurs at 1700 yr BP (1620 cal. yr BP; 0.1 m), with a return to cooler climatic conditions in the southern Bellingshausen Sea and an expansion in the extent and seasonal persistence of sea ice, highlighted by the dramatically increased absolute and relative abundance of sea ice type 1 species (particularly *F. curta*, *F. cylindrus*, *F. obliquecostata*, *F. vanheurckii*, *A. actinochilus* and *S. microtrias* rs) (Figure 7.31). This is potentially a regional reflection of the onset of the Late Holocene Neoglacial.

8.3.5 VC243 and VC237

The discussion of these two cores is combined because both lie in the Prince Gustav Channel (PGC) and by splicing the records a near full Holocene history is documented. Based on the ^{14}C chronology, discussed in Chapter 6.2.6, there is approximately 1400 ^{14}C years of overlap between the records, with core depths between 4.6 – 5.9 m in VC243 equivalent in age to core depths 2.1 – 3 m in VC237. The base of post-glacial deposition was not reached in the longer record (VC237), so the initial period of sub-ice shelf deposition is not documented. The onset of post-glacial marine deposition in PGC

is proposed to have occurred between 16700 – 11500 yr BP (19950 – 13400 cal. yr BP), based on sedimentological analyses of a suite of cores by Pudsey et al. (2006).

Diatom assemblage data in this study is combined with previous analyses of ice rafted debris provenance (Pudsey and Evans, 2001; Pudsey et al., 2006) to reveal differing ice shelf histories and ocean conditions between core sites. It is difficult from diatom assemblage data to differentiate between ice shelf and summer (permanent) sea ice deposition, so the inferences about the timing of ice shelf retreat relies on the previously published provenance work (Pudsey and Evans, 2001; Pudsey et al., 2006). As Pudsey et al. (2006) observed, no distinct coarse grained layers from the influx of terrigenous material are present (Figures 6.7 and 6.8), suggesting ice shelf collapse was not instantaneous. This is supported by the observation that each of the transitions in diatom data are subtle (Figures 7.38, 7.40, 7.51 and 7.53) suggesting that the changes in ice shelf stability during the Holocene were not sudden events. Stratigraphic differences in diatom community structure record changes in regional oceanography, which are supported by carbon and nitrogen stable isotope data (Figure 7.47). Additional palaeoceanographic information is provided by the changing distribution of pigments derived from primary producers (Figures 7.49 and 7.50), reflecting ch anges in the overall community composition and ecology of surface waters. The ecological affinities and environmental interpretation of individual pigments preserved in core VC243 were detailed in Table 8.2.

- **Zone VC237-i: Floating ice shelf conditions**
  ^{14}C age = 11130 – 9880 yr BP
  Cal. Age = 13030 – 11290 cal. yr BP
  Depth = 6 – 5.2 m

This zone in core VC237 is characteristic of sub-ice shelf deposition, with diatoms being advected under the ice shelf from the surrounding areas of sea ice and open ocean. This is supported by higher degree of diatom fragmentation (Figure 7.52). As a consequence, diatom abundance is likely to be revealing information about transportation processes and distance to open water, rather than local diatom production. MS values through this interval are no higher than any other time throughout the Holocene (Figure 6.8), suggesting that diatom abundance is not controlled by dilution factors through increased contribution from terrigenous material. This zone is characterised by low total diatom, CRS absolute and relative abundance, although both progressively increase towards zone VC237-ii (Figure 7.51). This suggests that diatom production in the surrounding areas of seasonally open ocean was progressively

increasing in duration and / or proximity to the PGC, or that coastal currents were increasing in strength, acting to sweep more diatom frustules under the ice shelf.

Conditions in the productive areas surrounding PGC are likely to have been dominated by super-cooled waters, streaming from the base of the melting ice shelf and freshly calved material. Such conditions mimic autumnal hydrology, characterised by expansive areas of cool water and waxing of new sea ice (sea ice type 2), and explain the overwhelming dominance of the non-CRS assemblage by *T. antarctica* warm rs, together with elevated absolute and relative abundance of *P. glacialis* (Figure 7.53). Sea ice type 1 conditions, characterised by active meltwater stratification, were not common during this zone because associated sea ice type 1 species (e.g. *F. curta – F. cylindrus*) and cool open ocean species, linked with the marginal sea ice zone (e.g. *T. gracilis*), are in relatively low absolute and relative abundances. This suggests that the fast ice edge and open ocean were some distance from the core site, or currents were not in the optimum configuration or strength to transport such frustules under the ice shelf.

- **Zone VC237-ii: Retreat of ice shelf from site VC237**
  ^{14}C age = 9880 – 7530 yr BP
  Cal. Age = 11290 – 8360 cal. yr BP
  Depth = 5.2 – 3.7 m

The observation of mixed source ice rafted debris in core VC237 between 9250 – 3320 yr BP (10420 – 3550 cal. yr BP; 4.8 – 1 m) (Figure 6.10) was used by Pudsey et al. (2006) to propose that the ice shelf had retreated from the core site. However, from MS (Figure 6.8) and diatom assemblages (Figure 7.53) there is no obvious ice shelf collapse signal in core VC237; no dramatic influx of ice rafted debris, increase in sedimentation rate or abrupt change in the diatom species assemblage. Changes do occur in the diatom assemblage, but they are subtle and gradual through this zone. Conditions on the EAP were slowly ameliorating, with the progressive increase in the proximity and duration of open water, and length of the growing season. This is highlighted by the reasonably monotonic increase in total diatom abundance between 11130 – 8000 yr BP (13030 – 8880 cal. yr BP; 6 – 4 m; zone VC237-i into VC237-ii) (Figure 7.51).

Shifts in the non-CRS assemblage in this zone suggest the establishment of spring melt conditions at 9410 yr BP (10640 cal. yr BP; 4.9 m) in close proximity to PGC. Although sea ice melt and associated expansion of meltwater-stratified surface waters was probably not an annual event and multi-year ice was still abundant, changes in the diatom community suggests gradual climatic amelioration, including longer periods of

open water in the region, towards 7530 yr BP (8360 cal. yr BP; 3.7 m), consistent with the absence of the ice shelf at this site. This is based on shifts in the absolute and relative contributions from sea ice type 2 species towards sea ice type 1 species (Figure 7.53). Although the non-CRS assemblage in this zone is still dominated by *T. antarctica* warm rs, absolute and relative abundance of this species and *P. glacialis* are reduced, whereas *F. curta*, *F. cylindrus* and *F. vanheurckii* all display an increase in absolute and relative abundance. This anti-correlation between sea ice type 2 species and sea ice type 1 species at the transition between zone VC237-i and VC237-ii is again witnessed at the transition between zone VC237-ii and VC237-iii, and between zone VC243-i and VC243-ii. It is worth noting that there is still a high degree of fragmentation at this time (Figure 7.52), which could be used to argue that transportation mechanisms, rather than distance to the marginal sea ice zone, were also important in explaining the observed change in diatom assemblage.

- **Zone VC237-iii into Zone VC243-i: Retreat of ice shelf from site VC243**
  ^{14}C age = 7530 – 5030 yr BP (VC237);
  6350 – 4380 yr BP (VC243)
  Cal. Age = 8360 – 5800 cal. yr BP (VC237);
  7300 – 4960 cal. yr BP (VC243)
  Depth = 3.7 – 2.1 m (VC237);
  5.8 – 4 m (VC243)

These two linked zones between the two cores are characterised by the influence exerted by the retreating ice shelf and associated iceberg calving on the local marine environment. Both cores record high MS values through these zones (Figures 6.7 and 6.8), reflecting increased inputs of terrigenous material from melting of remnants of the ice shelf and icebergs. Nevertheless, diatom productivity in the PGC is still inferred to be low-moderate, based on fluctuating mid-range total diatom and CRS absolute abundance values from 8000 yr BP (8880 cal. yr BP; 4 m in zone VC237-ii) (Figure 7.51) and running through zone VC237-iii into zone VC243-i (Figure 7.38).

As mentioned previously, the transition from zone VC237-ii into VC237-iii reflects the continued expansion and duration of regional open water during spring, with more extensive areas of seasonal stratified surface water in the central part of PGC. This is based on the decrease in sea ice type 2 species abundance and an increase in sea ice type 1 species abundance (particularly *F. curta*, *F. cylindrus*, *F. obliquecostata*, *F. sublinearis*, *F. vanheurckii*, *Navicula* species) (Figure 7.53). The retreat of the floating ice shelf eventually exposed core site VC243 by 5260 yr BP (6050 cal. yr BP; 4.8 m) (Pudsey et al., 2006). In core VC243, the diatom assemblage in zone VC243-i reflects

this freshly disintegrated ice shelf – seasonally open water environment; the typical sea ice type 2 taxa, *T. antarctica* warm rs, dominates the assemblage in vast numbers (Figure 7.40). The community structure in zone VC243-i (6350 – 4380 yr BP; 7300 – 4960 cal. yr BP; 5.8 – 4 m) (Figure 7.40) is equivalent to the assemblage in zone VC237-i (11130 – 9410 yr BP; 13030 – 10640 cal. yr BP; 6 – 4.9 m) (Figure 7.53), and furthermore, is very similar to the assemblages seen in the WAP cores immediately following ice sheet retreat. Both zone VC243-i and VC237-i are recording the retreat of the PGC Ice Shelf and immediate post-ice shelf conditions, dominated by super-cooled water streaming from beneath the melting ice. The difference in timing between these zones (~4700 ^{14}C years; 4400 cal. years) between two very close core localities (~9 km) highlights either the extremely slow nature of retreat of the PGC Ice Shelf, or two separate break-up events during the Early to Mid-Holocene.

The carbon and nitrogen stable isotopic signal through zone VC243-i (Figure 7.47) provides further clues to the oceanographic regime at this time. Similar to the isotope record from VC306, on a broad scale $\delta^{15}N_{org}$ has an inverse relationship to diatom abundance and productivity in core VC243. Nutrient utilisation is highest in zone VC243-i, when overall diatom productivity is low. Reconciling these two observations requires for nutrient inputs to be much smaller, resulting in more rapid exhaustion of the nutrient pool. Keeping the interpretation strictly oceanic requires either a smaller volume of upwelling water reaching the surface or different water masses (with low NO_3^- pool). Potentially the abundance of freshly calved material and super-cooled water prevented the upwelling of more nutrient-rich deep water into the PGC.

- **Zone VC243-ii: Culmination of Mid-Holocene climatic optimum – open channel, under the influence of seasonal sea ice**
  ^{14}C age = 4380 – 1650 yr BP
  Cal. Age = 4960 – 1550 cal. yr BP
  Depth = 4 – 1.5 m

This zone is characterised by the diminishing influence of the retreating ice shelf, which is replaced by continued expansion of seasonally open water and spring melt conditions deeper into PGC. This is based on the decline in sea ice type 2 species, an increase in cool open ocean species (particularly *T. gracilis*) between 4380 – 2740 yr BP (4960 – 2840 cal. yr. BP; 4 – 2.5 m), followed by increased abundance of sea ice type 1 species (*F. curta*, *F. cylindrus* and *T. antarctica* cold rs) between 2740 – 1430 yr BP (2840 – 1340 cal. yr BP; 2.5 – 1.3 m) (Figure 7.40). Decreased terrigenous inputs and increased biogenic productivity is inferred from the decline in MS values (Figure 6.7), which is

mirrored by an increase in total diatom and CRS absolute abundance (Figure 7.38), initiated between ~ 3840 – 3290 (~ 4270 – 3530 cal. yr BP; 3.5 – 3 m) and peaking between 2740 – 1430 yr BP (2840 – 1340 cal. yr BP; 2.5 – 1.3 m). Further evidence of higher total primary production in the surface water of PGC at this time is provided by carbon and nitrogen stable isotope (Figure 7.47) and sedimentary pigment data (Figures 7.49 and 7.50). Peak diatom abundance between 2740 – 1430 yr BP (2840 – 1340 cal. yr BP; 2.5 – 1.3 m) is matched by less negative $\delta^{13}C_{org}$ values (enriched in ^{13}C; heavier), peak total Chl *a* and total carotenoids concentrations, together with preservation of native Chl *a*.

Carbon and nitrogen stable isotope data provides further information about oceanographic conditions. Similar to the stable isotopic signal in core VC306, $\delta^{15}N_{org}$ in zone VC243-ii becomes less positive when productivity is inferred to increase (Figure 7.47). This suggests lower relative nutrient utilisation, despite higher productivity. Reconciling the two requires that the balance between nutrient inputs (size of NO_3^- pool) and outputs (utilisation by phytoplankton) has shifted towards a larger nutrient supply compared to phytoplankton demand. The increased supply of nutrients is potentially explained by more intense upwelling and increased flux of water around James Ross Island following removal of the PGC Ice Shelf and / or increased glacial run-off and subglacial melting leading to nutrient-rich meltwater plumes during the retreat of land-based ice on James Ross Island and the Trinity Peninsula. The C_{org}/N_{org} ratio (Figure 7.47) suggests that the dominant source of the nutrients was marine-derived.

Pigment distributions support the diatom-based reconstruction for the PGC at this time and reveal further information about changes in the total phytoplankton community. Firstly, higher number of chlorophyll derivatives (Figure 7.50) suggests a more complex marine ecosystem in PGC than during other times through the Holocene. This complexity likely reflects the presence of more diverse environments (sea ice, ice edge, open ocean) and consequently enabling a greater range of degradation processes to occur (e.g. photo-oxidation and grazing). Grazing is most intimately linked with abundance of purpurins (Keeley, 2006), which are also more concentrated in this interval. Carotenoids are also in elevated abundance (Figures 7.49 and 7.50), reflecting the increased requirement for photo-protection under open water conditions. Specifically, the ratio of Diatox to total chlorophylls can be used as an index of light history (Claustre et al., 1994a); this ratio is higher in zone VC243-ii than zone VC243-

iii (Figure 7.49), again reflecting the absence of an ice shelf in PGC in zone VC243-ii. In addition, higher values of Diatox to total chlorophylls are often associated with nutrient-limited populations (Claustre et al., 1994b). This is consistent with open water blooms exhausting nutrients during the period of ice shelf absence and extended seasonal open water conditions, but is not supported by $\delta^{15}N_{org}$ data. Finally, elevated concentrations of the carotenoid Monadox between 2740 – 1760 yr BP (2840 – 1680 cal. yr BP; 2.5 – 1.6 m) (Figure 7.50) provides insight into a key change in the total phytoplankton community structure. Monadox is derived from cryptophytes (Jeffrey et al., 1997), which are a major portion of the primary producer assemblage that would have been unrepresented if it were not for pigment analysis. Recent work by Moline et al. (2004) documents a re-current shift in phytoplankton community structure in nearshore coastal AP waters, from diatoms to cryptophytes. The shift was observed in consecutive years (1991-1996) during the austral summer and was correlated in time and space with increased glacial meltwater runoff and reduced surface water salinities (Moline et al., 2004). The observed elevated concentration of Monadox in the upper portion of zone VC243-ii therefore records massive cryptophyte blooms, likely to be associated with meltwater-driven stratification of surface waters, corroborating the diatom-based interpretation from elevated abundances of sea ice type 1 species. The decline in cryptophytes at 1760 yr BP (1680 cal. yr BP; 1.6 m) (Figure 7.50) pre-dates the reduction in total diatom abundance at 1650 yr BP (1550 cal. yr BP; 1.5 m) (Figure 7.38), suggesting that cryptophytes may be more sensitive to changes in surface water conditions, specifically the reduction in meltwater inputs, increased perennial sea ice (both of which act to increase surface water salinity), and the gradual reformation of the PGC Ice Shelf into the Late Holocene (zone VC243-iii).

- **Zone VC243-iii: Ice shelf reformed**
  ^{14}C age = 1650 – 0 yr BP
  Cal. Age = 1550 – 0 cal. yr BP
  Depth = 1.5 – 0 m

This zone documents re-formation of the ice shelf over core site VC243 at 1650 yr BP (1550 cal. yr BP; 1.5 m), revealed through changes in ice rafted debris provenance (Pudsey et al., 2006), together with reduced phytoplankton production (this study; Figure 7.38). Increasing ice thickness and reduced light levels subsequently lead to a decline in total diatom and CRS absolute abundance between 1650 – 670 yr BP (1550 – 621 cal. yr BP; 1.5 – 0.6 m) (Figure 7.38), decreasing C_{org} and N_{org} contents (Figure 7.47) and lower concentrations of sedimentary pigments (Figure 7.50). Similar to the

record of PGC Ice Shelf disintegration, no dramatic shifts in the diatom assemblage are evident during ice shelf re-formation (Figure 7.40), suggesting it was a gradual process. Furthermore, no precursor oceanographic events are detected from the diatom assemblage (e.g. change to cool open ocean assemblage) and stable isotope data (e.g. shift to more positive $\delta^{15}N_{org}$ values, which could develop if nutrient supply provided by upwelling was not sufficient to meet phytoplankton demand). This is an important conclusion, especially when considering the driving mechanisms of Holocene climate events, and will be discussed further during the synthesis of AP records (section 8.4.1). Ice shelf growth is likely to have been a slow process, driven by the continual expansion and seasonal persistence of sea ice, together with the coalescence of glacier tongues from James Ross Island and Trinity Peninsula into a reformed ice shelf. The non-CRS diatom assemblage reveals that perennial sea ice soon became established and once again diatoms were advected under the ice shelf from a proximal source of seasonally open water. The interpretation of diatom transport is supported by the observed higher levels of diatom fragmentation in this zone (Figure 7.39). Although still in moderate abundance, sea ice type 1 species fall in numbers across the transition into zone VC243-iii (Figure 7.40), reflecting the shorter length of the growing season for these spring bloom species. Benthic diatoms, including *Cocconeis* and *Achnanthes* species, show higher abundance, possibly associated with stable perennial sea ice substrates (Scott and Marchant, 2005). A decline in concentrations of the carotenoid Monadox (Figure 7.50) also provides further supporting evidence for the proposed Late Holocene ice shelf presence in PGC. The link between Monadox and cryptophytes has already been discussed in zone VC243-ii. Correspondingly, the observed reduction of Monadox concentrations through zone VC243-iii and total absence in the sediment after 560 yr BP (590 cal. yr BP; 0.5 m) suggests the converse to observations of Moline et al. (2004); reduced glacial meltwater runoff and increased surface water salinities due to the presence of a floating ice shelf in PGC resulting in the loss of cryptophytes from the Late Holocene phytoplankton assemblage. This is an extremely interesting result and demonstrates the value of pigment analyses in identifying important components of the primary producer community that leave no morphological fossils (e.g. diatom frustules).

Finally, the most recent 700 yr (635 – 0 cal. yr BP; 0.6 – 0 m) of this core record contains evidence of the onset of the second Holocene disintegration of the PGC Ice Shelf, eventually culminating in the ice shelf collapse witnessed in 1995. This period is characterised by the progressive retreat of regional sea ice extent towards the continent

up to the present day, based on high absolute and relative abundances of *F. curta*, *T. antarctica* cold rs and *P. glacialis* (Figure 7.40). A return to higher primary production, associated with more proximal open ocean conditions, is also suggested from sedimentary pigments, which record increased preservation of native Chl *a* and Phorb *a* between 450 – 120 yr BP (502 – 140 cal. yr BP; 0.4 – 0.1 m) (Figure 7.50). However, an alternative explanation could be that the higher concentration of native pigments at the core top is a function of the younger sediment at this stratigraphic level, having had less time to undergo primary degradation through diagenetic processes. Finally, there is also a notable increase in the ratio of C_{org}/N_{org} after 700 yr BP (635 cal. yr BP; 0.6 m) (Figure 7.47). Remineralisation can be excluded as a cause because there is no concurrent shift towards heavier $\delta^{13}C_{org}$ and $\delta^{15}N_{org}$ values. The change in the ratio of C_{org}/N_{org} is proposed to be related to input of continental organic matter, which has a much higher C_{org}/N_{org} ratio than phytoplankton. From sedimentological information (Figure 6.7) a pronounced concentration of clasts are observed at these core depths, likely to originate from a mass movement event. This general instability in PGC sediments could also signify increased sub-ice shelf melting and subglacial meltwater inputs from James Ross Island, periodically delivering more terrigenous material and triggering mass movement events.

8.3.6 VC205

Core VC205, from Erebus and Terror Gulf (northern EAP) records highly variable depositional regimes, of both biogenic and terrigenous sedimentation, through the Mid- to Late Holocene. Clear stratigraphic changes exist in the sedimentary record, reflecting changes in regional oceanography and sea ice extent. This record is intimately linked with changes in the nearby PGC and its associated ice shelf history; events in core VC205 are therefore compared with reconstructions from cores VC237 and VC243 in section 8.4.

- **Zone VC205-i: Mid-Holocene climatic optimum**
  ^{14}C age = 5610 – 5230 yr BP
  Cal. Age = 6390 – 6010 cal. yr BP
  Depth = 5.1 – 3.5 m

This zone is characterised by very high sedimentation rates (410 cm ka^{-1}) (Figure 6.11), paired with low MS values (Figure 6.9) and high total diatom abundance (Figure 7.60). Primary production is predicted to have been extremely high in the newly exposed PGC and surrounding bays, following ice shelf retreat from the main channel. The high

sedimentation rate witnessed at this site is believed to be controlled by sediment focusing processes, with coastal currents flushing biogenic material northwards to be deposited in the Erebus and Terror Gulf basin. However, high abundance of vegetative valves and delicate forms (e.g. *Corethron pennatum*) (Figure A2.14) indicates good preservation, which would suggest rapid export of diatoms from the surface waters to the sediment and that a proportion of the biogenic material in this zone was locally sourced and had undergone minimal transportation. A potential mechanism to produce rapid sinking of diatoms from surface waters is quick onset of mixing and break-down of stratification at the transition into autumn (similar to that inferred for rapid deposition of *Rhizosolenia* mats; Kemp et al., 1999).

Diatom species present in elevated relative abundance through this period are typically sea ice type 1 species (particularly *F. cylindrus*, *F. obliquecostata*, *F. ritscheri*, *F. sublinearis*, *F. vanheurckii* and to a lesser extent *F. curta*) together with *Navicula* species and *T. antarctica* cold rs (Figure 7.62). These species indicate that a seasonal cycle of sea ice advance and retreat was well established in the Erebus and Terror Gulf and PGC during the Mid-Holocene climatic optimum. [The equivalent zone in PGC is VC237-iii (Figure 7.53), which also records increased abundance of sea ice type 1 species, used to infer the continued expansion and duration of open water during spring.] *F. kerguelensis* is in low abundance in all the EAP cores, however, during this zone, this typically open ocean diatom forms a minor component of the assemblage (Figure 7.62). *E. antarctica* rs also record moderate abundance; typically *E. antarctica* var. *antarctica* (asymmetric, proposed sub-polar form). This suggests that surface waters were comparatively warm, with open ocean conditions present for a significant proportion of the year.

- **Zone VC205-ii: Culmination of PGC Ice Shelf retreat and deglaciation of James Ross Island**
  ^{14}C age = 5230 – 4360 yr BP
  Cal. Age = 6010 – 4940 yr cal. BP
  Depth = 3.5 – 2.2 m

The transition into zone VC205-ii marks a relatively abrupt change in the depositional regime and environmental conditions at this core site. Although sedimentation rates remain high, total diatom abundance dramatically decreases (Figure 7.60), whereas MS values increase (Figure 6.9). It is likely that both these conditions reflect increased terrigenous input to the sediment, diluting the biogenic signal, together with a matched decrease in surface water productivity. Diatom assemblage data suggests that reduced

productivity is linked to poorly developed surface water stratification through this zone. The seasonal cycle of sea ice melt (sea ice type 1 conditions) is inferred to have been suppressed by prolonged periods of autumn-like conditions, characterised by super-cooled shelf waters (sea ice type 2 conditions). These suggestions are based on the observation that, in general, all species exhibiting high abundance (particularly sea ice type 1 species) in zone VC205-i, decline dramatically in absolute numbers and relative percentage through the transition into zone VC205-ii, whereas *T. antarctica* warm rs display a marked increase in relative abundance (Figure 7.62). The onset of this zone is coincident with a proposed second phase of PGC ice shelf break-up, exposing core site VC243 at 5260 yr BP (6050 cal. yr BP) (as discussed in section 8.3.5), related to Mid-Holocene climatic optimum conditions. Sea ice type 2 conditions in the Erebus and Terror Gulf could potentially be linked to the final phase of ice shelf retreat in the PGC and deglaciation of James Ross Island and would account for the increased terrigenous inputs described above. It has long been suggested that ice shelves act to buttress inland ice and their removal leads to discharge of continental ice (Weertman, 1974; Thomas, 1979); this has been confirmed by recent satellite data that shows several glaciers which drain the former Larsen-A and Larsen-B, PGC and the Wordie Ice Shelves have accelerated since their demise (Rott et al., 2002; Scambos et al., 2004). This process could have occurred in the Mid-Holocene following the disappearance of the PGC Ice Shelf, leading to acceleration of land based ice from James Ross Island and the Trinity Peninsula, increased iceberg calving and terrigenous sediment delivery to basins such as those found in Erebus and Terror Gulf. An alternative explanation for the sedimentological and diatom abundance changes witnessed in this zone is that glacier advance, driven by climatic cooling, delivered large volumes of terrigenous material to the Erebus and Terror Gulf. Glacial re-advance between ~5000 – 4600 yr BP (~4400 – 4100 cal. yr BP) has been proposed for several northern AP settings, including northern James Ross Island (Ingólfsson et al., 2004; Hjort et al., 1997) (although not supported by Sterken, 2009) and Hope Bay (Zale, 1994). The two scenarios (ice shelf collapse versus glacial re-advance) will be more fully discussed when regional reconstructions are explored (section 8.4).

- **Zone VC205-iii: Mid-Holocene stabilisation, followed by Late Holocene Neoglacial**
  ^{14}C age = 4360 – 0 yr BP
  Cal. Age = 4940 – 0 cal. yr BP
  Depth = 2.2 – 0 m

This zone is characterised initially by ameliorating climatic conditions between 4360 – 2280 yr BP (4940 – 2270 cal. yr BP; 2.2 – 1.1 m), followed by deterioration into the Late Holocene Neoglacial towards the present. Amelioration of environmental conditions in both the Erebus and Terror Gulf region and PGC is inferred from higher diatom primary production and reduced terrigenous inputs, revealed through increased total diatom and CRS absolute abundance (Figure 7.60) and lower MS values (Figure 6.9). Although diatom concentrations are higher, sedimentation rates throughout this zone are not as high as witnessed in zone VC205-i, indicating primary production has not returned to levels seen prior to 5230 yr BP (6010 cal. yr BP; 3.5 m) and / or reduced sediment focusing processes (e.g. reduced vigour of coastal currents or their reconfiguration). Diatom assemblage data indicates re-establishment of the seasonal sea ice cycle, with associated stratified spring water column conditions. This interpretation is based on increased absolute and relative abundances of typical sea ice type 1 species (particularly *F. curta*, *F. cylindrus*, *F. sublinearis*, *F. vanheurckii* and *P. glacialis*) (Figure 7.62). Increased numbers of benthic genera such as *Cocconeis* and *Navicula* suggest transport of species typically associated with nearshore shallow habitats into the region, consistent with coastal areas being exposed to seasonally open water during the climatic optimum conditions.

After ~2280 yr BP (2070 cal. yr BP; 1.1 m) Late Holocene climatic deterioration is proposed, characterised by more persistent sea ice and diminishing periods of spring meltwater driven stratification. This interpretation is based on a decline in sea ice type 1 species absolute and relative abundance (and a slight increase in *T. antarctica* warm rs relative abundance) (Figure 7.62). Terrigenous sedimentary inputs also increased once again, based on higher MS values (Figure 6.9) that are not matched by a decline in total diatom abundance (Figure 7.60). Possible causes of increased input of terrigenous material at this locality include: (i) increased iceberg frequency, as glacier fronts advance and actively calve into the Weddell Sea; (ii) increased sediment-laden subglacial meltwater inputs from the James Ross Island and the Trinity Peninsula. This inferred climatic deterioration from ~2280 yr BP (2070 cal. yr BP) slightly predates reformation of the PGC Ice Shelf at ~1650 yr BP (1550 cal. yr B.P) and may be an oceanographic precursor of conditions that led to the advance and coalescence of glaciers witnessed around PGC in the Late Holocene.

8.4 Discussion

8.4.1 Were Holocene climate events peninsula-wide and synchronous?

This section addresses the first primary questions posed in Chapter 1.2; were Holocene climatic events peninsula-wide and synchronous? Where spatial and temporal discrepancies exist, do these patterns provide clues to forcing mechanisms? In the discussion of climatic episodes, comparisons will be made between cores studied in this investigation (Figure 8.4), and then expanded to include other regional marine and terrestrial records. Unfortunately there are no long ice cores from the AP with which to compare this data; the nearest full Holocene records are to the south (Siple Dome and Byrd) and east (Berkner Island) (Figure 2.4). These records do not fully represent AP Holocene conditions (Bentley et al., 2009), and further, display significant climatic contrasts to ice core records from the East Antarctic Ice Sheet (Masson et al., 2000; Das and Alley, 2008). Discussion of the ice core records from both the West and East Antarctic Ice Sheets is therefore confined to section 8.4.2, although some of the three main climatic events focused on in this AP comparison (section 8.4.1) are based on well-observed features from the continental ice core records (e.g. Early Holocene warmth, evident in ice core records between 11000 – 9500 cal. yr BP (~9600 – 8450 yr BP) (Ciais et al., 1992; Masson et al., 2000; Masson-Delmotte et al., 2004)).

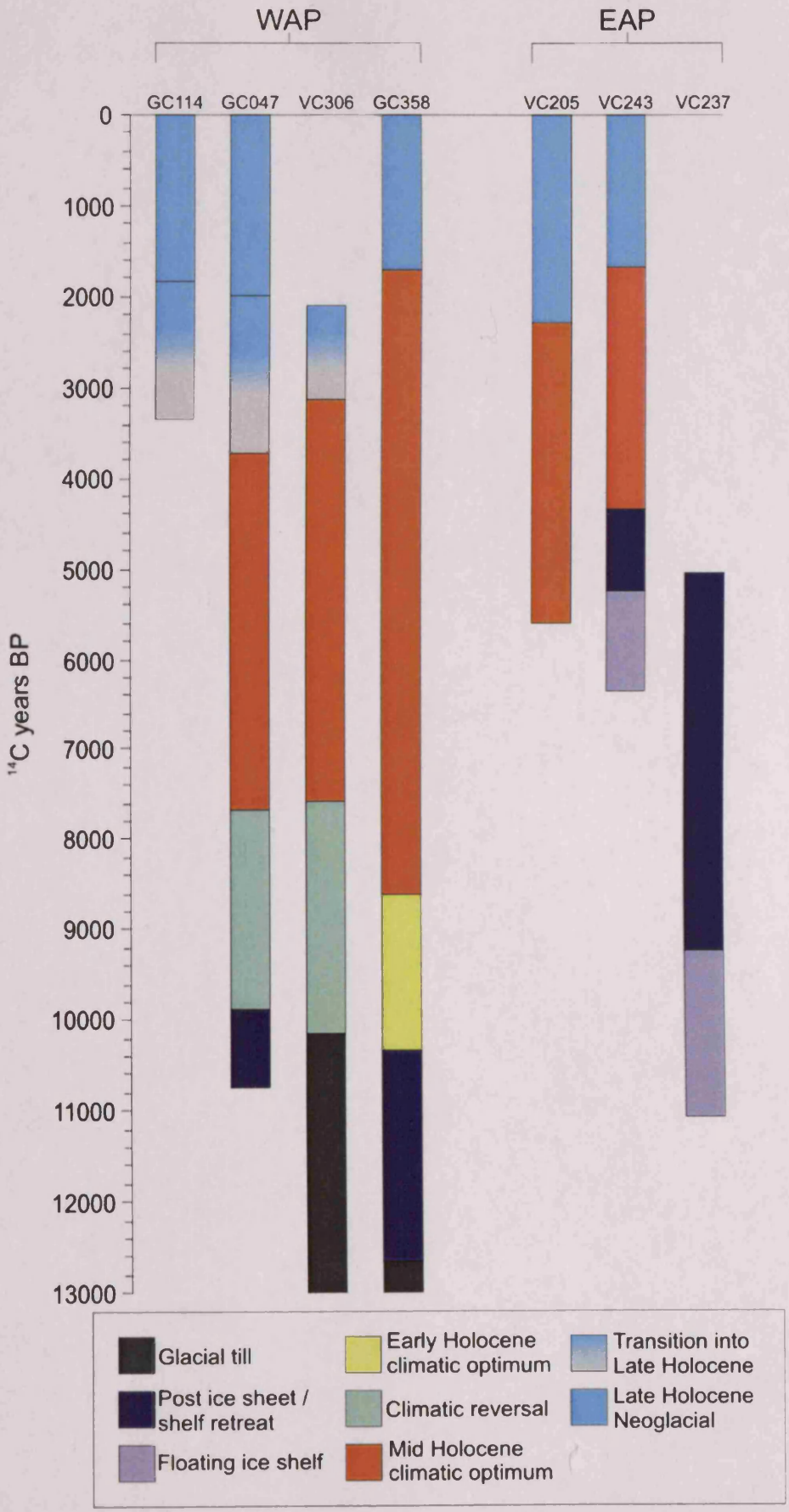


Figure 8.4
Comparison of Holocene events between AP marine cores. WAP = West Antarctic Peninsula; EAP = East Antarctic Peninsula.

8.4.1.1 Deglaciation – Early Holocene transition

In Antarctica it is believed that ice sheet recession commenced later and continued longer than in the Northern Hemisphere, and may still be under way (Stone et al., 2003). There is considerable variability in the timing of retreat along the AP and around the Antarctic continent. The fact that ice sheet retreat is likely to have occurred over a prolonged period in Antarctica leads to some difficulty identifying and demarcating individual Holocene climatic events because they can be obscured by the deglaciation signal. In this section, deglaciation is approached from two perspectives. Firstly, it is viewed as a single event at individual core sites – the retreat of grounded ice from the seafloor sediments at that locality, enabling sub-ice shelf or marine deposition to occur. From this viewpoint, focus will be placed on the timing of that initial event and compared along the AP, with possible forcing mechanisms proposed for the spatial patterns observed. Secondly, deglaciation is seen to represent a more regional and prolonged phenomenon – the manifestation of the impacts of progressive retreat of the ice sheet landward, such as re-organisation of coastal currents, inputs of glacial ice, and changing meltwater and nutrient fluxes. From this viewpoint, regional environmental reconstructions are explored, i.e. what was the initial AP post-deglaciation environment like and did its development follow the same pattern between localities?

Retreat of grounded ice

In Antarctic shelf sedimentary settings, retreat of grounded ice typically involves a transition from terrigenous-rich glacial till to more biogenic-rich homogenous mud. However, for a number of reasons it is often difficult to precisely delimit the first post-glacial sediments in marine cores. Firstly, the transition from glacial to glacio-marine deposition is often gradational, with the progressive reduction (increase) in terrigenous (biogenic) material up-core. For example, the ice sheet may have lifted off the seafloor, becoming a floating ice shelf under which biogenic material can be swept, thus giving a false impression of glacio-marine sedimentation. Finally, initial post-glacial deposition is often devoid of microfossils, making it difficult to accurately date the transition. Such complications mean that all radiocarbon dates taken at or close to the deglaciation sediment transition (particularly those derived from AIOM, because of contamination issues discussed in Chapter 6.2.2.) are, by convention, viewed as minimum ages for deglaciation.

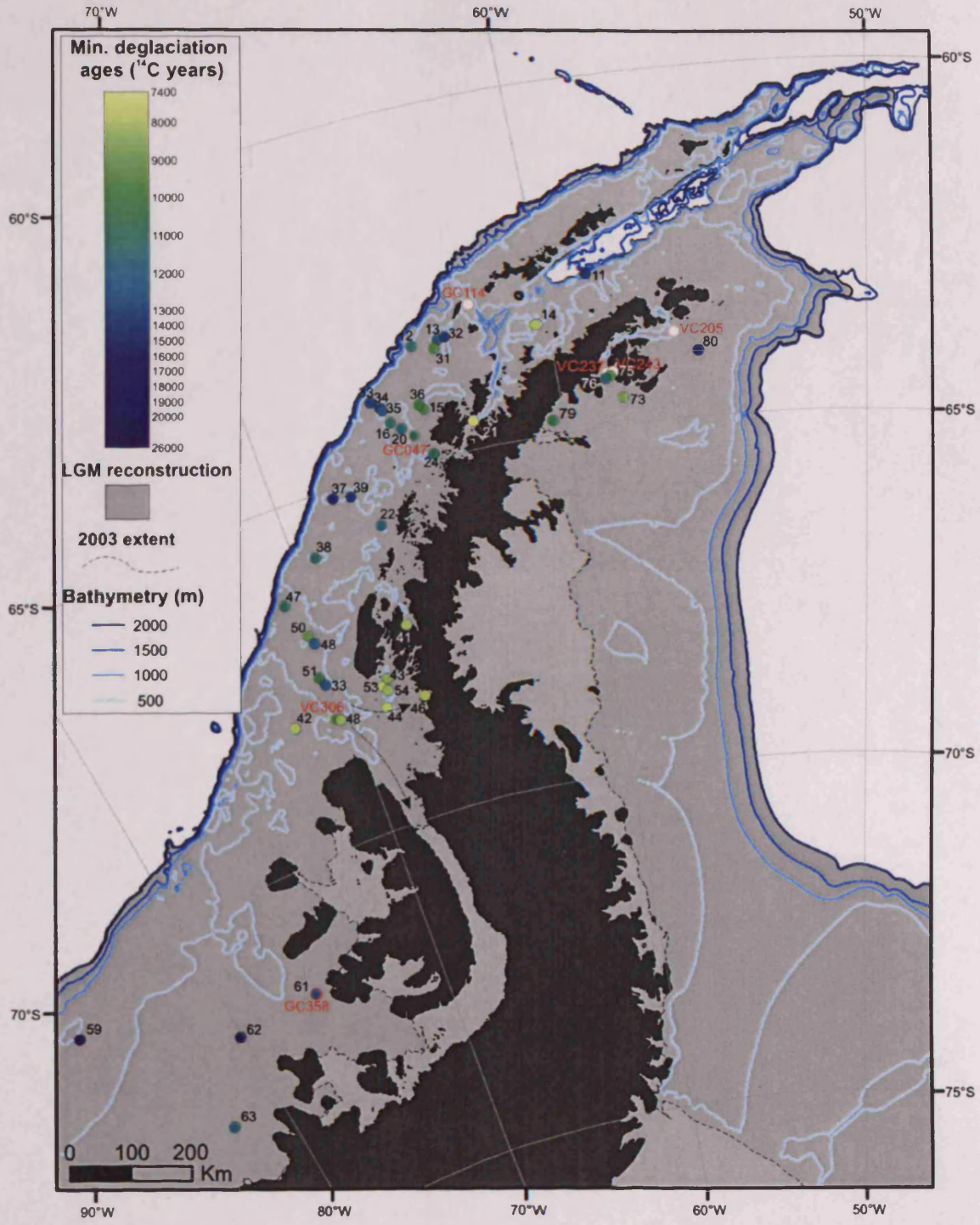


Figure 8.5
Minimum deglaciation ages from published marine records from the Antarctic Peninsula (AP) continental shelf, provided by dating the transition between sub-glacial and glacio-marine sediments. Table A2.20 contains details of source publication, ^{14}C ages and marine reservoir correction. White circles highlight core localities used in this investigation that do not contain the deglaciation sedimentary sequence. Dashed arrows in Marguerite Bay represent two ice sheet retreat trajectories, discussed in the text. Last Glacial Maximum (LGM) reconstructions adapted from Anderson et al. (2002) and Heroy and Anderson (2007).

Two cores analysed in this investigation record the deglaciation – Early Holocene sediment transition (VC306 and GC358), and in a further core (GC047) the presence of CRS ooze at the base of the core potentially marks the onset of open marine deposition at the core site (Figure 8.4). As highlighted in Figure 8.5, dates of the earliest post-glacial sediments not surprisingly suggest progressive ice sheet retreat from the outer continental shelf towards the AP coast. In this investigation, approximate ice sheet retreat rates were calculated by mapping the timing of deglaciation at core sites and the distance between localities, in transects from the outer continental shelf to coastal AP settings, following bathymetric troughs (likely the earliest ice sheet retreat pathways) (Figure 8.6 and Figure 8.7). The method has reproduced particularly well the previously proposed Marguerite Bay rapid palaeo-ice-stream retreat, inferred from geophysical data of palaeo-landforms (Ó Cofaigh et al., 2005a; 2008; Anderson et al., 2008; Dowdeswell et al., 2008), providing some validation for the technique, in spite of errors associated with AIOM radiocarbon dates. Retreat rates varied between regions (Figure 8.6 and Figure 8.7), with some areas experiencing relatively rapid, two-phase ice sheet recession (offshore Anvers Island (core GC047) and Marguerite Bay (core VC306)), whereas in other areas retreat was reasonably gradual and monotonic (southern Bellinghausen Sea (core GC358)). The EAP followed a completely different pattern again, with very episodic retreat, and two periods of ice shelf break-up in the PGC (cores VC237 and VC243). The reconstructed retreat rates for the outer WAP continental shelf (discussed in detail below) are comparable with that inferred for deglaciation of the western Ross Sea (0.1 km/yr) by Bindschadler (1998).

Of the three cores preserving the removal of grounded ice, core GC358 in the southern Bellingshausen Sea records the earliest retreat of the ice sheet at 12650 yr BP (15020 cal. yr BP). Comparing the timing of deglaciation at this core site with other published data along the AP (Figure 8.5 and Table A2.20), suggests that ice sheet retreat in the southern Bellingshausen Sea predates that of northern WAP and coastal EAP sites by several thousand years. The observation of an early deglaciation at this coastal, southern Bellingshausen Sea core site, together with the suggestion that ice sheet retreat from the outer continental shelf in this area had occurred at ~26000 yr BP (~30000 cal. yr BP) (Hillenbrand et al., 2007), are unexpected findings for a number of reasons. Firstly, the timing goes against glacio-isostatic and glaciological models, which suggest onset of deglaciation in Antarctica started several thousand years later (~12000 – 9000 cal. yr BP; ~10250 – 8100 yr BP) (Tushingham and Peltier, 1991; Peltier, 1994; Nakada et al.,

2000), although this is a continent-wide average. Secondly, the geographical expression of initial retreat in the AP to be in the south also contradicts models, which suggest retreat began in the northern AP at 14000 – 13000 cal. yr BP and gradually progressed southwards over the next 6000 years (Huybrechts, 2002). Furthermore, recession of the ice sheet in the southern AP prior to northern AP areas is not analogous with recent rapid warming trends, which display the converse pattern, evidenced by the progressive retreat of small tidewater glaciers over the past 50 years (Cook et al., 2005) and the collapse of AP ice shelves as the -5 °C to -9 °C isotherms shift southwards (Hodgson et al., 2006a; Morris and Vaughan, 2003). Published reconstructions of post-LGM retreat would also imply that glacial retreat was initiated in the north (~18000 cal. yr BP) and progressed southward (to Marguerite Bay by ~14000 cal. yr BP) (Anderson et al., 2002; Heroy and Anderson, 2007). However, three previous studies (Ó Cofaigh et al., 2005b; 2008; Hillenbrand et al., 2007) and this investigation have extended the AP palaeoenvironmental transect into previously un-surveyed southern AP localities. The authors of these previous studies conclude that the southern Bellinghausen Sea has potentially been overlooked in previous deglaciation reconstructions, as seabed morphological features and their orientation suggest that ice flow into this area played a significant role in drainage of the WAIS (Ó Cofaigh et al., 2005b; 2008; Hillenbrand et al., 2007), contrasting present drainage patterns, whose main exit gates are into the Ross, Amundsen and Weddell seas (Bindschadler, 1998).

Ice sheet retreat rates in the southern Bellingshausen Sea have been reconstructed in Figure 8.6 (diamond symbols) and the dates show a chronological progression landwards. If the chronology of core GC358 (and others used in the study of Hillenbrand et al. 2007) is correct, this would suggest that ice sheet retreat from the outer WAP continental shelf occurred initially in the southern Bellingshausen Sea at ~26000 yr BP (#59; Hillenbrand et al., 2007), with moderately paced recession towards the middle shelf (~0.036 km/yr) between 26000 and 19000 yrs BP (record #62; Hillenbrand et al., 2007). Retreat subsequently slowed towards coastal AP localities and core site GC358 (#61) (~0.014 km/yr) between 19000 and 12650 yr BP (~22800 – 15020 cal. yr BP). Because of the paucity of data points, it is not possible to fully assess whether retreat was monotonic or more sporadic, with localised periods of stability and subsequent rapid retreat. Geophysical data suggests the latter was more likely; the absence of grounding-zone wedges from the outer shelf trough suggest that ice stream retreat across this region was rapid, which progressed until the ice stream grounding

zone stabilised on the middle – inner shelf, subsequently taking on a more episodic style of retreat (Ó Cofaigh et al., 2008).

The model proposed of a two-phased ice sheet retreat in the southern Bellingshausen Sea (Figure 8.6) is similar in style to the deglaciation history of Marguerite Bay (core VC306) and northern WAP shelf settings (core GC047), although retreat occurred later in these regions and, particularly for Marguerite Bay, is predicted to have occurred more rapidly. Geophysical data from the continental shelf reveals very well preserved landforms and a lack of sequential retreat moraines, suggesting that the ice streams retreated rapidly in this area (Ó Cofaigh et al., 2005a; 2008; Anderson et al., 2008; Dowdeswell et al., 2008) and presence of deep iceberg scours, which reflect calving of the ice sheet margin (Anderson et al., 2005). Ice sheet retreat from the outer shelf of Marguerite Bay is suggested to have been underway by 11195 yr BP (~13090 cal. yr BP) (#47; Pope and Anderson, 1992). In core VC306, from the mid-shelf, the sediment transition marking removal of grounded ice is at 10150 yr BP (11800 cal. yr BP). A rudimentary deglaciation history and approximate retreat rates are proposed in Figure 8.6. In this region two coastal tie-points exist: (1) an epishelf lake sediment core from Moutonnée Lake, on the Ablation Point Massif of Alexander Island, that records an Early Holocene absence of the George VI Ice Shelf between 8170 and 7300 yr BP (9600 and 7730 cal. yr BP) (#55; Smith et al., 2007a); and (2) a marine sediment core from Neny Fjord, recording an open marine influence at 8130 yr BP (9170 cal. yr BP) (#46; Heroy and Anderson, 2007). These two dates provide end points of two ice sheet retreat trajectories in Marguerite Bay (dashed arrows marked on Figure 8.5): (1) running along the length of Marguerite Trough to George VI Sound (Figure 8.6, square symbols); and (2) running along the length of Marguerite Trough, then retreating through tributary bathymetric troughs lying roughly parallel with the 68°S line of latitude, towards the AP coast and Neny Fjord (Figure 8.6, triangle symbols). From the reconstructions in Figure 8.6, ice sheet recession in Marguerite Bay appears to have occurred in two main phases: initially rapid retreat (~0.23 km/yr) from the outer to middle shelf along Marguerite Trough, including core site VC306 (#52), between 11195 and 10150 yr BP (13090 and 11800 cal. yr BP); followed by a period of slow retreat (~0.004 km/yr) or even relative stability, where the ice sheet was potentially pinned landwards of core site VC306 (between Adelaide Island to the north and Alexander Island to the south), between 10150 and ~8000 yr BP (11800 – ~9000 cal. yr BP);

proceeded by a second period of very rapid retreat (~2.4 km/yr) and collapse of the ice sheet through inner Marguerite Bay around ~8000 yr BP (9000 cal. yr BP).

Moving into the northern WAP region, although core GC047 does not record the typical ice retreat sediment transition, initial biogenic sedimentation is characteristic of the deglaciation phase witnessed in other marine records. The base of core GC047 is dated at 10750 yr BP (12720 cal. yr BP), which is a comparable age to deglaciation recorded in other marine records from the Anvers Trough region (Figure 8.5). By plotting these ice sheet retreat markers from cores along Anvers Trough, approximate retreat rates and timings can be inferred (Figure 8.7). Based on the similarity between the ^{14}C date from the base of core GC047 (open square) and the linear trendline through dates on the middle-to-inner shelf, it is predicted that only a small portion (~ 250 years; ~ 8.5 cm (assuming the same linear sedimentation rate of 34 cm ky^{-1})) of immediate post-deglaciation deposition is missing from core GC047.

Numerous marine cores and geophysical data have been analysed from the northern WAP to reconstruct retreat of the AP Ice Sheet, summarised in Figure 8.5 and Table A2.20. In the north, glacial retreat was underway in Bransfield Strait by 14435 yr BP (17500 cal. yr BP) (#11; Banfield and Anderson, 1995), continuing south to the outer shelf of Anvers Trough by 13650 – 12790 yr BP (16230 – 15090 cal. yr BP) (record #34, #33 and #35; Heroy and Anderson, 2007). Palaeo-ice streams, glacial flowlines and retreat models for the Anvers Trough and Palmer Deep basin were reconstructed based on geophysical mapping of bedform features by Domack et al. (2006) and are summarised on Figure 8.8. The model Domack et al. (2006) propose is for calving bay re-entrants to cause recession of the ice stream progressively from the outer to middle shelf and inland to Palmer Deep basin. In this scenario, retreat occurred more rapidly over the deep trough while ice remained grounded on the shallower banks at either side, facilitating the development of sedimentary regimes in which varved sediments were deposited in the trough (Domack et al., 2006). This style of deglacial sedimentation is discussed further under the heading "The post-glacial marine environment" (p8-57), where comparisons are made between the immediate post-deglaciation sedimentation in the cores studied in this investigation.

The retreat rate reconstructions for Anvers Trough (Figure 8.7) suggest that ice retreat was a relatively rapid process in the outer portion of the trough (~0.14 km/yr), potentially slowing (~0.015 km/yr) towards the middle section of the shelf (#16), which

records removal of grounded ice at 11230 yr BP (13110 cal. yr BP) (Pudsey et al., 1994). Ice sheet retreat from the inner section of Anvers Trough, towards core site GC047 and Palmer Deep basin (#22; Domack et al., 2001), was again relatively rapid (~0.098 km/yr). The substantial break-in-time for removal of grounded ice between the relatively coastal Palmer Deep site at ~11300 yr BP (13180 cal. yr B.P; Domack et al., 2001) and inner coastal and fjord settings, such as Gerlache Strait at 7480 yr BP (8370 cal. yr BP) (#21; Harden et al., 1992 – corrected in this investigation by using the core top age), suggests that the final stages of retreat towards the AP coast were either characterised by very slow retreat (0.0062 km/yr) (scenario (a) on Figure 8.7) or a period of ice sheet stability, followed by rapid collapse and inshore retreat (scenario (b) on Figure 8.7). A similar trend is witnessed in Biscoe Strait, with relatively early retreat from outer to middle shelf settings between 15421 – 11360 yr BP (18760 – 13230 cal. yr BP) (#37, #38, #39; Heroy and Anderson, 2007) followed by a several thousand year gap before nearshore coastal settings experienced seasonally open marine conditions, such as Lallemand Fjord prior to 8128 yr BP (9170 cal. yr BP) (#41; Shevenell et al., 1996). Timing of ice sheet retreat from Lallemand Fjord has been subsequently modified by Taylor et al. (2001) to 10580 cal. yr BP (~9350 yr BP), who assumed a constant sedimentation rate and extrapolated the radiocarbon chronology to the base of unit III defined by Shevenell et al. (1996).

On land, ice sheet retreat from the northern WAP displays significant temporal variability. Parts of the coast of King George Island in the South Shetland Islands were ice-free by ~9500 cal. yr BP (~8500 yr BP) and some lake basins began to accumulate sediments ~9500 – 9000 cal. yr BP (~8500 – 8090 yr BP) (Mäusbacher et al., 1989; Hjort et al., 2003), whereas other islands in the same chain did not become free of ice until much later in the Holocene, e.g. Byers Peninsula on Livingston Island appear to have remained ice covered until 5000 – 3000 cal. yr BP (~4400 – 2870 yr BP) (Björck et al., 1996).

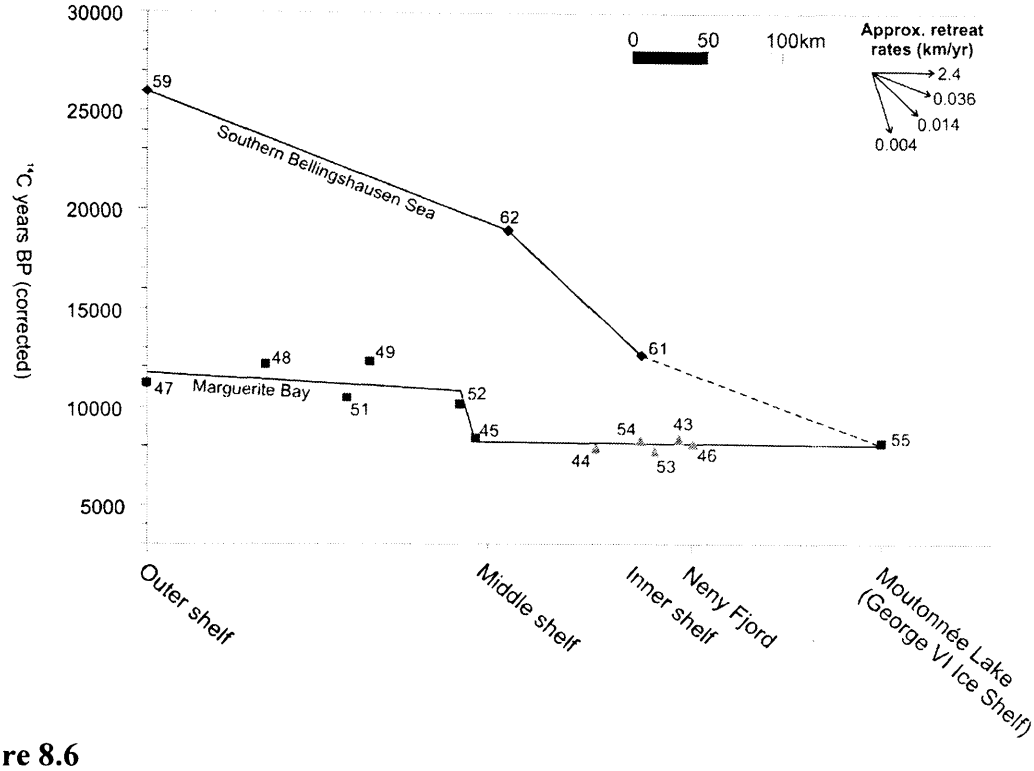


Figure 8.6
History of ice sheet retreat and associated rates for the southern Bellingshausen Sea (diamond symbols; core GC358) and Marguerite Bay (square and triangle symbols; core VC306), inferred from sediment transitions in marine cores marking the removal of grounded ice (numbered as shown in Figure 8.5 and Table A2.20). Site bathymetry is shown in Figure 8.5. It is worth noting that the chronology for Marguerite Bay is more robust and with no conflicting ages between marine sediments compared to that for the southern Bellingshausen Sea (as discussed in Chapter 6.2.5).

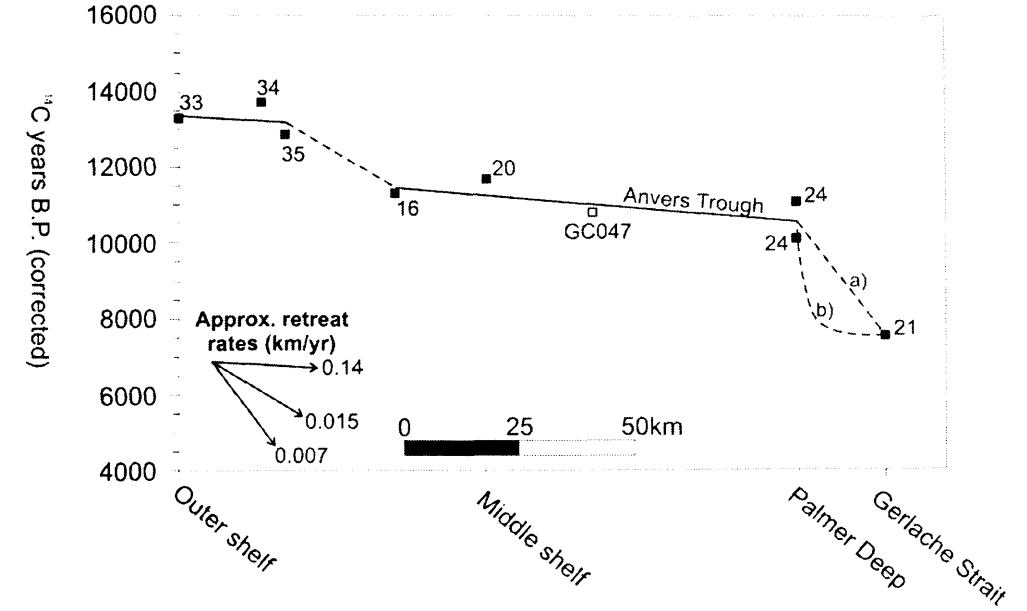


Figure 8.7
History of ice sheet retreat and associated rates for Anvers Trough (core GC047), inferred from sediment transitions in marine cores marking the removal of grounded ice (numbered as shown in Figure 8.5 and Table A2.20). Dashed line labelled (a) represents scenario of gradual retreat of ice sheet between Palmer Deep and Gerlache Strait; (b) represents scenario of a period of ice sheet stability, followed by rapid retreat and collapse of ice sheet from coastal localities. Site bathymetry is shown in Figure 8.5.

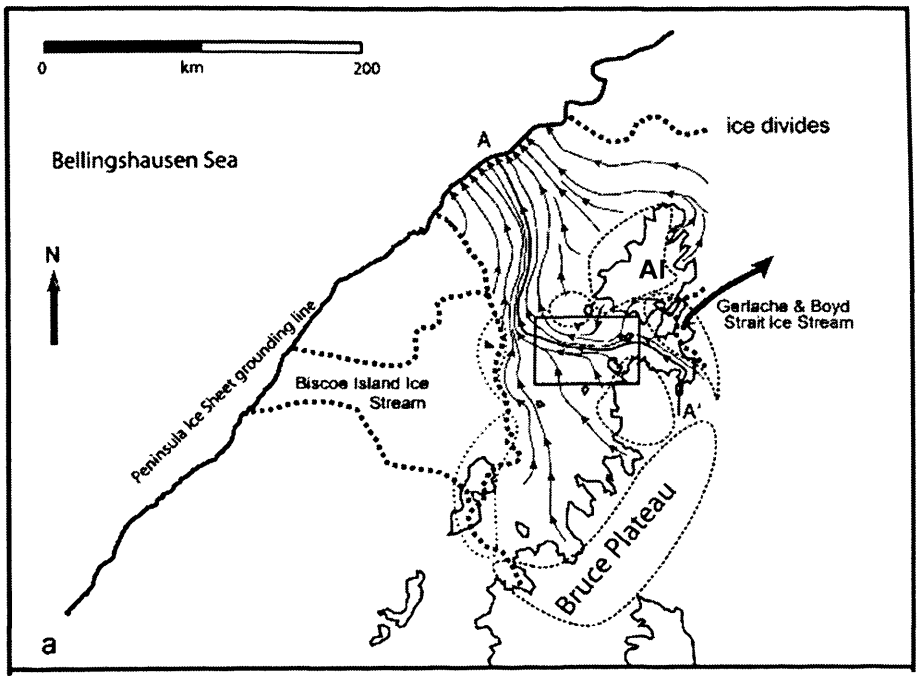


Figure 8.8
Regional outline of the ice stream outlet system in the vicinity of Anvers Island (AI) and reconstructed grounding line position of Antarctic Peninsula Ice Sheet during the LGM. Ice flow directions = parallel, thin sold lines, ice domes = dotted lines; drainage divides = bold dashed lines. (Source: Domack et al., 2006).

Addressing cross-peninsula patterns of ice sheet retreat, it has been suggested that removal of ice from the much colder EAP occurred differently to that of the more maritime WAP (Evans et al., 2005; Sugden et al., 2006). The ice sheet on the EAP is inferred to have drained mainly through fast-flowing palaeo-ice streams, rather than meltwater release processes, with variable recession rates, ranging from staggered retreat punctuated by still-stands across the mid-shelf, to rapid and continuous in the troughs (e.g. PGC, Larsen Inlet and Greenpeace Trough) (Evans et al., 2005). However, the exact timing of retreat is poorly constrained, due to the paucity of well-dated records from the northern EAP and the problems with radiocarbon dating because of contamination issues particularly prevalent on the EAP (discussed in Chapter 6.2.2). The three EAP cores studied in this investigation did not recover the sediment transition marking the removal of grounded ice; consequently the timing of ice sheet retreat is inferred from previously published data (Figure 8.5). The outer EAP shelf (Vega Trough) records removal of grounded ice at 15170 yr BP (18510 cal. yr BP) (#80; Heroy and Anderson, 2007). For coastal EAP localities, previous reconstructions in the PGC, infer that removal of grounded ice and establishment of seasonally open marine conditions nearby took place some time between 16700 – 11450 yr BP (19950 – 13370

cal. yr BP) (Pudsey et al., 2006). In the Larsen-A region (Greenpeace Trough), the transition from grounded ice to ice shelf was completed by 10770 cal. yr BP (~ 9500 yr BP) (#79; Brachfeld et al., 2003). The fact that diatoms are present throughout core VC237 suggests that seasonally open marine conditions were sufficiently close to PGC, allowing diatoms to be advected under the floating ice shelf, from at least 11130 yr BP (13030 cal. yr BP). Retreat of the ice shelf in PGC was a very gradual, or two-phased, process (Figure 8.4 and discussed in section 8.3.5) and complete absence did not occur until the Mid-Holocene (5260 yr BP; 6050 cal. yr BP; core VC243) (Pudsey and Evans, 2001; this study). The final tie-point on the EAP for recession of the AP ice sheet is provided by onshore studies from James Ross Island, suggesting that retreat occurred prior to ~ 7400 yr BP (~8250 cal. yr BP) (Hjort et al., 1992; Hjort et al., 1997), to between 7000 – 6000 yr BP (~7850 – 6850 cal. yr BP) (Ingólfsson et al., 1992; 2004). Hope Bay, at the northern tip of the AP, was ice-free by 6300 cal. yr BP (~5500 yr BP) (Zale, 1994).

The timing of ice sheet recession is different between the EAP and WAP. The outer shelf regions of the EAP experiences retreat at ~15000 yr BP (~18500 cal. yr BP), which is slightly earlier than similar latitude sites on the outer WAP shelf (e.g. outer Anvers Trough between ~14000 – 13000 yr BP; ~17250 – 15850 cal. yr BP; #34, #33 and #35; Heroy and Anderson, 2007). Whereas retreat from EAP inner shelf settings between ~11000 – 10000 yr BP (~12900 – 11500 cal. yr BP) is comparable with similar inner shelf localities on the WAP (e.g. Palmer Deep at ~11300 yr B.P; 13180 cal. yr BP; Domack et al., 2001). However, the acceleration of retreat rates over the WAP inner shelf was not experienced on the EAP; the synchronicity of retreat from WAP coastal and fjord settings (e.g. Gerlache Strait and Lallemand Fjord) at ~8000 yr BP (~9000 cal. yr BP) predates the EAP, as full exposure to seasonally open marine conditions did not occur in PGC until the Mid-Holocene (~ 5000 yr BP; 5750 cal. yr BP). Further, the Larsen-B Ice Shelf has remained intact throughout the Holocene period (Domack et al., 2005), until its recent collapse in March 2002 (Scambos et al., 2003), but it is not clear if this was due to temperature or ice stability factors (Domack et al., 2005). The climatic and oceanographic contrasts present across the modern-day AP (as discussed in Chapters 2.3.3 and 2.5) are likely to have been in operation during deglaciation and would explain the delayed and more subdued response of the EAP ice sheet and ice shelves compared to the WAP.

- **Wider context and mechanisms**

Potential forcing mechanisms for ice sheet recession are now assessed in an attempt to explain the observed variability along the AP and specifically the timing for removal of grounded ice at individual core sites studied in this investigation. Previously invoked mechanisms to explain termination of the last glacial period, together with amplifiers to facilitate the continued retreat of ice sheets, in approximate chronological order and highlighted on Figure 8.9, include:

1) Increase in Northern Hemisphere summer insolation between 24000 and 10000 cal. yr BP (~20000 – 8900 yr BP) and peaking at ~12300 cal yr BP (~10400 yr BP) (Berger and Loutre, 1991; Imbrie et al., 1992; Petit et al., 1999; Alley et al., 2002; Kawamura et al., 2007). If summer insolation at high Northern latitudes is the pace-maker of global glacial and interglacial cycles, some strong inter-hemispheric connection must exist to transmit the signal to Antarctica. Whereas the statistical coherence between Northern summer forcing and Antarctic temperatures is well established (Jouzel et al., 2007), a consensus on the physical mechanism that transports the Northern Hemisphere climate signal to Antarctica has not yet been agreed.

2) Increase in Southern Hemisphere spring insolation between 18000 and 17000 cal. yr BP (~14700 – 13800 yr BP) (Stott et al., 2007). This mechanism is proposed to influence the retreat of sea ice, leading to enhanced Ekman transport to the Southern Ocean and decreased stratification due to stronger air-sea fluxes, further causing enhanced ventilation of the deep sea and subsequent rise in atmospheric CO_2 (Stott et al., 2007).

3) Changes in the duration of Southern Hemisphere summer radiative forcing (Hubers and Denton, 2008). Models suggest that a longer summer, as opposed to a more intense one, produces warmer annual average atmospheric temperature; patterns produced by the models are coherent and in phase with proxies of Antarctic atmosphere temperature (Hubers and Denton, 2008). The duration of the Southern summer covaries almost identically with Northern summer insolation intensity (Hubers and Denton, 2008), which as discussed in point (1) reached a peak at ~12300 cal yr BP (~10400 yr BP) (Berger and Loutre, 1991).

4) Oceanographic controls, through the bipolar seesaw mechanism, whereby changes in the strength of the Atlantic meridional overturning circulation

(AMOC) affect the distribution of heat between the South Atlantic and North Atlantic and more widely (Broecker et al., 1998; Vellinga et al., 2002; Barker et al., 2009). Put simply, a vigorous AMOC is thought to deliver heat to the North Atlantic at the expense of the Southern Ocean (Steig, 2006). Reconstructions for the last deglaciation (18000 – 14600 cal. yr BP; ~14700 – 12400 yr BP) suggest that AMOC was much reduced (McManus et al., 2004; Carlson et al., 2008), resulting from large influxes of freshwater into the North Atlantic (Broecker and Denton, 1990), and causing an immediate decrease in the northward heat transport (Vellinga et al., 2002). As a result, surface air temperatures over the North Atlantic cool and those over the South Atlantic warm (Barker et al., 2009). Associated indirect effects include the southward shift of the Intertropical Convergence Zone (ITCZ) (Vellinga et al., 2002) and the Southern Hemisphere westerly wind belts (Timmermann et al., 2005; Lamy et al., 2007; Anderson et al., 2009; Toggweiler, 2009). Southward shift in the westerly wind belt is suggested to have occurred at 17000 cal. yr BP (~13800 yr BP) and more significantly, concurrent with the rise in CO_2 levels and before warming in Antarctica (Anderson et al., 2009). This led Anderson et al. (2009) to propose a direct link between increased ventilation of deep water through wind-driven upwelling and the deglacial rise in atmospheric CO_2. Furthermore, modelling studies suggest a direct consequence of the increased westerly wind strength is a contemporaneous intensification of the ACC (Rind et al., 2001), which has been inferred in the South Atlantic from benthic foraminiferal data (Barker et al., 2009).

The implication for the AP is that southward migration of the westerly wind belt and intensification of the ACC at ~18000 cal. yr BP (~14700 yr BP) could provide a mechanism to promote increased UCDW upwelling. The flux of warm UCDW onto the continental shelf of the AP is thought to be related to a combination of the continuity and strength of the ACC (Klinck and Smith, 1993; Hofmann and Klinck, 1998), therefore impingement of the ACC along the WAP shelf break could potentially enable UCDW to interact with the ice sheet and facilitate basal melting. If this was a plausible mechanism for driving ice sheet retreat, it reinforces conclusions based on model studies that ice shelves are susceptible to the effects of changing ocean currents on the rate of bottom melting (Shepherd et al., 2003; Payne et al., 2004; Smith et al., 2007b).

5) Increase in atmospheric greenhouse gas concentrations (CO_2 and CH_4) (Petit et al., 1999; Shackleton, 2000). On a global scale it is reasonable to assume that greenhouse gases have contributed significantly (possibly about half; 2 – 3 °C) to the globally averaged glacial-interglacial temperature change (Petit et al., 1999). Increases in CO_2 and CH_4 concentrations and changes in Antarctica temperature occur quasi-synchronously during the last termination (and the three previous terminations) in the Vostok ice record (Blunier et al., 1997; Petit et al., 1999), whereas in the EPICA Dome C record CO_2 and CH_4 appear to lag Antarctic temperature changes (Jouzel et al., 2007). Potentially past CO_2 variability is driven by ocean-atmosphere gas exchanges through changes in Antarctic sea ice cover and Southern Ocean surface, deep water stratification or upwelling (Toggweiler, 1999; Stephens and Keeling, 2000; Sigman and Boyle, 2000; Anderson et al., 2009).

6) Sea level rise. During the period from the LGM to the onset of the Holocene, sea level rose by just over 60 m, with the steepest rise termed melt-water pulse (MWP) 1A, beginning just before 14000 cal. yr BP (~12000 yr BP) (Fairbanks, 1989; Bard et al., 1990), with sea levels rising by 15 – 25 m in a period of less than 500 years (Clark et al., 1996; 2002) and a further rapid rise at 11000 cal. yr BP (~9700 yr BP) (MWP 1B) (Fairbanks, 1989). There is also evidence of a smaller, but significant, increase of ~10 m, around 19000 cal. yr BP (~15800 yr BP) (termed 19ka-MWP) (Yokoyama et al., 2001; Clark et al., 2004). Rising sea levels would aid floatation of the marine-based WAIS and cause rapid ice sheet retreat from the AP continental shelf.

As summarised by Severinghaus (2009, p1094): "The chain of causality for the last deglaciation began with Earth's spin-axis (precession), but this gradual change was amplified in an unsteady cascade of events by ice cover, meltwater, ocean circulation and CO_2 in the atmosphere." With regards to the spatial variability in the timing of ice sheet retreat along the AP, a number of points are worth discussing (as highlighted in Figure 8.9).

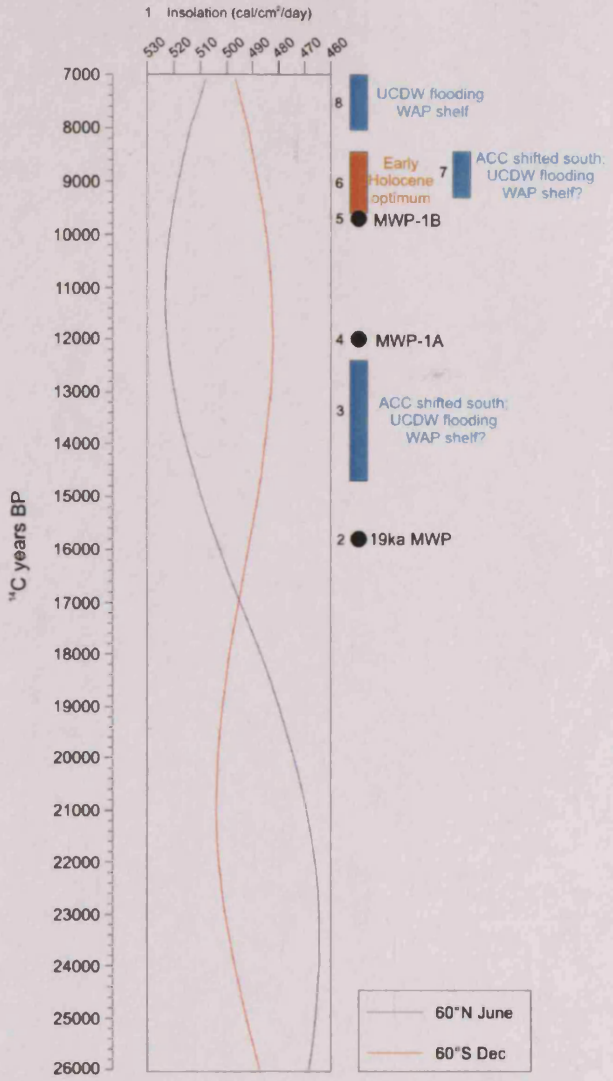


Figure 8.9
Forcing mechanisms contributing to Antarctic deglaciation: 1 = Summer insolation curve for Northern and Southern Hemisphere (Berger and Loutre, 1991); 2 = 19ka meltwater pulse (MWP) (Yokoyama et al., 2001; Clark et al., 2004); 3 = Southward shift of the Southern Hemisphere westerly wind belt and ACC (Timmermann et al., 2005; Lamy et al., 2007; Anderson et al., 2009; Toggweiler, 2009), through reduced strength of Atlantic meridional overturning circulation (AMOC), potentially causing incursion of UCDW onto the WAP shelf; 4 = Meltwater pulse (MWP) 1A (Fairbanks, 1989; Bard et al., 1990); 5 = Meltwater pulse (MWP) 1B (Fairbanks, 1989); 6 = Early Holocene climatic optimum recorded in Antarctic ice cores (Ciais et al., 1992; Masson et al., 2000; Masson-Delmotte et al., 2004); 7 = Southward shift of the Southern Hemisphere westerly wind belt and ACC, revealed through proxy data in South America (Lamy et al., 2001; 2002; McCulloch and Davies, 2001; Mayr et al., 2007); 8 = UCDW flooding the WAP (diatom and stable isotope data in this study).

The early recession of the ice sheet in the southern Bellingshausen Sea at ~26000 yr BP (~30000 cal. yr BP) is an important result when considering deglaciation mechanisms and is being addressed fully by Hillenbrand et al. (in prep.). What factors could cause this region to respond differently or independently to the rest of the AP? In this investigation, emphasis is placed on possible reasons for removal of grounded ice from the coastal core site GC358 at 12650 yr BP (15020 cal. yr BP). As discussed in Chapter 2.6.3, the present-day oceanographic regime of the southern Bellingshausen Sea is characterised by the ubiquitous presence of UCDW (Jenkins and Jacobs, 2008). UCDW is around 3 °C warmer than the surface freezing point and when it has access to the base of an ice shelf high melt rates result (Shoosmith et al., 2008). The inferred southerly position of the ACC ~18000 cal. yr BP (~14700 yr BP) could mean that it was impinging on the outer continental shelf. The wide, deep opening of the Belgica Trough

at the shelf break could have enabled UCDW to flood the shelf, using the trough as a conduit to reach coastal localities and facilitate sub-glacial melting. Although glacio-isostacy is difficult to infer for the LGM, if the suggestions of Ó Cofaigh et al. (2005b; 2008) and Hillenbrand et al. (2007) that the southern Bellingshausen Sea provided one of the main exits for WAIS drainage are correct, then potentially the increased ice load would have resulted in depression of the continental crust and made any UCDW influence or sea level rise (driven by 19ka-MWP) more effective in floating grounded ice in this area. Furthermore, early retreat specifically from core site GC358 could be controlled to some degree by the surrounding geography, glaciological regime and drainage patterns. Today, most terrestrial ice on Alexander Island (directly to the north of this core site) flows to the north; potentially the same occurred during deglaciation, with this core site in the shadow of Beethoven Peninsula (Figure 2.10b).

Again, considering the southerly latitude of Marguerite Bay, ice sheet retreat is slightly earlier than glacio-isostatic and glaciological model predictions, which place initiation at ~12000 – 9000 cal. yr BP; ~10250 – 8100 yr BP) (Tushingham and Peltier, 1991; Peltier, 1994; Nakada et al., 2000). Instead the earlier, rapid retreat of the ice sheet from the outer to mid-shelf between 11195 – 10150 yr BP (~13090 – 11800 cal. yr BP) could be a response to the rapidly rising sea levels associated with MWP-1A (14000 cal. yr BP; ~12000 yr BP) (Figure 8.9). Floatation mechanisms, facilitated by the shoreward dipping shelf profile, could have lifted the ice sheet from the sediments enabling rapid flow (Dowdeswell et al., 2008; Ó Cofaigh et al., 2008) and sub-glacial melting processes to ensue. The subsequent period of grounding line stability between ~10000 and 8000 yr BP (~11500 – 8870 cal. yr BP) in the ice sheet recession histories of Marguerite Bay and Anvers Trough potentially suggests that either glacio-dynamic / topographic controls are also important in some specific settings (e.g. presence of grounding line pinning points), or that a period of relative "climatic cooling" occurred. Diatom assemblage data in cores GC047 and VC306, together with carbon and nitrogen stable isotope results from core VC306, provide further clues to the oceanographic conditions at this time and are discussed more fully under the heading "occurrence of an Early Holocene climatic reversal" (p8-61).

Following the inferred pause in recession of the ice sheet on the WAP, a second phase of rapid retreat occurred towards coastal localities at ~8000 yr BP (8870 cal. yr BP). A potential precursor signal is provided by increased abundances of *E. antarctica* rs in the three cores recording the post-deglaciation environment (GC358, VC306 and GC047).

This species has been tentatively linked with the occurrence of localised iceberg meltwater lenses (Burckle, 1984) and iron enrichment (Armand et al., 2008). Noticeably increased abundance of this species occurs at 10320 yr BP (12210 yr BP) in core GC358, 9500 yr BP (10860 cal. yr BP) in core VC306, and 9000 yr BP (10200 cal. yr BP) in core GC047. The observation of very rapid retreat in inner WAP shelf areas and synchronicity of removal of grounded ice from very coastal WAP localities (Moutonnée Lake – George VI Ice Shelf, #55; Neny Fjord, #46; Lallemand Fjord, #41; Gerlache Strait, #21) at ~8000 years (~8870 cal. yr BP) is important when considering ice shelf collapse mechanisms and glacier dynamics. Recent observations have shown that several glaciers have accelerated since the collapse of their buttressing ice shelves (Rignot et al., 2004: 2005; Dupont and Alley, 2005). It is therefore likely that the instability produced by the rapid retreat of the ice sheet from inner Marguerite Bay (together with atmospheric and oceanic influences (Smith et al. 2007a)), would have had knock-on consequences for the stability of the George VI Ice Shelf, leading to its eventual collapse in the Early Holocene (8170 yr BP; 9600 cal. yr BP) (Smith et al., 2007a: 2007b). Sub-glacial melting processes are also likely to have been important during ice sheet retreat from Marguerite Bay and the southern Bellingshausen Sea, due to the shelf profile in this area, containing deep inner basins that facilitate the intrusion of warm UCDW into inner shelf settings. Reconstructions from the AP marine cores used in this investigation suggest that UCDW influence was present on the WAP at ~8000 yr BP (~8870 cal. yr BP), coincident with this second phase of rapid recession of the ice sheet from inner bay and fjord settings and establishment of re-current sea ice cycle in Marguerite Bay and Anvers Shelf. However, large scale connection through variations in AMOC and associated heat fluxes to Antarctica (discussed in point 4) cannot be inferred for the oceanographic changes and ice sheet retreat at ~8000 yr BP (~8870 cal. yr BP) because during the last 11500 cal. yrs (9300 yrs), except for a brief reduction 8200 cal. yr BP (~7370 yr BP) (Alley et al., 1997; Barber et al., 1999), circulation appears to have remained locked in its conveyor mode, with active meridional overturning (Denton and Broecker, 2008); another mechanism must be inferred to drive warm UCDW onto the shelf at this time.

Both the strength and position of the ACC are important in controlling the flux of UCDW onto the WAP shelf (Klinck and Smith, 1993; Hofmann and Klinck, 1998). An intensification of the ACC is has been modelled to be a direct consequence of increased westerly wind strength (Rind et al., 2001). Between 11500 and 9500 cal. yr BP (~9300

– 8450 yr BP) a more southerly position for the ACC is inferred from a compilation of data, including SST data from the Peru-Chile Current, a northern extension of the ACC (Lamy et al., 2001; 2002), pollen data in the Magellen Strait region of southernmost South America (McCulloch and Davies, 2001) and pollen evidence in Patagonia (Mayr et al., 2007) (Figure 8.9). In theory, a more southerly position of the ACC at this time could provide a mechanism to promote greater UCDW upwelling onto the WAP shelf. This would act to facilitate sub-glacial melting, on an already weakened ice sheet through high surface melting rates resulting from elevated Early Holocene atmospheric temperatures (Figure 8.9). However, there is no direct evidence in the cores studied in this investigation or the Palmer Deep record for the presence of this warm ocean current between ~9300 – 8450 yr BP (11500 and 9500 cal. yr BP). A potential explanation is because the grounding line remained largely fixed in mid-shelf settings, leading to the dominance of cool shelf waters and reduced cross-shelf circulation (as suggested in this study for Marguerite Bay and Anvers Shelf; Figure 8.3), no accommodation space for UCDW existed on the WAP shelf. The importance of cross-shelf circulation near the shelf break to "pull" UCDW into the interior was modelled by Dinniman and Klinck (2004). Once the trend of ice sheet retreat had been re-initiated on the WAP and sea ice cover reduced, important cross-shelf currents would become established and facilitate the intrusion of UCDW into more coastal WAP settings, irrespective of shifts in the latitudinal position of the Southern Westerlies and ACC. The pollen records in southern Patagonia suggest that the Southern Westerlies moved north by 9500 – 9200 cal. yr BP (~8450 – 8210 yr BP) (McCulloch and Davies, 2001; Mayr et al., 2007), but they may not have reached their modern configuration at this time (Bentley et al., 2009). Evidence of increased precipitation in Chile, occurring in two phases at 8000 cal. yr BP (~7200 yr BP) and 6000 cal. yr BP (~5200 yr BP) was used to suggest that there was southward movement of the Westerlies also at this time (Jenny et al., 2002). This latter suggestion would fit with the reconstructions from this investigation, suggesting UCDW presence on the WAP after ~7600 yr BP (8300 cal. yr BP). Further understanding of the regional oceanography in the Early Holocene presents one of the challenges to both the palaeoclimate and modelling disciplines. However, an oceanographic forcing mechanism would help explain the cross-peninsula differences at this time, with the thicker ice shelves on the east remaining stable and protected from this warm oceanographic pulse.

One of the motivations for constraining the timing of deglaciation is to assess the contribution Antarctic ice sheets provided to meltwater pulses and associated sea level rise. There has been much debate as to whether the source of the meltwater pulses came from Northern high latitudes (Peltier, 1994; Kennett and Shackleton, 1975; Keigwin et al., 1991) or Southern high latitudes (Clark et al., 2002; Denton and Hughes, 2002; Bassett et al., 2007). The deglaciation history presented for the AP suggests that large-scale retreat had started before 14000 cal. yr BP (~12000 yr BP), so it is possible that some of MWP-1A originated from the Southern Hemisphere, as modelled by Bassett et al. (2007). The early drainage of the ice sheet through the southern Bellingshausen Sea, potentially initiated as early as 26000 yr BP, could potentially have contributed to the 19ka-MWP. The model of Denton and Hughes (2002) suggests that Antarctica contributed 14 m to eustatic sea level equivalent since the LGM rise, 2.9 m of which came from the AP sector. However, as Heroy and Anderson (2007) note, the extended duration of ice sheet retreat in the AP (~9000 years) means that the actual contribution to either MWP-1A or -1B is likely to be a small fraction of the total 2.9 m.

The post-deglaciation marine environment

The initial post-deglaciation environment on the AP is revealed through diatom assemblage data. In two of the WAP cores (GC358 and GC047), immediate post-deglaciation biogenic sedimentation is overwhelmingly dominated by CRS, recording their Holocene maximum abundance at this time. Mass sedimentation of CRS immediately after ice sheet retreat has also been observed in several other published records from Antarctica, including Palmer Deep (#25 and #27; Leventer et al., 1996; 2002) and sites on the East Antarctic margin (#22; Taylor and McMinn, 2001; #123; Leventer et al., 2006). Deposition of these mono-specific layers requires both high primary productivity (phytoplankton blooms), resting spore formation and mass sedimentation; each resulting from different processes and a change in environmental conditions. However, the only recorded expression in the sediment cores is sedimentation of resting spore formation; high primary productivity, together with minimal transportation and dissolution processes, are inferred from the large numbers of resting spores that reach the sediment. Causes or factors promoting large phytoplankton blooms, that would have been common in the post-deglaciation environment, include low salinity, surface water stratification (Nelson et al., 1987), which would have developed through active melt of the retreating ice sheet, and large nutrient inputs (Martin et al., 1990). Enhanced micronutrient iron input has been proposed previously

as a fertilisation mechanism for extremely large glacial – Holocene transition blooms (Stickley et al., 2005; Leventer et al., 2006). Melting sea and glacial ice provide a potential nutrient source, as iron-rich dust originally accumulated on the ice sheet via aeolian transport (Rea, 1994; Wolff et al., 2006) is subsequently released by ablation processes. Incubation and large-scale ecosystem experiments demonstrate that iron fertilisation promotes large diatom blooms in the Southern Ocean (Martin et al., 1990; Boyd et al., 2000; Boyd and Law, 2001; Coale et al., 2004), suggesting that this is a likely scenario. Another possible source of the elevated nutrients, suggested for Iceberg Alley (East Antarctic margin) (#136; Stickley et al., 2005), is incursion of UCDW. As discussed above, upwelling of warm UCDW is proposed to be a plausible mechanism for facilitating ice sheet retreat from WAP localities, so potentially could have been a source of nutrients for initial post-deglaciation diatom blooms recorded in these AP cores. The subsequent formation of resting spores and their mass sedimentation requires quite different processes to those that promote high productivity, although as discussed in Chapter 3.2.2, exactly what triggers resting spore formation is poorly understood. In the ice-dominated post-deglaciation AP environment likely attributing factors include: (1) depletion of surface water nutrients, which occurs frequently at the end of phytoplankton bloom events; (2) break-down of stratification and deep mixing of the water column, due to reduced meltwater input or increased storm frequency; and (3) fluctuations in light levels, which can occur when (i) cells are mixed or sink below the pycnocline; (ii) self-limitation occurs due to extremely high phytoplankton stocks; or (iii) sea ice cover increases and cells are advected under the ice.

In cores GC047 and GC358, the overwhelming dominance of CRS is only observed in one or two sample depths, lasting ~230 and ~860 ^{14}C years, respectively. In core GC358, this may be attributed in some degree to the very low sedimentation rate experienced at this core site. However, a more likely interpretation is that CRS bloom conditions were only prevalent for a short period of the post-deglaciation environment, associated with the immediate retreat of grounded ice, rather than the more prolonged ice sheet retreat towards the Early Holocene climatic optimum. In this scenario, water column stratification would progressively break-down as the meltwater, derived from the retreating ice front, becomes increasingly distal from the core site. Surface water nutrients would also soon be depleted by the large phytoplankton blooms and exhausted, through reduced ablation from glacier and sea ice, or reduced deep water sources, leading to a decline in primary production.

In exceptional circumstances, through development of very specific environmental conditions, post-deglaciation diatom production and sedimentation were dramatically amplified above today's levels (e.g. Palmer Deep and core site GC407). These resulted from the combined effects of nutrient-rich melt from both glacial and seasonal sea ice and intense surface water stratification; an environment in which diatoms flourished. In the Palmer Deep record, the period between 13180 – 11460 cal. yr BP (~11300 – 10120 yr BP) is proposed to be warmer than modern (Leventer et al., 2002), based on the rhythmically laminated intervals of *Chaetoceros* ooze (biogenic laminae; > ~1000 Mv/g) and mud (terrigenous laminae; < ~1000 Mv/g) (Leventer et al., 2002; Maddison et al., 2005). The model Leventer et al. (2002) propose for such sedimentation and extremely high primary productivity involves a combination of estuarine circulation and glacier proximal conditions, whereby warmer sub-polar conditions leads to large spring blooms of *Chaetoceros*, followed by influx of silt and clay via estuarine overflow, causing a frontal boundary and mass sedimentation of CRS. This type of sedimentation is not found today in any modern setting along the AP or elsewhere in Antarctica (Leventer et al., 2002). Recent analysis of the Palmer Deep record using the TEX_{86} palaeotemperature proxy has shown that Holocene SSTs were warmest (5 – 6 °C) in the Early Holocene (12000 – 10500 cal. yr BP; ~10300 – 9300 yr BP) (Shevenell et al., 2007). The Palmer Deep regional reconstruction suggests an environment strongly influenced by the presence and position of the adjacent ice sheet (Domack et al., 2001; Leventer et al., 2002; Sjunneskog and Taylor, 2002; Taylor and Sjunneskog, 2002; Maddison et al., 2005). Domack et al. (2002) propose that the Gerlache Strait and Bismarck Strait remained largely blocked by ice, leaving the Palmer Deep basin partially encircled by tidewater glaciers (those grounded at the calving line below or near sea level) or ice shelves. This would have resulted in constricted circulation and further enhanced stratification across the basin; ideal conditions for diatom bloom species (Domack et al., 2001; Leventer et al., 2002; Sjunneskog and Taylor, 2002; Maddison et al., 2005). In the cores analysed in this investigation, comparable sedimentation regimes and diatom assemblages were only observed in core GC047 (see section 8.3.2, p8-16), interestingly, the most proximal core to the Palmer Deep site. Zone GC047-i (10750 – 9870 yr BP; 12720 – 11280 cal. yr BP) is characterised by exceptionally high diatom abundance (>1000 Mv/g, comparable to the biogenic laminae in Palmer Deep), with diatom assemblages indicative of seasonal sea ice melt and associated stable, stratified upper water column. Similar to the reconstruction for Palmer

Deep, offshore Anvers Island represents a more distal member of glacier proximal conditions and intense surface water stratification.

More commonly observed in AP cores, the post-deglaciation non-CRS assemblage is dominated by *T. antarctica* warm rs, particularly apparent in Marguerite Bay (core VC306) and again offshore Anvers Island (core GC047), plus the immediate post-ice shelf absence environment in the EAP cores. High abundance of *T. antarctica* rs (unspecified variety) have been observed in other deglacial sedimentary sequences, including Palmer Deep (#24; Taylor and Sjunneskog, 2002; Maddison et al., 2005), Bransfield Strait (#14; Heroy et al., 2008) and Prydz Bay (#120; Taylor and McMinn, 2002). In the Prydz Bay example, high abundances of *T. antarctica* rs (unspecified variety), together with *F. curta*, were used to infer a reduction in seasonal sea ice cover, probably with no permanent sea ice edge present, and an increase in the duration of open water (Taylor and McMinn, 2002), whereas in Bransfield Strait high abundances were attributed to the ice-edge environment (Heroy et al., 2008). Large fluxes of *T. antarctica* warm rs to the sediment require comparably high concentrations of vegetative valves in the surface water. Shelf waters containing newly forming platelet ice and frazil ice (typical of late summer – early autumn conditions; sea ice type 2) would easily develop in the post-deglaciation marine environment through interaction with the proximal grounded ice and ice shelves. Further support for this environmental reconstruction is provided by the observation that *T. antarctica* warm rs dominate the non-CRS assemblage throughout the Holocene in the EAP sediment cores (VC234, VC237 and VC205). Elevated abundance of this species in the WAP post-deglaciation environment suggests surface water conditions comparable to the EAP, characterised by super-cooled surface water and active ice crystal formation. Furthermore, in the northern WAP (core VC306 and GC047) typical sea ice type 1 species are in low abundance compared to Mid-Holocene levels, suggesting that the seasonal cycle of sea ice advance and retreat had not become established in WAP coastal waters at this time (before 7580 yr BP; 8390 cal. yr BP in Marguerite Bay and before 7680 yr BP; 8280 cal. yr BP in Anvers Trough). Potentially fast ice extended further offshore at this time, or was built up behind or blown against ice fronts and icebergs. The latter has been observed in recent years in McMurdo Sound (Ross Sea) when a very large iceberg (B-15) detached from the Ross Ice Shelf and became stranded at the entrance of the Sound; preventing the usual ocean circulation purging the annual sea ice cover and multi-year ice quickly built up (Remy et al., 2008). Associated with increased ice thickness and

strong decrease in bulk salinity, autotrophic productivity was observed to decrease over consecutive years (Remy et al., 2008). Ocean modelling also suggests that icebergs facilitate the formation of sea ice, through the addition of fresh water and surface water cooling (Jongma et al., 2009). In the immediate post-deglaciation environment, the increased relative importance of sea ice type 2 conditions, compared to sea ice type 1 conditions suggests that diatom productivity was characterised by a short growing season, with the annual – perennial cycle consisting of: (i) isolated areas of the sea ice breaking up periodically, leading to development of a meltwater environment and CRS deposition ("spring-type" conditions; sea ice type 1); (ii) followed by a more prolonged period of super-cooled surface waters, leading to the blooms of *T. antarctica* vegetative ("autumn-type" conditions; sea ice type 2); and (iii) rapid return to more consolidated ice conditions and associated reduction in light intensity, leading to resting spore formation and low primary production ("winter-type" conditions).

Occurrence of an Early Holocene "climatic reversal"?

The AP "climatic reversal" was first documented in the Palmer Deep record between ~10000 – 8250 yr BP (11460 – 9070 cal. yr BP) (Domack et al., 2001; Domack, 2002). This interval in the Palmer Deep record is characterised by several cold indicators: lower diatom abundance and a mixed assemblage, with sea ice, sub-polar, and late season associated diatom species (Sjunneskog and Taylor, 2002; Taylor and Sjunneskog, 2002) and benthic foraminiferal record reflecting the influence of cold shelf water (Ishman and Sperling, 2002). The Palmer Deep Basin experienced higher terrigenous input through this interval, shown by higher coarse-fraction abundance, higher MS and mass accumulation rates (Domack, 2002). Explanations for these observations in the Palmer Deep record include resurgence of grounded glacial ice over the basin, indicating climatic cooling (Domack et al., 2001: 2002), and opening of a passage through Gerlache and Bismarck Straits, leading to reduced upper water column stratification, reconfiguration and increased vigour of surface water currents (Taylor and Sjunneskog, 2002; Sjunneskog and Taylor, 2002). The timing, diatom assemblages and environmental reconstructions of the "climatic reversal" in the Palmer Deep record is very similar to zones GC047-ii (9870 – 7680 yr BP; 11280 – 8280 cal. yr BP) and VC306-i (10150 – 7580 yr BP; 11800 – 8390 cal. yr BP) from Anvers Shelf and Marguerite Bay, respectively (Figure 8.4). The "climatic reversal" inferred from the Palmer Deep record has not been widely observed in the AP and a comparable signal in

cores GC047 and VC306 provide two further data points, suggesting that the event was not localised to the Palmer Deep Basin.

Zone VC306-i (10150 – 7580 yr BP; 11800 – 8390 cal. yr BP) and zone GC047-ii (9870 – 7680 yr BP; 11280 – 8280 cal. yr BP) are characterised by low total diatom abundance and diatom assemblages indicative of cool shelf waters, with poorly developed surface water stratification, together with a stable isotope signal in core VC306 indicating limited upwelling. The shelf water-dominant regime proposed for Marguerite Bay (core VC306) during this early post-ice sheet retreat phase (10150 – 7580 yr BP; 11800 – 8390 cal. yr BP) potentially results from the close proximity of a relatively stable ice front. Well-mixed, supercooled shelf waters would quickly develop through interaction with the ice sheet, or floating ice shelf, together with lack of warming influence from UCDW and reduction in fresh meltwater fluxes (which typically promotes surface water stability). Such conditions would mimic autumn-type sea ice formation, leading to the observed high abundance of sea ice type 2 diatom species (*T. antarctica* warm rs) during this interval. The marginal sea ice zone (and associated sea ice type 1 assemblage) is likely to have been located offshore; a suggestion supported by a core from the South Scotia Sea (#84; Bak et al., 2007), with diatom assemblages indicating that the spring sea ice edge covered the core site before 8300 yr BP (~9280 cal. yr BP). I propose that the early post-ice sheet retreat environmental reconstruction for Marguerite Bay is also transferable to offshore Anvers Island (zone GC047-ii; 9870 – 7680 yr BP; 11280 – 8280 cal. yr BP), with shelf waters dominant and active coastal currents, resulting in a well-mixed water column and associated lower diatom abundance. Cool shelf waters could indicate the re-circulation of the AP coastal current, carrying Weddell Sea Transitional Water to more southerly WAP localities and strengthening the cool shelf water signal along route.

- **Wider context and mechanisms**

Explaining the presence of a "climatic reversal" within a widely documented period of Early Holocene warmth in other proxy records has been difficult. Bentley et al. (2009) suggest that the "climatic reversal" represents: (1) a local response to deglaciation with increased glacial meltwater causing more persistent sea ice and perhaps a standstill or even re-advance of the grounding line around the Palmer Deep basin; or (2) discharge of ice from glaciers following collapse of buttressing ice shelves through mechanisms seen on the AP today (Rott et al., 2002; Rignot et al., 2004; Scambos et al., 2004). The data

presented in this study supports Bentley et al.'s first argument; the occurrence of this "climatic reversal" signal coincident with a proposed period of grounding line stability in the deglaciation histories of Marguerite Bay and Anvers Trough (and potentially elsewhere on the WAP), would suggest this reflects a stall in ice sheet recession on the WAP. An important observation is that this event is only observed in marine records, suggesting an oceanographic control, rather than an atmospheric one. From the evidence (diatom, plus carbon and nitrogen stable isotopic) specifically in core VC306, it is likely that this oceanographic factor is the competitive interaction between cool shelf waters and warm UCDW (Figure 8.3). This mechanism has also been implied for observed variability in the Late Holocene record from Palmer Deep (670 cal. years BP to present) (Shevenell and Kennett, 2002).

Occurrence of an Early Holocene climatic optimum?

Distinguishing the diatom signal of deglaciation from the ice-core based Early Holocene climatic optimum conditions between 11000 – 9500 cal. yr BP (~9600 – 8450 yr BP) (discussed fully in section 8.4.2.1) has proved difficult in this investigation. Early Holocene climatic conditions clearly were warmer than the preceding glacial period, evidenced by the contraction of the ice sheet exposing four of the core sites studied in this investigation, however, it is not easy to determine whether this retreat was driven by significantly elevated atmospheric or oceanic temperatures, or a combination of both. Removal of grounded ice from two core sites (VC306 and VC237) did occur during this period and it is likely that a combination of factors played a part, including insolation, eustatic sea level rise and warm oceanographic influences. As discussed in section 8.4.1.1, ice sheet recession from the outer AP continental shelf was underway before 11000 cal. yr BP (~9600 yr BP). Further, ice sheet retreat reconstructions for the WAP (Figure 8.6 and Figure 8.7) suggest that the ice-core based Early Holocene warmth preceded the periods of rapid ice sheet retreat (Figure 8.9); a lag of ~1600 years (~2000 cal. years) is witnessed between initial onset of elevated atmospheric temperatures and retreat and collapse of inner shelf and coastal ice shelves. Potentially the ice sheet was progressively thinning by surface melting processes through elevated atmospheric temperatures, eventually collapsing from inner shelf areas due to the presence of UCDW on the WAP continental shelf.

A distinct Early Holocene warmth is not widely noted in the AP marine environment, mainly because a pre-requisite for recording this event is that the site was free from grounded ice at this time (11000 – 9500 cal. yr BP; ~9600 – 8450 yr BP). Three records

from this investigation fulfil this requirement (cores GC047, VC306 and GC358); the two former core localities (Anvers Shelf and Marguerite Bay, together with Palmer Deep) were experiencing a "climatic reversal" at this time. Other sites in Bransfield Strait (#14; Heroy et al., 2008) and Lallemand Fjord (#41; Taylor et al., 2001) were also exposed to seasonally open water conditions at this time and hint at warmer conditions, but not to levels suggested by ice core data. In the records from the southern Bellingshausen Sea (core GC358), Bransfield Strait and Lallemand Fjord, elevated diatom abundance, used to infer high productivity and optimum conditions, was not reached until after ~8000 yr B.P; (~8900 cal. yr BP) (discussed in section 8.4.1.2). The Early Holocene (10320 – 8600 yr BP; 12210 – 9570 cal. yr BP) in the southern Bellingshausen Sea was characterised by low relative abundance of typical sea ice type 1 species and occurrences of *E. antarctica* var. *antarctica* (sub-polar form), particularly around 9460 yr BP (10710 cal. yr BP), suggesting minimal seasonal sea ice and influence of UCDW, acting to facilitate melting of glacial ice. In Lallemand Fjord (#41), the diatom assemblage between 10580 – 7890 cal. yr BP (~9350 – 7050 yr BP) was used to suggest that sea ice cover was unconsolidated and oscillating seasonally over water exposed by the nearby retreating Müller Ice Shelf (Taylor et al., 2001).

- **Wider context and mechanisms**

The Early Holocene (11000 – 9500 cal. yr BP; ~9600 – 8450 yr BP) is clearly a period of complex variability in Antarctica: ice core records from the continent imply atmospheric warmth (see section 8.4.2.1); the South Atlantic records maximum Holocene SST and contraction of marginal sea ice towards Antarctica (see section 8.4.2.1); several coastal AP localities (Palmer Deep, Anvers Shelf and Marguerite Bay) allude to climatic cooling or at least stabilisation of the deglaciation trend; and several AP localities (Ronne Entrance and Lallemand Fjord) suggest presence of unconsolidated sea ice and connection with open ocean influences. Reconciling these very different environmental reconstructions and assigning forcing mechanisms is difficult.

One mechanism proposed to explain the Early Holocene warmth in Antarctica is connection with the Northern Hemisphere, through the Atlantic thermohaline circulation and associated southward shift of the Southern Hemisphere Westerlies and ACC (as discussed in point 4 on page 8-50). There is no direct evidence in these AP marine records for such mechanisms driving Early Holocene warmth and the impact of

thermohaline circulation on the AP remains speculative. As discussed previously, potentially the delay between the inferred southerly position of the ACC and evidence for upwelling of UCDW in these WAP marine cores is because no accommodation space existed on the WAP shelf because the grounding line remained largely fixed in mid-shelf settings and cool shelf waters were spatially pervasive (Figure 8.3). Another mechanism to explain the Early Holocene warmth is that annual solar insolation values were at their highest in the Early Holocene (Bentley et al., 2009). However, as Bentley et al. (2009) note, solar insolation declined gradually whereas the Early Holocene warm period ended fairly abruptly; therefore, some other mechanism was likely involved, or there are non-linear thresholds in the AP climate system.

In summary, the reconstruction for the AP in the suggested Early Holocene climatic optimum, evident in ice core records between 11000 – 9500 cal. yr BP (~9600 – 8450 yr BP), is for an environment strongly marked by progressive ice sheet recession and associated meltwater inputs, and relative insensitivity to atmospheric forcing. The grounding line is suggested to have been relatively stationary and stable (due to glacio-dynamic / oceanographic controls) and the marginal sea ice zone was progressively contracting towards this ice front (possibly aided by warmer atmospheric conditions and the southerly position of the ACC).

After the Early Holocene climatic optimum

After 9500 cal. yr BP (~8450 yr BP), several dramatic changes occurred on the AP, including renewed vigour of ice sheet retreat rates, WAP ice shelf collapse events and reconfiguration of regional ocean circulation. If the ice core-based Early Holocene climatic optimum was pervasive across the whole of the Antarctic continent (evidence for and against this is presented in section 8.4.2.1), an important question is: to what extent did the preceding period of warmth precondition or accelerate AP ice sheet recession?

Ice sheet retreat reconstructions and radiocarbon data (Figure 8.6, Figure 8.7 and Table A2.20) suggest that retreat in northern WAP inner shelf, coastal bays and fjords was synchronous at 8035 ± 315 yr BP (~8950 ± 370 cal. yr BP) (#41, #43, #46, #44, #53, #54, #21, #55). Recent studies of Holocene stability of George VI Ice Shelf propose that in the Early Holocene this ice shelf collapsed (8170 – 7300 yr BP; 9600 – 7730 cal. yr BP) (Bentley et al., 2005; Smith et al., 2007a; 2007b). Observations that this occurred immediately after the period of maximum Holocene warmth (from ice cores; Masson-

Delmotte et al., 2004) and coincided with an influx of warmer ocean water onto the WAP shelf between 9000 – 6700 cal. yr BP (~8000 – 5900 yr BP) (from the Palmer Deep diatom record; Leventer et al., 2002) provided two possible causal mechanisms (Smith et al., 2007a; 2007b). Supporting evidence for an oceanographic forcing factor is provided by the diatom and stable isotope record from Marguerite Bay (core VC306), which records a dramatic onset of open ocean influence (*F. kerguelensis*), establishment of a re-current sea ice cycle (sea ice type 1 species) and increased upwelling of nutrient-rich UCDW ($\delta^{15}N_{org}$ signal suggesting larger nutrient supply compared to phytoplankton demand) at 7580 yr BP (8390 cal. yr BP). In summary, it is believed that a combination of atmospheric, oceanographic and glacio-dynamic factors (instability produced by the rapid retreat of the ice sheet from the inner shelf) led to the ice shelf collapse in inner coastal settings of the WAP.

Elsewhere, in Bransfield Strait (record #14), the period between 9000 – 6800 cal. yr BP (~8100 – 6000 yr BP) was characterised by increased total diatom abundance and species associated with cold open water and reduced summer sea ice (*F. kerguelensis* and *T. gracilis*) (Heroy et al., 2008). The authors use this to infer retreat of the ice shelf, ameliorating conditions and increased intrusion of surface water from the outer continental shelf and from the Weddell Sea approaching modern circulation (Heroy et al., 2008). Furthermore, in the South Atlantic (50 – 53°S) several cores record the onset of cooling, after the Early Holocene climatic optimum, between 9000 and 7000 cal. yr BP (~8100 – 6100 yr BP) (Bianchi and Gersonde, 2004) and sea ice expansion and surface ocean cooling after 9300 cal. yr BP (~8300 yr BP) (Nielsen et al., 2004). This Early Holocene cooling in the South Atlantic has been attributed to expansion of the Weddell Sea Gyre circulation at that time (Bianchi and Gersonde, 2004). Although the sea ice record from Bransfield Strait (reduced summer sea ice) appears to contradict the record from the South Atlantic (sea ice expansion and surface cooling), both suggest greater connection with the Weddell Sea and highlight a common feature associated with expansion of the Weddell Sea Gyre circulation. As shelf areas of the Weddell Sea progressively experienced ice sheet recession, there would be a concurrent increase in EAP shelf circulation and surface water cooling; however, these surface waters are also able to pass through shallow openings around the tip of the AP and impact the oceanographic regime of the northern WAP. Seasonal differences in insolation (Figure 8.10; Renssen et al., 2005) could also potentially explain the observed difference in sea ice extent between Bransfield Strait and the South Atlantic. Spring temperatures

between 9000 – 7000 cal. yr BP (~8100 – 6100 yr BP) were between 2 – 2.7 °C above pre-industrial levels (Renssen et al., 2005). Spring is the time of sea ice retreat in Antarctica, so possibly elevated spring-time temperatures at this time facilitated the rapid and extensive retreat towards the AP coast; this would lead to Bransfield Strait experiencing open ocean conditions in summer. Additionally, autumn temperatures at this time were between 0.5 – 1.4 °C below pre-industrial levels (Renssen et al., 2005). As suggested by Crosta et al. (2005), based on diatom records from East Antarctica partnered with the insolation modelling studies of Renssen et al. (2005), spring sea ice melted earlier in the year, but also autumn sea ice freezing occurred earlier in the year during the Early- to Mid-Holocene. In other words, the summer and winter sea ice boundaries were becoming more and more geographically divergent between 9000 – 7000 cal. yr BP (~8100 – 6100 yr BP); summer sea ice progressively contracted towards the AP coast, reaching Bransfield Strait, due to elevated spring temperatures, whereas winter sea ice progressively expanded outwards, reaching into the South Atlantic, due to cooler autumn temperatures.

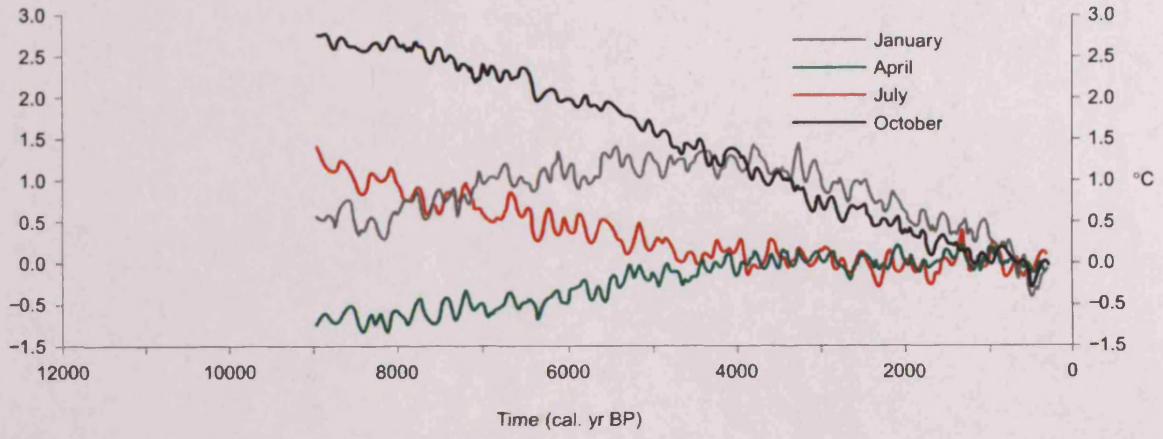


Figure 8.10
Modelled Holocene monthly surface temperatures (°C), averaged over the area south of 60°S (Renssen et al., 2005).

8.4.1.2 Mid-Holocene climatic optimum

A peninsula-wide marine inferred Mid-Holocene climatic optimum is witnessed in all cores analysed in this investigation (excluding core GC114, which only recovered Late Holocene sediments) (Figure 8.4). The climatic optimum manifests itself in these marine records as a period of elevated primary production, evidenced by higher overall

diatom abundances and species assemblages associated with active spring meltwater stratification (*Chaetoceros* species and typical sea ice type 1 assemblage). However, diatom assemblages from individual core localities and different sides of the AP reflect the complex nature of both the timing and local expression of the climatic optimum (Figure 8.11).

In the northern WAP (cores GC047 and VC306), onset of the climatic optimum is abrupt, occurring roughly coevally between localities (~7600 yr BP; 8300 cal. yr BP) (Figure 8.4), and is represented by the establishment of a re-current seasonal sea ice cycle. Whereas previously sea ice was persistent across the AP shelf (as discussed in section 8.4.1.1) and cool shelf waters dominated, near-complete recession of the ice sheet from the continental shelf facilitated the inland retreat of summer sea ice into coastal AP settings. Elevated abundances of *F. kerguelensis*, *Proboscia* and *Rhizosolenia* species also indicate there was exchange with outer shelf waters, with substantial periods of seasonally open water. This is further supported by the carbon and nitrogen stable isotope record from core VC306 (see section 8.3.3, p8-21), potentially highlighting the role UCDW played in breaking-up the Early Holocene multi-year ice cover in Marguerite Bay (and ice sheet retreat from inner coastal settings, discussed in section 8.4.1.1). Vertical time-dependent sea ice and mixed layer models have highlighted the importance of UCDW intrusions onto the Marguerite Bay shelf in both the heat and salt budgets of the area (Smith and Klinck, 2002). It is also worth noting carbon and nitrogen stable isotope-based interpretations for Marguerite Bay (core VC306) corroborate suggestions of sustained presence of UCDW between 9000 and 3600 cal. yr BP (~8050 – 3350 yr BP) in the Palmer Deep, based on the marine isotope record ($\delta^{18}O$ and $\delta^{13}C$ from benthic foraminfera) (#26; Shevenell and Kennett, 2002). However, both of these are at odds with the benthic foraminifera faunal record for the same period in Palmer Deep, which suggests these basins were filled with saline shelf water and an associated absence of UCDW (Ishman and Sperling, 2002). Although the contradiction between Marguerite Bay reconstructions and the benthic foraminifera record in Palmer Deep can possibly be explained due to spatial variability of UCDW influences in the Mid-Holocene, this mechanism cannot be inferred when two proxies in the same record (Palmer Deep) are conflicting. Resolving this is crucial if we are to understand the role UCDW plays in shaping the climate of the AP.

Lallemand Fjord (#41), situated between Anvers Shelf (core GC047) and Marguerite Bay (core VC306), similarly records a relatively warm period between ~7890 – 3850

cal. yr BP (~7050 – 3550 yr BP), characterised by high primary productivity, open water diatom taxa, high TOC and scattered ice rafted debris (Taylor et al., 2001). This was used to infer a more open marine, ice distal environment (Taylor et al., 2001), although variability in primary production, which in turn is thought to reflect variation in sea ice extent, was evident through this period (Shevenell et al., 1996). This is particularly notable around 7310 – 5390 cal. yr BP (6450 – 4650 yr BP), where low TOC values correspond with deposition of the sea ice-associated assemblage (Taylor et al., 2001). Following on from the suggestion made in this study for the establishment of a re-current seasonal sea ice cycle on the WAP at ~7600 yr BP (8300 cal. yr BP), potentially the marine record from Lallemand Fjord is also reflecting the close proximity of the marginal sea ice zone at this time, resulting in variable deposition of open ocean diatom species (during periods when the summer sea ice boundary retreats fully into Lallemand Fjord and the inner fjord experiences open water conditions) and sea ice species (during periods when the summer sea ice boundary lies offshore of Lallemand Fjord and the inner fjord experiences open pack ice conditions during summer). Another period in the record from Lallemand Fjord, between 4200 – 2700 cal. yr BP (~3800 – 2600 yr BP), is highlighted for having high TOC values and was used to infer "true" climatic optimum conditions (Shevenell et al., 1996) and agrees with the timing of the Mid-Holocene climatic optimum recorded in terrestrial records (Figure 8.11). It is worth noting however, that the diatom data does not suggest climatic optimum conditions at this time, instead climatic cooling is inferred from 3850 cal. yr BP (~3550 yr BP) towards the present (Taylor et al., 2001).

Comparing the proposed timing of the Mid-Holocene climatic optimum in Marguerite Bay (core VC306) and offshore Anvers Island (core GC047) with other localities on the WAP, it becomes apparent that many discrepancies exist (Figure 8.11). Firstly, the Palmer Deep record suggests that onset of the Mid-Holocene climatic optimum occurred abruptly at 9000 cal. yr BP (~8050 yr BP) and spanned the period until 3700 cal. yr BP (~3450 yr BP). This onset is slightly earlier than that proposed for the two northern WAP in this investigation and record #15 (Yoon et al., 2002), but the transition into Late Holocene climatic deterioration is roughly synchronous (~3400 yr BP; ~3600 cal. yr BP) between Palmer Deep and cores VC306 and GC047. Mid-Holocene warmth in the Palmer Deep record is characterised by high mass accumulation rate, maxima in biogenic and TOC flux (Domack, 2002) and a diatom assemblage characterised by *F. kerguelensis* and *Rhizosolenia*, plus high occurrence of *E. antarctica* var. *antarctica*

(sub-polar) laminae (Taylor and Sjunneskog, 2002). The latter observation was used to infer southward incursion of warm, northern surface water into Palmer Deep (Leventer et al., 2002). The timing of the peak of *E. antarctica* var. *antarctica* rs is overlapping between Palmer Deep (~8300 – 5900 yr BP; 9100 – 6800 cal. yr BP) and Anvers Shelf (6950 – 5190 yr BP; 7780 – 5960 cal. yr BP). In Palmer Deep, diatom data further suggests the climatic optimum may be divided into two warm phases, separated by an interval of cooling between ~7000 – 5000 cal. yr BP (~6100 – 4400 yr BP) (Taylor and Sjunneskog, 2002). This suggestion of a cooler interval is based on the decrease in total diatom abundance, alternating deposition of *F. kerguelensis* and *Cocconeis* assemblage and disappearance of *E. antarctica* var. *antarctica* (sub-polar) laminae (Taylor and Sjunneskog, 2002). On the nearby Anvers Shelf (core GC047), a comparable decline in both forms of *E. antarctica* rs abundance is observed after 5190 yr BP (5960 cal. yr BP), but in this study, this is inferred to represent the diminished influence of melting glacier and sea ice, due to reduced nutrient fertilisation processes, and the greater impact of outer shelf oceanographic influences, with longer periods of open water (high *F. kerguelensis* relative abundance and reduced sea ice type 1 abundance). This period between 5190 – 3380 yr BP (5960 – 3630 cal. yr BP) is proposed to signify peak climatic optimum conditions offshore Anvers Island, not climatic cooling. Potentially the Mid-Holocene climatic optimum in the combined records from Marguerite Bay (core VC306) and offshore Anvers Island (GC047) record the progressive southward and inland migration of the marginal sea ice zone from ~7600 yr BP (8300 cal. yr BP), finally oscillating to the south of Anvers Island by 5190 yr BP (5960 cal. yr BP), through a combination of atmospheric warming and active UCDW influences.

In another WAP locality (Bransfield Strait; #14), the inferred Mid-Holocene warmth (6800 – 5900 cal. yr BP; ~6000 – 5200 yr BP) is again characterised by highest total diatom abundance and peak abundance of *E. antarctica* var. *antarctica* (Heroy et al., 2008). However, this period is significantly shorter than that observed in cores GC047, VC306 and Palmer Deep which, together with a series of records from the outer WAP shelf (#12 and #13; Yoon et al., 2002), suggests a Mid-Holocene climatic optimum between ~6000 – 2500 cal. yr BP (~5200 – 2450 yr BP). The later onset in these northerly, offshore sites (#14, #13 and #12) (~2300 – <3000 cal. years; ~1600 – <2850 ^{14}C years) suggests that the Mid-Holocene climatic optimum was more pervasive in mid-shelf to coastal areas of the AP. This could potentially be due to coastal areas experiencing more stability in surface ocean conditions and more regular sea ice cover,

compared to outer shelf areas that are more susceptible to storm influences and sensitive to subtle climatic changes via sea ice cover. The quick demise into inferred cooler late Mid-Holocene conditions after 5900 cal. yr BP (~5100 yr BP) in the record from Bransfield Strait (#14) was proposed based on higher abundances of *T. antarctica* rs, together with *A. actinochilus* and *T. gracilis*, indicating colder surface water and increased winter sea ice (Heroy et al., 2008). Interestingly, this transition in the Bransfield Strait, attributed to a shift in predominant water masses, with possible increased intrusion of colder water from the Weddell Sea, increased wave action and prolonged sea ice cover (Heroy et al., 2008), is coeval with inferred peak climatic conditions for the Anvers Shelf record (core GC047). As described above, this interval (5190 – 3380 yr BP; 5960 – 3630 cal. yr BP) of reduced sea ice type 1 influence and greater connection with outer shelf water masses, could also signify increased intrusion of Weddell Sea waters, with active shelf circulation dispersing the previously persistent meltwater driven stratification and hence discouraging development of the sea ice type 1 assemblage.

The Mid-Holocene phase in the record from the southern Bellingshausen Sea (core GC358) is more subdued than northern WAP localities, but is proposed to be of long duration (8600 – 1700 yr BP; 9570 – 1620 cal. yr BP) (Figure 8.4). The typical indicators used elsewhere to infer the Mid-Holocene climatic optimum (e.g. elevated total diatom abundance, species adapted to exploit active spring meltwater stratification) are not apparent. The proposed warmer conditions are based on the mixed assemblage containing elevated abundance of: (1) *E. antarctica* var. *recta* rs, suggesting localised meltwater lenses derived from continued ice shelf retreat; (2) marginal sea ice species (*Rhizosolenia* and *Proboscia* species), suggesting periods of open water did occur, but potentially not annually; and (3) typical cool water species (*T. antarctica* cold rs and *A. actinochilus*). This mix suggests that the re-current sea ice cycle had not propagated as far south as the southern Bellingshausen Sea, instead the summer sea ice boundary was oscillating around Marguerite Bay during the Mid-Holocene.

On the EAP, a very different expression of the Mid-Holocene climatic optimum is evident again. In the PGC, progressive amelioration of environmental conditions through the Early to Mid-Holocene and the subsequent retreat of the PGC Ice Shelf from core locality VC237 at 9250 yr BP (10420 cal. yr BP), lead to high productivity in the marginal ice edge environment, as observed in the modern-day Weddell Sea (Garrison et al., 1987; 1993; Nelson et al., 1987; 1989; Smith and Nelson, 1990; Kang

and Fryxell, 1993; Kang et al., 1995; 2001; Park et al., 1999; Hoppema et al., 2000). This environment is characterised by water column stabilisation by meltwater inputs. Therefore the transition into the Mid-Holocene climatic optimum is initially inferred from increased abundance of sea ice type 1 species exploiting this environment, reflecting the continued expansion and duration of open water during spring, and associated seasonally stratified surface water. In the record from Erebus and Terror Gulf (core VC205), there is an associated high abundance of sea ice type 1 species, together with extremely high sedimentation rates and total diatom abundance between 5610 – 5230 yr BP (6390 – 6010 cal. yr BP). The second phase of PGC Ice Shelf collapse, exposing core site VC243 at 5260 yr BP (6050 cal. yr BP) (Pudsey and Evans, 2001; this study) and causing a very different style of sedimentation and diatom assemblage in core VC205 after 5230 yr BP (6010 yr BP), is likely to reflect the continued amelioration of Mid-Holocene climatic conditions. Between 4390 – 1650 yr BP (4960 – 1550 cal. yr BP) the PGC was exposed to seasonally open marine conditions and sea ice type 1 species dominated as the marginal ice zone penetrated into the channel; this period reflects peak Mid-Holocene climatic optimum conditions for the EAP. This is in agreement with lake sediment records from Beak Island (PGC) which suggest wetter and milder conditions between 3500 – 1700 cal. yr BP (3250 – 1780 yr BP) (Sterken, 2009). The nearby Larsen-A Ice Shelf also records fluctuations in extent and increased proximity to seasonally open water between 4000 – 1400 cal. yr BP (~3650 – 1500 yr BP), based on ice-rafted debris provenance data (Pudsey et al., 2006) and open water indicator diatom species (Brachfeld et al., 2003). Although Holocene climatic amelioration appears to have been a very gradual process on the EAP, exemplified by the progressive retreat of the PGC Ice Shelf from 9250 yr BP (10420 cal. yr BP) onwards, peak Mid-Holocene climatic optimum conditions on the EAP were not fully established until 4390 yr BP (4960 cal. yr BP); several thousand years after that on the WAP (Figure 8.4).

In addition to the asynchronous nature of the Mid-Holocene climatic optimum between WAP and EAP marine records, it also appears that the oceanic reflection in WAP marine records (both those in this investigation and several published records, discussed above) predates terrestrial and ice-core evidence from the AP and Antarctic continent. WAP cores from this investigation place the marine climatic optimum between 7950 – 2740 yr BP (8750 – 2870 cal. yr BP), whereas the "Antarctic Consensus" is that the climatic optimum occurred much later, between 4500 – 2800 cal. yr BP (~4050 – 2700

yr BP) (Bentley et al., 2009). This Mid-Holocene Hypsithermal is proposed largely from lake sediment records from the South Shetland Islands (Björck et al., 1996a; Lee et al., 2008), James Ross Island (Björck et al., 1996b), Signy Island (Jones et al., 2000; Hodgson and Convey, 2005) and terrestrial sediments, such as moss banks (Björck et al., 1991). There is some ice core evidence, such as the Plateau Remote core which records warmer conditions between 4000 – 2500 cal. yr BP (~3700 – 2400 yr BP) (Mosley-Thompson, 1996), together with the synthesis of several ice core records, suggesting some evidence of relative warmth between 4500 – 2000 cal. yr BP (~4050 – 2050 yr BP) (Ciais et al., 1994) (Figure 8.14). Similar to the Palmer Deep reconstructions (Domack, 2002), the WAP cores analysed in this investigation suggest prolonged exposure to warm oceanographic influences through the Mid-Holocene (~8000 – 2700 yr BP; ~8700 – 2900 cal. yr BP), resulting in the establishment of re-current sea ice cycles and the progressive shift towards longer periods of open water in the northern WAP after ~5200 yr BP (~6000 cal. yr BP).

Another striking difference between Mid-Holocene palaeoclimate records is that in a few areas, particularly around the northern tip of the AP, the period between ~5000 – 4600 yr BP (~5760 – 5300 cal. yr BP) is characterised by glacial re-advance, including: northern James Ross Island (Hjort et al., 1997); Hope Bay (Zale, 1994); King George Island (Mäusbacher, 1991); Brabant Island, Palmer Archipelago (Hansom and Flint, 1989); and George VI Ice Shelf after 5700 yr BP (~6500 cal. yr BP) (Sugden and Clapperton, 1980; 1981; Clapperton and Sugden 1982; Hjort et al., 2001). Marine records from fjord settings on King George Island also identify cold waters and extensive sea ice cover between 6200 – 4000 cal. yr BP (~5400 – 3700 yr BP) (Yoon et al., 2000) and diatom data in Palmer Deep suggests relative cooling between ~7000 – 5000 cal. yr BP (6100 – 4400 yr BP) (Taylor and Sjunneskog, 2002). In this investigation, only core VC205 from the Erebus and Terror Gulf potentially alludes to a scenario of glacier advance, although as discussed above, it is equally plausible that the signal reflects PGC Ice Shelf collapse. All the other marine records studied in this investigation, together with Lallemand Fjord (Taylor et al., 2001) and most Palmer Deep proxies (Domack, 2002) do not document a period of climatic cooling at this time. Hjort et al. (1997) suggest that the glacial advance might be a regional response to increased precipitation, due to warming and increased cyclonic activity in the Mid-Holocene; such factors would have greater impact on terrestrial records rather than marine ones.

- **Wider context and mechanisms**

Explaining the regional differences highlighted above, together with the discrepancies between marine and terrestrial data, is intriguing and may be important for understanding the patterns of regional rapid warming experienced in the modern-day AP. Firstly addressing regional differences, based on the marine cores used in this investigation and other published proxy records, the AP can be divided into a number of regions based on the character of the Mid-Holocene climatic optimum (Figure 8.11):

1) WAP troughs (e.g. Anvers Trough, Palmer Deep, Marguerite Bay, Belgica Trough, plus Lallemand Fjord (Taylor et al., 2001)?) record prolonged, yet variable, Mid-Holocene climatic optimum; dissimilar to terrestrial and ice core records, and instead reflecting a possible connection with ACC and Southern Westerlies?

2) WAP shelf edge (e.g. Bransfield Strait) record very different and variable Mid-Holocene climatic optimum signals; record #14 – early and short (Heroy et al., 2008), whereas cores #12, #13 and #15 – early and longer (Yoon et al., 2002); possible connection with Weddell Sea?

3) EAP and WAP coastal areas (e.g. Lallemand Fjord (Shevenell et al., 1996)?) record late and short Mid-Holocene climatic optimum; highlighting possible connections with AP terrestrial records, through impacts of glacier fluctuations linked to terrestrial and / or atmospheric forcing?

Expanding briefly on point 1, a multi-proxy approach reconstructing SSTs over the last 8000 yrs suggests that higher palaeotemperatures in the Peru-Chile Current (northern extension of the ACC) between 8000 – 4000 cal. yr BP (~7200 – 3670 yr BP) (Lamy et al., 2002), together with less humid conditions, peaking between 6000 – 5300 cal. yr BP (~5200 – 4600 yr BP) (Lamy et al., 2001). Several other palaeoclimate records from Patagonia point towards Mid-Holocene aridity (e.g. Jenny et al., 2002; Gilli et al., 2005). These observations in South America most likely reflect the poleward displacement of the Southern Westerly wind belt, resulting in decreased advection of cold and nutrient-rich water by the ACC and re-distribution of rainfall patterns (Lamy et al., 2002; Gilli et al., 2005). The position of the Southern Westerlies is dependent on the location of the SE Pacific anticyclone in the north and the circum-Antarctic low pressure belt in the south, together with steep SST gradients within the ACC (Pittock et al., 1978; Aceituno et al., 1993). The poleward migration of the Southern Westerlies at

this time is possibly the result of an intensification and / or southward migration of the SE Pacific anticyclone (an atmospheric situation resembling modern-day La Niña conditions; Markgraf et al., 1992), which is supported by Early to Mid-Holocene palaeoclimate reconstructions (e.g. Rodbell et al., 1999; Moy et al., 2002) and model simulations (Clement et al., 2000). This connection between large-scale Southern Hemisphere atmospheric circulation patterns (e.g. Hadley cell intensity) (Lamy et al., 2002) and localised forcing on the AP (UCDW) suggests that oceanic and atmospheric changes occurring in the SE Pacific have been important in shaping events on the AP throughout the Holocene.

Secondly, explaining the difference between marine and terrestrial data, potentially these proxies are responding to environmental conditions expressed at different times of the year (Bentley et al., 2009). Renssen et al. (2005) also highlighted this possibility; model outputs suggest that the temperature evolution differed substantially from season to season through the Holocene, with summer temperatures experiencing thermal maximum between 6000 – 3000 cal. yr BP (~5300 – 2900 yr BP), while spring temperature is highest at 9000 cal. yr BP (~8100 yr BP) and autumn temperature peaks at present (Figure 8.10). Consequently, part of the variations in the timing of maximum warmth seen between different proxies could be related to the seasonal dependence of the proxies (Renssen et al., 2005). In other words, marine diatom-based reconstructions preferentially reflect spring conditions (periods of retreating sea ice and increased abundance of sea ice type 1 species), leading to the timing of the Mid-Holocene climatic optimum in the marine realm occurring between ~8000 – 2700 yr BP (~8800 – 2900 cal. yr BP) (this study), which is several thousand years before the terrestrial equivalent. Whereas productivity in onshore lakes may have been responding to summer insolation-driven loss of lake ice and catchment snow (Bentley et al., 2009), leading to a late Mid-Holocene climatic optimum. This theory about the bias towards spring in marine records is supported by observations from surface sediments that show dominance by spring assemblages, with summer species almost completely absent (Pike et al., 2008).

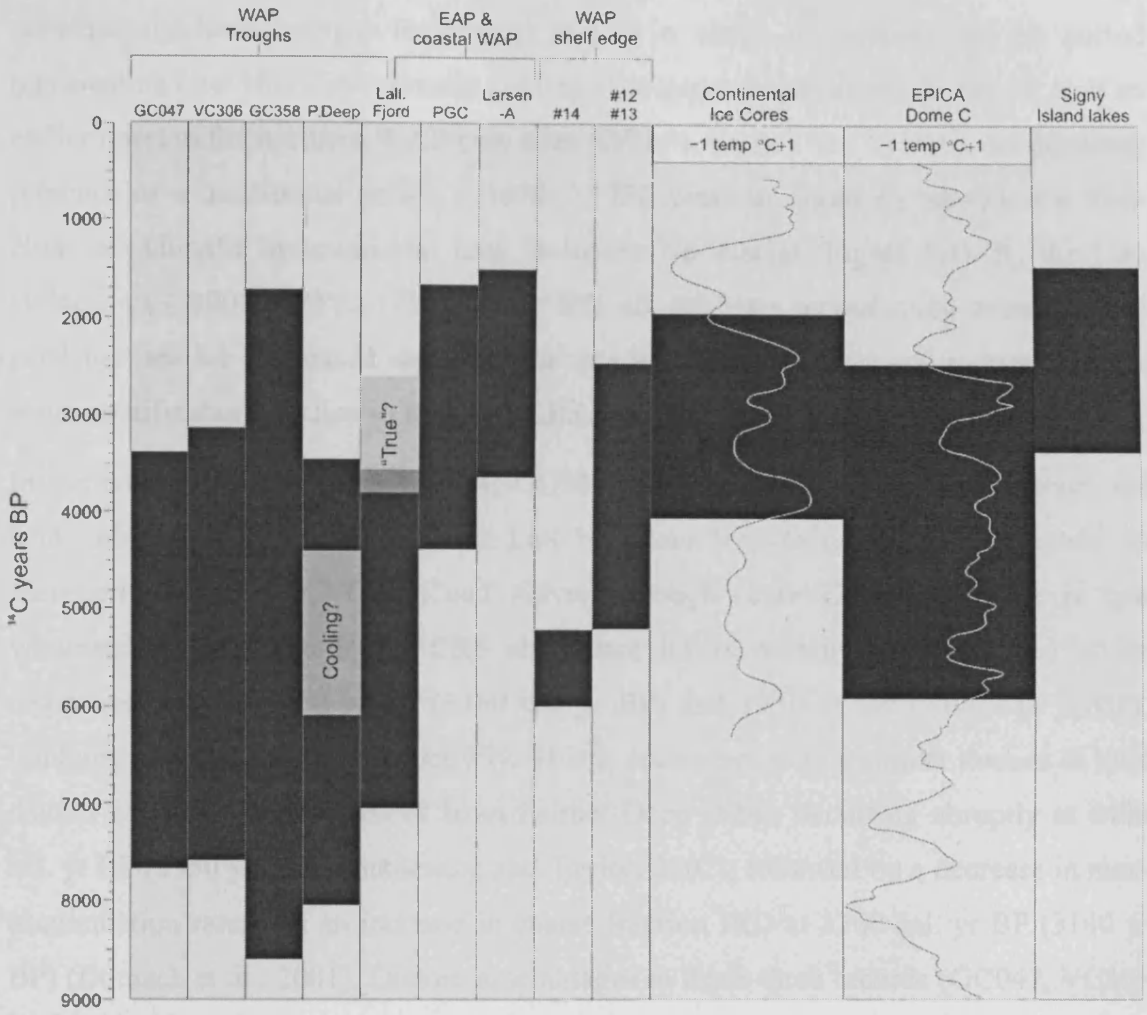


Figure 8.11
Compilation of Mid-Holocene climatic optimum records in the AP marine cores used in this investigation, together with published marine records: P.Deep = Palmer Deep (#24); Lall. Fjord = Lallemand Fjord (#41); PGC = Prince Gustav Channel (cores VC243, VC237 and VC205)). Diatom data in Palmer Deep suggests a period of cooling (Taylor and Sjunneskog, 2002). Diatom data in Lallemand Fjord (Taylor et al., 2001) suggest Mid-Holocene climatic optimum before TOC values, used by Shevenell et al. (1996) to infer "true" climatic optimum conditions. Continental ice cores represent a compilation of records (Dome C, Vostok and Komsomolskaia) (Ciais et al., 1994) and EPICA Dome C (Jouzel et al., 2007). Signy Island lake sediment record of Mid-Holocene Hypsithermal (Hodgson and Convey, 2005).

8.4.1.3 Late Holocene Neoglacial

In all of the records studied in this investigation, a clear change in environmental conditions is witnessed in the Late Holocene. However, the initial onset, duration and regional expressions of proposed Late Holocene Neoglacial are different between localities. The term Neoglacial was originally defined by Porter and Denton (1967, p205) as "the climatic episode characterised by rebirth and / or growth of glaciers following maximum shrinkage during the Hypsithermal interval". The term has

subsequently been applied frequently, and to a range of proxies, for the period representing Late Holocene climatic cooling. The generalised pattern for the AP is of an earlier onset in the northern WAP core sites (GC114, GC047 and VC306), documenting presence of a transitional period (~1030 – 1750 years in duration) between the Mid-Holocene climatic optimum and Late Holocene Neoglacial (Figure 8.4). By the Late Holocene (~1800 yr BP; ~1730 cal. yr BP) all AP sites record more extensive and persistent sea ice (increased abundance of sea ice type 1 species) and reduced surface water stratification (decline in total and CRS abundance).

In the northern WAP (cores GC114, GC047 and VC306), the transition between the Mid-Holocene climatic optimum and Late Holocene Neoglacial is relatively subtle. In Marguerite Bay (core VC306) and Anvers Trough (core GC407), change is first witnessed in total diatom and CRS abundance levels, which start to decline in the respective areas at 3130 yr BP (3360 cal. yr BP) and 3950 yr BP (4400 cal. yr BP), implying reduced primary productivity. This is coincident with a similar decline in total diatom abundance in the record from Palmer Deep (#24), occurring abruptly at 4400 cal. yr BP (3950 yr BP) (Sjunneskog and Taylor, 2002), followed by a decrease in mass accumulation rates and an increase in coarse fraction IRD at 3360 cal. yr BP (3140 yr BP) (Domack et al., 2001). Diatom assemblages in these three records (GC047, VC306 and Palmer Deep) record a decline in *F. kerguelensis* abundance, increase in *T. gracilis* and sea ice type 1 species, suggesting reduced connection with open ocean influences (UCDW) and longer periods of sea ice cover (section 8.3.2 (p8-19); 8.3.3 (p8-23); Taylor and Sjunneskog, 2001 for the respective cores). Similarly, in Lallemand Fjord, combined diatom, sedimentary and geochemical data suggest that the climatic deterioration occurred prior to 3850 cal. yr BP (~3560 yr BP), even up to 4420 cal. yr BP (~3950 yr BP) (Taylor et al., 2002). This transition from a seasonally open water environment to one influenced by more dense sea ice was possibly linked to the ice shelf at the head of Lallemand Fjord being in closer proximity (Taylor et al., 2002). Previous suggestions of the timing of Late Holocene climatic deterioration in Lallemand Fjord imply that it occurred sometime prior to 2000 cal. yr BP (~2030 yr BP) (Domack and McClennen, 1996).

At a coeval time (3360 – 2620 yr BP; 3600 – 2750 cal. yr BP), the record from Bransfield Strait (core GC114) suggests open connection between Weddell Sea and Bransfield Strait water masses, inferred from higher abundances of *T. antarctica* warm rs (conclusions similar to those suggested by Abelmann and Gersonde, 1991; Bárcena et

al., 1998; Heroy et al., 2008). This is coincident with the Mid-Holocene climatic optimum on the EAP (Figure 8.4), when sea ice would have retreated significantly in the summer months, enabling density differences in the surface water to develop and activation of shelf currents, which potentially can flow around the tip of the AP and into Bransfield Strait. This is the first inference of a Holocene "interconnection" between the marine environment of the EAP and WAP. A reduction in cross-peninsula contrasts develops because the EAP is experiencing comparatively warmer conditions (EAP Mid-Holocene climatic optimum) and the consequences for the WAP (via increased Weddell Sea influx) is climatic instability and comparatively cooler conditions. A longer Holocene record from Bransfield Strait (#14) also records a shift in predominant water masses, with colder water, increased wave action and prolonged sea ice cover (Heroy et al., 2008). This suggestion was based on increased abundance of *T. antarctica* (unspecified variety), together with *T. gracilis* and *A. actinochilus* (Heroy et al., 2008). However, these conditions were observed for the period between 5900 – 2600 cal. yr BP (~5200 yr BP – 2520 yr BP), which is significantly longer than other WAP localities that experienced Mid-Holocene climatic optimum conditions at this time (as discussed in section 8.4.1.2). In core GC114, increased abundance of *T. antarctica* warm rs between 3360 – 2620 yr BP (3600 – 2750 cal. yr BP) was also used to infer influence of colder water, possibly derived from the Weddell Sea. Potentially this signal in core GC114 is equivalent to the latter phases of the inferred period of instability in record #14 from the Bransfield Strait. However, because core GC114 only spans the last 3360 yrs (3600 cal. yrs) it is not possible to substantiate the suggestions of Heroy et al. (2008) for prolonged instability in Bransfield Strait from the Mid into Late Holocene.

Following the extended transitional period in the records from the northern WAP, both cores GC114 and GC047 document increased abundances of *Proboscia* and *Rhizosolenia* species at ~1900 yr BP (~1840 cal. yr BP). This potentially signifies the onset of large-scale changes in the water column structure of the WAP, characterised by deeper mixing. Both these species are able to survive at depth, due to their ability to grow in limited light (Goldman, 1993) and to regulate their buoyancy (Moore and Villareal, 1996; Villareal et al., 1996); increased abundance in the sedimentary record at this time reflects the ability of these species to survive at greater depths, where potentially other diatoms would not be able to. A marked increase of *Probosica* spp., *Rhizosolenia* spp. and *T. lentiginosa* abundance is also noted in record #14 (Bransfield Strait) from 2600 cal. yr BP (~2520 yr BP), used to indicate presence of cold open water

masses (Heroy et al., 2008). The origin of the reduction of water column stratification and deeper mixing in cores GC114 and GC047 may be increased storm frequency and wave action; mechanisms also inferred for reduced diatom abundance observed in other marine records from the northern WAP, e.g. Palmer Deep record #24 (Taylor and Sjunneskog, 2002); records #7, #8 and #10 (Bárcena et al., 1998: 2002); and record #14 (Heroy and Anderson, 2008).

This period of transition between the Mid-Holocene climatic optimum and Late Holocene Neoglacial is less obvious or absent in the southern Bellingshausen Sea (core GC358) and records from the EAP (cores VC243 and VC205) (Figure 8.4). In the southern Bellingshausen Sea, the non-CRS diatom assemblage records the progressive change from marginal sea ice, with open ocean influences prior to 3420 yr BP (3700 cal. yr BP) to a more sea ice-dominated environment, particularly notable after 1700 yr BP (1620 cal. yr BP). In the PGC on the EAP, the transition from maximum productivity, inferred from high diatom abundance and sedimentary pigment concentration, into ice shelf reforming phase, inferred from ice rafted debris province studies (Pudsey and Evans, 2001) and diatom evidence (this study), was particularly abrupt, occurring at 1650 yr BP (1550 cal. yr BP). The Larsen-A Ice Shelf is also suggested to have reformed at a similar time (~1400 cal yr BP; ~1500 yr BP) (Brachfeld et al., 2003). In the wider EAP region, the first suggestion of deteriorating conditions is witnessed at ~2280 yr BP (2070 cal. yr BP), as increased terrigenous fluxes impact the sediment character in the Erebus and Terror Gulf (core VC205). This observation is presumed to reflect advancing glaciers and more frequent icebergs, and the decline in sea ice type 1 species suggests perennial sea ice was more common in the Late Holocene on the EAP.

Terrestrial AP evidence of the Late Holocene Neo glacial include glacier advances, noted particularly on the South Shetland Islands, although most are poorly dated or un-dated (Ingólfsson et al., 1998), together with numerous biological proxy records in lakes and other sites showing temperature-related decline in production ~1400 – 1300 cal. yr BP (~1500 – 1380 yr BP) (Björck et al., 1991; Jones et al., 2000; Hodgson and Convey, 2005). Terrestrial expression of cold climatic conditions lags the WAP marine records (cores GC114, GC047 and VC306, plus Palmer Deep – #24 and Lallemand Fjord – #41) by several thousand years, but is coeval with southern WAP (core GC358) and EAP marine settings (cores VC243 and VC205). In summary, the climatic contrasts between the WAP marine and AP terrestrial realm appear to have been further pronounced

during the onset of the Late Holocene Neoglacial (~3360 – 2690 yr BP; 3600 – 2810 cal. yr BP). Continuing warmth on land (i.e. the ongoing Mid-Holocene climatic optimum) may be attributable to the relatively high summer insolation (Bentley et al., 2009).

- **Wider context and mechanisms**

The proposed connection between terrestrial climatic conditions and regional insolation highlights a remaining puzzle; Holocene insolation seems to be out of phase with inferred climatic interpretations of the Mid-Holocene climatic optimum and the Late Holocene Neoglacial (Domack, 2002; Taylor et al., 2001; Shevenell and Kennett, 2002). The summer insolation curve for 60°S reaches a maximum in the last 2000 cal. yrs with a minimum in the Early to Mid-Holocene (Berger and Loutre, 1991). A potential explanation for this discrepancy is that variability in seasonal temperatures, driven by the complex seasonal patterns of insolation changes through the Holocene (Renssen et al., 2005; Figure 8.10), are more important than annual averaged insolation inputs. As shown in Figure 8.10, modelled spring (October), summer (January) and winter (July) temperature show a decline through the Late Holocene (~1 °C between 3000 – 0 cal. yr BP; ~2870 – 0 yr BP). Cooler temperatures during these months (and potentially reduced UCDW influence, as discussed below) would have the effect of increasing the longevity of sea ice cover, through reduced melting in the spring and summer months as surface waters remain closer to the freezing point. Alternatively, additional forcing mechanisms may be accountable for the observed Late Holocene climatic deterioration.

Onset of the Late Holocene Neoglacial (<3950 yr BP; <4400 cal. yr BP) appears to be reflected first in the deep trough settings of the WAP (Marguerite Bay, Anvers Trough and Palmer Deep) and some coastal localities (Lallemand Fjord); this observation potentially provided clues as to forcing mechanisms for the climatic deterioration. Similar to observations of spatial variability during the Mid-Holocene climatic optimum, potentially the WAP troughs (e.g. Anvers Trough, Palmer Deep, Marguerite Bay) are acting differently and recording greater connection with the ACC and Southern Westerlies, whereas the northern WAP (e.g. Bransfield Strait) is experiencing greater connection with the EAP, via Weddell Sea Transitional Water. The much later response witnessed on the EAP and in the southern WAP (e.g. southern Bellingshausen Sea) may be a function of the more extensive sea ice typically found in these areas; potentially sea

ice could act as a buffer to climate perturbations or display less sensitivity to forcing mechanisms. The difference in albedo between sea ice and the sea surface, means that sea ice serves as a barrier to energy exchange between the atmosphere and ocean (Anderson, 1999) and acts as a strong amplifier through the positive ice-albedo and ice-insulation feedbacks (Renssen et al., 2005).

To date, the most detailed reconstructions for the AP oceanographic conditions during the Late Holocene interval is provided by the isotopic data from Palmer Deep (# 26; Shevenell and Kennett, 2002). Consistent and rapid alterations in shelf water temperatures of 1 – 1.5 °C are inferred (Shevenell and Kennett, 2002), which are significant differences for the Antarctic shelf (Domack, 2002). Such oscillations were also highlighted in TEX_{86} sea surface temperature data from Palmer Deep, with the long-term Holocene record of cooling (~3 °C) punctuated by millennial scale temperature variability (Shevenell et al., 2007). These observations are believed to document oscillating presence of cool shelf water and warmer UCDW (Shevenell and Kennett, 2002; Ishman and Sperling, 2002; Shevenell et al., 2007). This suggestion is supported by the diatom-based reconstructions from Palmer Deep, that record alternating periods of more intense (seasonally persistent) sea ice and open water (Sjunneskog and Taylor, 2002; Taylor and Sjunneskog, 2002). Such changes were inferred to reflect atmospheric forcing via westerly wind strength on the axial flow of the ACC; predominantly offshore winds could push the southern boundary of the ACC away from the western AP continental shelf, thereby depressing the volume of UCDW in the Palmer Deep (Shevenell and Kennett, 2002). Thus the Southern Westerlies may be implicated in fluctuations of oceanographic conditions on the WAP during the Late Holocene Neoglacial (Bentley et al., 2009). In central Chile, there is evidence of decreasing temperatures and increasing continental precipitation during the Late Holocene (from 4000 cal. yr BP; 3700 yr BP), which also points to an equatorward shift of both the ACC and the Southern Westerlies (Lamy et al., 2001; 2002). Likewise in southern Chile, shifts in woodland vegetation have been inferred to reflect step-wise shifts in the position of the Southern Westerlies, bringing wetter conditions to the region through the Late Holocene (Moreno et al., 2009a).

The "flickering" variability in oceanographic conditions, exemplified by the isotope and TEX_{86} record from Palmer Deep, potentially suggests the influence of ENSO on the AP climatic regime during the Late Holocene, suggesting teleconnections between the tropical Pacific and Southern Ocean (Domack and Mayewski, 1999; Bentley et al.,

2009). The effect of ENSO on the climate and oceanography of the AP has been directly observed in recent decades. Meredith et al. (2004) report the impacts of the 1997/1998 ENSO event for the Marguerite Bay area, showing that the winter of 1998 was characterised by low sea ice concentrations, high atmospheric temperatures and a high frequency of northerly winds. Thus, if these findings are representative of the wider WAP region, then the winter following an El Niño year appears to be associated with relative warmth in this region. Similarly, Harangozo (2000) showed from recent meteorological data the impact of ENSO events on the AP, particularly the Amundsen-Bellingshausen Sea region (anomalously high atmospheric pressures) and Weddell Sea areas (lower atmospheric pressures). There are increasing numbers of proxy records that reconstruct the Holocene evolution of ENSO, including lake records from southwestern Equador analysing clastic laminae (Moy et al., 2002), from Galapagos Islands (Riedinger et al., 2002), mollusc analysis at archaeological sites along the north and central coast of Peru (Sandweiss et al., 2001). These suggest suppression of El Niño prior to 7000 cal. yr BP (~6100 yr BP), followed by increased ENSO frequency, intensified at ~4000 cal. yr BP (~3670 yr BP) (Rodbell et al., 1999), with variability reaching a peak by 1200 cal. yr BP (~1270 yr BP) (Moy et al., 2002). Addressing the causes of increased frequency of ENSO at 7000 cal. yr BP (~6100 yr BP) coupled ocean-atmosphere models suggest that changes in seasonal insolation due to orbital parameters may be attributable (Clement et al., 1999; 2000).

Potentially some of the Late Holocene climate variability experienced on the AP resulted from fluctuation in ENSO intensity. Further, it is possible that the associated impacts did not propagate to the southern WAP or across the AP, helping to explain the less complex Late Holocene climate reconstructions in this investigation for the southern Bellingshausen Sea and EAP. If ENSO has played a role in forcing AP climate then winter air temperatures along the WAP should have started to warm (and sea ice coverage decreased) around 7000 cal. yr BP (~6100 yr BP), and should have shown significant variability since then, reaching maximum warmth (sea ice reaching minimum extent) at 1200 cal. yr BP (~1270 yr BP) (Bentley et al., 2009). Do the marine records used in this investigation corroborate this suggestion? There is support from warmth on the WAP after 7000 cal. yr BP (~6100 yr BP) (see section 8.4.1.2), but sea ice extent is inferred to have increased in extent through the Late Holocene. This suggests that additional factors are needed to explain changes in Holocene AP sea ice extent and duration.

Modelling studies of Renssen et al. (2005) have successfully replicated the long-term character observed in Antarctic palaeoclimate records, which record a warmer Early Holocene and climatic deterioration into the Late Holocene. The simulated response of sea ice concentration and thickness shows an increase through the Holocene, with March (end of summer) sea ice cover displaying the same trend as summer temperatures (Figure 8.10; Renssen et al., 2005). These trends in sea ice area and surface temperatures can be explained by a combination of a delayed response to local orbital forcing and the long-term memory of the Southern Ocean, with sea ice acting as a strong amplifying factor (Renssen et al., 2005). In other words, once sea ice had started to increase in concentration along the WAP (possibly through greater connection with the Weddell Sea) a positive albedo feedback would lead to more sea ice formation, which in turn would further enhance the cooling.

Finally, in a number of records from the northern WAP (Palmer Deep, #24), overprinted on the general trend of reduced primary productivity over the last 3000 yrs is a high frequency oscillation in diatom abundance, which correlates with an approximate 250 year cyclicity recognised in magnetic susceptibility, organic carbon, nitrogen and siliceous microfossil data (Leventer et al., 1996; Bárcena et al., 1998, 2002; 2006; Domack, 2001). These changes in primary productivity are mainly controlled by sea ice conditions and surface water stability and stratification. This cyclicity / periodicity could be related to the effect of the 200-year sun-spot activity cycle on the oceanic system (Bárcena et al., 2006). Unfortunately little is known about solar influence on these restricted oceanic areas from Antarctica. Further, Shevenell and Kennett (2002) suggest that such cycles could be directly linked with westerly wind fluctuations (as inferred for the Palmer Deep record, as discussed above). For the majority of cores used in this investigation, such cyclicity is not evident, perhaps because higher resolution sampling is needed. In core GC114, total diatom abundance does display cycles, however, their periodicity (~440 – 660 ^{14}C years) is different to those observed by Leventer et al. (1996) and Bárcena et al. (1998; 2002; 2006) (200 – 300 years).

8.4.1.4 Summary

Palaeoclimate reconstructions have revealed the complex spatial and temporal evolution of the AP through the Holocene; climate events were peninsula-wide, but not synchronous. These patterns are summarised on a series of schematic maps representing each of the three different Holocene time slices: Deglaciation – Early Holocene (Figure 8.12a); Mid-Holocene (Figure 8.12b); and Late Holocene (Figure 8.12c).

- **Deglaciation – Early Holocene** (12650 – 8450 yr BP; 15020 – 9500 cal. yr BP)

The first phase of AP ice sheet retreat occurred relatively rapidly along the WAP, with earliest onset in the southern Bellingshausen Sea (~26000 yr BP; ~30000 cal. yr BP) and core GC358 exposed to seasonally open marine influences by 12650 yr BP (15020 cal. yr BP). Bransfield Strait, Anvers Trough, Biscoe Trough and Marguerite Bay followed suit from 14435 yr BP (17500 cal. yr BP), with grounded ice removed from core sites VC306 and GC047 by 10150 yr BP (11800 cal. yr BP) and 10750 yr BP (12720 cal. yr BP) respectively. Following this rapid retreat on the WAP, the grounding line appears to have been relatively stable for ~2000 years, possibly due to glacio-dynamic factors (presence of pinning points) or through oceanographic controls (lack of UCDW influence), in spite of elevated Early Holocene atmospheric temperatures. The post-deglaciation – Early Holocene marine environment was characterised by super-cooled shelf waters and active ice crystal formation (sea ice type 2 conditions), developed through interaction with the relatively stable ice front, stagnant icebergs and persistent and extensive fast ice. Sea ice cover would break-up in isolated patches, but in general sea ice was a multi-year feature along both the WAP and EAP shelf. The EAP, specifically the PGC, was slowly experiencing the lift-off of grounded ice from seafloor sediments, yet remaining as a floating ice shelf for the duration of this time-slice.

- **Mid-Holocene** (8450 – 3700 yr BP; 9500 – 4100 cal. yr BP)

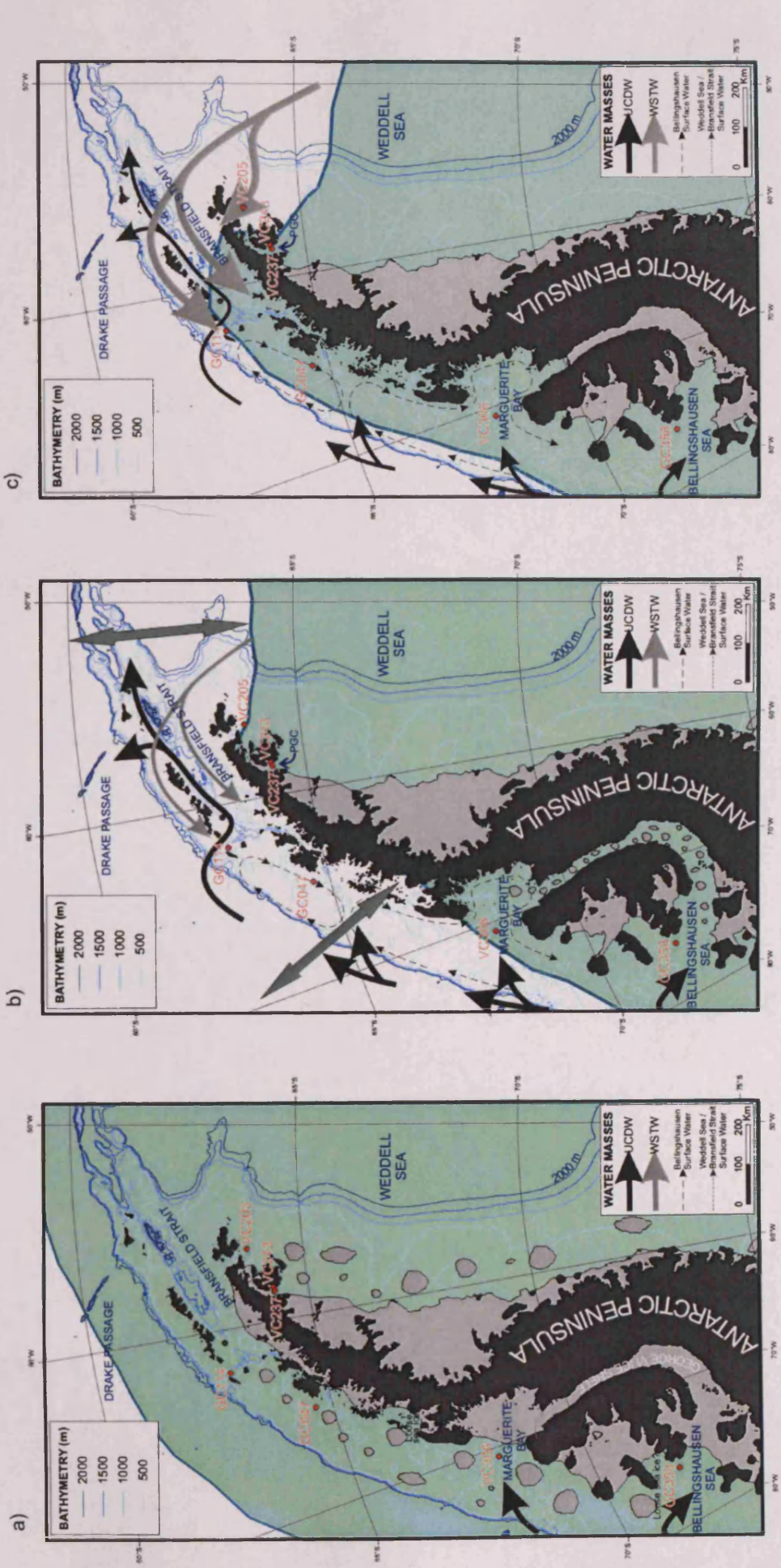
At ~8450 yr BP (9500 cal. yr BP), several dramatic changes took place on the AP, including renewed vigour of ice sheet retreat rates, disappearance of George VI Ice Shelf, establishment of a re-current sea ice cycle and large-scale oceanographic changes, specifically the flooding of UCDW onto the WAP shelf and Weddell Sea circulation approaching its modern configuration. The WAP experienced a marine Mid-Holocene climatic optimum significantly earlier (~7600 yr BP; ~8300 cal. yr BP) than the EAP and terrestrial environment (~4390 yr BP; ~4960 cal. yr BP). This is likely to

reflect a connection between the maritime WAP and the ACC and Southern Westerlies; whereas the continental EAP records the impacts of glacier fluctuations linked to terrestrial and / or atmospheric forcing. On the WAP, the persistent presence of UCDW is likely to have prevented multi-year ice becoming established; the marginal sea ice zone is proposed to have oscillated around Marguerite Bay each summer; and potentially summer and winter sea ice boundaries became progressively geographically divergent through this period (green arrow on Figure 8.12b). On the EAP, the position of marginal sea ice zone was progressively moving southward over successive cycles, directly influencing the PGC by 4390 yr BP (4960 cal. yr BP), once elevated Mid-Holocene atmosphere temperatures had caused the demise of the PGC Ice Shelf.

- **Late Holocene** (3700 yr BP – present; 4100 cal. yr BP – present)

Transition into the Late Holocene Neoglacial is first witnessed on the WAP, occurring subtly from ~3700 yr BP (4100 cal. yr BP). This transition period, coincident with peak climatic optimum conditions for the EAP, suggests greater cross-peninsula connection at this time, through the influence of cool Weddell Sea shelf currents and reduced UCDW upwelling on the WAP. By 1800 yr BP (1730 cal. yr BP), both sides of the AP were experiencing more extensive and persistent sea ice cover, reduced surface water stratification (through reduced meltwater and potentially increased storm frequency) and the PGC Ice Shelf had re-formed. It is suggested that the seasonal pattern of insolation is more important than annual input. The Late Holocene potentially also experienced the impacts of more frequent ENSO events, leading to spatially variable environmental conditions, particularly on the WAP.

Figure 8.12 (next page)
Holocene palaeoclimate reconstructions for the AP during:
a) Deglaciation – Early Holocene (12650 – 8450 yr BP; 15020 – 9500 cal. yr BP);
b) Mid-Holocene (8450 – 3700 yr BP; 9500 – 4100 cal. yr BP);
c) Late Holocene (3700 yr BP – present; 4100 cal. yr BP – present).
Note changes in the position of the ice sheet; presence and absence of George VI and Prince Gustav Channel Ice Shelves; iceberg numbers (grey blocks); position of the summer sea ice boundary (green block) and variability in its geographic extent through the annual cycle (green arrow); and strength and position of ocean currents.


a)
b)
c)
BATHYMETRY (m)
2000
1500
1000
500
DRAKE PASSAGE
BRANSFIELD STRAIT
WEDDELL SEA
ANTARCTIC PENINSULA
MARGUERITE BAY
BELLINGSHAUSEN SEA
2000m
WATER MASSES
UCDW
WSTW
Bellingshausen Surface Water
Weddell Sea / Bransfield Strait Surface Water
0
100
200
Km
PGC
VC205
VC237
VC243
VC196
GC041
GC037
GC038
GC039
GC036
GC035
GC034
GC033

8.4.2 *Do AP Holocene climate events display similar phasing and duration to circum-Antarctic and global trends?*

This section addresses the second of the primary questions posed in Chapter 1.2: do AP Holocene climate events display similar phasing and duration to circum-Antarctic and global trends? It is not intended to be an exhaustive review of Antarctic and global palaeoclimate records; focus is placed on the relative timing of events compared to the AP trends revealed during this investigation. Referenced Antarctic ice core localities and individual Holocene palaeoclimate proxy records are provided in Figure 2.15, A1.1 – A1.4, with a brief summary of the study and source reference given in Table A1.1.

8.4.2.1 *Deglaciation – Early Holocene transition*

Ice cores from the Antarctic continent provide the most detailed and chronologically well-constrained records of climatic events during the last deglaciation. Inland ice cores from Byrd, Dome C, Dome B, Dome Fuji and Vostok, together with Southern Ocean SST reconstructions show a similar sequence of climatic variability, with a slow increase from glacial to interglacial conditions and a cold reversal (the Antarctic Cold Reversal) at the end of the deglaciation (~14000 cal. yr BP; ~12000 yr BP) (Blunier and Brook, 2001 and references therein). Associated with the Antarctic Cold Reversal, the record of deuterium excess from EPICA Dome C suggests that an Oceanic Cold Reversal also took place in the southern Indian Ocean, 800 years after the Antarctic Cold Reversal (Stenni et al., 2001). Onset of ACR cooling at EPICA Dome C, ahead of cooling in the Subantarctic, suggests a steepening of the meridional temperature gradient between the EAIS and Subantarctic Ocean, probably associated with an intensification of mid- to high-latitude atmospheric circulation from 14000 – 11500 cal. yr BP (during the Bølling-Allerød warming in the Northern Hemisphere) (Stenni et al., 2001). The inland ice core records listed above, together with a recently drilled ice core from the Atlantic sector of Antarctica (EPICA Dronning Maud Land), suggest an out-of-phase relationship with Northern Hemisphere high latitudes at this time, with a direct relationship between the duration of warming across Antarctica and cold, stadial conditions (the Younger Dryas) over Greenland (EPICA Community Members, 2006). In the Southern Hemisphere mid-latitudes, one suite of terrestrial and marine palaeoclimate records has been interpreted as reflecting an in-phase relationship with the Northern Hemisphere (e.g. Andres et al., 2003; Denton and Hendry, 1994; Denton et al., 1999); whereas other records suggest an Antarctic signal prevails (e.g Lamy et al.,

2004; Turney et al., 2003). A recent study by Moreno et al. (2009b) from southwestern Patagonia observed an apparent blend of Greenlandic and Antarctic cold phases between 14800 – 12600 cal. yr BP (12500 – 10700 yr BP), and hypothesised that their co-occurrence at this latitude is controlled by the position of the Antarctic Polar Front, acting to modulate the location of these cold events in regions to the north and south of it.

Retreat of grounded ice

There are a number of similarities and differences in the timing and character of deglaciation of the WAIS and EAIS.

Similarities:

- Excluding the anomalously early recession of the AP ice sheet in the southern Bellingshausen Sea, onset of retreat from the outer continental shelf in the northern WAP at ~14400 yr BP (~17500 cal. yr BP) (this study; Figure 8.5) appears to be roughly coeval or predate (<3000 ^{14}C years) retreat of the WAIS, in areas that also experienced grounded ice at the shelf break (Figure 8.13). Earlier retreat on the WAP is not an unexpected finding because of the Peninsula's northerly location, extending into the relatively warm ACC (Huybrechts, 2002).

- Retreat in several settings (Pine Island Bay and Marie Byrd Land; Lowe and Anderson, 2002) followed a similar two-phase retreat style to the WAP identified in this study, although the exact timing is different between localities.

- Synchronous ice sheet retreat from WAP coastal localities shown by this study to be between ~9000 – 8000 yr BP (~10100 – 8850 cal. yr BP) appears to be extendable to the inner Ross Sea (Conway et al., 1999) and the Windmill Islands (Hodgson et al., 2003).

- There was significant retreat of the WAIS after 7000 yr BP (7830 cal. yr BP) in the Ross Sea (Anderson et al., 2002) and Marie Byrd Land (Stone et al., 2003); comparable with the late recession of the AP ice sheet identified by this study on the EAP. This has important implications for global sea level rise during this period, adding support to modelling studies (e.g. Nakada and Lambeck, 1988) suggesting that continued deglaciation of Antarctic into the Holocene is needed

to explain sea level changes on tectonically stable coasts far from the influence of glacio-isotatic rebound (Stone et al., 2003).

Differences:

- During the LGM, much of the WAIS (AP: this study; Pine Island Bay: Lowe and Anderson, 2002; eastern and central Ross Sea: Shipp et al., 1999) is suggested to have been grounded at the shelf break (Figure 8.13); whereas expansion of EAIS is inferred to have only reached mid-shelf settings in the majority of locations (western Ross Sea: Shipp et al., 1999; Northern Victoria Land: Anderson et al., 2002; Windmill Islands: Harris et al., 1997; Prydz Bay: Anderson et al., 2002; Mac Robertson Land: Harris and O'Brien, 1998). Most of the large volume changes were concentrated to the WAIS (including the AP) (Huybrechts, 2002), mainly laterally through large ice streams, pinned to the shelf edge, whereas less expansion of the EAIS took place (Denton and Hughes, 2002).
- Retreat of the WAIS is generally suggested to have started later and continued well into the Holocene (e.g. ~14400 yr BP (~17500 cal. yr BP) for northern WAP; ~6000 yr BP (~6850 cal. yr BP) for northern EAP; this study; Figure 8.5), compared to retreat of the EAIS, which in some areas occurred prior to the LGM (Anderson et al., 2002; Figure 8.13). The earlier retreat of the EAIS is likely to have occurred through insolation and CO_2 driven changes; whereas later onset for the WAIS can be explained by the ice streams being more susceptible to deglaciation sea level rise, which occurred after deglaciation had been initiated. As highlighted by Huybrechts (2002), the role of sea level is particularly interesting and supports the view that the Antarctic ice sheet follows events on the Northern Hemisphere continents by oceanic teleconnections.

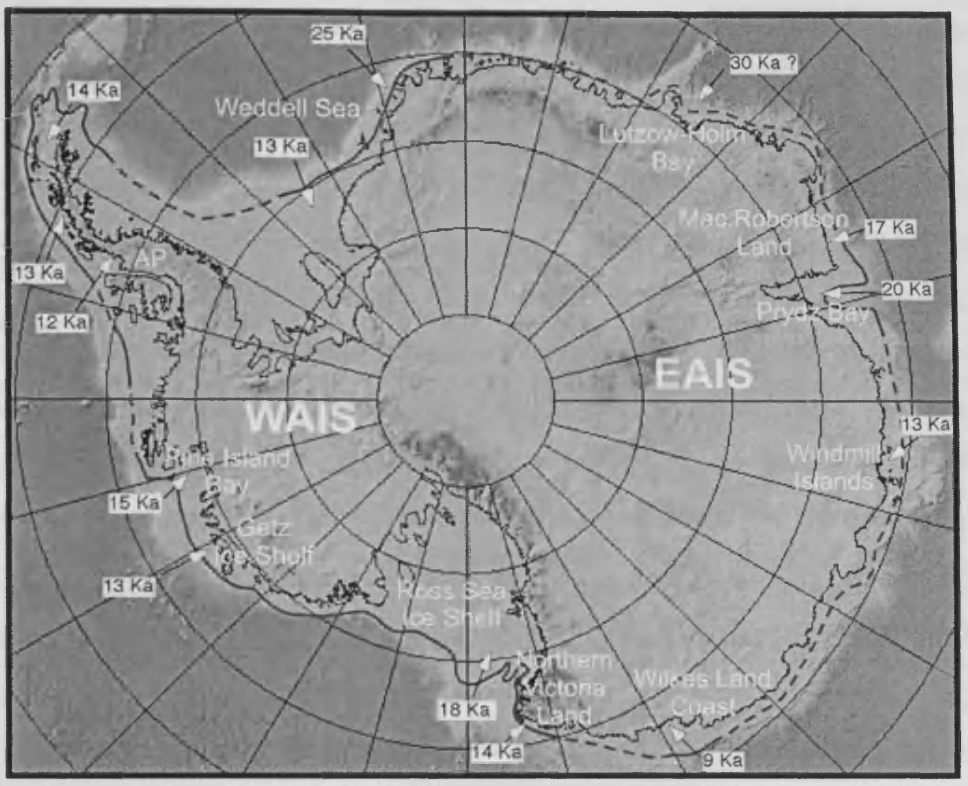


Figure 8.13
Circum-Antarctic LGM ice sheet reconstruction and oldest radiocarbon ages from glacial-marine deposits, representing approximate age of initial ice sheet retreat from the shelf. Deeper grey shades indicate the continental slope and abyssal plain. (Source: Anderson et al., 2002, with place names added).

Occurrence of an Early Holocene "climatic reversal"?

The proposed "climatic reversal" witnessed in this study in the northern WAP between ~10000 – 7680 yr BP (11460 – 8280 cal. yr BP), is not observed in Antarctic ice core records or circum-Antarctic marine records. This suggests that the event was not climatically driven, rather reflecting a localised stall in the ice sheet retreat trend, due to bathymetric, glacio-dynamic or sea level controls.

Occurrence of an Early Holocene climatic optimum?

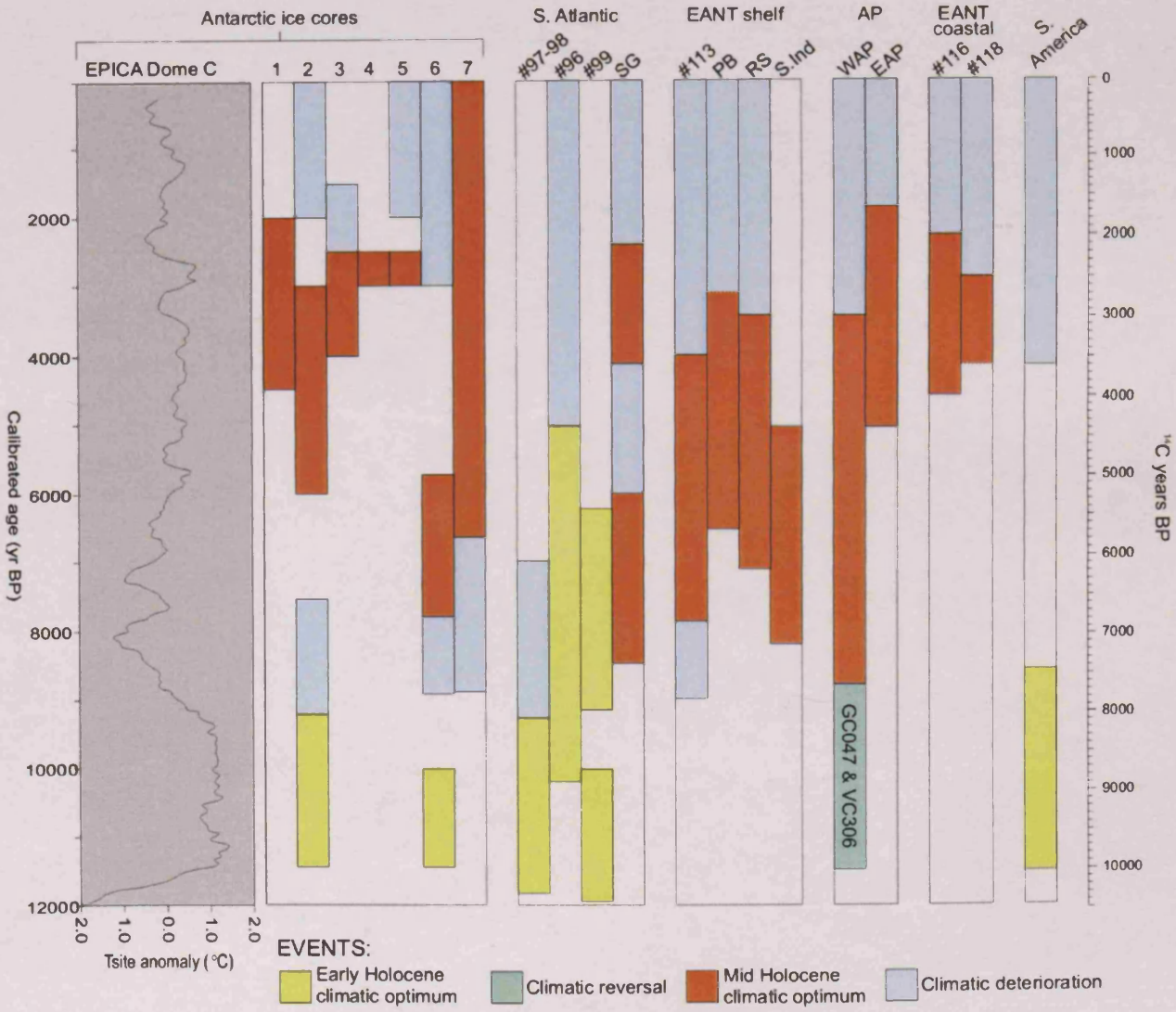
Antarctic ice core records provide clear evidence suggesting that the Early Holocene (11000 – 9500 cal. yr BP; ~9600 – 8450 yr BP) was a widespread period of significant warmth on the Antarctic continent (Ciais et al., 1992; Masson et al., 2000; Masson-Delmotte et al., 2004), with temperatures increased by 0.2 to 2.5 °C (Masson et al., 2000). However, the mechanisms behind the Early Holocene climatic optimum are not fully understood (Masson-Delmotte et al., 2004).

In circum-Antarctic marine records an Early Holocene climatic optimum is less well-documented, particularly in records from the AP. Several cores from the South Atlantic

(#96 – #99) display the clearest coherence with Antarctic ice-core records, suggesting warmest Holocene SST and low sea ice cover (Hodell et al., 2001; Bianchi and Gersonde, 2004; Nielsen et al., 2004) (Figure 8.14). The second period of warmth observed in record #99 partly overlaps with the Holocene climatic optimum in several northern WAP sites (Palmer Deep: Domack et al., 2001; cores GC047 and VC306: this investigation). In these South Atlantic records, the Early Holocene optimum displays a close affinity to northern latitude summer insolation, leading the authors to suggest that orbital forcing was the main driving mechanism (Hodell et al., 2001; Nielsen et al., 2004; Bianchi and Gersonde, 2004), causing expansion of the Polar Front Zone southward, at the expense of the seasonal sea ice zone (Bianchi and Gersonde, 2004).

In southern South America, the Early Holocene displays considerable climatic variability; warm, dry conditions are inferred from pollen records between 11000 – 8000 cal. yr BP (10010 – 7450 yr BP) (Moreno and León, 2003; Moreno et al., 2004; Vargas-Ramirez et al., 2008), whereas another record slightly to the north suggests higher amounts of either precipitation or meltwater from 12810 cal. yr BP (10800 yr BP) (Skerken et al., 2008); consistent with a rise in SE Pacific SSTs and associated increase in moisture supply to the Andes (Lamy et al., 2004). Dramatic climatic reorganisations were occurring globally in the Early Holocene and the regional expression is very different between localities.

Figure 8.14
Holocene climatic events for the circum-Antarctic and South America. Antarctic ice core records: EPICA Dome C = Jouzel et al., 2007; 1 = Synthesis of Ciais et al., 1994; 2 = Central EAIS (Masson et al., 2000); 3 = Plateau Remote (Mosley-Thompson, 1996); 4 = Byrd (Masson et al., 2000); 5 = Dominion Range (Masson et al., 2000); 6 = Taylor Dome (Masson et al., 2000); 7 = Siple Dome (Johnsen et al., 1972; Das and Alley, 2008). South Atlantic marine records: #96 (Hodell et al., 2001); #97-98 (Bianchi and Gersonde, 2004); #99 (Nielsen et al., 2004). SG = South Georgia lake sediment record (Rosqvirst et al., 1999; 2003). EANT shelf: #113 (Crosta et al., 2007); PB = Prydz Bay encompassing records #124 (Taylor and Leventer, 2003), #135 (Taylor and McMinn, 2001) and #128 (Hemer and Harris, 2003). RS = Ross Sea based on record #102 (Cunningham et al., 1999); S.Ind = Subantarctic Indian Ocean (Stenni et al., 2001). AP = Antarctic Peninsula; WAP = West Antarctic Peninsula; EAP = East Antarctic Peninsula. EANT coastal: #116 (Hodgson et al., 2004); #118 (McMinn et al., 2001). S. America based on a compilation of palaeoclimate proxies, as discussed in the text.



After the Early Holocene climatic optimum

On the AP, the period after the Early Holocene climatic optimum (i.e. after 9600 cal. yr BP; ~8450 yr BP) witnessed several dramatic changes, including renewed vigour of ice sheet retreat rates, WAP ice shelf collapse events and reconfiguration of regional ocean circulation, culminating in a large-scale reduction of sea ice cover along the WAP and establishment of a re-current sea ice cycle. These observations made during this study suggest ameliorating climatic conditions; a trend that is apparently out-of-phase with circum-Antarctic, and possibly global patterns (Figure 8.14). Some Antarctic ice cores (Dome C, EPICA Dome C and Taylor Dome) and marine records (Adélie Land margin and South Atlantic) show evidence for a period of cooling, centred at ~8000 cal. yr BP (~7150 yr BP), with temperatures reconstructions at EPICA Dome C to be ~2 °C cooler than the preceding Early Holocene climatic optimum (Masson-Delmotte et al., 2004). However, although the EPICA Dome C site is recording cold temperatures, an increase in deuterium excess indicates temperatures in the Subantarctic Indian Ocean (the source area for Dome C precipitation) were warmer than today (Stenni et al., 2001; Masson-Delmotte et al., 2004). This is a similar scenario to that observed during the Antarctic Cold Reversal and suggests large changes in atmospheric transport were occurring in response to an increased meridional temperature gradient (Masson-Delmotte et al., 2004). This gradient results from the opposite annual insolation trends at low (increase) and high southern latitudes (decrease), leading to increased relative contribution from tropical zones to Antarctic moisture (Masson-Delmotte et al., 2004). If the warmth inferred for the Subantarctic Indian Ocean was a pervasive feature in the Southern Ocean, climatic amelioration on the AP could reflect closer connection with maritime influences, compared to the EAIS which is potentially more closely connected with continental influences.

8.4.2.2 Mid-Holocene climatic optimum

There is consensus in Antarctic palaeoclimate studies that the Mid-Holocene experienced a climate warmer than today (Hodgson et al., 2004). However, similar to the spatial and temporal complexity inferred for the AP in this study (see section 8.4.1.2), considerable variability exists in the timing and localised reflection around the Antarctic continent and between proxies.

Inland Antarctic ice cores generally show low variability through the Holocene. A Mid-Holocene climatic optimum signal is present in the majority of cores; however there are considerable disparities in the timing of onset (Figure 8.14). In the Ross Sea sector,

warm conditions are recorded much earlier than the EAIS sites; between 7800 – 5800 cal. yr BP (~7000 – 5100 yr BP) at Taylor Dome (Stager and Mayewski, 1997), compared to between 4500 – 2000 cal. yr BP (~4050 – 2050 yr BP) from a compilation of EAIS records (Ciais et al., 1994). An associated drop in Na concentrations in the Taylor Dome record at 7800 cal. yr BP (~7000 yr BP) was proposed to reflect a reduction of meridional circulation, possibly related to a decline in the extent of Antarctic sea ice that might have shifted circumpolar air masses poleward (Stager and Mayewski, 1997). Similarly, at Siple Dome, warm conditions are inferred from 6600 cal. yr BP (~5800 yr BP) and into the Late Holocene from an increase in melt layer frequency (Das and Alley, 2008). This is interpreted to reflect an increasing marine influence on the Ross Sea sector (Das and Alley, 2008) (discussed further in section 8.4.2.3).

Marine sedimentary data from the Ross Sea (#102) also suggests that between 6200 – 3000 yr BP (7100 – 3200 cal. yr BP) productivity was higher and seasonal spring sea ice melt occurred earlier (relative to today) (Cunningham et al., 1999) (Figure 8.14). This diatom-based marine interpretation, together with the ice core data from Taylor Dome, corroborates suggestions made in this investigation that sea ice cover was reduced on the WAP and a re-current sea ice cycle established by ~7600 yr BP (~8300 cal. yr BP). Furthermore, lake records from South Georgia record general climatic improvement after 8200 cal. yr BP (~7400 yr BP) (Rosqvirst et al., 1999). This reconstruction for a reduction in sea ice cover at ~7600 yr BP (~8300 cal. yr BP), over a broad area (from the Ross Sea, along the WAP and to South Georgia) suggests a connection between these localities, possibly through SE Pacific forcing mechanisms. A more poleward location of storm tracks of the Southern Westerlies has been used to explain drier, yet colder and variable, conditions in South America between ~7000 – 5000 yr BP (7800 – 5750 cal. yr BP) (Markgraf and Seltzer, 2001; Lamy et al., 2001; Gilli et al, 2005; Sterken et al., 2008).

The onset of the Mid-Holocene climatic optimum in the marine environment of the WAP from ~8000 yr BP (8850 cal. yr BP) (this study) appears to be the first circum-Antarctic expression of this Holocene climatic event (Figure 8.14). These reconstructions for non-synchronous Mid-Holocene climatic optimum conditions between West and East Antarctica is consistent with model outputs for Holocene climate evolution (Renssen et al., 2005). Simulated summer (October to April) temperatures suggest that the peak thermal optimum was 2000 to 1000 years earlier in

West Antarctica (7000 – 5000 cal. yr BP; 6100 – 4400 yr BP) than in East Antarctica (5500 – 4000 cal. yr BP; 4800 – 3700 yr BP) (Renssen et al., 2005). In their model, this difference is caused by the relatively strong reduction of sea ice in the Early Holocene in the western sector of the Southern Ocean relative to the eastern sector, resulting in relatively high Early Holocene temperatures in western Antarctica compared with the eastern part of the continent (Renssen et al., 2005).

Finally, the observation that Mid-Holocene climatic optimum conditions were in-phase between the marine environment of the EAP, together with coastal AP localities, and the terrestrial climate (see Figure 8.11) is also found in several circum-Antarctic coastal proxy records. In the Windmill Islands, warmer and more humid conditions are inferred from peak diatom concentration between ~4000 – 2000 yr BP (4500 – 1980 cal. yr BP) (#116: Hodgson et al., 2003). Similarly, in Ellis Fjord (#118) a transition occurs at 2500 yr BP (2570 cal. yr BP) from a period of reduced temporal sea ice cover to a much larger sea ice extent (McMinn et al., 2001).

8.4.2.3 Late Holocene Neoglacial

In general, the Late Holocene Neoglacial appears to be a circum-Antarctic feature. It is widely documented in East Antarctic ice core records (apart from Dome C) (Masson et al., 2000), with temperature at EPICA Dome C decreasing by ~1°C at 3000 cal. yr BP (~2850 yr BP) (Masson-Delmotte et al., 2004). All continental shelf marine cores record more extensive sea ice, with onset being roughly synchronous with the climatic deterioration witnessed on the WAP (~3000 yr BP; 3200 cal. yr BP) (this study) (Figure 8.14). This suggests similar forcing mechanisms were in operation in areas exposed to ACC influences. Late Holocene climatic deterioration is also evident in Southern Hemisphere mid-latitudes. In general, the Americas are characterised by a far greater degree of regionalisation of climate patterns during the Late Holocene (Markgraf and Seltzer, 2001). In southern South America, more humid conditions have prevailed from 4000 cal. yr BP (~3650 yr BP) (Lamy et al., 2001 and references therein), with an associated advances of glaciers, maybe as early as ~5000 – 4000 yr BP (~5700 – 4500 cal. yr BP) (Porter, 2000). These climatic shifts were potentially caused by changes in seasonal insolation, with Late Holocene austral summers warmer and austral winters cooler than today (Gilli et al., 2005). This resulted in a general strengthening and equatorward shift of the Southern Westerlies during the Late Holocene (Markgraf et al., 1992; Gilli et al., 2005).

However, some anomalies are also evident in the Late Holocene circum-Antarctic climate. In the South Atlantic, marine core #96 suggests abrupt cooling of SSTs, sea ice advance and increased delivery of ice-rafted debris at 5000 cal. yr BP (~4400 yr BP) (Hoddell et al., 2001); significantly earlier than the Late Holocene Neoglacial on the AP. In another South Atlantic core (#99), Nielsen et al. (2004) infer Late Holocene warming. Explaining the anti-phase behaviour between the climate trend of the eastern South Atlantic Ocean and the Pacific sector of the Southern Ocean (Lamy et al., 2002) and WAP (Palmer Deep and this study), Nielsen et al. (2004) proposed that a climatic divide was present during the Late Holocene through Patagonia, the Drake Passage, and between West and East Antarctica. Furthermore, in two ice cores from the WAIS, Mid-Holocene climatic optimum conditions are suggested to have extended into the Late Holocene; in Byrd, a temperature increase of ~2 °C in suggested from 4500 cal. yr BP (4000 yr BP) (Johnsen et al., 1972), which is similar in magnitude to the Mid- to Late-Holocene temperature increase derived from melt layer calibration in Siple Dome of Das and Alley (2008). Such a Mid- to Late Holocene temperature rise is absent in all East Antarctic ice core records and continental shelf marine cores. Das and Alley (2008) suggest that the Late Holocene melt record from Siple Dome provides evidence of increasing marine influence on the climate of West Antarctica, with periods of increased cyclogenesis, perhaps related to variations in ENSO, allowing this climate signal to more easily reach West Antarctica. This highlights the fact that the same forcing mechanism (increased storm frequency and ENSO) can cause very different responses (variable sea ice cover on the AP and propagation of a maritime signal into the WAIS interior, leading to warming).

8.4.2.4 Summary

On a broad-scale, AP Holocene climate events show an increasing degree of synchronicity with circum-Antarctic trends as time progresses: (1) retreat of the WAIS and EAIS was out-of phase and highly diachronous; (2) onset of the Mid-Holocene climatic optimum was roughly synchronous between: (a) the WAP and circum-Antarctic mid-shelf settings, suggesting the ACC acts as a circum-Antarctic teleconnection, driven ultimately by the strength and position of the Southern Westerlies; and (b) the EAP and coastal circum-Antarctic settings, suggesting connection with the Antarctic terrestrial character, as revealed through continental ice cores; and (3) Late Holocene Neoglacial was roughly synchronous around the continent. The different character of AP Holocene climate evolution, compared to circum-

Antarctic trends, is partly attributable to the contrasting extents of the West and East Antarctic Ice Sheets at the LGM. The much expanded WAIS was slower to respond to deglacial warming than the EAIS, with the ramifications of ice sheet retreat felt on the AP well into the Mid-Holocene.

8.5 Chapter summary

This chapter has discussed regional patterns in AP fossil diatom assemblages, which are linked to cross-peninsula and latitudinal environmental differences. Trends of consistent diatom species associations were explored and habitat types defined. Holocene climatic and oceanographic conditions were reconstructed for each of the seven AP core localities, utilising diatom assemblage data, stable isotopes and sedimentary pigments. Individual sediment records were compared between marine locations and integrated with published palaeoclimate data from the AP and Antarctic continent. This synthesis has revealed the complex nature of Antarctic climate evolution through the Holocene.

9 Conclusions

This chapter summarises the main conclusions from this investigation, addressing the two primary research questions posed in Chapter 1.2, and concludes by suggesting priorities for future research.

9.1 Conclusions from AP palaeoclimate reconstructions

(1) Were Holocene climatic events peninsula-wide and synchronous? Where spatial and temporal discrepancies exist, do these patterns provide clues to forcing mechanisms?

Palaeoclimate reconstructions for the AP have revealed that Holocene climatic events were peninsula-wide, but not synchronous. From the onset of Antarctic deglaciation to the present, climatic trends have displayed an earlier onset and longer duration on the WAP compared to the EAP; a similar trend to that witnessed during the recent decades of rapid warming on the AP. This discrepancy is suggested to reflect a connection between the WAP and SE Pacific, through coupled ocean-atmosphere interactions (position of Southern Westerlies and ENSO frequency); whereas the EAP is more closely connected with the terrestrial response of the Antarctic continent to climate change and the stable oceanographic and cryospheric influences of the Weddell Sea.

Deglaciation – Early Holocene transition

- WAP deglaciation occurred in two phases. The first phase of ice sheet retreat was relatively rapid, following the bathymetric troughs of the Belinga Trough, southern Bellinghausen Sea (from ~26000 yr BP; ~30000 cal. yr BP and retreating from core site GC358 by 12650 yr BP; 15020 cal. yr BP); Anvers Trough (from 13650 yr BP; 16230 cal. yr BP and retreating from core site GC047 by 10150 yr BP; 11800 cal. yr BP) and Marguerite Trough (from 11195 yr BP; 13090 cal. yr BP and retreating from core site VC306 by 10750 yr BP; 12720 cal. yr BP). Early deglaciation of the WAP troughs highlights the importance of localised controls, such as bathymetry and oceanographic influences which, when paired with deglaciation sea level rise, facilitate floatation and unhinging of the ice sheet. Following this rapid ice sheet retreat on the WAP, the grounding line appeared to have been relatively stable for ~2000 years in Marguerite Bay and Anvers Trough, possibly due to glacio-dynamic factors (presence of pinning points) or through oceanographic controls (lack of a warm UCDW influence), in spite of elevated

Early Holocene atmospheric temperatures. The second phase of ice sheet retreat occurred very rapidly, with retreat rates accelerating across the inner WAP shelf from ~8450 yr BP (9500 cal. yr BP). Diatom assemblages and stable isotope data suggested that upwelling of warm UCDW was a contributing factor, causing increased basal melting of the ice sheet and previously perennial WAP sea ice cover, together with the dispersal of post-deglaciation cool shelf waters.

- EAP deglaciation occurred episodically, with the ice shelf in Prince Gustav Channel (PGC) undergoing two periods of break-up: (1) retreating from core site VC237 at ~9250 yr BP (10420 cal. yr BP); and (2) retreating from core site VC243 at ~5260 yr BP (6050 cal. yr BP). The harsher continental climate of the EAP, with frequent perennial sea ice cover and cool shelf waters, was slower to respond to deglacial warming than the milder maritime WAP. Full retreat of the PGC Ice Shelf was potentially triggered by the Mid-Holocene climatic optimum.
- If the proposed link between upwelling of UCDW and acceleration of ice sheet retreat rates on the WAP at ~8000 yr BP (~8870 cal. yr BP) is correct, then the rapidity of retreat and associated dramatic changes in the WAP marine environment should be a cause for concern in the modern-day AP; there is evidence that surface water temperatures off the WAP have increased by 1 °C (Meredith and King, 2005) and furthermore, that mid-depth waters in the Southern Ocean have warmed since the 1950s (Gille, 2002; Fyfe, 2006). This temperature trend has clear implications for melt rates beneath a number of AP ice shelves and glaciers (e.g. George VI Ice Shelf and Pine Island Bay).

Mid-Holocene climatic optimum

- Although the Mid-Holocene climatic optimum is a well-documented climate feature of the AP, the event is highly diachronous. The AP can be divided into a number of regions based on the character of the Mid-Holocene climatic optimum, which reflects different forcing mechanisms: (1) WAP trough cores recorded prolonged (~7600 – 3400 yr BP; ~8300 – 3600 cal. yr BP) yet variable marine optimum conditions, dissimilar in timing to terrestrial and ice core records, and instead reflecting a connection with UCDW, possibly via the position of the ACC and Southern Westerlies; (2) WAP shelf edge cores recorded very different and variable climatic optimum signals: (a) early and short (~6000 – 5100 yr BP; ~6800 – 5900 cal. yr BP); or (b) early and longer (~5200 – 2450 yr BP; ~6000 – 2500

cal. yr BP), highlighting a possible connection with oceanographic influences of the Weddell Sea and sensitivity to subtle climatic changes via sea ice cover; (3) EAP and WAP coastal areas recorded a late and short climatic optimum (~4400 – 1650 yr BP; ~4960 – 1550 cal. yr BP), through impacts of glacier fluctuations linked to terrestrial and / or atmospheric forcing.

- Sedimentary pigments supported the interpretations provided by diatom assemblages, with the Mid-Holocene climatic optimum in PGC (core VC243) characterised by a more complex marine ecosystem than at other times during the Holocene. Elevated concentrations of the carotenoid Mondoxanthin revealed that large cryptophyte blooms developed in the Mid-Holocene environment of PGC, exploiting the reduced surface water salinities following ice shelf retreat and increased glacial meltwater runoff. This highlights the value of this proxy in providing additional information on the total phototrophic community, particularly the components that leave no morphological fossils.
- If the Mid-Holocene climatic optimum is a representative analogy for regional trends on the AP in the current warming world, it is likely future climate events and their impacts will display considerable spatial and temporal heterogeneity. Critical factors determining the localised expression are: (i) temperature and strength of UCDW upwelling; (ii) sea ice feedback mechanisms; and (iii) atmospheric temperatures and their rate of change. There is some evidence that the sequence of events witnessed during the Mid-Holocene climatic optimum, is being replayed in the modern-day, yet the rate of change is much faster, and even synchronous, today. In the Mid-Holocene, WAP sea ice extent and thickness was one of the first parameters to respond to climatic amelioration, followed by the collapse of one EAP ice shelf (PGC) several thousand years later; in the last 30 years, sea ice concentrations have dramatically decreased in the Bellingshausen Sea and Amundsen Sea (Parkinson, 2004), with collapse of several AP ice shelves also occurring during the last two decades (Hodgson et al., 2006a).

Late Holocene climatic deterioration

- Onset of Late Holocene climatic deterioration occurred earlier in the WAP marine environment, at ~3700 yr BP (~4100 cal. yr BP), compared to the EAP, southern WAP and terrestrial environment, which display a roughly synchronous onset at ~1700 yr BP (~1620 cal. yr BP). This study has shown that the transition into Late

Holocene climatic deterioration on the WAP was coincident with peak climatic optimum conditions for the EAP, suggesting greater cross-peninsula connection at this time. Retreat of sea ice cover on the EAP allowed cool shelf currents to develop and flow around the tip of the AP, impacting the northern WAP to produce relatively cooler surface water conditions and increased sea ice cover.

- Recent rapid AP warming has caused a reduction in EAP sea ice extent and thickness; it will be interesting to see if this has knock-on consequences for the WAP, as suggested by the transition into Late Holocene climate deterioration, with greater oceanographic, sea ice and climatic instability via cross-peninsula connections.

(2) Do AP Holocene climate events display similar phasing and duration to circum-Antarctic and global trends?

On a broad-scale, AP Holocene climate events show a similar pattern to circum-Antarctic and Southern Hemisphere trends, characterised by a warm Mid-Holocene and cooler Late Holocene. However, significant discrepancies in the timing of onset and duration of events are evident between localities and proxy records. AP palaeoclimate records show much greater variability compared to circum-Antarctic trends and generally earliest onset occurs in the WAP. This can be attributed to the dynamics of the WAIS, AP ice shelves and patterns of sea ice growth and decay having more affect in the maritime AP. Climate events in modern-day Antarctica are displaying a similar trend, with the AP identified as the most sensitive portion; this spatial and temporal complexity is likely to continue into the future and stresses the need for further palaeoclimate and modelling studies to address questions about how the climate system is linked spatially. This study has highlighted that no simple and universal pattern of Holocene climate exists; instead the character and cause of climate events is different between regions, reflecting differences in the sensitivity of climate proxies and the potential that the same forcing mechanism can cause very different responses.

9.2 Future research

This study of the palaeoclimate history of the AP has highlighted a number of gaps in our knowledge of both the trends in environmental change and associated mechanisms. Research priorities and questions to be addressed in future work include:

- Palaeoclimate reconstructions based on Antarctic marine sediments are hampered by the accuracy of chronological controls. Radiocarbon dating is the main method used for dating marine material, yet is subject to variable marine reservoir effects and incorporation of reworked carbon, whose effect is heterogeneous and often unknown. Although progress has been made in understanding these influences and new chronological techniques have been employed (e.g. palaeomagnetic intensity dating: Brachfeld et al., 2003; Willmott et al., 2006; and step-combustion radiocarbon dating: Rosenheim et al., 2007; 2008), there is still a need for more rigorous dating techniques, such as the development of compound-specific radiocarbon dating.

- Re-evaluation of glacio-isostatic and glaciological models for AP deglaciation is needed; ice sheet retreat reconstructions from marine sediments studied here suggests that onset of deglaciation started several thousand years earlier than models would predict, and in the southern Bellingshausen Sea, not the northern AP.

- There is a need for long ice cores to be recovered from the AP, which retrieve the glacial-interglacial transition or at a minimum the Early – Mid-Holocene. Ice core records from the continental interior, and those from south or east of the AP, are not fully representative of the regional pattern for the peninsula. However, recent drilling in 2008 at James Ross Island appears to have captured the glacial-interglacial transition and the full Holocene (Bentley et al., 2009); this record will hopefully fill this gap in AP palaeoclimate research.

- Low accumulation and relatively high bioturbation at each of these marine core localities has meant that it has not been possible to resolve climate events of short duration, such as the Little Ice Age, Medieval Warm Period and some ENSO effects; higher resolution cores are necessary to address such events and for comparison with recent warming trends. High accumulation core sites would also enable further refinement of the timing and character of longer duration Holocene climatic events, such as the Mid-Holocene climatic optimum.

- This study has highlighted the potential for sedimentary pigment datasets to reconstruct total primary production. Wider application of this proxy in the marine realm would provide a more comprehensive assessment of total primary production and environmental conditions prevalent at the time of sediment deposition.
- The forcing mechanisms behind AP climatic events require further understanding, particularly the role of Southern Westerlies, their connection with the ACC and upwelling of UCDW, together with ENSO variability. This will require a combined approach of additional proxy reconstructions from the AP, SE Pacific and South America, together with modelling studies. Understanding and modelling spatial variability in UCDW upwelling along the AP is of critical importance, as warm ocean perturbations are increasingly being linked to basal melting of AP ice shelves (Shepherd et al., 2004; Thoma et al., 2008). With respect to investigating the impacts of ENSO on the high latitudes, one of the most attractive means to address this is through sea ice reconstructions, as the sea ice cycle is very dependent on atmospheric circulation. High resolution diatom-based studies would provide this opportunity, potentially incorporating the use of isoprenoid lipids in diatoms; a relatively new technique applied in Arctic sea ice reconstructions (e.g. Massé et al., 2008; Andrews et al., 2009), yet not extensively applied in the Antarctic marine realm.

A

Abelmann, A., and Gersonde, R. (1991). Biosiliceous Particle-Flux in the Southern-Ocean. *Marine Chemistry* **35,** 503-536.

Absy, J. M., Schröder, M., Muench, R., and Hellmer, H. H. (2008). Early summer thermohaline characteristics and mixing in the western Weddell Sea. *Deep Sea Research Part II: Topical Studies in Oceanography* **55,** 1117-1131.

Aceituno, P., Fuenzalida, H., and Rosenblüth, B. (1993). Climate along the extratropical west coast of South America. *In* "Earth system responses to global change." (H. A. Mooney, E. R. Fuentes, and B. I. Kronberg, Eds.), pp. 61–69. Academic Press.

Ackley, S. F. (1996). Sea ice: Encyclopedia of applied physics, pp. 81-103. Hanover, VCH Publishers.

Ackley, S. F., Buck, K., and Taguchi, S. (1979). Standing crop of algae in the sea ice of the Weddell Sea region. *Deep-Sea Research Part a-Oceanographic Research Papers* **26,** 269-281.

Ahn, I. Y., Chung, H., Kang, J.-S., and Kang, S.-H. (1997). Diatom composition and biomass variability in nearshore waters of Maxwell Bay, Antarctica, during the 1992/1993 austral summer. *Polar Biology* **17,** 123-130.

Airs, R. L. (2002). "Analysis of complex pigment distributions using high resolution liquid chromatography." University of York. PhD thesis.

Airs, R. L., Atkinson, J. E., and Keely, B. J. (2001). Development and application of a high resolution liquid chromatographic method for the analysis of complex pigment distributions. *Journal of Chromatography A* **917,** 167-177.

Al-Handal, A. Y., and Wulff, A. (2008). Marine epiphytic diatoms from the shallow sublittoral zone in Potter Cove, King George Island, Antarctica. *Botanica Marina* **51,** 411-435.

Alldredge, A. L., and Gotschalk, C. C. (1989). Direct observations of the mass flocculation of diatom blooms - characteristics, settling velocities and formation of diatom aggregates. *Deep-Sea Research Part A - Oceanographic Research Papers* **36,** 159-171.

Alldredge, A. L., and Silver, M. W. (1982). Abundance and production rates of floating diatom mats (Rhizosolenia castracanei and R. imbricata va. shrubsolei) in the eastern Pacific Ocean. *Marine Biology* **66,** 83-88.

Alldredge, A. L., and Silver, M. W. (1988). Characteristics, dynamics and significance of marine snow. *Progress in Oceanography* **20,** 41-82.

Allen, C. S. (2003). "Late Quaternary Palaeoceanography of The Scotia Sea, southwest Atlantic: Evidence from the Diatom Record." Cardiff University. PhD thesis.

Allen, C. S., Pike, J., Pudsey, C. J., and Leventer, A. (2005). Submillennial variations in ocean conditions during deglaciation based on diatom assemblages from the southwest Atlantic. *Paleoceanography* **20,** PA2012, doi:10.1029/2004PA001055.

Alley, R. B., Brook, E. J., and Anandakrishnan, S. (2002). A northern lead in the orbital band: North-south phasing of Ice-Age events. *Quaternary Science Reviews* **21,** 431-441.

Alley, R. B., Mayewski, P. A., Sowers, T., Stuiver, M., Taylor, K. C., and Clark, P. U. (1997). Holocene climatic instability: A prominent, widespread event 8200 yr ago. *Geology* **25,** 483-486.

Altabet, M. A. (2005). Isotopic Tracers of the Marine Nitrogen Cycle: Present and Past. *In* "Handook of Environmental Chemistry." pp. 2-39.

Altabet, M. A., and Francois, R. (2001). Nitrogen isotope biogeochemistry of the Antarctic Polar Frontal Zone at 170 W. *Deep-Sea Research II* **48,** 4247-4273.

Amblas, D., Urgeles, R., Canals, M., Calafat, A. M., Rebesco, M., Camerlenghi, A., Estrada, F., De Batist, M., and Hughes-Clarke, J. E. (2006). Relationship between continental rise development and palaeo-ice sheet dynamics, Northern Antarctic Peninsula Pacific margin. *Quaternary Science Reviews* **25,** 933-944.

Amos, A. F. (1987). Racer: physical oceanography of the western Bransfield Strait. *Antarctic Journal of Unites States* **22,** 137-140.

Anderson, J. B. (1999). "Antarctic Marine Geology." Cambridge University Press, Cambridge.

Anderson, J. B., Lowe, A., Mosola, A., and Oakes, L. (2005). Extent of West Antarctic Ice Sheet During the LGM, Timing of Retreat and Potential Contribution to MWP Ia. *In* "American Geophysical Union, Fall Meeting." San Francisco, U.S.A.

Anderson, J. B., and Oates-Fretwell, L. (2008). Geomorphology of the onset area of a paleo-ice stream, Marguerite Bay, Antarctic Peninsula. *Earth Surface Processes and Landforms* **33,** 503-512.

Anderson, J. B., and Shipp, S. S. (2001). Evolution of the West Antarctic Ice Sheet. *In* "The West Antarctic Ice Sheet: Behavior and Environments." (R. Alley, and R. Bindschadler, Eds.), pp. 45–57. Antarctic Research Series. American Geophysical Union, Washington, DC.

Anderson, J. B., Shipp, S. S., Lowe, A. L., Wellner, J. S., and Mosola, A. B. (2002). The Antarctic Ice Sheet during the Last Glacial Maximum and its subsequent retreat history: a review. *Quaternary Science Reviews* **21,** 49-70.

Anderson, R. F., Ali, S., Bradtmiller, L. I., Nielsen, S. H. H., Fleisher, M. Q., Anderson, B. E., and Burckle, L. H. (2009). Wind-Driven Upwelling in the Southern Ocean and the Deglacial Rise in Atmospheric CO2. *Science* **323,** 1443-1448.

Andres, M. S., Bernasconi, S. M., McKenzie, J. A., and Rohl, U. (2003). Southern Ocean deglacial record supports global Younger Dryas. *Earth and Planetary Science Letters* **216,** 515-524.

Andrews, J. T., Belt, S. T., Olafsdottir, S., Massé, G., and Vare, L. L. (2009). Sea ice and marine climate variability for NW Iceland/Denmark Strait over the last 2000 cal yr BP. *The Holocene* **19,** 773-782.

Andrews, J. T., Domack, E. W., Cunningham, W. L., Leventer, A., Licht, K. J., Jull, A. J. T., DeMaster, D. J., and Jennings, A. E. (1999). Problems and possible solutions concerning radiocarbon dating of surface marine sediments, Ross Sea, Antarctica. *Quaternary Research* **52,** 206-216.

Armand, L. K. (1997). "The use of diatom transfer functions in estimating sea-surface temperature and sea-ice in cores from the southeast Indian Ocean." Australian National University. PhD thesis.

Armand, L. K. (2000). An Ocean of Ice - advances in the estimation of past sea ice in the Southern Ocean. *GSA Today* **10,** 1-7.

Armand, L., and Zielinski, U. (2001). Diatom species of the genus Rhizosolenia from Southern Ocean sediments: distribution and taxonomic notes. *Diatom Research* **16,** 259-294.

Armand, L. K., and Leventer, A. (2003). Palaeo Sea Ice Distribution - Reconstruction and Palaeoclimatic Significance. *In* "Sea Ice. An Introduction to its Physics, Chemistry, Biology and Geology." (D. N. Thomas, and G. S. Dieckmann, Eds.), pp. 333-372. Blackwell Science Ltd.

Armand, L. K., Crosta, X., Romero, O., and Pichon, J. J. (2005). The biogeography of major diatom taxa in Southern Ocean sediments: 1. Sea ice related species. *Palaeogeography Palaeoclimatology Palaeoecology* **223,** 93-126.

Armand, L. K., Crosta, X., Quéguiner, B., Mosseri, J., and Garcia, N. (2008). Diatoms preserved in surface sediments of the northeastern Kerguelen Plateau. *Deep Sea Research Part II: Topical Studies in Oceanography* **55,** 677-692.

Arrigo, K. R. (2003). Primary production in sea ice. *In* "Sea Ice: An introduction to its physics, chemistry, biology and geology." (D. N. Thomas, and G. S. Dieckmann, Eds.), pp. 143-183. Blackwell Science Ltd, Oxford.

Arrigo, K. R., Lubin, D., van Dijken, G. L., Holm-Hansen, O., and Morrow, E. (2003). Impact of a deep ozone hole on Southern Ocean primary production. *Journal of Geophysical Research-Oceans* **108,** C5, ISI:000183179200001.

Arrigo, K. R., and McClain, C. R. (1994). Spring phytoplankton production in the western Ross Sea. *Science* **266,** 261-263.

Ashworth, A. C., and Cantrill, D. J. (2004). Neogene vegetation of the Meyer Desert Formation (Sirius Group) Transantarctic Mountains, Antarctica. *Palaeogeography, Palaeoclimatology, Palaeoecology* **213,** 65-82.

B

Badger, M. R., Andrews, T. J., Whitney, S. M., Ludwig, M., Yellowlees, D. C., Leggat, W., and Dean Price, G. (1998). The diversity and coevolution of Rubisco, plastids, pyrenoids and chloroplast-based CO_2-concentrating mechanisms in algae. *Canadian Journal of Botany* **76,** 1052-1071.

Bak, Y. S., Yoo, K. C., Yoon, H. I., Lee, J. D., and Yun, H. (2007). Diatom evidence for Holocene paleoclimatic change in the South Scotia Sea, West Antarctica. *Geosciences Journal* **11,** 11-22.

Banfield, L. A., and Anderson, J. B. (1995). Seismic facies investigation of the late Quaternary glacial history of Bransfield Basin, Antarctica. *Antarctic Research Series* **86,** 123-140.

Barber, D. C., Dyke, A., Hillaire-Marcel, C., Jennings, A. E., Andrews, J. T., Kerwin, M. W., Bilodeau, G., McNeely, R., Southon, J., Morehead, M. D., and Gagnon, J. M. (1999). Forcing of the cold event of 8,200 years ago by catastrophic drainage of Laurentide lakes. *Nature* **400,** 344-348.

Bárcena, M. A., Fabrés, J., Isla, E., Flores, J. A., Sierro, F. J., Canals, M., and Palanques, A. (2006). Holocene neoglacial events in the Bransfield Strait (Antarctica). Palaeoceanographic and palaeoclimatic significance. *Scientia Marina* **70,** 607-619.

Bárcena, M. A., Gersonde, R., Ledesma, S., Fabres, J., Calafat, A. M., Canals, M., Sierro, F. J., and Flores, J. A. (1998). Record of Holocene glacial oscillations in Bransfield Basin as revealed by siliceous microfossil assemblages. *Antarctic Science* **10,** 269-285.

Bárcena, M. Á., Isla, E., Plaza, A., Flores, J. A., Sierro, F. J., Masqué, P., Sanchez-Cabeza, J. A., and Palanques, A. (2002). Bioaccumulation record and paleoclimatic significance in the Western Bransfield Strait. The last 2000 years. *Deep Sea Research Part II: Topical Studies in Oceanography* **49,** 935-950.

Bard, E. (1988). Correction of accelerator mass spectrometry ^{14}C ages measured in planktonic foraminifera: Paleoceanographic implications. *Palaeoceanography* **3,** 635-645.

Bard, E. (1994). The North Atlantic atmosphere-sea surface 14C gradient during the Younger Dryas climatic event. *Earth & Planetary Science Leters* **126,** 275-287.

Bard, E., B., H., G., F. R., and A., Z. (1990). Calibration of the ^{14}C timescale over the past 30,000 years using mass spectrometric U-Th ages from Barbados corals. *Nature* **345,** 405-410.

Barker, S., Broecker, W. S., Clarke, E., and Hajdas, I. (2007). Radiocarbon age offsets of foraminifera resulting from differential dissolution and fragmentation within the sedimentary bioturbated zone. *Paleoceanography* **22,** PA2205, doi:10.1029/2006PA001354,.

Barker, S., Diz, P., Vautravers, M. J., Pike, J., Knorr, G., Hall, I. R., and Broecker, W. S. (2009). Interhemispheric Atlantic seesaw response during the last deglaciation. *Nature* **457,** 1097-1102.

Baroni, C., and Orombelli, G. (1994). Abandoned penguin rookeries as Holocene palaeoclimatic indicators in Antarctica. *Geology* **22,** 23-26.

Bassett, S. E., Milne, G. A., Bentley, M. J., and Huybrechts, P. (2007). Modelling Antarctic sea-level data to explore the possibility of a dominant Antarctic contribution to meltwater pulse IA. *Quaternary Science Reviews* **26,** 2113-2127.

Beardsley, R. C., Limeburner, R., and Brechner Owens, W. (2004). Drifter measurements of surface currents near Marguerite Bay on the western Antarctic Peninsula shelf during austral summer and fall, 2001 and 2002. *Deep-Sea Research Part II: Topical Studies in Oceanography* **51,** 1947-1964.

Bentley, M. J., and Anderson, J. B. (1998). Glacial and marine geological evidence for the ice sheet configuration in the Weddell Sea Antarctic Peninsula region during the Last Glacial Maximum. *Antarctic Science* **10,** 309-325.

Bentley, M. J., Hodgson, D. A., Smith, J. A., Ó Cofaigh, C., Domack, E. W., Larter, R. D., Roberts, S. J., Brachfeld, S., Leventer, A., Hjort, C., Hillenbrand, C.-D., and Evans, J. (2009). Mechanisms of Holocene palaeoenvironmental change in the Antarctic Peninsula region. *The Holocene* **19,** 51-69.

Bentley, M. J., Hodgson, D. A., Sugden, D. E., Roberts, S. J., Smith, J. A., Leng, M. J., and Bryant, C. (2005). Early Holocene retreat of the George VI Ice Shelf, Antarctic Peninsula. *Geology* **33,** 173-76.

Berger, A., and Loutre, M. F. (1991). Insolation values for the climate of the last 10 million years. *Quaternary Science Reviews* **10,** 297-317.

Berkman, P. A., Andrews, J. T., Bjorck, S., Colhoun, E. A., Emslie, S. D., Goodwin, I. D., Hall, B. L., Hart, C. P., Hirakawa, K., Igarashi, A., Ingolfsson, O., Lopez-Martinez, J., Lyons, W. B., Mabin, M. C. G., Quilty, P. G., Taviani, M., and Yoshida, Y. (1998). Circum-Antarctic coastal environmental shifts during the Late Quaternary reflected by emerged marine deposits. *Antarctic Science* **10,** 345-362.

Berkman, P. A., and Forman, S. L. (1996). Pre-bomb radiocarbon and the reservoir correction for calcareous marine species in the Southern Ocean. *Geophysical Research Letters* **23,** 363-366.

Bianchi, C., and Gersonde, R. (2004). Climate evolution at the last deglaciation: the role of the Southern Ocean. *Earth and Planetary Science Letters* **228,** 407-424.

Biddanda , B., and Benner, R. (1997). Carbon, nitrogen and carbohydrate fluxes during the production of particulate and dissolved organic matter by marine phytoplankton. *Limnology and Oceanography* **42,** 506-518.

Bindschadler, R. (1998). GEOSCIENCE:Future of the West Antarctic Ice Sheet. *Science* **282,** 428-429.

Björck, S., Håkansson, H., Olsson, S., Ellis-Evans, C., Humlum, O., and Lirio, J. M. (1996a). Late Holocene palaeoclimatic records from lake sediments on James Ross Island, Antarctica. *Paleogeography, Paleoclimatology, Paleoecology* **113,** 195–220.

Björck, S., Hjort, C., Ingólfsson, Ó., Zale, R., and Ising, J. (1996b). Holocene deglaciation chronology from lake sediments. *In* "Geomorphological map of Byers Peninsula, Livingston Island. British Antarctic Survey Geomap Series, Sheet 5-A." (J. L. Lopez-Martinez, M. R. A. Thomson, and J. W. Thomson, Eds.).

Björck, S., Malmer, N., Hjort, C., Sandgren, P., Ingólfsson, Ó., Wallén, B., Smith, R. I. L., and Jönsson, B. L. (1991). Stratigraphic and paleoclimatic studies of a 5500-year-old moss bank on Elephant Island, Antarctica. . *Arctic and Alpine Research* **23,** 361-74.

Black, T. H. (1983). The preparation and reactions of diazomethane. *Aldrichimica Acta* **16,** 3-10.

Blunier, T., and Brook, E. J. (2001). Timing of millennial-scale climate change in Antarctica and Greenland during the last glacial period. *Science* **291,** 109-112.

Blunier, T., Schwander, J., Chappellaz, J., Parrenin, F., and Barnola, J. M. (2004). What was the surface temperature in central Antarctica during the last glacial maximum? *Earth and Planetary Science Letters* **218,** 379-388.

Blunier, T., Schwander, J., Stauffer, B., Stocker, T., Dallenbach, A., Indermuhle, A., Tschumi, J., Chappellaz, J., Raynaud, D., and Barnola, J. M. (1997). Timing of the Antarctic cold reversal and the atmospheric CO2 increase with respect to the Younger Dryas event. *Geophysical Research Letters* **24,** 2683-2686.

Bodén, P. (1991). Reproducibility in the random settling method for quantitative diatom analysis. *Micropaleontology* **37,** 313-319.

Bodungen, B. V., Smetacek, V. S., Tilzer, M. M., and Zeitzschel, B. (1986). Primary Production and Sedimentation During Spring in the Antarctic Peninsula Region. *Deep-Sea Research Part a-Oceanographic Research Papers* **33,** 177-194.

Bondevik, S., Mangerud, J., Birks, H. H., Gulliksen, S., and Reimer, P. (2006). Changes in North Atlantic Radiocarbon Reservoir Ages During the Allerod and Younger Dryas. *Science* **312,** 1514-1517.

Bowman, S. (1990). "Radiocarbon dating." British Museum Publications, London. pp64.

Boyd, P. W., and Law, C. S. (2001). The Southern Ocean Iron RElease Experiment (SOIREE)--introduction and summary. *Deep Sea Research Part II: Topical Studies in Oceanography* **48,** 2425-2438.

Boyd, P. W., Watson, A. J., Law, C. S., Abraham, E. R., Trull, T., Murdoch, R., Bakker, D. C. E., Bowie, A. R., Buesseler, K. O., Chang, H., Charette, M., Croot, P., Downing, K., Frew, R., Gall, M., Hadfield, M., Hall, J., Harvey, M., Jameson, G., LaRoche, J., Liddicoat, M., Ling, R., Maldonado, M. T., McKay, R. M., Nodder, S., Pickmere, S., Pridmore, R., Rintoul, S., Safi, K., Sutton, P., Strzepek, R., Tanneberger, K., Turner, S., Waite, A., and Zeldis, J. (2000). A mesoscale phytoplankton bloom in the polar Southern Ocean stimulated by iron fertilization. *Nature* **407,** 695-702.

Brachfeld, S., Domack, E., Kissel, C., Laj, C., Leventer, A., Ishman, S., Gilbert, R., Camerlenghi, A., and Eglinton, L. B. (2003). Holocene history of the Larsen-A Ice Shelf constrained by geomagnetic paleointensity dating. *Geology* **31,** 749-752.

Brathauer, U., and Abelmann, A. (1999). Late Quaternary Variations in Sea Surface Temperatures and their Relationship to Orbital Forcing Recorded in the Southern Ocean (Atlantic Sector). *Paleoceanography* **14,** doi:10.1029/1998PA900020.

Brichta, M., and Nöthig, E.-M. (2003). Proboscia inermis: A key diatom species in Antarctic autumn. *In* "Abstract AGU Chapman conference: The role of Diatom Production and Si flux and Burial in the Regulation of Global Cycles."

British Antarctic Survey RRS Cruise Report (2002) Marine geology and geophysics on the continental shelf and slope of the Antarctic Peninsula and in the Weddell Sea. Pudsey, C. J., and contributors. pp. 72. British Antarctic Survey.

British Antarctic Survey RRS *James Clark Ross* Cruise JR104 report (2004) Marine geology and geophysics, Bellingshausen Sea. Larter, R. D., Tait, A., Pudsey, C. J., Preston, M. O., O' Cofaigh, C., Morris, P., Hillenbrand, C.-D., Evans, J., Dowdeswell, J. A., and Bremner, S. F. pp. 68. British Antarctic Survey.

Britton, G. (1993). Structure and nomenclature. *In* "Carotenoids in Photosynthesis." (A. Young, and G. Britton, Eds.). Chapman & Hall, London.

Broecker, W. S. (1998a). Paleocean circulation during the last deglaciation: A bipolar seesaw? *Paleoceanography* **13,** 119-121.

Broecker, W. S. (1998b). The end of the present interglacial: How and when? *Quaternary Science Reviews* **17,** 689-694.

Broecker, W. S., and Denton, G. H. (1990). The role of ocean-atmosphere reorganizations in glacial cycles. *Quaternary Science Reviews* **53,** 305-341.

Broecker, W. S., and Peng, T. (1982). "Tracers in the sea." Lamont Doherty Geological Observatory, New York. pp690.

Brook, E. J., White, J. W. C., Schilla, A. S. M., Bender, M. L., Barnett, B., Severinghaus, J. P., Taylor, K. C., Alley, R. B., and Steig, E. J. (2005). Timing of millennial-scale climate change at Siple Dome, West Antarctica, during the last glacial period. *Quaternary Science Reviews* **24,** 1333-1343.

Buffen, A., Leventer, A., Rubin, A., and Hutchins, T. (2007). Diatom assemblages in surface sediments of the northwestern Weddell Sea, Antarctic Peninsula. *Marine Micropaleontology* **62,** 7-30.

Burckle, L. H. (1984a). Diatom Distribution and Paleoceanographic Reconstruction in the Southern-Ocean - Present and Last Glacial Maximum. *Marine Micropaleontology* **9,** 241-261.

Burckle, L. H. (1984b). Ecology and Paleoecology of the Marine Diatom Eucampia-Antarctica (Castr) Mangin. *Marine Micropaleontology* **9,** 77-86.

Burckle, L. H., and Cirilli, J. (1987). Origin of Diatom Ooze Belt in the Southern-Ocean - Implications for Late Quaternary Paleoceanography. *Micropaleontology* **33,** 82-86.

Burckle, L. H., Gersonde, R., and Abrams, N. (1990). Late Pliocene-Pleistocene paleoclimate in the Jane Basin region: ODP Site 697. *Proceedings of the Ocean Drilling Program, Scientific Results* **113,** 803-809.

Burckle, L. H., Jacobs, S. S., and McLaughlin, R. B. (1987). Late Austral Spring Diatom Distribution between New-Zealand and the Ross Ice Shelf, Antarctica - Hydrographic and Sediment Correlations. *Micropaleontology* **33,** 74-81.

Burckle, L. H., and Stanton, D. (1975). Distribution of displaced Antarctic diatoms in the Argentine Basin. *Nova Hedwigia* **53,** 283-292.

Burkhardt, S., Riebesell, U., and Zondervan, I. (1999a). Effects of growth rate, CO_2 concentration, and cell size on the stable carbon isotope fractionation in marine phytoplankton. *Geochimica et Cosmochimica Acta* **63,** 3729-3741.

Burkhardt, S., Riebesell, U., and Zondervan, I. (1999b). Stable carbon isotope fractionation by marine phytoplankton in response to daylength, growth rate, and CO2 availability. *Marine Ecology Progress Series* **184,** 31-41.

Butzin, M., Prange, M., and Lohmann, G. (2005). Radiocarbon simulations for the glacial ocean: The effects of wind stress, Southern Ocean sea ice and Heinrich events. *Earth and Planetary Science Letters* **235,** 45-61.

C

Carlson, A. E., Oppo, D. W., Came, R. E., LeGrande, A. N., Keigwin, L. D., and Curry, W. B. (2008). Subtropical Atlantic salinity variability and Atlantic meridional circulation during the last deglaciation. *Geology* **36,** 991-994.

Carpenter, E. J., Harbison, G. R., Madin, L. P., Swanberg, N. R., Biggs, D. C., Hulbert, E. M., McAlister, V. L., and McCarthy, J. J. (1977). Rhizosolenia mats. *Limnology and Oceanography* **22,** 739-741.

Cassar, N., Laws, E. A., Bidigare, R. R., and Popp, B. N. (2004). Bicarbonate uptake by Southern Ocean phytoplankton. *Global Biogeochemical Cycles* **18,** doi:10.1029/2003GB002116.

Cassar, N., Laws, E. A., and Popp, B. N. (2006). Carbon isotopic fractionation by the marine diatom Phaeodactylum tricornutum under nutrient- and light-limited growth conditions. *Geochimica et Cosmochimica Acta* **70,** 5323-5335.

Ciais, P., Jouzel, J., Petit, J. R., Lipenkov, V., and White, J. W. C. (1994). Holocene temperature variations inferred from six Antarctic ice cores. *Annals of Glaciology* **20,** 427-436.

Ciais, P., Petit, J. R., Jouzel, J., Lorius, C., Barkov, N. I., Lipenkov, V., and Nicolaïev, V. (1992). Evidence for an early Holocene climatic optimum in the Antarctic deep ice-core record. *Climate Dynamics* **6,** 169-177.

Clapperton, C. M., and Sugden, D. E. (1982). Late Quaternary glacial history of George VI Sound area, West Antarctica. *Quaternary Research* **18,** 243-267.

Clark, P. U., Alley, R. B., Keigwin, L. D., Licciardi, J. M., Johnsen, S. J., and Wang, H. (1996). Origin of the First Global Meltwater Pulse Following the Last Glacial Maximum. *Paleoceanography* **11,** 563–577.

Clark, P. U., McCabe, A. M., Mix, A. C., and Weaver, A. J. (2004). Rapid Rise of Sea Level 19,000 Years Ago and Its Global Implications. *Science* **304,** 1141-1144.

Clark, P. U., Mitrovica, J. X., Milne, G. A., and Tamisiea, M. E. (2002). Sea-Level Fingerprinting as a Direct Test for the Source of Global Meltwater Pulse IA. *Science* **295,** 2438-2441.

Clarke, A., Meredith, M. P., Wallace, M. I., Brandon, M. A., and Thomas, D. N. (2008). Seasonal and interannaul variability in temperature, chlorophyll and macronutrients in Ryder Bay, northern Marguerite Bay, Antarctica. *Deep Sea Research Part II: Topical Studies in Oceanography* **55,** 1988-2006

Clarke, A., Murphy, E. J., Meredith, M. P., King, J. C., Peck, L. S., Barnes, D. K. A., and Smith, R. C. (2007). Climate Change and the marine ecosystem of the western Antarctic Peninsula. *Philosophical Transactions of the Royal Society B Biological Sciences* **362,** 149-166.

Claustre, H. (1994). The trophic status of various oceanic provinces as revealed by phytoplankton pigment signatures. *Limnology and Oceanography* **39,** 1206-1210.

Claustre, H., Kerhervé, P., Marty, J. C., and Prieur, L. (1994). Phytoplankton photoadaptation related to some frontal physical processes. *Journal of Marine Systems* **5,** 251-265.

Clement, A. C., Seager, R., and Cane, M. A. (1999). Orbital controls on the El Nino/Southern Oscillation and the tropical climate. *Palaeoceanography* **14,** 441-456.

Clement, A. C., Seager, R., and Cane, M. A. (2000). Suppression of El Nino during the Mid-Holocene by Changes in the Earth's Orbit. *Paleoceanography* **15,** 731–737.

CLIMAP. (1981). Seasonal reconstructions of the Earth's surface at the last glacial maximum. *In* "Map Chart Series MC-36." (G. S. o. America, Ed.).

Coale, K. H., Johnson, K. S., Chavez, F. P., Buesseler, K. O., Barber, R. T., Brzezinski, M. A., Cochlan, W. P., Millero, F. J., Falkowski, P. G., Bauer, J. E., Wanninkhof, R. H., Kudela, R. M., Altabet, M. A., Hales, B. E., Takahashi, T., Landry, M. R., Bidigare, R. R., Wang, X., Chase, Z., Strutton, P. G., Friederich, G. E., Gorbunov, M. Y., Lance, V. P., Hilting, A. K., Hiscock, M. R., Demarest, M., Hiscock, W. T., Sullivan, K. F., Tanner, S. J., Gordon, R. M., Hunter, C. N., Elrod, V. A., Fitzwater, S. E., Jones, J. L., Tozzi, S., Koblizek, M., Roberts, A. E., Herndon, J., Brewster, J., Ladizinsky, N., Smith, G., Cooper, D., Timothy, D., Brown, S. L., Selph, K. E., Sheridan, C. C., Twining, B. S., and Johnson, Z. I. (2004). Southern Ocean Iron Enrichment Experiment: Carbon Cycling in High- and Low-Si Waters. *Science* **304,** 408-414.

Comiso, J. C. (2003). Large-scale characteristics and variability of the global sea ice cover. *In* "Sea Ice: An introduction to its physics, chemistry, biology and geology." (D. N. Thomas, and G. S. Dieckmann, Eds.), pp. 112-142. Blackwell Science.

Convey, P. (2001). Terrestrial ecosystem responses to climate changes in the Antarctic. *In* ""Fingerprints" of Climate Change - Adapted Behaviour and Shifting Species Ranges" (G.-R. Walther, C. A. Burga, and P. J. Edwards, Eds.), pp. 17–42. Kluwer Academic, New York.

Conway, H., Hall, B. L., Denton, G. H., Gades, A. M., and Waddington, E. D. (1999). Past and Future Grounding-Line Retreat of the West Antarctic Ice Sheet. *Science* **286,** 280-283.

Cook, A. J., Fox, A. J., Vaughan, D. G., and Ferrigno, J. G. (2005). Retreating glacier fronts on the Antarctic Peninsula over the past half-century. *Science* **308,** 541-544.

Cooke, D. W., and Hays, J. D. (1982). Estimates of Antarctic Ocean seasonal sea-ice cover during glacial intervals. *In* "Antarctic Geoscience, International union of Geological Sciences." (C. Craddock, Ed.), pp. 1017–1025. The Union of Wisconsin Press, Madison, WI.

Cortese, G., and Gersonde, R. (2007). Morphometric variability in the diatom Fragilariopsis kerguelensis : implications for Southern Ocean paleoceanography. *Earth and planetary science letters* **257,** 526-544.

Craig, H. (1957). The natural distribution of radiocarbon and the exchaneg time of carbon dioxide between the atmosphere and sea. *Tellus* **9,** 1-17.

Cremer, H., Roberts, D., McMinn, A., Gore, D., and Melles, M. (2003). The Holocene Diatom Flora of Marine Bays in the Windmill Islands, East Antarctica. *Botanica Marina* **46,** 82-106.

Cremer, H., Heiri, O., Wagner, B., and Wagner-Cremer, F. (2007). Abrupt climate warming in East Antarctica during the early Holocene. *Quaternary Science Reviews* **26,** 2012-2018.

Crosta, X., Pichon, J. J., and Labracherie, M. (1997). Distribution of Chaetoceros resting spores in modern peri-Antarctic sediments. *Marine Micropaleontology* **29,** 283-299.

Crosta, X., Pichon, J. J., and Burckle, L. H. (1998). Application of modern analog technique to marine Antarctic diatoms: Reconstruction of maximum sea-ice extent at the Last Glacial Maximum. *Paleoceanography* **13,** 284-297.

Crosta, X., and Shemesh, A. (2002). Reconciling down core anticorrelation of diatom carbon and nitrogen isotopic ratios from the Southern Ocean. *Paleoceanography* **17,** 10-1.

Crosta, X., Sturm, A., Armand, L., and Pichon, J. J. (2004). Late Quaternary sea ice history in the Indian sector of the Southern Ocean as recorded by diatom assemblages. *Marine Micropaleontology* **50,** 209-223.

Crosta, X., Crespin, J., Billy, I., and Ther, O. (2005a). Major factors controlling Holocene delta C-13(org) changes in a seasonal sea-ice environment, Adelie Land, East Antarctica. *Global Biogeochemical Cycles* **19,** ISI:000234506200004.

Crosta, X., Romero, O., Armand, L. K., and Pichon, J. J. (2005b). The biogeography of major diatom taxa in Southern Ocean sediments: 2. Open ocean related species. *Palaeogeography Palaeoclimatology Palaeoecology* **223,** 66-92.

Crosta, X., and Koç, N. (2007). Diatoms: From Micropaleontology to Isotope Geochemistry. *In* "Developments in Marine Geology." pp. 327-369. Elsevier.

Crosta, X., Debret, M., Denis, D., Courty, M. A., and Ther, O. (2007). Holocene long- and short-term climate changes off Adelie Land, East Antarctica. *Geochemistry, Geophysics, Geosystems* **8,** 1-15.

Crosta, X., Denis, D., and Ther, O. (2008). Sea ice seasonality during the Holocene, Adélie Land, East Antarctica. *Marine Micropaleontology* **66,** 222-232.

Cunningham, W. L., and Leventer, A. (1998). Diatom assemblages in surface sediments of the Ross Sea: relationship to present oceanographic conditions. *Antarctic Science* **10,** 134-146.

Cunningham, W. L., Leventer, A., Andrews, J. T., Jennings, A. E., and Licht, K. J. (1999). Late Pleistocene-Holocene marine conditions in the Ross Sea, Antarctica: evidence from the diatom record. *Holocene* **9,** 129-139.

Curran, M. A. J., van Ommen, T. D., Morgan, V. I., Phillips, K. L., and Palmer, A. S. (2003). Ice Core Evidence for Antarctic Sea Ice Decline Since the 1950s. *Science* **302,** 1203-1206.

Curry, P., and Pudsey, C. J. (2007). New Quaternary sedimentary records from near the Larsen C and former Larsen B ice shelves; evidence for Holocene stability. *Antarctic Science* **19,** 355-364.

D

Daintith, J. (2008). A Dictionary of Chemistry. Oxford University Press; Oxford Reference Online.

Dale, A. L., and Dale, B. (2002). Application of ecologically based statistical treatments to micropalaeontology. *In* "Quaternary Environmental Micropalaeontology." (S. K. Haslett, Ed.), pp. 259 - 286. Arnold, London.

Danzeglocke, U., Jöris, O., and Weninger, B. (2008). CalPal-2007online (online version).

Das, S. B., and Alley, R. B. (2008). Rise in frequency of surface melting at Siple Dome through the Holocene: Evidence for increasing marine influence on the climate of West Antarctica. *Journal of Geophysical Research D: Atmospheres* **113,** D02112, doi:10.1029/2007JD008790.

De Angelis, H., and Skvarca, P. (2003). Glacier surge after ice shelf collapse. *Science* **299,** 1560-1562.

de Baar, H. J. W., de Jong, J. T. M., Bakker, D. C. E., Löscher, B. M., Veth, C., Bathmann, U., and Smetacek, V. (1995). Importance of iron for phytoplankton spring blooms and CO_2 drawdown in the Southern Ocean. *Nature* **373,** 412-415.

De La Rocha, C. L., Jacot des Combes, H., Gersonde, R., and Abelmann, A. (2005). The O, Si, and N isotopic composition of sedimentary opal: a status report. *In* "Biogeochemical Controls on Palaeoceanographic Proxies." The Geological Society, London.

de Vries, H. (1958). Variation in concentration of radiocarbon with time and location on Earth. *In* "Proceedings Koninklijke Nederlandse Akademie van Wetenschappen." pp. 94–102.

de Vries, H. (1959). Measurement and use of natural radiocarbon. *In* "Researches in Geochemistry." (P. H. Abelson, Ed.), pp. 169–189. Wiley, New York.

DeConto, R. M., and Pollard, D. (2003). Rapid Cenozoic glaciation of Antarctica induced by declining atmospheric CO_2. *Nature* **421,** 245-249.

DeConto, R. M., Pollard, D., Wilson, P., Palike, H., Lear, C., and Pagani, M. (2008). Thresholds for Cenozoic bipolar glaciation. *Nature* **455,** 653-656.

DeFelice, D. R., and Wise, S. W. (1981). Surface lithofacies, biofacies and diatom diversity patterns as models for delineation of climatic change in the south east Atlantic Ocean. *Marine Micropaleontology* **6,** 29-70.

Delaygue, G., Stocker, T. F., Joos, F., and Plattner, G. K. (2003). Simulation of atmospheric radiocarbon during abrupt oceanic circulation changes: Trying to reconcile models and reconstructions. *Quaternary Science Reviews* **22,** 1647-1658.

Delmonte, B., Petit, J. R., Krinner, G., Maggi, V., Jouzel, J., and Udisti, R. (2005). Ice core evidence for secular variability and 200-year dipolar oscillations in atmospheric circulation over East Antarctica. *Climate Dynamics* **24,** 641-654.

Delmonte, B., Petit, J. R., and Maggi, V. (2002). Glacial to Holocene implications of the new 27000-year dust record from the EPICA Dome C (East Antarctica) ice core. *Climate Dynamics* **18,** 647-660.

Denis, D., Crosta, X., Schmidt, S., Carson, D. S., Ganeshram, R. S., Renssen, H., Bout-Roumazeilles, V., Zaragosi, S., Martin, B., Cremer, M., and Giraudeau, J. (2009). Holocene glacier and deep water dynamics, Adélie Land region, East Antarctica. *Quaternary Science Reviews* **28,** 1291-1303.

Denis, D., Crosta, X., Zaragosi, S., Romero, O., Martin, B., and Mas, V. (2006). Seasonal and subseasonal climate changes recorded in laminated diatom ooze sediments, Adelie Land, East Antarctica. *The Holocene* **16,** 1137-1147.

Denton, G. H., and Broecker, W. S. (2008). Wobbly ocean conveyor circulation during the Holocene? *Quaternary Science Reviews* **27,** 1939-1950.

Denton, G. H., and Hendy, C. H. (1994). Younger Dryas Age advance of Franz-Josef Glacier in the Southern Alps of New Zealand. *Science* **264,** 1434-1437.

Denton, G. H., Heusser, C. J., Lowell, T. V., Moreno, P. I., Andersen, B. G., Heusser, L. E., Schluchter, C., and Marchant, D. R. (1999). Interhemispheric linkage of paleoclimate during the last glaciation. *Geografiska Annaler Series a-Physical Geography* **81,** 107–153.

Denton, G. H., and Hughes, T. J. (2002). Reconstructing the Antarctic Ice Sheet at the Last Glacial Maximum. *Quaternary Science Reviews* **21,** 193-202.

Dieckmann, G. S., and Hellmer, H. H. (2003). The importance of sea ice: an overview. *In* "Sea Ice: An introduction to its physics, chemistry, biology and geology." (D. N. Thomas, and G. S. Dieckmann, Eds.), pp. 1-21. Blackwell Science.

Dierssen, H. M., Smith, R. C., and Vernet, M. (2002). Glacial meltwater dynamics in coastal waters west of the Antarctic peninsula. *Proceedings of the National Academy of Sciences of the United States of America* **99,** 1790-1795.

Dinnimann, M. S., and Klinck, J. M. (2004). A model of circulation and cross-shelf exchange on the west Antarctic Peninsula continental shelf. *Deep-Sea Research: Part II* **51,** 2003-2022.

Domack, E. (1992). ^{14}C ages and reservoir corrections for the Antarctic Peninsula and Gerlache Strait area. *Antarctic Journal of the United States* **27,** 63-64.

Domack, E. (2002). A synthesis for site 1098: Palmer Deep. *In* "Proceedings of the Ocean Drilling Program, Scientific Results." (P. F. Barker, A. Camerlenghi, G. D. Acton, and A. T. S. Ramsay, Eds.), pp. 1-14.

Domack, E., Amblas, D., Gilbert, R., Brachfeld, S., Camerlenghi, A., Rebesco, M., Canals, M., and Urgeles, R. (2006). Subglacial morphology and glacial evolution of the Palmer deep outlet system, Antarctic Peninsula. *Geomorphology* **75,** 125-142.

Domack, E., Duran, D., Leventer, A., Ishman, S., Doane, S., McCallum, S., Amblas, D., Ring, J., Gilbert, R., and Prentice, M. (2005). Stability of the Larsen B ice shelf on the Antarctic Peninsula during the Holocene epoch. *Nature* **436,** 681-685.

Domack, E., Ishman, S., Stein, A. B., McClennen, C. E., and Jull, A. J. T. (1995). Late Holocene Advance of Muller Ice Shelf, Antarctic Peninsula: Sedimentological, Geochemical and Palaeontological Evidence. *Antarctic Science* **7,** 159-170.

Domack, E., Jacobson, E., Shipp, S., and Anderson, J. (1999). Late Pleistocene retreat of the West Antarctic Ice-Sheet system in the Ross Sea: Part 2 - Sedimentologic and stratigraphic signature. *GSA Bulletin* **111,** 1517-1536.

Domack, E., Leventer, A., and Burnettet, A. (2003). "Antarctic Peninsula Climate Variability: Historical and Paleoenvironmental Perspectives." American Geophysical Union.

Domack, E., Leventer, A., Dunbar, R., Taylor, F., Brachfeld, S., and Sjunneskog, C. (2001). Chronology of the Palmer Deep site, Antarctic Peninsula: a Holocene palaeoenvironmental reference for the circum-Antarctic. *Holocene* **11,** 1-9.

Domack, E., O'Brien, P., Harris, P., Taylor, F., Quilty, P. G., De Santis, L., and Raker, B. (1998). Late Quaternary sediment facies in Prydz Bay, East Antarctica and their relationship to glacial advance onto the continental shelf. *Antarctic Science* **10,** 236-246.

Domack, E. W., and Ishman, S. (1992). Magnetic susceptibility of Antarctic glacial marine sediments. *Antarctic Journal of the United States* **27,** 64-65.

Domack, E. W., Jull, A. J. T., Anderson, J. B., Linick, T. W., and Williams, C. R. (1989). Application of Tandem Accelerator Mass-spectrometre dating to Late Pleistocene-Holocene sediments of the East Antarctic Continental Shelf. *Quaternary Research* **31,** 277-287.

Domack, E. W., Jull, A. J. T., and Donahue, D. J. (1991a). Holocene chronology for the unconsolidated sediments at Hole 740A: Prydz Bay, East Antarctica. *In* "Proceedings of the Ocean Drilling Program, Scientific Results." (J. Barron, and B. Larsen, Eds.), pp. 747-750.

Domack, E. W., Jull, A. J. T., and Nakao, S. (1991b). Advance of East Antarctic outlet glaciers during the Hypsithermal: Implications for the volume state of the Antarctic ice sheet under global warming. *Geology* **19,** 1059-1062.

Domack, E. W., and Mayewski, P. A. (1999). Bi-polar linkages: evidence from late-Holocene and Greenland ice-core records. *The Holocene* **9,** 247-51.

Domack, E. W., and McClennen, C. E. (1996). Accumulation of glacial marine sediments in fjords of the Antarctic Peninsula and their use as late Holocene palaeoenvironmental indicators. *In* "Foundations for ecological research west of the Antarctic Peninsula." (R. M. Ross, E. Hofmann, and L. B. Quetin, Eds.), pp. 135–154. Antarctic Research Series. American Geophysical Union.

Domack, E. W., and Williams, C. R. (1990). Fine-structure and suspended sediment transport in three Antarctic fjords. *In* "Antarctic Research Series." (C. R. Bentley, Ed.), pp. 71-89. American Geophysical Union.

Dowdeswell, J. A., Cofaigh, C. O., and Pudsey, C. J. (2004a). Continental slope morphology and sedimentary processes at the mouth of an Antarctic palaeo-ice stream. *Marine Geology* **204,** 203-214.

Dowdeswell, J. A., O Cofaigh, C., and Pudsey, C. J. (2004b). Thickness and extent of the subglacial till layer beneath an Antarctic paleo-ice stream. *Geology* **32,** 13-16.

Dowdeswell, J. A., Ottesen, D., Evans, J., Cofaigh, C., and Anderson, J. B. (2008). Submarine glacial landforms and rates of ice-stream collapse. *Geology* **36,** 819-822.

Draggan, S. (2009). Antarctic Peninsula. *In* "Encyclopedia of Earth." (C. J. Cleveland, Ed.). Environmental Information Coalition, National Council for Science and the Environment, Washington, D.C.

Dunbar, R., Anderson, J., Domack, E. W., and Jacobs, S. S. (1985). Oceanographic influences on sedimentation along the Antarctic continental shelf. *Antarctic Research Series* **43,** 291-312.

Dunbar, R. B. (1984). Sediment trap experiments on the Antarctic continental margin. *Antarctic Journal of the United States* **19,** 70-71.

Dunbar, R. B., Leventer, A. R., and Stockton, W. L. (1989). Biogenic Sedimentation in Mcmurdo Sound, Antarctica. *Marine Geology* **85,** 155-179.

Dupont, T. K., and Alley, R. B. (2005). Assessment of the importance of ice-shelf buttressing to ice-sheet flow. *Geophysical Research Letters* **32,** 10.1029/2004GL022024.

E

Edwards, R. L., Beck, J. W., Burr, G. S., Donahue, D. J., Chappell, J. M. A., Bloom, A. L., Druffel, E. R. M., and Taylor, F. W. (1993). A large drop in atmospheric 14C/12C and reduced melting in the Younger Dryas, documented with 230Th ages of corals. *Science* **260,** 962-968.

Eicken, H. (1992). The role of sea ice in structuring Antarctic ecosystems. *Polar Biology* **12,** 3-13.

El-Sayed, S. Z. (1990). Plankton. *In* "Antarctic sector of the Pacific." (G. P. Glasby, Ed.), pp. 95–125. Elsevier, Amsterdam.

El-Sayed, S. Z., and Weber, L. H. (1982). Spatial and temporal variations in phytoplankton biomass and primary productivity in the Southwest Atlantic and the Scotia Sea. *Polar Biology* **1,** 83-90.

Emslie, S. D. (2001). Radiocarbon dates from abandoned penguin colonies in the Antarctic Peninsula region. *Antarctic Science* **13,** 289-295.

EPICA Community Members. (2004). Eight glacial cycles from an Antarctic ice core. *Nature* **429,** 623-628.

EPICA Community Members. (2006). One-to-one coupling of glacial climate variability in Greenland and Antarctica. *Nature* **444,** 195-198.

ESRI ArcMap (2006) version 9.2

Ettwein, V. J., Stickley, C. E., Maslin, M. A., Laurie, E. R., Rosell-Melé, A., Vidal, L., and Brownless, M. (2001). Fluctuations in productivity and upwelling intensity at Site 1083 during the intensification of the Northern Hemisphere glaciation (2.40-2.65 Ma). *In* "Proceedings of the Ocean Drilling Program, Scientific Results." (G. Wefer, W. H. Berger, and C. Richter, Eds.), pp. 1-25.

Evans, J., Pudsey, C. J., Ó Cofaigh, C., Morris, P., and Domack, E. (2005). Late Quaternary glacial history, flow dynamics and sedimentation along the eastern margin of the Antarctic Peninsula Ice Sheet. *Quaternary Science Reviews* **24,** 741-774.

Everitt, D. A., and Thomas, D. P. (1986). Observations of seasonal changes in diatoms at inshore localities near Davis Station, East Antarctica. *Hydrobiologia* **139,** 3-12.

F

Fairbanks, R. G. (1989). A 17,000-year glacio-eustatic sea level record: Influence of glacial melting rates on the Younger Dryas event and deep-ocean circulation. *Nature* **342,** 637-642.

Fairbanks, R. G. (2005). Marine Radiocarbon Reservoir Age. http://radiocarbon.ldeo.columbia.edu/research/resage.htm

Fenner, J., Schrader, H. J., and Wienigk, H. (1976). Diatom phytoplankton studies in the Southern Pacific Ocean, composition and correlation to the Antarctic Convergence and its paleoecological significance. *Initial Reports of the Deep-Sea Drilling Project* **35,** 757- 813

Ferrario, M. E., Sar, E. A., and Vernet, M. (1998). Chaetoceros resting spores in the Gerlache Strait, Antarctic Peninsula. *Polar Biology* **19,** 286-288.

Fetterer, F., Knowles, K., Meier, W., Savoie, M., 2002. Sea Ice Index. National Snow and Ice Data Center. National Snow and Ice Data Center, Boulder, CO, digital media. updated 2007.

Fietz, S., Nicklisch, A., and Oberhansli, H. (2007). Phytoplankton response to climate changes in Lake Baikal during the Holocene and Kazantsevo Interglacials assessed from sedimentary pigments. *Journal of Paleolimnology* **37,** 177-203.

Fleming, E. A., and Thomson, J. W. (1979). Northern Graham Land and South Shetland Islands Geological map, 1: 500000, BAS 500G.

Flower, B., and Kennett, J. P. (1994). The middle Miocene climatic transistion: East Antarctic ice sheet development, deep ocean circulation and global carbon cycling. *Palaeogeography, Palaeoclimatology, Palaeoecology* **108,** 537-555.

Foldvik, A., Gammelsrød, T., Østerhus, S., Fahrbach, E., Rohardt, G., Schröder, M., Nicholls, K. W., Padman, L., and Woodgate, R. A. (2004). Ice shelf water overflow and bottom water formation in the Southern Weddell Sea. *Journal of Geophysical Research* **109,** doi:10.1029/2003JC002008.

Foster, T. D., and Carmack, E. C. (1976). Temperature and salinity structure in the Weddell Sea. *Journal of Physical Oceanography* **6,** 36-44.

Fox, A. J., and Cooper, A. P. R. (1994). Measured Properties of the Antarctic Ice Sheet Derived from the SCAR Antarctic Digital Database. *Polar Rec.* **30,** 201-206.

Francis, J. E., Ashworth, A., Cantrill, D. J., Crame, J. A., Howe, J., Stephens, R., Tosolini, A.-M., and Thorn, V. (2007). 100 million years of Antarctic climate evolution: evidence from fossil plants. *In* "10th International Symposium of Antarctic Earth Sciences. Antarctica: A keystone in a Changing World." (A. K. Cooper, P. J. Barrett, H. Stagg, B. Storey, E. Stump, and W. Wise, Eds.), pp. 19-27. The National Academies Press, University of California, Santa Barbara.

Francis, J. E., and Poole, I. (2002). Cretaceous and early Tertiary climates of Antarctica: evidence from fossil wood. *Palaeogeography, Palaeoclimatology, Palaeoecology* **182,** 47-64.

Francois, R., Altabet, M. A., and Burckle, L. H. (1992). Glacial to Interglacial Changes in Surface Nitrate Utilization in the Indian Sector of the Southern Ocean as Recorded by Sediment d15N. *Paleoceanography* **7,** 589-606.

Francois, R., Altabet, M. A., Yu, E. F., Sigman, D. M., Bacon, M. P., Frank, M., Bohrmann, G., Bareille, G., and Labeyrie, L. D. (1997). Contribution of Southern Ocean surface-water stratification to low atmospheric CO_2 concentrations during the last glacial period. *Nature* **389,** 929-935.

Francois, R., Bacon, M. P., Altabet, M. A., and Labeyrie, L. D. (1993). Glacial/Interglacial Changes in Sediment Rain Rate in the SW Indian Sector of Subantarctic Waters as Recorded by 230Th, 231Pa, U, and d15N. *Paleoceanography* **8,** 611-629.

Froneman, P. W., Perissinotto, R., McQuaid, C. D., and Laubscher, R. K. (1995). Summer distribution of net phytoplankton in the Atlantic sector of the Southern Ocean. *Polar Biology* **15,** 77-84.

Fryxell, G. A. (1983). "Survival strategies of the algae." Phycological Society of America, Botanical Society of America.

Fryxell, G. A. (1989). Marine-phytoplankton at the Weddell Sea ice edge - seasonal changes at the specific level. *Polar Biology* **10,** 1-18.

Fryxell, G. A. (1990). Planktonic marine diatom winter stages: Antarctic alternatives to resting spores. *In* "Proceedings of the 11th International Diatom Symposium." pp. 437-448. Memoirs of the Californian Academy of Sciences.

Fryxell, G. A., Kang, S.-H., and Reap, M. E. (1987). AMERIEZ 1986: phytoplankton at the Weddell Sea ice edge. *Antarctic Journal of the United States* **22,** 173-175.

Fryxell, G. A., and Kendrick, G. A. (1988). Austral spring microalgae across the Weddell Sea ice edge; spatial relationships found along a northward transect during AMERIEZ 83. *Deep-Sea Research Part A. Oceanographic Research Papers* **35,** 1-20.

Fryxell, G. A., and Prasad, A. (1990). Eucampia-Antarctica Var Recta (Mangin) Stat Nov (Biddulphiaceae, Bacillariophyceae) - Life Stages at the Weddell Sea Ice Edge. *Phycologia* **29,** 27-38.

Fryxell, G. A., Theriot, E. C., and Buck, K. R. (1984). Phytoplankton, ice algae, and choanoflagellates from AMERIEZ, the Southern Atlantic and Indian Oceans. *Antarctic Journal of the United States* **19,** 107-109.

Fyfe, J. C. (2006). Southern Ocean warming due to human influence. *Geophysical Research Letters* **33,** L19701.

G

Garabato, A. C. N., Heywood, K. J., and Stevens, D. P. (2002). Modification and pathways of Southern Ocean Deep Waters in the Scotia Sea. *Deep-Sea Research Part I-Oceanographic Research Papers* **49,** 681-705.

García, M. A., Castro, C. G., Ríos, A. F., Doval, M. D., Rosón, G., Gomis, D., and López, O. (2002). Water masses and distribution of physico-chemical properties in the Western Bransfield Strait and Gerlache Strait during Austral summer 1995/96. *Deep Sea Research Part II: Topical Studies in Oceanography* **49,** 585-602.

Garibotti, I. A., Vernet, M., Ferrario, M. E., Smith, R. C., Ross, R. M., and Quetin, L. B. (2003). Phytoplankton spatial distribution patterns along the western Antarctic Peninsula (Southern Ocean). *Marine Ecology-Progress Series* **261,** 21-39.

Garrison, D. L. (1991). Antarctic sea ice biota. *American Zoologist* **31,** 17-33.

Garrison, D. L., Ackley, S. F., and Buck, K. R. (1983). A physical mechanism for establishing algal populations in frazil ice. *Nature* **306,** 363-365.

Garrison, D. L., and Buck, K. R. (1989). The biota of Antarctic pack ice in the Weddell Sea and Antarctic Peninsula regions. *Polar Biology* **10** 211-219.

Garrison, D. L., Buck, K. R., and Fryxell, G. A. (1987). Algal assemblages in Antarctic pack ice and in ice-edge plankton. *Journal of Phycology* **23,** 564–572.

Gersonde, R. (1984). Siliceous microorganisms in sea ice and their record in sediments in the Southern Weddell Sea (Antarctica). *8th Diatom-Symposium,* 549-566.

Gersonde, R. (1990). The palaeontological significance of fossil diatoms from high latitude oceans. *In* "Polar Marine Diatoms." (L. K. Medlin, and J. Priddle, Eds.), pp. 57-63. British Antarctic Survey, Cambridge.

Gersonde, R., Crosta, X., Abelmann, A., and Armand, L. (2005). Sea-surface temperature and sea ice distribution of the Southern Ocean at the EPILOG Last Glacial Maximum--a circum-Antarctic view based on siliceous microfossil records. *Quaternary Science Reviews* **24,** 869-896.

Gersonde, R., and Wefer, G. (1987). Sedimentation of biogenic siliceous particles in Antarctic waters from the Atlantic sector. *Marine Micropaleontology* **11,** 311-332.

Gersonde, R., and Zielinski, U. (2000). The reconstruction of Late Quaternary Antarctic sea-ice distribution - the use of diatoms as a proxy for sea ice. *Palaeogeography, Palaeoclimatology, Palaeoecology* **162,** 263-286.

Gilbert, R., and Domack, E. W. (2003). Sedimentary record of disintegrating ice shelves in a warming climate, Antarctic Peninsula. *Geochemistry, Geophysics, Geosystems* **4** 1038.

Gille, S. T. (1994). Mean sea surface height of the Antarctic Circumpolar Current from Geosat data: Method and application. *Journal of Geophysical Research* **99,** 18,255-18,273.

Gille, S. T. (2002). Warming of the Southern Ocean since the 1950s. *Science* **295,** 1275-1277.

Gilli, A., Ariztegui, D., Anselmetti, F. S., McKenzie, J. A., Markgraf, V., Hajdas, I., and McCulloch, R. D. (2005). Mid-Holocene strengthening of the Southern Westerlies in South America -- Sedimentological evidences from Lago Cardiel, Argentina (49°S). *Global and Planetary Change* **49,** 75-93.

Gleitz, M., Bartsch, A., Dieckmann, G. S., and Eicken, H. (1998). Composition and succession of sea ice diatom assemblages in the eastern and southern Weddell Sea, Antarctica. *In* "Antarctic Sea Ice: Biological Processes, Interactions and Variability." (M. P. Lizotte, and K. R. Arrigo, Eds.), pp. 107-120. Antarctic Research Series.

Gleitz, M., Grossmann, S., Scharek, R., and Smetacek, V. (1996). Ecology of diatom and bacterial assemblages in water associated with melting summer sea ice in the Weddell Sea, Antarctica. *Antarctic Science* **8,** 135-146.

Gleitz, M., and Thomas, D. N. (1992). Physiological responses of a small Antarctic diatom (*Chaetoceros* sp.) to simulated environmental constraints associated with sea-ice formation. *Marine Ecology Progress Series* **88,** 271-278.

Gleitz, M., and Thomas, D. N. (1993). Variation in phytoplankton standing stock, chemical composition and physiology during sea-ice formation in the southeastern Weddell Sea, Antarctica. *Journal of Experimental Marine Biology and Ecology* **173,** 211-230.

Gloersen, P., Campbell, W. J., Cavalieri, D. J., Comiso, J. C., Parkinson, C., and Zwally, H. J. (1992). Arctic and Antarctic sea ice, 1978-1987: Satellite passive microwave observations and analysis pp. 290. NASA Special Publication, Washington D.C.

Goldman, J. C. (1993). Potential role of large oceanic diatoms in new primary production. *Deep Sea Research* **40,** 189-168.

Gordon, A. L. (1998). Western Weddell Sea thermohaline stratification. *Antarctic Research Series* **75,** 215-240.

Gordon, A. L. (2001). Interocean Exchange. *In* "Ocean Circulation and Climate. Observing and Modelling the Global Ocean." (G. Siedler, J. Church, and J. Gould, Eds.), pp. 303-314. Academic Press.

Gordon, A. L., and Comiso, J. C. (1988). Polynyas in the Southern-Ocean. *Scientific American* **258,** 90-97.

Gordon, A. L., and Huber, B. A. (1984). Thermohaline stratification below the Southern Ocean sea ice. *Journal of Geophysical Research* **89,** 641-648.

Gordon, A. L., and Huber, B. A. (1990). Southern Ocean winter mixed layer. *Journal of Geophysical Research* **95,** 11655–11672.

Gordon, A. L., Huber, B. A., Hellmer, H. H., and Ffield, A. (1993). Deep and Bottom Water of the Weddell Sea's Western Rim. *Science* **262,** 95-97.

Gordon, A. L., Mensch, M., Dong, Z., Smethie Jr., W. M., and de Bettencourt, J. (2000). Deep and bottom water of the Bransfield Strait eastern and central basins. *Journal of Geophysical Research* **105** 11,337-11,346.

Gordon, A. L., and Nowlin Jr, W. D. (1978). The basin waters of the Bransfield Strait. *Journal of Physical Oceanography* **8,** 258-264.

Gordon, A. L., Visbeck, M., and Huber, B. (2001). Export of Weddell Sea Deep and Bottom Water. *Journal of Geophysical Research-Oceans* **106,** 9005-9017.

Gordon, J. E., and Harkness, D. D. (1992). Magnitude and geographic variation of the radiocarbon content in Antarctic marine life: implications for reservoir corrections in radiocarbon dating. . *Quaternary Science Reviews* **11,** 696-708.

Gracia, E., Canals, M., Farran, M., Prieto, M. J., Sorribas, J., and Team, T. G. (1996). Morphostructure and evolution of the central and eastern Bransfield basins (NW Antarctic Peninsula). *Marine Geophysical Research* **18,** 429-448.

Gudmundsson, G. H. (2006). Fortnightly variations in the flow velocity of Rutford Ice Stream, West Antarctica. *Nature* **444,** 1063-1064.

H

Hammer, Ø., and Harper, D. (2006). "Paleontological Data Analysis." Blackwell Publishing, Oxford.

Hansom, J. D., and Flint, C. P. (1989). Short notes. Holocene ice fluctuations on Brabant Island, Antarctic Peninsula. *Antarctic Science* **1,** 165-166.

Harangozo, S. A. (2000). A search for ENSO teleconnections in the west Antarctic Peninsula climate in austral winter. *International Journal of Climatology* **20,** 663-669.

Harden, S. L., DeMaster, D. J., and Nittrouer, C. A. (1992). Developing sediment geochronologies for high-latitude continental shelf deposits: a radiochemical approach. *Marine Geology* **103,** 69-97.

Hargraves, P. E., and French, F. W. (1983). Diatom resting spores: significance and strategies. *In* "Survival strategies in algae." (G. A. Fryxell, Ed.), pp. 49-68. Cambridge University Press, New York.

Harradine, P. J., Harris, P. G., Head, R. N., Harris, R. P., and Maxwell, J. R. (1996). Steryl chlorin esters are formed by zooplankton herbivory. *Geochimica et Cosmochimica Acta* **60,** 2265-2270.

Harris, P. G., Zhao, M., Rosell-Mele, A., Tiedemann, R., Sarnthein, M., and Maxwell, J. R. (1996). Chlorin accumulation rate as a proxy for Quaternary marine primary productivity. *Nature* **383,** 63-65.

Harris, P. T., Brancolini, G., Armand, L., Busetti, M., Beaman, R. J., Giorgetti, G., Presti, M., and Trincardi, F. (2001). Continental shelf drift deposits indicate non-steady state Antarctic bottom water production in the Holocene. *Marine Geology* **179,** 1-8.

Harris, P. T., and O'Brien, P. E. (1998). Bottom currents, sedimentation and ice-sheet retreat facies successions on the Mac Robertson shelf, East Antarctica. *Marine Geology* **151,** 47-72.

Harris, P. T., Taylor, F., Domack, E., DeSantis, L., Goodwin, I., Quilty, P. G., and O'Brien, P. E. (1997). Glacimarine siliciclastic muds from Vincennes Bay, East Antarctica; preliminary results of an Exploratory Cruise in 1997. *Terra Antarctica* **4,** 11-20.

Hasle, G. R. (1969). An analysis of the phytoplankton of the Pacific Southern Ocean: abundance, composition, and distribution during the Brategg Expedition, 1947-1948 Hvalradets Skrifter. *In* "Scientific Results of Marine Biological Research." pp. 52. Universitetsforlaget, Oslo.

Hasle, G. R. (1973). Some marine plankton genera of the diatom family Thalassiosiraceae. . *In* "Second symposium on recent and fossil marine diatoms." pp. 1-49. Beihefte zur Nova Hedwigia, London.

Hasle, G. R. (1976). The biogeography of some marine planktonic diatoms. *Deep-Sea Research and Oceanographic Abstracts* **23,** 319-338.

Hasle, G. R., and Syvertsen, E. E. (1997). Marine Diatoms. *In* "Identifying Marine Phytoplankton." (C. R. Tomas, Ed.), pp. 5-385. Academic Press Ltd, London.

Hemer, M. A., Post, A. L., O'Brien, P. E., Craven, M., Truswell, E. M., Roberts, D., and Harris, P. T. (2007). Sedimentological signatures of the sub-Amery Ice Shelf circulation. *Antarctic Science* **19,** 497-506.

Heroy, D. C., and Anderson, J. B. (2005). Ice-sheet extent of the Antarctic Peninsula region during the Last Glacial Maximum (LGM)—Insights from glacial geomorphology. *Geological Society of America Bulletin* **117,** 1497-1512.

Heroy, D. C., and Anderson, J. B. (2007). Radiocarbon constraints on Antarctic Peninsula Ice Sheet retreat following the Last Glacial Maximum (LGM). *Quaternary Science Reviews* **26,** 3286-3297.

Heroy, D. C., Sjunneskog, C., and Anderson, J. B. (2008). Holocene climate change in the Bransfield Basin, Antarctic Peninsula: evidence from sedimnt and diatom analysis. *Antarctic Science* **20** 69-87.

Hesse, P. P., and McTainsh, G. H. (1999). Last Glacial Maximum to Early Holocene Wind Strength in the Mid-latitudes of the Southern Hemisphere from Aeolian Dust in the Tasman Sea. *Quaternary Research* **52,** 343-349.

Hillenbrand, C.-D., Benetti, S., Ehrmann, W., Larter, R. D., Ó Cofaigh, C., Dowdeswell, J. A., Grobe, H., and Graham, A. G. C. (2007). Glacial dynamics of the West Antarctic Ice Sheet in the southern Bellingshausen Sea during the last glacial cycle. *USGS OFR-2007, Extended Abstract 150* U.S. Geological Survey and The National Academies, 1-4.

Hjort, C., Bentley, M. J., and Ingolfsson, O. (2001). Holocene and pre-Holocene temporary disappearance of the George VI Ice Shelf, Antarctic Peninsula. *Antarctic Science* **13,** 296-301.

Hjort, C., Ingólfsson, O., Bentley, M. J., and Björck, S. (2003). Late Pleistocene and Holocene glacial and climate history of the Antarctic Peninsula regions: a brief overview of land and lake sediments. *In* "Antarctic Peninsula climate variability: historical and paleoenvironmental perspectives." (E. W. Domack, A. Leventer, A. Burnett, R. Bindschadler, P. Convey, and M. Kirby, Eds.), pp. 95-102. American Geophysical Union.

Hjort, C., Ingolfsson, O., and Bjorck, S. (1992). The last major deglaciation in the Antarctic Peninsula region - a review of recent Swedish Quaternary Research. *In* "Recent Progress in Antarctic Earth Science." (Y. Yoshida, and e. al, Eds.), pp. 741-743. Terra Scientific Publishing Company (TERRAPUB), Tokyo.

Hjort, C., Ingolfsson, O., Moller, P., and Lirio, J. M. (1997). Holocene glacial history and sea-level changes on James Ross Island, Antarctic Peninsula. *Journal of Quaternary Science* **12,** 259-273.

Hodell, D. A., Kanfoush, S. L., Shemesh, A., Crosta, X., Charles, C. D., and Guilderson, T. P. (2001). Abrupt cooling of Antarctic surface waters and sea ice expansion in the South Atlantic sector of the Southern Ocean at 5000 cal yr B.P. *Quaternary Research* **56,** 191-198.

Hodgson, D. A., Bentley, M. J., Roberts, S. J., Smith, J. A., Sugden, D. E., and Domack, E. W. (2006a). Examining Holocene stability of Antarctic Peninsula Ice Shelves. *EOS Transactions* **87,** 305-312.

Hodgson, D. A., and Convey, P. (2005). A 7000-year Record of Oribatid Mite Communities on a Maritime-Antarctic Island: Responses to Climate Change. *Arctic, Antarctic, and Alpine Research* **37,** 239-245.

Hodgson, D. A., Doran, P. T., Roberts, D., and McMinn, A. (2004). Paleolimnological studies from the Antarctic and subantarctic islands. *In* "Long-term Environmental Change in Arctic and Antarctic Lakes." (R. Pienitz, M. S. V. Douglas, and J. P. Smol, Eds.), pp. 419-474. Springer, Netherlands.

Hodgson, D. A., McMinn, A., Kirkup, H., Cremer, H., Gore, D., Melles, M., Roberts, D., and Montiel, P. (2003). Colonization, succession, and extinction of marine floras during a glacial cycle: A case study from the Windmill Islands (east Antarctica) using biomarkers. *Paleoceanography* **18,** 12-1.

Hodgson, D. A., Verleyen, E., Squier, A. H., Sabbe, K., Keely, B. J., Saunders, K. M., and Vyverman, W. (2006b). Interglacial environments of coastal east Antarctica: comparison of MIS 1 (Holocene) and MIS 5e (Last Interglacial) lake-sediment records. *Quaternary Science Reviews* **25,** 179-197.

Hofmann, E. E., and Klinck, J. M. (1998a). Hydrography and circulation of the Antarctic continental shelf: 150°E to the Greenwich meridian. *In* "The Sea." (A. R. Robinson, and K. H. Brink, Eds.), pp. 997-1042. John Wiley & Sons, Inc.

Hofmann, E. E., and Klinck, J. M. (1998b). Thermohaline variability of the waters overlying the West Antarctic Peninsula continental shelf. *In* "Ocean, Ice, and Atmosphere: Interactions at the Antarctic Continental Margin." pp. 67-81. Antarctic Research Series. American Geophysical Union.

Hofmann, E. E., Klinck, J. M., Lascara, C. M., and Smith, D. A. (1996). Water mass distribution and circulation west of the Antarctic Peninsula and including the Bransfield Strait. *In* "Foundations for Ecological Research west of the Antarctic Peninsula." pp. 61-80. Antarctic Research Series. American Geophysical Union.

Hofmann, M., Wolf-Gladrow, D. A., Takahashi, T., Sutherland, S. C., Six, K. D., and Maier-Reimer, E. (2000). Stable carbon isotope distribution of particulate organic matter in the ocean: a model study. *Marine Chemistry* **72,** 131-150.

Holm-Hansen, O., Amos, A. F., Nelson, S. S., Villafane, V., and Helbling, E. W. (1994). In situ evidence for a nutrient limitation of phytoplankton growth in pelagic Antarctic waters. *Antarctic Science* **6,** 315-324.

Holm-Hansen, O., El-Sayed, S. Z., Franceschini, G. A., and Cuhel, R. L. (1977). Primary production and the factors controlling phytoplankton growth in the Southern Ocean. *In* "Proceedings of the Third SCAR Symposium of Antarctic Biology on Adaptations within Antarctic Ecosystems." pp. 11–50.

Horner, R. A. (1985). Taxonomy of sea ice microalgae. *In* "Sea ice biota." (R. A. Horner, Ed.), pp. 147-157.

Houghton, J. T., Ding, Y., Griggs, D. J., Noguer, M., van den Linden, P. J., Dai, X., Maskell, K., and Johnson, C. A. (2001). "Climate Change 2001: The Scientific Basis." Cambridge University Press, Cambridge.

Hughen, K., Southon, J., Lehman, S., Bertrand, C., and Turnbull, J. (2006). Marine-derived 14C calibration and activity record for the past 50,000 years updated from the Cariaco Basin. *Quaternary Science Reviews* **25,** 3216-3227.

Hughen, K. A., Baillie, M. G. L., Bard, E., Bayliss, A., Beck, J. W., Bertrand, C. J. H., Blackwell, P. G., Buck, C. E., Burr, G. S., Cutler, K. B., Damon, P. E., Edwards, R. L., Fairbanks, R. G., Friedrich, M., Guilderson, T. P., Kromer, B., McCormac, F. G., Manning, S. W., Bronk Ramsey, C., Reimer, P. J., Reimer, R. W., Remmele, S., Southon, J. R., Stuiver, M., Talamo, S., Taylor, F. W., van der Plicht, J., and Weyhenmeyer, C. E. (2004). Marine04 Marine radiocarbon age calibration, 26 - 0 ka BP. *Radiocarbon* **46,** 1059-1086.

Hughen, K. A., Southon, J. R., Lehman, S. J., and Overpeck, J. T. (2000). Synchronous Radiocarbon and Climate Shifts During the Last Deglaciation. *Science* **290,** 1951-1954.

Hughes, T. (1973). Is the West Antarctic Ice Sheet disintegrating? *Journal of Geophysical Research* **78,** 7884-7910.

Huybers, P., and Denton, G. (2008). Antarctic temperature at orbital timescales controlled by local summer duration. *Nature Geosci* **1,** 787-792.

Huybrechts, P. (2002). Sea-level changes at the LGM from ice-dynamic reconstructions of the Greenland and Antarctic ice sheets during the glacial cycles. *Quaternary Science Reviews* **21,** 203-231.

I

Iizuka, Y., Horikawa, S., Sakurai, T., Johnson, S., Dahl-Jensen, D., Steffensen, J. r. P., and Hondoh, T. (2008). A relationship between ion balance and the chemical compounds of salt inclusions found in the Greenland Ice Core Project and Dome Fuji ice cores. *Journal of Geophysical Research* **113,** D07303.

Imbrie, J., Boyle, E. A., Clemens, S. C., Duffy, A., Howard, W. R., Kukla, G., Kutzbach, J., Martinson, D. G., McIntyre, A., Mix, A. C., Molfino, B., Morley, J. J., Peterson, L. C., Pisias, N. G., Prell, W. L., Raymo, M. E., Shackleton, N. J., and Toggweiler, J. R. (1992). On the Structure and Origin of Major Glaciation Cycles 1. Linear Responses to Milankovitch Forcing. *Paleoceanography* **7,** 701-738.

Ingólfsson, Ó. (2004). The Quaternary Glacial and Climate History of Antarctica. *In* "Quaternary Glaciations of the World, Part III." (J. Ehlers, and P. L. Gibbard, Eds.), pp. 3-43. Kluwer, Dordrecht, .

Ingólfsson, O., Hjort, C., Berkman, P. A., Björck, S., Colhoun, E., Goodwin, I. D., Hall, B., Hirakawa, K., Melles, M., Moller, P., and Prentice, M. L. (1998). Antarctic glacial history since the Last Glacial Maximum: an overview of the record on land. *Antarctic Science* **10,** 326-344.

Ingólfsson, O., Hjort, C., Bjorck, S., and Smith, R. I. L. (1992). Late Pleistocene and Holocene Glacial History of James-Ross-Island, Antarctic Peninsula. *Boreas* **21,** 209-222.

Ishman, S. E., and Sperling, M. R. (2002). Benthic foraminiferal record of Holocene deep-water evolution in the Palmer Deep, western Antarctic Peninsula. *Geology* **30,** 435-438.

Ivany, L. C., Van Simaeys, S., Domack, E. W., and Samson, S. D. (2006). Evidence for an earliest Oligocene ice sheet on the Antarctic Peninsula. *Geology* **34,** 377-380.

J

Jaeger, J. M., Nittrouer, C. A., DeMaster, D. J., and R.B., D. (1996). Advection of suspended sediment in the Ross Sea and implications for the fate of biogenic material. *Journal of Geophysical Research* **101,** 18479-18488.

Jamieson, S. S. R., and Sugden, D. E. (2007). Landscape evolution of Antarctica. *In* "10th International Symposium of Antarctic Earth Sciences. Antarctica: A keystone in a Changing World." (A. K. Cooper, P. J. Barrett, H. Stagg, B. Storey, E. Stump, and W. Wise, Eds.), pp. 39-54. The National Academies Press, University of California, Santa Barbara.

Jasper, J. P., and Hayes, J. M. (1990). A carbon-isotopic record of CO_2 levels during the last quaternary. *Nature* **347,** 462-464.

Jeffery, S. W., and Humphrey, G. F. (1975). New spectrophotometric equations for determining chlorophylls a, b, c1, and c2 in higher plants, algae and natural phytoplankton. *Biochemie and Physiologie der Pflanzen* **167,** 191-194.

Jeffrey, S. W., Mantoura, R. F. C., and Bjørland, T. (1997). Data for identification of 47 key phytoplankton pigments. *In* "Phytoplankton Pigments in Oceanography." (S. W. Jeffrey, R. F. C. Mantoura, and S. W. Wright, Eds.), pp. 449-559. UNESCO, Paris.

Jenkins, A. (1999). The Impact of Melting Ice on Ocean Waters. *Journal of Physical Oceanography* **29,** 2370-2381.

Jenkins, A., and Jacobs, S. (2008). Circulation and melting beneath George VI Ice Shelf, Antarctica. *Journal of Geophysical Research* **113,** CO4013.

Jenny, B., Valero-Garcés, B. L., Villa-Martínez, R., Urrutia, R., Geyh, M., and Veit, H. (2002). Early to mid-Holocene aridity in central Chile and the southern Westerlies: The Laguna Aculeo record (34°S). *Quaternary Research* **58,** 160-170.

Johansen, J. R., and Fryxell, G. A. (1985). The genus Thalassiosira (Bacillariophyceae): studies on species occurring south of the Antarctic Convergence Zone. *Phycologia* **24,** 155-179.

Johnsen, S. J., Dansgaard, W., Clausen, H. B., and Langway, C. C. (1972). Oxygen isotope profiles through the Antarctic and Greenland ice sheets. *Nature* **235,** 429-434.

Jones, V. J. (2007a). Diatom Introduction. *In* "Encyclopedia of Quaternary Science." (S. A. Elias, Ed.), pp. 24-32. Elsevier Science.

Jones, C. M. (2007b). Introduction to Computational Statistics: Multivariate Data Analysis - Cluster Analysis. *In* "Undergraduate Maths module handout: MA0263." pp. 82-94. Cardiff University.

Jones, V. J., Hodgson, D. A., and Chepstow-Lusty, A. (2000). Palaeolimnological evidence for marked Holocene environmental changes on Signy Island, Antarctica. *The Holocene* **10,** 43-60.

Jongma, J. I., Driesschaert, E., Fichefet, T., Goosse, H., and Renssen, H. (2009). The effect of dynamic-thermodynamic icebergs on the Southern Ocean climate in a three-dimensional model. *Ocean Modelling* **26,** 104-113.

Jordan, R. W., Priddle, J., Pudsey, C. J., Barker, P. F., and Whitehouse, M. J. (1991). Unusual Diatom Layers in Upper Pleistocene Sediments from the Northern Weddell Sea. *Deep-Sea Research Part a-Oceanographic Research Papers* **38,** 829-843.

Jordan, R. W., and Pudsey, C. J. (1992). High-resolution diatom stratigraphy of Quaternary sediments from the Scotia Sea. *Marine Micropaleontology* **19,** 201-237.

Jouzel, J., Masson-Delmotte, V., Cattani, O., Dreyfus, G., Falourd, S., Hoffmann, G., Minster, B., Nouet, J., Barnola, J. M., Chappellaz, J., Fischer, H., Gallet, J. C., Johnsen, S., Leuenberger, M., Loulergue, L., Luethi, D., Oerter, H., Parrenin, F., Raisbeck, G., Raynaud, D., Schilt, A., Schwander, J., Selmo, E., Souchez, R., Spahni, R., Stauffer, B., Steffensen, J. P., Stehni, B., Stocker, T. F., Tison, J. L., Werner, M., and Wolff, E. W. (2007). Orbital and millennial antarctic climate variability over the past 800,000 years. *Science* **317,** 793-796.

Jouzel, J., Vaikmae, R., Petit, J.-R., Martin, M., Duclos, Y., Stievenard, M., Lorius, C., Toots, M., Melie`res, M.-A., Burckle, L. H., Barkov, N. I., and Kotlyakov, V. M. (1995). The two-step shape and timing of the last deglaciation in Antarctica. *Climate Dynamics* **11,** 151-161.

K

Kaczmarska, I., Barbrick, N. E., Ehrman, J. M., and Cant, G. P. (1993). Eucampia Index as an indicator of the late Pleistocene oscillations of the winter sea-ice extent at the ODP Leg 119 Site 745B at the Kerguelen Plateau. *Hydrobiologia* **269-270,** 103-112.

Kang, J.-S., Kang, S. H., Lee, J. H., and Lee, S. H. (2002). Seasonal variation of microalgal assemblages at a fixed station in King George Island, Antarctica, 1996. *Marine Ecology-Progress Series* **229,** 19-32.

Kang, S. H., and Fryxell, G. A. (1992). Fragilariopsis-Cylindrus (Grunow) Krieger - the Most Abundant Diatom in Water Column Assemblages of Antarctic Marginal Ice-Edge Zones. *Polar Biology* **12,** 609-627.

Kang, S. H., and Fryxell, G. A. (1993). Phytoplankton in the Weddell Sea, Antarctica: composition, abundance and distribution in water-column assemblages of the marginal ice- edge zone during austral autumn. *Marine Biology* **116,** 335-348.

Kang, S. H., and Lee, S. H. (1995). Antarctic phytoplankton assemblage in the western Bransfield Strait region, February 1993: composition, biomass, and mesoscale distributions. *Marine Ecology-Progress Series* **129,** 253-267.

Kawamura, K., Parrenin, F., Lisiecki, L., Uemura, R., Vimeux, F., Severinghaus, J. P., Hutterli, M. A., Nakazawa, T., Aoki, S., Jouzel, J., Raymo, M. E., Matsumoto, K., Nakata, H., Motoyama, H., Fujita, S., Goto-Azuma, K., Fujii, Y., and Watanabe, O. (2007). Northern Hemisphere forcing of climatic cycles in Antarctica over the past 360,000[thinsp]years. *Nature* **448,** 912-916.

Keeley, J. E., and Rundel, P. A. W. (2003). Evolution of CAM and C4 Carbon-Concentrating Mechanisms. *International Journal of Plant Sciences* **164,** S55-S77.

Keely, B. J. (2006). Geochemistry of Chlorophylls. *In* "Biochemistry, Biophysics and Biological Functions of Chlorophylls." (B. Grimm, R. Porra, W. Rudiger, and H. Scheer, Eds.), pp. 535-561. Advances in Photosynthesis and Respiration.

Keigwin, L. D., Jones, G. A., Lehman, S. J., and Boyle, E. A. (1991). Deglacial Meltwater Discharge, North Atlantic Deep Circulation, and Abrupt Climate Change. *Journal of Geophysical Research* **96,** 16,811–16,826.

Keller, K., and Morel, F. M. M. (1999). A model of carbon isotopic fractionation and active carbon uptake in phytoplankton. *Marine Ecology Progress Series* **182,** 295-298.

Kellogg, D. E., and Kellogg, T. B. (1987). Microfossil distributions in modern Amundson Sea sediments. *Marine Micropalaeontology* **12,** 203-222.

Kellogg, T. B. (1987). Glacial-interglacial changes in global deep-water circulation. *Paleoceanography* **2,** 259-271.

Kemp, A. E. S., Pearce, R. B., Koizumi, I., Pike, J., and Rance, S. J. (1999). The role of mat-forming diatoms in the formation of Mediterranean sapropels. *Nature* **398,** 57-61.

Kemp, A. E. S., Pike, J., Pearce, R. B., and Lange, C. B. (2000). The "Fall Dump" - a new perspective on the role of a "shade flora" in the annual cycle of diatom production andexport flux. *Deep-Sea Research Part II - Topical Studies in Oceanography* **47,** 2129-2154.

Kennedy, D. S., and Anderson, J. B. (1989). Quaternary glacial history of Marguerite Bay, Antarctic Peninsula. *Quaternary Research* **31,** 255-276.

Kennett, J. P. (1978). Development of planktonic biogeography in Southern-Ocean during Cenozoic. *Marine Micropalaeontology* **3,** 301-345.

Kennett, J. P., and Shackleton, N. J. (1975). Laurentide Ice Sheet Meltwater Recorded in Gulf of Mexico Deep-Sea Cores. *Science* **188,** 147-150.

Kennett, J. P., and Shackleton, N. J. (1976). Oxygen isotopic evidence for development of psychrosphere 38 myr ago. *Nature* **260,** 513-515.

Khim, B., Yoon, H. I., Kang, C. Y., and Bahk, J. J. (2002). Unstable climatic oscillations during the late Holocene in the eastern Bransfield Basin, Antarctic Peninsula. *Quaternary Research* **58,** 234-245.

King, J. C., Turner, J., Marshall, G. J., Connolley, W. M., and Lachlan-Cope, T. A. I. e., vol. 79, , Washington D.C. pp 17-30. (2003). Antarctic Peninsula Climate Variability And Its Causes As Revealed By Analysis Of Instrumental Records. *In* "Antarctic Peninsula Climate Variability: A historical and Paleoenvironmental Perspective." (E. Domack, A. Burnett, P. Convey, M. Kirby, and R. Bindschadler, Eds.), pp. 17-30. Antarctic Research Series. American Geophysical Union, Washington D.C.

Kirby, M. E., Domack, E. W., and McClennen, C. E. (1998). Magnetic stratigraphy and sedimentology of Holocene glacial marine deposits in the Palmer Deep, Bellingshausen Sea, Antarctica: implications for climate change? *Marine Geology* **152,** 247-259.

Klinck, J. M. (1998). Heat and salt changes on the continental shelf west of the Antarctic Peninsula between January 1993 and January 1994. *Journal of Geophysical Research C: Oceans* **103,** 7617-7636.

Klinck, J. M., Hofmann, E. E., Beardsley, R. C., Salihoglu, B., and Howard, S. (2004). Water-mass properties and circulation on the west Antarctic Peninsula Continental Shelf in Austral Fall and Winter 2001. *Deep-Sea Research Part II: Topical Studies in Oceanography* **51,** 1925-1946.

Klinck, J. M., and Smith, D. A. (1993). Effect of wind changes during the Last Glacial Maximum on the circulation in the Southern Ocean. *Paleoceanography* **8,** 427-433.

Kominz, M. A., Browning, J. V., Miller, K. G., Sugarman, P. J., Mizintseva, S., and Scotese, C. R. (2008). Late Cretaceous to Miocene sea-level estimates from the New Jersey and Delaware coastal plain coreholes: an error analysis. *Basin Research* **20,** 211-226.

Kovach, W. L. (2002). Multi-Variate Statistical Package (MVSP). Program and Manual.

Krebs, W. N. (1983). Ecology of neritic marine diatoms, Arthur Harbor, Antarctica. *Micropaleontology* **29,** 267-297.

Krebs, W. N., Lipps, J. H., and Burckle, L. H. (1987). Ice diatom floras, Arthur Harbor Antarctica. *Polar Biology* **7,** 163–171.

L

Lagabrielle, Y., Goddéris, Y., Donnadieu, Y., Malavieille, J., and Suarez, M. (2009). The tectonic history of Drake Passage and its possible impacts on global climate. *Earth and Planetary Science Letters* **279,** 197-211.

Lamy, F., Hebbeln, D., Röhl, U., and Wefer, G. (2001). Holocene rainfall variability in southern Chile: a marine record of latitudinal shifts of the Southern Westerlies. *Earth and Planetary Science Letters* **185,** 369-382.

Lamy, F., Kaiser, J., Arz, H. W., Hebbeln, D., Ninnemann, U., Timm, O., Timmermann, A., and Toggweiler, J. R. (2007). Modulation of the bipolar seesaw in the Southeast Pacific during Termination 1. *Earth and Planetary Science Letters* **259,** 400-413.

Lamy, F., Kaiser, J., Ninnemann, U., Hebbeln, D., Arz, H. W., and Stoner, J. (2004). Antarctic Timing of Surface Water Changes off Chile and Patagonian Ice Sheet Response. *Science* **304,** 1959-1962.

Lamy, F., Rahlemann, C., Hebbeln, D., and Wefer, G. (2002). High- and low-latitude climate control on the position of the southern Peru-Chile Current during the Holocene. *Paleoceanography* **17.**

Lange, M. A., Ackley, S. F., Wadhams, P., Dieckmann, G. S., and Eicken, H. (1989). Development of sea ice in the Weddell Sea. *Annals of Glaciology* **12,** 92-96.

Lange, M. A., and Eicken, H. (1991). Textural characteristics of sea ice and the major mechanisms of ice growth in the Weddell Sea. *Annals of Glaciology* **15,** 204-209.

Law, R. A. (1983). Preparing strewn slides for quantitative microscopical analysis: a test using calibrated microspheres. *Micropaleontology* **29,** 60-65.

Laws, E. A., Popp, B. N., Bidigare, R. R., Kennicutt, M. C., and Macko, S. A. (1995). Dependence of phytoplankton carbon isotopic composition on growth rate and [CO2]aq: theoretical considerations and experimental results. *Geochimica et Cosmochimica Acta* **59,** 1131-1138.

Lawver, L. A., Gahagan, L. M., and Coffin, M. F. (1992). The development of seaways around Antarctica. *In* "Antarctic Research Series." pp. 7-30.

Lawver, L. A., Sloan, B. J., Klepeis, K. A., and von Herzen, R. P. (1996). Migration of an active plate boundary, Scotia Sea; evidence from multibeam bathymetry. *EOS, Transactions of the American Geophysical Union* **77,** 947.

Lear, C. H., Elderfield, H., and Wilson, P. A. (2000). Cenozoic deep-sea temperatures and global ice volumes from Mg/Ca in benthic foraminiferal calcite. *Science* **287,** 269-272.

Leavitt, P. R. (1993). A review of factors that regulate carotenoid and chlorophyll deposition and fossil pigment abundance. *Journal of Palaeolimnology* **9,** 109-127.

Lee, K., Yoon, S. K., and Yoon, H. I. (2008). Holocene paleoclimate changes determined using diatom assemblages from Lake Long, King George Island, Antarctica. *Journal of Paleolimnology,* **42,** 1-10.

Lehmann, M. F., Bernasconi, S. M., Barbieri, A., and McKenzie, J. A. (2002). Preservation of organic matter and alteration of its carbon and nitrogen isotope composition during simulated and in situ early sedimentary diagenesis. *Geochimica et Cosmochimica Acta* **66,** 3573-3584.

Leventer, A. (1991). Sediment Trap Diatom Assemblages from the Northern Antarctic Peninsula Region. *Deep-Sea Research Part a-Oceanographic Research Papers* **38,** 1127-1143.

Leventer, A. (1992). Modern distribution of diatoms in sediments from the George V Coast, Antarctica. *Marine Micropaleontology* **19,** 315-332.

Leventer, A. (1998). The fate of Antarctic "sea-ice diatoms" and their use as paleoenvironmental indicators. *In* "Antarctic sea ice biological processes, interactions and variability: American Geophysical Union Antarctic Research Series." (M. Lizotte, and K. Arrigo, Eds.), pp. 121-137.

Leventer, A., Domack, E., Barkoukis, A., McAndrews, B., and Murray, J. (2002). Laminations from the Palmer Deep: A diatom-based interpretation. *Paleoceanography* **17,** ISI:000178940200002.

Leventer, A. (2003). Particulate flux from sea ice in Polar waters. *In* "Sea Ice: An introduction to its physics, chemistry, biology and geology." (D. N. Thomas, and G. S. Dieckmann, Eds.), pp. 303-332. Blackwell Science.

Leventer, A. (2006). Approaches to the use of marine diatoms in fingerprinting glacial ice retreat. *In* "2006 Philadelphia Annual Meeting." Geological Society of America.

Leventer, A., Domack, E., Dunbar, R., Pike, J., Stickley, C., Maddison, E. J., Brachfeld, S., Manley, P., and McClennen, C. E. (2006). Marine sediment record from the East Antarctic margin reveals dynamics of ice sheet recession. *GSA Today* **16,** 4-10.

Leventer, A., Domack, E. W., Ishman, S. E., Brachfeld, S., McClennen, C. E., and Manley, P. (1996). Productivity cycles of 200-300 years in the Antarctic Peninsula region: Understanding linkages among the sun, atmosphere, oceans, sea ice, and biota. *Geological Society of America Bulletin* **108,** 1626-1644.

Leventer, A., and Dunbar, R. B. (1987). Diatom Flux in Mcmurdo Sound, Antarctica. *Marine Micropaleontology* **12,** 49-64.

Leventer, A., and Dunbar, R. B. (1988). Recent diatom record of McMurdo Sound, Antarctica: implications for the history of sea ice extent. *Palaeoceanography* **3,** 259-274.

Leventer, A., and Dunbar, R. B. (1996). Factors influencing the distribution of diatoms and other algae in the Ross Sea. *Journal of Geophysical Research* **101,** 18,489-18,500.

Licht, K. J., Jennings, A. E., Andrews, J. T., and Williams, K. M. (1996). Chronology of late Wisconsin ice retreat from the western Ross Sea, Antarctica. *Geology* **24,** 223-226.

Ligowski, R., Godlewski, M., and Lukowski, A. (1992). Sea ice diatoms and ice edge planktonic diatoms at the northern limit of the Weddell Sea pack ice; Proceedings of the National Institute of Polar Research Symposium. *Polar Biology* **5,** 9-20.

Lipenkov, V., Ekaykin, A. A., Barkov, N. I., and Pourchet, M. (1998). On the relation between surface snow density in Antarctica and wind speed. *Data of Glaciological Studies* **85,** 148-158.

Liu, J., Curry, J. A., and Martinson, D. G. (2004). Interpretation of recent Antarctic sea ice variability. *Geophysical Research Letters* **31**. L02205, doi:10.1029/2003GL018732

Longhi, M. L., Schloss, I. R., and Wiencke, C. (2003). Effect of Irradiance and Temperature on Photosynthesis and Growth of Two Antarctic Benthic Diatoms, Gyrosigma subsalinum and Odontella litigiosa. *Botanica Marina* **46,** 276-284.

López, O., García, M. A., Gomis, D., Rojas, P., Sospedra, J., and Sánchez-Arcilla, A. (1999). Hydrographic and hydrodynamic characteristics of the eastern basin of the Bransfield Strait (Antarctica). *Deep Sea Research Part I: Oceanographic Research Papers* **46,** 1755-1778.

Lourey, M. J., Trull, T. W., and Sigman, D. M. (2003). Sensitivity of d15N of nitrate, surface suspended and deep sinking particulate nitrogen to seasonal nitrate depletion in the Southern Ocean. *Global Biogeochemical Cycles* **17,** 1081.

Lowe, A. L., and Anderson, J. B. (2002). Reconstruction of the West Antarctic ice sheet in Pine Island Bay during the Last Glacial Maximum and its subsequent retreat history. *Quaternary Science Reviews* **21,** 1879-1897.

Ludlam, G. J., Rothschild, K. J., Pancost, R. D., Freeman, K. H., Wakeham, S. G., and Robertson, C. Y. (1997). Controls on carbon isotope fractionation by diatoms in the Peru upwelling region. *Geochimica et Cosmochimica Acta* **61,** 4983-4991.

Lythe, M., Vaughan, D. G., and Consortium, T. B. (2001). 'BEDMAP: A New Ice Thickness and Subglacial Topographic Model of Antarctica'. *Journal of Geophysical Research* **106,** 11335–11352.

M

MacAyeal, D. R., Scambos, T. A., Hulbe, L. C., and Fahnestock, M. (2003). Catastrophic ice shelf breakup by an ice shelf fragment capsize mechanism. *Journal of Glaciology* **49,** 22-36.

MacIntyre, S., Alldredge, A. L., and Gotschalk, C. C. (1995). Accumulation of marine snow at density discontinuities in the water column. *Limnology and Oceanography* **40,** 449-468.

Maddison, E. J., Pike, J., Leventer, A., and Domack, E. W. (2005). Deglacial seasonal and sub-seasonal diatom record from Palmer Deep, Antarctica. *Journal of Quaternary Science* **20,** 435-446.

Maddison, E. J., Pike, J., Leventer, A., Dunbar, R., Brachfeld, S., Domack, E., Manley, P., and McClennen, C. (2006). Post-glacial seasonal diatom record of the Mertz Glacier Polynya, East Antarctica. *Marine Micropaleontology* **60,** 66-88.

Markgraf, V., and Seltzer, G. O. (2001). Pole-equator-pole paleoclimates of the Americas integration: toward the big picture. *In* "Interhemispheric Climate Linkages." (V. Markgraf, Ed.), pp. 433–442. Academic Press, London.

Marrari, M., Daly, K. L., and Hu, C. (2008). Spatial and temporal variability of SeaWiFS chlorophyll a distributions west of the Antarctic Peninsula: Implications for krill production. *Deep Sea Research Part II: Topical Studies in Oceanography* **55,** 377-392.

Martin, J. H., Gordon, R. M., and Fitzwater, S. E. (1990). Iron in Antarctic waters. *Nature* **345,** 156-158.

Martinson, D. G., Stammerjohn, S. E., Iannuzzi, R. A., Smith, R. C., and Vernet, M. (2008). Western Antarctic Peninsula physical oceanography and spatio-temporal variability. *Deep Sea Research Part II: Topical Studies in Oceanography* **55,** 1964-1987.

Maslin, M., and Swann, G. E. A. (2005). Isotopes in Marine Sediments. *In* "Isotopes in Palaeoenvironmental Research." (M. J. Leng, Ed.). Springer, Netherlands.

Masqué, P., Isla, E., Sanchez-Cabeza, J. A., Palanques, A., Bruach, J. M., Puig, P., and Guillén, J. (2002). Sediment accumulation rates and carbon fluxes to bottom sediments at the Western Bransfield Strait (Antarctica). *Deep Sea Research Part II: Topical Studies in Oceanography* **49,** 921-933.

Massé, G., Rowland, S. J., Sicre, M.-A., Jacob, J., Jansen, E., and Belt, S. T. (2008). Abrupt climate changes for Iceland during the last millennium: Evidence from high resolution sea ice reconstructions. *Earth Planetary Science Letters* **269,** 564-568.

Masson-Delmotte, V., Stenni, B., and Jouzel, J. (2004). Common millennial-scale variability of Antarctic and Southern Ocean temperatures during the past 5000 years reconstructed from the EPICA Dome C ice core. *Holocene* **14,** 145-151.

Masson, V., Vimeux, F., Jouzel, J., Morgan, V., Delmotte, M., Ciais, P., Hammer, C., Johnsen, S., Lipenkov, V. Y., Mosley-Thompson, E., Petit, J. R., Steig, E. J., Stievenard, M., and Vaikmae, R. (2000). Holocene climate variability in Antarctica based on 11 ice-core isotopic records. *Quaternary Research* **54,** 348-358.

Matsumoto, K., and Key, R. M. (2004). Natural radiocarbon distribution in the deep ocean. *In* "Global Environmental Change in the Ocean and on Land." (E. Shiyomi, Ed.), pp. 45-58. TERRAPUB.

Mäusbacher, R., Müller, J., and Schmidt, R. (1989). Evolution of post-glacial sedimentation in Antarctic lakes (King George Island). *Zeitschrift für Geomorphologie* **33,** 219–34.

Mayewski, P. A., Lyons, W. B., Zielinski, G., Twickler, M., Whitlow, S., Dibb, J., Grootes, P., Taylor, K., Whung, P. Y., Fosberry, L., Wake, C., and Welch, K. (1995). An Ice-core based, late Holocene history for the Transantarctic Mountains, Antarctica. *In* "Contributions to Antarctic Research IV." pp. 33-45.

Mayewski, P. A., Rohling, E. E., Stager, J. C., Karlen, W., Maasch, K. A., Meeker, L. D., Meyerson, E. A., Gasse, F., van Kreveld, S., Holmgren, K., Lee-Thorp, J., Rosqvist, G., Rack, F., Staubwasser, M., Schneider, R. R., and Steig, E. J. (2004). Holocene climate variability. *Quaternary Research* **62,** 243-255.

Mayewski, P. A., Twickler, M. S., Whitlow, S. I., Meeker, L. D., Yang, Q., Thomas, J., Kreutz, K., Grootes, P. M., Morse, D. L., Steig, E. J., Waddington, E. D., Saltzman, E. S., Whung, P. Y., and Taylor, K. C. (1996). Climate change during the last deglaciation in Antarctica. *Science* **272,** 1636-1638.

Mayhew, S. (2004). "A Dictionary of Geography; Oxford Reference Online." Oxford University Press.

Mayr, C., Wille, M., Haberzettl, T., Fey, M., Janssen, S., Lücke, A., Ohlendorf, C., Oliva, G., Schäbitz, F., Schleser, G. H., and Zolitschka, B. (2007). Holocene variability of the Southern Hemisphere westerlies in Argentinean Patagonia (52°S). *Quaternary Science Reviews* **26,** 579-584.

McCoy, F. W. (1980). Photographic analysis of coring. *Marine Geology* **38,** 263-282.

McCoy, F. W., and von Herzen, R. P. (1971). Deep-sea corehead camera photography and piston coring. *Deep Sea Research* **18,** 361-373.

McCulloch, R. D., and Davies, S. J. (2001). Late-glacial and Holocene palaeoenvironmental change in the central Strait of Magellan, southern Patagonia. *Palaeogeography, Palaeoclimatology, Palaeoecology* **173,** 143-173.

McManus, J. F., Francois, R., Gherardi, J. M., Keigwin, L. D., and Brown-Leger, S. (2004). Collapse and rapid resumption of Atlantic meridional circulation linked to deglacial climate changes. *Nature* **428,** 834-837.

McMinn, A. (2000). Late Holocene increase in sea ice extent in fjords of the Vestfold Hills, eastern Antarctica. *Antarctic Science* **12,** 80-88.

McMinn, A., and Hodgson, D. A. (1993). Summer phytoplankton succession in Ellis Fjord, eastern Antarctica. *J. Plankton Res.* **15,** 925-938.

McQuoid, M. R., and L.A., H. (1996). Diatom resting stages. *Journal of Phycology* **32,** 889-902.

Melles, M., Verkulich, S. R., and Hermichen, W.-D. (1994). Radiocarbon dating of lacustrine and marine sediments from the Bunger Hills, East Antarctica. *Antarctic Science* **6,** 375-378.

Meng, L. (1994). How accurate is the random settling method of quantitative diatom analysis? A test using *Lycopodium* spore tablets. *Micropaleontology* **40,** 261-266.

Meredith, M. P., and King, J. C. (2005). Rapid climate change in the ocean west of the Antarctic Peninsula during the second half of the 20th century. *Geophys. Res. Lett.* **32,** 10.1029/2005GL024042.

Meredith, M. P., Murphy, E. J., Hawker, E. J., King, J. C., and Wallace, M. I. (2008). On the interannual variability of ocean temperatures around South Georgia, Southern Ocean: Forcing by El Niño/Southern Oscillation and the Southern Annular Mode. *Deep Sea Research Part II: Topical Studies in Oceanography* **55,** 2007-2022.

Meredith, M. P., Renfrew, I. A., Clarke, A., and King, J. C. (2004). Impact of the 1997/98 ENSO on upper ocean characteristics in Marguerite Bay, western Antarctic Peninsula. *Journal of Geophysical Research* **109,** C09013.

Michels, J., Dieckmann, G. S., Thomas, D. N., Schnack-Schiel, S. B., Krell, A., Assmy, P., Kennedy, H., Papadimitriou, S., and Cisewski, B. (2008). Short-term biogenic particle flux under late spring sea ice in the western Weddell Sea. *Deep Sea Research Part II: Topical Studies in Oceanography* **55,** 1024-1039.

Miller, K. G., Kominz, M. A., Browning, J. V., Wright, J. D., Mountain, G. S., Katz, M. E., Sugarman, P. J., Cramer, B. S., Christie-Blick, N., and Pekar, S. F. (2005). The Phanerozoic Record of Global Sea-Level Change. *Science* **310,** 1293-1298.

Miller, K. G., Wright, J. D., and Fairbanks, R. G. (1991). Unlocking the Ice House: Oligocene-Miocene Oxygen Isotopes, Eustasy, and Margin Erosion. *Journal of Geophysical Research* **96,** 6829-6848.

Miller, K. G., Wright, J. D., Katz, M. E., Browning, J. V., Cramer, B. S., Wade, B. S., and Mizintseva, S. F. (2007). A view of Antarctic ice-sheet evolution from sea-level and deep-sea isotope changes during the Late Cretaceous-Cenozoic. *In* "10th International Symposium of Antarctic Earth Sciences. Antarctica: A keystone in a Changing World." (A. K. Cooper, P. J. Barrett, H. Stagg, B. Storey, E. Stump, and W. Wise, Eds.), pp. 55-70. The National Academies Press, University of California, Santa Barbara.

Mitchell, B. G., and Holm-Hansen, O. (1991). Observations and modeling of the Antarctic phytoplankton crop in relation to mixing depth. *Deep Sea Research* **38,** 981-1007.

Mix, A. C., Bard, E., and Schneider, R. (2001). Environmental processes of the ice age: land, oceans, glaciers (EPILOG). *Quaternary Science Reviews* **20,** 627-657.

Moffat, C., Beardsley, R. C., Owens, B., and van Lipzig, N. (2008). A first description of the Antarctic Peninsula Coastal Current. *Deep Sea Research Part II: Topical Studies in Oceanography* **55,** 277-293.

Moisan, T. A., and Fryxell, G. A. (1993). The distribution of Antarctic diatoms in the Weddell Sea during austral winter. *Botanica Marina* **36** 489-497.

Moline, M. A., Claustre, H., Frazer, T. K., Schofield, O., and Vernet, M. (2004). Alteration of the food web along the Antarctic Peninsula in response to a regional warming trend. *Global Change Biology* **10,** 1973-1980.

Montes-Hugo, M., Doney, S. C., Ducklow, H. W., Fraser, W., Martinson, D., Stammerjohn, S. E., and Schofield, O. (2009). Recent Changes in Phytoplankton Communities Associated with Rapid Regional Climate Change Along the Western Antarctic Peninsula. *Science* **323,** 1470-1473.

Moore, J. K., and Villareal, T. A. (1996). Size-ascent rate in positively buoyant marine diatoms. *Limnology and Oceanography* **41,** 1514-1520.

Moore, T. C. (1973). Method of randomly distributing grains for microscopic examination. *Journal of Sedimentary Petrology* **43,** 904-906.

Moreno, P. I. (2004). Millennial-scale climate variability in northwest Patagonia over the last 15000 yr. *Journal of Quaternary Science* **19,** 35-47.

Moreno, P. I., François, J. P., Villa-Martínez, R. P., and Moy, C. M. (2009a). Millennial-scale variability in Southern Hemisphere westerly wind activity over the last 5000 years in SW Patagonia. *Quaternary Science Reviews* **28,** 25-38.

Moreno, P. I., Kaplan, M. R., Francois, J. P., Villa-Martinez, R., Moy, C. M., Stern, C. R., and Kubik, P. W. (2009b). Renewed glacial activity during the Antarctic cold reversal and persistence of cold conditions until 11.5 ka in southwestern Patagonia. *Geology* **37,** 375-378.

Moreno, P. I., and León, A. L. (2003). Abrupt vegetation changes during the last glacial to Holocene transition in mid-latitude South America. *Journal of Quaternary Science* **18,** 787-800.

Moreton, S. G. (1999). "Quaternary tephrochronology of the Scotia Sea and Bellingshausen Sea, Antarctica." Cheltenham and Gloucester College of Higher Education.

Moreton, S. G., and Smellie, J. L. (1998). Identification and correlation of distal tephra layers in deep-sea sediment cores, Scotia Sea, Antarctica. *Annals of Glaciology* **27,** 285-289.

Morgan, V., Delmotte, M., van Ommen, T., Jouzel, J., Chappellaz, J., Woon, S., Masson-Delmotte, V., and Raynaud, D. (2002). Relative Timing of Deglacial Climate Events in Antarctica and Greenland. *Science* **297,** 1862-1864.

Morris, E. M., and Vaughan, D. G. (2003). Spatial and temporal variation of surface temperature on the Antarctic Peninsula and the limit of viability of ice shelves. *Antarctic Research Series* **79,** 61-68.

Mosley-Thompson, E. (1996). Holocene Climate Changes Recorded in an East Antarctica Ice Core. *In* "Climatic Variations and Forcing Mechanisms of the Last 2,000 Years." (P. Jones, R. Bradley, and J. Jouzel, Eds.), pp. 263-279. NATO Advanced Research, Berlin., Berlin.

Moy, C. M., Seltzer, G. O., Rodbell, D. T., and Anderson, D. M. (2002). Variability of El Nino/Southern Oscillation activity at millennial timescales during the Holocene epoch. *Nature* **420,** 162-165.

Mulvaney, R., Alemany, O., and Possenti, P. (2007). The Berkner Island (Antarctica) ice-core drilling project. *Annals of Glaciology* **47,** 115-123.

Murray, T., Smith, A. M., King, M. A., and Weedon, G. P. (2007). Ice flow modulated by tides at up to annual periods at Rutford Ice Stream, West Antarctica. *Geophysical Research Letters* **34**.

MSVP (2002) Kovach Computing Services, version 3.1

N

Nakada, M., Kimura, R., Okuno, J., Moriwaki, K., Miura, H., and Maemoku, H. (2000). Late Pleistocene and Holocene melting history of the Antarctic ice sheet derived from sea-level variations. *Marine Geology* **167,** 85-103.

Nakada, M., and Lambeck, K. (1988). The melting history of the late Pleistocene Antarctic Ice Sheet. *Nature* **333,** 36-40.

Neftel, A., Oeschger, H., Staffelbach, T., and Stauffer, B. (1988). CO2 record in the Byrd ice core 50,000-5,000 years bp. *Nature* **331,** 609-611.

Nelson, D. M., and Smith Jr, W. O. (1986). Phytoplankton bloom dynamics of the western Ross Sea ice edge--II. Mesoscale cycling of nitrogen and silicon. *Deep Sea Research Part A. Oceanographic Research Papers* **33,** 1389-1412.

Nelson, D. M., and Smith Jr., W. O. (1991). Sverdrup revisited: Critical depths, maximum chlorophyll levels and the control of Southern Ocean productivity by the irradiance-mixing regime. *Limnology and Oceanography* **36,** 1650-1661.

Nelson, D. M., Smith, W. O., Jr., Gordon, L. I., and Huber, B. A. (1987). Spring Distributions of Density, Nutrients, and Phytoplankton Biomass in the Ice Edge Zone of the Weddell-Scotia Sea. *Journal of Geophysical Research* **92,** 10.1029/JC092iC07p07181.

Neori, A., and Holm-Hansen, O. (1982). Effect of temperature on rate of photosynthesis in Antarctic phytoplankton. *Polar Biology* **1,** 33-38.

Nielsen, S. H. H., Koc, N., and Crosta, X. (2004). Holocene climate in the Atlantic sector of the Southern Ocean: Controlled by insolation or oceanic circulation? *Geology* **32,** 317-320.

Nikolaiev, V. I., Kotlyakov, V. M., and Smirnov, K. E. (1988). Isotopic studies of the ice core from the Komsomolskaia station, Antarctica. *Data of Glaciological Studies of the USSR Academy of Sciences* **63,** 97-102.

O

Ó Cofaigh, C., Dowdeswell, J. A., Allen, C. S., Hiemstra, J. F., Pudsey, C. J., Evans, J., and Evans, D. J. A. (2005a). Flow dynamics and till genesis associated with a marine-based Antarctic palaeo-ice stream. *Quaternary Science Reviews* **24,** 709-740.

Ó Cofaigh, C., Dowdeswell, J. A., Evans, J., and Larter, R. D. (2008). Geological constraints on Antarctic palaeo-ice-stream retreat. *Earth Surface Processes and Landforms* **33,** 513-525.

Ó Cofaigh, C., Larter, R. D., Dowdeswell, J. A., Hillenbrand, C. D., Pudsey, C. J., Evans, J., and Morris, P. (2005b). Flow of the West Antarctic Ice Sheet on the continental margin of the Bellingshausen Sea at the Last Glacial Maximum. *Journal of Geophysical Research-Solid Earth* **110,** ISI:000233588500002.

Ó Cofaigh, C., Pudsey, C. J., Dowdeswell, J. A., and Morris, P. (2002). Evolution of subglacial bedforms along a paleo-ice stream, Antarctic Peninsula continental shelf. *Geophysical Research Letters* **29,** 10.1029/2001GL014488.

Omoto, K. (1983). The problem and significance of radiocarbon geochronology in Antarctica. *In* "Antarctic Earth Science." (R. L. Oliver, P. R. James, and J. B. Jago, Eds.), pp. 205-209. Cambridge University Press, Cambridge.

Oppenheimer, M. (1998). Global warming and the stability of the West Antarctic Ice Sheet. *Nature* **393,** 325-332.

Orsi, A. H., Johnson, G. C., and Bullister, J. L. (1999). Circulation, mixing, and production of Antarctic Bottom Water. *Progress in Oceanography* **43,** 55-109.

Orsi, A. H., Nowlin Jr, W. D., and Whitworth Iii, T. (1993). On the circulation and stratification of the Weddell Gyre. *Deep Sea Research Part I: Oceanographic Research Papers* **40,** 169-203.

Orsi, A. H., Whitworth, T., and Nowlin, W. D. (1995). On the Meridional Extent and Fronts of the Antarctic Circumpolar Current. *Deep-Sea Research Part I-Oceanographic Research Papers* **42,** 641-673.

Osborn, T. J. (1997). Thermohaline oscillations in the LSG OGCM: Propagating anomalies and sensitivity to parameterizations. *Journal of Physical Oceanography* **27,** 2233-2255.

Ostrom, N. E., Macko, S. A., Deibel, D., and Thompson, R. J. (1997). Seasonal variation in the stable carbon and nitrogen isotope biogeochemistry of a coastal cold ocean environment. *Geochimica et Cosmochimica Acta* **61,** 2929-2942.

P

Palmisano, A. C., and Sullivan, C. W. (1985). Growth, metabolism, and dark Survival in sea ice microalgae. *In* "Sea Ice Biota." (R. A. Horner, Ed.), pp. 131-146. CRC Press, Boca Raton.

Pancost, R. D., Freeman, K. H., Wakeham, S. G., and Robertson, C. Y. (1997). Controls on carbon isotope fractionation by diatoms in the Peru upwelling region. *Geochimica et Cosmochimica Acta* **61,** 1983-4991.

Parkinson, C. L. (2004). Southern Ocean sea ice and its wider linkages: Insights revealed from models and observations. *Antarctic Science* **16,** 387-400.

Patterson, M., and Leventer, A. (2008). The polar marine diatom *Eucampia antarctica*: A test of its paleoceanographic utility. *In* "The Geological Society of America, Northeastern Section - 43rd Annual Meeting." GSA, Buffalo, New York (U.S.A.).

Payne, A. J., Vieli, A., Shepherd, A. P., Wingham, D. J., and Rignot, E. (2004). Recent dramatic thinning of largest West Antarctic ice stream triggered by oceans. *Geophysical Research Letters* **31,** 10.1029/2004GL021284.

Peltier, W. R. (1994). Ice age paleotopography. *Science* **265,** 195-201.

Peng, T. H., and Broecker, W. S. (1984). The impacts of bioturbation on the age difference between benthic and planktonic foraminifera in deep-sea sediments. *Nuclear Instruments and Methods in Physics Research; Section B* **233,** 346–352.

Petit, J.-R., Briat, M., and Royer, A. (1981). Ice age aerosol content from East Antarctic ice core samples and past wind strength. *Nature* **293,** 391-394.

Petit, J.-R., Jouzel, J., Raynaud, D., Barkov, N. I., Barnola, J.-M., Basile, I., Bender, M., Chappellaz, J., Davis, J., Delaygue, G., Delmotte, M., Kotlyakov, V. M., Legrand, M., Lipenkov, V., Lorius, C., Pepin, L., Ritz, C., Salzman, E., and Stievenard, M. (1999). Climate and atmospheric history of the past 420 000 years from the Vostok ice core, Antarctica. *Nature* **399,** 429–436.

Pichon, J.-J., Bareille, G., Labracherie, M., Labeyrie, L. D., Baudrimont, A., and Turon, J. L. (1992a). Quantification of the biogenic silica dissolution in Southern Ocean sediments. *Quaternary Research* **37,** 361-378.

Pichon, J.-J., Labracherie, M., Labeyrie, L. D., and Duprat, J. (1987). Transfer functions between diatom assemblages and surface hydrobiology in the Southern Ocean. *Palaeograography, Palaeoclimatology, Palaeoecology* **61,** 79-95.

Pichon, J. J., Labeyrie, L. D., Bareille, G., Labracherie, M., Duprat, J., and Jouzel, J. (1992b). Surface water temperature changes in the high latitudes of the Southern Hemisphere over the last glacial-interglacial cycle. *Paleoceanography* **7,** 289-318.

Pierce, D. W., Barnett, T. P., and Mikolajewicz, U. (1995). Competing role of heat and freshwater flux in forcing thermohaline oscillations. *Journal of Physical Oceanography* **25,** 2046-2064.

Pike, J., Allen, C. S., Leventer, A., Stickley, C., and Pudsey, C. J. (2008). Comparison of contemporary and fossil diatom assemblages from the western Antarctic Peninsula shelf. *Marine Micropaleontology* **67,** 274-287.

Pike, J., and Kemp, A. E. S. (1999). Diatom mats in Gulf of California sediments: Implications for the palaeoenvironmental interpretation of laminated sediments and silica burial. *Geology* **27,** 311-314.

Pittock, A. B., Frakes, L. A., Jenssen, D., Peterson, J. A., and Zillman, J. W. (1978). Climatic change and variability - a southern perspective, pp. 325. Cambridge University Press

Pope, P. G., and Anderson, J. B. (1992). Late Quaternary Glacial History of the Northern Antarctic Peninsula's western continental shelf: Evidence from the marin record. *In* "Contributions to Antarctic Research III, Antarctic Research Series." (D. H. Elliot, Ed.), pp. 63-91. American Geophysical Union.

Popp, B. N., Laws, E. A., Bidigare, R. R., Dore, J. E., Hanson, K. L., and Wakeham, S. G. (1998). Effect of Phytoplankton Cell Geometry on Carbon Isotopic Fractionation. *Geochimica et Cosmochimica Acta* **62,** 69-77.

Porter, S. C., and Denton, G. H. (1967). Chronology of neoglaciation in the Northern American Cordillera. *American Journal of Science* **265,** 177-210.

Presti, M., De Santis, L., Busetti, M., and Harris, P. T. (2003). Late Pleistocene and Holocene sedimentation on the George V continental shelf, East Antarctica. *Deep-Sea Research Part II: Topical Studies in Oceanography* **50,** 1441-1461.

Prézelin, B. B., Hofmann, E. E., Mengelt, C., and Klinck, J. M. (2000). The linkage between Upper Circumpolar Deep Water (UCDW) and phytoplankton assemblages on the west Antarctic Peninsula continental shelf. *Journal of Marine Research* **58,** 165-202.

Priddle, J. (1990). The Antarctic Planktonic Ecosystem. *In* "Polar Marine Diatoms." (L. K. Medlin, and J. Priddle, Eds.), pp. 25-34. British Antarctic Survey, Natural Environment Research Council (NERC).

Priddle, J., and Fryxell, G. A. (1985). "Handbook of the Common Plankton Diatoms of the Southern Ocean. Centrales except the Genus *Thalassiosira.*" British Antarctic Survey, Cambridge.

Priddle, J., Jordan, R. W., and Medlin, L. K. (1990). Family Rhizosoleniaceae. *In* "Polar marine diatoms." (L. K. Medlin, and J. Priddle, Eds.), pp. 115-127. British Antarctic Survey, Cambridge.

Pritchard, H. D., and Vaughan, D. G. (2007). Widespread acceleration of tidewater glaciers on the Antarctic Peninsula. *Journal of Geophysical Research* **112,** F03S29.

Pudsey, C. J., Barker, P. F., and Larter, R. D. (1994). Ice-Sheet Retreat from the Antarctic Peninsula Shelf. *Continental Shelf Research* **14,** 1647-1675.

Pudsey, C. J., and Evans, J. (2001). First Survey of Antarctic Sub-Ice Shelf Sediments Reveals Mid-Holocene Ice Shelf Retreat. *Geology* **29,** 787-790.

Pudsey, C. J., Murray, J. W., Appleby, P., and Evans, J. (2006). Ice shelf history from petrographic and foraminiferal evidence, Northeast Antarctic Peninsula. *Quaternary Science Reviews* **25,** 2357-2379.

R

Rathburn, A. E., Pichon, J. J., Ayress, M. A., and De Deckker, P. (1997). Microfossil and stable-isotope evidence for changes in Late Holocene palaeoproductivity and palaeoceanographic conditions in the Prydz Bay region of Antarctica. *Palaeogeography, Palaeoclimatology, Palaeoecology* **131,** 485-510.

Rau, G. H., Chavez, F. P., and Friederich, G. E. (2001). Plankton $^{13}C/^{12}C$ variations in Monterey Bay, California: evidence of non-diffusive inorganic carbon uptake by phytoplankton in an upwelling environment. *Deep Sea Research Part I: Oceanographic Research Papers* **48,** 79-94.

Rau, G. H., Sullivan, C. W., and Gordon, L. I. (1991). d13C and d15N variations in Weddell Sea particulate organic matter. *Marine Chemistry* **35,** 355-369.

Rea, D. K. (1994). The paleoclimatic record provided by eolian deposition in the deep sea: The geologic history of wind. *Reviews of Geophysics* **32,** doi: 10.1029/93RG03257.

Redfield, A. C., Ketchum, B. H., and Richards, F. A. (1963). The influence of organisms on the composition of seawater. *In* "The sea: ideas and observations on progress in the study of the seas, 2: pp. 26-77 " (N. Hill, Ed.), pp. 26-77. Interscience.

Reimer, P. J., Baillie, M. G. L., Bard, E., Bayliss, A., Beck, J. W., Bertrand, C. J. H., Blackwell, P. G., Buck, C. E., Burr, G. S., Cutler, K. B., Damon, P. E., Edwards, R. L., Fairbanks, R. G., Friedrich, M., Guilderson, T. P., Hogg, A. G., Hughen, K. A., Kromer, B., McCormac, F. G., Manning, S. W., Ramsey, C. B., Reimer, R. W., Remmele, S., Southon, J. R., Stuiver, M., Talamo, S., Taylor, F. W., van der Plicht, J., and

Weyhenmeyer, C. E. (2004). IntCal04 Terrestrial radiocarbon age calibration, 26 - 0 ka BP. *Radiocarbon* **46,** 1029-1058.

Remy, J. P., Becquevort, S., Haskell, T. G., and Tison, J. L. (2008). Impact of the B-15 iceberg "stranding event" on the physical and biological properties of sea ice in McMurdo Sound, Ross Sea, Antarctica. *Antarctic Science* **20,** 593-604.

Renfrew, I. A., and Anderson, P. S. (2002). The surface climatology of an ordinary katabatic wind regime in Coats Land, Antarctica. *Tellus* **54,** 463-484.

Renssen, H., Goosse, H., Fichefet, T., Masson-Delmotte, V., and Koc, N. (2005). Holocene climate evolution in the high-latitude Southern Hemisphere simulated by a coupled atmosphere-sea ice-ocean-vegetation model. *The Holocene* **15,** 951-964.

Riaux-Gobin, C., Treguer, P., Poulin, M., and Vetion, G. (2000). Nutrients, algal biomass and communities in land-fast ice and seawater off Adelie Land, Antarctica. *Antarctic Science* **12,** 160-171.

Riebesell, U. (1992). The formation of large marine snow and its sustained residence in surface waters. *Limnology and Oceanography* **37,** 63-76.

Riebesell, U. (2000). Photosynthesis: Carbon fix for a diatom. *Nature* **407,** 959-960.

Riebesell, U., Burkhardt, S., Dauelsberg, A., and Kroon, B. (2000). Carbon isotope fractionation by a marine diatom: Dependence on the growth-rate-limiting resource. *Marine Ecology Progress Series* **193,** 295-303.

Riebesell, U., Schloss, I., and Smetacek, V. (1991). Aggregation of algae released from melting sea ice: implications for seeding and sedimentation. *Polar Biology* **11,** 239-248.

Riedinger, M. A., Steinitz-Kannan, M., Last, W. M., and Brenner, M. (2002). A similar to 6100 C-14 yr record of El Nino activity from the Galapagos Islands. *Journal of Palaeolimnology* **27,** 1-7.

Rignot, E., Casassa, G., Goginen, P., Krabill, W., Rivera, A., and Thomas, R. (2004). Accelerated ice discharge from the Antarctic Peninsula following the collapse of Larsen B ice shelf. *Geophysical Research Letters* **31,** L18401.

Rignot, E., Casassa, G., Gogineni, S., Kanagaratnam, P., Krabill, W., Pritchard, H., Rivera, A., Thomas, R., Turner, J., and Vaughan, D. (2005). Recent ice loss from the Fleming and other glaciers, Wordie Bay, West Antarctic Peninsula. *Geophysical Research Letters* **32,** L07502.

Rind, D., Russell, G., Schmidt, G., Sheth, S., Collins, D., DeMenocal, P., and Teller, J. (2001). Effects of glacial meltwater in the GISS coupled atmosphere-ocean model 2. A bipolar seesaw in Atlantic Deep Water production. *Journal of Geophysical Research D: Atmospheres* **106,** 27355-27365.

Rintoul, S. R., Hughes, C. W., and Olbers, D. (2001). The Antarctic Circumpolar Current System. *In* "Ocean Circulation and Climate. Observing and Modelling the Global Ocean." (G. Siedler, J. Church, and J. Gould, Eds.), pp. 271-302. Academic Press.

Roberts, D., van Ommen, T. D., McMinn, A., Morgan, V., and Roberts, J. L. (2001). Late-Holocene East Antarctic climate trends from ice-core and lake-sediment proxies. *Holocene* **11,** 117-120.

Roberts, S. J., Hodgson, D. A., Bentley, M. J., Smith, J. A., Millar, I. L., Olive, V., and Sugden, D. E. (2008). The Holocene history of George VI Ice Shelf, Antarctic Peninsula from clast-provenance analysis of epishelf lake sediments. *Palaeogeography, Palaeoclimatology, Palaeoecology* **259,** 258-283.

Robinson, R. S., and Sigman, D. M. (2008). Nitrogen isotopic evidence for a poleward decrease in surface nitrate within the ice age Antarctic. *Quaternary Science Reviews* **27,** 1076-1090.

Rodbell, D. T., Seltzer, G. O., Anderson, D. M., Abbott, M. B., Enfield, D. B., and Newman, J. H. (1999). An ~15,000-Year Record of El Nino-Driven Alluviation in Southwestern Ecuador. *Science* **283,** 516-520.

Romero, O. E., Armand, L. K., Crosta, X., and Pichon, J. J. (2005). The biogeography of major diatom taxa in Southern Ocean surface sediments: 3. Tropical/Subtropical species. *Palaeogeography Palaeoclimatology Palaeoecology* **223,** 49-65.

Rosenheim, B., Domack, E., Hayes, J., Day, M. B., Schrum, H., and Roberts, M. (2007). A proposed community wide analytical netwrok using a new approach to radiocarbon dating of Antarctic glacial marine sediments. *In* "10th International Symposium on Antarctic Earth Sciences." The National Academies Press, Santa Barbara, California, USA.

Rosenheim, B. E., Day, M. B., Domack, E., Schrum, H., Benthien, A., and Hayes, J. M. (2008). Antarctic sediment chronology by programmed-temperature pyrolysis: methodology and data treatment. *Geochemistry, Geophysics, Geosystems* **9,** Q04005.

Rosqvist, G. C., Rietti-Shati, M., and Shemesh, A. (1999). Late glacial to middle Holocene climatic record of lacustrine biogenic silica oxygen isotopes from a Southern Ocean island. *Geology* **27,** 967-970.

Rosqvist, G. C., and Schuber, P. (2003). Millennial-scale climate changes on South Georgia, Southern Ocean. *Quaternary Research* **59,** 470-475.

Ross, R. M., Quetin, L. B., Martinson, D. G., Ianuzzi, R. A., Stammerjohn, S. E., and Smith, R. C. (2008). Palmer LTER: Patterns of distribution of five dominant zooplankton species in the epipelagic zone west of the Antarctic Peninsula, 1993-2004. *Deep Sea Research Part II: Topical Studies in Oceanography* **55,** 2086-2105.

Rott, H., Rack, W., Skvarca, P., and De Angelis, H. (2002). Northern Larsen Ice Shelf, Antarctica: further retreat after collapse. *Annals of Glaciology* **34,** 277–282.

Rott, H., Skvarca, P., and Agler, T. (1996). Rapid collapse of Northern Larsen Ice Shelf. *Antarctic Science* **271,** 788-792.

Round, F. E., Crawford, R. M., and Mann, D. G. (1990). "The Diatoms. Biology and Morphology of the Genera." Cambridge University Press, Cambridge.

Rowan, K. S. (1989). "Photosynthetic pigments of algae." Cambridge University Press, Cambridge.

S

Sakshaug, E., and Holm-Hansen, O. (1984). Factors governing pelagic production in polar oceans. *In* "Marine phytoplankton and productivity, lecture notes coastal and estuarine studies." (O. Holm-Hansen, L. Bolis, and R. Gilles., Eds.), pp. 1-18.

Sandweiss, D. H., Maasch, K. A., Burger, R. L., Richardson, J. B., Rollins, H. B., and Clement, A. (2001). Variation in Holocene El Niño frequencies: Climate records and cultural consequences in ancient Peru. *Geology* **29,** 603-606.

Scambos, T., Hulbe, C., and Fahnestock, M. (2003). Climate-induced ice shelf disintegration in the Antarctic Peninsula. *Antarctic Research Series* **79,** 79-92.

Scambos, T., Raup, B., Bohlander, J., and compilers. (2001, updated 2006). Images of Larsen B Ice Shelf, November 2002 - April 2006. Boulder, CO: National Snow and Ice Data Center.

Scambos, T. A., Bohlander, J. A., Shuman, C. A., and Skvarca, P. (2004). Glacier acceleration and thinning after ice shelf collapse in the Larsen-B embayment, Antarctica. *Geophysical Research Letters* **31,** 1-4.

Scambos, T. A., Hulbe, C., Fahnestock, M., and Bohlander, J. (2000). The link between climate warming and break-up of ice shelves in the Antarctic Peninsula. *Journal of Glaciology* **46,** 516-530.

Scherer, R. P. (1994). A new method for the determination of absolute abundance of diatoms and other silt-sized sedimentary particles. *Journal of Paleolimnology* **12,** 171-179.

Schlosser, P. (1994). The distribution of 14C and 39Ar in the Weddell Sea. *Journal of Geophysical Research* **99,** 10275-10287.

Schmitz, W. J. (1996). "On the World Ocean Circulation. Volume I: Some Global Features / North Atlantic Circulation."

Schwarz, J., and Schodlok, M. (2008). Icebergs boost phytoplankton growth in the Southern Ocean. *In* "Nature Precedings." 10101/npre.2008.1706.1

Schweitzer, P. N. (1995). Monthly averaged polar sea-ice concentration. U.S. Geological Survey Digital Data Series, Virginia.

Scott, F. J., and Marchant, H. J. (2005). Antarctic Marine Protists, pp. 563. Australian Biological Resources Study, Canberra.

Scott, F. J., and Thomas, D. P. (2005). Diatoms. *In* "Antarctic Marine Protists." (F. J. Scott, and H. J. Marchant, Eds.). Australian Biological Resources Study, Canberra.

Scott, P., McMinn, A., and Hosie, G. (1994). Physical parameters influencing diatom community structure in eastern Antarctic sea ice. *Polar biology* **14,** 507-517.

Seidov, D., Barron, E., and Haupt, B. J. (2001). Meltwater and the global ocean conveyor: northern versus southern connections. *Global and Planetary Change* **30,** 257-270.

Severinghaus, J. P. (2009). Climate change: Southern see-saw seen. *Nature* **457,** 1093-1094.

Sewell, D. R. (1998). A note for Novices. *Radiocarbon* **40,** xi.

Shackleton, N. J. (2000). The 100,000-Year Ice-Age Cycle Identified and Found to Lag Temperature, Carbon Dioxide, and Orbital Eccentricity. *Science* **289,** 1897-1902.

Shackleton, N. J., and Kennett, J. P. (1975). Paleotemperature history of the Cenozoic and the initiation of Antarctic glaciation: oxygen and carbon isotope analyses in DSDP Sites

277, 279, and 281. *In* "Initial Reports. DSDP, 29." (J. P. Kennett, and R. E. Houtz, Eds.), pp. 743-755. U.S. Government Printing Office, Washington.

Shemesh, A., Burckle, L. H., and Froelich, P. N. (1989). Dissolution and preservation of Antarctic diatoms and the effect on sediment thanatocoenoses. *Quaternary Research* **31,** 288-308.

Shemesh, A., Hodell, D., Crosta, X., Kanfoush, S., Charles, C., and Guilderson, T. (2002). Sequence of events during the last deglaciation in Southern Ocean sediments and Antarctic ice cores. *Paleoceanography* **17,** ISI:000180656400008.

Shepherd, A., Wingham, D., Payne, T., and Skvarca, P. (2003). Larsen Ice Shelf has progressively thinned. *Science* **302,** 856-859.

Shepherd, A., Wingham, D., and Rignot, E. (2004). Warm ocean is eroding West Antarctic Ice Sheet. *Geophysical Research Letters* **31,** L23402.

Shevenell, A. E., Domack, E. W., and Kernan, G. M. (1996). Record of Holocene climate change along the Antarctic Peninsula: Evidence from glacial marine sediments, Lallemand Fjord. *In* "The climate of the Southern Ocean." (P. a. P. o. t. R. S. Tasmania, Ed.), pp. 55-64.

Shevenell, A. E., Ingalls, A., and Domack, E. (2007). Orbital and atmospheric forcing of western Antarctic Peninsula climate in the Holocene: The TEX86 paleotemperature record of Palmer Deep. *In* "Antarctica: A Keystone in a Changing World - Online Proceedings of the 10th ISAES X." (A. K. Cooper, and C. R. Raymond, Eds.). USGS Open-File Report 2007-1047, Santa Barbara, USA.

Shevenell, A. E., and Kennett, J. P. (2002). Antarctic Holocene climate change: A benthic foraminiferal stable isotope record from Palmer Deep. *Paleoceanography* **17.**

Shipp, S., Anderson, J., and Domack, E. (1999). Late Pleistocene-Holocene retreat of the West Antarctic Ice-Sheet system in the Ross Sea: Part 1 - Geophysical results. *Geological Society of America Bulletin* **111,** 1486-1516.

Shoosmith, D. R., Jenkins, A., and Brandon, M. A. (2008). Oceanography of the Bellingshausen Sea and implications for west Antarctic Peninsula ice shelves. *In* "European Geophysical Union." (E. G. A. 2008, Ed.), pp. EGU2008-A-08526, Vienna, Austria.

Siedler, G., Church, J., and Gould, J. (2001). "Ocean circulation and climate: observing and modelling the global ocean." Academic Press.

Sievers, H. A., and Nowlin Jr, W. D. (1984). The stratification and water masses at Drake Passage. *Journal of Geophysical Research* **89,** 10,489 -10,514.

Sigman, D. M., and Boyle, E. A. (2000). Glacial/interglacial variations in atmospheric carbon dioxide. *Nature* **407,** 859-869.

Sikes, E. L., Samson, C. R., Guilderson, T. P., and Howard, W. R. (2000). Old radiocarbon ages in the southwest Pacific Ocean during the last glacial period and deglaciation. *Nature* **405,** 555-559.

Sjunneskog, C., and Taylor, F. (2002). Postglacial marine diatom record of the Palmer Deep, Antarctic Peninsula (ODP Leg 178, Site 1098) 1. Total diatom abundance. *Palaeoceanography* **17,** 10.1029/2000PA000563

Skinner, L. C., and McCave, I. N. (2003). Analysis and modelling of gravity- and piston coring based on soil mechanics. *Marine Geology* **199,** 181-204.

Skoog, D. A., West, D. M., Holler, F. J., and Crouch, S. R. (2000). "Analytical Chemistry: An Introduction (seventh edition)." Saunders College Publishing.

Skvarca, P., and De Angelis, H. (2003). Impact assessment of regional climatic warming on glaciers and ice shelves of the northeastern Antarctic Peninsula. *In* "AntarcticPeninsula Climate Variability." (E. Domack, A. Leventer, A. Burnett, R. Bindschadler, P. Convey, and M. Kirby, Eds.), pp. 69-78. Antarctic Research Series.

Smetacek, V., Scharek, R., Gordon, L. I., Eicken, H., Fahrbach, E., Rohardt, G., and Moore, S. (1992). Early spring phytoplankton blooms in Ice platelet layers of the southern Weddell Sea, Antarctica. *Deep-Sea Research Part A-Oceanographic Research Papers* **39,** 153-168.

Smith, D. A., Hofmann, E. E., Klinck, J. M., and Lascara, C. M. (1999). Hydrography and circulation of the west Antarctic Peninsula continental shelf. *Deep-Sea Research Part I-Oceanographic Research Papers* **46,** 925-949.

Smith, D. A., and Klinck, J. M. (2002). Water properties on the west Antarctic Peninsula continental shelf: a model study of effects of surface fluxes and sea ice. *Deep Sea Research Part II: Topical Studies in Oceanography* **49,** 4863-4886.

Smith, J. A., Bentley, M. J., Hodgson, D. A., Roberts, S. J., Leng, M. J., Lloyd, J. M., Barrett, M. S., Bryant, C., and Sugden, D. E. (2007a). Oceanic and atmospheric forcing of early Holocene ice shelf retreat, George VI Ice Shelf, Antarctica Peninsula. *Quaternary Science Reviews* **26,** 500-516.

Smith, J. A., Bentley, M. J., Hodgson, D. A., and Cook, A. J. (2007b). George VI Ice Shelf: past history, present behaviour and potential mechanisms for future collapse. *Antarctic Science* **19,** 131-142.

Smith, J. A., Hodgson, D. A., Bentley, M. J., Verleyen, E., Leng, M. J., and Roberts, S. J. (2006). Limnology of two antarctic epishelf lakes and their potential to record periods of ice shelf loss. *Journal of Paleolimnology* **35,** 373-394.

Smith Jr., W. O., and Nelson, D. M. (1986). Importance of ice-edge phytoplankton production in the Southern Ocean. *BioScience* **36,** 251-356.

Smith, K. L. J., Robison, B. H., Helly, J. J., Kaufmann, R. S., Ruhl, H. A., Shaw, T. J., Twining, B. S., and Vernet, M. (2007c). Free-Drifting Icebergs: Hot Spots of Chemical and Biological Enrichment in the Weddell Sea. *Science* **317,** 478-482.

Smith, R. C., Dierssen, H. M., and Vernet, M. (1996a). Phytoplankton biomass and productivity in the western Antarctic Peninsula. *In* "Foundations for Ecological Research West of the Antarctic Peninsula." (R. M. Ross, E. E. Hofmann, and L. B. Quetin, Eds.), pp. 333-356. Antarctic Research Series.

Smith, R. C., Stammerjohn, S. E., and Baker, K. (1996b). Surface air temperature variations in the western Antarctic Peninsula region. *In* "Foundations for Ecological Research West of the Antarctic Peninsula." (R. M. Ross, E. E. Hofmann, and L. B. Quetin, Eds.), pp. 105-121. Antarctic Research Series.

Smith, W. O. J., and Sakshaug, E. (1990). Polar Phytoplankton. *In* "Polar Oceanography, Part B: Chemistry, Biology and Geology." (W. O. J. Smith, Ed.), pp. 477-525. Academic Press.

Sneath, P. H. A., and Sokal, R. R. (1973). "Numerical Taxonomy." W.H. Freeman and Company, San Francisco.

Squier, A. H. (2003). "Pigments of photoautotrophs in lake sediments from the Larsemann Hills, east Antarctica." University of York. PhD thesis.

Squier, A. H., Hodgson, D. A., and Keely, B. J. (2002). Sedimentary pigments as markers for environmental change in an Antarctic lake. *Organic Geochemistry* **33,** 1655-1665.

Squier, A. H., Hodgson, D. A., and Keely, B. J. (2005). Evidence of late Quaternary environmental change in a continental east Antarctic lake from lacustrine sedimentary pigment distributions. *Antarctic Science* **17,** 361-376.

Stammerjohn, S., Martinson, D. G., Smith, R. C., Yuan, X., and Rind, D. (2008a). Trends in Antarctic annual sea ice retreat and advance and their relation to El Nino-Southern Oscillation and Southern Annular Mode variability. *Journal of Geophysical Research* **113,** doi:10.1029/2007JC004269.

Stammerjohn, S., and Smith, R. C. (1996). Spatial and temporal variability of western Antarctic Peninsula sea ice coverage. *In* "Foundations for ecological research west of the Antarctic Peninsula." pp. 81-104. American Geophysical Union.

Stammerjohn, S. E., Drinkwater, M. R., Smith, R. C., and Liu, X. (2003). Ice-atmosphere interactions during sea-ice advance and retreat in the western Antarctic Peninsula region. *Journal of Geophysical Research-Oceans* **108,** ISI:000186199300002.

Stammerjohn, S. E., Martinson, D. G., Smith, R. C., and Iannuzzi, R. A. (2008b). Sea ice in the western Antarctic Peninsula region: Spatio-temporal variability from ecological and climate change perspectives. *Deep Sea Research Part II: Topical Studies in Oceanography* **55,** 2041-2058.

Steig, E. J. (2006). Climate change: The south-north connection. *Nature* **444,** 152-153.

Steig, E. J., Brook, E. J., White, J. W. C., Sucher, C. M., Bender, M. L., Lehman, S. J., Morse, D. L., Waddington, E. D., and Clow, G. D. (1998). Synchronous climate changes in Antarctica and the North Atlantic. *Science* **282,** 92-95.

Stenni, B., Masson-Delmotte, V., Johnsen, S., Jouzel, J., Longinelli, A., Monnin, E., Rothlisberger, R., and Selmo, E. (2001). An Oceanic Cold Reversal During the Last Deglaciation. *Science* **293,** 2074-2077.

Stephens, B. B., and Keeling, R. F. (2000). The influence of Antarctic sea ice on glacial-interglacial CO_2 variations. *Nature* **404,** 171-174.

Sterken, M. (2009). "A paleolimnological reconstruction of Late-Quaternary environmental change along a transect from South America to the Antarctic Peninsula." Universiteit Gent. PhD thesis.

Sterken, M., Verleyen, E., Sabbe, K., Terryn, G., Charlet, F., Bertrand, S., Boe?s, X., Fagel, N., De Batist, M., and Vyverman, W. (2008). Late Quaternary climatic changes in southern Chile, as recorded in a diatom sequence of Lago Puyehue (40°40? S). *Journal of Paleolimnology* **39,** 219-235.

Stickley, C. E., Pike, J., Leventer, A., Dunbar, R., Domack, E. W., Brachfeld, S., Manley, P., and McClennan, C. (2005). Deglacial ocean and climate seasonality in laminated diatom sediments, Mac.Robertson Shelf, Antarctica. *Palaeogeography, Palaeoclimatology, Palaeoecology* **227,** 290-310.

Stocker, T. F., and Wright, D. G. (1996). Rapid changes in ocean circulation and atmospheric radiocarbon. *Paleoceanography* **11,** 773-795.

Stockwell, D. A., and Hargraves, P. E. (1984). Morphological variability within resting spores of the marine diatom genus Chaetoceros Ehrenberg. *In* "Proceedings of the Eighth International Diatom Symposium, Paris, Koenigstein." pp. 81–95.

Stockwell, D. A., Kang, S. H., and Fryxell, G. A. (1991). Comparisons of diatom biocoenoses with Holocene sediment assemblages in Prydz Bay, Antarctica. *In* "Proceedings of the Ocean Drilling Program, Scientific Results." (J. Barron, and B. Larsen, Eds.), pp. 667-673.

Stone, J. O., Balco, G. A., Sugden, D. E., Caffee, M. W., Sass Iii, L. C., Cowdery, S. G., and Siddoway, C. (2003). Holocene deglaciation of Marie Byrd Land, West Antarctica. *Science* **299,** 99-102.

Stonehouse, B. (2002). Encyclopedia of Antarctica and the southern oceans, pp. 391. Wiley, Chichester.

Stössel, A., Yang, K., and Kim, S.-J. (2002). On the Role of Sea Ice and Convection in a Global Ocean Model. *Journal of Physical Oceanography* **32,** 1194-1208.

Stott, L., Timmermann, A., and Thunell, R. (2007). Southern Hemisphere and Deep-Sea Warming Led Deglacial Atmospheric CO2 Rise and Tropical Warming. *Science* **318,** 435-438.

Stuiver, M. (1961). Variations in radiocarbon concentration and sunspot activity. *Journal of Geophysical Research* **66,** 273-276.

Stuiver, M., Braziunas, T. F., Becker, B., and Kromer, B. (1991). Climatic, solar, oceanic, and geomagnetic influences on late-glacial and holocene atmospheric 14C 12C change. *Quaternary Research* **35,** 1-24.

Stuiver, M., Denton, G.-H., Hughes, T. J., and Fastook, J. L. (1981). History of the marine ice sheet in West Antarctica during the last deglaciation: A working hypothesis. *In* "The Last Great Ice Sheets." (G. H. Denton, and T. J. Hughes, Eds.), pp. 319-436. John Wiley & Sons, New York.

Stuiver, M., and F., B. T. (1993). Modeling atmospheric ^{14}C influences and ^{14}C ages of marine samples back to 10,000 BC. *Radiocarbon* **35,** 137-189.

Stuiver, M., and Quay, P. D. (1980). Changes in atmospheric carbon-14 attributed to a variable Sun. *Science* **207,** 11-19.

Stuiver, M., and Reimer, P. J. (1993). Extended 14C database and revised CALIB radiocarbon calibration program. *Radiocarbon* **35,** 215-230.

Stuiver, M., Reimer, P. J., and Reimer, R. (2005). CALIB Manual.

Suess, H. E., and Revelle, R. (1957). Carbon dioxide exchange between the atmosphere and ocean and the question of an increase of atmospheric CO_2 during the past decades. *Tellus* **9,** 18-27.

Sugden, D. E., Bentley, M. J., and Ó Cofaigh, C. (2006). Geological and geomorphological insights into Antarctic ice sheet evolution. *Philosophical Transactions of the Royal Society A* **364,** 1607-1625.

Sugden, D. E., and Clapperton, C. M. (1980). West Antarctic Ice Sheet fluctuations in the Antarctic Peninsula area. *Nature* **286,** 378-381.

Sugden, D. E., Marchant, D. R., and Denton, G. H. (1993). The Case for a Stable East Antarctic Ice Sheet: The Background. *Geografiska Annaler. Series A, Physical Geography* **75,** 151-154.

Sullivan, C. W., Arrigo, K. R., McClain, C. R., Comiso, J. C., and Firestone, J. (1993). Distributions of Phytoplankton Blooms in the Southern Ocean. *Science* **262,** 1832-1837.

T

Talbot, H. M., Head, R. N., Harris, R. P., and Maxwell, J. R. (1999). Distribution and stability of steryl chlorin esters in copepod faecal pellets from diatom grazing. *Organic Geochemistry* **30,** 1163-1174.

Tanimura, Y. (1992). Distribution of diatom species in the surface sediments of Lützow Holm Bay, Antarctica. *In* "Centenary of Japanese Micropaleontology." (K. Ishizaki, and T. Saito, Eds.), pp. 399–411.

Taylor, F., and Leventer, A. (2003). Late Quaternary palaeoenvironments in Prydz Bay, East Antarctica: interpretations from marine diatoms. *Antarctic Science* **15,** 512-521.

Taylor, F., and McMinn, A. (2001). Evidence from diatoms for Holocene climate fluctuation along the East Antarctic margin. *Holocene* **11,** 455-466.

Taylor, F., and McMinn, A. (2002). Late Quaternary diatom assemblages from Prydz Bay, eastern Antarctica. *Quaternary Research* **57,** 151-161.

Taylor, F., McMinn, A., and Franklin, D. (1997). Distribution of diatoms in surface sediments of Prydz Bay, Antarctica. *Marine Micropaleontology* **32,** 209-229.

Taylor, F., and Sjunneskog, C. (2002). Postglacial marine diatom record of the Palmer Deep, Antarctic Peninsula (ODP Leg 178, Site 1098). *Palaeoceanography* **17,** 10.1029/2000PA000564.

Taylor, F., Whitehead, J., and Domack, E. (2001). Holocene paleoclimate change in the Antarctic Peninsula: evidence from the diatom, sedimentary and geochemical record. *Marine Micropaleontology* **41,** 25-43.

Thoma, M., Jenkins, A., Hollander, D., and Jacobs, S. (2008). Modelling Circumpolar Deep Water intrusions on the Amundsen Sea continental shelf, Antarctica. *Geophysical Research Letters* **35,** L18602.

Thomas, D. N., and Dieckmann, G. S. (2002). Antarctic Sea Ice--a Habitat for Extremophiles. *Science* **295,** 641-644.

Thomas, D. N., and Papadimitriou, S. (2003). Biochemistry of sea ice. *In* "Sea Ice: An introduction to its physics, chemistry, biology and geology." (D. N. Thomas, and G. S. Dieckmann, Eds.), pp. 267-302. Blackwell Science.

Thomas, R. H. (1979). The dynamics of marine ice sheets. *Journal of Glaciology* **24,** 167-177.

Timmermann, A., Krebs, U., Justino, F., Goosse, H., and Ivanochko, T. (2005). Mechanisms for millennial-scale global synchronization during the last glacial period. *Paleoceanography* **20,** 10.1029/2004PA001090.

Toggweiler, J. R. (1999). Variation of atmospheric CO2 by ventilation of the ocean's deepest water. *Paleoceanography* **14,** 571-588.

Toggweiler, J. R. (2009). CLIMATE CHANGE: Shifting Westerlies. *Science* **323,** 1434-1435.

Torsvik, T. H., Gaina, C., and Redfield, T. F. (2007). Antarctica and global paleogeography: from Rodinia, through Gondwanaland and Pangea, to the birth of the Southern Ocean and the opening of gateways. *In* "10th International Symposium of Antarctic Earth Sciences. Antarctica: A keystone in a Changing World." (A. K. Cooper, P. J. Barrett, H. Stagg, B. Storey, E. Stump, and W. Wise, Eds.), pp. 125-140. The National Academies Press, University of California, Santa Barbara.

Tortell, P. D., Rau, G. H., and Morel, F. M. M. (2000). Inorganic carbon acquisition in coastal Pacific phytoplankton communities. *Limnology and Oceanography* **45,** 1485-1500.

Tortell, P. D., Reinfelder, J. R., and Morel, F. M. M. (1997). Active uptake of bicarbonate by diatoms. *Nature* **390,** 243-244.

Tréguer, P., and Jacques, G. (1992). Dynamics of nutrients and phytoplankton, and fluxes of carbon, nitrogen and silicon in the Antarctic Ocean. *Polar Biology* **12,** 149-162.

Tréguer, P., Kamatani, A., Gueneley, S., and Queguiner, B. (1989). Kinetics of dissolution of Antarctic diatom frustules and the biogeochemical cycle of silicon in the Southern Ocean. *Polar Biology* **9,** 397-403.

Troedson, A. L., and Riding, J. B. (2002). Upper Oligocene to Lowermost Miocene Strata of King George Island, South Shetland Islands, Antarctica: Stratigraphy, Facies Analysis, and Implications for the Glacial History of the Antarctic Peninsula. *Journal of Sedimentary Research* **72,** 510-523.

Truesdale, R. S., and Kellogg, T. B. (1979). Ross Sea Diatoms: Modern assemblage distributions and their relationship to ecologic, oceanographic and sedimentary conditions. *Marine Micropaleontology* **4,** 13-31.

Trull, T. W., and Armand, L. (2001). Insights into Southern Ocean carbon export from the d13C of particles and dissolved inorganic carbon during the SOIREE iron release experiment. *Deep Sea Research, Part II,* **48,** 2655-2680.

Turner, J., Colwell, S. R., Marshall, G. J., Lachlan-Cope, T. A., Carleton, A. M., Jones, P. D., Lagun, V., Reid, P. A., and Iagovkina, S. (2005). Antarctic climate change during the last 50 years. *International Journal of Climatology* **25,** 279-294.

Turner, J. T. (2002). Zooplankton fecal pellets, marine snow and sinking phytoplankton blooms. *Aquatic Microbial Ecology* **27,** 57-102.

Turney, C. S. M., McGlone, M. S., and Wilmshurst, J. M. (2003). Asynchronous climate change between New Zealand and the North Atlantic during the last deglaciation. *Geology* **31,** 223-226.

Tushingham, A. M., and Peltier, W. R. (1991). Ice-3G: a new global model of late Pleistocene deglaciation based upon geophysical predictions of post-glacial relative sea level change. *Journal of Geophysical Research* **96,** 4497-4523.

V

van Beek, P., Reyss, J.-L., Paterne, M., Gersonde, R., van der Loeff, M. R., and Kuhn, G. (2002). ^{226}Ra in barite: Absolute dating of Holocene Southern Ocean sediments and reconstruction of sea-surface reservoir ages. *Geology* **30,** 731-734.

van Lipzig, N. P. M., King, J. C., Lachlan-Cope, T. A., and van den Broeke, M. R. (2004). Precipitation, sublimation, and snow drift in the Antarctic Peninsula region from a regional atmospheric model. *Journal of Geophysical Research* **109,** D24109.

Vargas-Ramirez, L., Roche, E., Gerrienne, P., and Hooghiemstra, H. (2008). A pollen-based record of late glacial–Holocene climatic variability in the southern lake district, Chile. *Journal of Paleolimnology* **39,** 197-217.

Vaughan, D. G. (1993). Implications of the break-up of Wordie Ice Shelf, Antarctica for sea level. *Antarctic Science* **5,** 403-408.

Vaughan, D. G. (2008). Press Release - Antarctic ice shelf 'hangs by a thread' (BAS Press Department, Ed.), Cambridge, U.K.

Vaughan, D. G., and Doake, C. S. M. (1996). Recent atmospheric warming and retreat of ice shelves on the Antarctic Peninsula. *Nature* **379,** 328-331.

Vaughan, D. G., Marshall, G. J., Connolley, W. M., Parkinson, C., Mulvaney, R., Hodgson, D. A., King, J. C., Pudsey, C. J., and Turner, J. (2003). Recent rapid regional climate warming on the Antarctic Peninsula. *Climatic Change* **60,** 243-274.

Vaughan, D. G., and Spouge, J. R. (2002). Risk Estimation of Collapse of the West Antarctic Ice Sheet. *Climatic Change* **52,** 65-91.

Vellinga, M., and Wood, R. A. (2002). Global climatic impacts of a collapse of the Atlantic thermohaline circulation. *Climate Change* **54,** 251-267.

Venegas, S. A., and Drinkwater, M. R. (2001). Sea ice, atmosphere and upper ocean variability in the Weddell Sea, Antarctica. *Journal of Geophysical Research-Oceans* **106,** 16747-16765.

Villareal, T. A. (1988). Positive buoyancy in the oceanic diatom Rhizosolenia debyana H. Peragallo. *Deep-Sea Research Part A - Oceanographic Research Papers* **35,** 1037-1045.

Villareal, T. A., and Fryxell, G. A. (1983). Temperature effects of the valve structure of the bipolar diatoms *Thalassiosira antarctica* and *Porosira glacialis*. *Polar Biology* **2,** 163-169.

Villareal, T. A., Woods, S., J.K., M., and Culver-Rymsza, K. (1996). Vertical migration of Rhizosolenia mats and their significance to NO3- fluxes in the central North Pacific gyre. *Journal of Plankton Research* **18,** 1103-1121.

Von Gyldenfeldt, A. B., Fahrbach, E., Garcia, M. A., and Schroder, M. (2002). Flow variability at the tip of the Antarctic Peninsula. *Deep-Sea Research Part II: Topical Studies in Oceanography* **49,** 4743-4766.

Vostok. Federal Program, World Ocean, Antarctic Research and Investigation, Subprogram Russian Antarctic Expedition. http://www.aari.aq

W

Wadhams, P. (2000). "Ice in the Ocean." Gordon and Breach Science Publishers, Amsterdam.

Wallace, M. I., Meredith, M. P., Brandon, M. A., Sherwin, T. J., Dale, A., and Clarke, A. (2008). On the characteristics of internal tides and coastal upwelling behaviour in Marguerite Bay, west Antarctic Peninsula. *Deep Sea Research Part II: Topical Studies in Oceanography* **55,** 2023-2040.

Walther, G.-R., Post, E., Convey, P., Menzel, A., Parmesan, C., Beebee, T. J. C., Fromentin, J.-M., Hoegh-Guldberg, O., and Bairlein, F. (2002). Ecological responses to recent climate change. *Nature* **416,** 389-395.

Warner, N. R., and Domack, E. W. (2002). Millennial- to decadal-scale paleoenvironmental change during the Holocene in the Palmer Deep, Antarctica, as recorded by particle size analysis. *Paleoceanography* **17**.

Watanabe, K. (1982). Centric diatom communities found in the Antarctic sea ice. *Antarctic Record, National Institute of Polar Research* **7,** 119-126.

Watanabe, O., Jouzel, J., Johnsen, S., Parrenin, F., Shoji, H., and Yoshida, N. (2003). Homogeneous climate variability across East Antarctica over the past three glacial cycles. *Nature* **422,** 509-512.

Weaver, P. P. E., and Schultheiss, P. J. (1990). Current methods for obtaining, logging and splitting marine sediment cores. *Marine Geophysical Researches* **12,** 85-100.

Weertman, J. (1974). Stability of the junction of an ice sheet and ice shelf. *Journal of Glaciology* **13,** 3-11.

Wefer, G., Fischer, G., Futterer, D. K., and Gersonde, R. (1988). Seasonal particle flux in the Bransfield Strait, Antarctica. *Deep Sea Research* **35,** 891-898.

Whitaker, T. M., and Richardson, M. G. (1980). Morphology and chemical composition of a natural population of an ice-associated Antarctic diatom Navicula glaciei. *Journal of Phycology* **16,** 250-257.

Whitehead, J. M., and McMinn, A. (1997). Paleodepth determination from Antarctic benthic diatom assemblages. *Marine Micropaleontology* **29,** 301-318.

Willmott, V., Domack, E. W., Canals, M., and Brachfeld, S. (2006). A high resolution relative paleointensity record from the Gerlache-Boyd paleo-ice stream region, northern Antarctic Peninsula. *Quaternary Research* **66,** 1-11.

Wolff, E. W., Fischer, H., Fundel, F., Ruth, U., Twarloh, B., Littot, G. C., Mulvaney, R., Rothlisberger, R., de Angelis, M., Boutron, C. F., Hansson, M., Jonsell, U., Hutterli, M. A., Lambert, F., Kaufmann, P., Stauffer, B., Stocker, T. F., Steffensen, J. P., Bigler, M., Siggaard-Andersen, M. L., Udisti, R., Becagli, S., Castellano, E., Severi, M., Wagenbach, D., Barbante, C., Gabrielli, P., and Gaspari, V. (2006). Southern Ocean

sea-ice extent, productivity and iron flux over the past eight glacial cycles. *Nature* **440,** 491-496.

Woodworth, M., Goni, M., Tappa, E., Tedesco, K., Thunell, R., Astor, Y., Varela, R., Diaz-Ramos, J. R., and Muller-Karger, F. (2004). Oceanographic controls on the carbon isotopic compositions of sinking particles from the Cariaco Basin. *Deep Sea Research I* **51,** 1955-1974.

Wright, S. W., and Jeffrey, S. W. (2006). Pigment markers for phytoplankton production. *In* "Marine Organic Matter: Biomarkers, Isotopes and DNA." (J. K. Volkman, Ed.), pp. 71-104. Springer-Verlag, Berlin.

Y

Yokohama, Y., Deckker, P. D., Lambeck, K., Johnson, P., and Fifield, L. K. (2001). Sea-level at the last glacial maximum: evidence from northwestern Australia to constrain ice volumes for oxygen isotope stage 2. *Palaeogeography Palaeoclimatology Palaeoecology* **165,** 281-297.

Yoon, H. I. (1999). Glaciomarine sediments on the Northern Antarctic peninsula's western continental shelf. *Korea Ocean Res. Dev. Inst. Open File Report* **BSPM 99027-00-1233-9,** 288-376.

Yoon, H. I., Khim, B. K., Yoo, K. C., Bak, Y. S., and Lee, J. I. (2007). Late glacial to Holocene climatic and oceanographic record of sediment facies from the South Scotia Sea off the northern Antarctic Peninsula. *Deep Sea Research Part II: Topical Studies in Oceanography* **54,** 2367-2387.

Yoon, H. I., Park, B. K., and al, e. (2002). Glaciomarine sedimentation and its paleoclimatic implications on the Antarctic Peninsula shelf over the last 15 000 years. *Palaeogeography, Palaeoclimatology, Palaeoecology* **185,** 235-254.

Z

Zachos, J. C., Breza, J. R., and Wise, S. W. (1992). Early Oligocene ice-sheet expansion on Antarctica: Stable isotope and sedimentological evidence from Kerguelen Plateau, southern Indian Ocean. *Geology* **20,** 569-573.

Zachos, J. C., Quinn, T. M., and Salamy, K. A. (1996). High-resolution (10^4 years) deep-sea foraminiferal stable isotope records of the Eocene-Oligocene climate transition. *Palaeoceanography* **11,** 251-266.

Zale, R. (1994). Changes in size of the Hope Bay Adélie penguin rookery as inferred from Lake Boeckella sediment. *Ecography* **17,** 297-304.

Zemmelink, H. J., Houghton, L., Dacey, J. W. H., Stefels, J., Koch, B. P., Schröder, M., Wisotzki, A., Scheltz, A., Thomas, D. N., Papadimitriou, S., Kennedy, H., Kuosa, H., and Dittmar, T. (2008). Stratification and the distribution of phytoplankton, nutrients, inorganic carbon, and sulfur in the surface waters of Weddell Sea leads. *Deep Sea Research Part II: Topical Studies in Oceanography* **55,** 988-999.

Zhou, M., Niiler, P. P., and Hu, J.-H. (2002). Surface currents in the Bransfield and Gerlache Straits, Antarctica. *Deep Sea Research Part I: Oceanographic Research Papers* **49,** 267-280.

Zielinski, U., and Gersonde, R. (1997). Diatom distribution in Southern Ocean surface sediments (Atlantic sector): Implications for paleoenvironmental reconstructions. *Palaeogeography, Palaeoclimatology, Palaeoecology* **129,** 213-250.

Zwally, H. J., Comiso, J. C., Parkinson, C. L., Cavalieri, D. J., and Gloersen, P. (2002). Variability of Antarctic sea ice 1979 - 1998. *Journal of Geophysical Research* **107,** 10.1029/2000JC000733

Zwally, H. J., Parkinson, C. L., and Comiso, J. C. (1983). Variability of Antarctic Sea Ice and Changes in Carbon-Dioxide. *Science* **220,** 1005-1012.

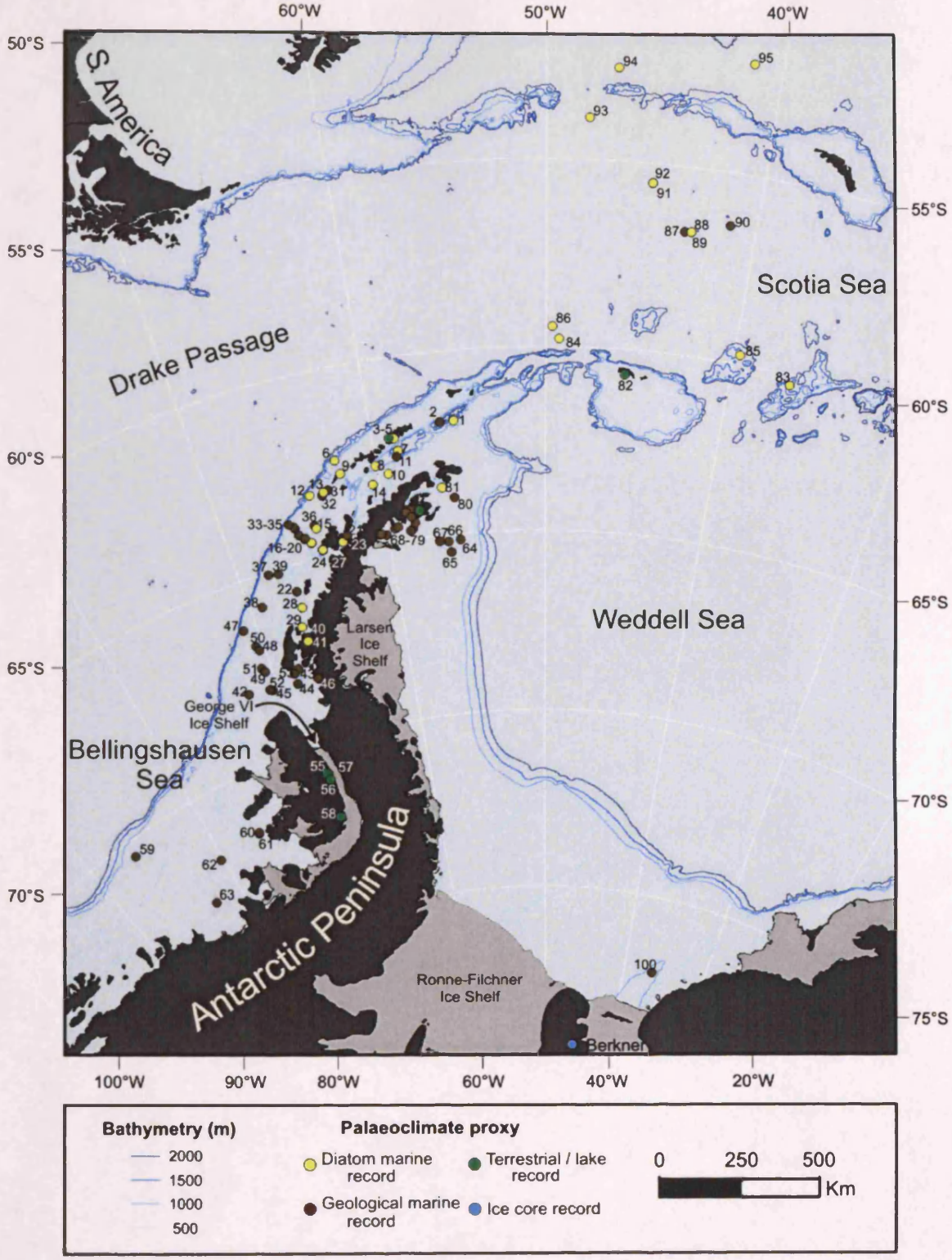


Figure A1.1
Palaeoclimate proxy records from the Antarctic Peninsula (AP), surrounding Weddell Sea, Bellingshausen Sea, Drake Passage and Scotia Sea, colour-coded based on the proxy used and numbered, with full details of each proxy record and the source publication in Table A1.1.

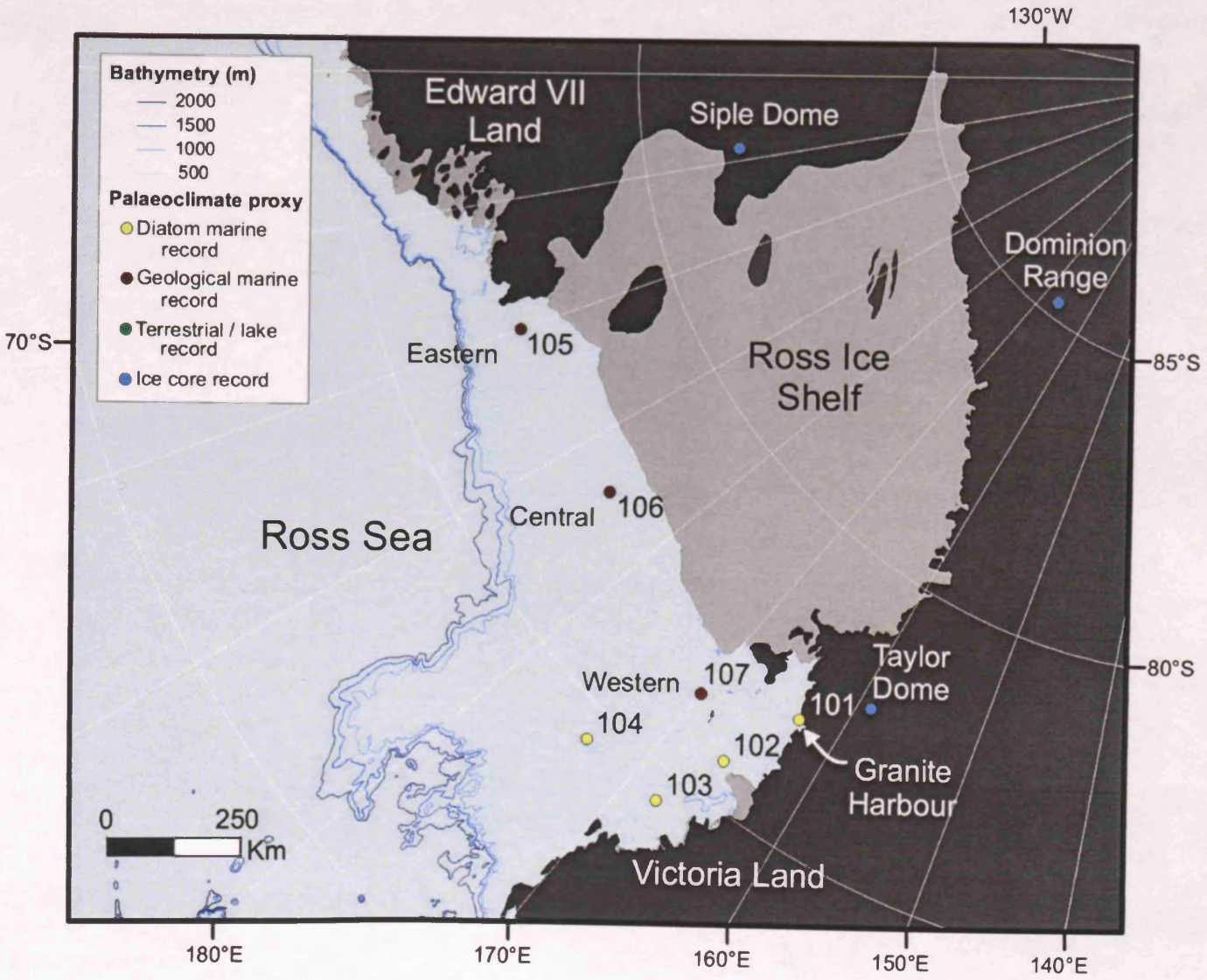


Figure A1.2
Palaeoclimate proxy records from the Ross Sea Embayment, colour-coded based on the proxy used and numbered, with full details of each proxy record and the source publication in Table A1.1. Numerous geophysical surveys and geological coring studies have been undertaken in the Ross Sea and are not all detailed on this map (see Anderson et al., 1980: 1984; Licht et al., 1996; 1999; Shipp et al., 1999; Anderson et al., 2002).

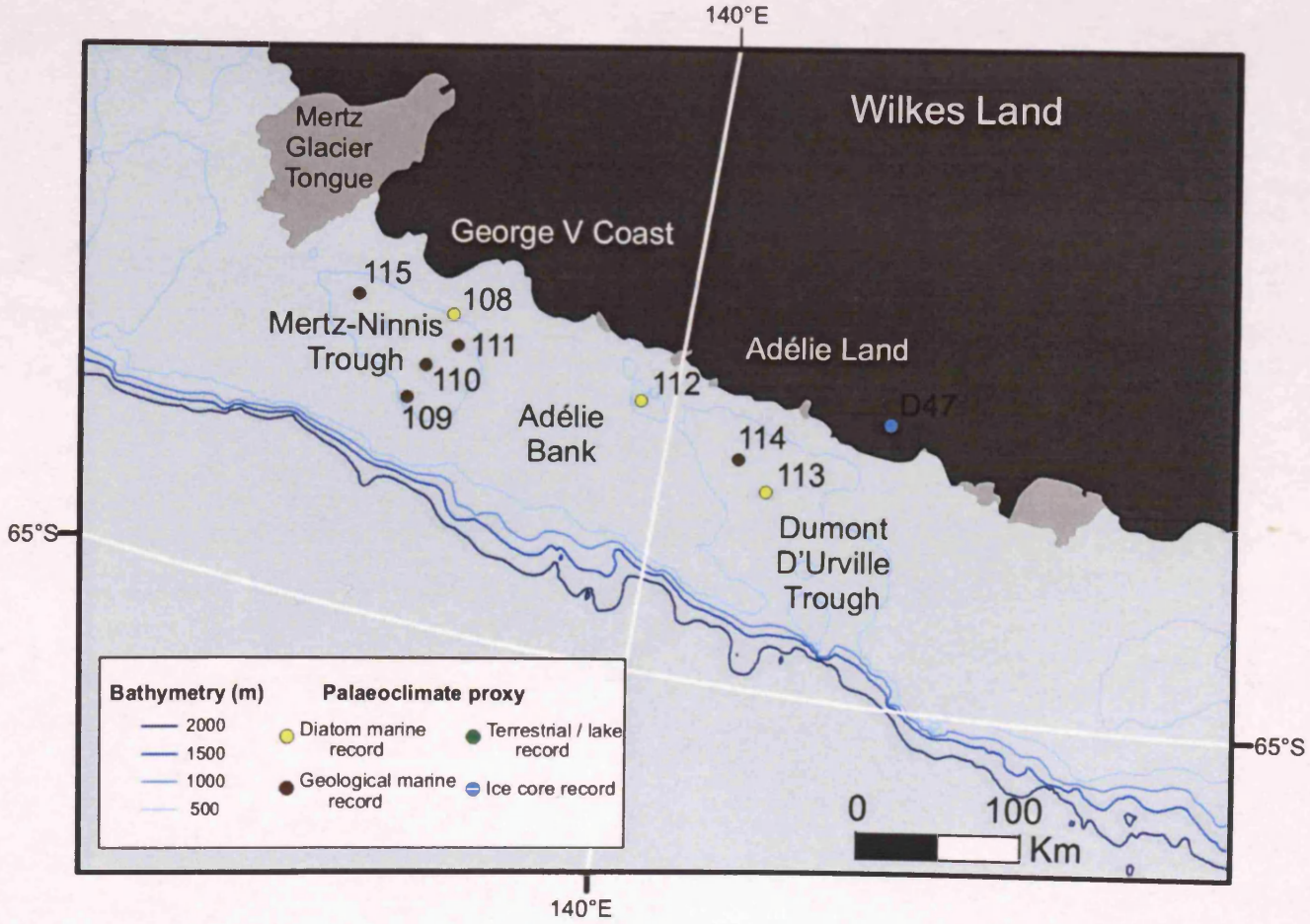


Figure A1.3
Palaeoclimate proxy records from the East Antarctic Margin, encompassing the George V and Adélie Coast, colour-coded based on the proxy used and numbered, with full details of each proxy record and the source publication in Table A1.1.

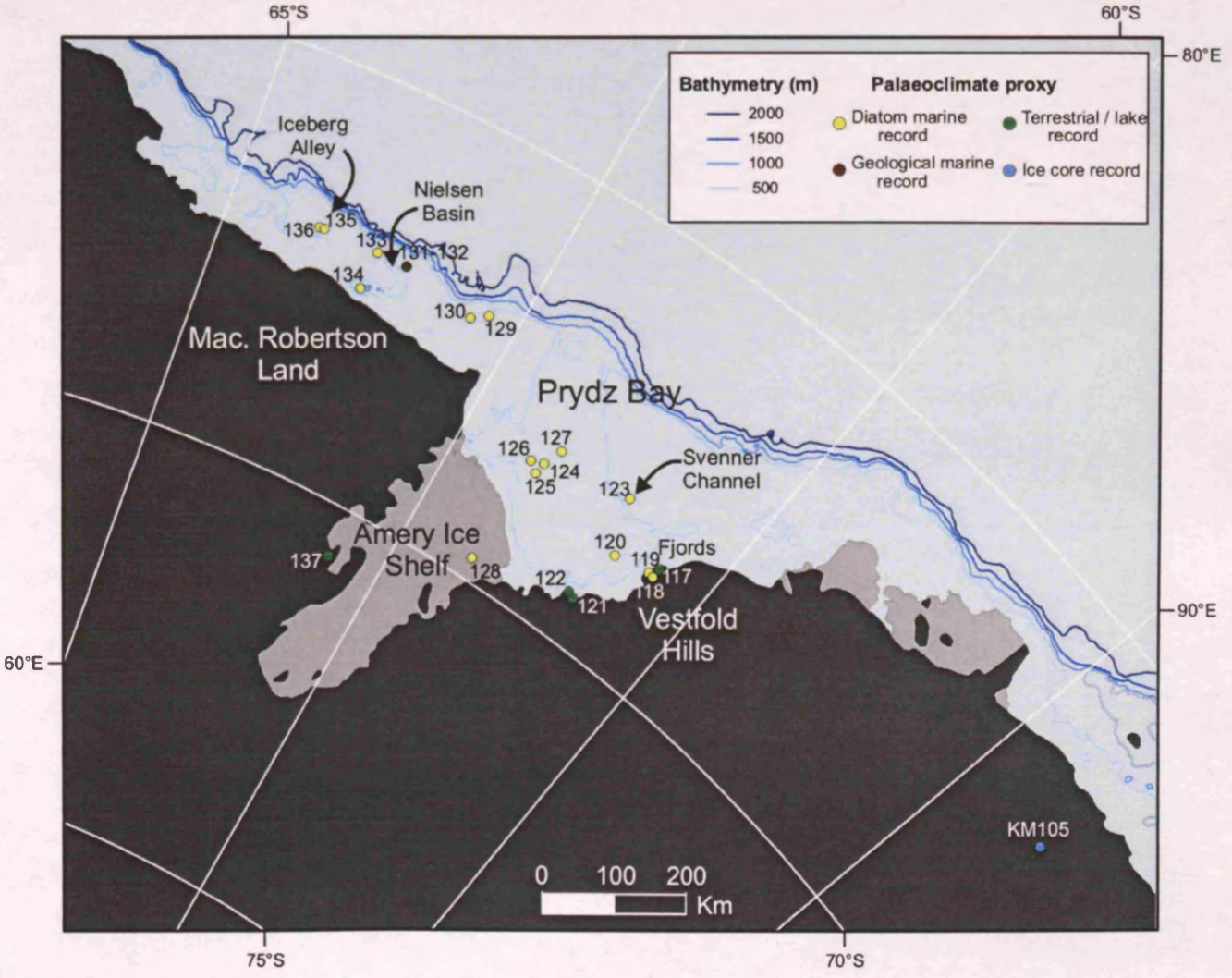


Figure A1.4
Palaeoclimate proxy records from the East Antarctic Margin, encompassing Prydz Bay and the Mac. Robertson Shelf, colour-coded based on the proxy used and numbered, with full details of each proxy record and the source publication in Table A1.1.

Table A1.1
Antarctic palaeoclimate records; original site identification, source publication and brief summary. Colour-coded on Figures A1.1 – A1.4: Diatom = yellow; Geological = brown; Terrestrial / lake = green; Ice core = blue.

Map ref	Proxy	Core / site ID	Reference	Summary of study
1	Diatom	Gebra-2	Bàrcena et al. (1998)	Micropalaeontological (diatoms and radiolarian) and geochemical analyses reveal a sequence of Neoglacial events over last 3000 yrs.
2	Geological	A9-EB2	Khim et al. (2002)	Late Holocene cyclically laminated (diatom-rich and terrigenous) sediments identify several Neoglacial events, the Little Ice Age and Medieval Warm Period.
3	Diatom	MC-01	Yoon et al. (2004)	Fjord sediment cores from King George Island containing diamicton, which documenting advance of the glacier front at ~1700 yrs BP.
4	Terrestrial / lake	LS-1	Lee et al. (2008)	Lake sediment record from King George Island, with fluctuations in the diatom community recording Late Holocene climate oscillations.
5	Diatom	PC-01	Yoon et al. (2004)	Same study as record number 3.
6	Diatom	NCS 09	Yoon et al. (2002)	Full Holocene diatom record, focusing on sediment properties and foraminiferal assemblage, with the latter documenting periodic influence of more corrosive Weddell Sea water into the area.
7	Diatom	Gebra-1	Bàrcena et al. (1998)	Same study as record number 1.
8	Diatom	A-6	Bàrcena et al. (2002; 2006)	Micropalaeontological (diatoms and radiolarian) and geochemical analyses reveal a sequence of Neoglacial events over last 3000 yrs, overprinted by high frequency (solar?) cycles (200-300 yr).
9	Diatom	GC 114	Moreton (1999); This study	Volcanic glass shards within the sediment analysed for major element compositions to assess potential tephrachronological correlations
10	Diatom	A-3	Barcena et al. (2002; 2006)	Same study as record number 8.
11	Geological	DF82-48	Banfield and Anderson, (1995)	Reconstruction of the glacial history of Bransfield Strait from seismic data.
12	Diatom	GC 03	Yoon et al. (2002)	Full Holocene diatom record, focusing on sediment properties and diatom assemblage, documenting warm period between 6000 and 2500 yr BP, followed by Late Holocene cooling.
13	Diatom	GC 1702	Yoon et al. (2002)	Same study as record number 12.
14	Diatom	NBP_PC61	Heroy et al. (2008)	Full Holocene diatom record, identifying five separate climate regimes, most notably a significantly shorter Mid Holocene Climatic Optimum (6800 – 5900 cal. yr BP).

15	Diatom	GC 02	Yoon et al. (2002)	Same study as record number 12.
16	Geological	GC 51	Pudsey et al. (1994)	Geophysical survey and marine coring, revealing timing of deglaciation and rapid retreat style of ice sheet across the outer and middle shelf of the WAP.
17	Geological	TC 48	Pudsey et al. (1994)	Same study as record number 16.
18	Diatom	GC 047	Pudsey et al. (1994); This study	Same study as record number 16.
19	Geological	TC 46	Pudsey et al. (1994)	Same study as record number 16.
20	Geological	GC049	Pudsey et al. (1994)	Same study as record number 16.
21	Geological	PC83	Harden et al. (1992)	Assessing Antarctic sediment chronologies using ^{210}Pb and ^{14}C dating methods.
22	Geological	PD88-42	Pope and Anderson, (1992)	Reconstruction of the timing of retreat of AP Ice Sheet since the LGM.
23	Diatom	NBP_KC18B&C	Domack et al. (2001)	Incorporated in the Palmer Deep multi-proxy study (see record number 24).
24	Diatom	ODP-1098C	Domack et al. (2001); Sjunneskog and Taylor (2002); Taylor and Sjunneskog (2002)	Ultra-high resolution record of Holocene palaeoclimate variability. Multi-proxy approach (sedimentology; diatoms; geochemistry; foraminifera) revealing five distinctive climate phases (as described in Chapter 2.3.2.3).
25	Diatom	PD92 30	Leventer et al. (1996)	Sedimentary, geochemical and diatom data reveals long-term Holocene climate variability, superimposed by 200-300 year cycles of productivity.
26	Diatom	LMG_KC1	Domack et al. (2001); Shevenell & Kennett (2002)	Same study as record number 24. Sedimentological and geochemical evidence for Late Holocene oceanographic fluctuations (UCDW and shelf waters) (Shevenell and Kennett, 2002).
27	Diatom	PC 92-30	Leventer et al. (2002); Shevenell and Kennett (2002)	Characterisation of the diatom composition in laminations from Palmer Deep record, with differences observed at glacial-interglacial transition and in Early Holocene (Leventer et al., 2002). Same study as record number 26 (Shevenell and Kennett, 2002).
28	Diatom	NBP_KC3	Domack et al. (2001)	Incorporated in the Palmer Deep multi-proxy study (see record number 24).
29	Diatom	NBP_KC1	Domack et al. (2001)	Incorporated in the Palmer Deep multi-proxy study (see record number 24).
30	Diatom	ODP-1098A	Maddison et al. (2005)	Deglacial laminated diatom record from Palmer Deep, reconstructing seasonal and sub-seasonal cycles in diatom productivity and assemblage composition.

31	Geological	PC-20	Heroy and Anderson, (2007)	Reconstruction of the timing of retreat of AP Ice Sheet since the LGM.
32	Geological	PC-22	Heroy and Anderson, (2007)	Same study as record number 31.
33	Geological	PC-25	Heroy and Anderson, (2007)	Same study as record number 31.
34	Geological	KC-26	Heroy and Anderson, (2007)	Same study as record number 31.
35	Geological	PC-24	Heroy and Anderson, (2007)	Same study as record number 31.
36	Geological	PC-23	Heroy and Anderson, (2007)	Same study as record number 31.
37	Geological	PC-55	Heroy and Anderson, (2007)	Same study as record number 31.
38	Geological	PC-30	Heroy and Anderson, (2007)	Same study as record number 31.
39	Geological	PC-57	Heroy and Anderson, (2007)	Same study as record number 31.
40	Geological	KC 72	Domack et al. (1995)	Late Holocene advance of Muller Ice Shelf across Lallemand Fjord, revealed through sedimentological, geochemical and foraminiferal data, during period of Little Ice Age, but attributed to exclusion of CDW in the fjord.
41	Diatom	PD92 GC1	Shevenell et al. (1996); Taylor et al. (2001)	Full Holocene record from Lallemand Fjord, using sedimentolgical, diatom and geochemical approaches to document climate variability over this period.
42	Geological	PC-52	Heroy and Anderson, (2007)	Same study as record number 31.
43	Geological	PC-48	Heroy and Anderson, (2007)	Same study as record number 31.
44	Geological	PC-49	Heroy and Anderson, (2007)	Same study as record number 31.
45	Geological	KC-51	Heroy and Anderson, (2007)	Same study as record number 31.
46	Geological	JPC-43	Heroy and Anderson, (2007)	Same study as record number 31.
47	Geological	NBP_PC76	Pope & Anderson (1992)	Same study as record number 22.
48	Geological	PD88-85	Pope & Anderson (1992)	Same study as record number 22.
49	Geological	PD88-99	Pope & Anderson (1992)	Same study as record number 22.
50	Geological	VC 304	Ó Cofaigh et al. (2005a)	Geophysical and geological data to reconstruct the configuration of a palaeo-ice stream that drained the AP Ice Sheet through Marguerite Bay during the last glacial cycle.
51	Geological	VC 307	Ó Cofaigh et al. (2005a)	Same study as record number 50.
52	Geological	VC 306	Ó Cofaigh et al. (2005a); This study	Same study as record number 50.
53	Geological	PC 111	Harden et al. (1992)	Same study as record number 21.
54	Geological	PC 112	Harden et al. (1992)	Same study as record number 21.

55	Terrestrial / lake	MLNB Core	Smith et al. (2007)	Epishelf lake record from Alexander Island to provide Holocene history of George VI Ice Shelf, using micropalaeontological, geochemical and sedimentological approaches. Highlighted the early Holocene absence of the ice shelf.
56	Terrestrial / lake	ML core	Smith et al. (2007); Roberts et al. (2008)	Same study as record number 55.
57	Terrestrial / lake	Ablation Lake	Roberts et al. (2008)	Building on the epishelf lake study of record number 55, integrating clast distribution and provenance data to support Holocene history of George VI Ice Shelf proposed.
58	Terrestrial / lake	Citadel Bastion	Roberts et al. (2008)	Same study as record number 57.
59	Geological	GC 374	Hillenbrand et al. (2006)	Geophysical and geological study assessing glacial-interglacial changes and the presence of large outlet drainage basins during late Quaternary glacial periods.
60	Geological	GC 359	Hillenbrand et al. (2007)	Same study as record number 59.
61	Geological	GC 358	Hillenbrand et al. (2007)	Same study as record number 59.
62	Geological	GC357	Hillenbrand et al. (2007)	Same study as record number 59.
63	Geological	GC 366	Hillenbrand et al. (2007)	Same study as record number 59.
64	Geological	VC 338	Evans et al. (2005)	Geophysical and geological study to reconstruct the glacial history, flow-dynamics and sedimentation of the AP Ice Sheet along its eastern margin.
65	Geological	VC 324	Evans et al. (2005)	Same study as record number 64.
66	Geological	VC 340	Evans et al. (2005)	Same study as record number 64.
67	Geological	VC 326	Evans et al. (2005)	Same study as record number 64.
68	Geological	VC 263	Evans et al. (2005)	Same study as record number 64.
69	Geological	VC 267	Pudsey et al. (2006); Evans et al. (2005)	Deglaciation history of the northern Larsen area from geological data and Mid Holocene break-up of the Prince Gustav Channel Ice Shelf from ice-rafted debris provenance studies and foraminiferal assemblages.
70	Geological	VC 256	Pudsey et al. (2006); Evans et al. (2005)	Same study as record number 69.
71	Geological	VC 247	Pudsey et al. (2006); Evans et al. (2005)	Same study as record number 69.
72	Geological	VC 270	Pudsey et al. (2006)	Same study as record number 69.
73	Geological	VC 275	Pudsey et al. (2006); Evans et al. (2005)	Same study as record number 69.
74	Geological	VC 276	Pudsey et al. (2006)	Same study as record number 69.
75	Geological	VC 244	Pudsey and Evans (2001)	Geophysical and geological study addressing questions on about past stability of the Prince Gustav

				Channel Ice Shelf. Using ice-rafted debris provenance analysis concluded that during the mid-Holocene (5000 – 2000 yr BP) the ice shelf was absent.
76	Geological	VC 236	Pudsey and Evans (2001)	Same study as record number 75.
77	Geological	VC 243	Pudsey and Evans (2001); This study	Same study as record number 75.
78	Geological	VC 237	Pudsey and Evans (2001); This study	Same study as record number 75.
79	Geological	KC-23	Brachfeld et al. (2003)	Holocene history of Larsen-A reconstructed using palaeomagnetic geointensity dating.
80	Geological	PC 04	Heroy and Anderson, (2007)	Same study as record number 31.
81	Diatom	VC 205	This study	
82	Terrestrial / lake	Signy Lakes	Jones et al. (2000)	Lake sediments from Signy Island containing macrofossil, diatom and pollen data to suggest a Holocene climatic optimum between 3800 – 1300 yr BP.
83	Diatom	PC287	Allen (2003)	Diatom record revealing palaeoceanographic changes in the Scotia Sea since the LGM, with reconstructions of the winter and summer sea ice limits.
84	Diatom	SS-01	Bak et al. (2007); Yoon et al. (2007)	Sedimentological, geochemical and micropalaeontological analyses to reconstruct sea ice coverage and oceanographic variability from the LGM and through the Holocene, highlighting Mid Holocene climatic optimum and Neoglacial.
85	Diatom	PC034	Allen (2003)	Same study as record number 83.
86	Diatom	SS-02	Yoon et al. (2007)	Same study as record number 84.
87	Geological	PC 79	Moreton (1999)	Same study as record number 9.
88	Diatom	KC081	Allen (2003)	Same study as record number 83.
89	Geological	KC 81	Moreton (1999)	Same study as record number 9.
90	Geological	PC 29	Moreton (1999)	Same study as record number 9.
91	Diatom	PC078	Allen (2003)	Same study as record number 83.
92	Diatom	PC290	Allen (2003)	Same study as record number 83.
93	Diatom	PC063	Allen (2003)	Same study as record number 83.
94	Diatom	PC036	Allen (2003)	Same study as record number 83.
95	Diatom	KC073	Allen et al. (2005)	Diatom record proximal to the Polar Front, reconstructing frontal migration, sea ice extent and NADW migration through the Holocene from the LGM.
96	Diatom	TTN057-13-PC4	Hodell et al. (2001)	Diatom and IRD record highlighting cooling of SSTs and sea ice advance at ~5000 cal. yr BP, marking the end of the Hypsithermal and onset of Neoglacial in South Atlantic.
97	Diatom	ODP-177-1094	Bianchi and Gersonde (2004)	Diatom-based SST reconstructions and planktonic foraminifera stable isotopes for deglaciation and Holocene in region of Polar Front. Highlights timing of deglacial warming and sea ice retreat; Antarctic Cold Reversal; Early Holocene climatic optimum;

				expansion of the Weddell Sea Gyre.
98	Diatom	ODP-177-1093	Bianchi and Gersonde (2004)	Same study as record number 97.
99	Diatom	TN057-17	Nielsen et al. (2004)	Decadal-scale record of Holocene SST and sea ice extent for full Holocene. Out-of-phase behaviour to Holocene climate trends of WAP; no abrupt Neoglacial cooling.
100	Geological	Cray Trough, Eastern Weddell Sea	Bentley and Anderson (1998); Anderson et al. (2002)	Glacial-marine sediments dated by radiocarbon methods to reconstruct LGM extent of the EAIS and its subsequent retreat.
101	Diatom	Granite Harbor	Leventer et al. (1993)	Late Holocene (last 1250 years) climatic events revealed through analysis of diatom assemblage data. Medieval Warm Period and Little Ice Age identified.
102	Diatom	NBP9501-31	Cunningham et al. (1999)	Transect of cores reconstructing retreat of LGM grounding line. Holocene diatom assemblages used to highlight changing oceanographic conditions, with Mid- to Late-Holocene warming and cooler Late Holocene.
103	Diatom	NBP9501-37	Cunningham et al. (1999)	Same study as record number 102.
104	Diatom	NBP9501-39	Cunningham et al. (1999)	Same study as record number 102.
105	Geological	Eastern Ross Sea	Licht et al., (1996): (1999); Shipp et al., (1999); Anderson et al., (2002)	Extensive geophysical and geological surveys reconstructing LGM ice extent and timing of retreat. Eastern and Central Ross Sea draws ice from the WAIS, whereas Western Ross Sea nourished by EAIS; leads to differences in LGM ice and retreat histories.
106	Geological	Central Ross Sea	Licht et al., (1996): (1999); Shipp et al., (1999); Anderson et al., (2002)	Same studies as record number 105.
107	Geological	Western Ross Sea	Licht et al., (1996): (1999); Shipp et al., (1999); Anderson et al., (2002)	Same studies as record number 105.
108	Diatom	NBP0101-KC10A	Maddison et al. (2006)	Laminated diatom record used to assess annual cyclicity in diatom assemblages, reflecting seasonal changes in nutrients, oceanographic regime and Mertz Glacier Polynya.
109	Geological	11GC03	Presti et al. (2003)	Sedimentological approach to reconstruct evolution of Mertz Drift deposit from LGM and through Holocene, specifically bottom current activity and palaeoproductivity.
110	Geological	17PC02	Presti et al. (2003)	Same study as record number 109.
111	Geological	26PC12	Presti et al. (2003)	Same study as record number 109.
112	Diatom	MD03-2597	Maddison, (2006)	Laminated diatom record used to assess annual cyclicity in diatom assemblages.

113	Diatom	MD03-2601	Crosta et al (2005: 2007: 2008); Denis et al. (2006: 2009)	Diatom and isotope analysis reconstructing inter-annual to millennial changes in environmental conditions from laminated sections (Denis et al. 2006); Holocene climate and ocean variability (long- and short-term (Crosta et al. 2007); Holocene sea ice seasonality (Crosta et al. 2008); Holocene glacier and deep-water fluctuations (Denis et al., 2009).
114	Geological	Core 302	Domack et al. (1991)	Sedimentological evidence for Mid Holocene advance of East Antarctic outlet glaciers, with grounding lines advancing between 7000 – 4000 cal. yr BP.
115	Geological	DF79-12	Domack et al. (1991)	Same study as record number 114.
116	Geological	Windmill Islands	Hodgson et al. (2003)	Sedimentary pigment study of two nearshore marine cores, reconstructing expansion of the ice sheet during the last glacial cycle and Holocene climate variability.
117	Terrestrial / lake	Ace Lake	Roberts et al. (2001)	Late Holocene lake sediment record, utilising diatom-salinity transfer function to produce high-resolution record of evaporation.
118	Diatom	Ellis Fjord	McMinn et al. (2001)	Geochemical and diatom study of two fjord cores to reconstruct Late Holocene sea ice extent.
119	Diatom	Abel Bay; Platcha Bay	McMinn (2000)	Geochemical and diatom study of two fjord cores to reconstruct Late Holocene sea ice extent. Several diatom-based indices proposed: "fast ice index"; "benthic index"; and "snow index".
120	Diatom	KROCK-15-GC29	Taylor and McMinn (2002)	Diatom-based study spanning the last 21000 ^{14}C yrs, covering the LGM, glacial retreat and Holocene open marine sedimentation, under the influence of variable sea ice extent.
121	Terrestrial / lake	Progress Lake	Squier et al. (2005); Hodgson et al. (2006)	Lake sediment record, using biogeochemical (sedimentary pigments), biological and sedimentological proxies to reconstruct the coastal environment during the last interglacial (MIS5e), LGM and Holocene.
122	Terrestrial / lake	Kirisjes Pond	Squier et al. (2002)	Lake sediment record, utilising sedimentary pigment analysis to identify period of marine incursion during Mid Holocene and subsequent re-isolation of the lake basin.
123	Diatom	JPC24	Leventer et al. (2006)	Glacial diamict and Holocene diatom sediments, with the transition radiocarbon dated and marked by deglacial laminations, highlighting a period of elevated primary production.
124	Diatom	NBP01-01-KC29B	Taylor and Leventer (2003)	Diatom-bearing marine sediments recording four distinct periods of

				sedimentation: pre-LGM interstadial; LGM; pre-Holocene interstadial; and Holocene. The latter period contains evidence of a Mid Holocene climatic optimum and Neoglacial episodes.
125	Diatom	NBP01-01-KC32	Taylor and Leventer (2003)	Same study as record number 124.
126	Diatom	NBP01-01-KC31	Taylor and Leventer (2003)	Same study as record number 124.
127	Diatom	NBP01-01-KC30B	Taylor and Leventer (2003)	Same study as record number 124.
128	Diatom	AM02	Hemer and Harris (2003)	Sub ice-shelf sediment core containing full record of glacial retreat and Holocene diatom ooze. Increase in sea ice diatom species during Mid Holocene used to infer retreat of the ice shelf at this time.
129	Diatom	GC 5	Rathburn et al. (1997)	Diatom and stable isotope analyses used to indicate changes in sea ice patterns and oceanographic conditions over the past 8000 yrs, although the chronology is poorly constrained.
130	Diatom	GC 35	Rathburn et al. (1997)	Same study as record number 129.
131	Geological	49/12GC12	Harris and O'Brien (1998); Harris (2001)	Sedimentological analysis of biosiliceous sediments, which record periods of intense cross-lamination, used to infer episodic and spatial variable bottom water production during the Holocene.
132	Geological	149/39GC38	Harris and O'Brien (1998); Harris (2001)	Same study as record number 131.
133	Diatom	JPC40	Leventer et al. (2006)	Glacial diamict and Holocene diatom sediments, with the transition radiocarbon dated and marked by deglacial laminations, highlighting a period of elevated primary production.
134	Diatom	KROCK-128-GC2	Taylor and McMinn (2001)	Relatively uniform Holocene diatom sediments recording late glacial ice retreat and establishment of sea ice conditions comparable to today; no evidence of Mid- to Late-Holocene high productivity events.
135	Diatom	KROCK-125-GC1	Taylor and McMinn (2001)	Holocene diatom sediments, recording variable Holocene sea ice extent and elevated primary production during the Mid- to Late-Holocene.
136	Diatom	JPC43B	Leventer et al. (2006); Stickley et al. (2005)	Deglacial laminated sediments, recording seasonal and longer-term information on the cryospheric and palaeoceanographic conditions at this time.
137	Terrestrial	Lz1005	Cremer et al. (2007)	Lake sediment core from Amery Oasis. Geochemical analyses reveal a period of relative warmth and ice-free conditions at ~8500 cal. yr BP; unique event for East Antarctica.

138	Ice core	EPICA DomeC	EPICA community members (2004)	Longest Antarctic ice core to date, with a complete record of Antarctic climate over the past 800,000 years and atmospheric methane and carbon dioxide records from 650,000 years ago to the present.
139	Ice core	Dominion Range	Mayewski et al. (1995); Masson et al. (2000)	Holocene climate variability reconstructed highlighting an Early Holocene and a late Holocene optimum (~3000 yr BP).
140	Ice core	Law Dome	Morgan et al. (1997); Masson et al. (2000)	High-resolution record constraining the timing of deglaciation events and arguing that changes in Antarctica are not a direct response to abrupt changes in North Atlantic thermohaline circulation.
141	Ice core	Dome Fuji	Watanabe et al. (2003); Iizuka et al. (2008)	Ice core record spanning the last 340,000 years and showing remarkable similarities to the Vostok record, in both large-amplitude changes, such as terminations, interglacials and interstadials and more subtle glacial events.
142	Ice core	Vostok	Petit et al. (1999); Masson et al. (2000)	Vostok ice core provided evidence of the nature of climate, and of climate feedbacks, over the past 420,000 years. Very close association between greenhouse gases and Antarctic temperature proxy.
143	Ice core	EPICA DML	EPICA community members (2006)	Ice core record at a resolution comparable with the Greenland ice core records, spanning the last 150,000 years. Reveals one-to-one coupling between all Antarctic warm events and Greenland Dansgaard–Oeschger Events, suggesting a bipolar seesaw phenomenon.
144	Ice core	KM105	Lipenkov et al. (1998); Masson et al. (2000)	Coastal site recording short-term Holocene isotopic fluctuations, with periodicities in the multi-decadal to centennial mode.
145	Ice core	D47	Ciais et al. (1992); Masson et al. (2000)	Coastal site recording Early Holocene climatic optimum and short-term Holocene isotopic fluctuations, with periodicities in the multi-decadal to centennial mode.
146	Ice core	Byrd	Neftel et al. (1988); Masson et al. (2000)	CO_2 record reconstructed from 50,000 – 5,000 years BP (Neftel et al. 1988). Holocene climate variability also reconstructed highlighting an Early Holocene and a late Holocene optimum (~3000 yr BP) (Masson et al., 2000).
147	Ice core	Komsomolskaia	Nikolaiev et al. (1988); Ciais et al. (1992); Masson et al. (2000)	Deglaciation trend very similar to Dome C.
148	Ice core	Dome B	Jouzel et al. (1995); Masson et al. (2000)	Deglaciation events reconstructed, highlighting the existence of the Antarctic cold reversal. Evidence for

				Early Holocene climatic optimum.
149	Ice core	Plateau Remote	Mosley-Thompson, (1996); Masson et al. (2000)	~4000 year dust history for East Antarctic Plateau, revealing multi-century and multi-decadal cycles. history of dust concentration and prolonged cool phase between 2500 – 1600 yr BP.
150	Ice core	Berkner Island	Mulvaney et al. (2007)	Results unpublished so far.
151	Ice core	Siple Dome	Brook et al. (2005); Das and Alley, (2008)	Comparison of Siple Dome with Greenland cores reveals that major millennial warming events preceded abrupt warming in Greenland during the LGM and glacial-interglacial transition (Brook et al., 2005). Holocene surface melt history reconstructed from melt layers in the ice core to reveal summer temperature increase in the Mid- to Late-Holocene (Das and Alley, 2008).
152	Ice core	Taylor Dome	Mayewski et al. (1996); Steig et al. (1998)	Ice core record of last deglaciation (16,000 – 10,000 yrs BP). Comparison with a record from central Greenland shows similar variability, suggesting that rapid climate change events also occurred in Antarctica and were synchronous with Northern Hemisphere events. Record also highlights Mid Holocene changes in temperature, circulation patterns and increased greenhouse gas concentrations.